Catalytic activities of Metallophthalocyanines towards Detection and Transformation of Pollutants

A thesis submitted in fulfillment of the requirement for the degree of

Doctor of Philosophy

of

Rhodes University

by

Bolade Oyeyinka Agboola

January 2007

DEDICATION

To my parents:

Mr. Gabriel Oyetunji Agboola

and

Mrs. Deborah Olanrele Agboola

ACKNOWLEDGEMENTS

Above all, all glory be to God, my creator in which all things are possible.

My gratitude and appreciation goes to my supervisor, Prof. Tebello Nyokong. Prof., your guidance and constructive criticisms in the past three years are invaluable and highly appreciated. Thank you Prof. for the opportunity given to me to do research in Gent University, Belgium.

Special thanks go to my host at Ghent University (Belgium) Prof. Paul Kiekens for giving me the opportunity to do part of my research at the University.

I would also like to thank the following:

- My co-supervisors, Dr. Westbroek and Dr. Ozoemena for their effective supervision
- S22 research group
- Chemistry Department of Rhodes University and its staff for their assistance in numerous ways
- World Laboratory, Switzerland and University of Ghent, Belgium for financial support

I would like to thank my sweetheart, Prue for always being there for me in all ways and at all times…*mo ni ife e.*

Finally, my family back home, Daddy, Mummy and my siblings Jumoke, Gbadebo, Adeola, Adekemi and Oyinlola, thank you all for your patience, unconditional love and support.

ABSTRACT

Syntheses, spectral, electrochemical and spectroelectrochemical studies of new thiol-derivatised MPc complexes were satisfactorily carried out. For the first time, spectroelectrochemistry gave evidence for the formation of Ni^{2+}/Ni^{+} process in a NiPc complex. Significant insights as to the nature of $Fe^{+}Pc$ and $Ni^{+}Pc$ spectra were obtained.

Transformations of chlorophenols using chemical and photochemical methods are presented. For cobalt tetrasulphophthalocyanine catalysed oxidation of chlorophenols using hydrogen peroxide as the oxidant, types of oxidation products formed depended on the solvent conditions. Photolysis of aqueous solutions of chlorophenols in the presence of immobilised non-transition metal phthalocyanine photosensitisers onto Amberlite® was carried out. For the first time, $MPcS_{mix}$ complexes were immobilised on Amberlite® for use in heterogeneous photocatalysis. Photolysis of the chlorophenols resulted mainly in the formation of chlorobenzoquinone derivatives. The generation of singlet oxygen ($^1O_2$) by these immobilised MPc photosensitisers was found to play a major role in their photoactivities.

Modifications of gold electrodes with the newly synthesised thiol-derivatised MPc complexes via electropolymerisation and SAM technique are presented. Cyclic voltammetry, impedance spectroscopy (NiPcs only) and spectroelectrochemical techniques (NiPcs only) confirmed that the complexes formed films on gold electrodes. Stable and well packed SAM films as evidenced by the voltammetric characterisation were obtained. For the first time, optimisation of the time for SAM formation based on CV technique was studied. First example of a formation of MnPc-SAM was achieved.

Catalytic activities of the NiPc towards chlorophenol depended on the nature of the NiPc in the polymer films and also anti-fouling ability of the films depended on polymer film thickness. The FeTBMPc polymer modified gold electrode showed the best catalytic activity in terms of peak potential, E_p when compared to reported work in literature for nitrite electrooxidation. Cyclic voltammetry and spectroscopy studies showed that the CoPcs, FePcs and NiPcs catalysed nitrite oxidation involve 2 electrons in total while that of MnPcs involve 1 electron. Better catalytic performance towards sulphite electrooxidation were obtained for the CoPcs, FePcs and MnPcs which have metal based redox processes within the range of the sulphite electrooxidation peak while the NiPcs which did not show metal based oxidation reaction performed less.

Table of Contents

LIST OF ABBREVIATIONS

A	=	Electrode surface area (cm^{-2})
Amb.	=	Amberlite$^{@}$
ADMA	=	Tetrasodium α,α-(anthracene-9,10-diyl) diethylmalonate
AFM	=	Atomic force microscopy
Ag	=	Silver wire pseudo-reference electrode
Ag/AgCl	=	Silver/silver chloride reference electrode
$AlPcS_4$	=	Aluminium (II) tetrasulphophthalocyanine
$AlPcS_{mix}$	=	Aluminium (II) sulphonated (mixed) phthalocyanine
AlOCPc	=	Octacarboxy phthalocyaninato aluminium (III)
BQ	=	Benzoquinone
ClAlPc	=	Chloroaluminium phthalocyanine
$(Cl)_2SnPc$	=	Bis (dichloro) phthalocyaninatotin(IV)
CME	=	Chemically modified electrode
CoTBMPc	=	Cobalt tetrakis (benzyl mercapto) phthalocyanine
CoTDMPc	=	Cobalt tetrakis (dodecylmercapto) phthalocyanine
C.E.	=	Counter electrode
CMEs	=	Chemically modified electrodes
CTTs	=	Charge transfer transitions
CV	=	Cyclic voltammetry
CV	=	Cyclic voltammogram
2-CP	=	2-chlorophenol
4-CP	=	4-chlorophenol

2,4-DCP	=	2,4-dichlorophenol
DCBQ	=	Dichlorobenzoquinone
DABCO	=	Diazabicyclooctane
DBU	=	1,8-diazabicyclo[5.4.0] undec-7-ene
D	=	Diffusion coefficient ($cm^2 s^{-1}$)
DMA	=	Dimethylacetamide
DMF	=	Dimethylformamide
DMSO	=	Dimethylsulfoxide
DPBF	=	1,3-diphenylisobenzofuran
EIS	=	Electrochemical impedance spectroscopy
EQCM	=	Electrochemical quartz crystal microbalance
E_i	=	Starting potential
E_f	=	Final potential
E_p	=	Peak potential
E_{pa}	=	Anodic peak potential
E_{pc}	=	Cathodic peak potential
E^o	=	Standard potential
$E^{o'}$	=	Formal redox potential
F	=	Faraday's constant
FeTBMPc	=	Iron tetrakis (benzyl mercapto) phthalocyanine
FeTDMPc	=	Iron tetrakis (dodecylmercapto) phthalocyanines
FTIR	=	Fourier transform infrared
GCE	=	Glassy carbon electrode

$GePcS_{mix}$	=	Germanium sulphonated (mixed) phthalocyanine
$(OH)_2GePc$	=	Bis(dihydroxo) phthalocyaninato germanium(IV)
HOMO	=	Highest occupied molecular orbital
^1H NMR	=	Proton nuclear magnetic resonance
I_{pa}	=	Anodic peak current
I_{pc}	=	Cathodic peak current
IR	=	Infrared
Ic	=	Internal conversion
Isc	=	Intersystem crossing
ITO	=	Indium tin oxide
L.B.	=	Langmuir-Blodgett
LMCT	=	Ligand-to-metal charge transfer
LoD	=	Limit of detection
LUMO	=	Lowest unoccupied orbital
MLCT	=	Metal-to-ligand charge transfer
MOCPc	=	Metallated octacarboxy phthalocyanine
MPc	=	Metallophthalocyanine
$^1MPc^*$	=	Excited singlet state of the MPc photosensitiser
$^3MPc^*$	=	Excited triplet state of the MPc photosensitiser
MPc-SAM	=	Metallophthalocyanine-self assembled monolayer
MPP	=	Metalloporphyrin
$MPcS_4$	=	Metallo-tetrasulphophthalocyanine
$MPcS_{mix}$	=	Metallo-sulphonated phthalocyanine

Mn(OAc)TBMPc	=	Manganese(III)acetate tetrakis (benzyl-mercapto) Pc
Mn(OAc)TDMPc	=	Manganese(III)acetate tetrakis (dodecyl-mercapto) Pc
NADH	=	Nicotinamide adenine dinucleotide
NIR	=	Near infra red
$NiPc(NH_2)_4$	=	Nickel tetraaminophthalocyanine
NiTBMPc	=	Nickel tetrakis (benzyl mercapto) phthalocyanine
NiTDMPc	=	Nickel tetrakis (dodecyl mercapto) phthalocyanine
[O]	=	Concentration of oxidised species (mol L^{-1})
$(OH)_2SiPc$	=	Bis(dihydroxo) phthalocyaninatosilicon(IV)
$(OH)_2SnPc$	=	Bis(dihydroxo) phthalocyaninatotin(IV)
OSWV	=	Osteryoung square wave voltammogram
OTEs	=	Optically transparent electrodes
OTTLE	=	Optically transparent thin layer electrode
Pc	=	Phthalocyanine
PCP	=	Pentachlorophenol
PDT	=	Photodynamic therapy
Pp	=	Porphyrin
PVC	=	Polyvinyl chloride
Pt	=	Platinum
QCM	=	Quartz crystal microbalance
RAIRS	=	Reflection-absorption infrared spectroscopy
R	=	Gas constant
[R]	=	Concentration of reduced species (mol L^{-1})

R.E.	=	Reference electrode
R_s	=	Solution resistance
ROS	=	Reactive oxygen species
SAM	=	Self-assembled monolayer
SCE	=	Standard calomel electrode
SECM	=	Scanning electrochemical microscopy
SEM	=	Scanning electron microscopy
SERS	=	Surface enhanced raman spectroscopy
$SiPcS_{mix}$	=	Silicon sulphonated (mixed) phthalocyanine
$SnPcS_{mix}$	=	Tin sulphonated (mixed) phthalocyanine
STM	=	Scanning tunneling microscopy
SWV	=	Square wave voltammetry
T	=	Temperature (K)
TCP	=	2,4,5-trichlorophenol
$TBABF_4$	=	Tetrabutylammonium tetrafluoroborate
TCP	=	Trichlorophenol
THF	=	Tetrahydrofuran
UV-Vis	=	Ultraviolet-visible
UPD	=	Underpotential deposition
VCE	=	Vitreous carbon electrode
W.E.	=	Working electrode
XPS	=	X-ray photoelectron spectroscopy
ZnPc	=	Zinc phthalocyanine

$ZnPcS_4$	=	Zinc (II) tetrasulphophthalocyanine
$ZnPcS_{mix}$	=	Zinc (II) sulphonated (mixed) phthalocyanine
ZnOCPc	=	Octacarboxy phthalocyaninato zinc (II)
ZnTBMPc	=	Zinc tetrakis (benzylmercapto) phthalocyanine
ZnTDMPc	=	Zinc tetrakis (dodecyl mercapto) phthalocyanine

LIST OF SYMBOLS

A	=	Rate of electron transfer
Φ_{Δ}	=	Singlet oxygen quantum yield
Φ_{Q}	=	Quantum yield of the quencher
$MPc_{\Delta\Phi}$	=	Singlet oxygen quantum yield in the presence of a MPc
$MPc_{Q\Phi}$	=	Quantum yield of the quencher in the presence of a MPc
ε	=	Extinction coefficient
Γ	=	Surface coverage or concentration
Γ_{ibf}	=	Ion barrier factor
π	=	Pi bonding
λ	=	Wavelength
π^*	=	Anti pi-bonding
A	=	Absorbance
A_o	=	Initial absorbance
A_f	=	Final absorbance
A_{eq}	=	Equilibrium absorbance
A_t	=	Absorbance at time, t
C	=	Molar concentration of analyte
C	=	Speed of light
C	=	Capacitance
C_{dl}	=	Double-layer capacitance
CPE	=	Constant phase electrode

C_t	=	Concentration of chlorophenol at time, t.
C_T	=	Total interfacial capacitance.
C_m	=	Monolayer capacitance
C_o	=	Initial concentration of chlorophenol
C_{Ox}	=	Concentration of the oxidised form of an analyte
C_{Red}	=	Concentration of the oxidised form of an analyte
C_s	=	Specific interfacial capacitance
d	=	Diameter
D	=	Diffusion coefficient
D_{ox}	=	Diffusion coefficient of the oxidised form of an analyte
D_{red}	=	Diffusion coefficient of the oxidised form of an analyte
E_{pa}	=	Anodic peak potential
E_{pc}	=	Cathodic peak potential
E	=	Potential
E^o	=	Standard potential
$E_{1/2}$	=	Half-wave potential
ΔE_p	=	Anodic-to-cathodic peak potential separation
f	=	Frequency
F	=	Faraday's constant
h	=	Plank's constant
Hz	=	Hertz
I_{abs}	=	Absorbed light

i_{pa} = Anodic peak current

i_{pc} = Cathodic peak current

k = Heterogeneous electron transfer coefficient

k_f = Rate of forward reaction

k_r = Rate of reverse/backward reaction

k_{obs} = Observed rate constant

K = Equilibrium constant

K_a = Dissociation constant

$K_{O/W}$ = Partition coefficient in the octanol-water system

K = Kelvin

N = Number of electron

N_A = Avogadro's constant

$O_2 (^3\Sigma_g)$ = Triplet state oxygen

$O_2 (^1\Delta_g)$ = Singlet state oxygen

q = Electrical charge

Q = Electrical charge (C)

Q_{Bare} = Integrated electrical charge due to bare gold electrode

Q_{SAM} = Integrated electrical charge due to MPc-SAM-modified gold electrode

r = Radius of electrode

R = Universal gas constant

R_{ct} = Charge transfer resistance

R_s = Resistance of electrolyte

Sub	=	Substrate
$Sub_{(ox)}$	=	Oxidised substrate
v	=	Scan rate
V	=	Volts
V	=	Volume of OTTLE cell (L)
Z_{im}	=	Imaginary impedance
Z_{re}	=	Real impedance
Z_w	=	Warburg impedance

LIST OF FIGURES

Figures 6.9: The variation of peak currents with scan number for the voltammetric response of 1 mM NO_2^- on (a) complex **35**, (b) complex **41**, (c) complex **36**, (d) complex **34**, (e) complex **40**, (f) complex **39**-poly 30 on gold electrode.

Figures 6.10: Plot of I_p vs. $[NO_2^-]$ (a) **35**, (b) **41** (c) **36** (d) **34** (e) **40** (f) **39**

Figures 6.11: Electrooxidation of 1 mM nitrite in phosphate buffer on *poly*-MPc, (a) E_p vs. log *v*, (b) I_p vs. $v^{1/2}$, (c) $I_p v^{1/2}$ vs. *v*. *Poly*-MPc: (i) **35**, (ii) **40**, (iii) **36**, (iv) **41**, (v) **34**, (vi) **39** modified Au electrode.

Figure 6.12: Electronic spectral changes of (a) complex **35** on addition of 1 mM nitrite solution in DMSO, (b) on addition of $NaBH_4$ to the final spectrum in (a).

Figure 6.13: Electronic spectral changes of complex **36** on addition of 1 mM nitrite solution in DMSO.

Figure 6.14: Electronic spectral changes of complex **34** on addition of 1 mM nitrite solution in DMSO.

Figure 6.15: Cyclic voltamogramms for 1 mM nitrite oxidation in phosphate buffer pH 7.4 solution at (a) an unmodified Au electrode, (b) *poly*-NiTDMPc-Au, (c) *poly*-NiTBMPc-Au, (d) *poly*-Ni(OH)TDMPc-Au and (e) *poly*-Ni(OH)TBMPc-Au.

Figure 6.16: The variation of peak currents with scan number for the voltammetric response of 1 mM NO_2^- on (a) *poly*-NiTDMPc-Au, (b) *poly*-NiTBMPc-Au, (c) *poly*-Ni(OH)TDMPc-Au and (d) *poly*-Ni(OH)TBMPc-Au. Buffer = pH 7.4.

Figure 6.17: The variation of peak currents with nitrite concentration for the voltammetric response on (a) *poly*-NiTBMPc-Au, (b) *poly*-NiTDMPc-Au, (c) *poly*-Ni(OH)TBMPc-Au and (d) *poly*-Ni(OH)TDMPc-Au. Buffer = pH 7.4.

Figure 6.18: (a) Cyclic voltamogramms of electrooxidation of 1 mM nitrite at different scan rates catalysed by *poly*-Ni(OH)TBMPc-Au electrode. Plot of (b) E_p vs. log *v*, (c) Ip vs. $v^{1/2}$ and (d) $I_p v^{-1/2}$ vs. v for electrooxidation of 1 mM nitrite solution on (i) *poly*-NiTBMPc-Au and (ii) *poly*-NiTDMPc-Au, (iii) *poly*-Ni(OH)TBMPc-Au and (iv) *poly*-Ni(OH)TDMPc-Au

Figure 6.19: Electronic spectral changes of (a) complex **37** on addition of 1 mM nitrite solution in DMSO to approx. 2 µM solution of the complexes in DMSO. (i) initial spectrum, (ii) final spectrum after 20 minutes.

Figure 6.20: Cyclic voltamogramms for 1 mM sulphite oxidation in phosphate buffer pH 7.4 solution at (i) unmodified gold electrode, (**a**) complex (ii) **34**, (iii) **35**, (iv) **36**, (v) **37**, (**b**) (vi) **39**, (vii) **40**, (viii) **41** and (ix) **42.**

Figure 6.21: Cyclic voltamogramms for 1 µM sulphite oxidation in phosphate buffer pH 7.4 solution at (i) unmodified gold electrode, complex (ii) **35**, (iii) **36**, (iv) **34** and (v) **37**

Figure 6.22: Plots of I_p vs. $[SO_3^{2-}]$ at complex (**a**) (i) **34**, (ii) **35**, (iii) **36**, (iv) **37**, (**b**) (v) **39**, (vi) **40**, (vii) **41** and (vii) **42**. Scan rate = 100 mV s^{-1}.

Figure 6.23: Plots of I_p vs. number of scans for repetitive cycling of 1 mM sulphite at complex (**a**) **34, 35**, **36, 37** (**b**) **39**, **40**, **41, 42.** Scan rate = 100 mV s^{-1}.

Figure 6.24: (a) Typical cyclic voltamogramms at different scan rates catalysed by complex **41**-SAM electrode, Plot of (b) E_p vs. log v, (c) I_p vs. $v^{1/2}$ on (d) I_p $v^{-1/2}$ vs. v for electrooxidation of 1 mM sulphite with complexes (i) **34**, (ii) **35**, (iii) **36**, (iv) **37**, (v) **39**, (vi) **40**, (vii) **41** and (viii) **42**.

LIST OF SCHEMES

LIST OF TABLES

CHAPTER 1

INTRODUCTION

1.1 Introduction to Metallophthalocyanines (MPcs)

Phthalocyanine (Pc) complexes are a special class of compounds that have similar structure to tetraazoporphyrin with additional four fused benzo rings (**1,** Figure 1.1).[1,2] Pcs were discovered in the 1900s.[2-5] Traditionally, they have been used as dyes and pigments due to their intense blue-green colour.[5] These class of molecules have high extinction coefficients which are of order of 10^5 M^{-1} cm^{-1} and they are thermally and chemically stable.[6-7] Phthalocyanines consists of 16 carbon and 8 nitrogen atoms and have a two-dimensional 18π electron conjugated system, in which more than 70 different metals and non-metals can be incorporated. Incorporation of different ring substituents in the peripheral and non peripheral positions is also possible. Many of Pc properties, for example, solubility can be varied by changing the central metal ions, axial ligands and ring substituents.[8,9]

As stated above, metallophthalocyanines (MPcs) are unique in terms of physical and chemical properties, which have resulted to a wide range of applications. Over the years phthalocyanine complexes have attracted many applications in areas such as catalysis[10-14], sensors[15-17] and photodynamic therapy (PDT).[18-22] New applications of MPcs are emerging, these include ink jet printing,[23] electrophotography,[23,24] photocopying and laser printing,[23,25] electrochromic display devices,[26-28] optical computer re-writable discs and information storage systems,[29-31] liquid crystal display devices,[9,32] photovoltaic cells,[33,34] fuel cells,[35] molecular electronics,[36] semi-conductor devices[1,37-39] and electrochemical sensors.[16,17,40]

MPcs especially the FePcs and MnPcs have been shown to have the ability to mimic the certain enzymes catalytic behaviour,[41-46] this enzyme-like catalytic behaviour will be further discussed later in this chapter.

Non-transition metal MPc complexes are widely used as photocatalysts for degradation of pollutants such as chlorophenols.[47-53] For use as photosensitisers in photodynamic therapy,[18-22,54-57] MPc complexes containing non-transition central metal ions such as Zn^{2+} and Al^{3+} are preferred.

MPcs containing redox active transition metal ions such as Co^{2+}, Fe^{2+} and Mn^{3+} are known to be effective electrocatalysts and electrochemical sensors under homogenous and heterogeneous conditions.[58-67]

This work focuses on the use of MPcs as photocatalysts and chemical/enzyme-like catalysts for the degradation of phenolic pollutants and electrocatalysts for detections of pollutants such as chlorophenols, nitrite and sulphite.

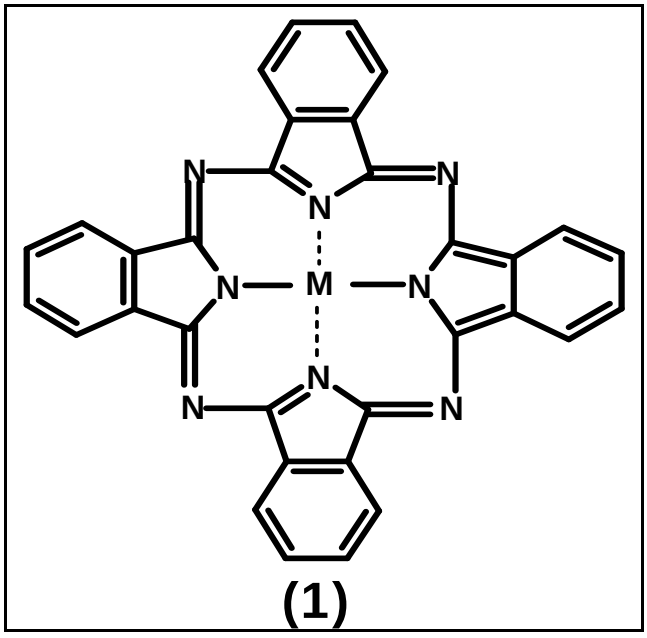

Figure 1.1: The structure of metallophthalocyanine (MPc)

1.1.1 General synthetic methods

Synthesis of phthalocyanines can be achieved using different routes depending on the type of phthalocyanines to be synthesised; metal free, symmetrical and asymmetrical metallophthalocyanines. Various precursors such as phthalonitrile, phthalic acid, phthalic acid anhydride, phthalimide, diiminoisoindoline and o-cyanobenzamide have been developed for this syntheses.[68-71] Phthalonitrile **(2),** phthalic anhydride **(3)**, phthalic acid **(4)** and phthalimide **(5)** Figure 1.2, are the most used precursors for the synthesis of MPcs.

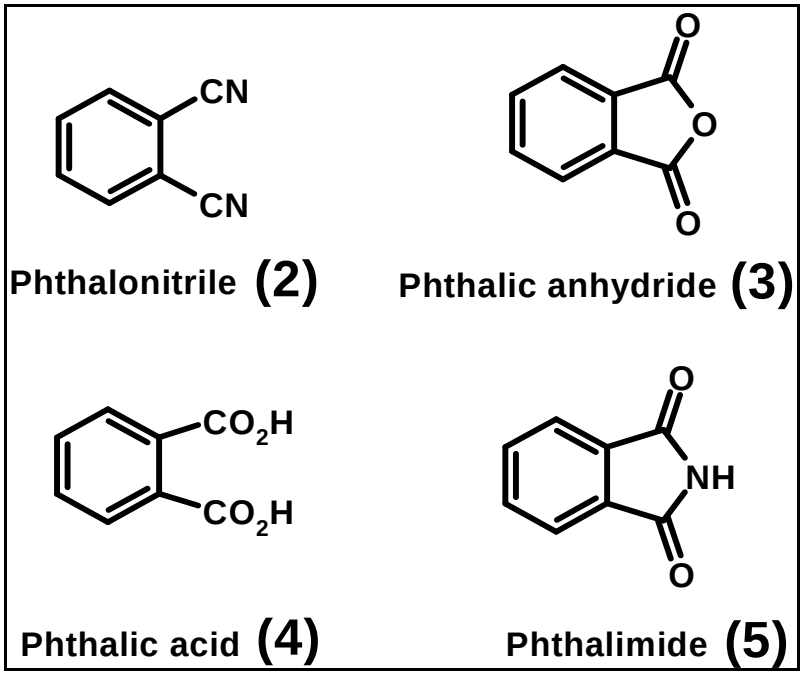

Figure 1.2: The structure of some MPcs precursors

In terms of choice of precursors for phthalocyanines synthesis, the use of phthalonitrile provides a mild and clean process[72] with high yields of very pure MPcs suitable for research purposes while the use of phthalic anhydride is relatively a cheap method but the MPcs obtained are usually not as pure as the former. Synthesis using phthalic anhydride

(3) also require the presence of nitrogen source such as urea and a catalyst such as ammonium molybdate or boric acid,[1] the latter is widely used for commercial purposes.

Scheme 1.1 shows the synthetic route for unsubstituted metal free phthalocyanines **(6)** from phthalonitrile **(2).** The synthesis occurs by simple heating of phthalonitrile with either (a) a base such as ammonia (NH_3) or 1,8-diazabicyclo[5.4.0]undec-7-ene (DBU), (b) labile metal or metal salt such as Li^+, Na^+ or K^+ in alcohol followed by addition of acid to yield the metal-free phthalocyanines or (c) organic reducing agents such as hydroquinone or 1,2,3,6-tetrahydropyridine which provide the two electrons and two protons required for cyclotetramerisation of the phthalonitrile.[73,74]

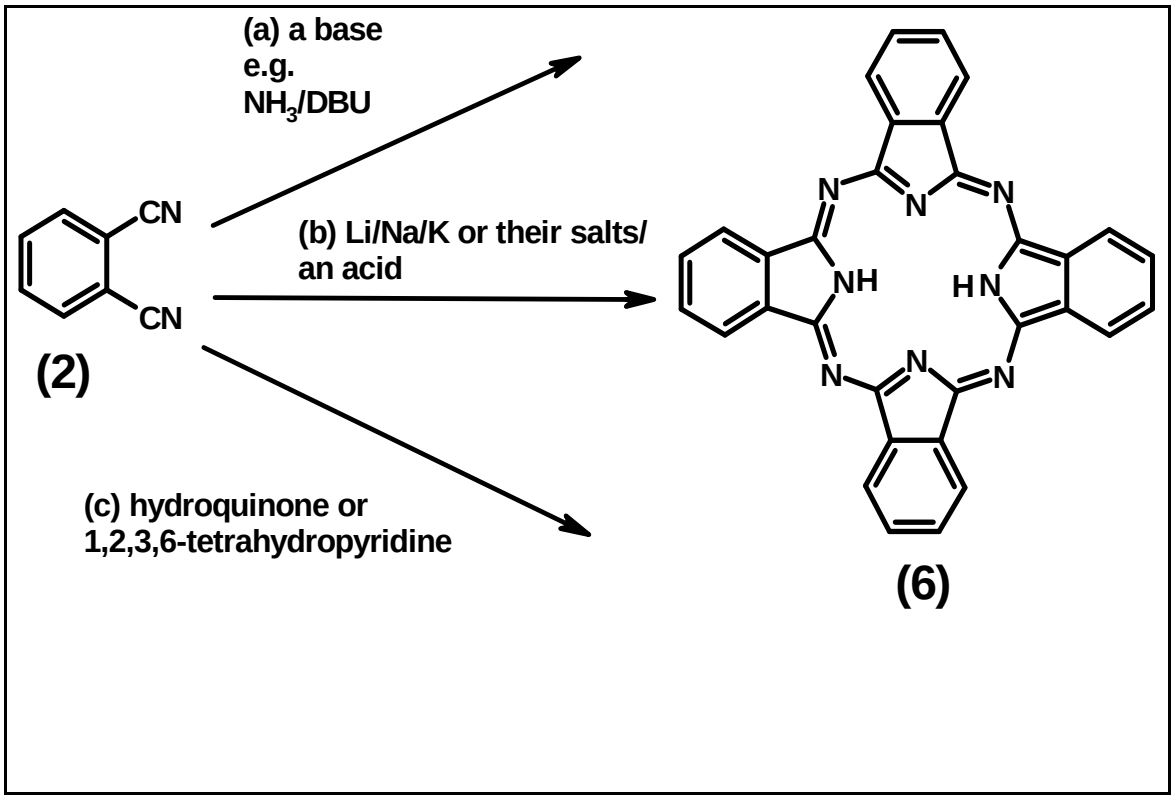

Scheme 1.1: Synthesis of MPcs from o-cyanobenzamide and phthalonitrile[73,74]

For the synthesis of metallated phthalocyanines, precursors such as phthalonitrile **(2)**, phthalic anhydride **(3),** phthalic acid **(4)**, and phthalimide **(5)** are often used, Scheme 1.2. Basically, the reactions involve cyclotetramerisation of the precursor by heating it at high temperature with a suitable metal or metal salt in the presence of a base such as DBU and in a suitable solvent such as dimethyl formamide (DMF), dimethyl sulphoxide (DMSO), hydroquinone and quinoline. Also unmetallated phthalocyanine **(6)** can be metallated by heating in the presence of metal or metal salt, using aromatic solvents such as 1-chloronaphthalene and quinoline.[75]

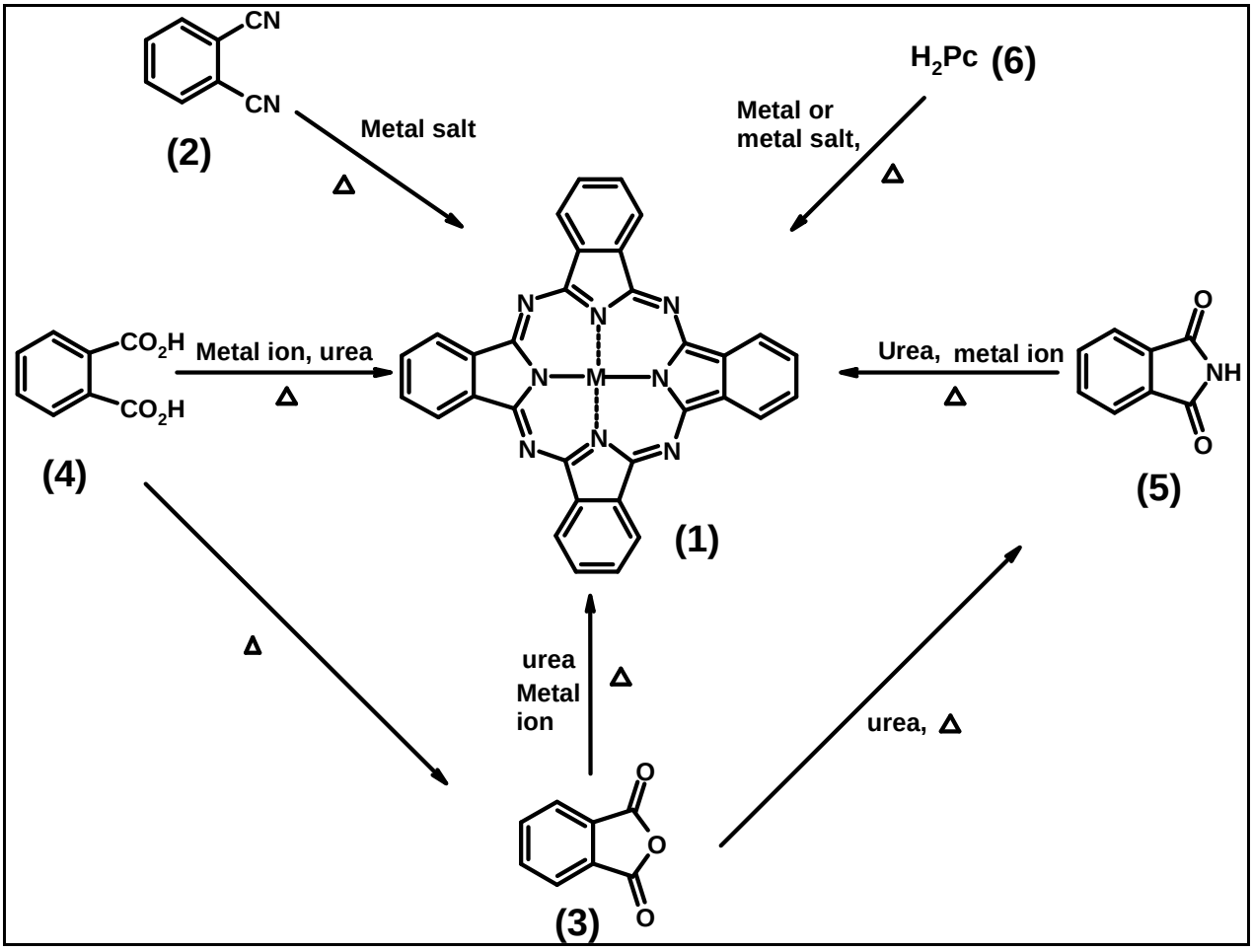

Scheme1.2: Synthesis of symmetrical MPcs from some precursors

By using mono (for tetrasubstituted MPcs) and di (for octasubstituted MPcs) substituted phthalonitrile **(7)** or substituted form of other precursors such as phthalic acid **(8)**, symmetrically substituted MPc **(9)** can be synthesised, some of the synthetic routes are shown in Scheme 1.3.

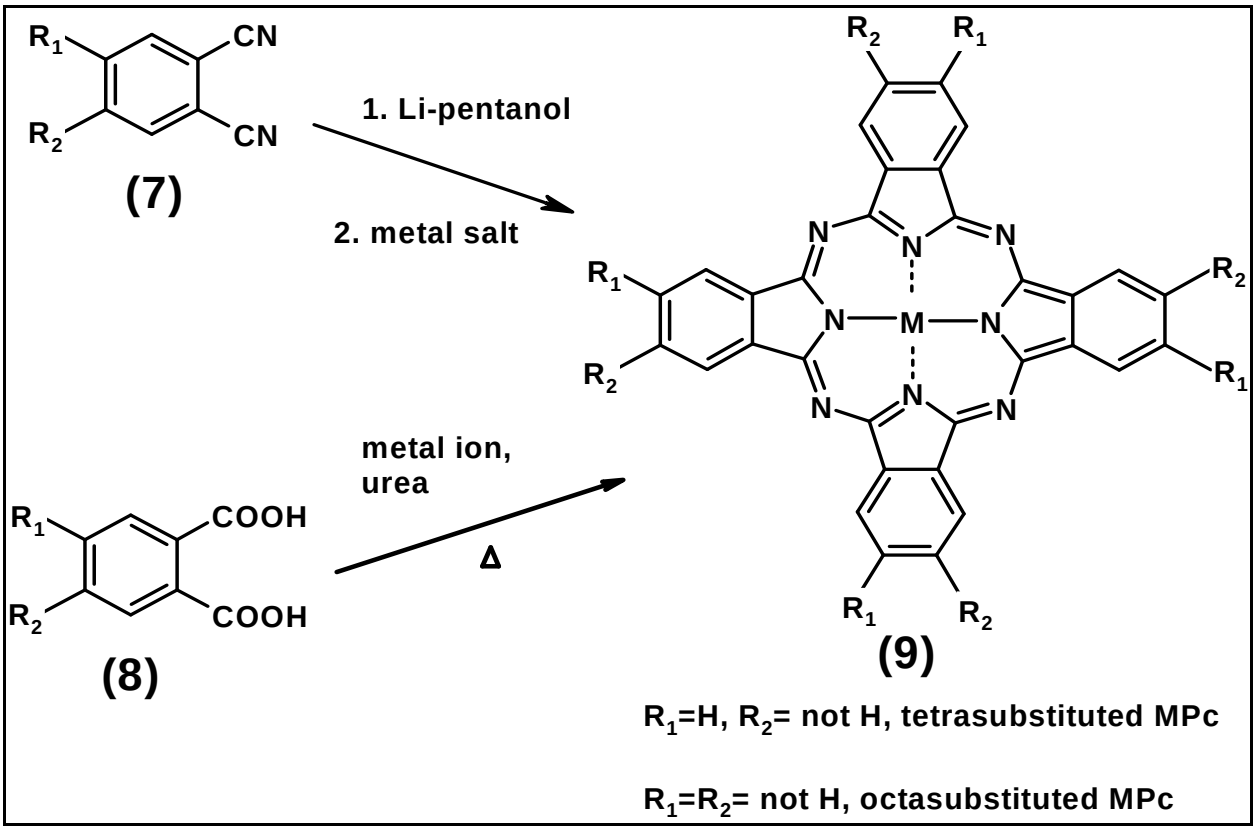

Scheme1.3: Synthesis of symmetrically substituted MPcs from some precursors

Introduction of ring substituents such as sulphonic[76] and carboxylic acid[77,78] to MPc complexes enable the complexes to be water soluble. Weber and Bush method[76] is a popular and effective way of synthesizing metallo-tetrasulphophthalocyanine ($MPcS_4$) **(10)**; the method involves refluxing at a high temperature (about 180^{o}C) a mixture of the

monosodium salt of the 4-sulphonic acid **(11)**, urea and appropriate metal salt in nitrobenzene in the presence of ammonium molybdate as catalyst, Scheme 1.4.

A mixture of sulphonated MPc complexes ($MPcS_{mix}$) can be obtained by direct sulphonation of unsubstituted MPc with oleum.[79]

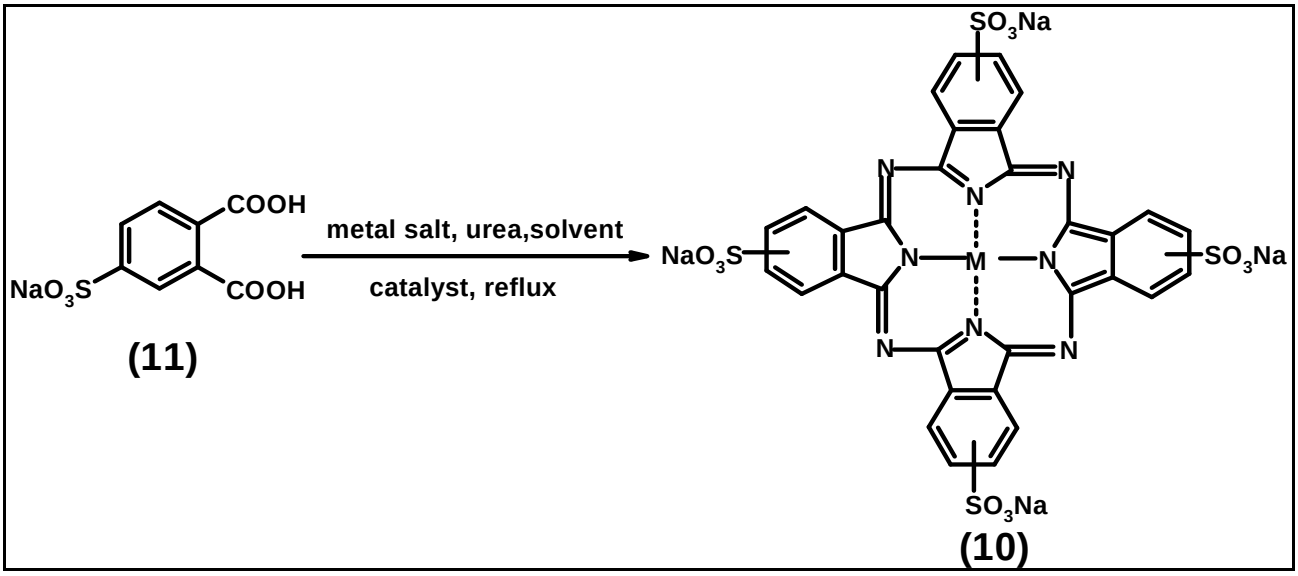

Scheme 1.4: General synthetic route for tetra sodium salt of metallo-tetrasulphophthalocyanine ($MPcS_4$)[76]

Metallated octacarboxy phthalocyanine (MOCPc) complexes **(12)** can be obtained using the reaction shown in Scheme 1.5. Basically, they are obtained from benzene-1,2,4,5-tetracarboxylic dianhydride **(13)** in the presence of urea using DBU as a catalyst.[77,78] Tetra-amido metallophthalocyanine **(14)** is obtained as the intermediate and is easily converted by acid hydrolysis to metallated octacarboxy phthalocyanine (MOCPc) complexes **(12)** by reacting it with aqueous sulphuric acid, H_2SO_4.

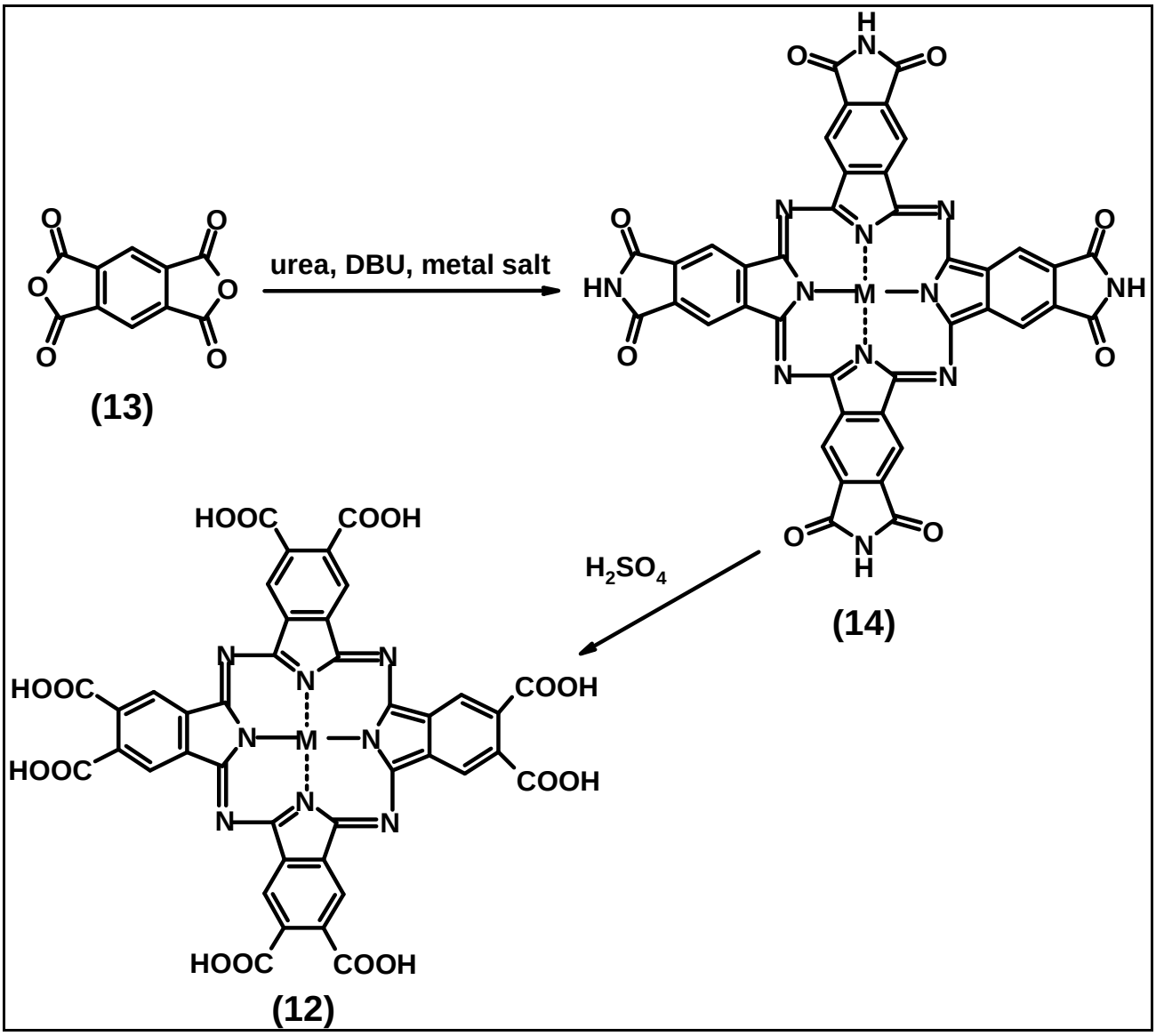

Scheme 1.5: Synthetic route for water-soluble octacarboxy-metallophthalocyanine, (MOCPc)[77,78]

In this work, water soluble metallo-sulphonated phthalocyanine ($MPcS_{mix}$, where S = SO_3^-) complexes, (Al^{3+}, Co^{2+}, Zn^{2+}, Ge^{4+}, Si^{4+} and Sn^{4+}) will be employed as catalysts for degradation of chlorophenols. The complexes will either be tetrasulphonated, $MPcS_4$ (where S = SO_3^-) or will contain a mixture of sulphonated groups, $MPcS_{mix}$. Octasubstituted MPcs with carboxylic groups will also be employed.

Thiol substituted MPcs will also be used in this work hence their general synthesis follows. The synthesis of thiol derivatised MPcs has been reported by some researchers.[58,80-93] Cook and co-workers[86-90] and Lieberman and co-workers[91-93] have been actively involved in the synthesis of thiol-derivatised phthalocyanines for the fabrication of self assembled monolayer (SAMs.). Thiol-derivatised MPcs with long chain alkyl ring substituents have been synthesised for the use as liquid crystals.[84] There are also thiol derivatised MPcs complexes which are used as IR absorbers[93] since the substituents are known to cause high red shift of the Q band.

The synthetic route adopted for the thiol derivatised MPcs synthesised in this work is shown in Scheme.1.6.[81] Basically, it is the cyclotetramerisation of monosubstituted thiol phthalonitrile **(15)** in the presence of the desired metal ion salt to give a tetrasubstituted thiol-derivatised MPc **(16)**.

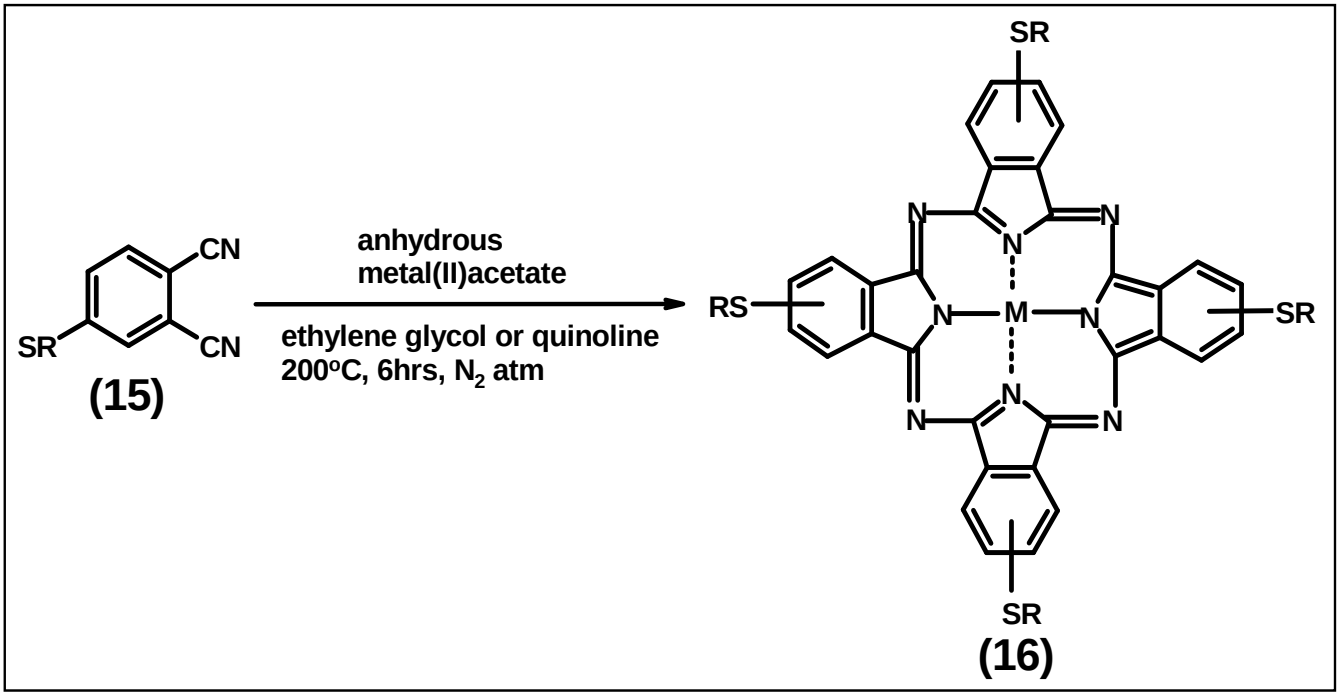

Scheme 1.6: Synthesis of symmetrical thiol derivatised MPc.[81]

Mechanisms in the formation MPcs

Since the preparation of phthalocyanines can be achieved via many routes, several mechanisms have been proposed. The mechanism of the formation of MPcs is basically the cyclotetramerisation of the precursor such as diiminoisoindoline **(17)** as shown in Scheme 1.7.[72] The first major step in the mechanism is the condensation reaction between the Pc precursors leading to formation of reactive intermediates with two isoindole unit. This is then followed by combination of the reactive species and central metal ion coordination which leads to MPc complex formation. Some intermediates isolated from these reactions have given some insights into how these complexes are formed even though the mechanism is not fully understood. The reaction leading to the formation of MPc complexes are generally thermodynamically feasible.[1]

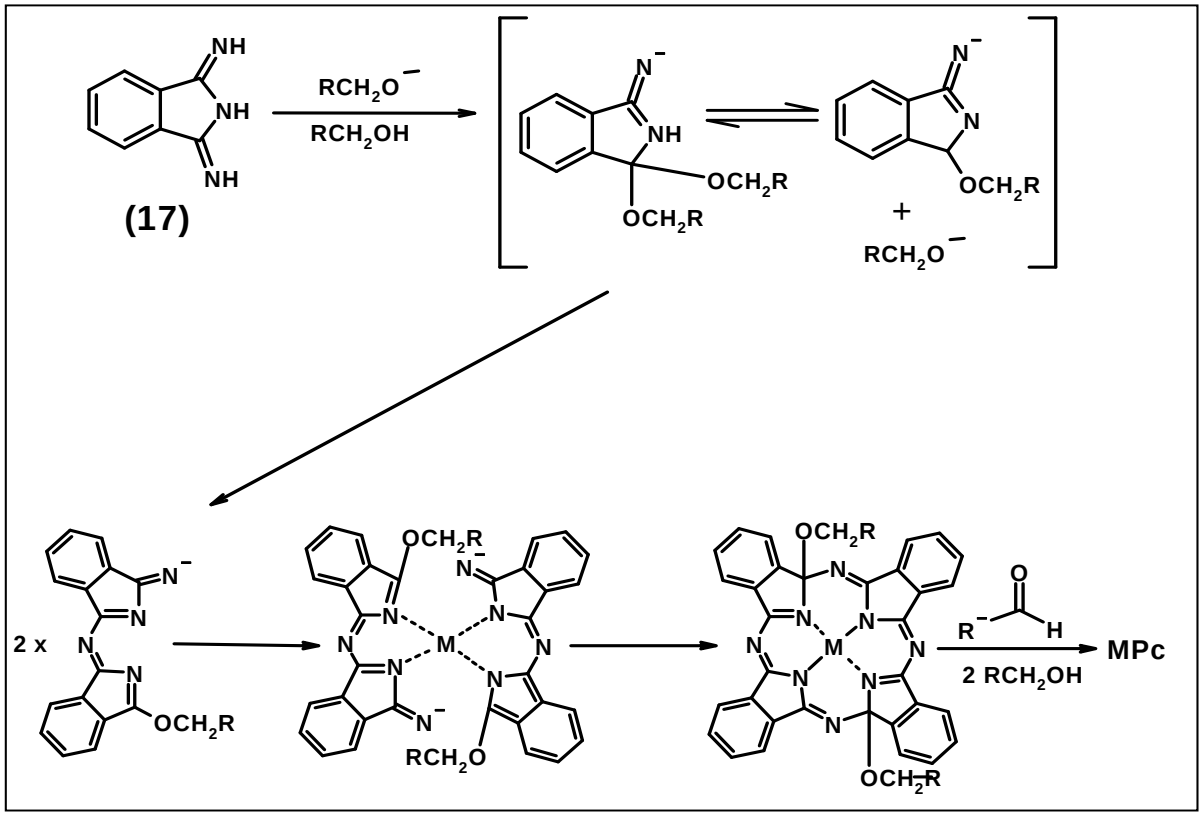

Scheme 1.7: Mechanistic scheme for MPcs forming reactions.

Aim of Thesis

The synthesis of thiol-derivatised benzyl mercapto and dodecyl-mercapto tetra substituted Co^{2+}, Fe^{2+}, Mn^{3+}, Ni^{2+} and Zn^{2+} MPc complexes will be carried out in this thesis. The choice of the first row transition central metal ions is because their macro complexes are known to be excellent electrocatalysts. Table 1.1 shows the list of some thiol-derivatised MPcs reported in literature. Sulphur containing groups as ring substituents will make the complexes to be suitable for gold electrode modification as SAMs. To date, there has been no reported work on the synthesis of a thiol-derivatised MPc containing Mn ion as the central metal despite the very rich and interesting Mn redox chemistry. In this work, benzyl mercapto ring substituents was chosen because it is a possible precursor for the synthesis of MPcs with –SH group (which are the ideal MPcs for SAM) and will be good for comparative studies with MPcs with long chain alkyl group. MPcs with dodecyl mercapto group were synthesised because long chain alkane thiols are known to form highly stable SAMs on gold. The influence of MPc ring substituents on the stability of SAMs should be of great interest and will be investigated in this thesis. Electropolymerisation of these complexes on gold electrodes will also be carried out and they will also be employed as electrocatalysts.

Table 1.1: List of known thiol-derivatised MPcs.

Thiol-derivatised MPc	**Metal free/ Central metal ion**	**References**
Octakis (hexylthio)-metallophthalocyanines	H^{+}, Zn^{2+}, Cu^{2+}	94
Octakis (phenylthio)-metallophthalocyanines	Co^{2+}, Fe^{2+}	95
Tetrakis (alkylthio)-metallophthalocyanines	H^{+}, Ni^{2+}	96
Octakis (hydroxyethylthiol)-metallophthalocyanines	H^{+}, Co^{2+}, Zn^{2+}, Ni^{2+}	97
Octakis (butylthiol and hydroxylthiol)-metallophthalocyanines	Zn^{2+}, Co^{2+}, Fe^{2+}	58, 67
1,4,8,11,15,18-Hexahexyl-22-[8-methylsulfonyloxy) octyl]-25-methyl-phthalocyanine	H^{+}	98
1,4,8,11,15,18-Hexahexyl-22-[3-(methylsulfonyloxy) propyl]-25-methyl-phthalocyanine	H^{+}	98
1,4,8,11,15,18-Hexahexyl-22-(8-mercaptooctyl)-25-methyl-phthalocyanine	H^{+}	98
1,4,8,11,15,18-Hexahexyl-22-(3-mercaptopropyl)-25-methyl-phthalocyanine	H^{+}	98
Octakis or tetrakis (Octylthiol or octylsulphonyl)-phthalocyanines	Cu^{2+}, Ni^{2+}	99
'Umbrella SiPc'	$Si^{4+}(CH_3)[O(CH_2)_2SH]$	91
'Octopus SiPc'	$Si^{4+}(OCH_3)_2$	91
1,(4)- and 2,(3)-(tetraphenylthio phthalocyaninato)-titanium(IV)oxide	Ti^{4+}=O	100
1,(4)- and 2,(3)-(tetrabenzylthio phthalocyaninato)-titanium(IV)oxide	Ti^{4+}=O	100

1.1.2 Spectral properties

1.1.2.1 Electronic spectra

Figure 1.3 shows typical electronic absorption spectrum of an MPc complex. The spectrum consists of distinct band in the visible spectrum called the Q band which is the most intense band and the B or Soret band[101,102] lying just to the blue of the visible region near 340 nm.

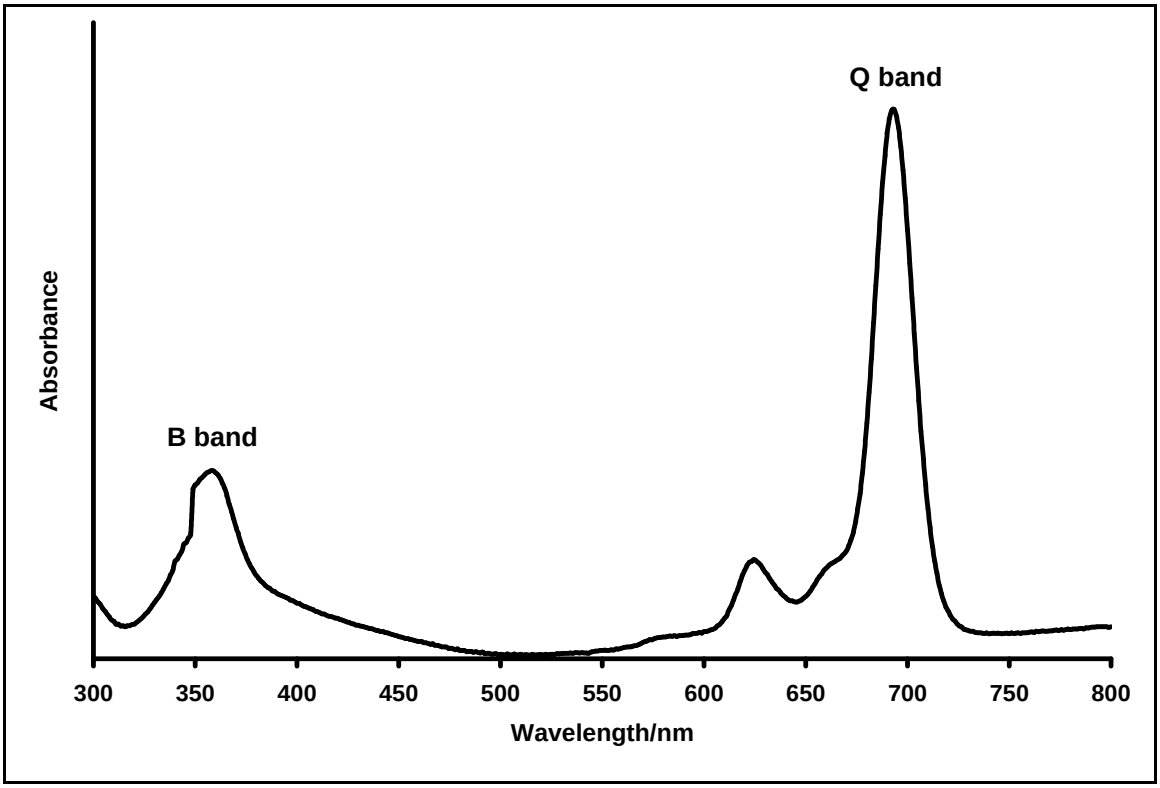

Figure 1.3: Typical electronic absorption spectrum of MPc

The origin of the UV-Visible spectrum is well explained by Gouterman's 4-orbital linear combination of atomic orbital model,[6] Scheme 1.8. According to the theory, the highest occupied molecular orbitals (HOMOs) of the MPc ring are the $a_{1u}(\pi)$ and $a_{2u}(\pi)$, the lowest unoccupied orbital (LUMO) of the MPc ring is the $e_g(\pi)$. The Q and B bands arise

from transitions from the $a_{1u}(\pi)$ (Q band), and $a_{2u}(\pi)$ and b_{2u} (B bands), respectively to the e_g orbital. There are other bands exhibited by MPcs, bands such as N, L and C bands which occur at high-energy (below 300 nm) in the ground state electronic absorption spectra of some diamagnetic MPcs such as ZnPcs and MgPcs.[103]

There are also possibilities of charge transfer transitions (CTTs)[7,8] which usually appear as weak absorption bands between Q and B bands. If the central metal has d-orbital lying within the HOMO-LUMO gap there is a possibility for the CTT occurring, which either can be metal to ligand (MLCT) or ligand to metal (LMCT), Scheme 1.8.

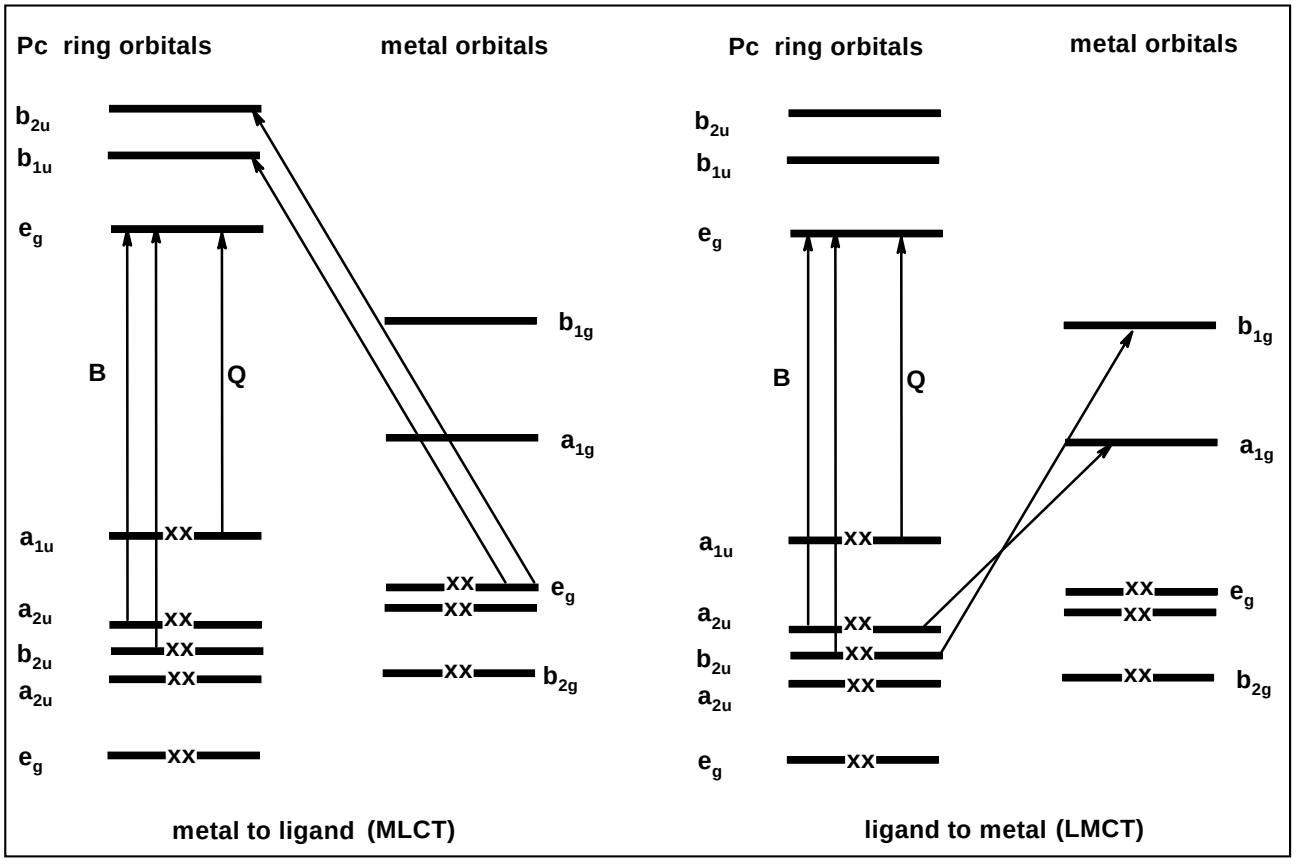

Scheme 1.8: Gouterman's 4-orbital linear combination of atomic orbital model.[6]

Metal oxidation or reduction is characterised by a shift in Q band without much lowering in intensity while ring oxidation will result in collapse of the Q band and formation of a broad peak at around 500 nm. This results in a 'hole' in the a_{1u} (π) level which allows transition from the low-lying, $e_g(\pi)$ level to the HOMO. Ring reduction also results in collapse of Q band followed by formation of new bands between 550 nm and 650 nm. Scheme 1.9 shows the energy level diagram for one-electron ring reduced or ring oxidised MPc complex.

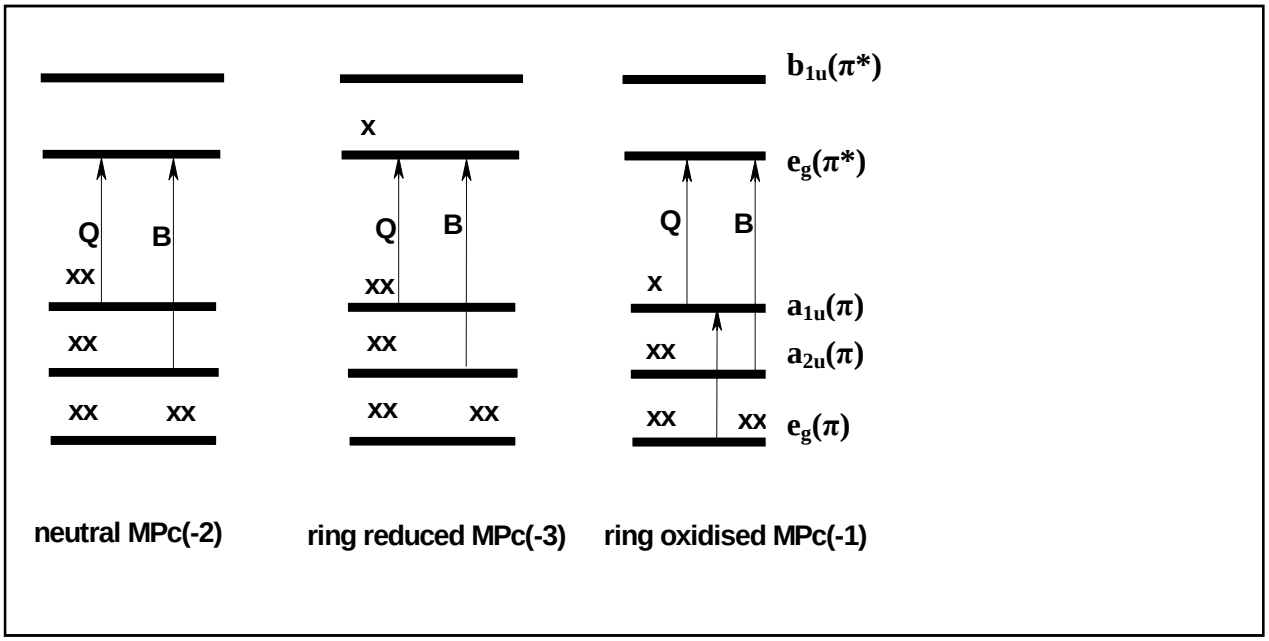

Scheme 1.9: Energy level diagram for one-electron ring reduced or ring oxidised MPc complex.

Aggregation in MPcs can be described as the association of molecules leading to dimers, oligomers or mixtures of both. Aggregation can be due to the following processes;[101] direct linkage or bridge between two or more phthalocyanine rings (i.e. intramolecular interaction),[104] covalent bonding between the metals as μ-oxo-links (especially MPc complexes of Fe and Si),[35,105] sandwich-type complex formation in which two MPc rings

share one central metal,[106-108] or by weak association whereby the peripheral substituents hold two rings in space.[109] The degree of aggregation in the latter type of MPc complexes in solutions depends on the π-π interaction, Van der Waal forces and hydrogen bonding between MPc molecules and/or with solvents. The effectiveness of these interactions depend on factors such as the closeness of the ring, the overlap position, the tilt angle the Pc ring adopt, the bulkiness of the peripheral groups, and the extinction coefficient[102] of the electronic bands involved. High concentration of MPc complexes encourages aggregation, since this will bring closeness of the neighboring MPc rings. The bulkier the peripheral groups, the less the aggregation, since bulkier groups reduces the closeness of the rings. Also, symmetrical MPcs tend to have more aggregation than the unsymmetrical ones; this can be attributed to the more effective overlap of the rings in symmetrical MPcs than in the unsymmetrical ones. The nature of solvents also plays a role in aggregation formation; aggregation tends to be more pronounced in polar solvents than in non polar solvents. In polar solvents, stronger interactions occurs, for example, hydrogen bonding occurs between water molecules and ring substituents such as sulphonated group. The effect of aggregation on the electronic spectra of MPcs can be seen by the blue shift in the Q band, splitting and broadening of the Q band.

The solid state spectra of MPc complexes can be studied mainly as thin films by electrodeposition on transparent electrodes such as indium tin oxide (ITO)[110] and immobilised on materials such as silica gel[111] and Amberlite®[112,113] Solid state spectra of MPc complexes are usually broader but not necessarily showing more aggregation behaviour than their respective solution spectra.

1.1.2.2 Infra red spectroscopy

The infra red (IR) spectra of MPc complexes are typically complex but similar. The main bands are the C-H stretching vibration at around 3030 cm^{-1}, C-C ring skeletal stretching vibrations at around 1600 and 1475 cm^{-1}, C-H out of plane bending vibrations at around 750-790 cm^{-1},[114] all these bands are from the aromatic ring of the MPc. The unmetallated phthalocyanines can be distinguished from the metallated ones by the presence of N-H stretching vibration at near 3298 cm^{-1} [115] in the former but absence of the band in the latter. For thiol derivatised MPcs, the prominent band is the aryl C-S stretching vibration which can be found at around 715-670 cm^{-1}.

1.1.2.3 ^{1}H NMR spectroscopy

Proton nuclear magnetic resonance (^{1}H-NMR) signal for symmetrical MPcs generally appears at lower field because of the deshielding effect of the induced secondary field in the phthalocyanine ring. The peripheral and non-peripheral H atoms resonances are of equal intensity for unsubstituted MPcs. The signals are generally broad for tetra-substituted MPcs because they exist as mixtures of isomers while the octa substituted MPcs in all cases exhibit well defined spectra because they exist as just one isomer. The ^{1}H-NMR signal for MPcs with transition metal ions such as Co^{2+}, Mn^{3+} and Fe^{2+} are usually broad because of the paramagnetism of the metal ions.

The incorporation of axial ligands or ring substituents can lead to more complicated ^{1}H-NMR spectra for MPc complexes and can also shift the signals to lower or higher field depending on the nature and positions of the substituents. Ideally, electron donating groups are expected to shift the ^{1}H-NMR signals to lower field while the reverse will be

the case for the electron withdrawing groups. For the same electron-donating ring substituents, ^{1}H-NMR signals usually shift to a lower field for the MPc complexes with substituents in non-peripheral positions than those with substituents in peripheral positions.[100]

1.1.3 Photochemistry

Non-transition metal MPcs complexes are well known red light photosensitisers. Non-transition metals such as Zn^{2+} and Al^{3+} are diamagnetic and have long triplet lifetimes and a relatively high triplet quantum yield suitable for photocatalytic purposes.[116,117] Non-transition MPcs produce singlet molecular oxygen ($^{1}O_2$, ($^{1}\Delta_g$)) on exposure to red light,[116,117] through Type II mechanism, Scheme 1.10. The energy transfer starts with the excitation of the sensitizer by irradiation with visible light, which yields the excited singlet state (^{1}MPc*) and then by intersystem crossing (isc) gives the excited triplet state (^{3}MPc*), equation 1.1, Scheme 1.10. This is followed by energy transfer from ^{3}MPc* to ground state (triplet) oxygen ($^{3}O_2$, ($^{3}\Sigma_g^{-}$)) resulting in generation of singlet oxygen ($^{1}O_2$, ($^{1}\Delta_g$)), equation 1.2. Although the excited singlet states of MPc (^{1}MPc*) have a higher energy (1.8-1.9 eV) than the triplet states (^{3}MPc*) (1.1 – 1.3 eV), the former has relatively lower lifetimes making the latter more important in photochemical process. The processes in Scheme 1.10 are feasible since the triplet states of MPcs are readily quenched by molecular oxygen. Singlet oxygen ($^{1}O_2$, ($^{1}\Delta_g$)) is the reactive species[22,118-120] during the photocatalytic applications of MPcs in areas such as photodynamic therapy and photodegradation of pollutants. The other possible process is the Type I mechanism, in this case, the triplet state of the MPc (^{3}MPc*) either reacts directly with a substrate

(equation 1.3) or molecular oxygen by electron transfer to generate the oxidised $MPc^{+\cdot}$ and superoxide radical ($O_2^{-\cdot}$), equation 1.4 in Scheme 1.10. Type II mechanism is known to be the predominating process in PDT and in photodegradation of pollutants such as chlorophenols. Equations 1.5 and 1.6 of Scheme 1.10 respectively show the reactions of $^1O_2$, and $O_2^{-\cdot}$ with substrates during photocatalysis processes.

$$MPc \xrightarrow{hv} {}^1MPc^* \xrightarrow{isc} {}^3MPc^* \quad (1.1)$$

$$O_2\ (^3\Sigma_g^-) + {}^3MPc^* \longrightarrow MPc + O_2\ (^1\Delta_g) \quad (1.2)$$

$$^3MPc^* + Sub \longrightarrow MPc^{-\cdot} + Sub^{+\cdot} \quad (1.3)$$

$$^3MPc^* + O_2 \longrightarrow MPc^{+\cdot} + O_2^{-\cdot} \quad (1.4)$$

$$O_2\ (^1\Delta_g) + Sub \longrightarrow Sub_{(ox)} \quad (1.5)$$

$$O_2^{-\cdot} + Sub \longrightarrow Sub_{(ox)} \quad (1.6)$$

isc = intersystem crossing

Sub = substrate

Scheme 1.10: Type I and Type II photoreaction mechanisms in MPc sensitiser

1.2 Basics of Electrochemistry

Electrochemistry is employed in this work for characterisation of MPcs and for electrocatalytic studies. Thus this section gives a brief overview of electrochemical techniques employed.

1.2.1 Cyclic voltammetry

Cyclic voltammetry (CV) is the most widely used electrochemical technique. The technique can be used to study electron transfer mechanisms in reactions including providing information on the reversibility, kinetics, formal reduction and oxidation potentials of a system.[121-126]

In a cyclic voltammetry experiment, the potential of an electrode is cycled from a starting potential, E_i to a final potential, E_f (the potential is also called the switching potential) and then back to E_i, Figure 1.4. The potential at which the peak current occurs is known as the peak potential, E_p. At this potential, the redox species has been depleted at the electrode surface and the current is diffusion limited. The magnitude of the Faradaic current, I_{pa} (anodic peak current) or I_{pc} (cathodic peak current), is an indication of the rate at which electrons are being transferred between the redox species and the electrode.

Cyclic voltammetric processes could be reversible, quasi-reversible and irreversible.

A **reversible process** obeys the Nernst reaction in which the electron transfer is rapid, allowing the assumption that the concentration of both the oxidised (O) and the reduced species (R) are in a state of equilibrium (equation 1.7). Figure 1.4 shows a typical CV for a reversible process. The electroactive species are stable and so the magnitudes of I_{pc} and

I_{pa} are equal and they are proportional to the concentrations of the active species. ΔE (E_{pa}-E_{pc}) should be independent of the scan rate, *v* but in practice ΔE slightly increases with *v*, this is due to the solution resistance, R_s between the reference and working electrodes.[127]

$$\mathbf{O} + ne^- \rightleftharpoons \mathbf{R} \qquad (1.7)$$

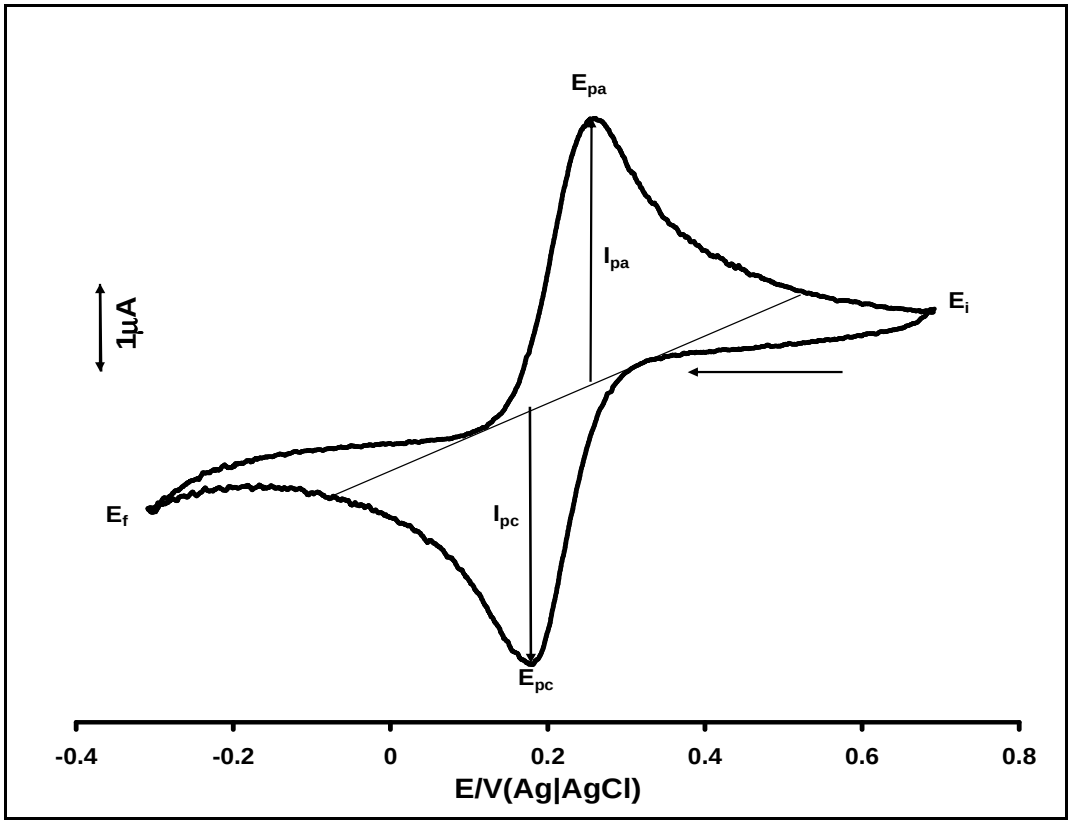

Figure 1.4: Typical cyclic voltammogram for a reversible process.

For a reversible process, the half-wave potential ($E_{1/2}$) equals the formal potential ($E^{o'}$) and are related to the standard potential (E^o) as follows (Equation 1.8):

$$E_{1/2} = E^{o'} = E^o + \frac{RT}{2F}\ln\frac{[O]}{[R]} \qquad (1.8)$$

where R = gas constant, T = temperature (K), F = Faraday's constant

[**O**] = concentration of oxidised species (mol L^{-1}), [**R**] = concentration of reduced species (mol L^{-1})

The formal redox potential, $E^{o'}$ can be calculated from equation 1.9:

$$E^{o'} = \frac{E_{pa} + E_{pc}}{2} \qquad (1.9)$$

where E_{pa} = anodic peak potential, E_{pc} = cathodic peak potential

The number of electron transferred in a reversible process can be calculated from equation 1.10:

$$\Delta E = E_{pc} - E_{pa} = \frac{RT}{nF}, \text{ at } 25\ ^{o}\text{C}\ \ \Delta E = \frac{0.059V}{n} \qquad (1.10)$$

n = number of electrons transferred, other symbols as in equation 1.8.

At 25^{o}C, the peak current of a reversible process is given by the Randles-Sevcik equation, 1.11

$$I_p = (2.69x10^5)n^{3/2}[O]A(D\nu)^{1/2} \qquad (1.11)$$

where I_p = peak current (A), A = electrode area (cm^{-2}), D = diffusion coefficient ($cm^2\ s^{-1}$), ν = scan rate ($V\ s^{-1}$).

Using the Randles-Sevcik equation (1.11), a linear plot of I_p vs. $\nu^{1/2}$ is obtained for a planar diffusion[126,128,129] to the electrode surface. Deviation from linearity indicates the presence of chemical reaction involving either the oxidised, reduced or both species.

For an **irreversible process**, only forward oxidation or reduction peak is observed but at times with a weak reverse peak, Figure 1.5. This process is usually due to slow electron exchange or slow chemical reactions at the electrode surface.[130] Nernst equation is not

applicable in this case since the rate of electron transfer is insufficient to maintain surface equilibrium and thus the oxidised [O] and reduced [R] species are not at equilibrium.

The peak current, I_p for irreversible process is given by equation 1.12.

$$I_p = (2.99 \times 10^5)\, n\, [(1-\alpha)n]^{1/2}\, A\, c\, (Dv)^{½} \qquad (1.12)$$

where α is the rate of electron transfer, c is the concentration of the active species in mol cm^{-3}. The rest of the symbols are as in above and they are listed in the Table of symbols.

For a totally irreversible system, ΔE_p is calculated from equation 1.13:

$$\Delta E_p = E^{o'} - RT/\alpha nF\, [0.78 - In(k^o/D^{1/2})\, In(\alpha nF/RT)^{1/2}] \qquad (1.13)$$

k^o = heterogeneous electron transfer coefficient (cms^{-1}). The rest of the symbols are as in above and they are listed in the Table of symbols.

At 25°C, the peak potential (E_p) and the half-peak potential ($E_{1/2}$) differ by 0.048/αn.

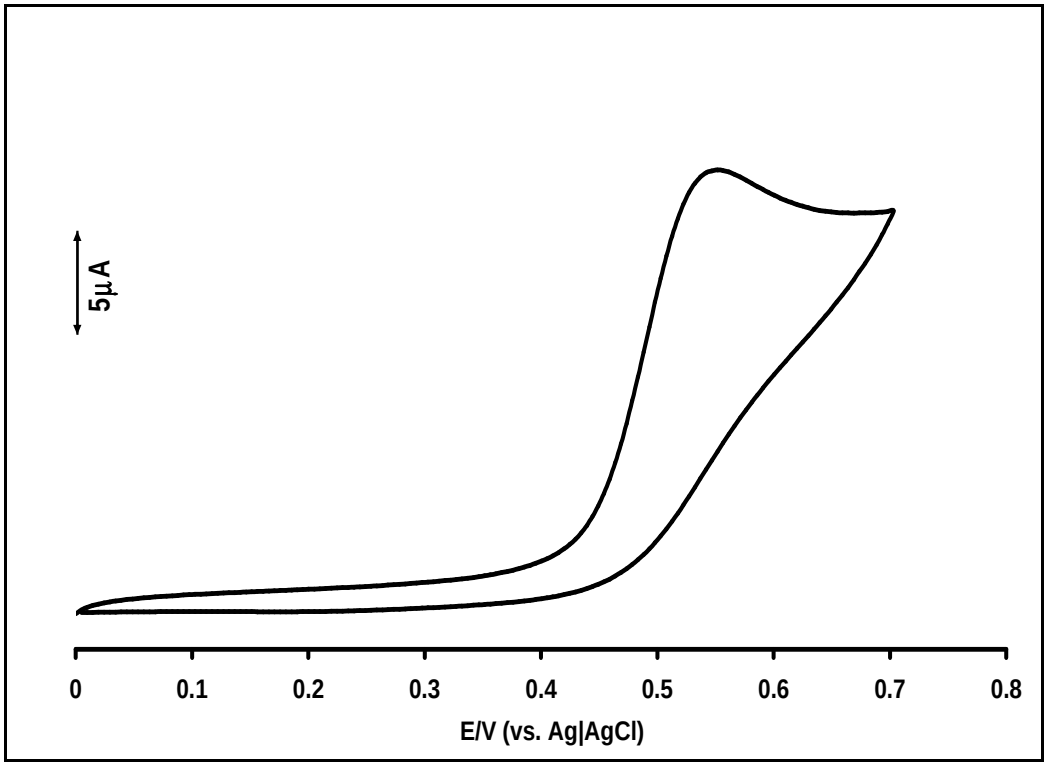

Figure 1.5: Typical Cyclic voltammogram for an irreversible process.

Quasi-reversible process is intermediate between reversible and irreversible systems. The current due to quasi-reversible processes is controlled by both mass transport and charge transfer kinetics.[125,131] The process occurs when the relative rate of electron transfer with respect to that of mass transport is insufficient to maintain Nernst equilibrium at the electrode surface.

For quasi-reversible process, I_p increases with $\upsilon^{1/2}$ but not in a linear relationship and $\Delta E > 59/n$ mV increases with increasing υ.

The CV experimental set up consist of a working electrode which can be gold, platinum, glassy carbon etc., a reference electrode against, which the potential is measured against can be standard calomel electrode (SCE) or silver|silver chloride (Ag|AgCl) and counter electrodes such as platinum wire can be used. During the CV, the solution is kept stationary and is therefore not stirred in order to avoid movement of ions to the electrode surface by mechanical means.

1.2.2 Square wave voltammetry (SWV)

This is a differential technique in which potential waveform composed of a symmetrical square wave of constant amplitude is superimposed on a base staircase potential.[131,132] It is the plot of the difference in the current measured in forward (i_f) and reverse cycle (i_r), plotted against the average potential of each waveform cycle. In this technique, the peak potential occurs at the $E_{1/2}$ of the redox couple because the current function is symmetrical around the potential.[133,134] The main advantages of SWV are excellent peak separation and high sensitivity.

1.2.3 Spectroelectrochemistry

It is a technique which combines spectroscopic and electrochemical techniques. It involves the use of a spectroscopic technique such as ultraviolet-visible light spectroscopy (UV-Vis) to monitor electrochemical processes which include study of species electrotransformation, elucidation of reaction mechanism and studies of reaction kinetics and thermodynamics.

With this technique, optically transparent electrodes (OTEs) are often employed.[127,130,135-144] Several types of OTEs are available, examples include fine wire mesh of metal minigrids, (which comprises several wires of platinum, gold, silver) and thin films of semiconductors such as doped tin oxide. Optically transparent thin layer electrode (OTTLE) cells incorporate these types of electrodes. The working volumes of OTTLE cells are very small in the range between 30-50 μL and thus the electrolysis time is very short, usually seconds.

The number of electrons (n) transferred during the redox process can be determined using the Faraday's law, given by equation 1.14.

$$n = Q/FVc \qquad (1.14)$$

where Q = amount of charge passed (C), V = volume of OTTLE cell (L). F = faraday constant, c = molar concentration of analyte.

This technique is useful for identification of species formed during MPcs electrochemical transformations, and also the number of electrons transferred can be deduced.

1.2.4 General electrochemistry of MPcs

MPcs have very rich and interesting electrochemical properties mainly due to their rich redox properties. The CV technique can be used to characterize newly synthesised MPcs, information such as the formal metal and ring based redox potentials, the influence of axial ligands and ring substituents on the electrochemical properties can be obtained from it. Figure 1.6[100] displays a typical cyclic voltammogram of an MPc complex showing both metal and ring based redox processes. In both positive and negative potential directions, metal based redox processes are in most cases (depending on the electrolyte system) firstly observed before the ring based ones for MPcs with redox active central metal ions.

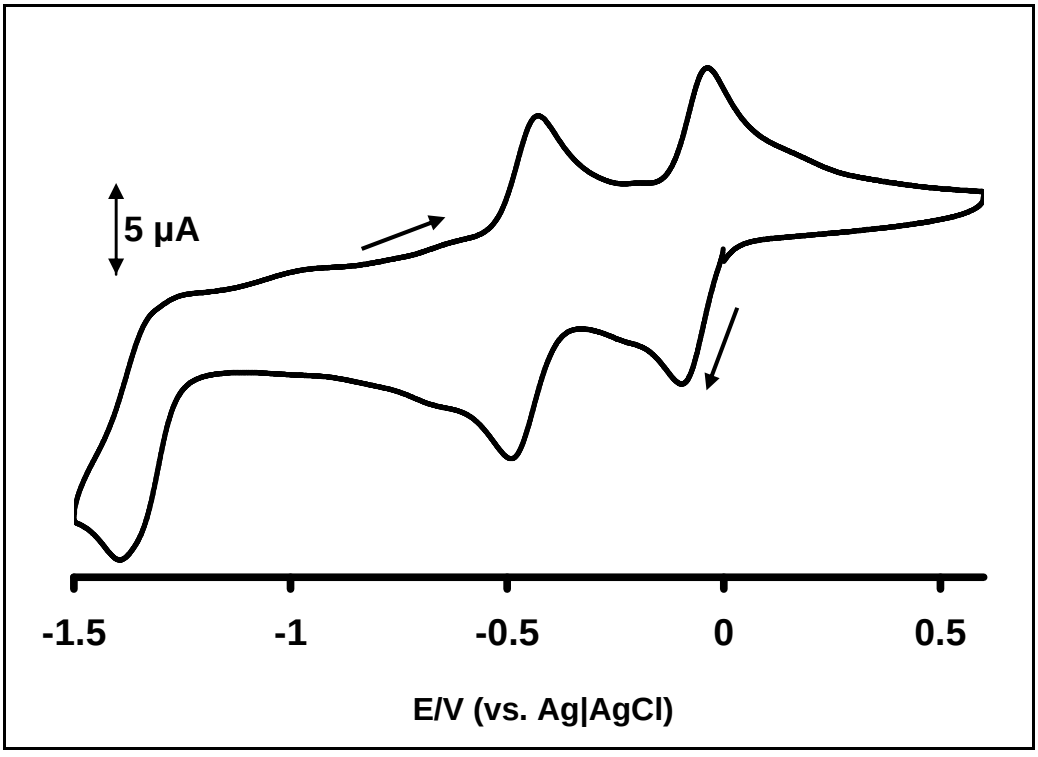

Figure 1.6: A cyclic voltammogram of an MPc showing both metal and ring based redox processes.[100]

At neutral state, the Pc ring has an oxidation state of -2 (Pc^{-2}).[145] The Pc ring can undergo oxidation by successive removal of up to two electrons from the HOMO (a_{1u}), leading to MPc^{-1} and MPc^{0} species respectively and it can undergo reduction by successive addition of up to four electrons to the LUMO (e_g), leading to MPc^{-3}, MPc^{-4}, MPc^{-5} and MPc^{-6} species respectively.[146-153] Because non-transition metal ions are not electroactive, their redox chemistry is similar to that of metal free Pcs and the complexes show redox activities of the Pc ring only. Factors such as solvent, electrolyte, axial ligands, ring substituents and aggregation can have significant influence on the redox properties of MPcs.[66,151,154-157]

1.2.5 Electrochemistry of thiol derivatised MPcs

The electrochemistry of thiol-derivatised MPcs has not received much attention. The effect of the sulphur in the thiol group is still not clear. As stated above, in phthalocyanines, up to four reversible ring reductions and two ring oxidations are possible, however the electrochemistry of thiol substituted MPc complexes is often different from that of other substituted MPc complexes. For example irreversible ring reductions have been reported,[94] often coupled with chemical reactions and adsorption of the reduction products. Overlaps of reduction couples to form one peak, and single step (irreversible) multi-electron oxidation accompanied by decomposition have also been reported.[83]

Aim of Thesis

The voltammetric and spectroelectrochemical properties of thiol derivatised MPcs complexes have not received much attention. In this work, newly synthesised thiol derivatised MPcs will be electrochemically and spectroelectrochemically characterised; the formal potential positions, the influence of the central metal ion and ring substituents on the formal potential positions, the nature of the electronic spectra in various oxidised and reduced species of the thiol derivatised MPcs will be studied. These investigations are important for better understanding of these complexes' behaviour during electrocatalysis.

1.3 Electrocatalysis

MPc complexes especially those containing transition metals are known to have good electrocatalytic properties. The physical and chemical stability of MPcs during electron transfer is a major factor that contributes to their suitability as electrocatalysts and makes them to be superior to metals and metal oxides in this regard. MPcs have been used extensively in both homogeneous and heterogeneous electrocatalysis; in heterogeneous catalysis, they are used to modify electrodes such as glassy carbon and gold electrodes and thus act as electron mediators or promoters during electrocatalysis. In general, metal based redox processes mediate catalytic reactions of MPcs,[61,144,158-163] but ring based catalyses have been reported.[164] The mechanism for the electrooxidation using MPcs as catalysts are shown in equations 1.15-1.17. Basically metal (equation 1.15) or ring oxidation (equation 1.17) occurs first followed by a chemical process leading to oxidation

of the analyte by the reactive oxidised catalyst, the latter is then regenerated. Equations 1.15 and 1.16 are metal based oxidation and equations 1.17 and 1.18 are ring based oxidation process.

$$M^{2+}Pc^{2-} \rightarrow M^{3+}Pc^{2-} + e^{-} \qquad (1.15)$$

$$M^{3+}Pc^{2-} + A \rightarrow M^{2+}Pc^{2-} + P \qquad (1.16)$$

$$M^{2+}Pc^{2-} \rightarrow M^{2+}Pc^{-} + e^{-} \qquad (1.17)$$

$$M^{2+}Pc^{-} + A \rightarrow M^{2+}Pc^{2-} + P \qquad (1.18)$$

where A is the analyte and P is the product

Electrocatalysis can be observed by comparing the CV of an analyte on modified electrode with that on bare electrodes; higher catalytic current, I_p and shift to a less positive peak potential in the CV of the former compared to the latter is an indication of electrocatalysis of oxidation of analyte. Typical example of catalysis is shown in Figure 1.7.

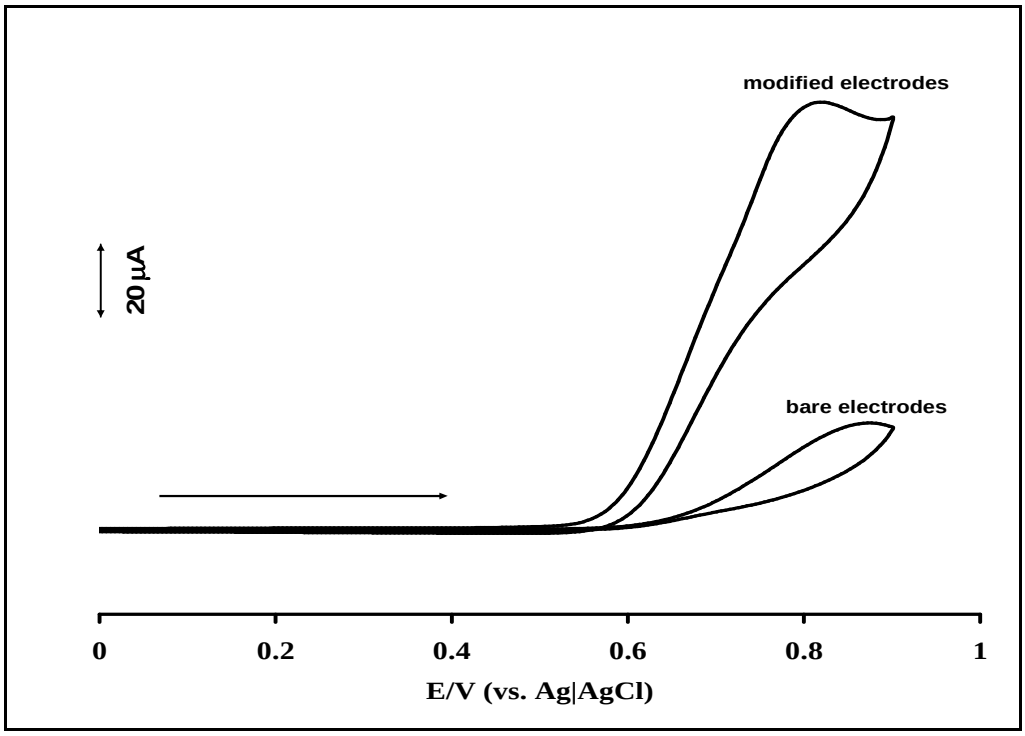

Figure 1.7: Cyclic voltammogram showing catalytic behaviour of an MPc-modified electrode catalyst towards the electrooxidation of an analyte.

Environmentally and biologically important molecules such as nitrite, sulphite, nitric oxide, sulphur dioxide, chlorophenols and many more have been electrooxidised by MPc chemically modified electrodes.

Chemically modified electrodes (CMEs) are electrodes coated with conducting materials for the purpose of improving the chemical and electrochemical properties of the electrodes. Macro molecules such as MPcs, metal Schiff bases and metalloporphyrins have been used to modify electrodes for use as electrocatalysts and sensors. These macromolecules act as electron mediators, increasing the rate of electron transfer at the electrode-solution interface and also lowering the potentials of redox processes. The modification introduces some chemical and electrochemical properties which the bare electrodes do not posses.[165-167]

Various techniques can be used to modify electrodes, these techniques include covalent bonding,[168,169] composite method,[170-173] dip dry,[174-177] drop dry,[63] spin coating,[91,178-183] electropolymerisation,[59,60,110,184-198] Langmuir-Blodgett technique,[90] vapour deposition[199] and self assembled monolayer (SAM).[86-93,200-202]

In this work electropolymerisation and SAM techniques will be used to modify gold electrodes and therefore these will be discussed in this section.

1.3.1 Electropolymerisation

Electropolymerisation is the most efficient method of depositing polymer films on electrodes. Electropolymerisation process involves the repetitive voltammetric scanning of the solution of the modifier monomers at the electrode surface within a specific potential window.[110,197,198] This can be oxidative[184-190] or reductive[191-193] voltammetric scanning in which the monomer forms radicals which combine to form polymers on electrodes. Electropolymerisation forms multilayered polymer coatings of the complexes forming a three-dimensional reaction zone at the electrode surface, thus improving the response sensitivity of the electrode.[203] It is a reproducible process and also it is possible to control the film thickness by varying the conditions for polymerisation process such as time, scan rate, potential range and the type of electrolytes. Various conducting surfaces such as metals, metal oxides and carbon based electrodes can be used as the depositing surface. Formation of new peaks (polymer peaks) is expected and at the same time as continuous growth of the monomer peaks. The peaks increase in size with film thickness until the process is complete.

A lot of work has been done on the study of mechanisms of polymer formations from monomers containing groups such as amino, polyaniline, polypyrrole and polythiophene groups.[204-206] Factors such as solubility of monomer, nature of solvent, electrode size and nature, and ability to form an insoluble polymer govern the polymer growth mechanism.[207] The mechanism of polymer growth of polypyrrole, polythiophene and polyaniline has been studied using cyclic voltammetry, electrochemical quartz crystal microbalance (EQCM) and spectroelectrochemical methods.[187,208-210]

Nyokong and Bedioui[211] have recently reviewed work done on electropolymerised thin films of phthalocyanines as electrocatalysts for biologically and environmentally important molecular materials. MPc complexes with ring substituents such as amino, pyrrole, sulphonate and mercaptopyrimidine groups have been used to modify various electrodes as polymer films for analytes such as glycine, chlorophenols, dopamine, L-cysteine, hydrazine and oxygen. Table 1.2 summarises some of the work carried out in this regard. To date, thiol-derivatised MPcs have not been used to modify electrodes by electropolymerisation; first attempts will be carried out in this work.

Table 1.2: Electrocatalysis of some analytes using poly-MPcs electrodes

MPc species[a]	**Electrode**[b]	**Analyte**	**Ep/ V vs. SCE**[c]	**Medium**	**References**
$CoPc(NH_2)_4$	GCE	Hydrazine	~-0.05	pH 13	212
$CoPc(NH_2)_4$	VCE	L-Cysteine	-0.13	0.5 M NaOH	213
$CrPc(NH_2)_4$	GCE	nitrite	0.76	pH 7.3	214
$MnPc(NH_2)_4$	GCE	glycine	-0.68	pH 4	60
$NiPc(NH_2)_4$	VCE	dopamine	~0.15	pH 7.4	215
MnTpPc	VCE	oxygen	-0.65	pH 4	216
NiTpPc	VCE or Pt	4-CP	0.39	0.1 M NaOH	217
Ni(OH)TpPc	VCE or Pt	4-CP	0.33	0.1 M NaOH	217
CoTpPc	GCE	L-Cysteine	0.46	pH 4	218
$NiPcS_4$	GCE	2-CP	0.16	pH 11	219

[a]TpPc= tetra-4-(pyrrol-1-yl) phenoxy phthalocyanine, [b]VCE = Vitreous carbon electrode, GCE= glassy carbon electrode, [c]To convert potential vs. Ag|AgCl to SCE, a correction factor of -0.0045 V is applied.[211]

1.3.2 Electrodeposition

Electrodeposition is also done in the same way as electropolymerisation, but unlike the latter polymers are not formed. The process occurs because the oxidised or reduced form of the modifier is less soluble in the depositing solvent and is adsorbed onto the electrodes without polymer formation. The first scan is generally similar to the subsequent scans.[220,221]

1.3.3 Self Assembled Monolayer (SAM)

Self assembled monolayers (SAMs) can be defined as the formation of highly ordered molecular assemblies formed by the adsorption of molecules from solution directly onto the surface of an appropriate substrate.[122,201,202] SAM technique has a number of advantages which include simplicity, reproducibility and formation of highly ordered and stable monolayers which are chemically bound onto gold electrodes.[222] Reported types of SAMs include chlorosilanes on silicon or glass,[201,223-226] carboxylic acids on metal oxides[227,228] and organosulphur compounds such as thiols and disulphides compounds on gold.[222,229-238] Gold has strong affinity for sulphur and the formation of gold sulphur bound is thermodynamically feasible with the Au-thiolate bond having bond strength of 44 kcal mol^{-1}.[239,240] It has been shown that SAMs formed on Au by alkane thiols with chain length of 12 or more are well-ordered and dense monolayers. These alkanethiols are known to form densely parked crystalline or liquid crystalline material on gold with attractive Van der Waal forces between the alkyl chains that enhances the stability and order of the SAMs.[241] Figure 1.8 shows a schematic representation of alkane thiols SAM on gold electrode.

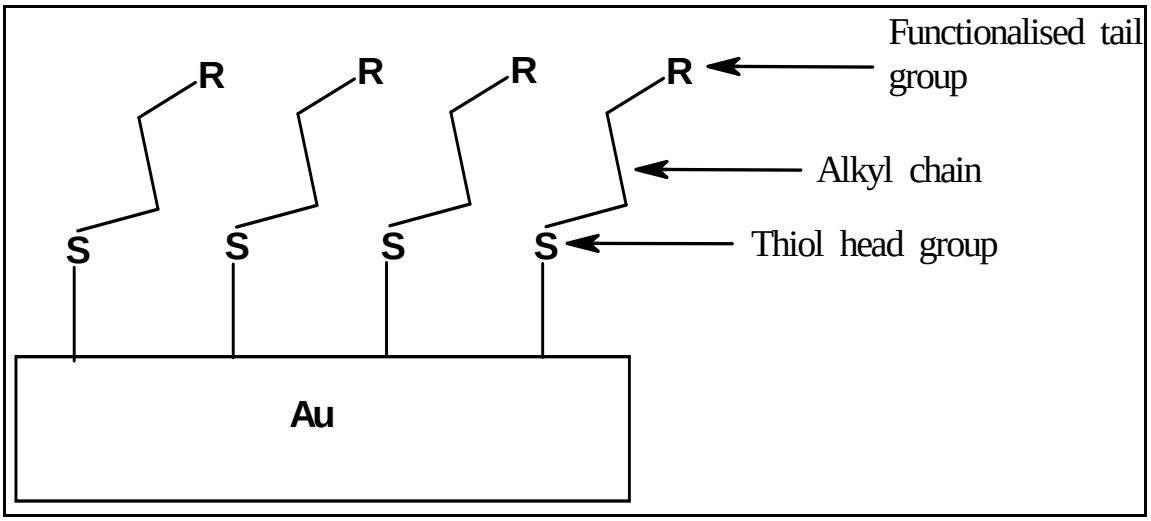

Figure 1.8: Schematic representation of alkane thiols SAM on gold.

Thiol derivatised MPc complexes have been used to form SAMs on gold electrodes especially for the purpose of using them as electrocatalysts.[58,82] However, the number of MPc complexes with thiol substituents is still limited and the electrochemistry of these molecules has not been fully explored, this is due to the fact that the synthesis of thiol-derivatised metallophthalocyanines is tedious and requires toxic chemical reagents. Hence, the study of thiol-derivatised MPc-SAMs has not received much attention.

Thiol-derivatised MPc-SAMs can adapt flat or vertical orientation on gold electrodes as shown schematically in Figure 1.9. Formation of MPc-SAMs on gold electrode gives the advantages of both enhancement of the Faradaic current of the adsorbed species relative to the charging current, (these will improve the sensing and selectivity) and creating chemically selective sites, which is the basis of an electrochemical sensor.[122,201]

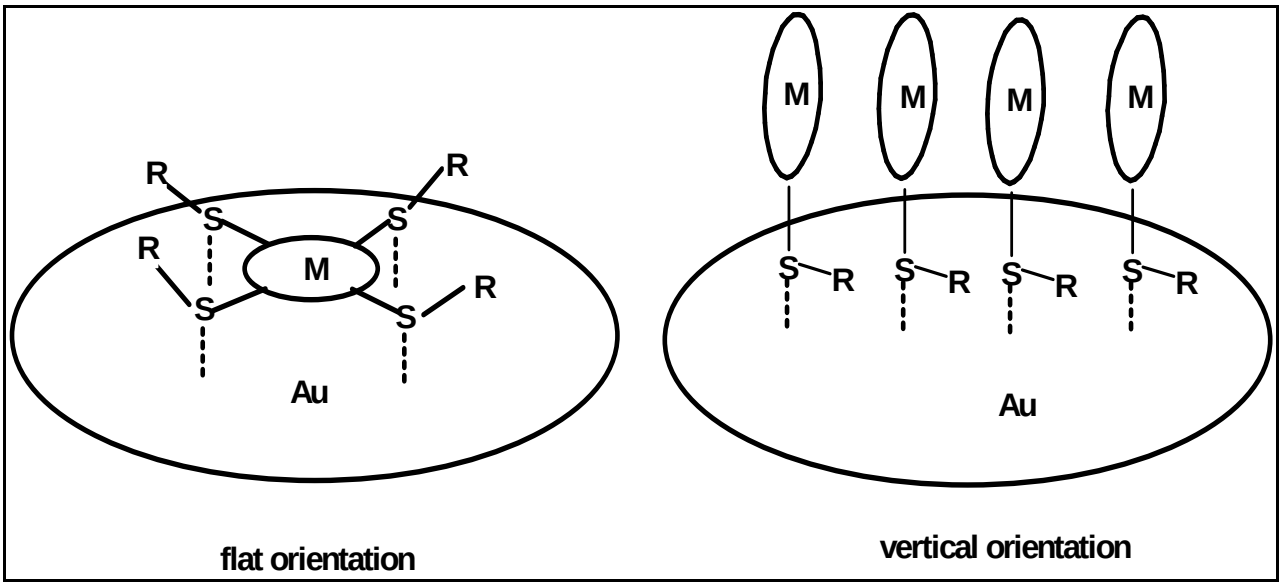

Figure 1.9: Schematic representation of thiol derivatised MPc SAM on gold.

The preparation of SAMs is simple and straight forward. Basically, the modifier is dissolved in a suitable solvent and purged with N_2 gas. The clean gold electrode is then immersed in the solution, SAM is allowed to form for about 24 hours or more depending on the solution concentration usually the higher the concentration the lower the deposition time; concentrations in millimolar to micromolar range are often employed. There has been no report on determination of the minimum time needed for SAM formation, in this work CV technique will be used to monitor SAM formation progress; hence finding the minimum time for SAM formation.

1.3.3.1 Characterisation of MPc-SAMs by Cyclic voltammetry (CV)

A number of non-electrochemical analytical tools[89-93,181] have been used for SAM characterisation namely infra red spectroscopy, X-ray photoelectron spectroscopy, ellipsometry and scanning probe measurements. Electrochemical techniques especially cyclic voltammetry (CV),[50,104] have proven to be effective for SAM characterisation. In this work, cyclic voltammetry will be used for SAM characterisation. A well formed MPc-SAM with flat orientation has a surface coverage concentration of about 10^{-10} mol cm^{-2}, free of pinholes (a pinhole is a site at which the electrode surface is exposed to the electrolyte) and also defect free (a defect is a site at which molecules or ions can approach the electrode surface at a distance shorter than the normal thickness of the SAM).[222,231,232] The surface roughness of gold electrode surface plays a role in determining whether or not the SAMs formed will have pinholes and defects or not; increase in surface roughness usually increases the chances of having pinholes and defects because it leads to formation of SAMs with poor uniformity.[201,202,242]

Cyclic voltammetry has been used to characterise SAMs in this work. For the determination of surface concentration, various methods can be used, these are explained below.

(i) For species that are surface confined, the peak current, I_p (μA) is directly proportional to the scan rate, v (V s^{-1}), equation (1.19).[201,202]

$$I_p = \frac{n^2 F^2 A \Gamma \nu}{4RT} \qquad (1.19)$$

where A = surface area of the electrode (cm^2), Γ = total surface coverage by electroactive species, n = number of electron transfer, *v* = scan rate, F = faraday constant, R = gas constant and T = temperature in Kelvin.

Γ may be also determined from equation 1.20

$$\Gamma = Q/ nFA \qquad (1.20)$$

where Q = quantity of charge in coulombs, the rest of the symbols have their usual meaning.

(ii) The surface concentration can be estimated by using charge, Q from either reductive or oxidative desorption of SAM in strong alkaline solution as illustrated by the equations 1.21, 1.22 shown below;

$$Au\text{-}SC_nX + ne^- + M^+ \longrightarrow Au^o + XC_nS^-M^+ \qquad (1.21)$$

$$Au\text{-}SC_nX + 4OH^- \longrightarrow Au^o + XC_nSO_2^- + 3e^- + 2H_2O \qquad (1.22)$$

where M^+ cation from the electrolyte is usually included in the equation for desorption because the peak is sensitive to the identity of the cation. X = the end group of the alkane thiol chain.

(iii) The surface concentration of the MPc complexes on gold electrode can also be estimated using the charge difference between the bare gold (Q_{Bare}) and the MPc-SAMs (Q_{SAM}) from the CVs obtained in basic media at bare and MPc modified gold electrodes. The difference is proportional to the fraction of the gold sites covered by the MPc-SAMs. This fraction is then divided by three to get the charge proportion of gold sites covered with MPc-SAM, according to equation 1.23.

$$Au.H_2O + 2H_20 \rightleftharpoons Au(OH)_3 + 3H^+ + 3e^- \quad (1.23)$$

The amount of gold sites covered by the MPc-SAM is then divided by the number of 'thiol arms' of the MPc followed by division with the surface area of the gold electrode to get the charge density proportional to each MPc molecule. These values can then be converted to the corresponding surface concentration (mol cm^{-2}) by dividing them with the Faraday constant (96485 C mol^{-1}). The surface concentration in number of molecules per area (in cm^2) can be obtained by simply multiplying the Γ_{MPc} (mol cm^{-2}) by the Avogadro's constant (N_A). Finally the inverse of the concentration in molecules per $Å^2$ correspond to the approximate surface area occupied per molecule.

Determination of ion barrier factor as shown in equation 1.24 is a measure of how pinholes free the SAM is; specifically how the monolayers effectively prevent ions from the electrolyte solution from reaching the electrode surface. It is the comparison of the total charges under the gold oxide striping peak at the bare gold (Q_{Bare}) and the SAM-modified gold electrode (Q_{SAM}).

$$\Gamma_{ibf} = 1 - Q_{SAM}/Q_{Bare} \quad (1.24)$$

where Γ_{ibf} = ion barrier factor

A well formed MPc-SAM should be able to block the gold surface oxidation redox process.[231,242] Blockage of this process indicates that the gold electrode surface is effectively covered and isolated by SAM of MPc and is free from pinholes and defects. Figure 1.10 shows typical CVs of both MPc-SAM and bare gold electrodes in basic media.

Other Faradaic processes[231,242] used for verifying the integrity of MPc-SAM formed on gold include underpotential deposition (UPD) of copper and solution redox chemistry $[Fe(H_2O)_6]^{3+}$/ $[Fe(H_2O)_6]^{2+}$of $Fe(NH_4)(SO_4)_2$ in perchloric acid solution.

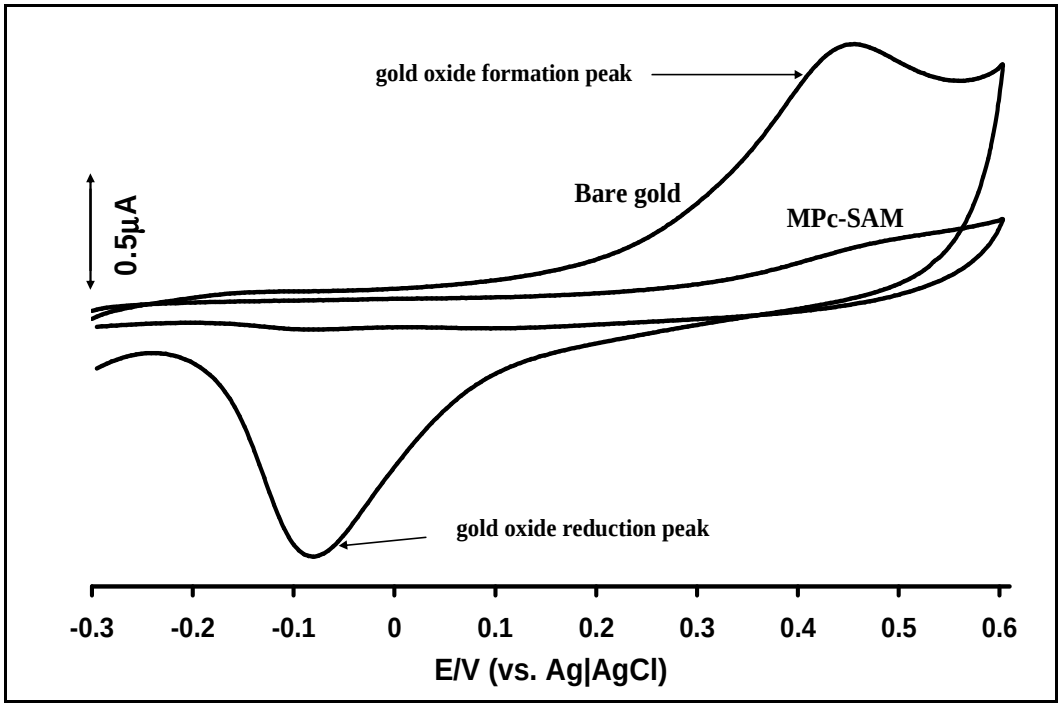

Figure 1.10: Typical CVs of both MPc-SAM and bare gold electrode basic media.

Work done on SAMs of phthalocyanines as electrocatalysts for biologically and environmentally important molecular materials has recently been reviewed.[211] Table 1.3 shows some selected work carried out in this regard. As the Table shows, it is only Co^{2+} and Fe^{2+} MPcs that have been used; in this work Mn^{3+} and Ni^{2+} thiol derivatised MPcs in addition to their Co^{2+} and Fe^{2+} counterparts will be used to form SAMs on gold. Also from Table 1.3, the applications have been limited to analysis of thiol compounds (L-cysteine, 2-mercaptoethanol, homocysteine, penicillamine and thiocyanate), hydrazine,

molecular oxygen and hydrogen peroxide. First examples of application of thiol-derivatised MPc-SAMs to sulphite electrooxidation will be carried out in this thesis.

Table 1.3: Electrocatalysis of some analytes using MPcs-SAM electrodes

MPc species[a]	**Electrode**[b]	**Analyte**	**Ep/ V vs. SCE**	**LoD / mol L^{-1}**	**Medium**	**References**
$CoPc(SC_4H_9)_8$	Au	L-Cysteine	0.38	$3.1 \pm 0.8 \times 10^{-7}$	pH 4	58
$FePc(SC_4H_9)_8$	VCE	L-Cysteine	0.29	3.1×10^{-7}	pH 4	82
$CoPc(SC_4H_9)_8$	Au	Homocysteine	0.48	$5.2 \pm 0.6 \times 10^{-7}$	pH 4	67
$CoPc(SC_4H_9)_8$	Au	Penicillamine	0.54	$2.7 \pm 0.6 \times 10^{-6}$	pH 4	67
$CoPc(SC_4H_9)_8$	Au	Thiocyanate	0.74	$1.1 \pm 0.8 \times 10^{-7}$	pH 4	67
FePc	4-MPy-Au	Thiocyanate	0.51	8.4×10^{-7}	pH 4	243, 244
$CoPc(NH_2)_4$	Au	O_2	-0.31	5×10^{-6}	pH 7	245
$CoPc(COOH)_4$	2-ME-Au	H_2O_2	0.56	5×10^{-7}	pH 4	246

[a]preformed SAM, [b]2-ME = 2- mercaptoethanol, 4-MPy = 4-mercaptopyridine

Aim of Thesis

A major part of the work described in this thesis is based on fabrication of MPc-SAMs on gold electrodes for potential applications in electrocatalysis and analysis. These thiol derivatised MPc-SAMs on gold will be characterised by the standard CV methods to ascertain the surface concentration of the complexes on gold electrodes and their integrity in terms of being free from defects and pinholes. For the first time, optimisation of the time for SAM formation based on CV technique will be studied.

1.3.4 Electrochemical Impedance Spectroscopy (EIS)

Electrochemical impedance spectroscopy (EIS) is a powerful tool for the investigations of the mechanisms of electrochemical reactions, the properties of porous electrodes, and for investigating passive surfaces.[247-251] EIS technique has been shown to be effective for probing the redox and structural features of a surface-confined species.[252] Impedance measurements include both the electrical resistance and resistance due to morphological state of the materials. Generally, a bare electrode should exhibit an almost straight line for the Nyquist plot (representation of impedance spectra) which is imaginary impedance versus the real impedance ($-Z_{im}$ versus Z_{re}) because electrochemical reactions at such electrode surfaces are expected to be a mass diffusional limiting electron-transfer processes.[253,254] For a modified electrode, the Nyquist plot shows characteristic semi-circle pattern due to barrier to the interfacial electron transfer. The interfacial barrier behaviour has been described by Randles equivalent circuit (Figure 1.11),[255-258] it incorporates various contributions to the interfacial barrier behaviour, these factors are the resistance of electrolyte (R_s), the charge transfer resistance (R_{ct}), double-layer

capacitance (C_{dl}) and Warburg impedance (Z_w). In the case of modified electrodes, C_{dl} is replaced by constant phase electrode (CPE). The R_{ct} value is influenced by the film thickness and the nature of the films on the electrodes.

Applications of EIS to modified electrodes characterisation have been reported.[246,253,254,259] EIS studies in $Fe(CN)_6^{3-/4-}$ electrolyte solution have been performed for SAMs of thiols with different alkyl chains and carboxylic acid (COOH) terminal group,[259] and the charge transfer resistance, R_{ct} was found to increase with the length of the alkyl chains and with pH. In the EIS study of the formation of SAMs of cysteamine functionalised with phosphate groups,[253] both R_{ct} values and the Nyquist semi-circle plots increased as stepwise build up of the three layers of cysteamine, glutaraldehyde and 2-amino-ethyl dihydrogen phosphate were formed. The biosensor consisting of preformed 2-mercapto ethanol SAM, followed by attachment tetra carboxyl acid metallophthalocyanine and the enzyme (Au-ME-CoTCAPc-GOx SAM)[246] for H_2O_2 analysis was characterised using EIS and the result was found to be comparable to that of CV characterisation. Films of electrodeposited poly-nickel(II)tetrasulphophthalocyanine (poly-NiTSPc)[254] with two different film thicknesses were characterised using EIS in pH 11 carbonate-hydrogencarbonate buffer as the electrolyte, it was shown that R_{ct} values was about twice higher for the thicker film.

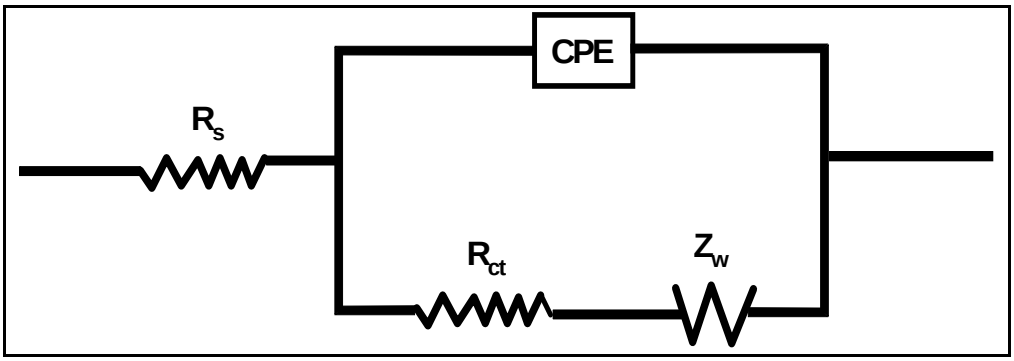

Figure 1.11: The CPE equivalent of circuit model showing the various factors for behaviour at the electrode thin film-electrolyte interface.

Aim of Thesis

In this work, EIS technique will be used to study the characteristics (nature and film thickness) of thiol derivatised NiPcs polymer films on gold electrodes. *Poly*-NiPcs are the only derivatives chosen for EIS studies because of the importance of differentiating between the *poly*-NiPc and poly-Ni(OH)Pc on Au electrode. A transformation from NiPc to Ni(OH)Pc only occurs for NiPc complexes.

1.4 Background on the analytes

The analytes chosen in these studies for catalysis using MPcs are chlorophenols, nitrite and sulphite. Below is a brief survey of these analytes.

1.4.1 Chlorophenols

The molecular structures of chlorophenols **(18-22)** studied in this work are shown in Figure 1.12.

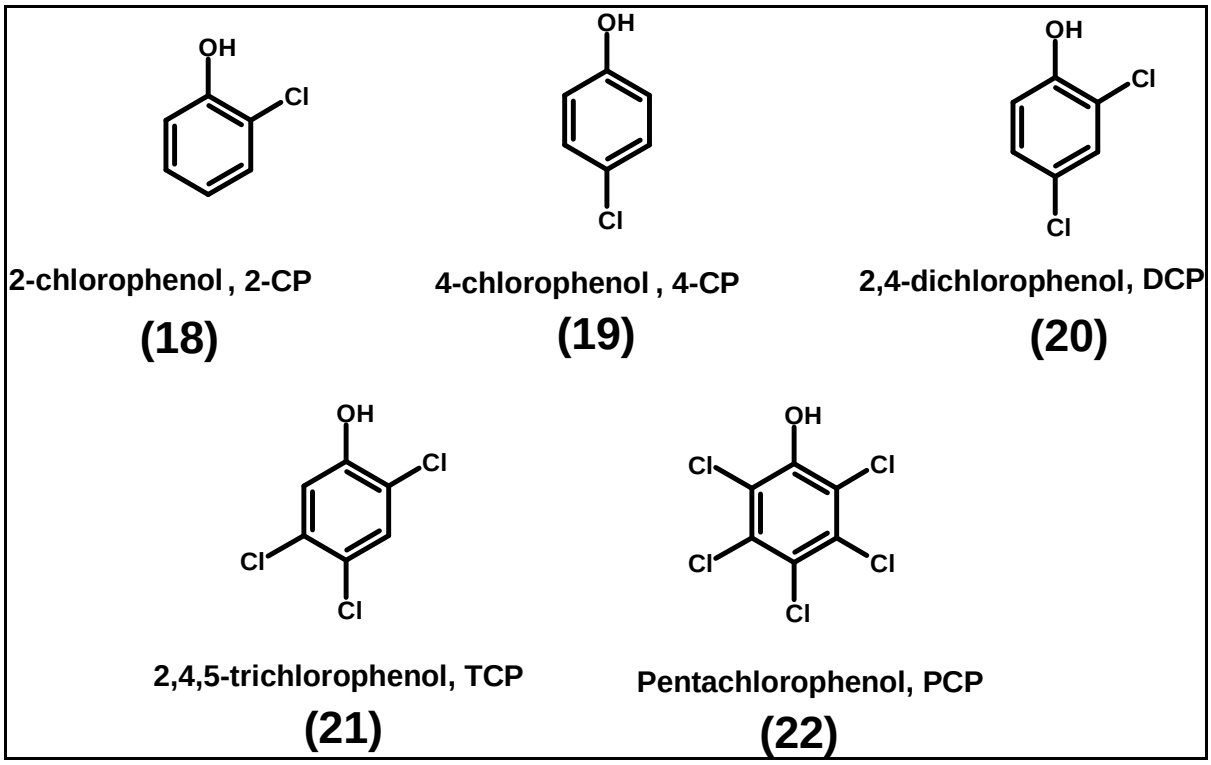

Figure 1.12: Molecular structure of chlorophenols

Rapid industrial and agricultural growth worldwide has led to more and more discharge of toxic substances such as chlorophenols as effluents. Chlorinated phenols such as 2-chlorophenol, 4-chlorophenol, 2,4-dichlorophenol, 2,4,5-trichlorophenol, and

pentachlorophenol are classified as priority pollutants by both the European Union (EU) and the United State Environmental Protection Agency (USEPA). According to both USEPA and EU the current admissible level for phenols in drinking water is set at 0.5 μg L^{-1} for total content and 0.1 μg L^{-1} for the individual phenol content, and 5 μg L^{-1} in bathing water.[260,261] Their toxicity depends on degree of chlorination and the positions of chlorine atoms relative to the hydroxyl group and it increases as the chlorine atom is further away from the hydroxyl group.[262,263] Chlorophenol toxicity also depends on pH and the presence of some other compounds accompanying them in the environment.[262-264] The physical and chemical properties of the chlorophenols of interest in this work are summarised in Table 1.4.[264] Chlorophenols undergo physical and chemical transformations in the environment, these transformations depend on the values of their dissociation constant (K_a) and the partition coefficient ($K_{O/W}$) in the octanol-water system. Both K_a and $K_{O/W}$ depend on the structures of the chlorophenols. The higher the number of chlorine atoms, the higher the dissociation constant (K_a) and partition coefficient ($K_{O/W}$). The $K_{O/W}$ values decrease as the water solubility of phenols increases. Chlorinated phenols are generally recalcitrant and in particular the polychlorinated ones exhibiting more resistance to biotransformation in the environment than the monochlorinated ones. Generally their resistance to degradation increases with the number of halogen substituents.[265-268]

Table 1.4: Physical-chemical properties of chlorophenols[264]

Compound	Molecular weight	Boiling point (^oC)	Melting point (^oC)	Solubility g L^{-1} at 20^oC	p*Ka*	Log $K_{O/W}$
2-chlorophenol	128.56	174.9	9.3	28	8.3-8.6	2.12-2.17
4-chlorophenol	128.56	217-219	42-44	27	9.1-9.4	2.35-2.50
2,4-dichlorophenol	163.00	Sublimes	45	4.50	7.5-8.1	2.75-3.30
2,4,5-trichlorophenol	197.45	Sublimes	67-70	0.948	7.0-7.7	3.72-4.10
Penta chlorophenol	266.34	300	190	0.014	4.7-4.9	5.01-5.86

Chlorophenols can be physically or chemical transformed in the environment by three major ways namely (i) biodegradation by bacteria in soil, these processes are slow because they are hindered by the chlorine atoms in chlorophenols which interfere with the action of many oxygenase enzymes that initiate the degradation of aromatic rings of the chlorophenols and (ii) photodegradation by UV light which can lead to photochemical processes such as photodissociation, photosubstitution, photoreduction and photooxidation[264]

Efficient chemical catalysts are needed to convert chlorinated phenols to more biodegradable molecules. Hitchman *et al.*[269] have reviewed the various methods for the degradation of chlorophenols, which ranges from biological to chemical and to

photochemical methods. MPc complexes containing electroactive central metals are preferred catalysts for the enzyme-like oxidation of chlorophenols since these complexes have a wide range of readily available oxidation states. Iron and manganese tetrasulphophthalocyanine ($MPcS_4$) complexes have been extensively studied as enzyme-like catalysts for the oxidation of chlorophenols in the presence of an environmentally clean hydrogen peroxide (H_2O_2) as the oxidant.[14,41-44]

Review of the use of MPcs as electrocatalysts for chlorophenols analysis will be dealt with in section 1.5.3.1.

1.4.2 Nitrite

Uses of nitrite are numerous,[270] these include (i) color fixative and preservation in meats, (ii) manufacturing diazo dyes, (iii) in the textile industry, (iv) photography, (v) manufacture of rubber chemicals, (vi) fertilizers in agriculture and (v) medicinal agents (used as a vasodilator,[271] bronchodilator,[272] intestinal relaxant, [273] and even as an antidote for cyanide poisoning[274]). Thus, nitrite ions are of both environmental and biological importance and because they are widely used, there have been toxicological studies on acute and chronic exposure to nitrite. Nitrite ions are known to react with amines forming nitrosamines which are known to be carcinogenic.[275-278] In the blood, they can inhibit oxygen intake of the body by oxidizing Fe^{2+} to Fe^{3+} of the hemoglobin, this condition is known as methemoglobinemia and infants are mostly affected by it. The United State Food and Drug Administration (USFDA) recognize 22-23 mg kg^{-1} body weight as the fatal dose of nitrite.[279-281] Various methods have been used to determine nitrite ions, traditionally, nitrite is determined quantitatively by spectroscopic methods,[282] this is

carried out by reacting nitrite with sulphanilamide and N-(1-naphthyl)ethylenediamine, the colour intensity of the complex formed can be used for quantitative determination of nitrite. However, this method suffers from interferences such as sulphide and sulphite. Chromatographic methods[283] have also been used for nitrite determination. Both spectroscopic and chromatographic methods have some disadvantages such as the use of complicated sample pre-treatment process, unsuitability for on-site monitoring and inability for detoxification. In order to tackle this problems, devices which are simple, inexpensive, stable and having the potential for the detoxification of these molecules are highly in demand. Electrochemical devices fall into this category,[15,214,284-287] which have more advantages over the other methods in terms of cost and time. Electrochemical determination of nitrite is either by reduction or oxidation. Polarographic and voltammetric methods for the detection of nitrite involve the catalytic reduction of nitrite in the presence of some polyvalent metal ions, such as molybdate and chromium. All of these methods suffer from poor sensitivity and are subject to interference from nitrate and molecular oxygen; hence detection using nitrite oxidation is preferred. The use of bare electrodes for the oxidation of nitrite requires high potentials and these electrodes tend to be poisoned by the species formed during the electrochemical process resulting in decrease in the electrode sensitivity and accuracy. The use of chemically modified electrodes for nitrite electrooxidation have been reported,[288] including the use of electrodes coated with thin films of mixed valence $CuPtCl_6$, silicotungstic heteropolyanions, enzymes, osmium polymers and ruthenium. A good way of lowering potentials for nitrite electrooxidation is by modification of the electrodes with complexes

such as MPcs. Review of the use of MPcs as electrocatalysts for nitrite analysis will be dealt with in section 1.5.3.2.

1.4.3 Sulphite

Sulphite (SO_3^{2-}) ions have antioxidant and antimicrobial activities and they are used as preservative for foods and beverages. Sulphite ions are used extensively in wine industry as inhibitor of yeasts and bacteria. In aqueous medium, the ions can exist in different forms depending on pH and the acid dissociation constant as shown in equation 1.25.[289,290]

$$SO_2 + H_2O \rightleftharpoons H_2SO_3 \overset{-H^+}{\rightleftharpoons} HSO_3^- \overset{-H^+}{\rightleftharpoons} SO_3^{2-} \quad (1.25)$$

Under physiological pH condition (pH 7.4), SO_2 exist as a mixture of hydrogen sulphite (HSO_3^-) and sulphite (SO_3^{2-}) with the latter, predominating.[289] In this work, electrocatalysis and analysis of sulphite will be carried out at pH 7.4 where it is expected that it exist mainly in SO_3^{2-} form. Sulphite ions are of great importance environmentally and biologically, it is the form in which sulphur dioxide (SO_2) gas exist in aqueous alkaline solution and thus can be used for the indirect measurement of SO_2. Atmospheric SO_2 can be absorbed by plant in the form of sulphite into chloroplast[290,291] and this can lead to increase in reactive oxygen species (ROS)[292-294] which can be very toxic to human beings. Methods for sulphite/SO_2 determination include absorption spectroscopy,[295] titrimetric,[296] ion chromatography[297] and electrochemical methods.[298,299] Electrochemical methods provide a simple, cost effective and a quick way of analysing sulphite/SO_2. Most works on electrocatalysis of sulphite/SO_2 involve electrode modification with macro complexes since these complexes are robust in nature and also provide catalytic sites for

sulphite electrooxidation to occur. Use of an amperometric sensor for SO_2 based on adsorption of (3-mercaptopropyl)-trimethoxysilane (MPS) on a glassy carbon (GC) electrode followed by complexation with silver has been reported; in the study, sulphite was used for the indirect determination of SO_2.[300] Copper hexacyanoferrate (CuHCF) modified with graphite electrode prepared by immobilisation method has been used for the determination of sulphite.[301] Review of the use of MPcs and metalloporphyrins as electrocatalysts for sulphite analysis will be dealt with in section 1.5.3.3.

1.5 Catalytic behavior of MPcs towards chlorophenols, nitrite and sulphite

Over the years, MPc complexes have been shown to exhibit interesting catalytic activities in various types of catalysis such as (i) chemical/enzyme-like catalysis, (ii) photocatalysis, and (iii) electrocatalysis. In this work, these three types of catalysis are studied using MPcs for the transformations of chlorophenols, nitrite and sulphite. Hence a review on the above catalysis types and their applications towards these analytes transformations are discussed below.

1.5.1 Enzyme-like catalytic transformation of chlorophenols

Enzyme-like catalysis mimic the catalytic reactions of biological enzymes. MPc enzyme-like processes can be divided into four categories namely (i) catalase-like oxidation

reactions,[302-309] (ii) peroxidase-like oxidation reactions,[310-313] (iii) oxidase-like oxidation reactions[312,314-319] and (iv) oxygenase-like oxidation reaction.[311,312,320-322]

(i) Catalase-like oxidation reactions

This type of reaction mimics the naturally occurring catalase. Catalase has an aproprotein and four molecules of protoheme IX and it is known to catalyse the decomposition of hydrogen peroxide (H_2O_2) into water and molecular oxygen as shown in equation 1.26.

$$2H_2O_2 \xrightarrow{\text{Catalase}} 2H_2O + O_2 \qquad (1.26)$$

$FePcS_4$, (where S = SO_3^-) complexes have been shown to be effective in the catalytic decomposition of H_2O_2 based on this type of catalysis.[310]

(ii) Peroxidase-like oxidation reaction

Catalysis of oxidation of proton donors (AH_2) such as vitamin C, phenols, aminophenol, *p*-aminobenzoic acid and *p*-phenylenediamine with H_2O_2 by naturally occurring heme enzyme peroxidase is well known, equation 1.27. $FePcS_8$ has been shown to be effective in the mimicking of the peroxidase-like oxidation reaction and it has been used as a catalyst, for example, for guaiacol oxidation.[313]

$$AH_2 + 2H_2O_2 \xrightarrow{\text{Peroxidase}} A + 2H_20 \qquad (1.27)$$

Sorokin and co workers[14,41-44] have extensively reported on peroxidases-like catalytic degradation of chlorophenols using $FePcS_4$ and $MnPcS_4$ (where S = SO_3^-) as catalysts in the presence of oxidants such as hydrogen peroxide and potassium hydrogen persulphate, formation of products like maleic acid and formic acid were reported.

(iii) Oxidase-like oxidation reaction

The oxidation-reduction enzymes are known to catalyse the reaction of sulfhydryl-containing substrates and hydrogen acceptors (equation 1.28) and reduced form of nicotinamide adenine dinucleotide (NADH) with O_2, equations 1.29. Attempts have been made to mimic these types of reactions using divalent and trivalent MPc complexes, several examples using MPc complexes for the catalyses of aerobic conversion of thiols to disulphide have been reported.[314-319]

$$SH_2 + A \xrightarrow{\text{Dehydrogenase}} S + AH_2 \qquad (1.28)$$

$$SH_2 + O_2 \xrightarrow{\text{Oxidase}} S + H_2O_2 \qquad (1.29)$$

where S represents sulfhydryl containing substrate

(iv) Oxygenase-like oxidation reaction

This is a synthetic model of cytochrome P-450 (equation 1.30). Cytochrome P-450 is an enzyme found in mammalian tissues such as liver and kidney, it catalyses the hydroxylation of non-polar substances such as drugs and pollutants thereby making them to be water soluble and easier to remove from the body.[302]

$$R_3C\text{-}H + O_2 + 2H^+ + 2e^- \xrightarrow{\text{P-450}} R_3C\text{-}OH + H_2O \qquad (1.30)$$

These types of reactions are mostly carried out using iron and manganese MPc complexes as catalysts. The active species in these reactions are generally believed to be the Fe-oxo and Mn-oxo species.[302] Several workers have used these type of reactions to oxidise industrially important molecules such as cyclohexene, styrene, and 3,5,5-trimethylcyclohex-3-en-1-one.[320-322] These reactions usually lead to the formation of an epoxide and can still lead to other oxidised products. Epoxidation of styrene[321] was

catalysed with the use of some MPc complexes; it was found that the FePc and MnPc performed significantly better than the NiPc and CoPc. Ito *et al.*[322] performed the oxidation of 3,5,5-trimethylcyclohex-3-en-1-one using molecular oxygen as the oxidant and the reaction was catalysed by Mn^{3+}, Mn^{2+}, Fe^{3+}, Fe^{2+}, Ni^{2+}, Cu^{2+} or Co^{2+}Pcs; Mn^{3+}Pc showed an excellent catalytic activity with a 93% yield 3,5,5-trimethylcyclohex-2-en-1,4-dione.

MPcs employed as chemical/enzyme-like catalysts for chlorophenols oxidation are listed in Table 1.5. Emphasis has been mainly on the investigation of catalysts/substrate ratio effects on the rate of reaction and the type of products formed. There has been no reported work on the effect of the influence of solvent composition on the type of products formed; this thesis will do investigation on that. Also $FePcS_4$ and $MnPcS_4$ have been mostly used, the mechanisms involve complicated steps via Fe-oxo and Mn-oxo species formation and $FePcS_4$ and $MnPcS_4$ spectra are relatively more complicated than that of $CoPcS_4$, the latter will be employed in this work.

Table 1.5: Data for the enzyme-like catalysis of chlorophenols transformation using MPc complexes

MPc/ medium[a]	Chlorophenol	Oxidant	Products[b]	(% Yield)	References
$FePcS_4$ in aqueous solution	TCP	H_2O_2	CMA, CFA, MA, FA, coupling products	24, 3, 1, 1, 27	323
$FePcS_4$ on Amb. IRA 400/ PVP	TCP	H_2O_2/ $KHSO_5$	Not stated		41
$FePcS_4$ in aqueous solution/ Amb. IRA 900	TCP	H_2O_2	Water soluble product, dimers and trimers CO_2, CO	69, 13, 11, 3	42
$FePcS_4$ in aqueous solution	TCP	H_2O_2	CMA, CFA, MA, FA, coupling products	24, 3, 1, 1, 27	46
$FePcS_4$ on silica	TCP	H_2O_2	CMA, CFA, MA, FA, coupling products	24, 3, 1, 1, 27	324
MOCPcs (M = Fe, Mn, Co)	TCP	H_2O_2	Formic acid, OA, chloropropenic acid, coupling products	Not stated	51

[a]Amb. = amberlite®, S = SO_3^-, PVP = poly (vinyl pyridine) polymer, [b]CMA = Chloromaleic acid, CFA = chlorofumaric acid, MA = maleic acid, FA = fumaric acid, OA = oxalic acid

Aim of Thesis

CoPc complexes have rich redox chemistry and because of their high catalytic activities, they have been more widely employed in electrocatalytic reactions than their FePc or MnPc counterparts. It is surprising therefore that, up to date; there has been no detailed literature report on the catalytic oxidation of chlorinated phenols by any CoPc complex. CoPc have been shown to mimic the oxygenase-like catalysis.[322]

This work will involve the use of $CoPcS_4$ catalyst for the H_2O_2 oxidation of 2-chlorophenol (2-CP) and 2,4,5-trichlorophenol (TCP). The effect of solvent on the type of products formed from the degradation of the chlorophenols using H_2O_2 as oxidant and $CoPcS_4$ as catalyst will explored. For a good understanding of the reactivities of $CoPcS_4$ in relation to the extent of aggregation, a mixture of water and methanol as well as water as sole solvent will be employed for the catalytic processes.

1.5.2 Photocatalytic oxidation of chlorophenols

The need for a facile phototransformation or photodegradation of phenols and chlorinated phenols to less harmful products has been of great research interest.[48-50,52,53,325,326] UV irradiation represents an important means of degradation of chlorophenols.[327] Regrettably, however, direct irradiation of chlorophenols in water generates more toxic organic compounds (like the polychlorinated dibenzo-p-dioxins) than the parent compound. Also, the semiconductor, titanium (IV) oxide (TiO_2) (band gap of 3.2 eV) widely used as a photocatalyst for the mineralisation of chlorophenols absorbs in the UV region where only approximately 4% of solar radiation is effective.[328-340] To overcome the above disadvantages, photosensitizers, which strongly absorb in the visible region are preferred. MPc photosensitizers are more efficient in photocatalytic reactions and also lead to the production of less harmful and relatively easily oxidised photoproducts such as chlorinated benzoquinones and hydroquinones.[48-50,52,53,325,326] Non-transition MPc complexes, such as Zn^{2+}, Al^{3+} and Si^{4+} exhibit excellent photosensitizing properties towards many environmentally relevant photo-assisted reactions. Photosensitised

transformation of organic substrates or pollutants in aqueous media with MPc photosensitisers mostly occur by the well-known Type II mechanism (section 1.1.3), which involves the generation of the highly oxidative singlet oxygen species responsible for the destruction of organic pollutants. Type I mechanism (section 1.1.3), which involves the participation of superoxide radical, may also take part in the reaction but this is generally limited.

An essential factor for these energy or electron transfer processes is the monomolecular distribution of the photosensitizers. Aggregated and dimeric MPc photosensitisers show significantly reduced photochemical activity compared to their unaggregated counterparts in energy transfer reactions probably due to enhanced radiationless excited state dissipation[341] and therefore, reduce the quantum yields of the singlet oxygen generation. Oxidative transformation of polychlorophenols by phthalocyanine and porphyrin complexes electrostatically bound onto supports such as Amberlite® and silica gel have been shown to result to disaggregation of the complexes, improved catalytic activity and higher stability.[51,113,324,342]

Table 1.6 gives a summary of MPcs as photocatalysts for visible light oxidation of chlorophenols. From literature, the main focus has been on the use of $MPcS_4$ and MOCPcs immobilised on supports. $MPcS_{mix}$ which are known to exhibit less aggregation than their $MPcS_4$ in aqueous solution have not been used as photocatalysts for chlorophenols transformation on support. $MPcS_{mix}$ and also $MPcS_4$ will be used as photocatalysts for chlorophenols oxidation in this thesis.

Table 1.6: Photocatalytic data for the transformation of chlorophenols using MPc complexes

MPc[a]/medium	Chlorophenol[b]	Oxidant[c]	Products[d]	References
$MPcS_4$, (M = Al or Zn), MOCPc (M = Al or Zn) in aqueous	4-CP	$^1O_2$	BQ	52
$MPcS_4$ (M = Al, Zn, Sn or Si) in aqueous solution	TCP/PCP	$^1O_2$	BQ derivatives	53
[Pc(-2)Nd(III)Pc (-2)]$^-$ solid particles in aqueous solution	4-CP	$^1O_2$	4-CC	343
$AlPcS_4$ on Amb. IRA 400	4-CP	H_2O_2	Not stated	344
$MPcS_4$ (M = Al, Zn, Ga) in aqueous solution	2-CP, 3-CP, 4-CP	$^1O_2$	MA and carbonates	49

[a]S = SO_3^-, [b]4-CP = 4-chlorophenol, 3-CP = 3-chlorophenol, 2-CP = 2-chlorophenol, TCP = trichlorophenol, PCP = pentachlorophenol, [c] $^1O_2$ = singlet oxygen, [d]BQ = benzoquinone, 4-CC = 4-chlorocatechol, MA = maleic acid,

Aim of Thesis

In this work, photocatalytic activities towards the phototransformation of chlorophenols of the following ring substituted non-transition metal MPc photosensitisers (i) tetra sulphonated ($MPcS_4$, M = Al^{3+} and Zn^{2+}) (ii) 'mixed sulphonated' ($MPcS_{mix}$, M = Si^{4+}, Al^{3+}, Zn^{2+}, Ge^{4+} and Sn^{4+}) and (iii) octacarboxy MOCPc, M = Al^{3+} and Zn^{2+}) all immobilised on Amberlite® support will be studied. Prior to this work, the 'mixed sulphonated' ($MPcS_{mix}$) types of photosensitisers have not been immobilised onto support

such as Amberlite® nor investigated for the phototransformation of organic pollutants such as the chlorophenols. These MPc photosensitizers are chosen because of their different photochemistry characteristics and hence possible different photoactivity towards the degradation of pollutants. By immobilising these MPc photosensitisers on Amberlite®, it is aimed that there will be improvement in their stabilities, ability to reuse them and preventing them from aggregating.

1.5.3 Electrocatalysis of chlorophenols, nitrite and sulphite oxidation using MPcs

Generally, electrochemical techniques offer a suitable means of both detecting and transforming environmentally and biologically important molecules like chlorophenols, nitrite and sulphite. Work done on the use of N_4-macrocyclic metal complexes (MPcs and metalloporphyrins, MPPs) modified electrodes as sensors for biologically and environmentally important molecules has been recently reviewed.[345] This section will deal with the review of the work done on the electrocatalysis of chlorophenols, nitrite and sulphite oxidation since the electrocatalysis part of this thesis involves that aspect.

1.5.3.1 Chlorophenol oxidation

Electrochemical techniques have the advantage over other techniques of their ability to both determine the quantity and also to transform chlorophenols into less toxic substances. Electrooxidation of chlorophenols on glassy carbon (GC),[346] platinum (Pt)[347-349] and on gold (Au) electrodes[350] have been reported, these electrodes showed instability

due to electrode fouling as a result of the formation of passivating polymer films derived from electrogenerated phenoxy radicals.[351,352] These polymers are formed by the coupling of phenoxy radicals to form dimeric or polymeric products, the coupling of the phenoxy radicals occurs through oxygen, using unpaired electrons, or through ortho or para-carbon atoms. The equation for the formation of the electrogenerated phenoxy radicals from phenol **(23)** is shown in Scheme 1.11.

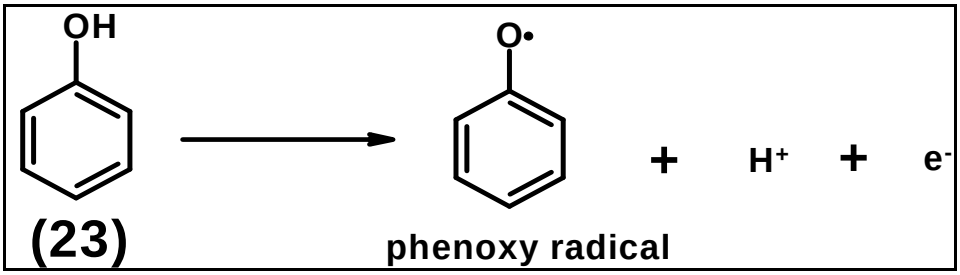

Scheme 1.11: Schematic representation of the formation of electrochemically generated phenoxy radicals

Factors such as the concentration of the phenol or the chlorinated derivative, the structure of the phenolic compounds and the operational conditions also play an important role in the extent of electrode passivation. Also for unmodified electrodes, the potentials for oxidation of chlorinated phenols are very high. For both Pt and Au,[347-350] the chlorophenols oxidation potentials are at the region where the metal oxides are formed. The quest for electrocatalysts and sensors which are stable and prevent electrode fouling is a major area of research and this has led to the use of macro complexes for electrode modifications. Chemically modified electrodes using transition metal macro complexes improves the performance of solid electrodes because of their robust nature and provision of catalytic sites at the electrode/solution interface.[353,354] Among these transition metal

macro complexes, the nickel macro complexes have been shown to be the most effective in this regard,[355] and improvements in terms of stability and electrocatalytic abilities towards chlorophenols and other analytes have been observed when these nickel macro complexes modified electrodes are repetitively cycled in strong alkaline media leading to the formation of O-Ni-O oxo bridges between the macro complexes,[215,356-358] which plays a key role in the improvement of their catalytic efficiency.

Table 1.7 gives a summary of MPcs used as electrocatalysts for chlorophenol oxidation. This Table shows that there has been very few MPc complexes employed for chlorophenol oxidation.

Table 1.7: Electrochemical data for the detection of chlorophenols using MPc complexes

MPc[a]	**Electrode[b]**	**Method of Modification**	**Analyte[c]**	**E_p / V (vs. SCE)**	**Medium**	**References**
CoPc	GCE	Drop dry	2-CP	1.05	0.05 H_2SO_4	359
CoPc	GCE	Drop dry	4-CP	1.06	0.05 H_2SO_4	359
NiTPhPyPc	VCE	Electro polymerisation	4-CP	~0.43	0.1M NaOH	360
Ni(OH) TPhPyPc	VCE	Electro polymerisation	4-CP	~0.35	0.1M NaOH	360
$NiPcS_4$	GCE/ITO	Electro polymerisation	2-CP	~0.25	pH 11	361

[a]TPhPy = tetra (pyrro-1-yl) phenoxy, [b]ITO = indium tin oxide, VCE = vitreous carbon electrode, GCE = glassy carbon electrode, [c]CP = chlorophenol

Aim of Thesis

This work will explore the use of gold electrode coated films of *poly*-NiPcs containing tetrakis benzylmercapto and tetrakis dodecylmercapto ring substituents for the electrooxidation of 4-CP and TCP. Elimination of electrode fouling by the polymer products from electrooxidation of chlorophenols has been a major challenge to researchers. Decrease in electrode fouling has been attributed to the bulkiness of MPc ring substituents group by their ability to allow analytes (chlorophenols) to catalytic sites because of the high porosity of the films despite the formation of polymer film products.[362,363] Benzylmercapto and tetrakis dodecylmercapto groups of the NiPcs were chosen for this purpose since they are bulky. In addition, the effects of the nature and thickness of the films on the electrodes' catalytic efficiency and stabilities against electrode fouling will be explored. This should be a significant contribution towards finding suitable electrocatalysts and sensors for chlorophenol electrooxidation.

1.5.3.2 Nitrite oxidation

Carbon electrodes modified with MPc complexes are known to lower both the reduction and oxidation potentials of nitrites.[364] The oxidation of nitrite on vitreous carbon electrode modified (by adsorption) with different CoPc has been investigated using CV and rotating disk electrode.[63] An amperometric nitrite sensor[287] based on a polymeric nickel tetraaminophthalocyanine film coated GC electrode has been developed; it showed a detection limit of 1×10^{-7} M and linear concentration range of 5×10^{-7} to 8×10^{-3} M for nitrite detection.

Table 1.8 gives a summary of MPc and metalloporphyrin complexes employed as electrocatalysts for nitrite oxidation. Nitrite oxidation generally occurs at potentials greater than 0.7 V (vs. SCE) on porphyrin and phthalocyanine modified electrodes (Table 1.8), with CoPcs being the most studied complexes. The central metals in MnPcs and FePcs are more easily oxidised (depending on substituents) compared to CoPc hence the former complexes may lower the overpotential for nitrite oxidation.

Table 1.8: Electrochemical data for the electrochemical detection of nitrite using MPc and MPP complexes

MPc[a]	**Electrode[b]**	**Method of Modification**	**E_p / V (SCE)**	**Medium**	**References**
CoPc	VCE	Drop dry	+0.87	pH 7.3	63
CoTPyP-$[Ru(bipy)_2Cl]_4$	GCE	Dip dry	+0.91	pH 4.7, 0.25 LiTFMS	365
CoTPyP-$[Ru(bipy)_2Cl]_4$: ZnTSPP	GCE	Drop dry	+0.72	0.2 M $BaClO_4$	366
CoTPyP-$[Ru(bipy)_2Cl]_4^+$/ ZnTSTPP	GCE	Drop dry	+0.76	pH 4.7	367
H_2TPyP-$[Ru(5\text{-}ClPhen_2Cl)]_4$	GCE or Pt	Electro polymerisation	+1.0	pH 4.5	368
FeTMPyP/ DNA	GCE	Electro deposition	+0.81	pH 9	369
$CrPc(NH_2)_4$	GCE/ITO	Electro polymerisation	+0.76 (vs. Ag|AgCl)	pH 7.3	214
$NiPc(NH_2)_4$	GCE	Electro polymerisation	+0.86	pH 2	287

[a]TPyP = tetrakis(3-pyridyl)porphine, TSPP = *meso*-tetrakis(*p*-sulphonatophenyl)porphine, TMPyP = tetra *meso* (3- and 4- pyridyl) porphyrin, DNA = deoxyribonucleic acid, phen = phenyl, bipy = bipyridine. [b]VCE = vitreous carbon electrode, GCE = glassy carbon electrode, ITO = indium tin oxide.

Aim of Thesis

This work thus explores a comparative study on the application of newly synthesised thiol derivatised MPcs (Co^{2+}, Fe^{2+}, Mn^{3+} and Ni^{2+}) towards nitrite electrooxidation. The possibility of lowering the overpotential by the use of MPcs with different central metal ions will be explored. The catalytic effect of the nature of the NiPcs films (*poly*-NiPc or *poly*-Ni(OH)Pc) will for the first time extended to electrooxidation of nitrite. Also, to further give insight to the understanding of the mechanisms behind electrooxidation of nitrite by MPcs (with different central transition metal ions) modified electrodes; interaction of nitrite ions with the MPcs will be studied using UV-Vis spectroscopy.

1.5.3.3 Sulphite oxidation

Electrocatalytic oxidation of sulphite in strongly acidic aqueous media by iron(II) tetrakis(4-sulphonatophenyl) porphine (FeTSPP) and manganese (III) tetra *meso* (3-pyridyl) porphine Mn(III)(4-TMPyP) immobilised on a zeolite molecular sieve has been reported, the oxidation of sulphite to sulphate was found to occur via Fe(III)($TSPP^{\cdot-}$) species and Mn(IV)(4-TMPyP) species,[370] respectively. Meso-pyridylporphyrins coordinated to four ruthenium bipyridyl porphyrin $[Ru(bipy)_2Cl]^+$ complexes form electrostatic active and stable nanomaterials by layer by layer electrostatic assembly films with $CuPcS_4$ anion, these were shown to have distinct catalytic activities towards nitrite and sulphite oxidation.[371] The indirect measurement of the SO_2 using aqueous solution of sulphite with adsorbed FePc on ordinary pyrolytic graphite (OPG) electrode has also been reported.[372]

Table 1.9 summarised MPc and metalloporphyrin complexes employed as electrocatalysts for sulphite. Reported work on the use of MPc and MPP modified electrodes as electrocatalysts for sulphite electrooxidation is limited and has been mostly on glassy carbon electrode. For the first time (i) a comparative effect of the central metal (first row transition metal; Co^{2+}, Fe^{2+}, Mn^{3+} and Ni^{2+} of the MPcs) on electrooxidation of sulphite and (ii) use of MPc-SAMs for electrooxidation of sulphite will be explored.

Table 1.9: Electrochemical data for the electrochemical detection of sulphite using MPc and MPP complexes

MPc[a]	**Electrode**	**Method of modification**	**E_p / V (SCE)**	**Medium**	**References**
Co(2-TMPyP)	GCE	Solution	+0.58	pH 2.2	373
CoTPyP-$[Ru(bipy)_2Cl]_4$	GCE	Dip dry	+0.91	pH 4.7, pH 0.25 LiTFMS	365
CoTPyP-$[Ru(bipy)_2Cl]^+$/ ZnTSTPP	GCE	Drop dry	+0.76	pH 4.7	367
Fe(2-TMPyP)	GCE	Solution	+0.82	pH 9.2	373
FeTSPP	GCE	Solution	+0.94	pH 2.0	370
Mn(2-TMPyP)	GCE	Solution	+0.30	pH 11.5	370
Zn(3-RPyP)/ $CuPcS_4$	Pt disk	Dip-coating	~+0.85	pH 6.8	371
FePc	OPG	Dip-dry	~+0.5	pH 5	372

[a]RPyP = 4-pyridyl porphine, TMPyP = tetra *meso* (3-pyridyl) porphine

Aim of Thesis

A comparative study on the potential use of MPc-SAMs of Co^{2+}, Fe^{2+}, Mn^{3+} and Ni^{2+} MPcs complexes, ring substituted with tetrakis benzylmercapto and dodecylmercapto as potential electrocatalysts and sensors for sulphite oxidation will be studied. The role of the central metal ion on the catalytic efficiency will be explored. The effect of the nature of the NiPcs films on the catalytic efficiency will also be explored.

1.6 Summary of Aim of Thesis

The aims of the thesis are summarised as follows:

i) Homogenous catalysis of chlorophenol transformations by monomeric and aggregated forms of cobalt tetrasulphonated phthalocyanine complex ($CoPcS_4$) **(24, Figure 1.13)**.

ii) Photocatalytic transformations of chlorophenols using sulphonated ($MPcS_4$ and $MPcS_{mix}$) and carboxyphthalocyanine (MOCPc) complexes of aluminium, zinc, tin, germanium and silicon **(25-33, Figure 1.13)**, immobilised on Amberlite$^{@}$.

iii) Syntheses and investigation of the electrochemical properties of alkanethiol-derivatised first row transition metal MPcs complexes **(34-43, Figure 1.14)** which are capable of forming self assembled monolayers (SAMs) and polymer films on gold electrodes.

iv) Fabrication and EIS, electrochemical and spectroelectrochemical characterisations of electrodes modified by thiol-derivatised MPcs complexes. Electrodes are modified by electropolymerisation and SAMs.

v) Investigation of the electrocatalytic properties of the MPcs complexes modified gold electrodes towards detection of some environmentally important analytes such as chlorophenols, nitrite and sulphite.

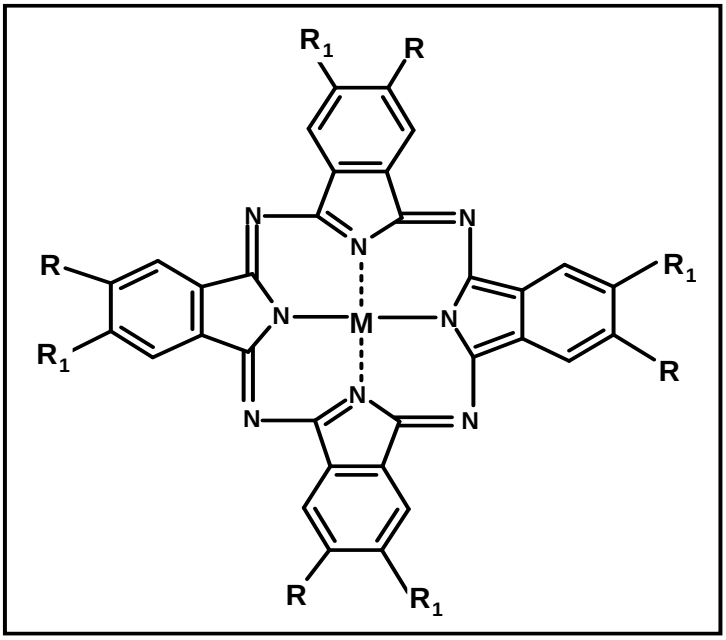

Complex	Central metal ion (M)	Complex number
$MPcS_4$, R = H, $R_1 = SO_3^-Na^+$	Co^{2+}	**24**
	$(OH)Al^{3+}$	**25**
	Zn^{2+}	**26**
MOCPc, $R = R_1 = COOH$	$(OH)Al^{3+}$	**27**
	Zn^{2+}	**28**
$MPcS_{mix}$, R = H, $(R_1)_n = SO_3^-Na^+$ (where n = 1, 2, 3 or 4)	$(OH)Al^{3+}$	**29**
	Zn^{2+}	**30**
	$(OH)_2Ge^{4+}$	**31**
	$(OH)_2Si^{4+}$	**32**
	$(OH)_2Sn^{4+}$	**33**

Figure 1.13: Structures of MPc complexes used for chlorophenols catalysis in this thesis

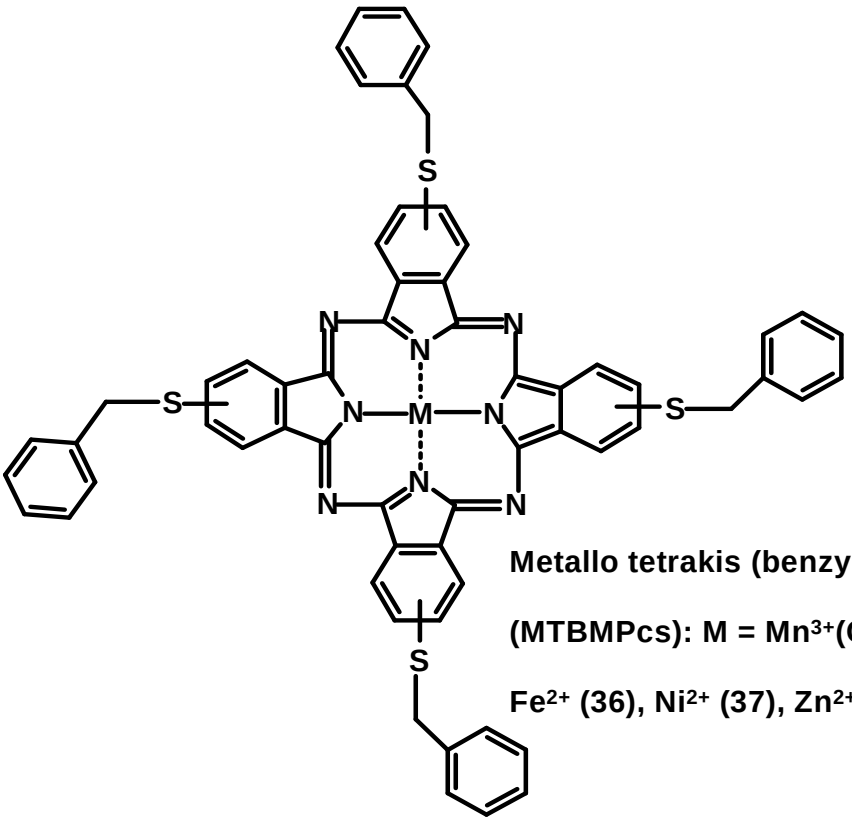

Metallo tetrakis (benzyl mercapto) phthalocyanines

(MTBMPcs): M = Mn^{3+}(OAc) (34), Co^{2+} (35),

Fe^{2+} (36), Ni^{2+} (37), Zn^{2+} (38)

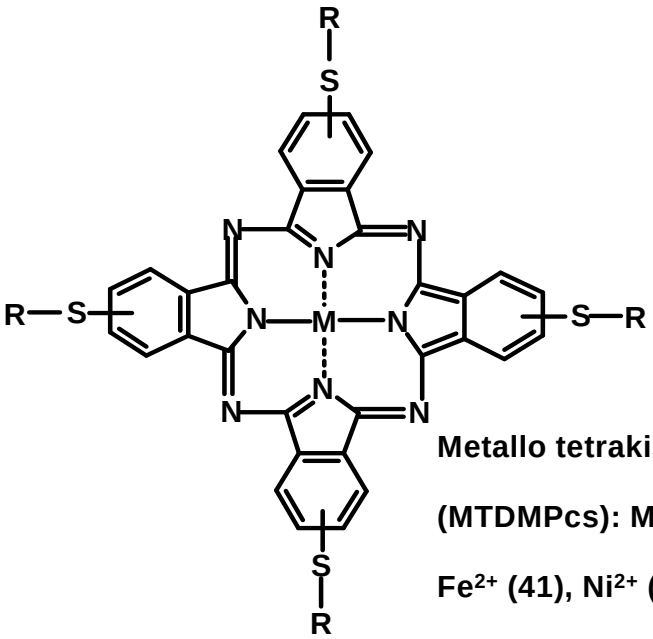

Metallo tetrakis (dodecyl mercapto) phthalocyanine

(MTDMPcs): M = Mn^{3+}(OAc) (39), Co^{2+} (40),

Fe^{2+} (41), Ni^{2+} (42), Zn^{2+} (43)

where R = $-CH_2(CH_2)_{10}CH_3$

Figure 1.14: Structures of thiol-derivatised MPc complexes studied in this thesis.

CHAPTER 2

EXPERIMENTAL

2.1 Materials

Phenol, dichlorobenzoquinone (DCBQ), benzoquinone (BQ), hydrogen peroxide (H_2O_2), 2, 4, 5-trichlorophenol (TCP), 2-chlorophenol (2-CP), amberlite® IRA-900 ion exchange resin, 4-chlorophenol, 2,4-dichlorophenol, 1,4-benzoquinone, 2-chloro-1,4-benzoquinone, 2,5-dichloro-1,4-benzoquinone, 2,3,4,5-tetrachloro-1,4-benzoquinone, anhydrous potassium carbonate, aluminium chloride, sodium azide, manganese(II)acetate salts, zinc acetate, tetrabutylammonium tetrafluoroborate {($TBABF_4$), recrystallised from ethanol and was used as electrolyte for all electrochemical experiments}, potassium carbonate, cobalt(II)chloride, zinc acetate, ferrous acetate and nickel(II)chloride hexahydrate were obtained from Sigma-Aldrich. Sodium nitrite was obtained from BDH. Silica gel 60 (0.04-0.063 mm) were purchased from Merck. Dichloromethane (DCM), DBU, maleic acid, pentachlorophenol (PCP) and fumaric acid were obtained from SAARCHEM (South Africa). Hydroquinone was obtained from May and Baker. (Cl)AlPc, ZnPc, $(OH)_2$GePc, $(OH)_2$SiPc, $(OH)_2$SnPc and copper(II)tetrasulphonated phthalocyanine (CuSO4) were available in our laboratory. Tetrasodium α,α-(anthracene-9,10-diyl) dimethylmalonate (ADMA) was a gift from Dr. V. Negrimovsky (from Organic Intermediates and Dyes Institute, Russia). Quinoline, ethylene glycol, dimethylsulfoxide (DMSO), dimethylformamide (DMF), dichloromethane (DCM), tetrahydrofuran (THF), diethyl ether, chloroform, methanol and ethanol were distilled prior to use. Where necessary, solutions used were deaerated by bubbling nitrogen prior to the experiments. Phosphate buffers were employed where needed.

2.2 Instrumentation

The UV/Vis absorption spectra were recorded with the use of Cary 500 UV/Vis/NIR spectrophotometer, Fourier transform infra red (FTIR) spectra (KBr pellets) were recorded on a Perkin-Elmer spectrum 2000 FT-IR spectrometer. ^{1}H-nuclear magnetic resonance (^{1}H-NMR, 400 MHz) was obtained in DMSO-d_6 or $CDCl_3$ using Bruker EMX 400 NMR spectrometer. MALDI-TOF spectra were obtained with Perspective Biosystems Voyager DE-PRO Biospectrometry Workstation and Processing Delayed Extraction at the University of Cape Town, Cape Town, South Africa. Mass spectra were recorded with Finnnigan LCQ-MS coupled with μ-Bondapak C-18 (390 x 3.00 mm diameter). Elemental analyses were performed with a Carlo Erba NA 1500 Nitrogen analyzer at the University of the Cape Town, Cape Town, South Africa. High Pressure Liquid Chromatography (HPLC) analysis was performed using Quad-Gradient HPLC system, Agilent 1100 series fitted with an analytical column, μ-Bondapak C-18 (390 x 3.00 mm) and connected to a variable wavelength UV-Vis detector (set at λ = 280 nm). Cyclic voltammetry (CV) and square wave voltammetry (SWV) data were obtained either using Autolab Potentiostat PGSTAT 30 (Eco Chemie, Utretch, The Netherlands) driven by the General Purpose Electrochemical Systems data processing software (GPES, software version 4.9, Eco Chemie) or Advanced Electrochemical System (Princeton Applied Research) Parstat 2273 equipment. Spectroelectrochemical data were obtained with the use of a home made optically transparent thin-layer electrochemical (OTTLE) cell which was connected to a Bioanalytic Systems (BAS) CV 27 voltammograph. A WTW pH meter was used for pH measurements.

2.3 Synthesis

2.3.1 Metallotetrasulphophthalocyanines ($MPcS_4$)[76]

Monosodium salt of 4-sulphophthalic acid (11).[148]

Equimolar mixture of 30% 4-sulphophthalic acid (12.3 g, 0.05 mol) and NaOH (2.0 g, 0.05 mol) was thoroughly mixed together in a flask. After 24 hours, the pink product crystallised out of the solution and was filtered off under pressure, washed with water and air dried. Yield: (88%). IR [(KBr) ν_{max}/ cm^{-1}]: 3440, 3065, 2655 and 2536 (O-H), 1745 and 1705 (C=O), 1595, 1574, 1496 and 1437 (C–C), 1396, 1375, 1280, 1242 and 1175 (C–O), 1070, 832, 794 and 720 (C–H).

Synthesis of metallotetrasulphophthalocyanines ($MPcS_4$),[76] Scheme 3.1

Cobalt ($CoPcS_4$) **(24)**, aluminum ($AlPcS_4$) **(25)** and zinc ($ZnPcS_4$) **(26)** tetrasulphophthalocyanine complexes were synthesised and purified using Weber and Busch method.[76] Monosodium salt of 4-sulphophthalic acid (4.32 g, 16 mmol), ammonium chloride (0.47 g, 9.0 mmol), urea (5.8 g, 97 mmol), ammonium molybdate (0.34 g, 0.03 mmol) and the metal salt (4.8 mmol) ($CoCl_2$ for cobalt(II)tetrasulphophthalocyanine, $CoPcS_4$ **(24)**, $AlCl_3$ for aluminium(III)tetrasulphophthalocyanine, $AlPcS_4$ **(25)** and $ZnCl_2$ for zinc(II)tetrasulphophthalocyanine, $ZnPcS_4$ **(26)** were thoroughly mixed together by grinding until a homogeneous mixture was formed. The mixture was added slowly to heated (180^oC) nitrobenzene (10 cm^3) in a three-necked round-bottomed flask fitted with a thermometer and a condenser under stirring over a period of 1 hour at 180-200^oC. Thereafter the mixture was heated for 6 hours at 200^oC. The crude product obtained was

a dark solid cake. The product was washed several times with methanol to remove nitrobenzene and then treated in a Soxhlet extraction apparatus with methanol for 24 hours to remove traces of nitrobenzene left. The final product was dried in an oven at ~ 120^{o}C for 24 hours after it was cooled to room temperature and filtered. The resulting product was then dissolved in 150 cm^{3} of 1.0 mol dm^{3} HCl saturated with NaCl and then heated to boiling. The mixture was cooled to room temperature, filtered, dissolved in 0.1 mol L^{-1} NaOH (70 cm^{3}) and then heated to 80^{o}C. The solid impurities were separated by centrifugation and then NaCl (27.0 g) was added to the filtrate and heated at 80^{o}C with stirring until the evolution of ammonia gas was complete (this was monitored using litmus paper). The crystallised product was separated by centrifugation and this last process was repeated twice. The product was then washed with 80% ethanol until it was chloride-free (detected by testing with 1.0 mol L^{-1} $AgNO_3$). Finally, the product was heated under reflux in 20 cm^{3} ethanol for 4 hours. Thereafter, cooled, filtered and dried in oven at 120^{o}C for 12 hours.

$CoPcS_4$ (24): Yield: (55%). IR [(KBr) ν_{max}/ cm^{-1}]: 1645 (C=C), 1577, 1523, 1497, 1399, 1342, 1193, 1148, 1111, 1076, 1038 (S=O), 925, 746, 694. UV-Vis [H_2O, λ_{max}/nm (log ε)]: 655 (5.12), 622 (4.98), 315 (5.02).

$AlPcS_4$ (25): Yield: (43%). IR [(KBr) ν_{max}/ cm^{-1}]: 3462 (O-H), 1642 (C=C), 1581, 1534, 1497, 1399, 1342, 1193, 1148, 1111, 1076, 1035 (S=O), 925, 830, 755, 699. UV-Vis [H_2O, λ_{max}/nm (log ε)]: 690 (5.2), 660 (5.1), 387 (4.92).

$ZnPcS_4$ (26): Yield: (58%). IR [(KBr) ν_{max}/ cm^{-1}]: 3451, 1644, 1586, 1397, 1344, 1198, 1154, 1107, 1077, 1037 (S=O), 925, 834, 735, 701. UV-Vis [H_2O, λ_{max}/nm (log ε)]: 692 (4.54), 652 (5.05), 376 (4.94).

2.3.2 Mixed sulphonated metallophthalocyanines ($MPcS_{mix}$), Scheme 3.2

$(OH)AlPcS_{mix}$ (**29**), $ZnPcS_{mix}$ (**30**), $(OH)_2GePcS_{mix}$ (**31**), $(OH)_2SiPcS_{mix}$ (**32**), and $(OH)_2SnPcS_{mix}$ (**33**) complexes were synthesised from (Cl)AlPc, ZnPc, $(OH)_2GePc$, $(OH)_2SiPc$ and $(OH)_2SnPc$, respectively, using fuming sulphuric acid (30% SO_3) according to literature procedure described for the synthesis of $AlPcS_{mix}$.[79] The required MPc (0.40 mmol) was placed in a round-bottomed flask and heated to 100^oC, thereafter, 1 cm^3 oleum was slowly added and the mixture stirred vigorously with the temperature kept at 100^oC. After 30 minutes, the reaction mixture was quenched by adding about 4 g of crushed ice onto it. The resulting mixture was adjusted to pH 7.0-7.5 using 1.0 mol L^{-1} NaOH solution to give a deep blue solution. The solution was evaporated to dryness and the residue Soxhlet extracted using methanol for 24 hours. Finally, the solvent was removed by evaporation and the solid product oven-dried at 120^oC.

$AlPcS_{mix}$ (29): Yield: (16%). IR [(KBr) ν_{max}/ cm^{-1}]: IR [(KBr) ν_{max}/ cm^{-1}]: 3435 and 3202 (O-H), 1732, 1635 and 1502, 1400, 1335, 1234, 1176, 1117, 1036 (S=O), 918, 756, 727. UV-Vis [H_2O, λ_{max}/nm (log ε)]: 681 (5.01), 608 (5.02), 355 (4.97).

$ZnPcS_{mix}$ (30): Yield: (18%). IR [(KBr) ν_{max}/ cm^{-1}]: 1737, 1626, 1548, 1394, 1226, 1212, 1154, 1086, 1045 (S=O), 984, 908. UV-Vis [H_2O, λ_{max}/nm (log ε)]: 675 (4.98), 616 (4.99).

$GePcS_{mix}$ (31): Yield: (12%). IR [(KBr) ν_{max}/ cm^{-1}]: 3444 and 3212 (O-H), 1728, 1627, 1550, 1396, 1223, 1215, 1148, 1091, 1041 (S=O), 974, 909, 747, 718. UV-Vis [H_2O, λ_{max}/nm (log ε)]: 677 (5.18), 639 (5.05), 607 (4.96), 349 (4.78).

$SiPcS_{mix}$ (32): Yield: (11%). IR [(KBr) ν_{max}/ cm^{-1}]: 3452 and 3215 (O-H), 1736, 1628, 1547, 1395, 1224, 1206, 1146, 1095, 1047 (S=O), 984, 908, 745, 713. UV-Vis [H_2O, λ_{max}/nm (log ε)]: 685 (5.11), 618 (4.98), 351 (4.96).

$SnPcS_{mix}$ (33): Yield: (11%). IR [(KBr) ν_{max}/ cm^{-1}]: 3464 and 3210 (O-H), 1734, 1585, 1396, 1312, 1197, 1142, 1080, 1043 (S=O), 886, 855, 811, 753, 722, 636, 572. UV-Vis [H_2O, λ_{max}/nm (log ε)]: 697 (5.24), 647 (4.86).

2.3.3 Synthesis of octacarboxymetallophthalocyanines (MOCPc),[77,78] Scheme 3.3

Octacarboxy phthalocyaninato aluminium(III), (AlOCPc) **(27)** and zinc(II) octacarboxyphthalocyaninatozinc(II), (ZnOCPc) **(28)** were prepared and purified according to the reported procedure.[77,78]

Benzene-1,2,4,5-tetracarboxylic dianhydride **(13)** (3.75 g, 17.25 mmol), urea (19.5 g, 0.33 mol), 1,8-diazabicyclo[5.4.0] undec-7-ene (DBU) (0.1 g, 0.7 mmol) and metal salt (23.5 mmol) (i.e. $AlCl_3$ for octacarboxy phthalocyaninato aluminium(III), (AlOCPc) (**27**) or zinc acetate for zinc(II) octacarboxyphthalocyaninatozinc(II), (ZnOCPc) (**28**)) were mixed together and placed in 100 ml two-necked flask fitted with a reflux condenser and a thermometer. The reaction mixture was heated at 250^oC under reflux for about 20 minutes and this resulted to formation of a fused product. Thereafter, the fused product was washed with water followed with acetone and finally with 6 mol L^{-1} HCl. The tetra-amide product **(14)** formed was dried and then hydrolysed by heating under reflux with 20% H_2SO_4 (3.0 cm^3) for 3 days. The product was washed with 200 cm^3 portions of 5% H_2SO_4, 100 cm^3 portions of water and acetone. The product was dried in the air and purified by column chromatography on an alumina column using 2% aqueous NaOH as eluent. The pure blue product **(27 or 28)** was filtered and then dried at 120^oC for 12 hours.

AlOCPc (27): Yield: (9.1%). IR [(KBr) ν_{max}/ cm^{-1}]: 3418 (O-H), 3235 (C-H), 1705 (C=O), 1641, 1618, 1507 and 1452 (C-C), 1378, 1282, 1249 and 1191 (C-O), 1154, 1133,

1075, 1038, 1016, 998, 912, 831 and 724 (C-H). UV-Vis [pH 10, λ_{max}/nm (log ε)]: 694 (5.10), 622 (4.85), 357 (4.99).

ZnOCPc (28): Yield: (11.5%). IR [(KBr) ν_{max}/ cm^{-1}]: 3421 (O-H), 3236 (C-H), 1702 (C=O), 1639, 1623, 1572 and 1451 (C-C), 1394, 1284, 1247 and 1184 (C-O), 1088, 1043, 1017, 982, 911 and 723 (C-H). UV-Vis [pH 10, λ_{max}/nm (log ε)]: 689 (5.26), 616 (5.11), 348 (4.95).

2.3.4 Synthesis of thiol-derivatised metallophthalocyanines

2.3.4.1 Synthesis of 4-nitrophthalonitrile,[375] Scheme 3.4

4-nitrophthalimide (44)

Fuming HNO_3 (60 mL) was slowly added to 360 ml of concentrated H_2SO_4 in the 1 L round bottom flask immersed in an ice bath. When the reaction mixture temperature cooled to ~ 12^oC, phthalimide **(5)**, 100.0 g (0.6 mol) was then added quickly under stirring and maintaining the temperature between 10^oC and 15^oC in an ice bath. The solution was then allowed to stand overnight at room temperature. The solution was poured on ice (~ 2 kg) while stirring to precipitate out the product which was a beige suspension and was isolated by filtration under reduced pressure. The solid product **(44)** was washed thrice with ice water. Yield: 58%. ^{1}H NMR $CDCl_3$: δ (ppm): 8.74 (d, 1H, Ar-H); 7.96 (s, 1H, N-H); 8.14 (d, 1H, Ar-H); 8.76 (dd, 1H, Ar-H). IR (KBr) v/ cm^{-1}: 1778 (s), 1717 (s) (CO-NH-CO), 1535 (vs) (NO_2 assym.), 1354 (vs) (NO_2 sym.).

4-nitrophthalamide (45)

4-Nitrophthalimide **(44)** (40 g, 0.2 mol), was added to 600 ml of 25% ammonia solution under stirring for 24 hours. Thereafter, another 200 ml 25% ammonia solution was added and the reaction mixture was left under stirring for another 24 hours. The resulting yellowish product was filtered off under reduced pressure and thoroughly washed several times with distilled water. The solid product, 4-nitrophthalamide **(45)** was dried in the oven at 100^{o}C. Yield: 83%. ^{1}HNMR $CDCl_3$: δ (ppm): 8.15 (d, 1H, Ar-H); 8.32 (dd, 1H, Ar-H); 8.46(d, 1H, Ar-H). IR (KBr) v/cm^{-1}: 3346 (NH_2 str), 1685 (s) (C=O str), 1620 (vs) (NH_2 def.).

4-nitrophthalonitrile (46)

Freshly distilled thionyl chloride, 25 mL (0.035 mol) was added slowly to 100 mL of dry dimethylfomamide (DMF) in a nitrogen atmosphere while stirring at 0 ^{o}C. The reaction mixture was further stirred for 2 hours and then 8.5 g (0.04 mol) of compound **45** was added to the mixture. The mixture was stirred for 5 hours at 0 ^{o}C and then at room temperature for 12 hours. The product was poured into 300 ml of ice water, filtered under reduced pressure and washed several times with distilled water. The product was recrystallised twice from methanol to yield yellow 4-nitrophthalonitrile **(46)**. Yield: 74%. ^{1}H NMR $CDCl_3$: δ (ppm): 8.15 (d, 1H, Ar-H); 8.56 (dd, 1H, Ar-H); 8.70 (d, 1H, Ar-H). IR (KBr) v/ cm^{-1}: 2230 (s) (C≡N) 1545 (vs) (NO_2 assym.), 1355 (vs) (NO_2 sym.).

2.3.4.2 Synthesis of monosubstituted thiol-derivatised phthalonitriles,[81] Scheme 3.5

4-(benzylmercapto) phthalonitrile (47)

A procedure similar to that reported[81] for the synthesis of 1,2-di(alkylthio)-4,5 dicyanobenzene was used in this work. Briefly 4.0 g (23 mmol) 4-nitrophthalonitrile (**46**) and 3.7 g (30 mmol) benzylmercapto thiol were dissolved in 20 ml DMSO and stirred strongly for 20 minutes under dry nitrogen atmosphere at room temperature. Thereafter, 10 g potassium carbonate was added portion wise for over 2 hours. The reaction was then left for another 12 hours to ensure complete reaction. The crude product was precipitated out from the reaction mixture and washed with water twice and then it was extracted with chloroform. Na_2CO_3 (5%) aqueous solution was added to the product in chloroform in a separating funnel, thoroughly mixed and then the aqueous layer removed. Thereafter, anhydrous Na_2SO_4 was added to remove traces of water, shaken and then decanted. The chloroform was then evaporated off and the light yellow solid product was crystallised from ethanol. Yield: 72%. IR (KBr) v (cm^{-1}): 1478, 1578, 2231 (ν_{CN}), 3026, 3060, 3069. ^{1}H NMR ($CDCl_3$): 4.30 (s, 2H, -*CH_2*), 7.28-7.38 (m, 5H, *phenyl*), 7.47-7.51 (dd, 1H, *benzyl*), 7.65 (d, 1H, *benzyl*), 7.58-7.62 (d-1H, *benzyl)*.

4-dodecylmercaptophthalonitrile (48)

The same procedure as for compound **47** was also used to make compound **48**, with 6.1 g (30 mmol) of dodecyl thiol being used in place of benzylmercapto. Yield: 62%. IR (KBr) v (cm^{-1}): 1465, 1579, 2228 (ν_{CN}), 2849, 2919. ^{1}H NMR ($CDCl_3$): 0.85 (t, 3H,-*CH_3*), 1.25 (m, 16H, -*CH_2*), 1.45 (m, 2H, -*CH_2*), 1.7 (m, 2H, -*CH_2*), 3.00 (t, 2H, -*CH_2*), 7.45-7.49 (dd, 1H, *benzyl*), 7.53-7.55 (d, 1H, *benzyl*), 7.60-7.63 (d, 1H, *benzyl*).

2.3.4.3 Thiol-derivatised tetrasubstituted phthalocyanine complexes,[81] Scheme 3.5

Manganese(III)acetate tetrakis (benzyl-mercapto) phthalocyanine, Mn(OAc)TBMPc (34)

4-(Benzylmercapto) phthalonitrile (**47,** 1 g, 4 mmol) was mixed with 0.182 g (1.05 mmol) anhydrous manganese(II)acetate and 6 ml ethylene glycol and then refluxed for 5 hours at 200^{o}C under N_2 atmosphere. The mixture was allowed to cool to room temperature and then excess methanol was added to precipitate out the crude reddish brown solid product which was then treated in a Soxhlet extraction apparatus with ethanol for 48 hours. The product was purified using silica gel column chromatography eluting twice with chloroform and THF. The pure complex was a deep red solid. Yield: 48%. IR (KBr) *v* (cm^{-1}): 696 (ν_{C-S}), 865 (ν_{Mn-O}), 1743 ($\nu_{C=O}$). λ_{max} (nm) (log ε) in DCM: 742 (5.1), 526 (4.8), 452 (4.4). Anal. Calcd. for $C_{60}H_{40}N_8S_4Mn$: %C, 66.79; %H, 3.86; %N, 10.06. Found: %C, 66.07; %H, 4.18; %N, 10.26. MALDI-TOF: $C_{62}H_{43}N_8S_4O_2Mn$. Calc. 1054.9 g mol^{-1}, found (M^+) 1054.3 g mol^{-1}.

Manganese(III)acetate tetrakis (dodecyl-mercapto) phthalocyanine, Mn(OAc)TDMPc (39)

Similar procedure as for the synthesis of complex **34** was also used for complex **39**. 4-Dodecylmercaptophthalonitrile (**48,** 1.3 g, 4 mmol) was used instead of compound **47**. The pure complex was a deep red solid. Yield: 41 %. IR (KBr) *v* (cm^{-1}): 698 (ν_{C-S}), 857 (ν_{Mn-O}), 1765 ($\nu_{C=O}$). λ_{max} (nm) (log ε) in DCM: 746 (4.9), 528 (4.6), 450 (4.3). Anal. Calcd. for $C_{80}H_{112}N_8S_4Mn$: %C, 69.01; %H, 8.07; %N, 7.86. Found: %C, 70.22; %H, 7.98; %N, 6.84. MALDI-TOF: $C_{82}H_{115}N_8S_4O_2Mn$: Calc. 1370.9 g mol^{-1}, found (M^+) 1370.5 g mol^{-1}.

Cobalt tetrakis (benzyl mercapto) phthalocyanine, CoTBMPc (35)

4-(Benzylmercapto) phthalonitrile (**47**, 1 g, 4 mmol) was mixed with 0.14 g (1.05 mmol) anhydrous cobalt chloride and 8 ml ethylene glycol and then refluxed for 4 hours at 200^{o}C under N_2 atmosphere. The mixture was allowed to cool to room temperature and then excess methanol was added to precipitate out the crude blue-green solid product which was then treated in a Soxhlet extraction apparatus with ethanol for 48 hours. The product was purified using silica gel column chromatography with chloroform as the eluting solvent. Yield: 47%. IR (KBr) *v* (cm^{-1}): 694 (ν_{C-S}). λ_{max} (nm) (log ε) in DCM: 676 (4.94), 613 (4.99), 325 (4.81). Anal. Calcd. for $C_{60}H_{40}N_8S_4Co.3H_2O$: C, 64.60; H, 3.59; N, 10.80; S, 11.49. Found: C, 64.78; H, 3.68; N, 9.24; S, 11.25. MALDI-TOF: $C_{60}H_{40}N_8S_4Co$. Calc. 1060.2 g mol^{-1}, found (M^+) 1059.1 g mol^{-1}.

Cobalt tetrakis (dodecylmercapto) phthalocyanine, CoTDMPc (40)

Similar procedure as in the synthesis of complex **35** was also used for complex **40**. 4-Dodecylmercaptophthalonitrile (**48,** 1.3 g, 4 mmol) was used instead of compound **47**. The blue-green product was purified by using silica gel column chromatography with chloroform-THF (ratio 3:1) as the eluting solvent. Yield: 33%. IR (KBr) *v* (cm^{-1}): 673 (ν_{C-S}). λ_{max} (nm) (log ε) in DCM: 684 (4.93), 623 (5.00), 310 (4.92). Anal. Calcd. for $C_{80}H_{112}N_8S_4Co$: C, 69.98; H, 8.22; N, 8.16; S, 9.34. Found: C, 70.55; H, 9.22; N, 8.35; S, 9.09. MALDI-TOF: $C_{80}H_{112}N_8S_4Co$: Calc. 1373.0 g mol^{-1}, found (M^+) 1372.6 g mol^{-1}.

Iron tetrakis (benzyl mercapto) phthalocyanine, FeTBMPc (36)

4-(Benzylmercapto) phthalonitrile (**47,** 1 g, 4 mmol) was mixed with anhydrous ferrous acetate (0.174 g, 1 mmol) and 4 ml quinoline. The mixture was refluxed for 7 hours at 200^{o}C under N_2 atmosphere. Thereafter, the reaction mixture was allowed to cool to room temperature and then excess methanol was added to precipitate out the crude green solid product which was then treated in a Soxhlet extraction apparatus for 48 hours to remove quinoline. The product was purified by using silica gel column chromatography with chloroform as the eluting solvent. Yield: 37 %. IR (KBr) *v* (cm^{-1}): 692 (ν_{C-S}). λ_{max} (nm) (log ε) in DCM: 705 (4.06), 675 (4.25), 638 (4.45), 349 (4.57). Anal. Calcd. for $C_{60}H_{40}N_8S_4Fe.3H_2O$: C, 64.80; H, 3.60; N, 10.08; S, 11.52. Found: C, 65.34; H, 3.78; N, 9.87; S, 9.47. MALDI-TOF: $C_{60}H_{40}N_8S_4Fe$: Calc. 1057.1 g mol^{-1}, found (M^+) 1056.4 g mol^{-1}.

Iron tetrakis (dodecylmercapto) phthalocyanines, FeTDMPc (41)

Similar procedure as in the synthesis of complex **36** was also used for complex **41**. 4-Dodecylmercaptophthalonitrile (**48,** 1.3 g, 4 mmol) was used instead of compound **47**. The green product was purified by using silica gel column chromatography with chloroform-THF (ratio 3:1) as the eluting solvent. Yield: 26 %. IR (KBr) *v* (cm^{-1}): 744 (ν_{C-S}). λ_{max} (nm) (log ε) in DCM: 712 (4.66), 586 (4.99), 422 (3.97), 350 (5.00), 310 (5.00). Anal. Calcd. for $C_{80}H_{112}N_8S_4Fe.5H_2O$: C, 65.76; H, 7.70; N, 7.70; S, 8.77. Found: C, 64.38; H, 7.54; N, 7.10; S, 7.94. MALDI-TOF: $C_{80}H_{112}N_8S_4Fe$. Calc. 1369.9 g mol^{-1}, found (M^+) 1369.9 g mol^{-1}.

Nickel tetrakis (benzyl mercapto) phthalocyanine, NiTBMPc (37)

4-(Benzylmercapto) phthalonitrile (**47,** 1 g, 4 mmol) was mixed with 0.136 g (1.05 mmol) anhydrous nickel(II)chloride and 3 ml quinoline and then refluxed for 4 hours at 200^{o}C under N_2 atmosphere. The mixture was allowed to cool to room temperature and then excess methanol was added to precipitate out the crude green solid product which was then treated in a Soxhlet extraction apparatus with ethanol for 24 hours. The product was purified using silica gel column chromatography with chloroform-THF (ratio 3:1) as the eluting solvent. Yield: 39%. IR (KBr) *v* (cm^{-1}): 685 (ν_{C-S}). λ_{max} (nm) (log ε) in DCM: 681 (4.82), 625 (5.05), 410 (5.00), 301 (5.00). Anal. Calcd. for $C_{60}H_{40}N_8S_4Ni.3H_2O$: C, 67.99; H, 3.80; N, 10.57, S, 12.10 Found : C, 67.43, H, 3.85; N,10.72; S,13.40. MALDI-TOF; $C_{60}H_{40}N_8S_4Ni$: Calc. 1059.9 g mol^{-1}, found (M^+) 1058.0 g mol^{-1}.

Nickel tetrakis (dodecyl mercapto) phthalocyanine, NiTDMPc (42)

NiTDMPc **(42)** has been synthesised before,[96] in this work the complex was synthesised according to literature[81] and gave satisfactory characterisation as follows: Yield: 31%. IR (KBr) *v* (cm^{-1}): 748 (ν_{C-S}). λ_{max}(nm) (log ε) in DCM: 685 (4.99), 632 (4.99), 400 (5.00), 310 (5.00). Anal. Calcd. for $C_{80}H_{112}N_8S_4Ni.4H_2O$: C, 69.99; H, 8.22; N, 8.16; S, 9.34. Found: C, 69.46; H, 8.20; N, 8.24; S, 9.58. MALDI-TOF; $C_{80}H_{112}N_8S_4Ni$: Calc. 1372.8 g mol^{-1}, found (M^+) 1372 g mol^{-1}.

Zinc tetrakis (benzylmercapto) phthalocyanine, ZnTBMPc (38)

4-(Benzylmercapto) phthalonitrile (**47,** 1 g, 4 mmol) was mixed with anhydrous zinc acetate (0.19 g, 1.05 mmol) and 4 ml quinoline. The mixture was refluxed for 7 hours at

200^{o}C under N_2 atmosphere. Thereafter, the reaction mixture was allowed to cool to room temperature and then excess methanol was added to precipitate out the crude green solid product which was then treated in a Soxhlet extraction apparatus with ethanol for 48 hours to remove quinoline. The green product was purified by using silica gel column chromatography with chloroform as the eluting solvent. Yield: 58%. IR (KBr) *v* (cm^{-1}): 692 (ν_{C-S}). λ_{max} (nm) (log ε) in DCM: 689 (5.22), 620 (4.99), 359 (4.81). ^{1}H NMR (DMSO d_6): 4.80 (s, 8H, -*CH$_2$*), 7.30-7.60 (m, 20H, -*phenyl*), 7.95 (m-4H, -*Pc*), 7.60-7.90 (m, 8H, -*Pc*). Anal. Calcd. for $C_{60}H_{40}N_8S_4Zn$: C, 67.56; H, 3.78; N, 10.51; S, 12.02. Found: C, 66.53; H, 3.73; N, 9.69; S, 12.01. MALDI-TOF: $C_{60}H_{40}N_8S_4Zn$: Calc. 1066.7 g mol^{-1}, found (M^+) 1066.0 g mol^{-1}.

Zinc tetrakis (dodecyl mercapto) phthalocyanine, ZnTDMPc (43)

Similar procedure as in the synthesis of complex **38** was also used for complex **43** synthesis except 4-dodecylmercaptophthalonitrile (**48,** 1.3 g, 4 mmol) was used instead of compound **47.** Yield: 49 %. IR (KBr) *v* (cm^{-1}): 668 (ν_{C-S}). λ_{max} (nm) (log ε) in DCM: 691 (5.4), 622 (4.99), 356 (4.97). ^{1}H NMR ($CDCl_3$): 0.95 (t, 12H, -*CH$_3$*), 1.20-1.50 (m, 80H, -*CH$_2$*), 2.20-2.90 (t, 8H, -*CH$_2$*), 6.50-7.80 (m, 12H –*Pc*). Anal. Calcd. for $C_{80}H_{112}N_8S_4Zn.3H_2O$: C, 66.99; H, 7.82; N, 7.82; S, 8.93. Found: C, 66.50; H, 7.95; N, 7.81; S, 8.53. MALDI-TOF: $C_{80}H_{112}N_8S_4Zn$: Calc. 1379.5 g mol^{-1}, found (M^+) 1379.5 g mol^{-1}.

2.3.5 Immobilisation of photosensitisers

The various MPc photosensitizer–Amberlite (represented as MPc-Amb.) ion exchange resin compositions were prepared using the established procedure.[41] Unbuffered water was employed to deposit sulphonated MPc complexes onto Amberlite® supports. In order to ensure ionisation of the MOCPcs, pH 8 boric acid buffer was employed for immobilisation of these complexes onto Amberlite® instead of unbuffered water. The resin was thoroughly washed with water and dried. A 0.01 g of the resin was suspended in 100 ml solution of MPc with an absorbance of approximately 1. The immobilisation of MPc was performed on a small scale of 0.01 g in order to have freshly prepared ones for each experiment. Also reproducibility was ensured by strictly using the same condition such as stirring rate, time of immobilisation and finally ensuring that the same number of moles of MPcs were immobilised on the amberlite as judged by the difference in the MPc absorbance before and after immobilisation. The reaction mixtures were left under gentle stirring with a magnetic stirrer and the reaction progress were monitored with Cary 500 UV-Vis-NIR spectrophotometer. For consistency, the immobilisation was carried out until the number of moles of MPc immobilised was 5×10^{-8} mol. The change in UV-Vis Q-band absorbance values of the various MPc in aqueous solutions was used to calculate the number of moles of the MPc photosensitizer.

Following immobilisation, the colored (light green or light blue) immobilised product obtained was first thoroughly washed with copious amount of distilled deionised water, then methanol and acetone, and finally dried in the oven at 70^{o}C for 24 hours. Diffused reflectance spectra of the solid MPc-resin were recorded with Cary 500 UV-Vis-NIR spectrophotometer.

2.4 Methods

2.4.1 Chlorophenol transformations

2.4.1.1 Chemical/Enzyme-like catalysis studies

Millipore water containing 60% methanol (v/v) (pH 3.4) or phosphate buffers (pH = 7 and pH = 10) were used to prepare all the solutions. The reaction mixtures containing 1.0 x 10^{-2} mol L^{-1} of substrate (2-CP or TCP), 1.0 x 10^{-2} mol L^{-1} of the oxidant (hydrogen peroxide) and the catalyst were stirred together in a sample vial for the desired time of reaction. Various amounts of the $CoPcS_4$ catalyst (0.1 to 2.5% of the total mixture) were employed in order to determine the optimal catalyst loading. Substrate conversions were monitored by HPLC. The mobile phase comprised of 70:30 methanol: water mixture, with a flow rate of 1 ml min^{-1}. The sample injection volume was 2 µL. The separation of the substrates and the products was achieved within 9 minutes for TCP and 4 minutes for 2-CP. The oxidation products were identified by spiking using standards and by retention times in HPLC traces. The nature of some of the products was further confirmed by mass to charge ratios of molecular ion peaks and fragmentation patterns as obtained from a liquid chromatograph connected to a mass spectrometer (LC/MS). The UV/VIS absorption spectra of the catalyst were monitored at regular intervals during the reaction using Cary 500 UV/Vis/NIR spectrophotometer. For the purpose of studying the effect of the central metal of the catalyst, $AlPcS_4$, $CuPcS_4$ and $NiPcS_4$ were also employed as catalysts, using 1% catalyst loading. The degradation reactions were monitored for up to 5 hours.

2.4.1.2 Photochemical studies

All photochemical studies were performed using a home-made photochemical set-up as shown in Scheme 2.1. Photolysis was performed in the visible region to avoid the effects of uncatalysed photodegradation of the chlorophenols in the ultra violet region. A 1 cm pathlength UV–Vis spectrophotometer quartz cell fitted with a tight-fitting stopper was employed for the photolysis studies. Briefly, the set-up comprised of a light source from a General Electric Quartz lamp (300 W); using a 600 nm glass (Schott) and water filters to filter off UV and far infrared radiations respectively. An interference filter (Intor, 700 nm with a bandwidth of 40 nm) was placed in the light path before the quartz cell containing the sample.

Typically, for the phototransformation of the chlorophenols (4-CP, 2,4-DCP, 2,4,5-TCP and PCP), a 2.5 ml solution of the substrate containing 5 x 10^{-8} mol of immobilised photosensitizer on Amberlite® was first saturated with oxygen and then photolysed under gentle stirring. The light intensity was measured with a power meter (Lasemate/A) and was found to be 5 x 10^{16} photons s^{-1} cm^{-2}. Kinetic studies were monitored with UV-VIS-NIR spectrophotometer or HPLC. Products identification (by spiking with standards and by comparing retention times) was carried out with the use of Quad-Gradient HPLC system, Agilent 1100 series fitted with an analytical column, μ-Bondapak-C18 (390 x 3.00 mm) and connected to a variable wavelength UV-VIS detector (set at λ = 280 nm). The mobile phase was made up of methanol/water (70:30) mixture. The volume of injected samples was 2 μL, and the elution rate was 1 ml min^{-1}.

Investigation of the singlet oxygen generation efficiencies of the immobilised photosensitizers was carried out by photolysis of an aqueous (unbuffered) solution of the

MPc containing tetrasodium α,α-(anthracene-9,10-diyl) dimethylmalonate (ADMA) as chemical scavenger for singlet oxygen. The participation of $^1O_2$ in the photolysis was further confirmed by the addition of sodium azide (which is a $^1O_2$ quencher) to the photolysis reaction containing the chlorinated phenols and the MPc photosensitizer.

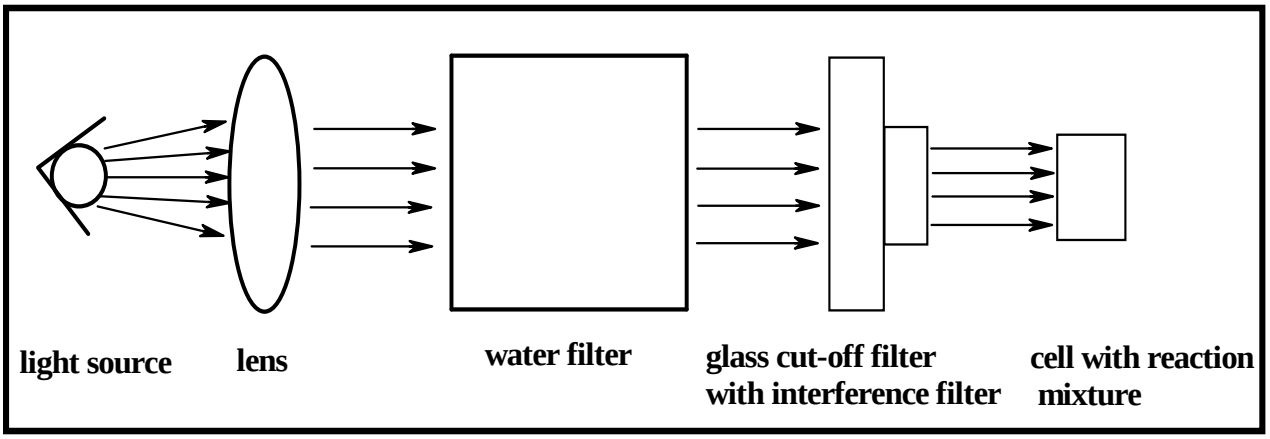

Scheme 2.1: Diagrammatic representation of the photochemical set-up.

2.4.2 Electrochemical methods

2.4.2.1 Characterisation of thiol-derivatised MPcs

Voltammetry data for the characterisation of thiol-derivatised MPc complexes were obtained with Autolab potentiostat PGSTAT 30 (Eco Chemie, Utretch, The Netherlands) driven by the General Purpose Electrochemical Systems data processing software (GPES, software version 4.9, Eco Chemie), using a three-electrode set-up. The working electrode was glassy carbon (GCE, 3.0 mm diameter); Ag|AgCl wire and platinum wire were pseudo reference and counter electrodes respectively. Square wave parameters were: step

potential 5 mV; amplitude 20 mV at a frequency of 25 Hz. All electrochemical experiments were carried out in nitrogen atmosphere.

2.4.2.2 Spectroelectrochemical characterisation of thiol-derivatised MPcs

Spectroelectrochemical data were obtained with the use of a home made optically transparent thin-layer electrochemical (OTTLE) cell, with the same construction as that described by Hartl and Denek.[376] The cell has as working and counter electrodes platinum grits and a piece of silver wire was used as the reference electrode. The OTTLE cell was connected to a BAS CV 27 voltammograph. Solutions of the complexes were introduced into the cell and electrolysis was performed at the appropriate potentials. Spectral changes during the electrolysis processes were monitored with a Cary 500 UV/Vis/NIR spectrophotometer.

For studies involving electronic spectra on indium titanium oxide (ITO), a 0.7 cm wide and 1 cm long ITO was placed against the wall of the 1 cm path length cell in the path of the light beam. Spectra were recorded on a Cary 500 UV/Vis/NIR spectrophotometer.

2.4.3 Electrode modification procedures

2.4.3.1 Electropolymerisation techniques

The working electrode was bare Au electrode, GCE or indium tin oxide, ITO; Ag|AgCl wire pseudo reference and platinum wire counter electrodes were employed. All electrochemical experiments were carried out in nitrogen atmosphere. Depositions of the complexes on gold, glassy carbon or ITO electrodes were performed by repetitive

scanning (CV) of the complexes solutions (1 mM) in DCM/$TBABF_4$ at the potential window from -0.5 to 1.2 V vs. Ag|AgCl at scan rate of 100 mV s^{-1}. Faradaic impedance measurements were performed using the Autolab FRA equipment with a 10 mV rms sinusoidal modulation, this was used to characterise the *poly*-NiPc and *poly*-Ni(OH)Pc films.

2.4.3.2 Self-assembling techniques

SAM studies were carried out using Advanced Electrochemical System (Princeton Applied Research) Parstat 2273 or Autolab potentiostat PGSTAT 30 (Eco Chemie, Utretch, The Netherlands) driven by the General Purpose Electrochemical Systems data processing software (GPES, software version 4.9, Eco Chemie) equipment with a three-electrode set-up consisting of either bare gold (r = 0.8 mm from Bioanalytical systems, BAS) or MPc-SAM modified gold electrodes, Ag|AgCl (3 M NaCl) or Ag|AgCl wire pseudo reference electrode and platinum wire counter electrode, the difference in the potentials is ~ 0.02 V. The gold electrodes were polished with slurries of 1.0 µm followed by 0.05 µm alumina on a SiC-emery paper (type 2400 grit) and then subjected to ultrasonic vibration in ethanol to remove residual alumina particles at the surface. The gold electrodes were then treated with 'Piranha' solution {1:3 (v/v) 30% H_2O_2 and conc. H_2SO_4} for about 1 minute, this step is necessary in order to remove organic contaminants and was followed by thorough rinsing with distilled water. The electrodes were rinsed with ethanol and finally with dichloromethane (DCM). Following this pre-treatment, the electrodes were then placed in nitrogen-saturated 1 mM solutions of the MPcs in DCM. After allowing the SAMs to form for a desired period of time, the

modified electrodes were then thoroughly rinsed with DCM and dried gently in a weak flowing nitrogen gas. The modified electrodes were stored in nitrogen-saturated phosphate buffer pH 4.0 at room temperature.

2.4.4 Electrocatalytic procedure

Experiments for electrocatalysis of chlorophenols oxidation were carried out using N_2 purged solutions in 0.1 M NaOH with the modified Au electrode (on Au by polymerisation) as the working electrode while Ag|AgCl and platinum electrodes were employed as reference and counter electrodes respectively.

For both electrocatalysis of nitrite (on Au by polymerisation) and sulphite oxidation (on Au by SAM), the experiments were carried out using N_2 purged solutions of the nitrite or sulphite in phosphate buffer (pH 7.4) solution using Au electrode modified with the complexes as the working electrodes while Ag|AgCl and platinum electrodes were employed as reference and counter electrodes respectively.

RESULTS AND DISCUSSION

Publications that resulted from these work are listed below and they are not referenced in this thesis:

1. Hydrogen peroxide oxidation of 2-chlorophenol and 2, 4, 5-trichlorophenol catalysed by monomeric and aggregated cobalt tetrasulphophthalocyanine. ***Bolade Agboola***, *Kenneth I. Ozoemena, Tebello Nyokong,* ***J. Mol. Catal. A: Chem. 227 (2005) 209.***

2. Comparative efficiency of immobilised non-transition metal phthalocyanine photosensitisers for the visible light transformation of chlorophenols. ***Bolade Agboola***, *Kenneth I. Ozoemena and Tebello Nyokong,* ***J. Mol. Catal. A: Chem. 248 (2006) 84.***

3. Synthesis and electrochemical characterisation of benzyl mercapto and dodecylmercapto tetra substituted cobalt, iron, and zinc phthalocyanines complexes. ***Bolade Agboola***, *Kenneth I. Ozoemena and Tebello Nyokong,* ***Electrochim. Acta, 51 (2006) 4379.***

4. Electrochemical properties of benzyl mercapto and dodecylmercapto tetra substituted nickel complexes: electrocatalytic oxidation of nitrite. ***Bolade O. Agboola***, *Kenneth I. Ozoemena and Tebello Nyokong,* ***Electrochim. Acta, 51 (2006) 6470.***

5. Synthesis and electrochemical properties of benzyl-mercapto and dodecyl-mercapto tetrasubstituted manganese phthalocyanine complexes. ***Bolade Agboola****, Kenneth I. Ozoemena, Philippe Westbroek and Tebello Nyokong,* ***Electrochim. Acta, 52 (2007) 2520.***

6. Voltammetric characterisation of the self-assembled monolayers (SAMs) of benzyl- and dodecyl-mercapto tetra substituted metallophthalocyanines complexes. ***Bolade Agboola****, Philippe Westbroek, Kenneth I. Ozoemena and Tebello Nyokong,* ***Electrochem. Commun., 9 (2007) 310.***

7. Comparative electrooxidation of nitrite by electropolymerised Co(II), Fe(II) and Mn(III) tetrakis benzylmercapto and dodecylmercapto metallophthalocyanines on gold electrodes. ***Bolade Agboola*** *and Tebello Nyokong,* ***Anal. Chim. Acta, 587 (2007) 116.***

8. Electrooxidation of chlorophenols by electropolymerised nickel (II) tetrakis benzylmercapto and dodecylmercapto metallophthalocyanines complexes on gold electrodes. ***Bolade Agboola*** *and Tebello Nyokong,* ***Electrochim. Acta, 52 (2007) 5039.***

9. Comparative electrooxidation of sulphite by self assembled monolayers (SAMs) of Co(II), Fe(II), Ni(II) and Mn(III) tetrakis benzylmercapto and dodecylmercapto metallophthalocyanines complexes on gold electrodes. ***Bolade Agboola*** *and Tebello Nyokong,* ***Talanta, In press (2007).***

CHAPTER 3

SYNTHESIS AND CHARACTERISATION

This chapter deals with the synthesis, spectral and electrochemical characterisation of the MPcs complexes used for transformation of chlorophenols, electrooxidation of chlorophenols, nitrite and sulphite.

Table 3.1 gives the list of the MPc complexes synthesised and their UV-Vis bands spectral data.

Table 3.1: List of complexes synthesised with their UV-Vis bands. $MPcS_4$ and $MPcS_{mix}$ complexes in water, MOCPc complexes in phosphate buffer pH 10, and MTBMPcs and MTDMPcs in DCM.

MPc complexes Abbreviations and Numbers	**Q band maxima[a,b]**
$CoPcS_4$ **(24)**	655 (m) (5.12) 622 (d) (4.98)
$AlPcS_4$ **(25)**	690 (m) (5.2) 660 (d) (5.1)
$ZnPcS_4$ **(26)**	692 (m) (4.54), 652 (d) (5.05)
$AlPcS_{mix}$ **(29)**	681 (5.01)
$ZnPcS_{mix}$ **(30)**	675 (m) (4.98), 616 (d) (4.99)
$GePcS_{mix}$ **(31)**	677 (5.18)
$SiPcS_{mix}$ **(32)**	685 (5.11)
$SnPcS_{mix}$ **(33)**	697 (m) (5.24), 647 (d) (4.86)
AlOCPc **(27)**	694 (5.10)
ZnOCPc **(28)**	689 (5.26)
MnTBMPc **(34)**	742 (5.1)
MnTDMPc **(39)**	746 (4.9)
CoTBMPc **(35)**	676 (4.94)
CoTDMPc **(40)**	684 (4.93)
FeTBMPc **(36)**	705 (m) (4.06), 675 (d) (4.25)
FeTDMPc **(41)**	712 (m) (4.66), 586 (d) (4.99)
NiTBMPc **(37)**	681(m) (4.82), 625 (m) (5.05),
NiTDMPc **(42)**	685 (m) (4.99), 632 (d) (4.99),
ZnTBMPc **(38)**	689 (5.22)
ZnTDMPc **(43)**	691 (5.4)

[a]m and d represent monomer and aggregate respectively,
[b] log ε values in bracket

3.1 Synthesis and Spectral Characterisation

3.1.1 Sulphonated and Carboxyl MPc derivatives

The tetrasulphonated and octacarboxy MPc complexes used for transformation of chlorophenols were synthesised and characterised as before[76-79] and their spectroscopic characterisations were consistent with literature.[76-79]

3.1.1.1 Sulphonated MPcs

The tetra sulphonated MPc complexes ($MPcS_4$) were synthesised using Weber and Busch method[76] shown in Scheme 3.1. High yields of the complexes were obtained as listed in Chapter 2, experimental section.

$MPcS_4$ complexes are generally known to exist as aggregates in equilibrium with monomers in aqueous solutions. From Figure 3.1, the spectra of (a) $CoPcS_4$ (**24**) (655, monomer; 622, aggregates) and (b) $ZnPcS_4$ (**26**) (692, monomer; 652, aggregates) are highly aggregated but (c) $AlPcS_4$ (**25**) showed much less aggregation in water.

The S=O vibrations which were observed in the 1030 – 1040 cm^{-1} region in the IR spectra are characteristic of $MPcS_4$ complexes. The O-H band appeared at 3462 cm^{-1} for $AlPcS_4$ (**25**) but was absent for both $CoPcS_4$ (**24**) and $ZnPcS_4$ (**26**), this is not unusual because the former has O-H axial ligand whereas the latter two do not.

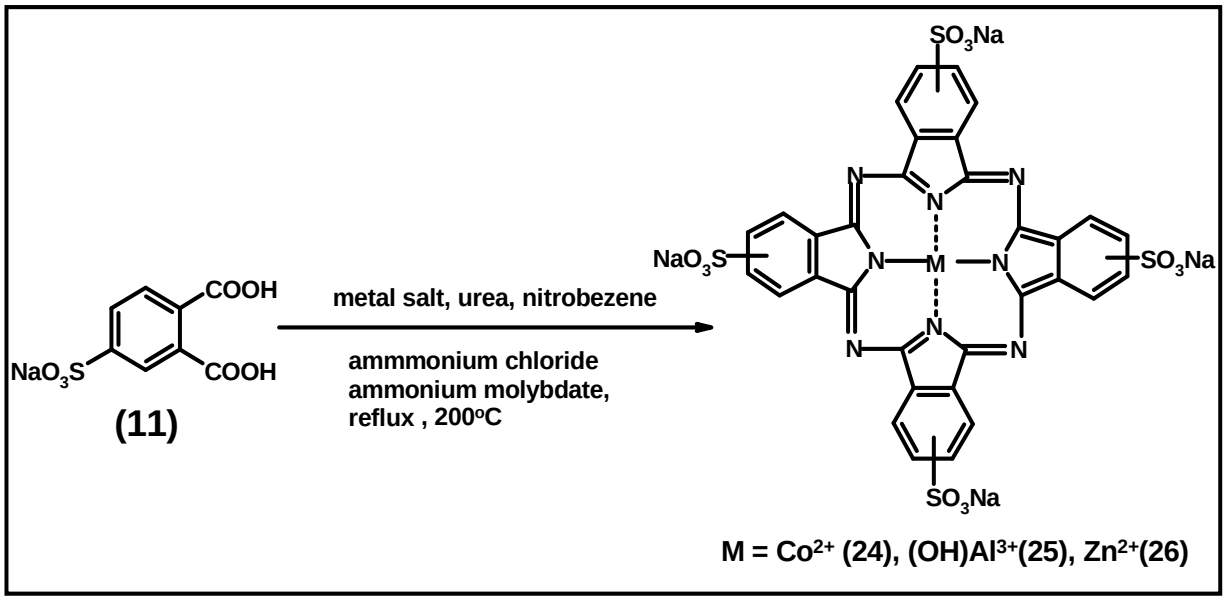

Scheme 3.1: Synthetic route for tetra sodium salt of Co^{2+}, $(OH)Al^{3+}$ and Zn^{2+} tetrasulphophthalocyanine ($MPcS_4$)

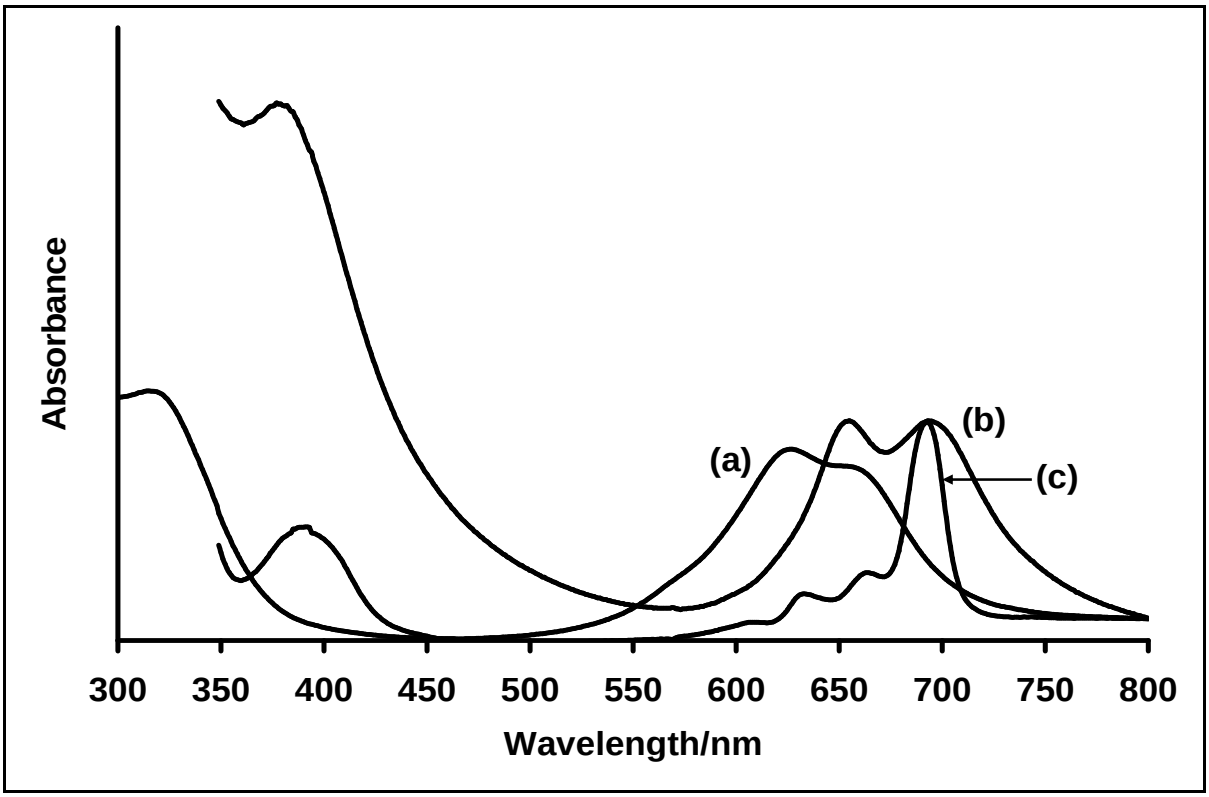

Figure 3.1: Electronic spectra of (a) $CoPcS_4$ (**24**), (b) $ZnPcS_4$ (**26**) and (c) $AlPcS_4$ (**25**) in water.

The synthesis and purification of the mixed sulphonated MPcs were carried out using an established procedure from literature,[79] Scheme 3.2. Appreciable yields (11-16%) of the complexes were obtained and were characterised using UV-Vis and IR spectra. Furthermore, HPLC analyses were carried out in order to know the extent of sulphonation in the complexes. The sulphonation process is not reproducible and therefore the fraction composition will vary from one experiment to the other even using the same MPc complex and that is why HPLC analysis is essential.

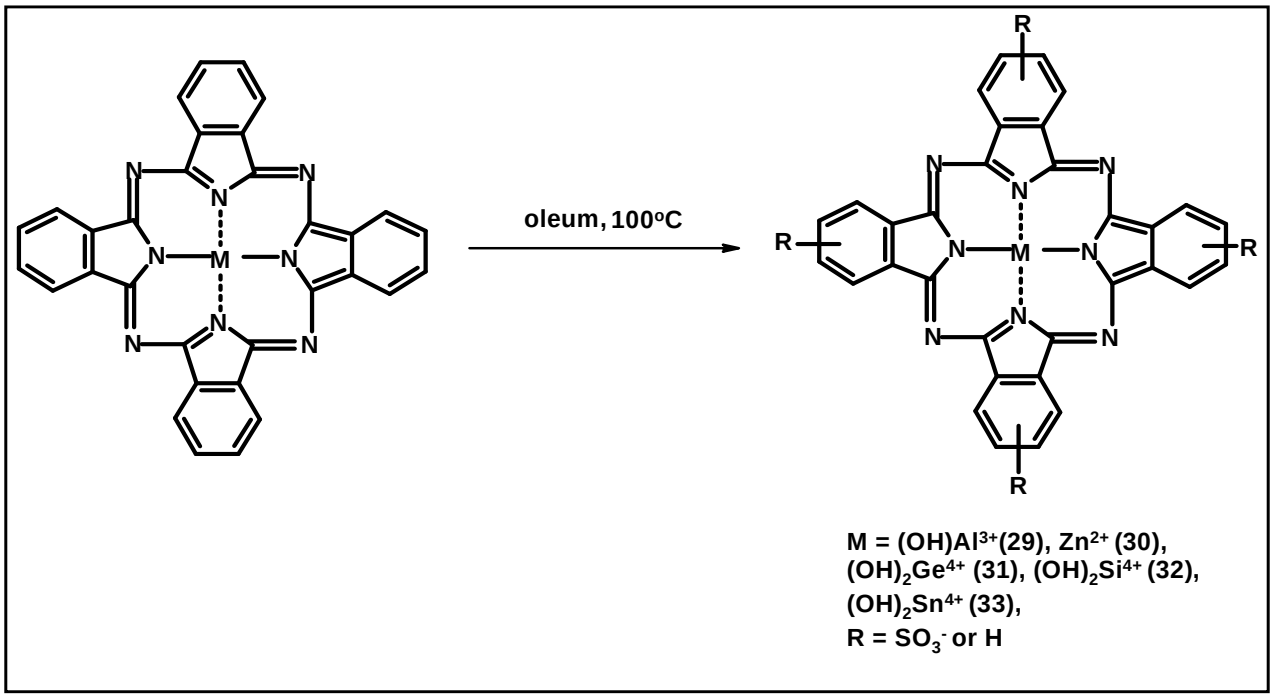

Scheme 3.2: Synthetic route for the mixed sulphonated MPcs[79]

Figure 3.2 showed the spectra of the $MPcS_{mix}$ in water; with the exception of $AlPcS_{mix}$(**29**), all other complexes showed either broadened or split Q band characteristic of aggregation behaviour. It has been shown in our laboratory[377] that these observations for $GePcS_{mix}$ (**31**) and $SiPcS_{mix}$ (**32**) (Figure 3.2a) were not due to aggregation but

probably due to the presence of unsymmetrical species while for $ZnPcS_{mix}$ (**30**) and $SiPcS_{mix}$ (**32**), they were due to aggregation as proven by the addition of Triton X-100 to the PBS 7.4 solutions of the complexes which resulted to lack of change in the intensities of the spectra of the former, $AlPcS_{mix}$ (**29**), $GePcS_{mix}$ (**31**), $SiPcS_{mix}$ (**32**) but for the latter, {$ZnPcS_{mix}$ (**30**) and $SnPcS_{mix}$ (**33**)} considerable increase in intensities of the low energy side of the Q bands were observed.

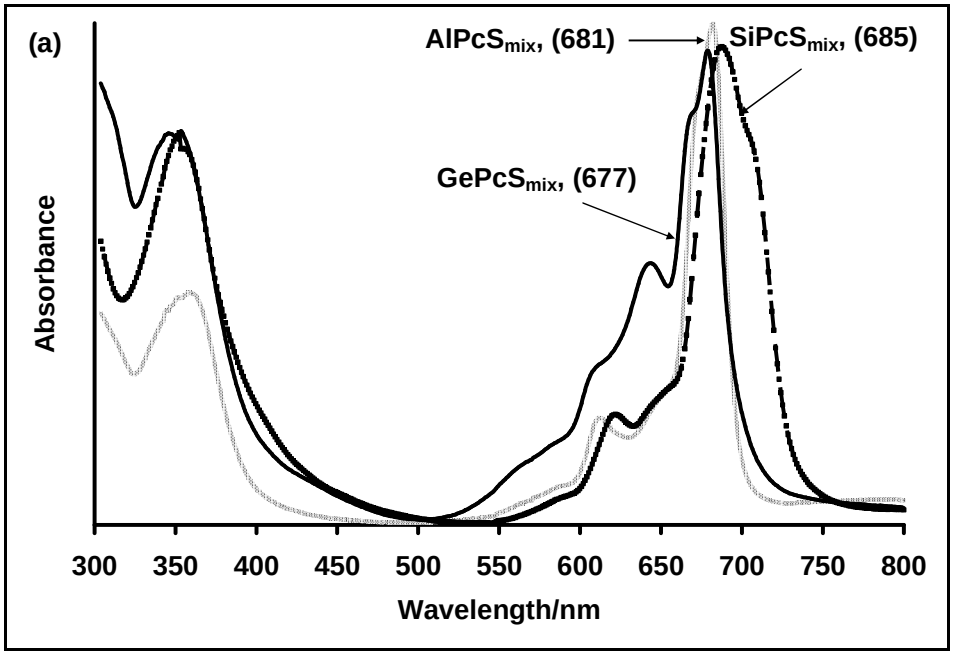

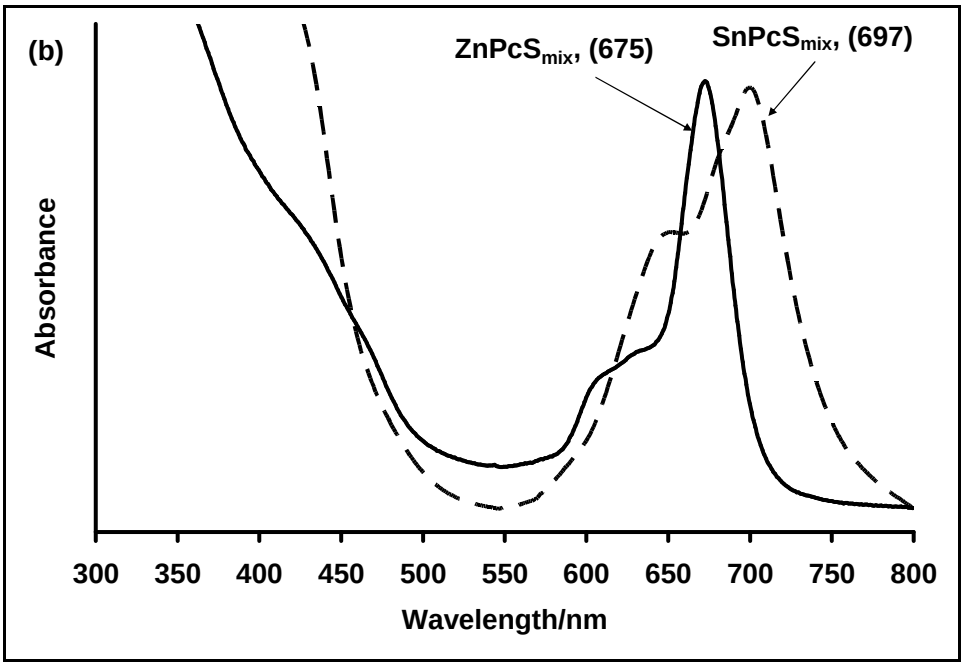

Figure 3.2: Electronic spectra of the $MPcS_{mix}$ in water, (a) $AlPcS_{mix}$ (**29**), $GePcS_{mix}$ (**31**), $SiPcS_{mix}$ (**32**) and (b) $ZnPcS_{mix}$ (**30**), $SnPcS_{mix}$ (**33**).

The characteristics bands of the S=O vibrations appeared for all the $MPcS_{mix}$ complexes in the 1030-1050 cm^{-1} region. While with the exception of $ZnPcS_{mix}$ (**30**), the O-H and weak M-O vibrations due to the OH axial ligands were observed respectively in the 3100-3300 cm^{-1} and 700-800 cm^{-1} regions.

The extent of sulphonation for each of the five $MPcS_{mix}$ (where M = Al, Ge, Si, Sn and Zn) complexes were obtained by HPLC. It is expected that the most highly sulphonated (most soluble) would be the first to be eluted from the chromatographic column, and so give the lowest retention time and that the monosulphonated fractions give the highest retention times. The HPLC signals with the lowest retention times (~ 1 minute) are assigned to the tetrasulphonated fractions, using the respective metal tetrasulphonated phthalocyanine as references. $AlPcS_{mix}$ (**29**), $GePcS_{mix}$ (**31**) and $SiPcS_{mix}$ (**32**) gave mainly the tetrasulphonated (Figure 3.3a) and $ZnPcS_{mix}$ (**30**) and $SnPcS_{mix}$ (**33**) (Figure 3.3b)

showed three main HPLC peaks confirming a large contribution of less sulphonated derivatives. The lack of aggregation behaviour of the former set of complexes could be due to the large fractions of the tetrasulphonated species while the aggregation behaviour of the latter maybe due to presence of large fractions of less sulphonated species. The extent of aggregation has been shown to decrease with increasing degree of sulphonation.[378]

The same $MPcS_{mix}$ batches for HPLC analyses were used for the photolysis studies to be discussed in Chapter 4.

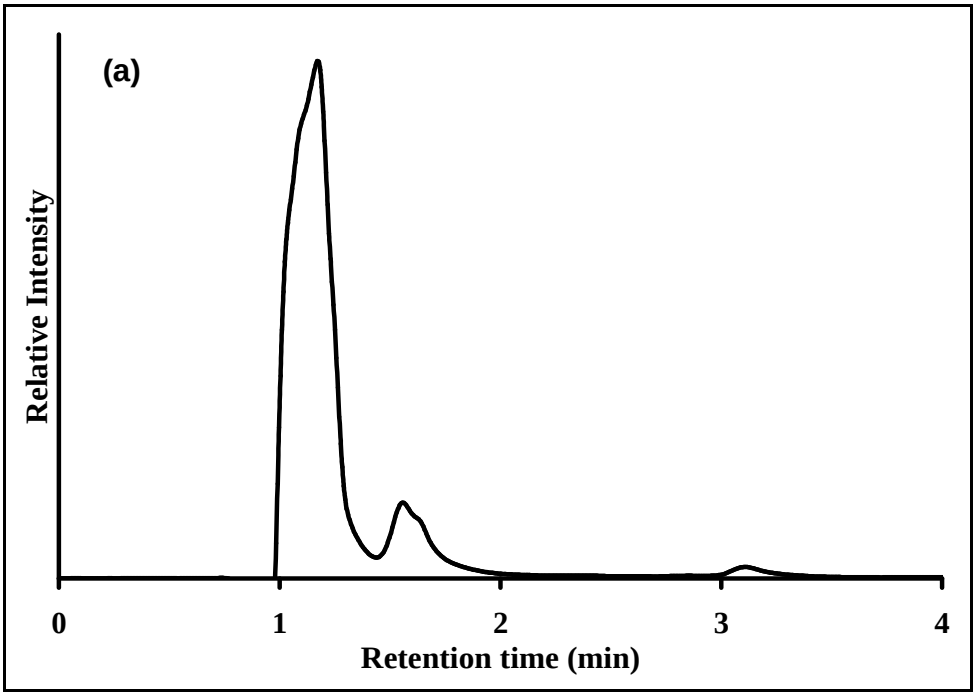

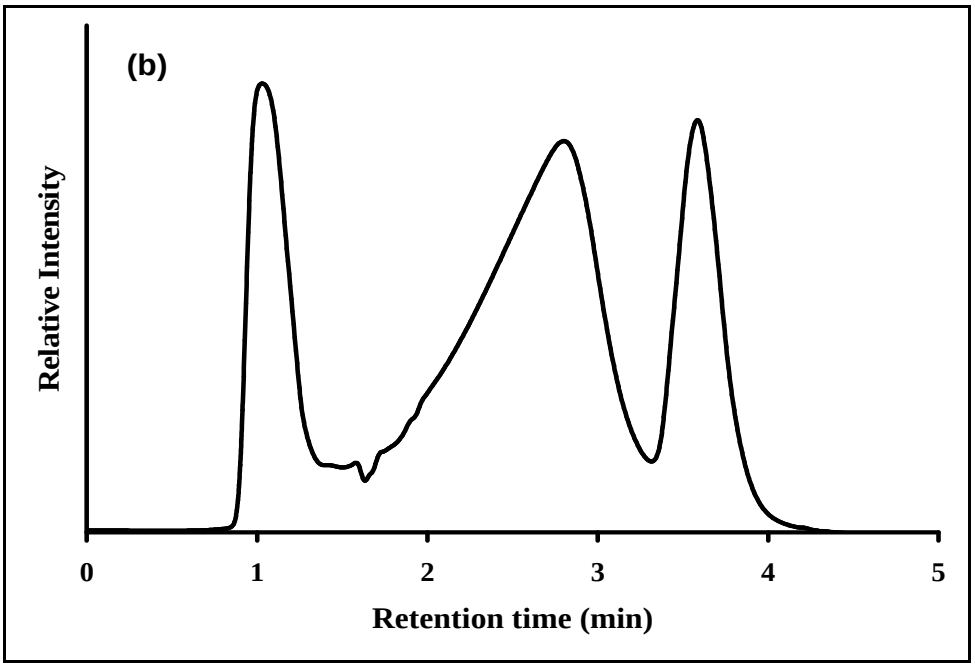

Figure 3.3: HPLC traces for (a) $GePcS_{mix}$ (**31**) and (b) $ZnPcS_{mix}$ (**30**)

3.1.1.2 Carboxyl MPcs

Synthesis of the MOCPcs were carried out using established methods from literature.[77,78] (Scheme 3.3). Generally, very low yields of the complexes were obtained.

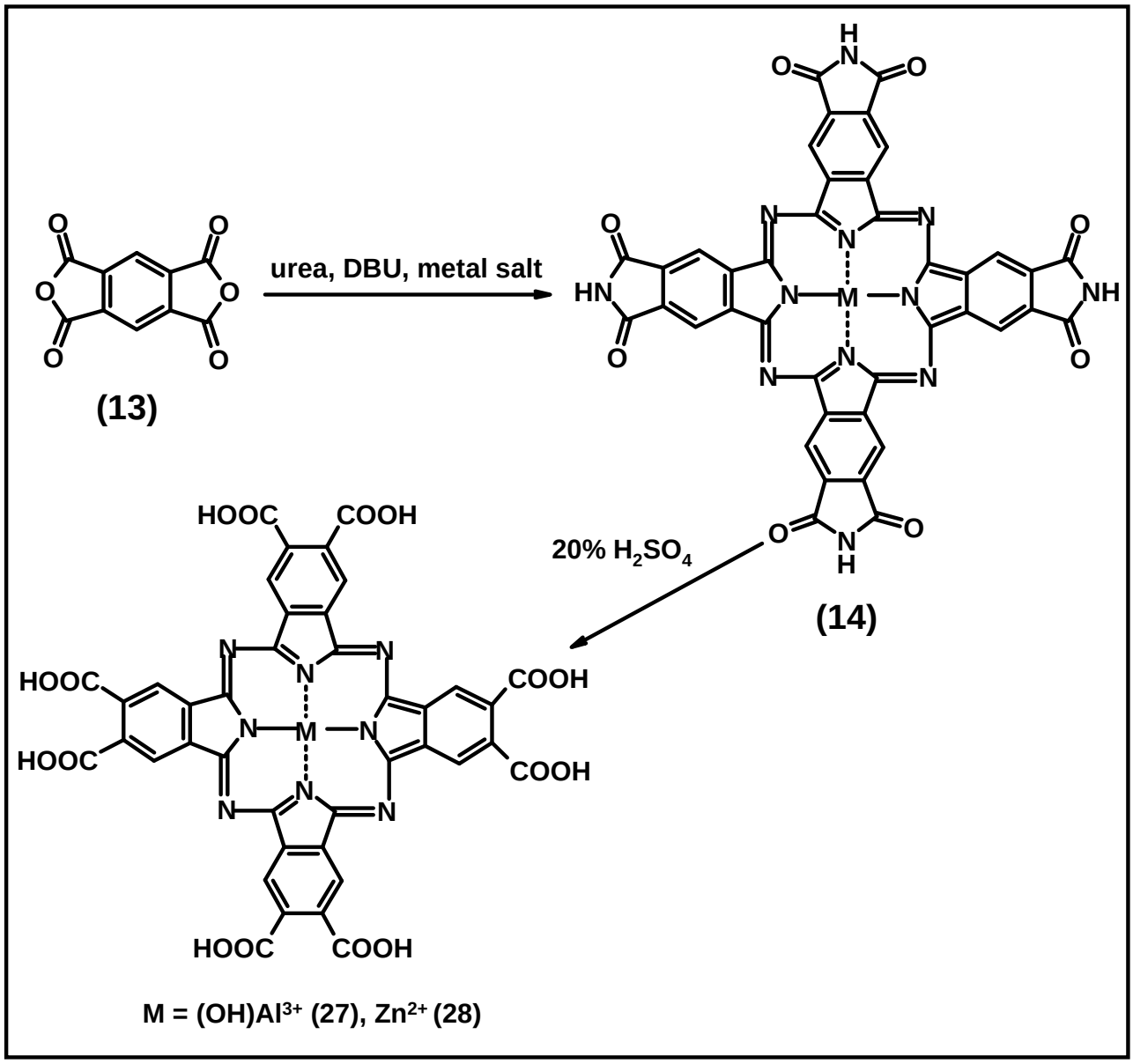

Scheme 3.3: Synthetic route for water-soluble $(OH)Al^{3+}$, Zn^{2+} octacarboxy-metallophthalocyanine, (MOCPc)[77,78]

Figure 3.4 shows the electronic spectra of AlOCPc (**27**) and ZnOCPc (**28**). Both complexes exhibited monomeric behaviour in phosphate buffer pH 10 as evidenced by the sharp Q band and no aggregated Q band.

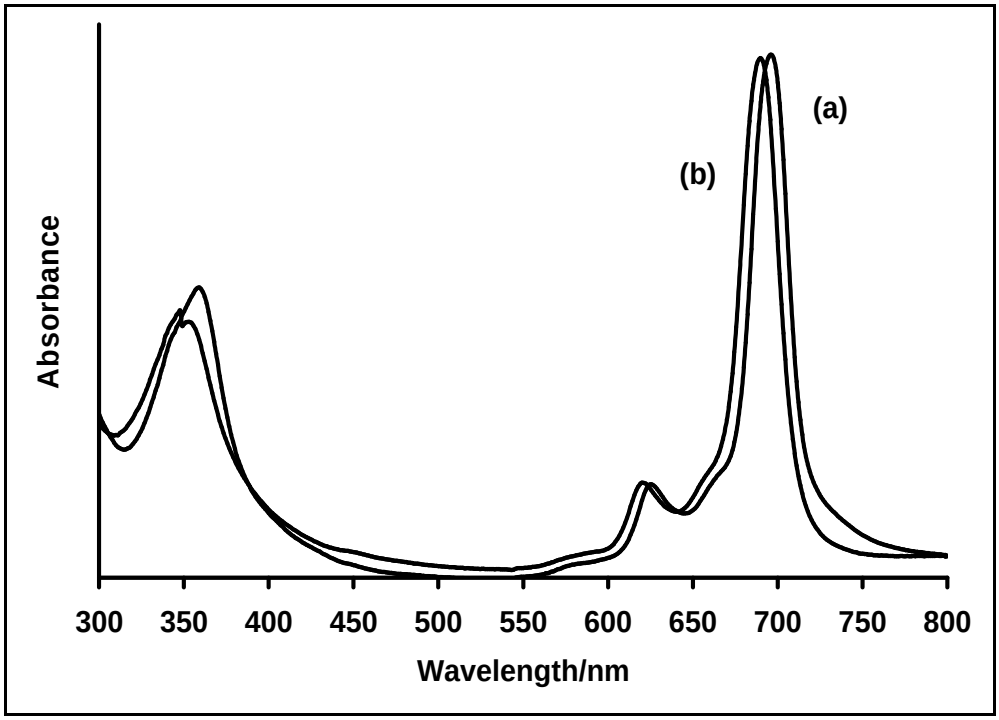

Figure 3.4: Electronic spectra of (a) AlOCPc (**27**) and (b) ZnOCPc (**28**) in phosphate buffer pH 10.

The FTIR data of both AlOCPc (**27**) and ZnOCPc (**28**) complexes showed characteristics bands of the complexes. Characteristic bands such as the O-H, C=O and C-O appeared at 3418, 1705 and 1191 cm^{-1} respectively for the former while for the latter they appeared at 3421, 1702 and 1184 cm^{-1}.

3.1.2 Thiol-derivatised MPcs

3.1.2.1 4-Nitro phthalonitrile (46), Scheme 3.4

The synthetic procedure is in three steps as shown in Scheme 3.4. High yields and satisfactory IR and NMR data were obtained for all the compounds. The ^{1}H NMR data for compounds (**44**), (**45**) and (**46**) gave expected number of protons (details in the

experimental section) indicating the purity of these compounds. The conversion of compound (**5**) to (**44**) was evidenced by the appearance of IR NO_2 bands at 1535 and 1354 cm^{-1} corresponding to assymetrical and symetrical NO_2 stretch. For the conversion of compound (**44**) to (**45**), the dissappearance of 1717 cm^{-1} (s) (CO-NH-CO) and appearance of 3346 cm^{-1} (NH_2 str), 1685 cm^{-1} (s) (C=O str), 1620 cm^{-1} (vs) (NH_2 def) confirmed the formation of compound (**45**). The synthesis of 4-nitro phthalonitrile (**46**) was comfirmed by the sharp and intense IR band at 2230 cm^{-1} corresponding to (C≡N) and others bands such as 545 cm^{-1} (vs) (NO_2 assym.), 1355 cm^{-1} (vs) (NO_2 sym.).

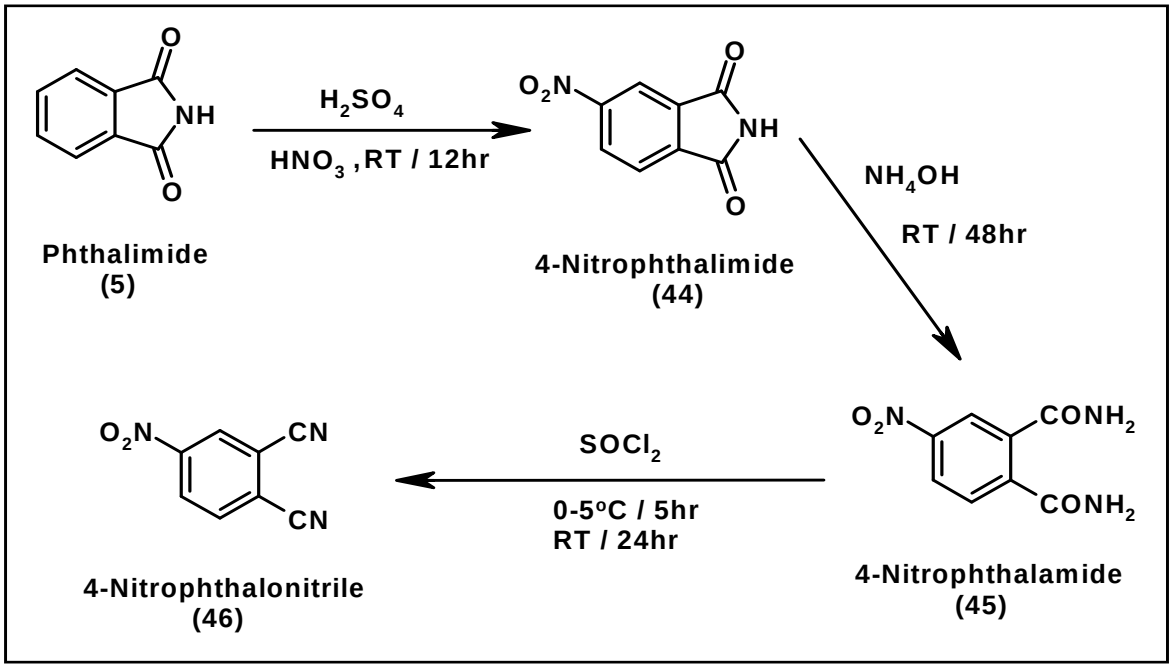

Scheme 3.4: Synthetic route for 4-nitro phthalonitrile[81]

3.1.2.2 Monosubstituted thiol-derivatised phthalonitrile

The syntheses of 4-(benzylmercapto) phthalonitrile (**47**) or 4-(dodecylthiol) phthalonitrile (**48**) were achieved by base (K_2CO_3) catalysed nucleophilic substitution of nitro groups in (**46**) using benzylmercapto or dodecylthiol respectively, Scheme 3.5. The substitution was performed in DMSO at room temperature in an inert nitrogen atmosphere. Satisfactory yields were obtained for the synthesis of compounds **47** and **48**.

The CN band in the IR spectrum of **47** was observed at 2231 cm^{-1} and at 2228 cm^{-1} for **48**. The protons in the ^{1}H-NMR spectrum of the phenyl substituent for **47** appeared as a multiplet integrating for 5 between 7.28 and 7.38 ppm, benzyl protons were observed between 7.47 and 7.65 ppm, the CH_2 protons at 4.30 ppm. For complex **48**, the CH_3 protons were observed at 0.85 ppm, the CH_2 protons between 1.25 and 3.00 ppm, and the benzyl protons between 7.45 and 7.63 ppm.

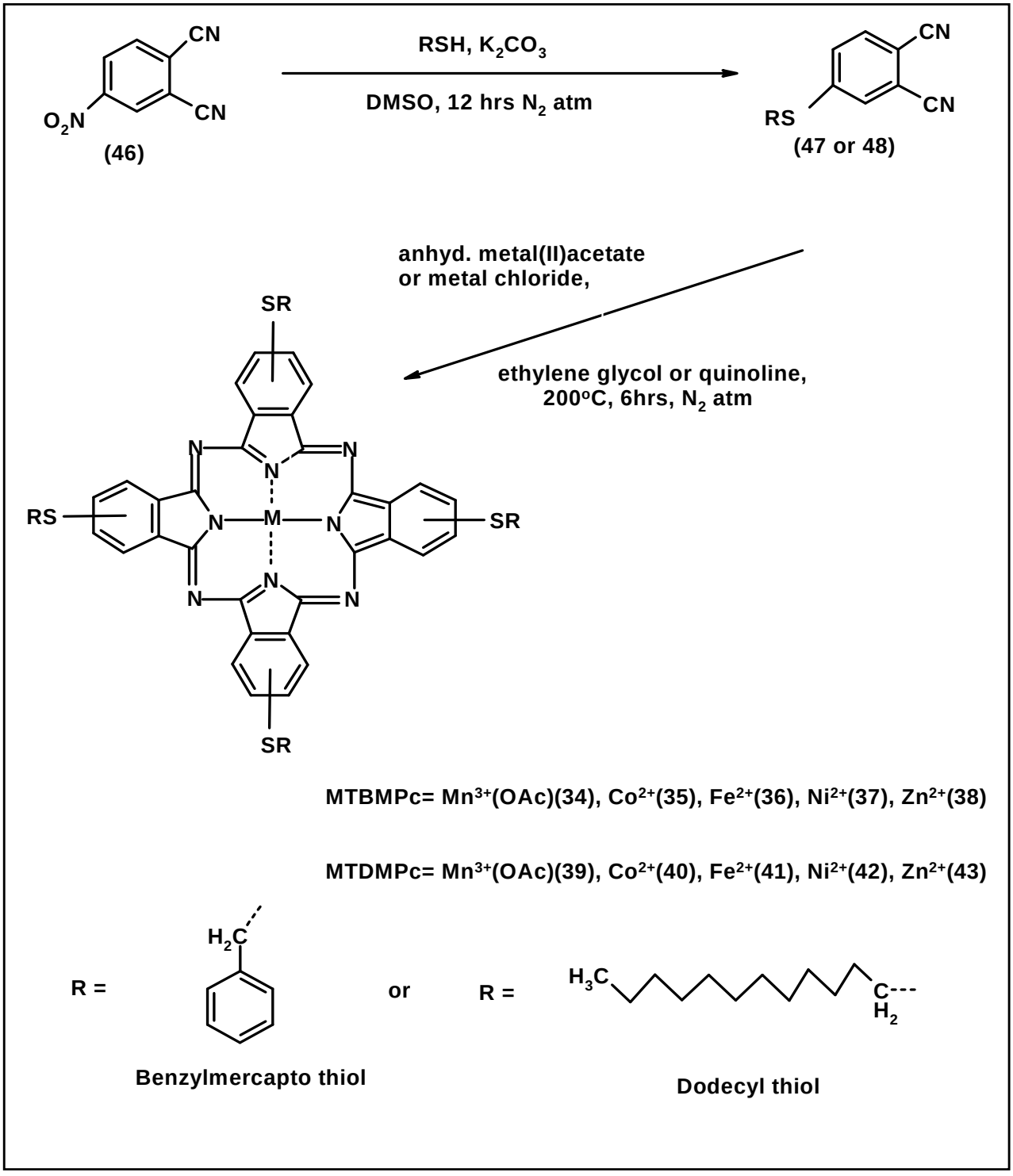

Scheme 3.5: Synthetic route for MTBMPc and MTDMPc complexes.[81]

3.1.2.3 Thiol-derivatised MPcs (Scheme 3.5)

Peripherally substituted tetrakis (benzylmercapto) or (dodecylthiol) phthalocyanines containing different central metals (Zn, Co, Fe, Ni, and Mn) were synthesised by cyclotetramerisation of 4-(benzyl mercapto) phthalonitrile (**47**) or 4-(dodecylthiol) phthalonitrile (**48**) in the presence of the required metal salts. Quinoline was used as the solvent for Fe (**36** and **41**), Ni (**37** and **42**) and Zn (**38** and **43**) phthalocyanine complexes while ethylene glycol was used as the solvent for synthesis of CoPc (**35** and **40**) and MnPc (**34** and **39**) derivatives.

All the metallophthalocyanine complexes were found to be soluble in less polar solvents such as DCM and chloroform while only the benzylmercapto substituted phthalocyanines (**34-38**) dissolved in the more polar solvents such as DMSO and DMF. The non-solubility of the (dodecylthiol) phthalocyanines in DMSO and DMF is not surprising; it is due to the presence of the highly non-polar long dodecylthiol alkyl chain.

The MPc complexes were characterised by several methods including UV-VIS, IR and ^{1}H NMR spectroscopies, and by MALDI-TOF mass spectroscopy and elemental analyses. Both MALDI-TOF and elemental analyses gave expected results as shown in the experimental section. For the MnPcs, IR bands at 865 cm^{-1} and 857 cm^{-1} correspond to the bond between Mn^{3+} and O atom of the acetate ion (Mn^{3+}─$OCOCH_3$) of complexes **34** and **39** respectively, while both complexes showed the C=O bands of the acetate ion at 1743 cm^{-1} and 1765 cm^{-1} respectively. Only the ZnPc derivatives were employed for ^{1}H-NMR analysis since the central metal is diamagnetic. Both complexes **38** and **43** exhibited broad peaks in the ^{1}H-NMR spectra probably due to the aggregation occurring at the high concentrations used.[379] The signals due to the Pc ring were observed from 7.60

to 7.95 ppm and integrated for a total of 12 protons for complex **38**, and for complex **43** the Pc ring protons were observed from 6.50 to 7.80 ppm. Hence the protons were more deshielded for complex **38** due to the presence of the phenyl ring. The protons due to the phenyl substituents for complex **38** integrated correctly and were observed at 7.30-7.60 ppm. For complex **43** the protons of the ring substituents integrated correctly.

The UV-Vis spectral Q band peak positions bands are listed in Table 3.1 in DCM. From the values of Q bands for the complexes in DCM, all the MTDMPc complexes with the long alkyl chain dodecylthiol ring substituent (**39-43**) exhibited red shift in Q band relative to their respective MTBMPc (**34-38**) counterparts. This observation may be due to the effect of the electron donating ability of the Pc ring substituent; dodecyl thiol group may have more electron donating ability than the benzyl mercapto group.

MnPcs

The MnPc complexes are deep red in colour due to absorption in the 400 to 500 nm region and the red shift of the Q band, typical of Mn^{3+}Pc complexes,[101,216,380,381] Figure 3.5. The UV-Vis bands at 452 and 526 nm for MnTBMPc, **34** and at 450 and 528 nm for MnTDMPc, **39** are charge transfer bands between metal and ligand. MALDI-TOF spectra showed the complexes without the acetate residue though the reason could not be ascertained but similar observation has been reported before.[381] However, elemental analysis of both complexes gave satisfactory results corresponding to the Mn(OAc)Pcs.

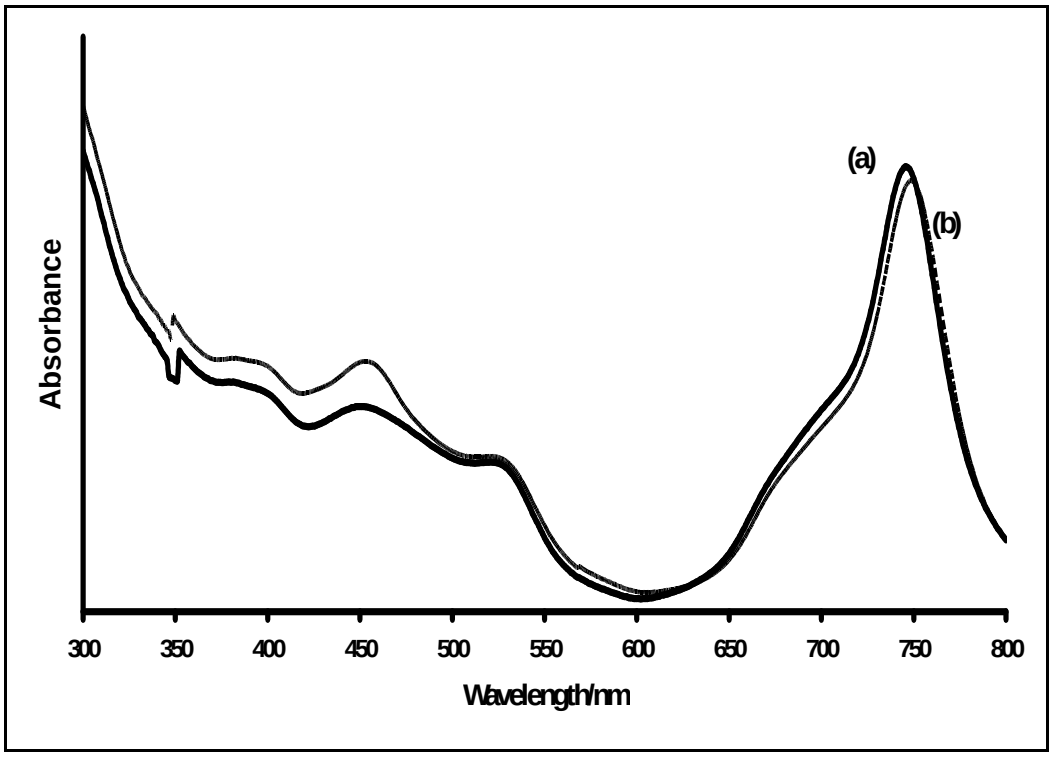

Figure 3.5: The UV-Visible spectra of (a) MnTBMPc (**34**) and (b) MnTDMPc (**39**) in DCM.

CoPcs

The spectra of CoPc complexes (**35** and **40**) are typical of monomeric species, Figure 3.6. The Q bands were observed at 676 and 684 nm for complexes **35** and **40** respectively in DCM. Both complexes obeyed Beer's Law behaviour at concentrations less than 1 x 10^{-5} M.

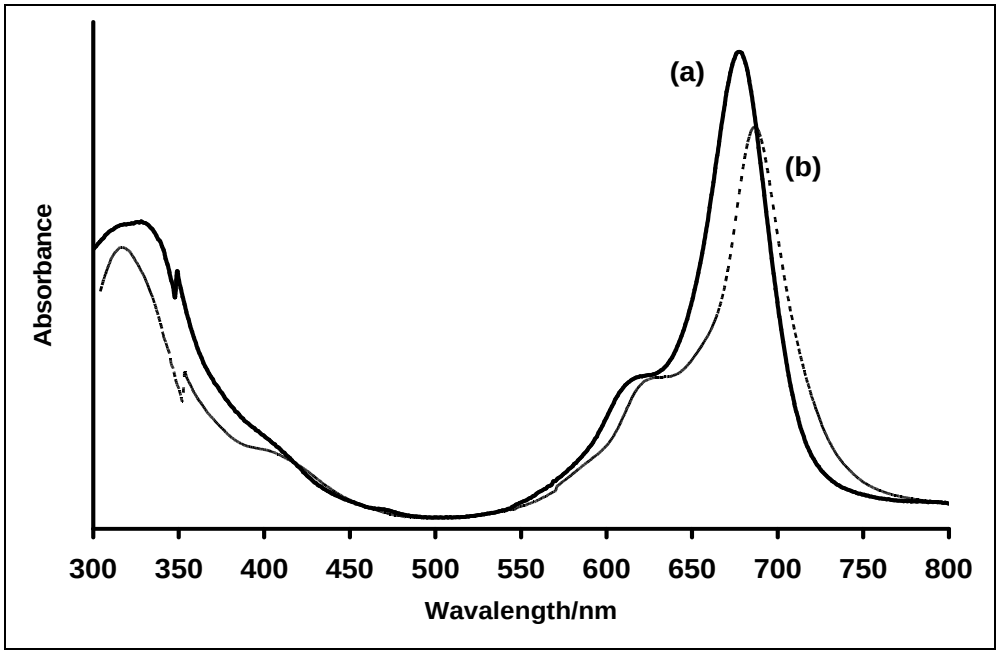

Figure 3.6: The UV-Visible spectra of (a) CoTBMPc (**35**) and (b) CoTDMPc (**40**) in DCM.

FePcs

For complex **36** the main absorption bands were observed at 675 and 705 nm in DCM, and for complex **41** the absorption band was at 712 nm in DCM, Figure 3.7. Aggregation in MPc complexes is typified by a broadened or split Q band, with the high energy band being due to the aggregate and the low energy band due to the monomer.[101] Complex **36** showed a split Q band in DCM while complex **41** Q band is broadened; both complexes can be said to be aggregated in DCM but there is more aggregation in complex **36** than in complex **41**, showing that the benzyl group on the former might increase aggregation due to possible π-π interactions between the neighboring Pcs.

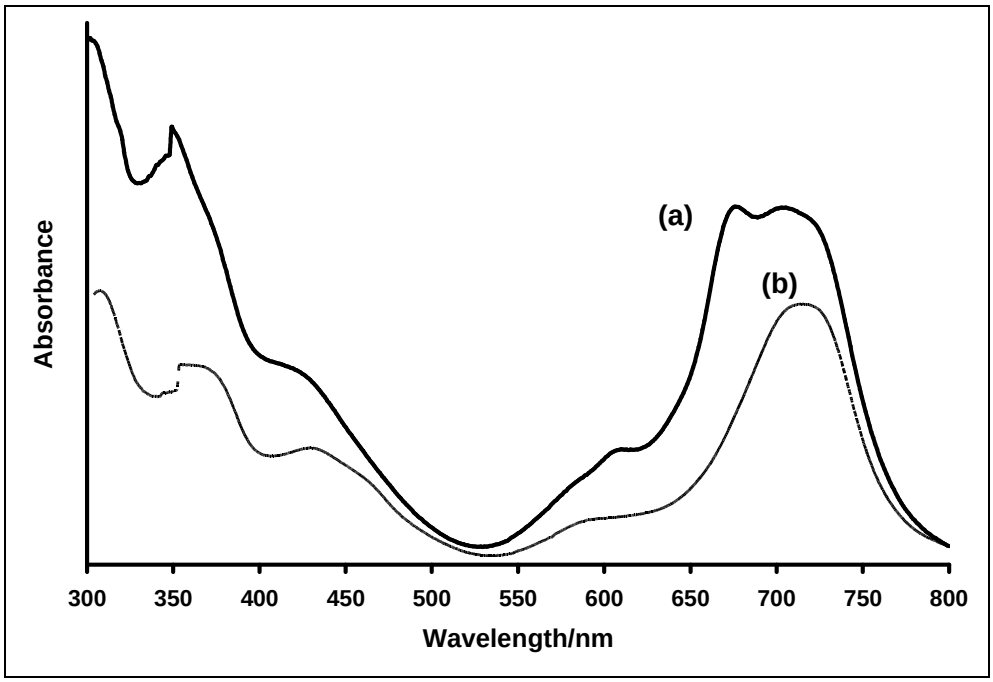

Figure 3.7: The UV-Visible spectra of (a) FeTBMPc (**36**) and (b) FeTDMPc (**41**) in DCM.

Figure 3.8 shows the UV-Vis spectra of complex **36** in DMF. The complex exhibited spectra typical of stacked monomer in FePc complexes,[44] which is normally observed near 630 nm. This suggests that the Q band observed for the complexes at 630 nm is due to the stacked monomer. Aggregation was evident even at concentrations as low as 3 x 10^{-6} M. Figure 3.8 also shows the effect of decreasing concentration on the spectra of complexes **36**. As the concentration was lowered for **36**, the peak due to the aggregate at 638 nm decreased at a faster rate compared to the monomer peak at 725 nm. These observations confirm that complex **36** is aggregated at high concentrations. Beer's law was not obeyed at concentration greater than 1.2 x 10^{-5} M.

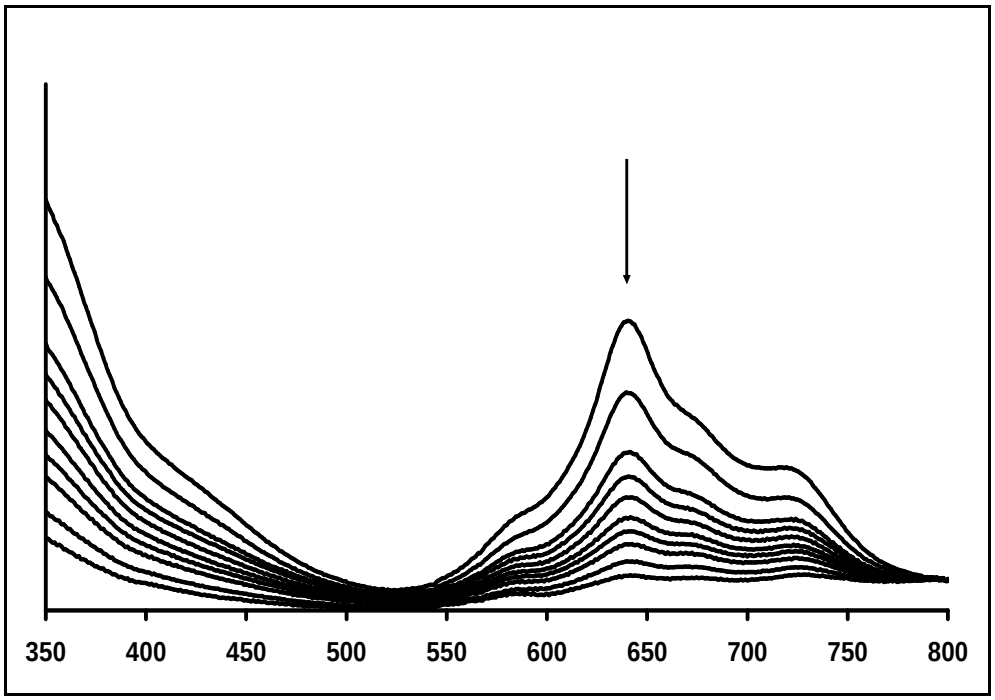

Figure 3.8: UV-VIS spectral changes observed for complex (**36**) in DMF as concentration is decreased. Starting concentration = 1.5 x 10^{-5} M.

NiPcs

UV/Vis spectra in Figure 3.9 shows considerable aggregation for both complexes as judged by split Q bands. NiTBMPc (**37**) showed more aggregation than NiTDMPc (**42**) at the same concentration as was the case for the FePc derivatives, in that the band due to the aggregated species at high energy was more pronounced than the band due to the monomeric species. For NiTDMPc (**42**), the band at low energy due to the monomeric species was more pronounced than the high energy band. The difference in the extent of aggregation maybe partly due to the influence of ring substituents, the former has benzylmercapto as the substituent, which can increase the π-π interaction of the molecules and thereby increasing aggregation as explained above.

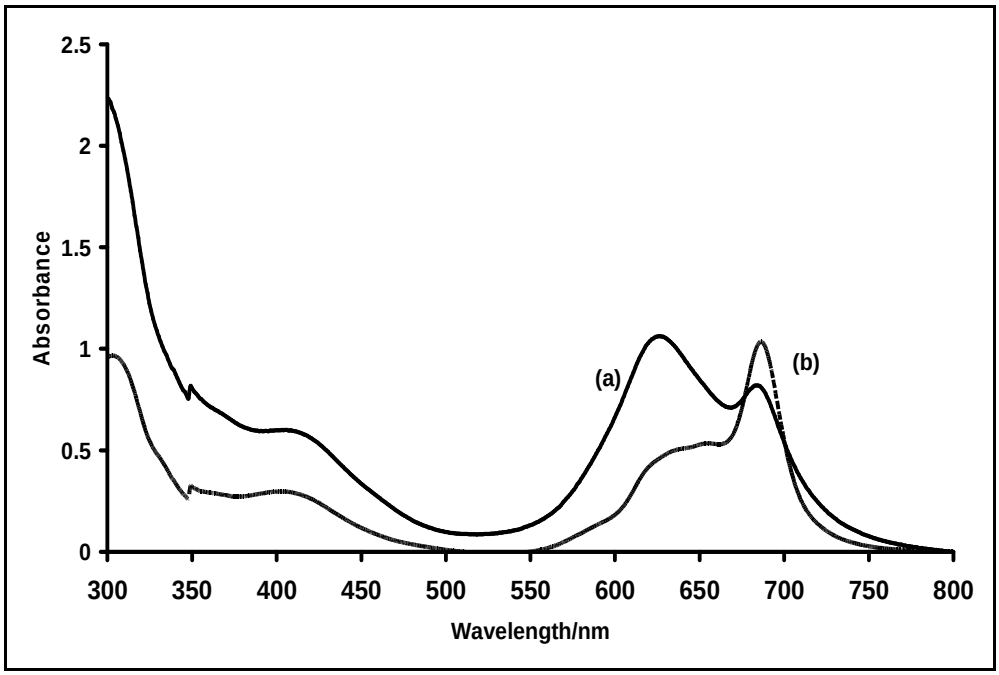

Figure 3.9: The UV-Visible spectra of (a) NiTBMPc (**37**) and (b) NiTDMPc (**42**) in DCM.

Figures 3.10 and 3.11 respectively show the effect of decreasing concentrations from 1.5 x 10^{-5} to 0.3 x 10^{-5} M on the UV-Vis spectra of NiTBMPc (**37**) and NiTDMPc (**42**) in the Q band region. The former has two Q bands at 625 and 681 nm, while the latter has a broad Q band at ~ 632 nm and a sharp Q band at 685 nm. As the concentrations of the complexes are decreased, the Q bands at relatively lower wavelengths (due to the aggregated species) became less pronounced compared to the lower energies (due to the monomer species), confirming the aggregated nature of the complexes.

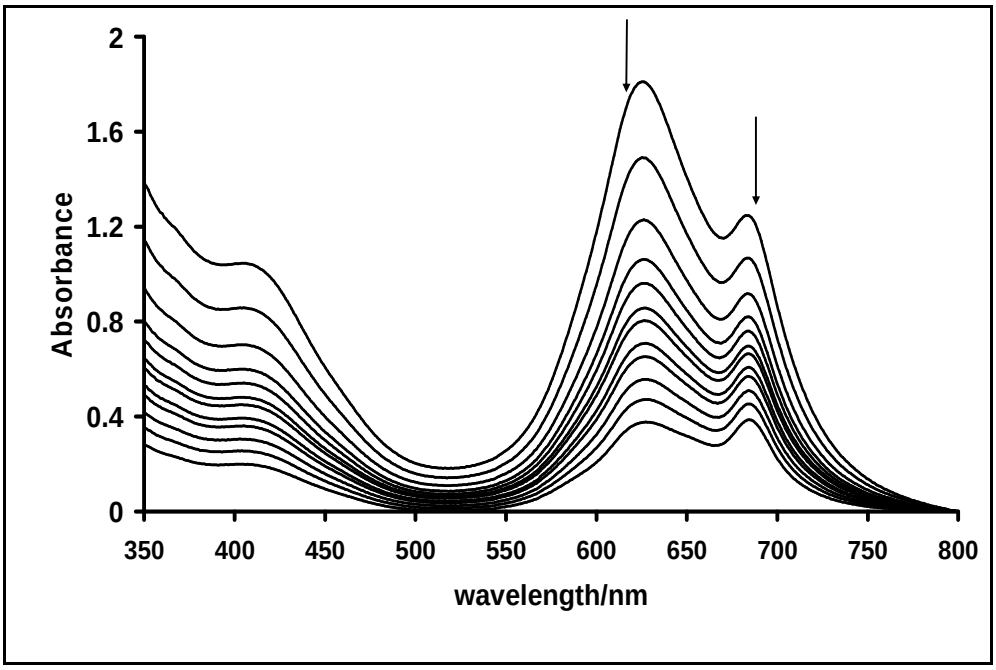

Figure 3.10: The UV-Visible spectral changes on dilution of NiTBMPc (**37**) in DCM.

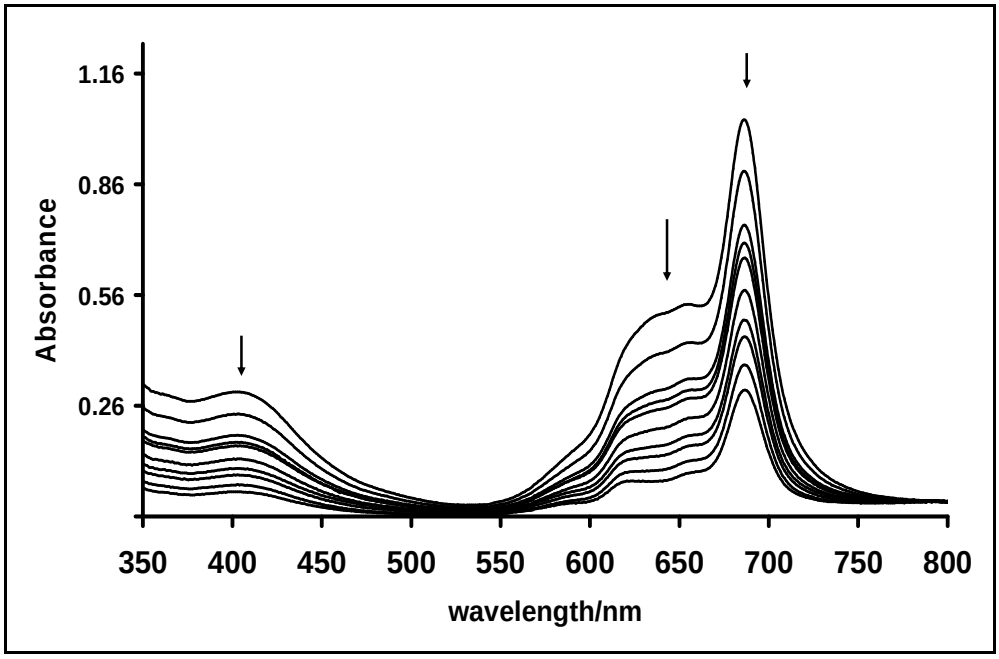

Figure 3.11: The UV-Visible spectral changes on dilution of NiTDMPc (**42**) in DCM.

ZnPcs

The spectra of Zn (**38** and **43**) phthalocyanine complexes are typical of monomeric species, Figure 3.12. The Q bands for complexes **38** and **43** were observed at 689 and 691 nm, respectively in DCM. Both complexes exhibited Beer's Law behaviour at concentrations less than 1 x 10^{-5} M.

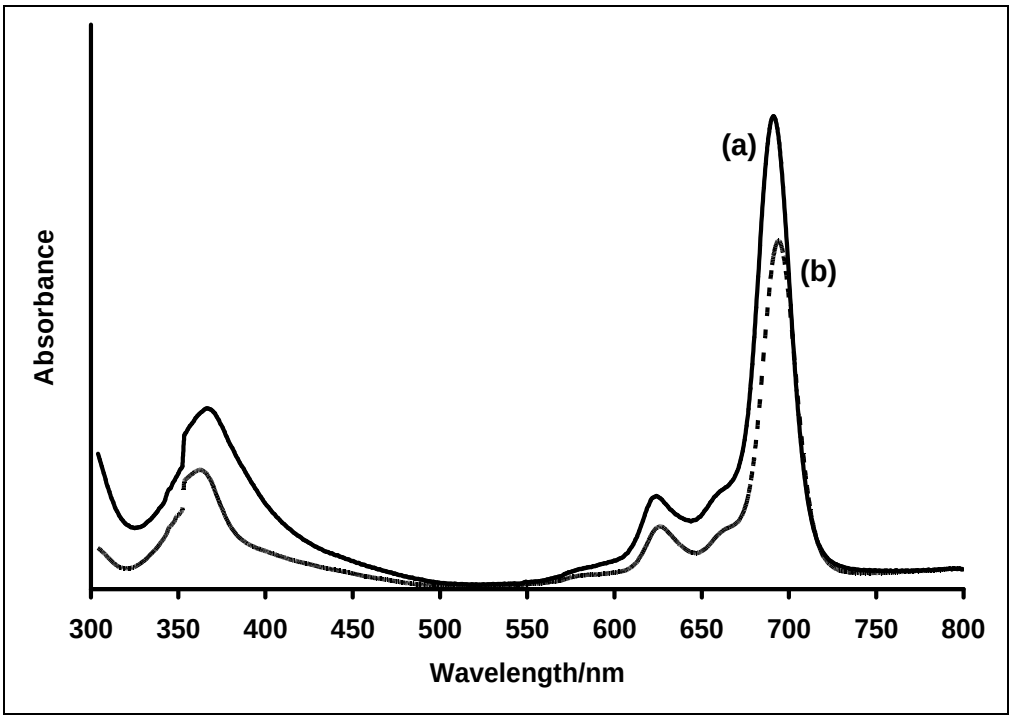

Figure 3.12: The UV-Visible spectra of (a) ZnTBMPc (**38**) and (b) ZnTDMPc (**43**) in DCM.

The differences in the aggregation behaviour of the complexes from one metal derivative to the other can be explained in terms of the central metal effects; the aggregation behaviour of both FePc and NiPc derivatives can be attributed to the former FePcs μ-oxo formation which could encourage interactions between neighboring molecules and the latter which has Ni atom in the 'in plane of the Pc ring' position thereby enabling neighboring Pc rings to interact more effectively. Less aggregation in ZnPc has been attributed[382,383] to Zn atom 'out of plane'

position in the Pc ring; this could also be the case for the monomeric behaviour of the ZnPc derivatives. The non-aggregation behaviour of the MnPc derivatives can be attributed to the presence of acetate axial ligand which can prevent aggregation from occurring.

3.2 Electrochemical characterisation of thiol derivatised MPcs

The solution redox properties of the complexes were studied using cyclic (CV) and square wave voltammetry (SWV) in DCM and DMF (DCM only for the MTDMPc complexes). The potential values and assignments are summarised in Table 3.2 a-d.

Table 3.2a: Summary of redox potentials ($E_{1/2}$ vs. Ag|AgCl) of the CoPc and FePc complexes in DCM containing $TBABF_4$. Values in brackets are in DMF for complexes **35** and **36** which were soluble in DMF.

Complex	**$M^{3+}Pc^{-}$/ $M^{3+}Pc^{2-}$ I**	**$M^{3+}Pc^{2-}$/ $M^{2+}Pc^{2-}$ II**	**$M^{2+}Pc^{2-}$/ $M^{+}Pc^{2-}$ III**	**$M^{+}Pc^{2-}$/ $M^{+}Pc^{3-}$ IV**	**$M^{+}Pc^{3-}$ / $M^{+}Pc^{4-}$ V**	**$M^{+}Pc^{4-}$/ $M^{+}Pc^{5-}$ VI**
CoTBMPc **(35)**	0.89, (0.89)	0.42, (0.42)	-0.40, (-0.38)	-0.84, (-1.41)	-	-
CoTDMPc **(40)**	0.66	0.44	-0.46	-	-	-
FeTBMPc **(36)**	0.82, (0.70)	0.44, (0.36)	-0.24, (-0.37)	-0.62, (-0.78)	-0.85, (-1.18)	-
FeTDMPc **(41)**	1.01	0.62	-0.53	-0.84	-1.16	-1.40

Table 3.2b: Summary of redox potentials ($E_{1/2}$ vs. Ag|AgCl) of the MnPc complexes in DCM containing $TBABF_4$.

Complex	**$Mn^{2+}Pc^{2-}$ /$Mn^{2+}Pc^{3-}$**	**$Mn^{3+}Pc^{2-}$ /$Mn^{2+}Pc^{2-}$**	**$Mn^{4+}Pc^{2-}$ /$Mn^{3+}Pc^{2-}$**	**$Mn^{4+}Pc^{-}$ /$Mn^{4+}Pc^{2-}$**
MnTBMPc **(34)**	-0.84	-0.08	~ 0.9	1.12
MnTDMPc **(39)**	-0.98	-0.26	~ 0.9	1.06

Table 3.2c: Summary of redox potentials ($E_{1/2}$ vs. Ag|AgCl) of the NiPcs in DCM containing $TBABF_4$.

Complex	**$Ni^{2+}Pc^{0}$/$Ni^{2+}Pc^{-}$**	**$Ni^{2+}Pc^{-}$ /$Ni^{2+}Pc^{2-}$**	**$Ni^{2+}Pc^{2-}$ /$Ni^{+}Pc^{2-}$**	**$Ni^{+}Pc^{2-}$ /$Ni^{+}Pc^{3-}$**	**$Ni^{+}Pc^{3-}$ /$Ni^{+}Pc^{4-}$**
NiTBMPc **(37)**	0.96	0.70	-0.25	-0.94	-
NiTDMPc **(42)**	0.99	0.73	-0.18	-0.93	-1.15

Table 3.2d: Summary of redox potentials ($E_{1/2}$ vs. Ag|AgCl) of the ZnPcs in DCM containing $TBABF_4$. Values in brackets are in DMF for complex **38** which was soluble in DMF.

Complex	**$Zn^{2+}Pc^{-}$/ $Zn^{2+}Pc^{2-}$**	**$Zn^{2+}Pc^{2-}$/ $Zn^{2+}Pc^{3-}$**	**$Zn^{2+}Pc^{3-}$/ $Zn^{2+}Pc^{4-}$**
ZnTBMPc **(38)**	0.36, (0.62)	-1.04, (-0.93)	-1.49, (-1.33)
ZnTDMPc **(43)**	0.46	-1.1	-

3.2.1 CoPcs

3.2.1.1 Voltammetry

For complex **35** more resolved voltammograms were observed in DMF than in DCM. Figure 3.13 shows the CV (Figure 3.13a) and SWV (Figure 3.13b) of complex **35** in DMF containing $TBABF_4$. Complex **35** showed excellent voltammetric behaviour, with four redox processes labelled **I** ($E_{½}$ = 0.89 V vs. Ag|AgCl), **II** ($E_{½}$ = 0.42 V vs. Ag|AgCl), **III** ($E_{½}$ = -0.38 V vs. Ag|AgCl), and **IV** ($E_{½}$ = -1.41 V vs. Ag|AgCl). Based on the well known[381] electrochemical behaviour of CoPc complexes in coordinating solvents such as DMF, couples **I, II, III** and **IV** in Figure 3.13 are assigned to $Co^{3+}Pc^{-}/Co^{3+}Pc^{2-}$, $Co^{3+}Pc^{2-}/Co^{2+}Pc^{2-}$, $Co^{2+}Pc^{2-}/Co^{+}Pc^{2-}$ and $Co^{+}Pc^{2-}/Co^{+}Pc^{3-}$ respectively. The ratios of the anodic to cathodic peak currents (I_a to I_c) for couples **II**, **III** and **IV** are close to unity, suggesting reversible redox processes but for couple **I** (which is expected to be ring oxidation), the anodic peak current was more pronounced compared to cathodic current (couple I ratio of I_a to I_c (13.7 µA/10.7 µA) is 1.15); this may be partly due to the decomposition upon oxidation commonly observed for thiol-derivatised MPc complexes.[83] For all couples anodic to cathodic peak separation (ΔE) was ≥ 90 mV (ΔE = 90 mV was obtained for ferrocene standard), suggesting slow electron transfer. Plots of square root of scan rate versus current (Figure 3.13c inset) were linear, suggesting diffusion control for all couples in Figure 3.13a. The peak currents are close in values for scan rate 50 mV s^{-1} but the difference became more significant as the scan rate increased, these may be due to decomposition especially oxidation reactions typical of thiol-derivatised metallophthalocyanines.

There was no effect on the voltammograms when the potential window was narrow (-1.0 to 1.0 V), or when starting at the rest potential of zero volts.

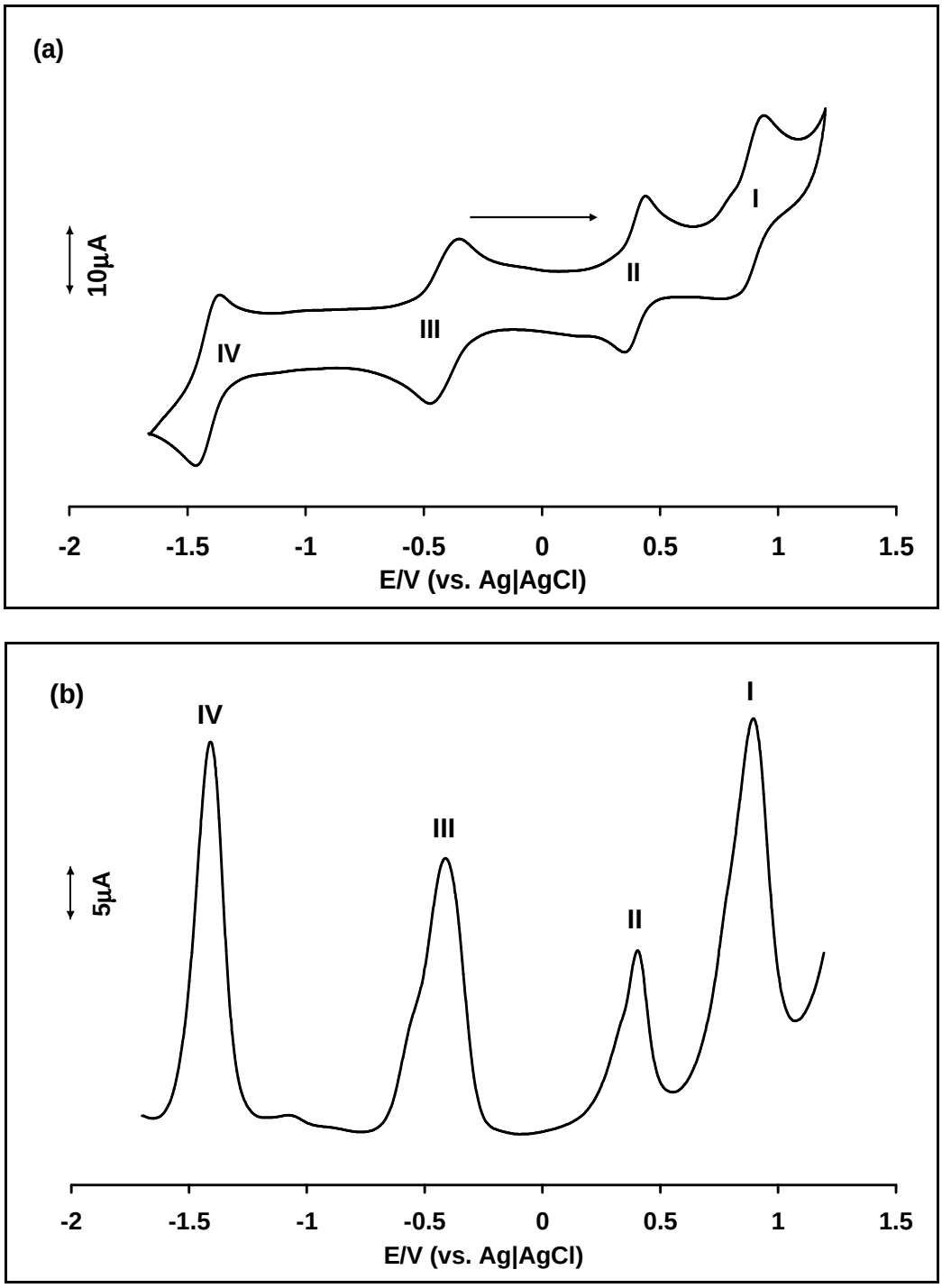
(a)
10µA
I
II
III
IV
-2
-1.5
-1
-0.5
0
0.5
1
1.5
E/V (vs. Ag|AgCl)
(b)
5µA
IV
III
II
I
-2
-1.5
-1
-0.5
0
0.5
1
1.5
E/V (vs. Ag|AgCl)

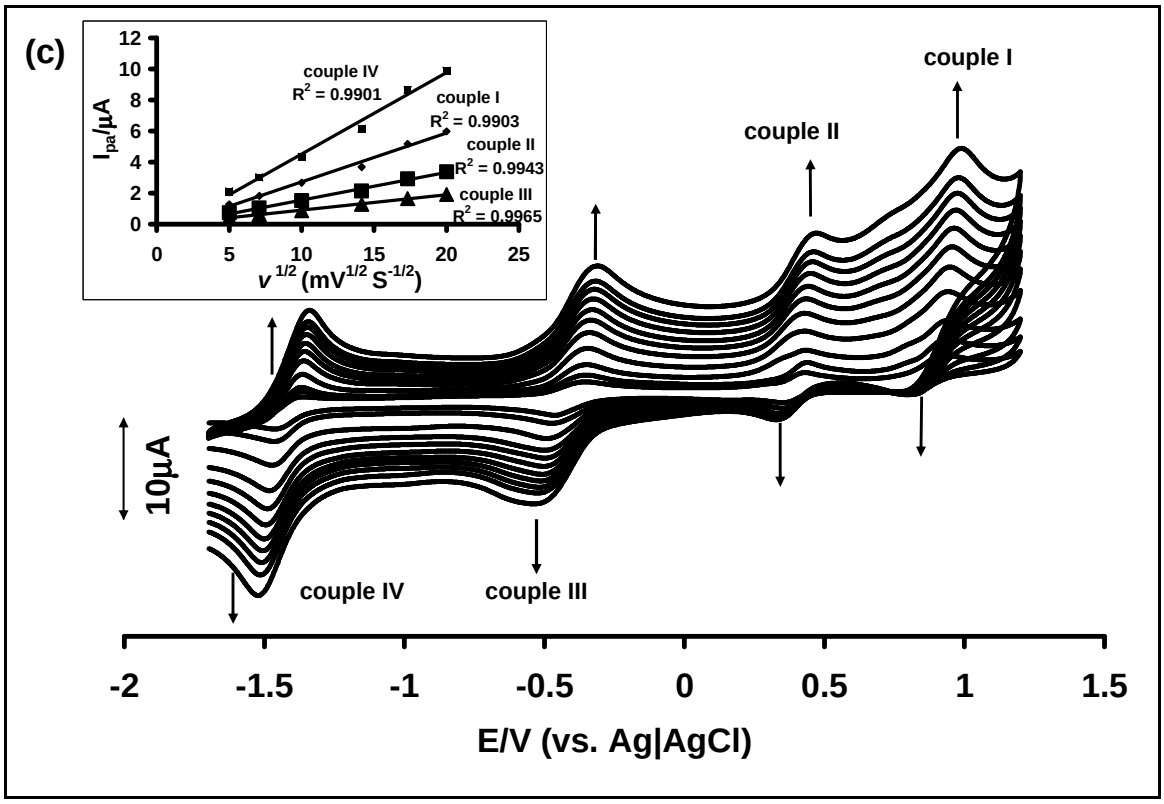

Figure 3.13: The (a) cyclic voltammogram, (b) square wave voltammogram and (c) cyclic voltammogram changes with scan rate and inset is the plot of current against square root of scan rate of complex (CoTBMPc, **35**) in DMF solution containing 0.1 M $TBABF_4$. Glassy carbon electrode used. Scan rate: 100 mV s^{-1}.

For complex **40**, three couples were observed and are assigned in Table 3.2a, and shown in Figure 3.14. The difference in the CV of **35** from that of **40** could still be due to the difference in the ring substituent. Couples **I** and **III** exhibited quasi-reversible behaviour in that ΔE was greater than 90 mV. Couple **II** however did not show a clear return peak, hence was irreversible. The couples showed diffusion control behaviour in that peak currents increased linearly with the square root of scan rate as was observed in Figure 3.14c.

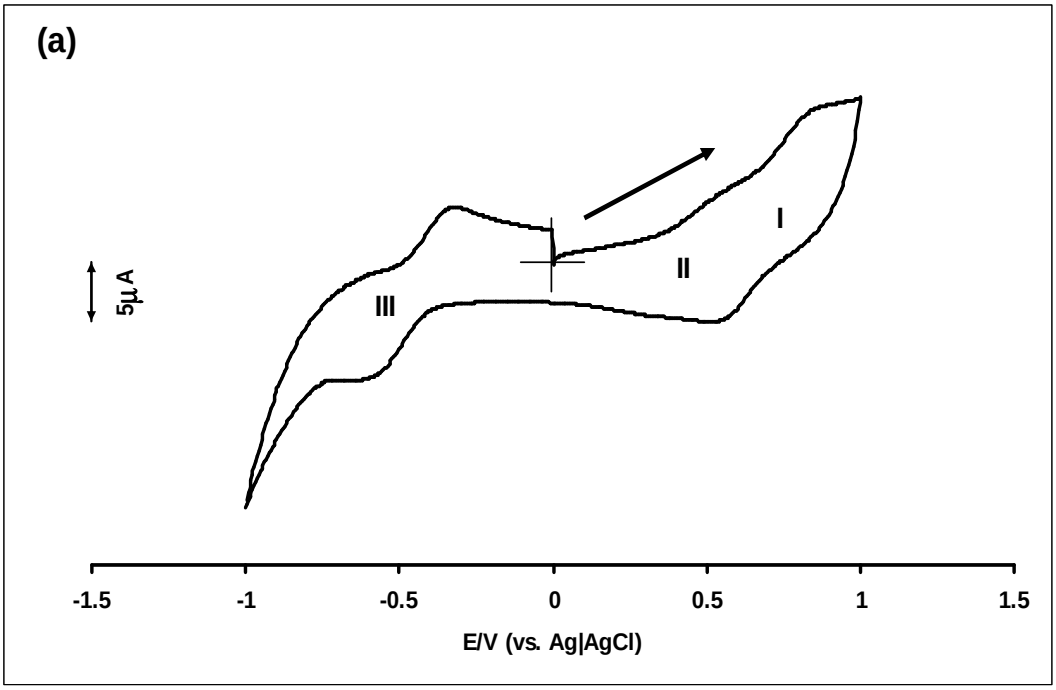
(a)
5µA
I
II
III
-1.5
-1
-0.5
0
0.5
1
1.5
E/V (vs. Ag|AgCl)

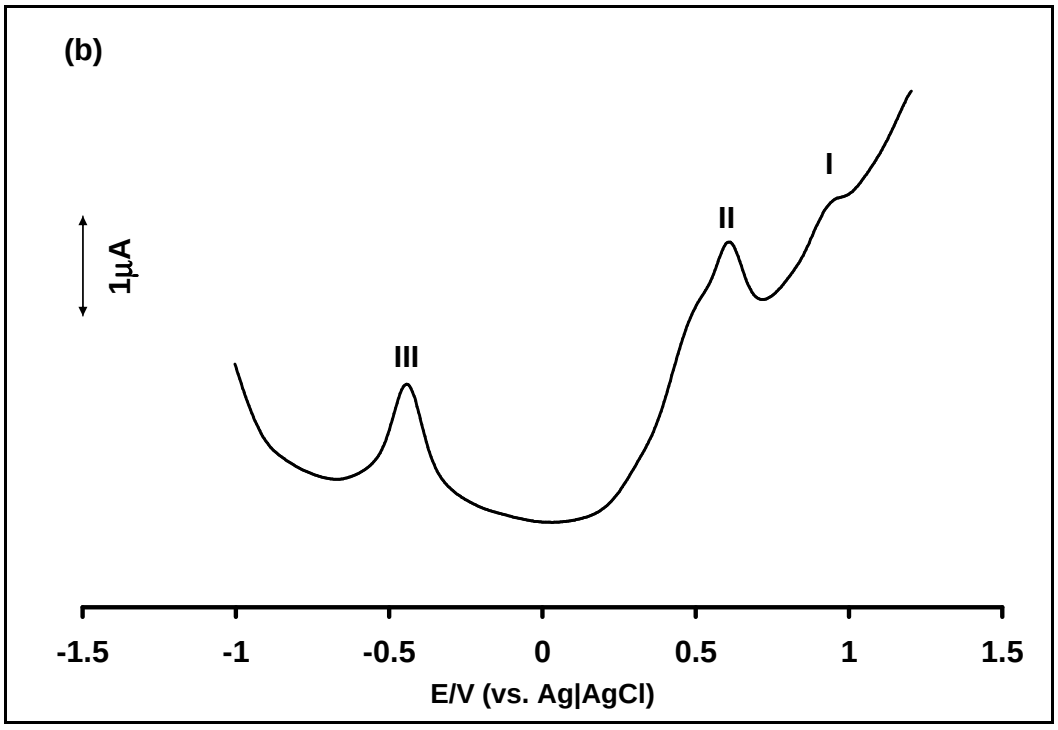
(b)
1µA
I
II
III
-1.5
-1
-0.5
0
0.5
1
1.5
E/V (vs. Ag|AgCl)

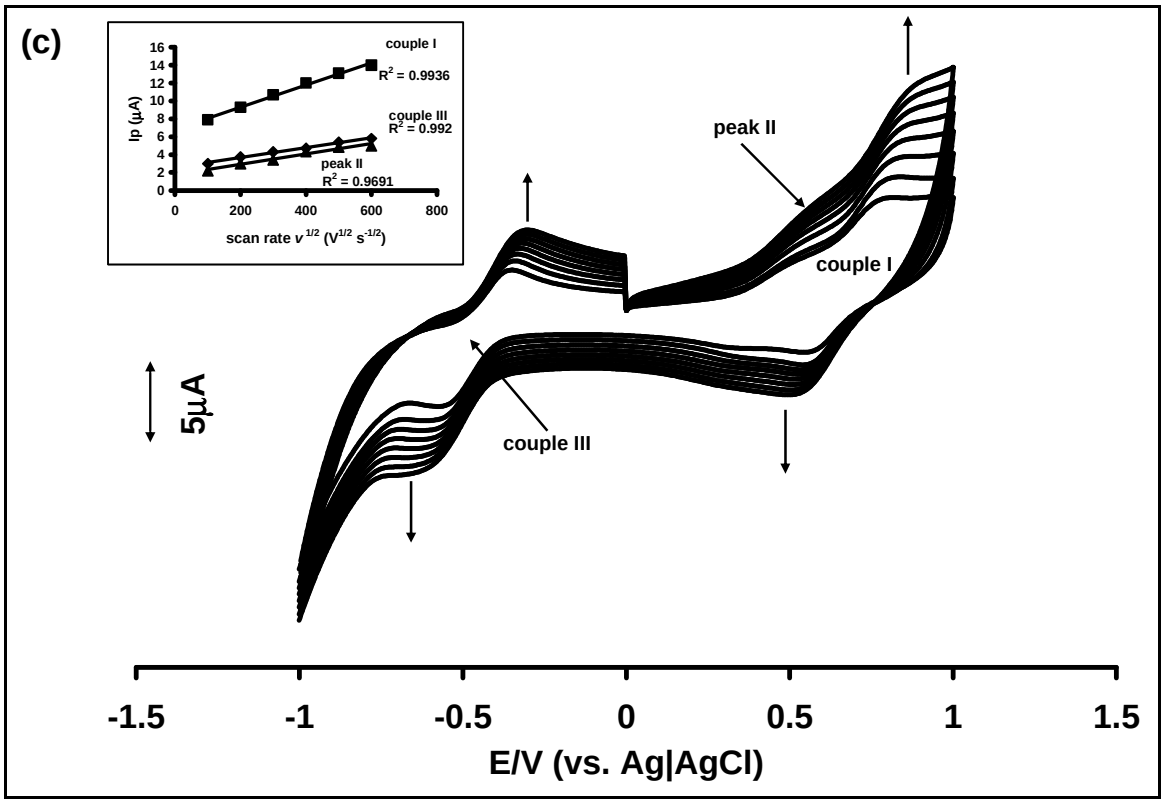

Figure 3.14: The (a) cyclic voltammogram, (b) square wave voltammogram and (c) cyclic voltammogram changes with scan rate and inset is the plot of current against square root of scan rate of complex (CoTDMPc, **39**) in DCM solution containing 0.1 M $TBABF_4$. Glassy carbon electrode used. Scan rate: 100 mV s^{-1}.

3.2.1.2 Spectroelectrochemistry

Spectroelectrochemical studies (Figure 3.15) were employed to confirm the assignments in the CV and SWV of complex **35**. The concentration of the complex was ~ 2 x 10^{-4} M for studies in OTTLE cell, at this high concentration, the aggregated species are present as judged by the broadening of the starting spectrum in Figure 3.15a, which shows the UV-VIS spectral changes of complex **35** during a controlled potential reduction of the complex at potential of couple **III**. The slight differences in the Q band maxima in Figure 3.15a (672 nm) compared to Figure 3.6 (676 nm) could be a result of the presence of

electrolyte in former. Upon reduction, the Q band shifted from 672 to 710 nm and increased in intensity. The spectral changes showed that upon reduction the Pc molecules become disaggregated as judged by the narrowing of the absorption bands. A new intense band was formed at 473 nm during reduction. New intense peaks between 400 and 500 nm are characteristic of $Co^{+}Pc$ species.[101] Also the shift in the Q band with increase or without decrease in intensity is typical of metal based reduction in MPc complexes. Thus spectral changes shown in Figure 3.15a clearly confirm that couple **III** is due to the reduction of $Co^{2+}Pc$ to $Co^{+}Pc$ (n was calculated to be approximately 1 from the equation, Q = nFVC). Furthermore, clear isobestic points at 690, 568 and 368 nm showed that the process is a clean reduction reaction involving two species. The reduction was reversible in that applying zero volts resulted in greater than 80% regeneration of the starting spectrum.

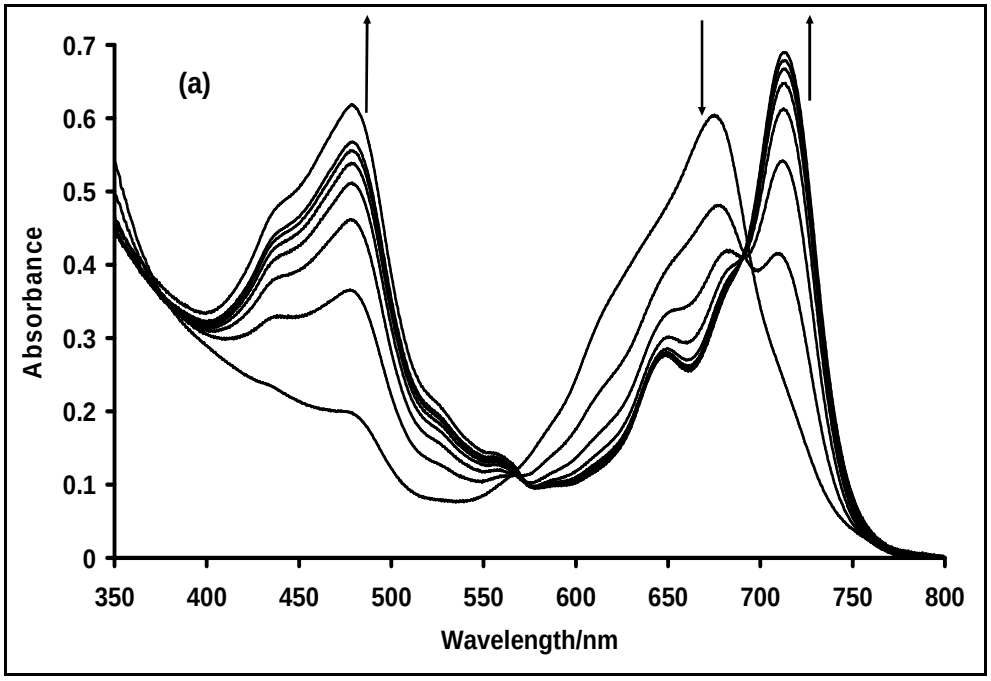

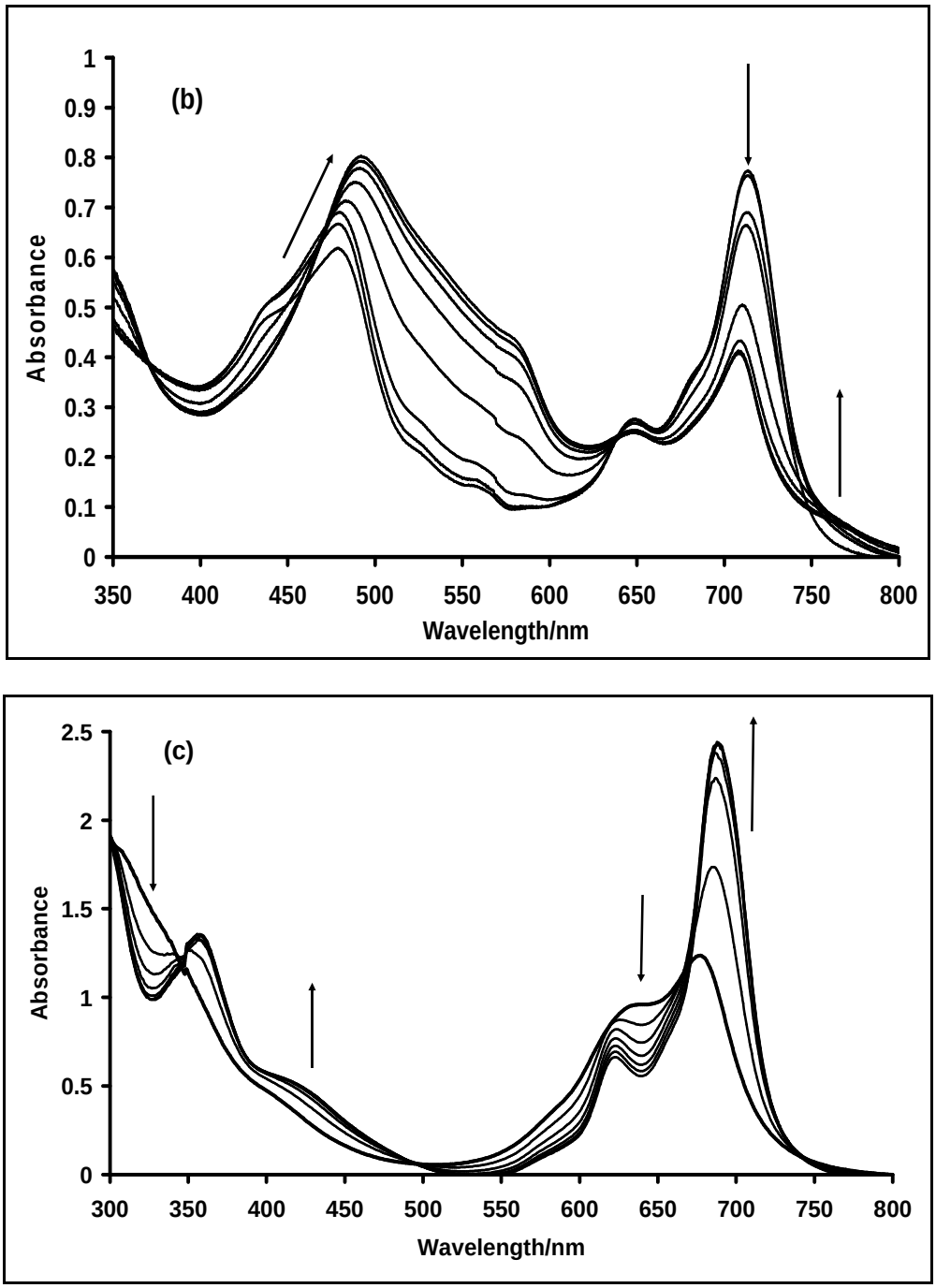

Figure 3.15: UV-Vis spectral changes for complex (CoTBMPc, **35**) observed using controlled potential electrolysis at (a) -0.6 V; (b) -1.6 V and (c) 0.6 V in DMF containing 0.1 M $TBABF_4$. The first scan in Figure 3.15b is the same as the last scan in Figure 3.15a.

Further reduction of the species formed in Figure 3.15a at potentials more negative than couple **IV** resulted in spectral changes shown in Figure 3.15b, which consisted of the decrease in the Q band and the shifting of the band at 473 to 485 nm, and the formation of new bands at 580 and 642 nm. Clear isobestic points at 637 and 368 nm showed that the process is a clean reduction reaction involving two species. The decrease in the Q band is characteristic of ring-based processes. Bands in the 500 to 600 nm region are typical[384] of ring based reduction and the formation of a Pc^{3-} species. Thus reduction at potentials of couple **IV** results in the formation of $Co^{+}Pc^{3-}$ species.

Oxidation at potentials more positive than couple **II** resulted in spectral changes shown in Figure 3.15c. The first spectrum shows aggregation with the monomer peak at 672 nm and the peak due to the aggregate at 628 nm. The differences in the starting spectrum in Figure 3.15 compared to Figure 3.6 could be a result of both aggregation and the presence of electrolyte in Figure 3.15c. Also the starting spectrum in Figure 3.15c is different from the starting spectrum in Figure 3.15a due to different extents of aggregation. For the sample employed for Figure 3.15c, the extent of aggregation is such that the Q band is split with the peak due to aggregated species observed at 628 nm and the monomer at 672 nm. Thus, the extent of aggregation varies from batch to batch depending on the concentration. The spectral changes observed during oxidation showed an increase of the monomer peak and its shifting from 672 to 687 nm. Since there was an increase in Q band intensity, the spectral changes in Figure 3.15c are due to the oxidation of Co^{2+} to the Co^{3+} species, showing that at potentials of couple **II** metal oxidation occurs, and that the couple is due to $Co^{3+}Pc^{2-}/Co^{2+}Pc^{2-}$ (n was calculated to be approximately 1 from the equation, Q = nFVC). Also, clear isobestic points at 671, 491 and 342 nm showed that the

process is a clean reduction reaction involving two species. The subsequent oxidations are expected to be on the ring in comparison with literature.[385] However, oxidation at potentials of couple **I** resulted in the loss in the intensity of the Q band, without significant increase in the 500 nm region of the spectrum which is typical for ring oxidation. These observations suggest decomposition as has been reported before[83] for other thiol substituted MPc complexes and confirm the irreversibility nature of process **I** in Figure 3.13.

Controlled potential reduction for complex **40** in DCM at potentials of couple **III** (Figure 3.16a) resulted in the formation of $Co^{+}Pc^{2-}$ as judged by the formation of a new peak at 476 nm and the shift of the Q band to a longer wavelength (711 nm) as discussed above for complex **35**. Figure 3.16b shows oxidation of complex **40** at potentials of couple **I**, the shift in Q band from 674 to 687 nm without loss in intensity again confirms metal oxidation and formation of $Co^{3+}Pc$. It should be noted that complex **40** was electrolysed in DCM since it does not dissolve in DMF as stated above. For both the metal oxidation and reduction, clear isobestic points were observed indicating that the processes are clean redox reactions involving two species.

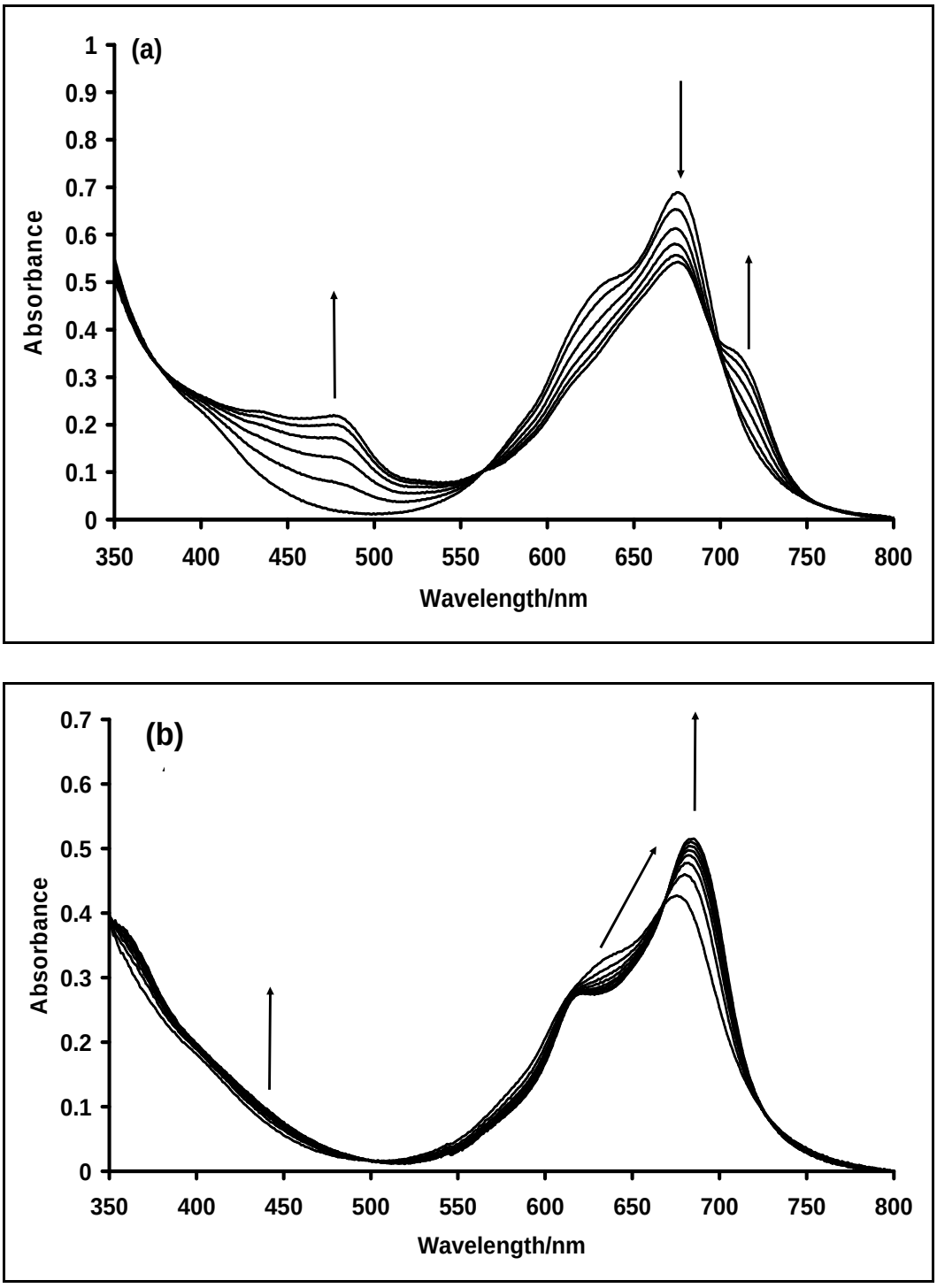

Figure 3.16: UV-Vis spectral changes of complex (CoTDMPc, **40**) observed using controlled potential electrolysis at (a) -0.7 V (process **III**) and (b) 0.7 V (process **II**) in DCM containing 0.1 M $TBABF_4$.

3.2.2 FePcs

3.2.2.1 Voltammetry

Figure 3.17 shows the CV and SWV of complex **36**. Five couples were observed labelled **I** to **V** in Figure 3.17. Couples **I** ($E_{½}$ = 0.70 V), **II** ($E_{½}$ = 0.36 V), **IV** ($E_{½}$ = -0.78 V) and **V** ($E_{½}$ = -1.18 V), showed clear return peaks but for **III** ($E_{½}$ = -0.37 V), the anodic component was weak. Thiol substituted MPc complexes often exhibit irreversible cyclic voltammetry behaviour.[94] Comparing the peak potentials (Table 3.2a) with those of documented FePc complexes, the couples are assigned **I**, **II**, **III**, **IV** and **V** to $Fe^{3+}Pc^{-}$ /$Fe^{3+}Pc^{2-}$, $Fe^{3+}Pc^{2-}$/$Fe^{2+}Pc^{2-}$, $Fe^{2+}Pc^{2-}$/$Fe^{+}Pc^{2-}$, $Fe^{+}Pc^{2+}$/$Fe^{+}Pc^{3-}$ and $Fe^{+}Pc^{3-}$/$Fe^{+}Pc^{4-}$ respectively.

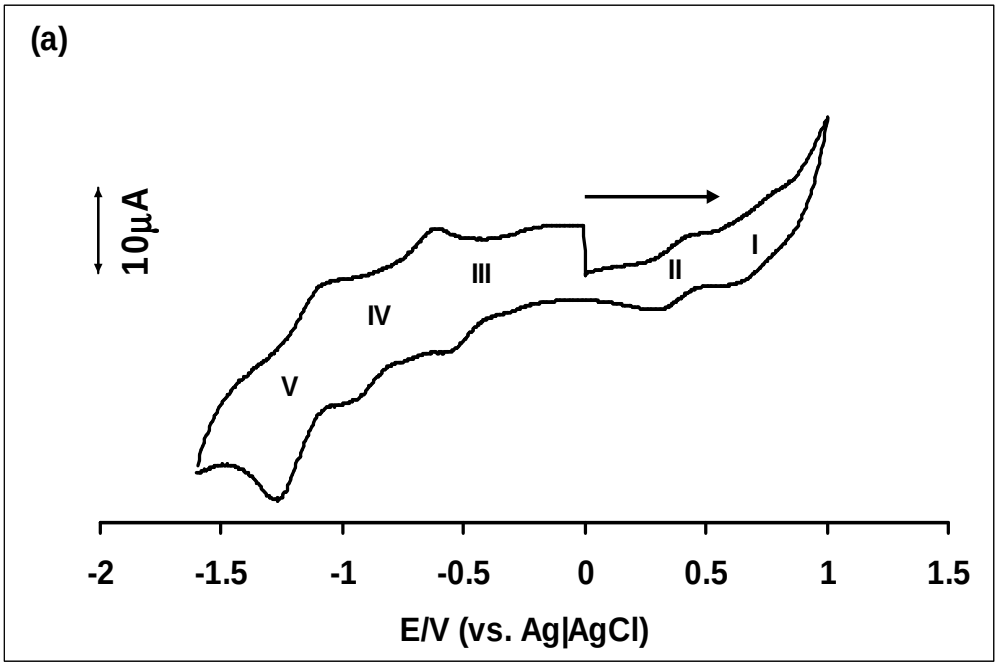

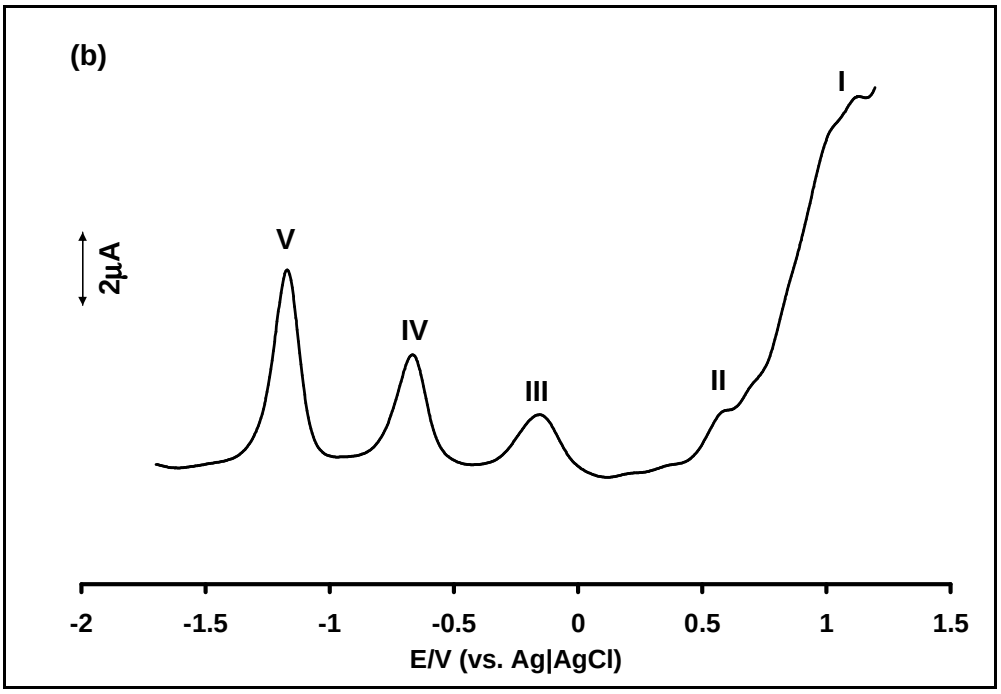

Figure 3.17: The (a) cyclic and (b) square wave voltammogram of complex (FeTBMPc, **36**) in DMF solution containing 0.1 M $TBABF_4$. Glassy carbon electrode used. Scan rate: 100 mV s^{-1}.

Complex **41** gave CV and SWV shown in Figure 3.18. Six processes ($E_{1/2}$) were observed at 1.01, 0.62, -0.53, -0.84, -1.16 and -1.40 V for couples, **I**, **II**, **III**, **IV, V** and **VI**, respectively. The anodic to cathodic currents were near unity for couples **I**, **II**, **III**, and **IV**. For the last two couples (**V** and **VI**) only weak return peaks were observed. However, diffusion control was observed for all couples, with linear variation of scan rate square root with peak current (not shown). The peaks are assigned in comparison with complex **36** and with literature,[385] Table 3.2a.

For both figures 3.17 and 3.18 which are for the FePc complexes, the difference in the peaks may be due to the closeness, possible overlap and sometimes irreversibility of the peaks often associated with thiol-derivatised metallophthalocyanines.

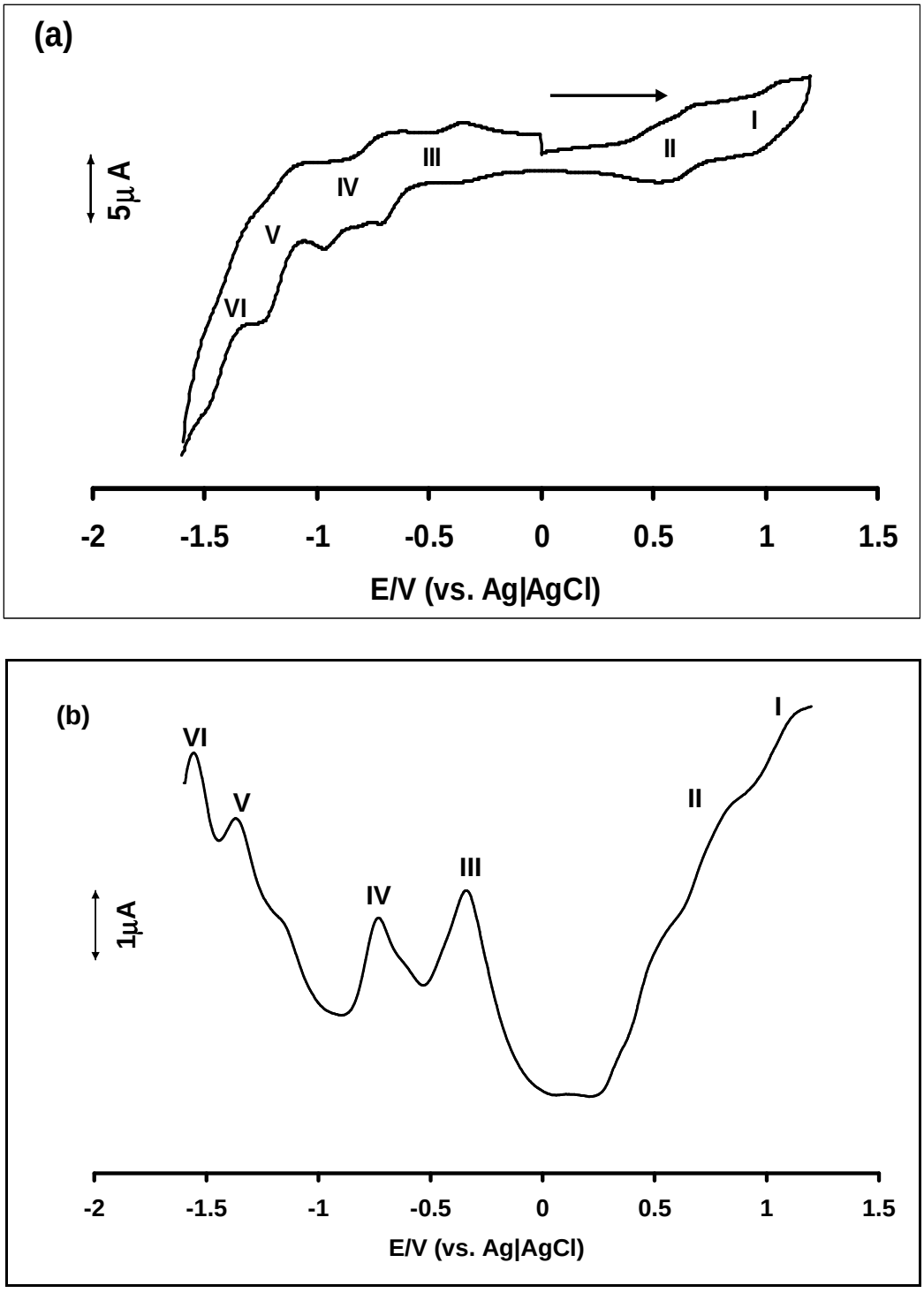

Figure 3.18: The (a) cyclic and (b) square wave voltammogram of complex (FeTDMPc, **41**) in DCM solution containing 0.1 M $TBABF_4$. Glassy carbon electrode used. Scan rate: 100 mV s^{-1}.

3.2.2.2 Spectroelectrochemistry

Spectroelectrochemistry (OTTLE) for complex **36** at potentials slightly more negative than couple **III** gave spectral changes shown in Figure 3.19a. Again the complex shows aggregation. Upon reduction, the peak due to aggregate at 636 nm decreased and a broad peak at 660 nm remained. Clear isobestic points at 677, 571 and 394 nm showed that the process is a clean reduction reaction involving two species. As already explained, in phthalocyanine chemistry, the lack of disappearance of the Q band on reduction or oxidation suggests a metal-based process. Thus the spectral changes shown in Figure 3.19a are typical of metal-based reduction, suggesting the formation of the $Fe^{+}Pc$ species. The spectrum of $Fe^{+}Pc$ species is not well known. It has been reported[386] that the presence of Fe^{+} disturbs the π-π* spectrum of the Pc resulting in a weak Q band and a pink solution. This work however shows that a relatively strong Q band is still present following reduction of $Fe^{2+}Pc$ to $Fe^{+}Pc$. Thus spectroelectrochemical studies here confirm that couple **III** is due to $Fe^{2+}Pc^{2-}$/ $Fe^{+}Pc^{2-}$. Oxidation at potentials of couple **II** resulted in spectral changes shown in Figure 3.19b, which consisted of the formation of a new peak at 649 nm, and the disappearance of the peak at 636 nm. These spectral changes are consistent with the oxidation of Fe^{2+} central metal to Fe^{3+} in phthalocyanines. It has also been reported[101] that the formation of $Fe^{3+}Pc$ species results in a split Q band for some complexes. The splitting is not evident in Figure 3.19b.

Spectroelectrochemistry of complex **41** confirmed that first oxidation and reduction occur at the central metal. Figure 3.20 shows spectral changes observed on oxidation of **41** at potentials of couple **II**. A new peak was observed at 671 nm with electrolysis time confirming central metal oxidation.

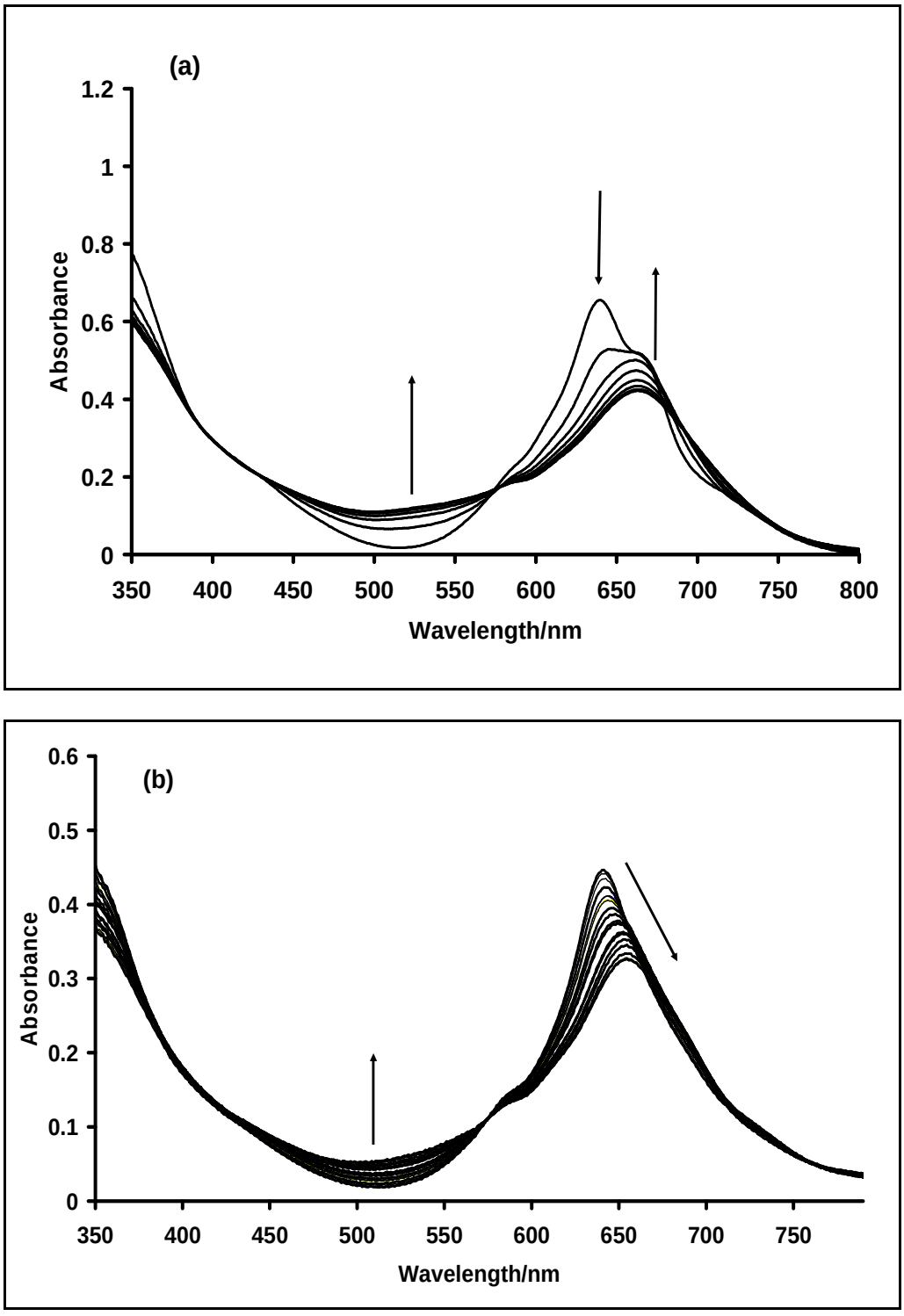

Figure 3.19: UV-Vis spectral changes of complex (FeTBMPc, **36**) observed using controlled potential electrolysis at (a) -0.6 V and (b) 0.6 V in DMF containing 0.1 M $TBABF_4$.

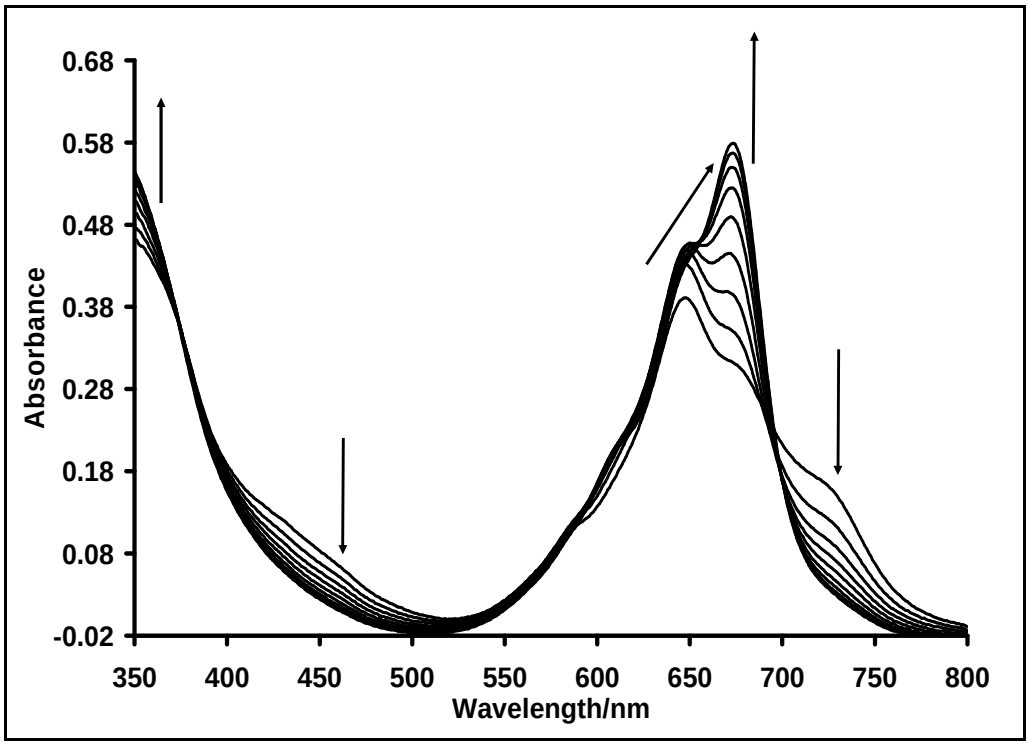

Figure 3.20: UV-Vis spectral changes of complex (FeTDMPc, **41**) observed using controlled potential electrolysis at 0.9 V in DCM containing 0.1 M $TBABF_4$.

3.2.3 MnPcs

3.2.3.1 Voltammetry

Figure 3.21 and 3.22 show the CVs and SWVs of MnTBMPc (**34**) and MnTDMPc (**39**) complexes in DCM (containing 0.1 M $TBABF_4$) respectively. Three quasi reversible redox processes were observed for both complexes with ΔE ranging from 100 to 240 mV. For MnTBMPc (**34**), the couples were observed at: $E_{½}$ = 1.12 V (**I**), $E_{½}$ = -0.08 V (**II**), $E_{½}$ = -0.84 V (**III**) vs. Ag|AgCl while for complex MnTDMPc (**39**), the three redox couples were observed at: $E_{½}$ = 1.06 V (**I**), $E_{½}$ = -0.26 V (**II**), $E_{½}$ = -0.98 V (**III**) vs. Ag|AgCl. A weak irreversible peak was observed at ~ 0.9 V for both complexes. This peak has been

observed before[60] for Mn^{3+} tetraaminophthalocyanine and was assigned using spectroelectrochemistry to a Mn^{4+}/Mn^{3+} redox process. Introduction of electron-donating groups to MPc ring is expected to lead to a thermodynamically easier oxidation and a more difficult reduction of the MPc complex.[152,387] This is because electron-donating group should increase the average electron density of the conjugated 18π-electron system of the phthalocyanine ring. MnTBMPc, **34** can be said to be more difficult to oxidise than MnTDMPc, **39** from the more positive $E_{1/2}$ value of its redox couple (**I**) while MnTDMPc, **39** can be said to be more difficult to reduce than MnTBMPc, **34** from the more negative $E_{1/2}$ of its redox couples (**II**) and (**III**).

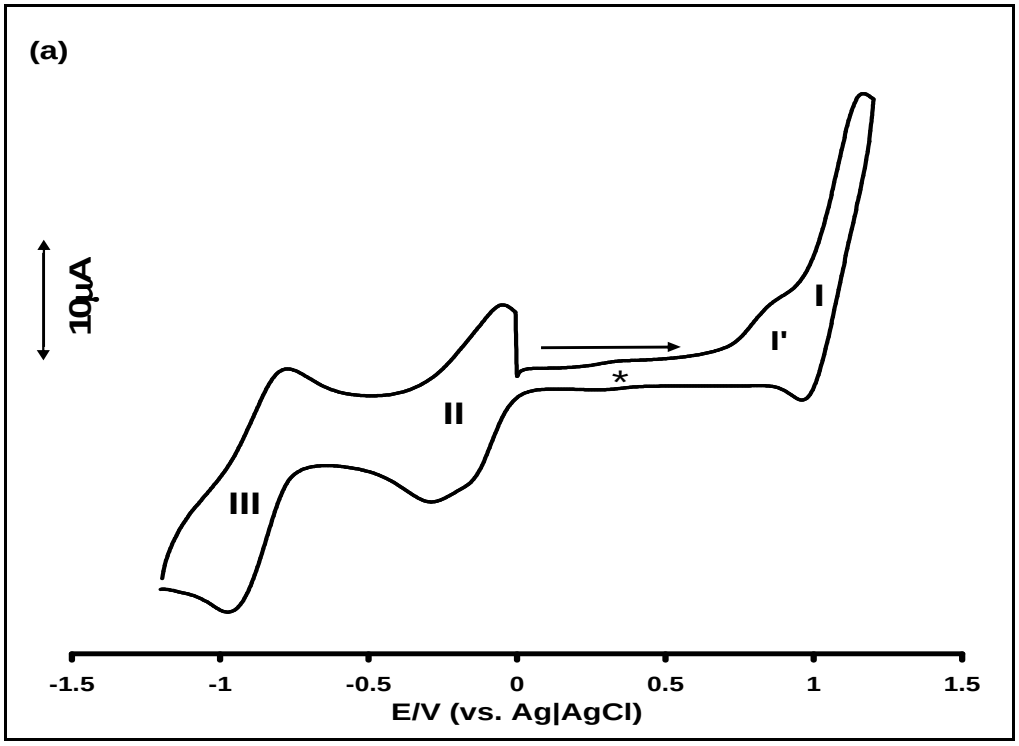

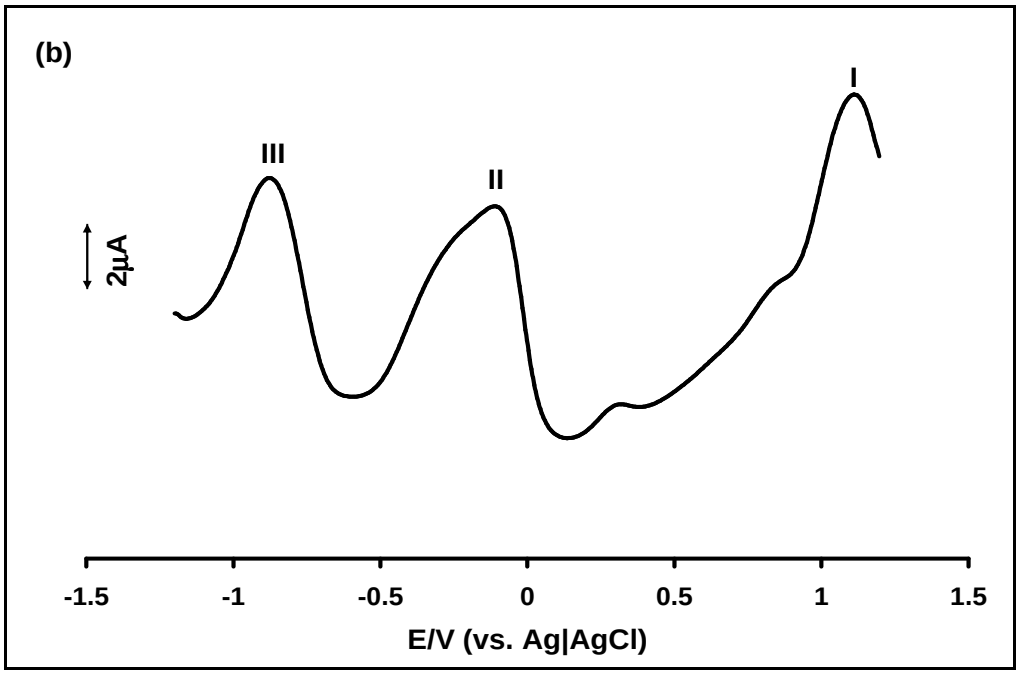

Figure 3.21: The (a) cyclic and (b) square wave voltammogram of complex (MnTBMPc, **34**) in DCM containing 0.1 M $TBABF_4$. Glassy carbon electrode used. Scan rate = 100 mV s^{-1}.

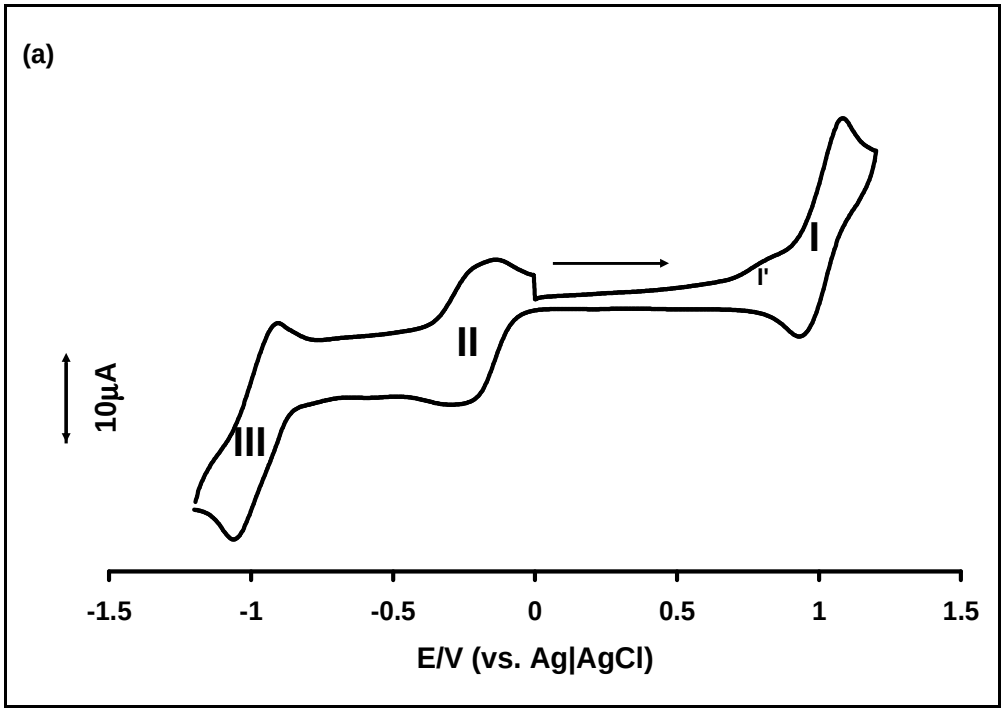

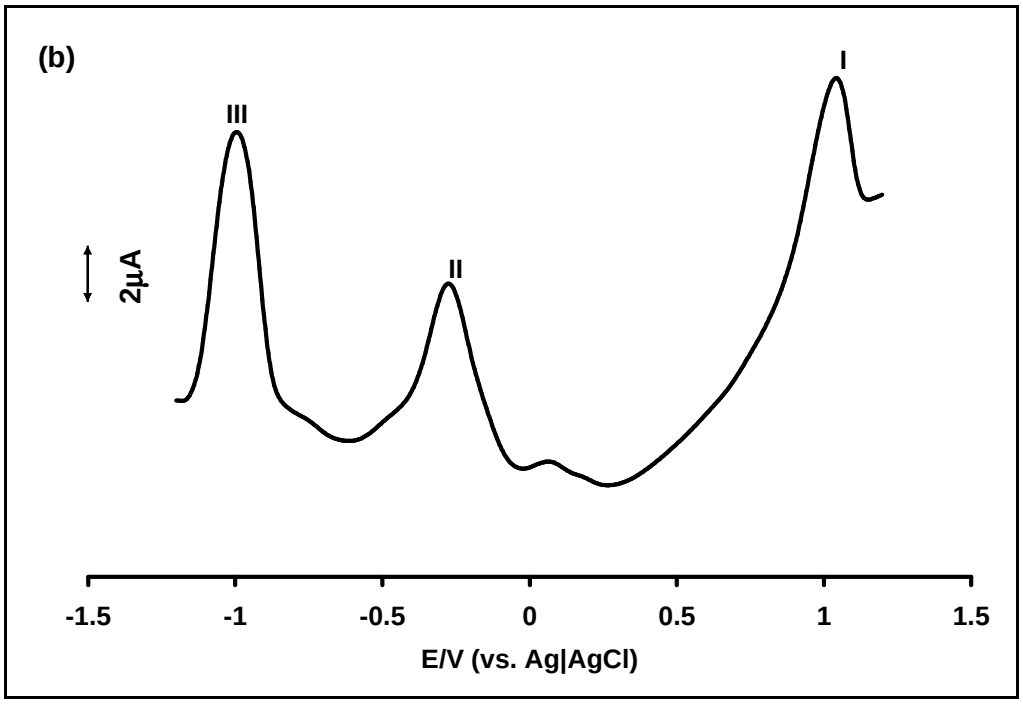

Figure 3.22: The (a) cyclic and (b) square wave voltammogram of complex (MnTDMPc, **39**) in DCM containing 0.1 M $TBABF_4$. Glassy carbon electrode used. Scan rate = 100 mV s^{-1}.

3.2.3.2 Spectroelectrochemistry

Spectroelectrochemical studies using optically transparent thin layer electrode (OTTLE) cell gave more insight into the origin of the redox couples observed during voltammetric studies of the complexes. Figure 3.23a shows the spectral changes observed during the reduction of complex **34** at potentials of process **II.** The initial spectrum in Figure 3.23a has more aggregated species than the one shown in Figure 3.5; this again is because a higher concentration of the complex was employed for the spectroelectrochemical studies. Upon reduction, there was a blue shift in the Q band from 742 to 701 nm and at the same time the colour of the complex changed from red to green, also the charge transfer bands at 523 and 455 nm decreased in intensities with the latter completely

disappearing and the former decreasing and shifting from 523 to 533 nm. A shift in the position of the Q band without a decrease in its intensity is indicative of metal based electro reduction reaction and a blue shift in the Q band upon reduction is typical of $Mn^{3+}Pc^{2-}$ to $Mn^{2+}Pc^{2-}$ reduction,[101] thus this confirmed that redox couple (**II**) in Figure 3.21 is due to redox couple $Mn^{3+}Pc^{2-}/Mn^{2+}Pc^{2-}$ (n was calculated to be approximately 1 from the equation, Q = nFVC). Furthermore, three clear isobestic points at 716, 558 and 402 nm indicate that it is a clean reduction, that is, only two species were present. As shown in Figure 3.23b, further reduction at potentials of process **III** to -1.2 V resulted in decrease in the intensity of the new Q band and at the same time there was increase in the band intensity between 400 and 600 nm typical of a ring based redox process.[384,388] Similar spectral changes were also observed for complex **39** for both redox couples (**II**) and (**III**) as shown in Figure 3.24a and b respectively. This observation confirmed that redox couple (**III**) is a ring based reduction, thus can be assigned to $Mn^{2+}Pc^{2-}/Mn^{2+}Pc^{3-}$. The first reduction in $Mn^{2+}Pc^{2-}$ complexes has been reported to occur at the ring to form $Mn^{2+}Pc^{3-}$ species as observed in this work, while other researchers have suggested metal reduction to the $Mn^{+}Pc^{2-}$ species.[101] As discussed earlier, there was a weak and broad anodic peak at around 0.9 V in Figures 3.21 and 3.22, this was attributed to Mn^{4+}/Mn^{3+} process. To confirm the origin of this peak, controlled potential electrolysis was conducted at 1.0 V; no visible change was observed in the UV/Vis spectra of both complexes thus the peak origin could not be confirmed. However, since the anodic peak current intensity is relatively small compared to that of redox couple (**I**), probably a negligible fraction of the complex transformed to the Mn^{4+}/Mn^{3+} species. The potential was then increased to 1.25 V in order to confirm the origin of redox couple (**I**) there was

a gradual decrease in the Q and B band peak intensity with time indicative of degradation. It is known that for thiol substituted MPc complexes, oxidation is often accompanied by decomposition.[83]

Based on the electrochemistry data above, the assignment of processes **I** to **III** can be confirmed as shown in Table 3.2b.

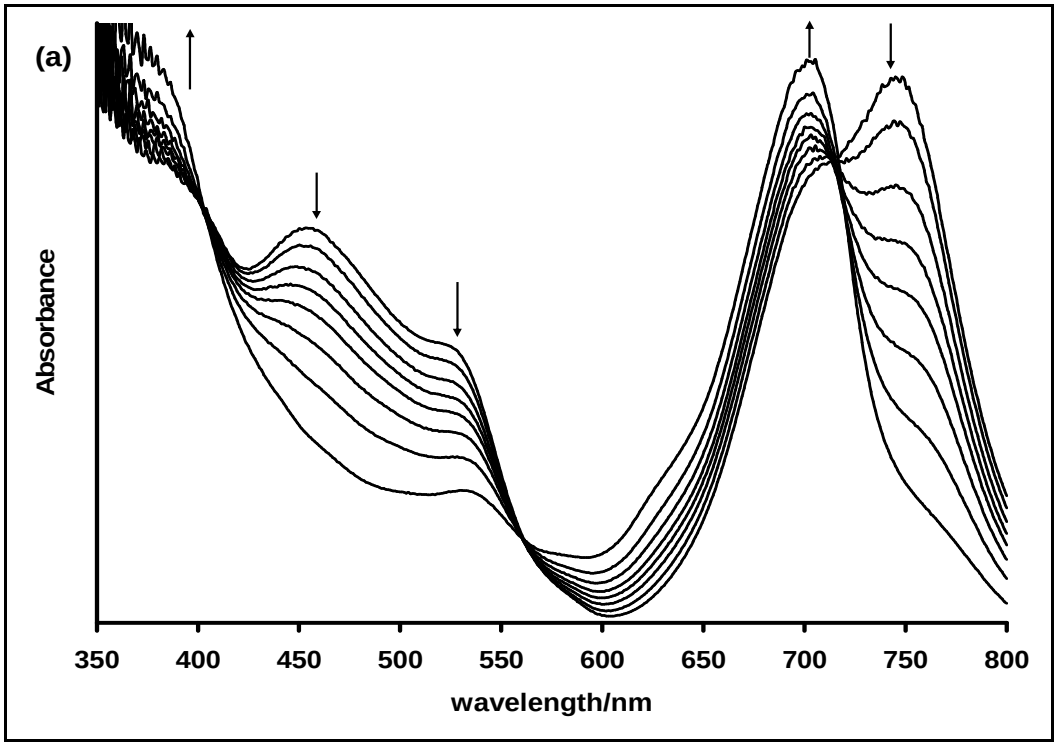

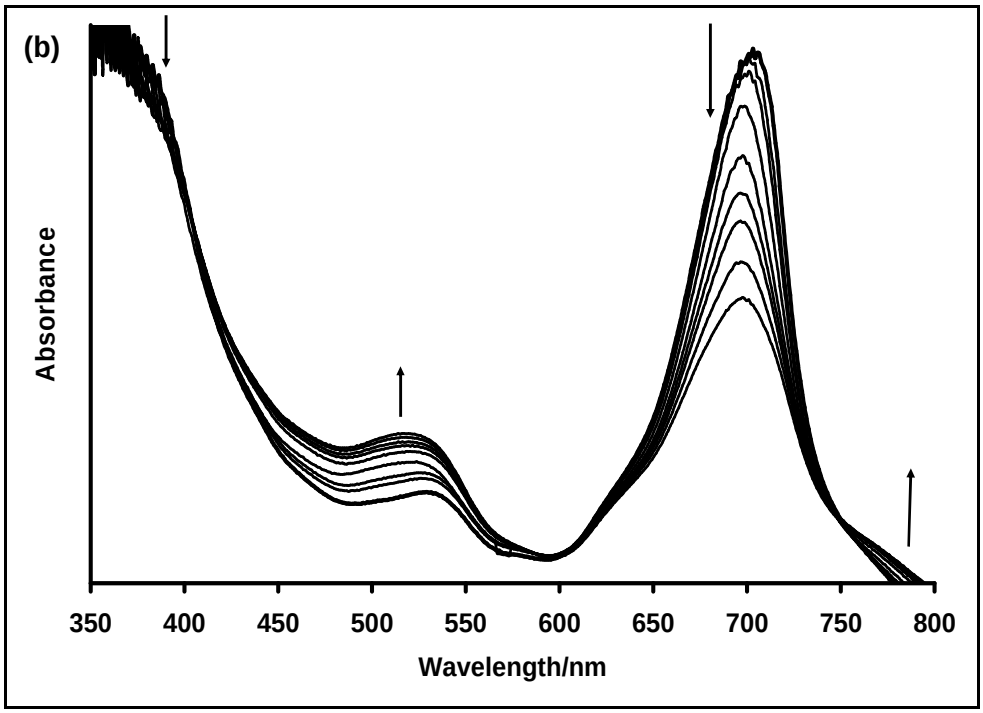

Figure 3.23: UV-Vis spectral changes for complex (MnTBMPc, **34**) observed using controlled potential electrolysis at (a) -0.5 V, (b) -1.15 V and (c) 1.25 V. The electrolyte solution was ~ 2 x 10^{-4} M of complex **34** in DCM containing 0.1 M $TBABF_4$ as the electrolyte.

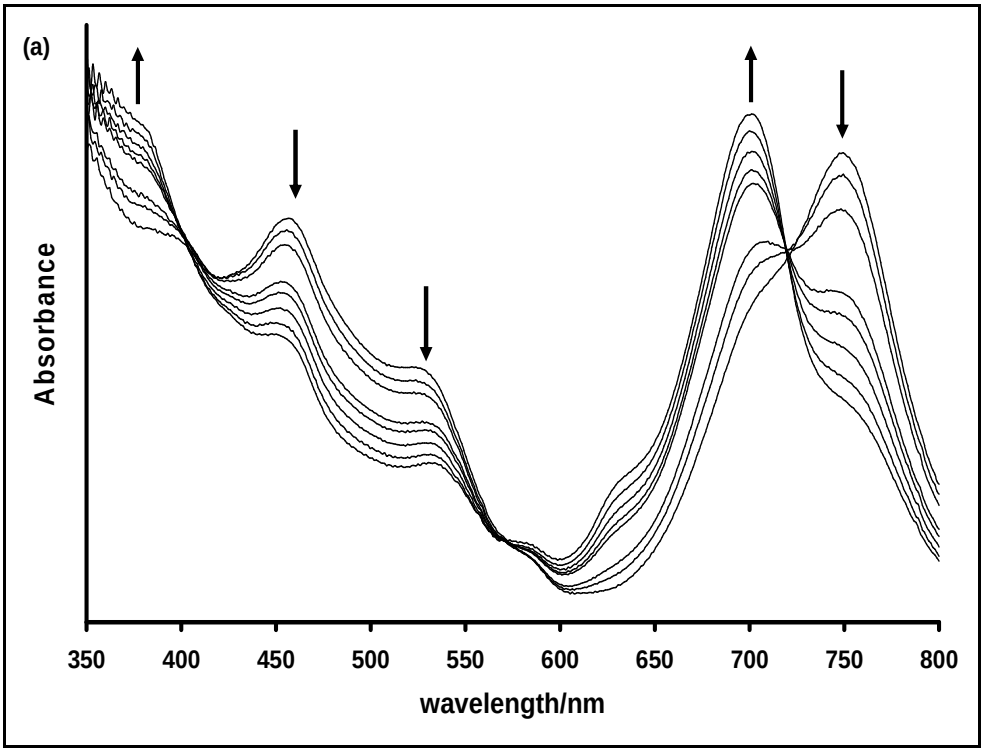

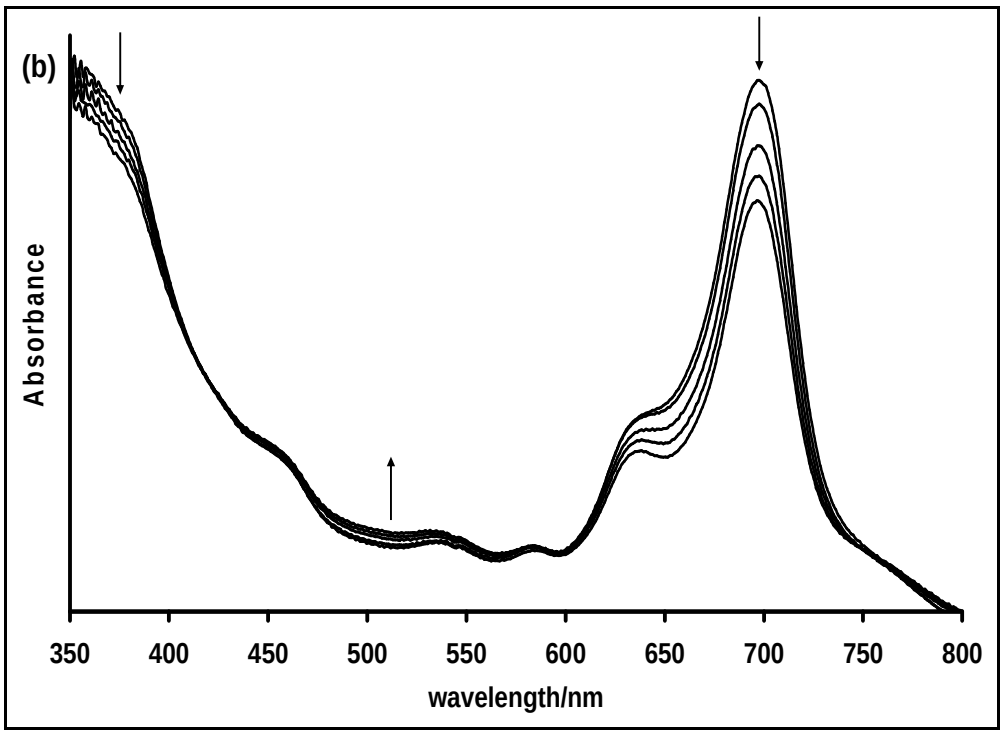

Figure 3.24: UV-Vis spectral changes for complex (MnTDMPc, **39**) observed using controlled potential electrolysis at (a) -0.5 V, (b) -1.15 V and (c) 1.2 V. The electrolyte solution was ~ 2 x 10^{-4} M of complex **39** in DCM containing 0.1 M $TBABF_4$ as the electrolyte.

3.2.4 NiPcs

3.2.4.1 Voltammetry

Figures 3.25 and 3.26 show the cyclic voltamogramms of NiTBMPc (**37**) and NiTDMPc (**42**) complexes in DCM (containing 0.1 M $TBABF_4$) respectively. Four redox processes were observed for NiTBMPc (**37**) complex while five redox processes were observed for NiTDMPc. For NiTBMPc (**37**) these were observed at: E_p = 0.96 V (**I**), E_p = 0.70 V (**II**), $E_{½}$ = -0.25 V (**III**) and $E_{½}$ = -0.94 V (**IV**) (vs. Ag|AgCl) while for NiTDMPc complex (**42**), the five redox couples were observed at: $E_{½}$ = 0.99 V (**I**), $E_{½}$ = 0.73 V (**II**), E_p = -0.18 V (**III**), $E_{½}$ = -0.93 V (**IV**), and $E_{½}$ = -1.15 V vs. Ag|AgCl. The couples were quasi-

reversible to irreversible. The irreversible behavior is typical of thiol substituted MPc complexes.[94] As stated above, redox processes are known to occur only on the ring for NiPc complexes in solution.[385] However, as is shown below, process **III** may be assigned to metal reduction for both complexes. The rest of the redox processes are assigned to ring reductions or oxidations.

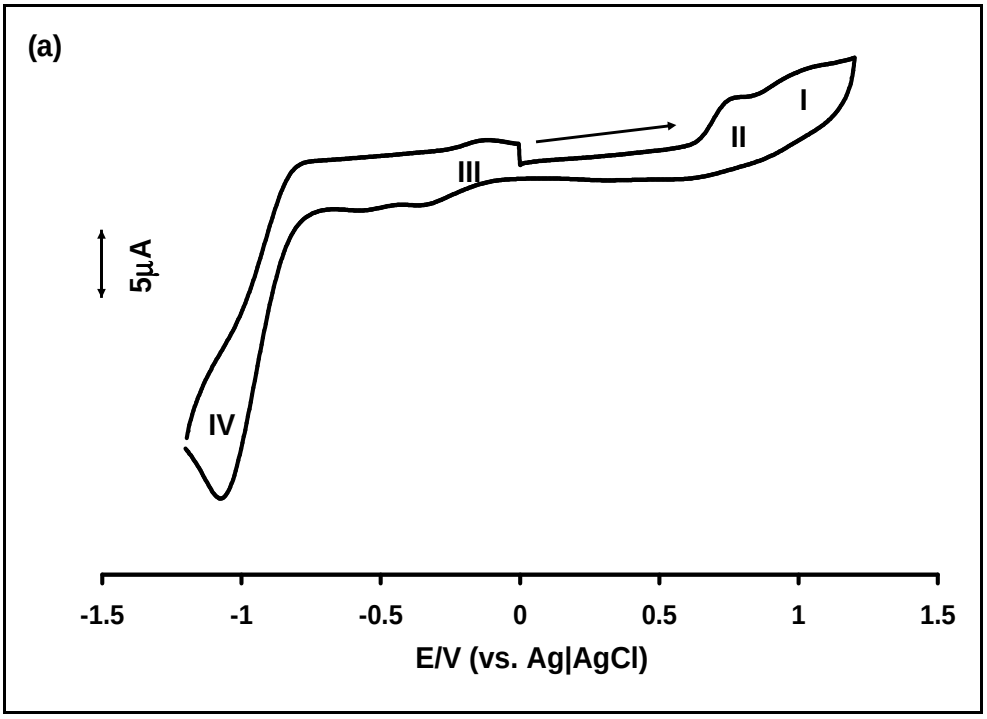

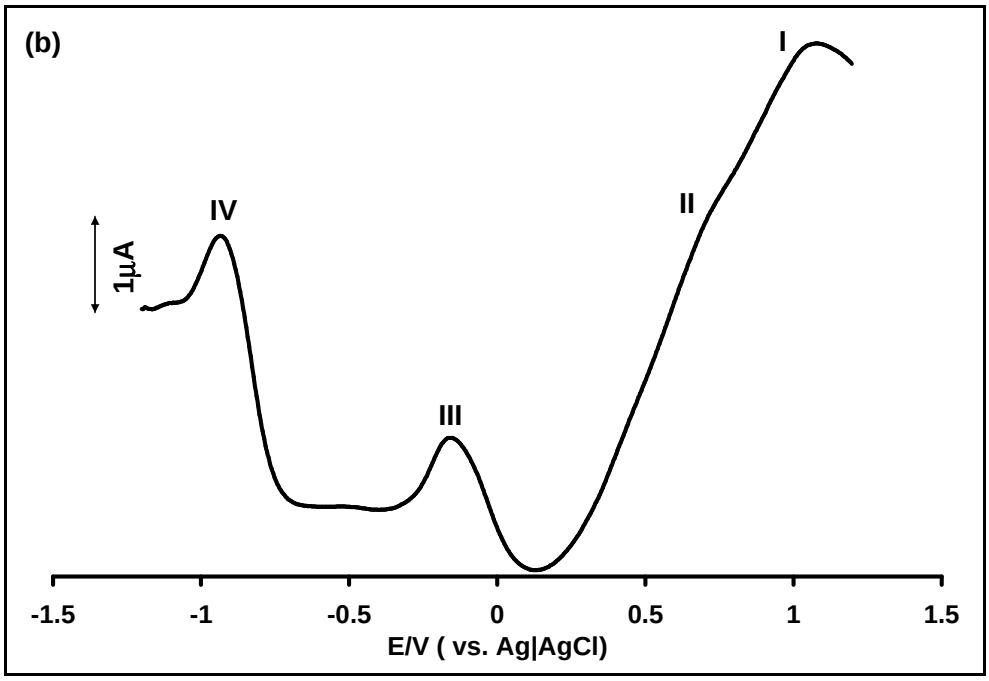

Figure 3.25: The (a) cyclic and (b) square wave voltammogram of complex (NiTBMPc, **37**) in DCM containing 0.1 M $TBABF_4$. Glassy carbon electrode used. Scan rate = 100 mV s^{-1}.

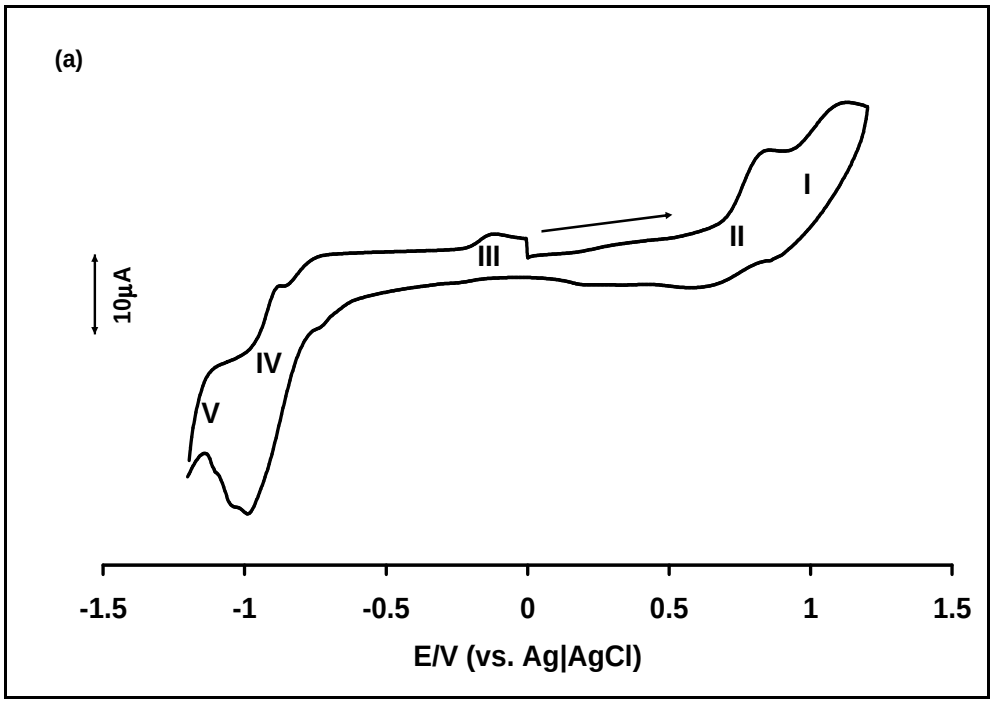

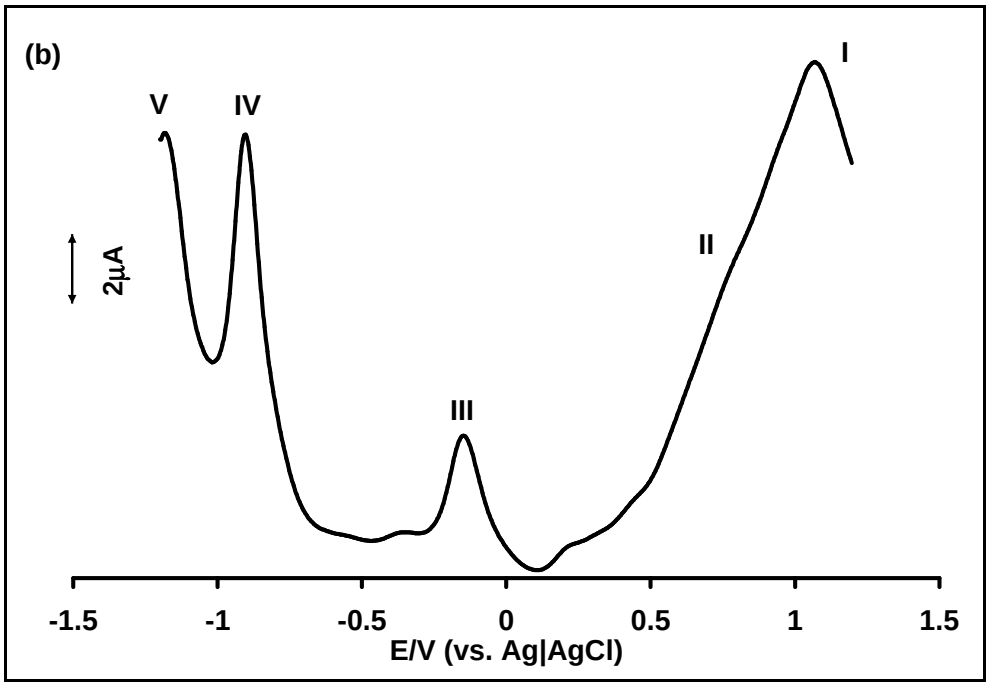

Figure 3.26: The (a) cyclic and (b) square wave voltammogram of complex (NiTDMPc, **42**) in DCM containing 0.1 M $TBABF_4$. Glassy carbon electrode used. Scan rate = 100 mV s^{-1}.

3.2.4.2 Spectroelectrochemistry

Spectroelectrochemical reduction of both complexes at potentials of process **III**, using optically transparent thin layer electrode (OTTLE) cell, resulted in spectral changes shown in Figure 3.27 and 3.28. The first spectrum for both complexes show broad peaks due to aggregation at concentrations employed for OTTLE cell studies. For NiTBMPc (**37**), these changes consisted of an increase in the bands in the Q band region, with sharp bands at 688 and 632 nm, and in the 400 to 500 nm region, two sharp bands were observed at 463 and 411 nm. The latter are charge transfer bands in MPc complexes. For NiTDMPc (**42**), sharp bands appear in the Q band region at 687, 634 and 608 nm, and charge transfer bands were observed at 463 and 412 nm. $M^{+}Pc$ species having bands

between 400 and 500 nm is not usual; a very good example is $Co^{+}Pc$ species which is well documented[101]. The spectral changes observed on reduction of the complexes suggest reduction of the central metal and the formation of $Ni^{+}Pc$ species.[385] Ring reduction would result in collapse of the Q bands and formation of new weak bands in the 500 to 600 nm region, due to the perturbation of the LUMO.[384] This is the first time electrochemical reduction of $Ni^{2+}Pc$ at the metal has been reported in solution.

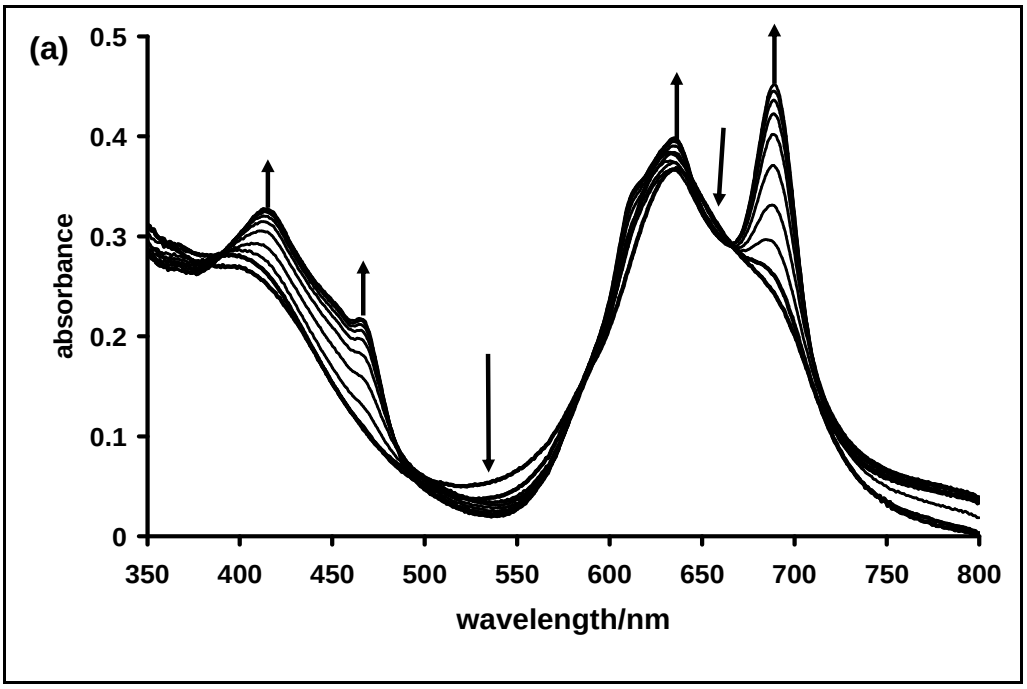

Figure 3.27: UV-Vis spectral changes observed during the reduction of complex (NiTBMPc, **37**) using controlled potential electrolysis at -0.4 V in DCM containing 0.1 M $TBABF_4$.

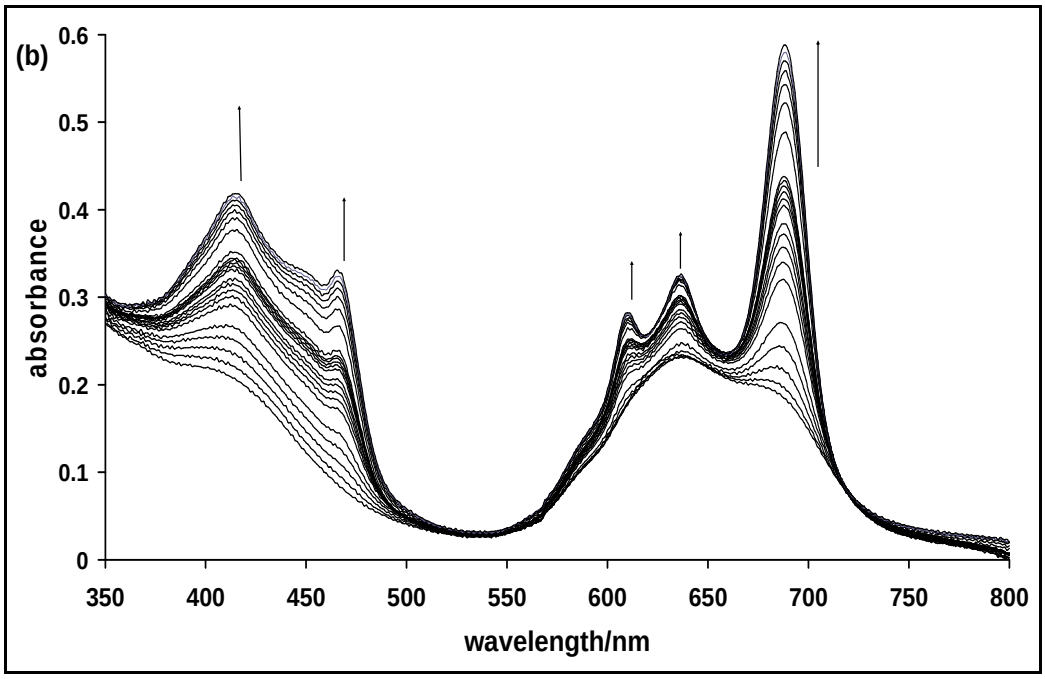

Figure 3.28: UV-Vis spectral changes observed during the reduction of complex (NiTDMPc, **42**) using controlled potential electrolysis at -0.4 V in DCM containing 0.1 M $TBABF_4$.

3.2.5 ZnPcs

3.2.5.1 Voltammetry

Figure 3.29 shows the CV and SWV for complex **38**. Three couples were observed all due to the phthalocyanine ring since the central metal is electroinactive.[385] The couples are assigned as shown in Table 3.2d. Complex **43** containing long chain thiol substituents showed less defined voltammograms, Figure 3.30 with two broad couples both due to ring-based processes, Table 3.2d. The difference in the CVs of the complexes could be due to the difference in the ring substituents.

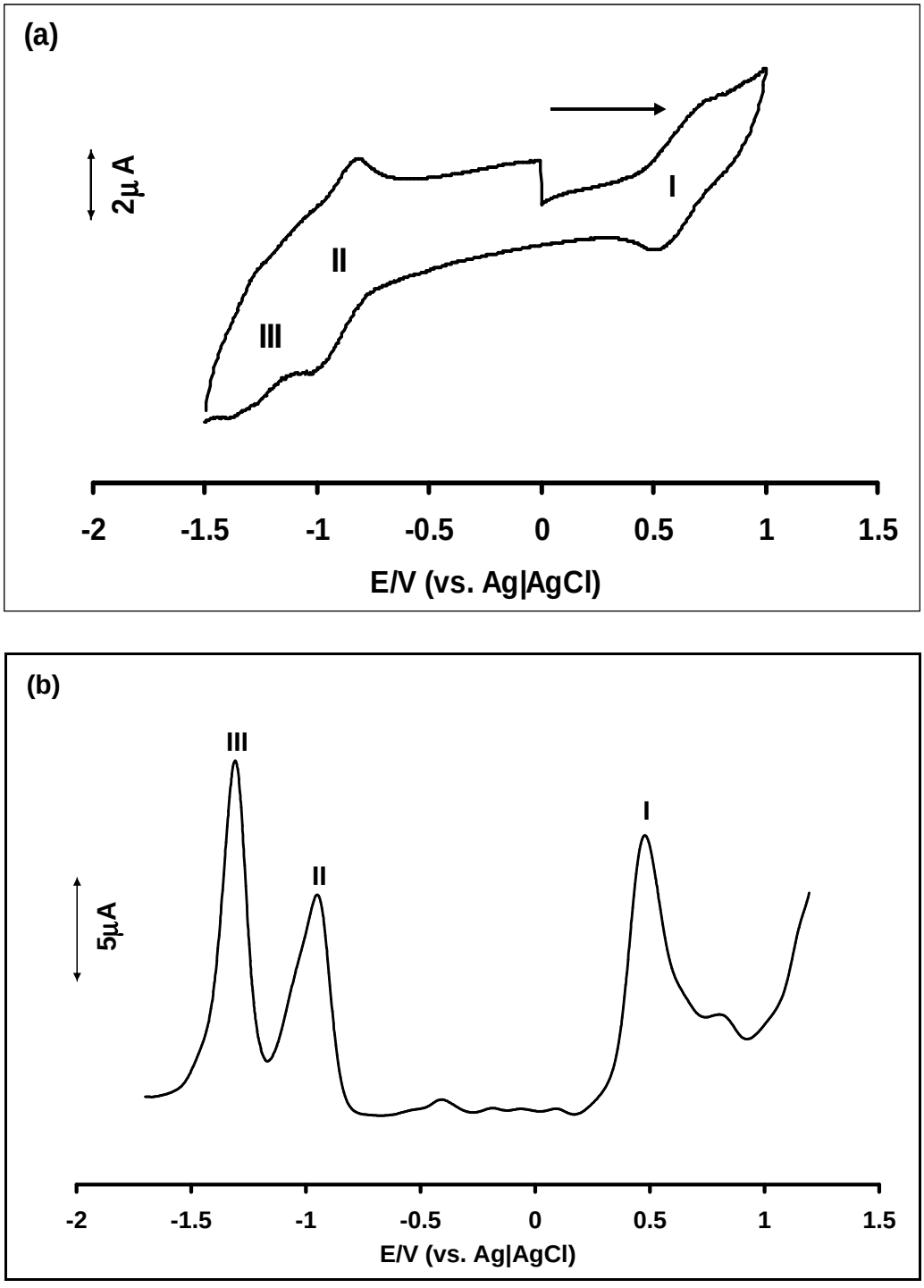

Figure 3.29: The (a) cyclic and (b) square wave voltammogram of complex (ZnTBMPc, **38**) in DMF containing 0.1 M $TBABF_4$. Glassy carbon electrode used. Scan rate = 100 mV s^{-1}.

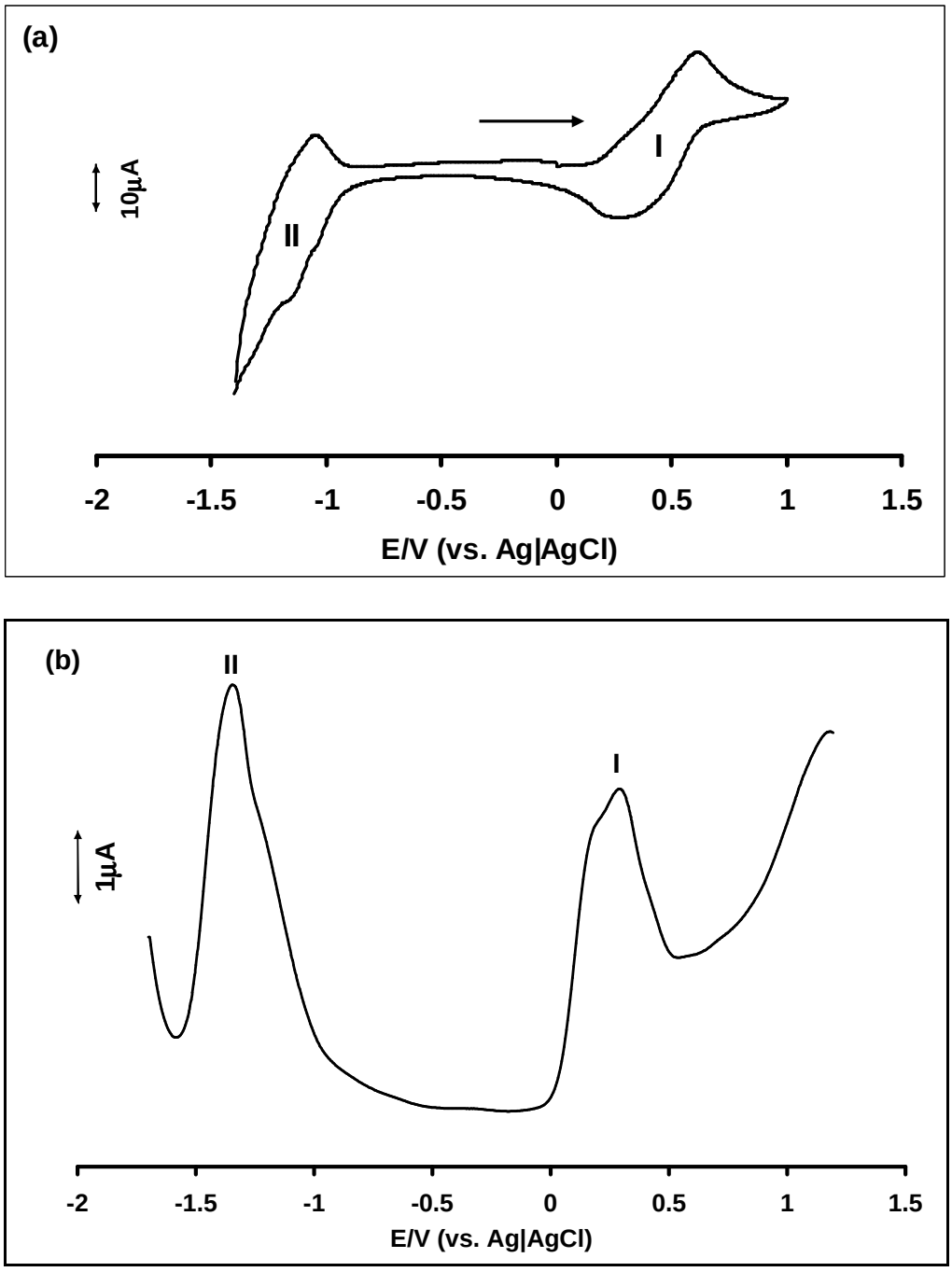

Figure 3.30: The (a) cyclic and (b) square wave voltammogram of complex (ZnTDMPc, **43**) in DCM containing 0.1 M $TBABF_4$. Glassy carbon electrode used. Scan rate = 100 mV s^{-1}.

3.2.5.2 Spectroelectrochemistry

Spectroelectrochemistry of complexes **38** and **43** showed similar trends and as expected the redox couples were ring based (Figures 3.31 and 3.32). Reduction at potentials of couple **II** gave similar spectral changes for both complexes, they were lowering in the Q band intensities without any shift and at the same time there were increases in the band intensities around 500 nm.

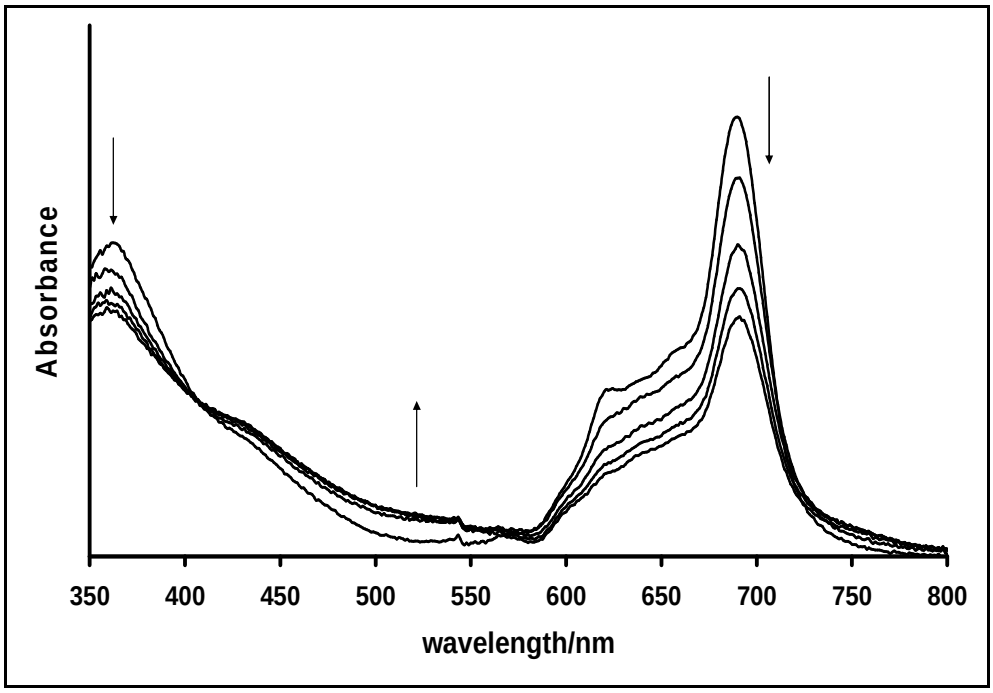

Figure 3.31: UV-VIS spectral changes of complex (**38**) observed using OTTLE cell controlled electrolysis at -1.45 V in DMF containing 0.1 M $TBABF_4$.

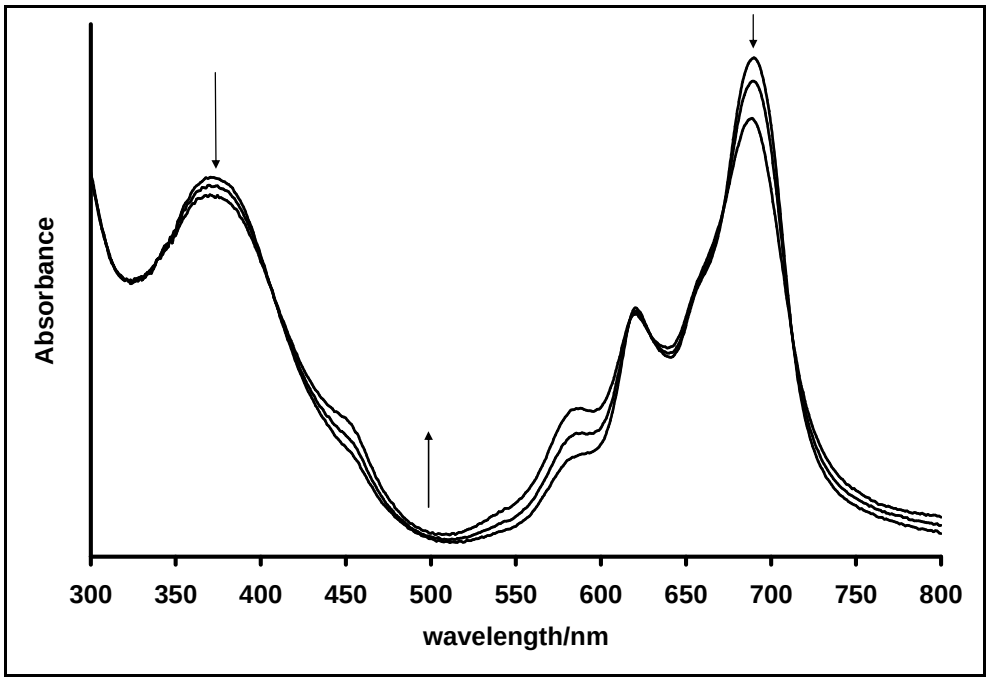

Figure 3.32: UV-Vis spectral changes of complex (**43**) observed using OTTLE cell controlled electrolysis at -1.45 V in DCM containing 0.1 M $TBABF_4$.

3.3 Conclusion

In conclusion, water soluble sulphonated and octacarboxy MPc complexes were synthesised and satisfactorily characterised by spectroscopic methods. UV-Vis spectra of most of the sulphonated MPc complexes showed aggregation behaviour in aqueous medium while the octacarboxy ones exhibited monomeric behaviour.

The synthesis, spectroscopic, and electrochemical characterisation of thiol substituted CoPc, FePc, MnPc, NiPc and ZnPc derivatives are presented. The synthesis of all the complexes gave high yields, also spectroscopic and electrochemical methods satisfactorily confirmed that the synthesis and purity of the complexes.

The CVs showed four, five to six redox processes for the CoPc, FePc and NiPc derivatives. As expected first oxidation and first reduction in CoPc, FePc and MnPc complexes occurred at the central metal. However ring oxidation was accompanied by decomposition. For the MnPc derivatives, three quasi reversible peaks were observed, one metal based and two ring based redox couples. Both complexes showed a broad and relatively small irreversible anodic peak at around 0.9 V which maybe due to $Mn^{3+}Pc^{2-}$ /$Mn^{4+}Pc^{2-}$ redox process. The complex MnTDMPc which has a more red shifted Q band in DCM was easier to reduce than the complex MnTBMPc and the other way around for oxidation, confirming the influence of electron donating ability of the ring substituents on the positions of the redox couples. Spectroelectrochemistry confirmed the first oxidation and reduction redox couples for CoPc, FePc, NiPc and MnPc to be metal based redox processes. Spectroelectrochemistry also confirmed that the redox couple (**II**) for both MnPc derivatives as a metal based reduction of $Mn^{3+}Pc$ to $Mn^{2+}Pc$ thus confirming the original state of the complexes as Mn^{3+}(Ac)Pc. For the first time, spectroelectrochemistry gave evidence for the formation of Ni^{+} process in a NiPc complex. The redox couples assigned to ring based processes were also confirmed by spectroelectrochemistry. Ring oxidation of the complexes resulted in decomposition. $Fe^{+}Pc$ showed a strong Q band in contrast to literature report.

The spectra of Ni^{+}, Fe^{+} and Co^{+} phthalocyanine complexes are not well known, and this work further gives some insight into the spectra of these species which would be helpful to other researchers.

CHAPTER 4

TRANSFORMATION OF CHLOROPHENOLS

This chapter deals with the transformation of chlorophenols using sulphonated and octacarboxy MPcs as catalysts. This chapter is mainly in two sections; (1) chemical/enzyme-like and (2) photocatalysis.

4.1 Chemical /Enzyme-like catalysis of chlorophenols transformation

4.1.1 $CoPcS_4$ catalyst loading and spectral characterisation

As discussed in chapter 3, $MPcS_4$ complexes are in general known to exist as aggregates in equilibrium with monomers in aqueous solutions. Their UV-Vis spectra thus consist of two peaks in the Q band region. The lower energy absorption band near 655 nm is associated with the monomeric species while the high energy absorption band near 622 nm is due to the aggregates species. In the presence of organic solvents, $MPcS_4$ complexes show monomeric behaviour. Figure 4.1 shows the spectra of $CoPcS_4$ (**24**) in water/methanol, pH 7 and pH 10 solutions. The presence of aggregates is evident under pH 7 and pH 10 conditions, as seen by a clear split in the Q band in the former and a broadened Q band in the latter. In water/methanol, $CoPcS_4$ (**24**) is monomeric. Thus Figure 4.1 shows that aggregation of the $CoPcS_4$ (**24**) increases as follows: water/methanol < pH 10 buffer < pH 7 buffer. The higher degree of aggregation in pH 7 than in pH 10 might be due to the nature of the buffer (phosphate buffer) which probably due to more interaction of the $CoPcS_4$ molecules with water molecules (by H-bonding) in pH 7 than in pH 10.

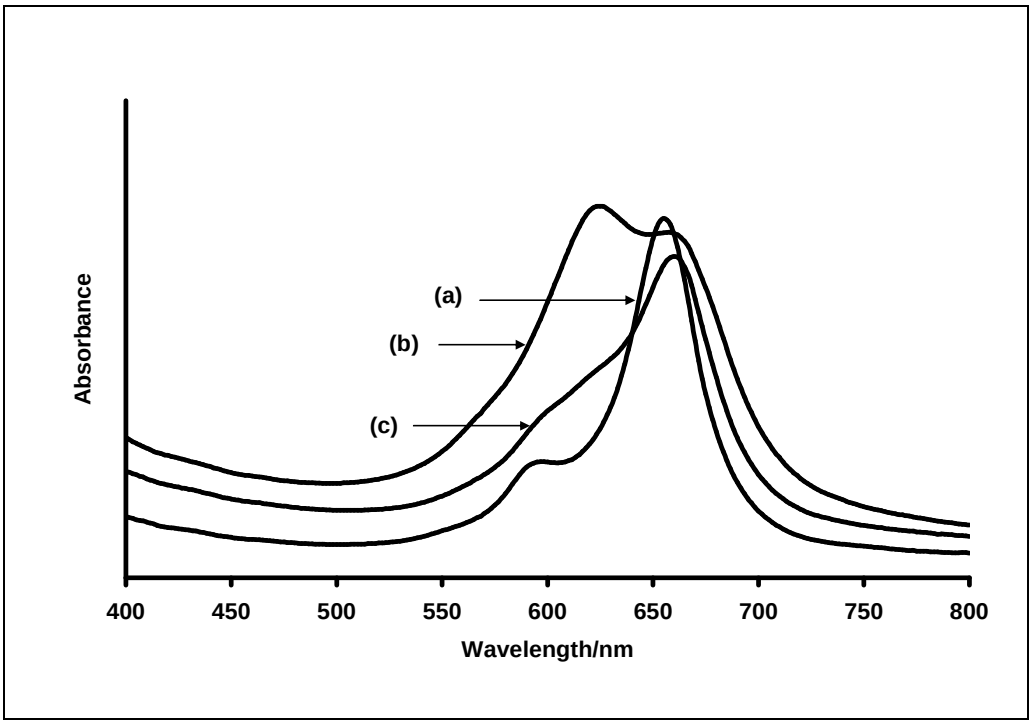

Figure 4.1: UV-Vis spectra of $CoPcS_4$ (**24**) in (a) water/methanol, (b) pH 7 and (c) pH 10. [$CoPcS_4$] ~ 1 x 10^{-6} mol L^{-1}.

The catalytic behaviour of $CoPcS_4$ (**24**) towards the oxidation of TCP and 2-CP was studied in water/methanol and also under the different pH conditions. pH 7 (for TCP) and 10 (for 2-CP) were so chosen because the pKa values of 2-CP and TCP are 8.55 and 6.23 respectively.[389]

The concentration of the oxidant (hydrogen peroxide) chosen in this work (1 x 10^{-2} mol L^{-1}) was found to effect the least destruction of the catalyst. The optimum amount of catalyst needed for the maximum conversion of the substrates was determined in water/methanol solvent mixture, after 5 hours reaction time, Figure 4.2. The results indicate that the catalytic conversion of the chlorophenols, under the experimental conditions employed here, is highly dependent on the $CoPcS_4$ (**24**) loading. Figure 4.2

shows that the maximum conversion of the 2-CP and TCP to products in water/methanol conditions were approximately 81 and 67%, respectively, at 1% $CoPcS_4$ (**24**) loading. Hence, most subsequent experiments were performed at 1% $CoPcS_4$ (**24**) loading, except for the pH studies described in section 4.1.2.

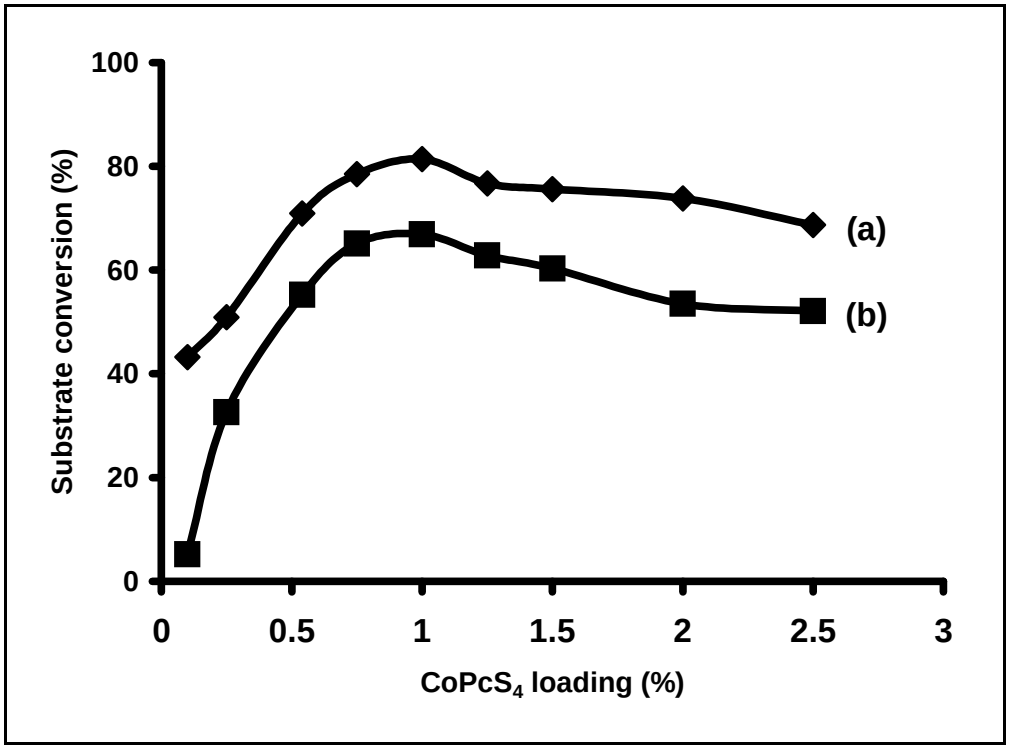

Figure 4.2: Effect of catalyst loading on the conversion of (a) 2-CP and (b) TCP water/methanol. [Hydrogen peroxide] = 1 x 10^{-2} mol L^{-1}. Starting concentration of the phenols = 1 x 10^{-2} mol L^{-1}. Reaction time was 2.5 hours.

It is well established that chlorophenols resist oxidative degradation and this resistance increases with the number of halogen substituents.[53,265-267,389] The lower conversion rate of the TCP, compared to the 2-CP, could therefore be attributed to the difficulty in catalytic oxidation of polychlorinated phenols compared to their unchlorinated and monochlorinated derivatives.

4.1.2 pH effect

Changes in the HPLC peak area of the substrates during the oxidative catalysis were monitored at pH 7, pH 10 and in water/methanol mixture for a 5-hour period. Figure 4.3 show the variation of substrate concentrations of 2-CP (Figure 4.3b and d) and TCP (Figure 4.3a and c) respectively with time, in the absence and presence of the $CoPcS_4$ (**24**) catalyst (0.5% catalyst loading was employed in this case), using the water/methanol solvent mixture. In the absence of the catalyst, oxidative transformation of the chlorophenols was observed, but much less than in the presence of the catalyst. The oxidation of 2-CP and TCP without the $CoPcS_4$ catalyst is not surprising, the presence of strong oxidant such as hydrogen peroxide facilitate such oxidation. The kinetic plots in Figures 4.3 show that the ratio of the slopes (2-CP : TCP) in the first two hours was 3:2 in the presence of the $CoPcS_4$ (**24**) catalyst. This result once again shows the difficulty in the oxidation of polychlorophenols compared to the monochlorophenols.

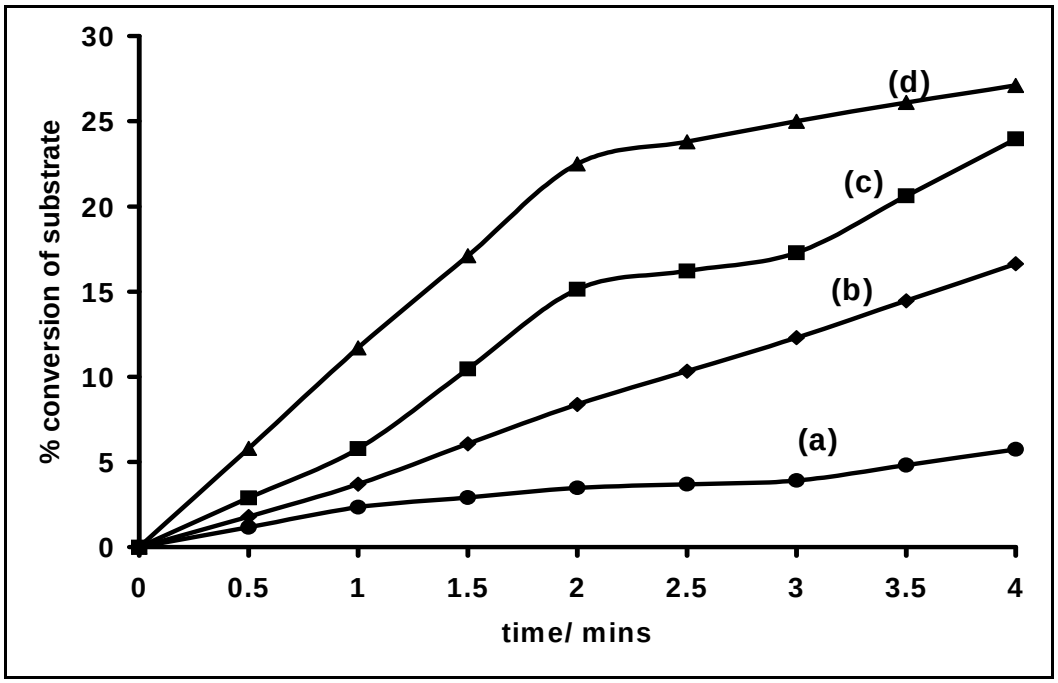

Figure 4.3: Percentage conversion vs. time for the H_2O_2 oxidised and $CoPcS_4$ (**24**) catalysed oxidation of TCP (a) and 2-CP (b) without catalyst, and TCP (c) and 2-CP (d) with $CoPcS_4$ (**24**) catalyst. [$CoPcS_4$] = 0.5% loading; $H_2O_2 = 10^{-2}$ mol L^{-1}. Solvent = water/methanol. Starting concentration of the phenols =1 x 10^{-2} mol L^{-1}.

Kinetic curves that are similar to those shown in Figures 4.3 were also observed at pH 7 for TCP and pH 10 for 2-CP. Comparative kinetic plots of the conversion of the substrates at different pH conditions (water/methanol (pH 3.4), and pH 7 and 10 for TCP and 2-CP, respectively) at 1% catalyst loading are shown in Figures 4.4 and 4.5 respectively for 2-CP and TCP.

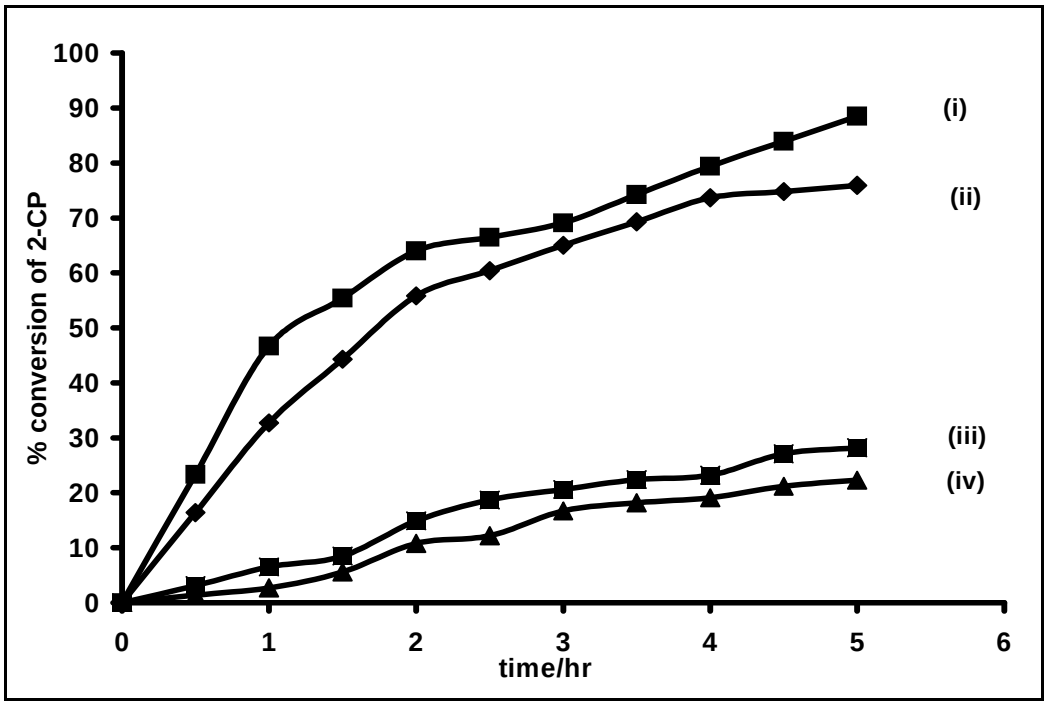

Figure 4.4: Effect of pH on the rate of oxidative degradation of 2-CP in pH 10 (curve i) and water/methanol (curve ii) in the presence of $CoPcS_4$ (**24**). Curves (iii) (pH 10) and curve (iv) (water/methanol) are in the absence of the $CoPcS_4$ (**24**) catalyst (1% loading). Starting concentration of 2-CP = 1 $x10^{-2}$ mol L^{-1}. $[H_2O_2]$ = 1 x 10^{-2} mol L^{-1}.

The percent conversion is lower in water/methanol for both 2-CP and TCP. From the pKa values of the chlorophenols, there are two species with different properties, which are in equilibrium in 2-CP or TCP solutions; these are the undissociated phenol (PhOH; below their pK_a values) and phenoxide ion (PhO^- above their pK_a values).[389] Since the equilibrium between these two forms is pH dependent, chemical transformations involving these compounds should be pH-dependent as well. The enhanced catalytic conversion of the substrates at pH 7 and pH 10, clearly reflect the significant contribution of the ionised forms of chlorophenols. It is interesting to see an appreciable degree of catalysis under the water/methanol (acid) conditions, Figures 4.4 and 4.5, curves (ii). For TCP (Figure 4.5, curve i), while catalysis is completed within the first one hour at pH 7.0

buffer solution, catalysis continues for several hours (> 5 hours) in water/methanol mixture (Figure 4.5, curve ii). This behaviour is possibly due to the enhanced solubility of the chlorophenols in co-organic solvent environment as well as the less aggregated conditions of the catalyst as shown in Figure 4.1.

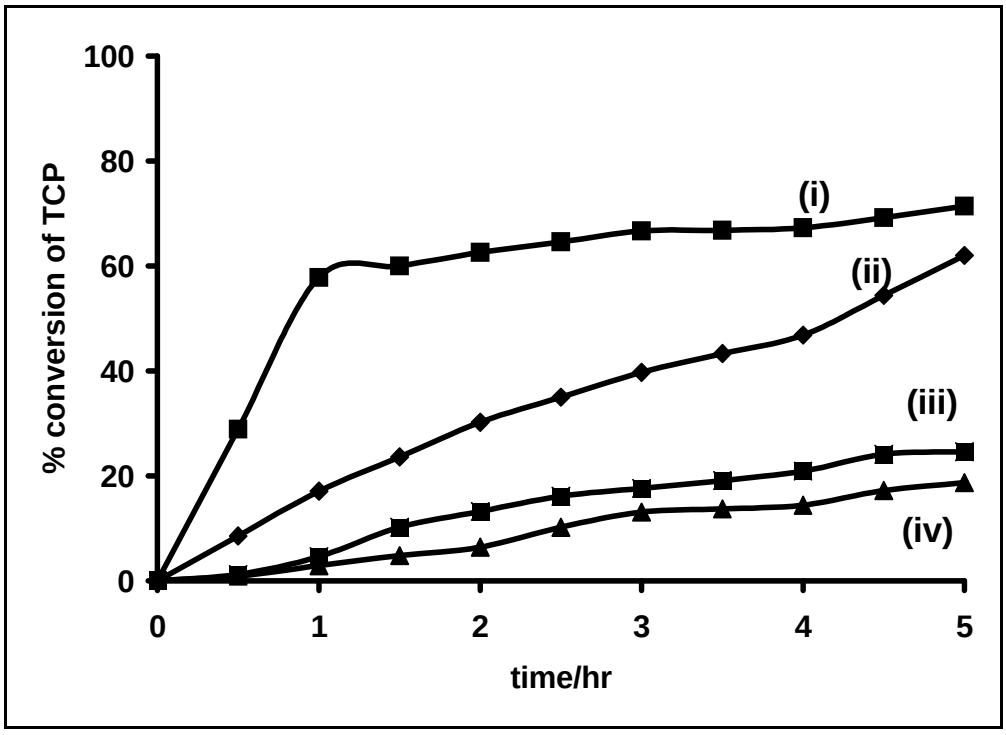

Figure 4.5: Effect of pH on the rate of oxidative degradation of TCP in pH 7 (curve i) and water/methanol (curve ii) in the presence of $CoPcS_4$ (**24**). Curves iii (pH 7) and curve iv (water/methanol) are in the absence of the $CoPcS_4$ (**24**) catalyst (1% loading). Starting concentration of TCP =1 x 10^{-2} mol L^{-1}. $[H_2O_2]$ = 1 x 10^{-2} mol L^{-1}.

4.1.3 Product identification

Figures 4.6 and 4.7 respectively show the HPLC traces obtained for the catalysis of 2-CP and TCP by H_2O_2 in the presence of $CoPcS_4$ (**24**) catalyst under water/methanol conditions and after 5 hours reaction time. New peaks started to emerge after about 60 minutes of reaction for both 2-CP and TCP. The peaks were clearly identified using HPLC by spiking with pure compounds and with LC-MS. For 2-CP the products are hydroquinone (HQ), phenol (PH), benzoquinone (BQ) and maleic acid (MA), Figure 4.6. The intensity of the product peaks increased with time while that of the parent 2-CP peak decreased. The formation of maleic acid is an indication that the catalytic oxidative degradation of these substrates including ring cleavages.

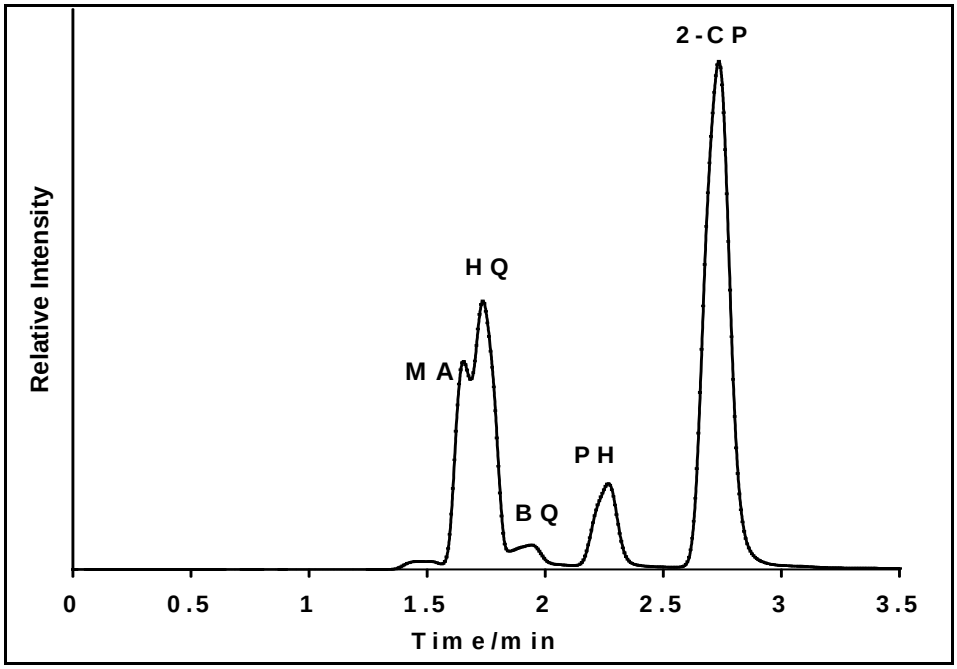

Figure 4.6: HPLC traces obtained after 5 hours of transformation of 2-chlorophenol in water/methanol mixture. Starting concentration of 2-CP =1 x 10^{-2} mol L^{-1}. [H_2O_2] = 1 x 10^{-2} mol L^{-1}. Catalyst: $CoPcS_4$ (**24**) (1% loading). HQ = hydroquinone, MA = maleic acid, BQ = benzoquinone, PH = phenol.

For TCP, peaks due to dichlorobenzoquinone (DCBQ), hydroquinone (HQ), phenol (PH) and maleic acid (MA) were observed, Figure 4.7. The first step when iron(II)tetrasulphonated phthalocyanine ($FePcS_4$)[14] and iron octacarboxyphthalocyanine (FeOCPc)[51] were employed as catalysts for hydrogen peroxide oxidation of TCP was reported to be the formation of dichlorobenzoquinone, which subsequently transformed to the formic acid, oxalic acid, 3-chloro-2-propenoic acid, dichloroacetate, and a small amount of oxidative coupling products.[51] In this work, however, it was observed that for TCP, after about 180 minutes of reaction, the phenol (PH) peak was formed and increased in intensity accompanied by a reduction in the peak intensity of the dichlorobenzoquinone. This trend is attributed to the transformation of dichlorobenzoquinone to mostly phenol and possibly other oxidative products.

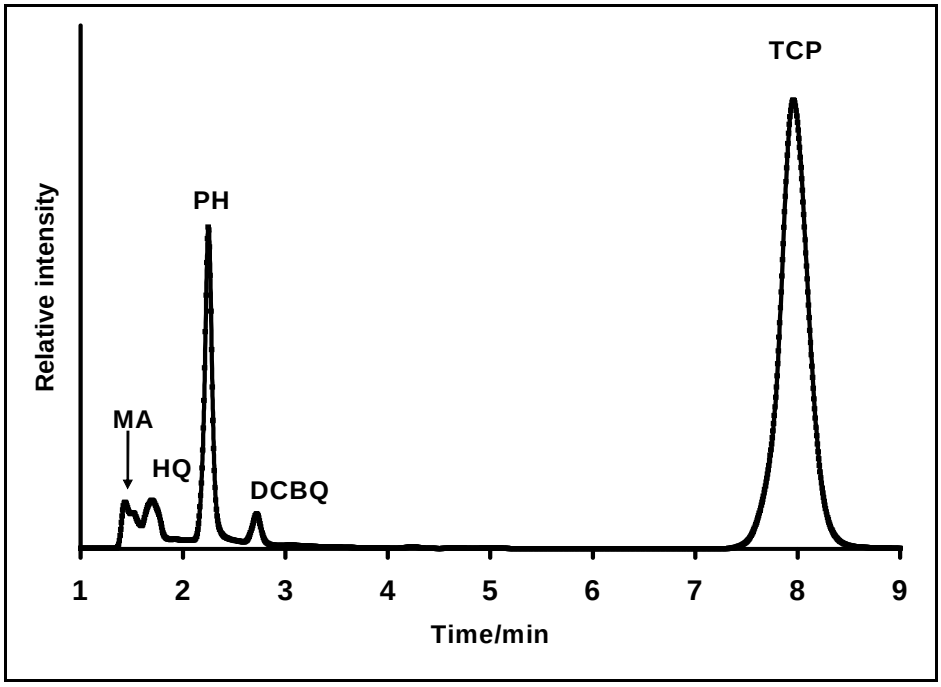

Figure 4.7: HPLC traces obtained after 5 hours of transformation of 2,4,5-trichlorophenol in water/methanol mixture. Starting concentration of TCP = 1 x 10^{-2} mol L^{-1}. [H_2O_2] = 1 x 10^{-2} mol L^{-1}. Catalyst: $CoPcS_4$ (**24**) (1% loading). DCBQ = dichlorobenzoquinone. Other abbreviations are as in Figure 4.6.

Figures 4.8 and 4.9 show the chromatograms of the 2-CP and TCP degradation respectively after 5 hours, under pH 10 and 7 conditions, respectively. The products formed under pH 7 and 10 conditions were different from those formed when methanol/water solvent mixture was employed. The main products of oxidation were benzoquinone (for 2-CP at pH 10, Figure 4.8) and 2,5-dichlorobenzoquinone (for TCP at pH 7, Figures 4.9). In both cases smaller amounts of maleic acid were formed. The formation of benzoquinone or dichlorobenzoquinone is desirable since these molecules are readily degraded. Thus fewer products were formed under pH 7 and 10 conditions in contrast to a wider variety of products formed in water/methanol solvent mixture. In particular, phenol is not formed at high pH. This proves that the use of different solvents and/or solution pH (hence the presence of either ionised or unionised forms of the phenols) is a determining factor in the type of oxidation products obtained during MPc catalysed oxidation of chlorophenols. The aggregated nature of $CoPcS_4$ (**24**) under pH 7 and 10 conditions may also contribute to the different products compared to when the monomeric form in water/methanol is employed.

In general, it should be stated that the oxidation products composition can not be accurately predicted and this could also depend on the experimental conditions.

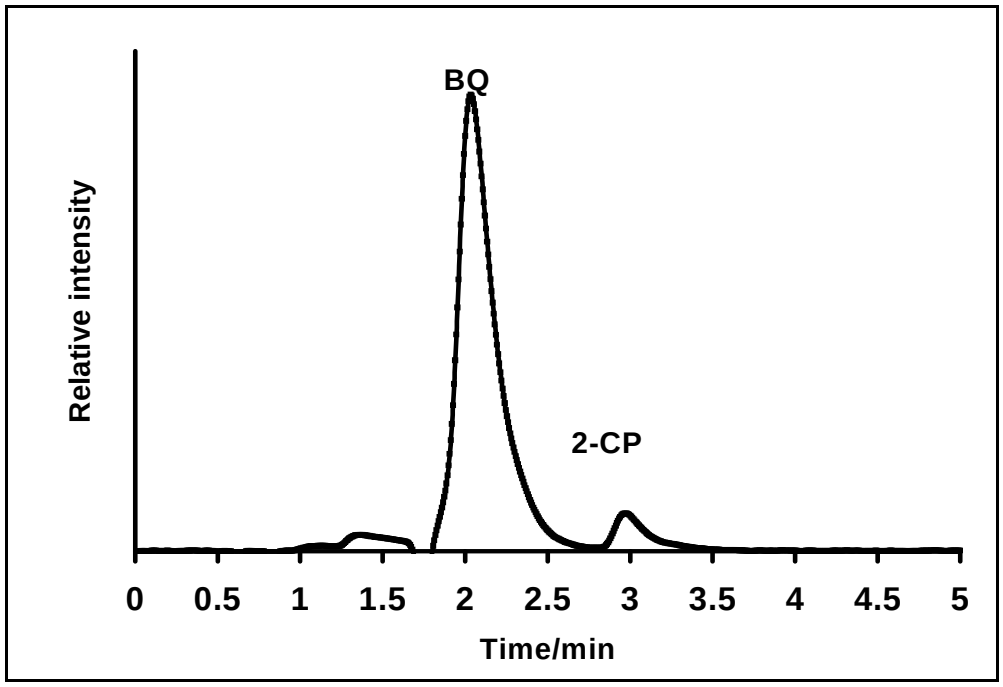

Figure 4.8: HPLC traces obtained after 5 hours of transformation of 2,4,5-trichlorophenol in pH 7.0 buffer solution. Starting concentration of TCP = 1 x 10^{-2} mol L^{-1}. [H_2O_2] = 1 x10^{-2} mol L^{-1}. Catalyst: $CoPcS_4$ (**24**) (1% loading).

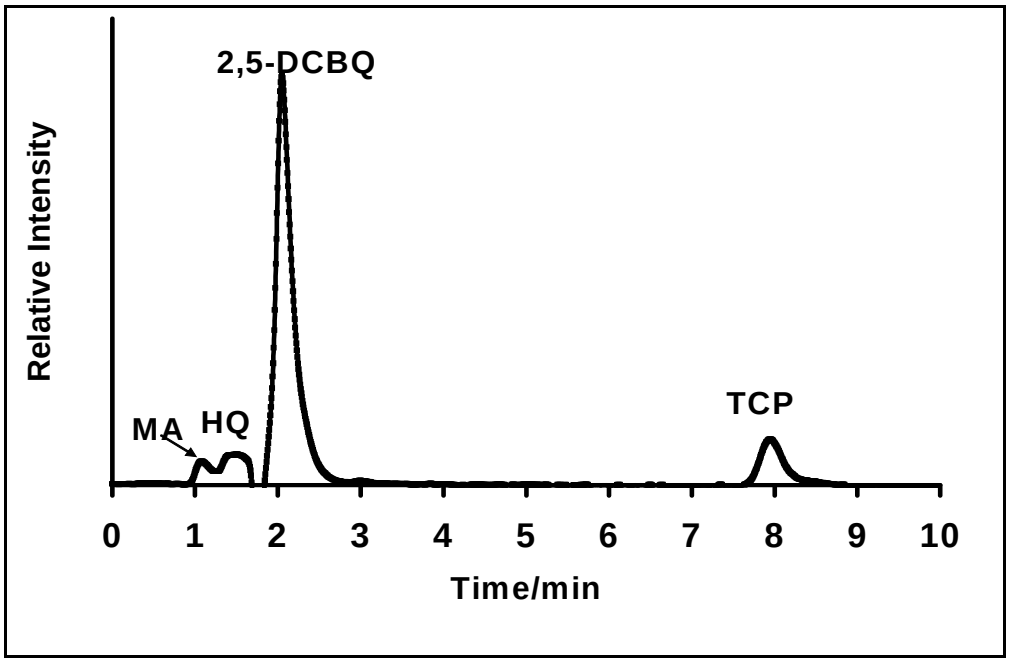

Figure 4.9: HPLC traces obtained after 5 hours of transformation of 2-chlorophenol in pH 10.0 buffer solution. Starting concentration of 2-CP = 1 x 10^{-2} mol L^{-1}. [H_2O_2] = 1 x 10^{-2} mol L^{-1}. Catalyst: $CoPcS_4$ (**24**) (1% loading).

4.1.4 The fate of the catalyst

Addition of hydrogen peroxide to $CoPcS_4$ (**24**) solutions in pH 7, resulted in the decrease in the intensity of the aggregate peak and the increase and shifting of the monomeric peak (Figure 4.10) showing that the aggregated form of $CoPcS_4$ (**24**) is monomerised by hydrogen peroxide oxidant. Thus under pH 7 or pH 10 conditions, the monomer is formed first on addition of hydrogen peroxide, followed by a shift to longer wavelengths (662 to 666 nm, Figure 4.10) which is an indication of oxidation of the central metal and the formation of the $Co^{3+}PcS_4$ species. The original spectrum could partly be regenerated by addition of sodium borohydride ($NaBH_4$), spectrum (iii) in Figure 4.10. Spectral studies on the fate of the $CoPcS_4$ (**24**) catalyst during the catalytic reaction were also undertaken in water/methanol solvent mixture. Addition of hydrogen peroxide to solutions of $CoPcS_4$ (**24**), resulted in spectral changes shown in Figure 4.11. There was a shift in the Q band from 660 to 665 nm, an increase in absorption in the 480 nm area as well as decrease in the intensity of the Q band. The shift in the Q band is consistent with metal oxidation of $Co^{2+}PcS_4$ to $Co^{3+}PcS_4$.[101] The broad peak around 480 nm suggests ring oxidation. Thus addition of hydrogen peroxide to solutions of $CoPcS_4$ (**24**) resulted in both metal and ring oxidation of $CoPcS_4$ (**24**), accompanied by degradation of the ring. Addition of reducing agents ($NaBH_4$) to solution of Figure 4.11, (following oxidation with hydrogen peroxide) resulted in the decrease in 480 nm peak and a shift of the Q band back to 660 nm. In the presence of 2-CP or TCP, spectral changes shown in Figure 4.12 were observed when using methanol/water. As catalysis progressed there was a gradual decrease in the intensity of the Q band of the $CoPcS_4$ (**24)** catalyst, Figure 4.12, suggesting catalyst degradation as is typical[390] of MPc catalysts in homogeneous

catalysis. There was an increase in background between 400 and 500 nm, which suggests the involvement of ring-based oxidation of the phthalocyanine ring during the catalytic oxidation of the phenols. However the shift in the Q band observed in the presence of hydrogen peroxide alone was not observed when both hydrogen peroxide and the phenols were present. This suggests that the $Co^{3+}PcS_4$ species is readily reduced back to the $Co^{2+}PcS_4$ species through oxidation of the phenols. The colour of the solution changed from blue to green to colourless as catalysis progressed. However the reaction products continued to form even after the catalyst had turned colourless, suggesting that once reaction intermediates are formed, the reaction can still proceed in the presence or absence of the original form of the catalyst. This indicates that the catalyst was still active even when the solution was colourless.

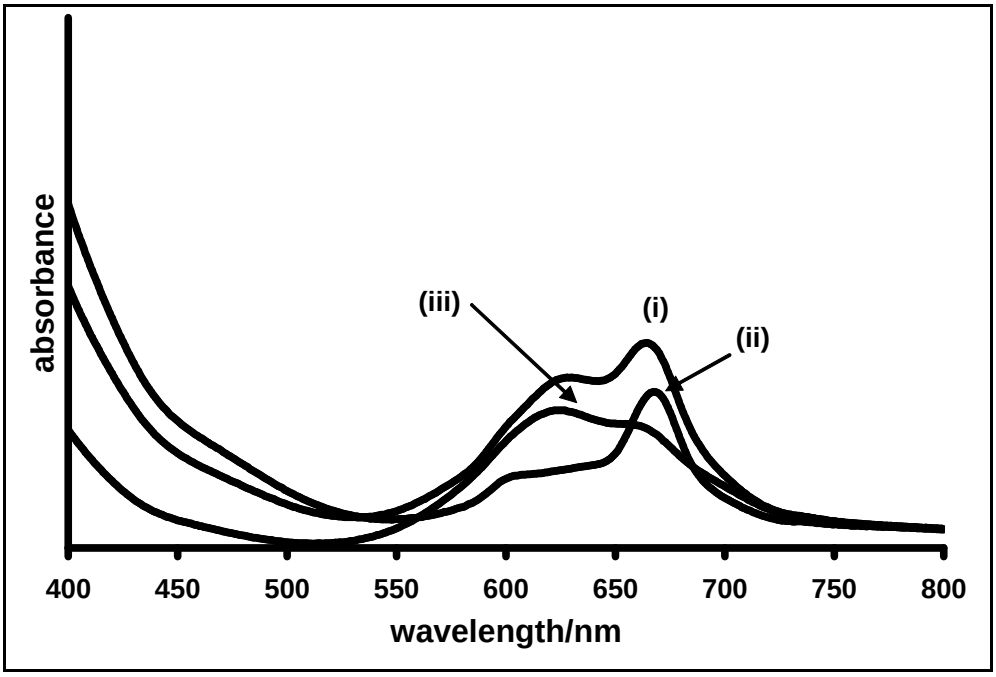

Figure 4.10: Electronic absorption spectra of 1 x 10^{-6} mol L^{-1} $CoPcS_4$ (**24**) in pH 7 (i) before, (ii) after addition of 0.02 M hydrogen peroxide. (iii) Spectrum obtained on addition of $NaBH_4$ to (ii).

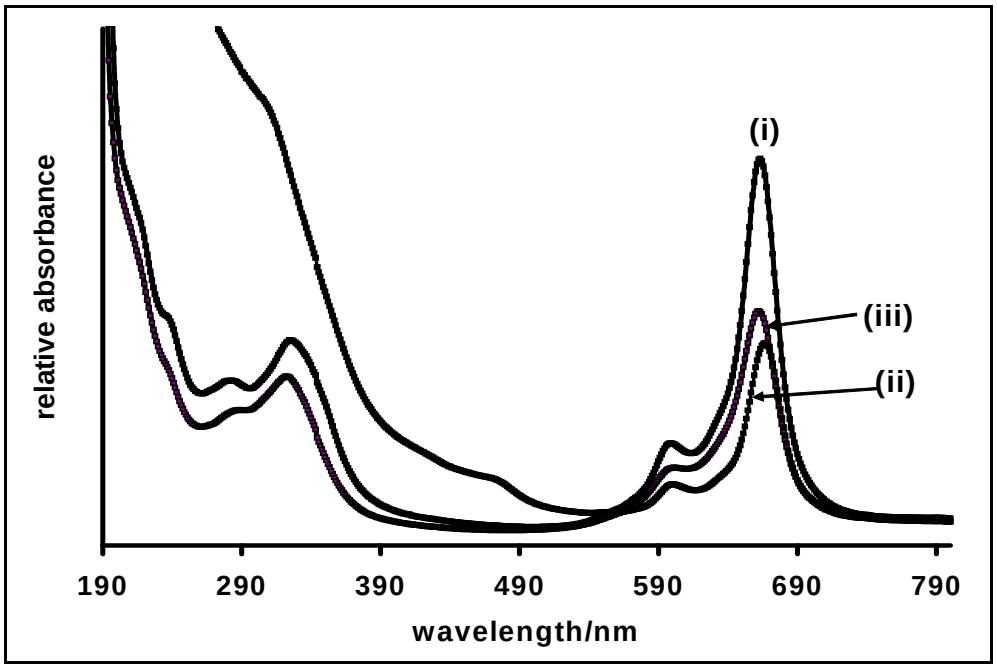

Figure 4.11: Electronic absorption spectra of 1 x 10^{-6} mol L^{-1} $CoPcS_4$ (**24**) in water/methanol solvent (i) before, (ii) after addition of 0.02 M H_2O_2. (iii) Spectrum obtained on addition of $NaBH_4$ to (ii).

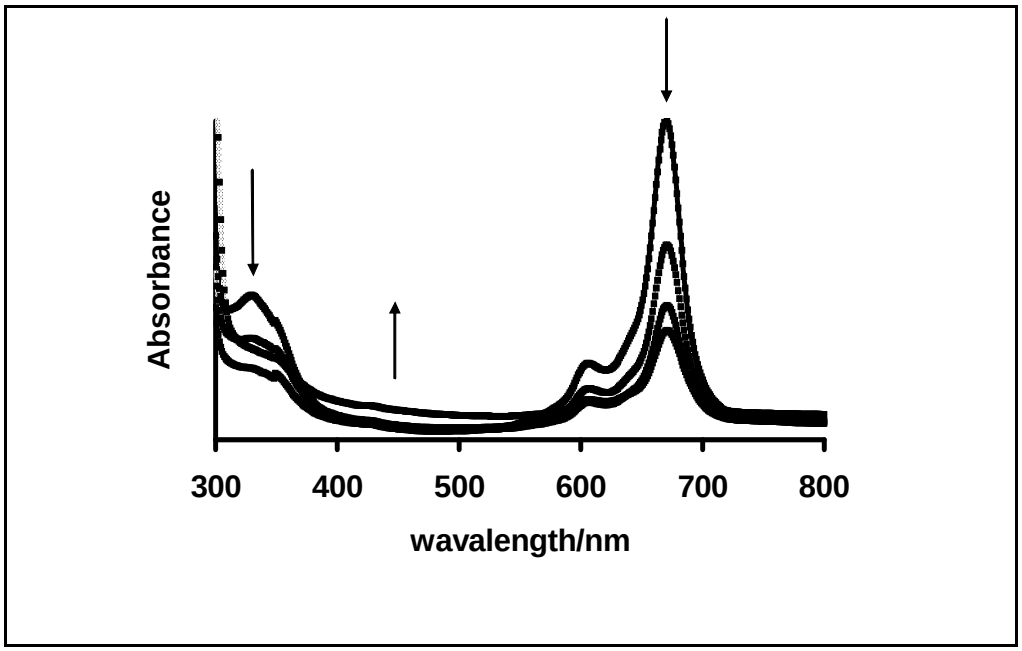

Figure 4.12: Electronic absorption spectral changes observed for 1 x 10^{-6} mol L^{-1} $CoPcS_4$ (**24**) in water/methanol solvent mixture as catalysis proceeds. Starting concentration of 2-CP = 1 x 10^{-2} mol L^{-1}. [H_2O_2] = 1 x 10^{-2} mol L^{-1}. Catalyst: $CoPcS_4$ (**24**) (1%).

4.1.5 Effects of the nature of MPc central metal ion

It is known that the central metal ion of the MPc catalyst has significant influence on the catalytic activities. Studies were carried out on other metallo-tetrasulphophthalocyanine ($MPcS_4$) complexes: $NiPcS_4$, $AlPcS_4$ and $CuPcS_4$, using similar experimental conditions as for $CoPcS_4$ (**24**). In contrast to $CoPcS_4$ (**24**), these other $MPcS_4$ complexes exhibited no measurable oxidative catalytic conversion of the chlorophenols investigated in this work (Figure 4.13, 2-CP and 4.14, TCP). The central Al and Cu metal ions in both AlTSPc and CuTSPc exist in only one oxidation state and hence cannot be oxidised. Surprisingly, however, Seelan and Sinha[391] recently reported that when CuPc and CoPc were encapsulated in zeolite-Y, CuPc exhibited higher phenol hydroxylation activity with H_2O_2 than CoPc. The authors attributed this observation to the changes in molecular and electronic structures of the MPc complexes on encapsulation. It may therefore be concluded that the enhanced catalytic activity observed in this present work for $CoPcS_4$ (**24**) over $CuPcS_4$ could partly be associated with the retention of the molecular and electronic structures of the MPc complexes in homogeneous catalysis for the former. There was no significant change in the intensity of the Q band during the H_2O_2 oxidation of phenols in the presence of $NiPcS_4$, $CuPcS_4$ and $AlPcS_4$, contrary to the observation for $CoPcS_4$ (**24**), where the Q band decreased in intensity as the reactions proceeded (Figure 4.12).

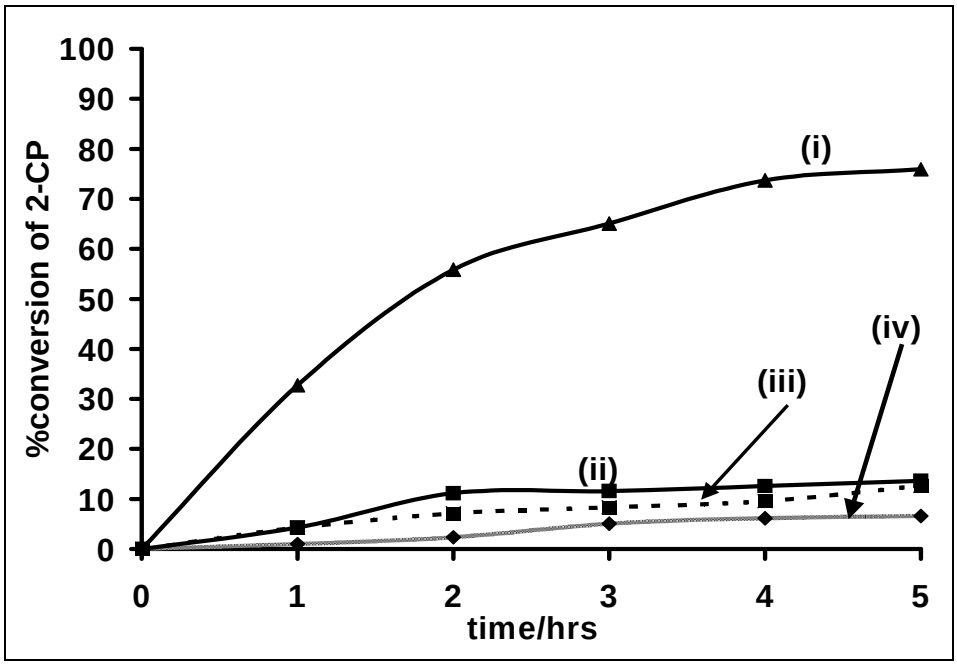

Figure 4.13: Comparative plots of percentage conversion of the 2-CP vs. time using (i) $CoPcS_4$, (ii) $NiPcS_4$ (iii) $CuPcS_4$ and (iv) $AlPcS_4$. $MPcS_4$ = 1% loading; $H_2O_2 = 1 \times 10^{-2}$ mol L^{-1}. Starting concentration of 2-CP $=1 \times 10^{-2}$ mol L^{-1}.

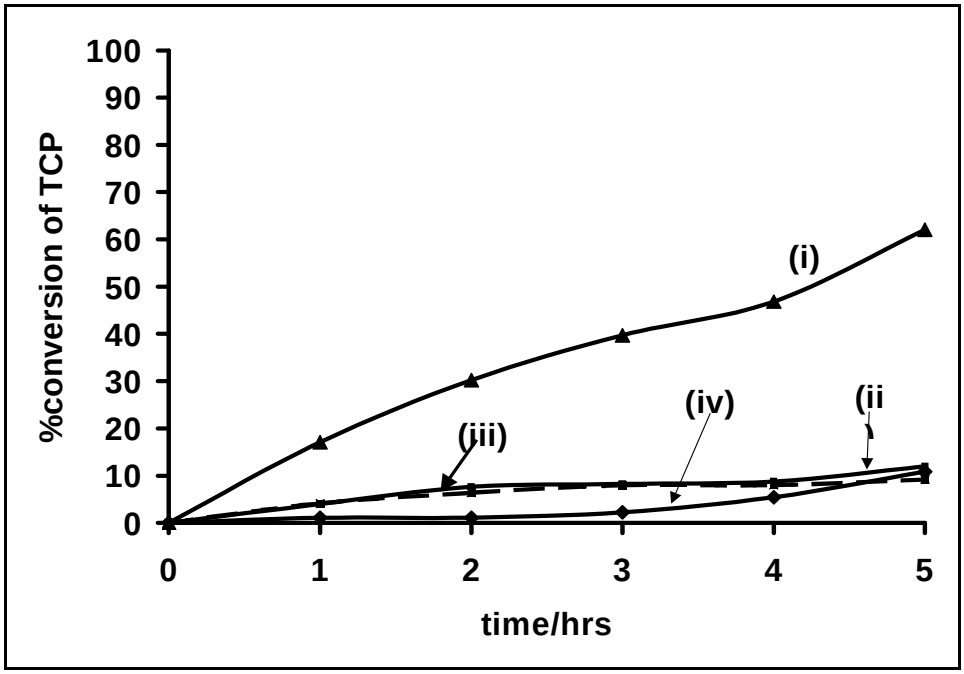

Figure 4.14: Comparative plots of percentage conversion of the TCP vs. time using (i) $CoPcS_4$, (ii) $NiPcS_4$ (iii) $CuPcS_4$ and (iv) $AlPcS_4$. $MPcS_4$ = 1% loading; $H_2O_2 = 1 \times 10^{-2}$ mol L^{-1}. Starting concentration of TCP $=1 \times 10^{-2}$ mol L^{-1}.

Figure 4.15 compares the changes in absorbance of the $CoPcS_4$ (**24**) and $NiPcS_4$ during the reaction. The Ni central metal ion in $NiPcS_4$ could be oxidised from +2 to +3; although this has been a subject of some controversy.[361,392-394] Recent reports have shown that $NiPcS_4$ has electrocatalytic activity towards 2-CP[361] and hydrazine[392] in the solid state, when adsorbed onto the electrode. The Ni^{3+}/Ni^{2+} redox couple has however not been observed electrochemically in solution. The lack of catalytic activity for the hydrogen peroxide oxidation of chlorophenols could be due to the absence of Ni^{3+}/Ni^{2+} couple in solution. As with nickel porphyrin complexes,[395] the Ni^{3+}/Ni^{2+} couple may occur in the solid state for NiPc complexes. NiPc complexes, like the main group MPcs (such as ZnPc and MgPc) whose metal ions have no accessible d-orbital levels lying in the HOMO-LUMO gap are redox-inactive with respect to their metal centers,[385] this situation is probably different for adsorbed NiPc complexes.

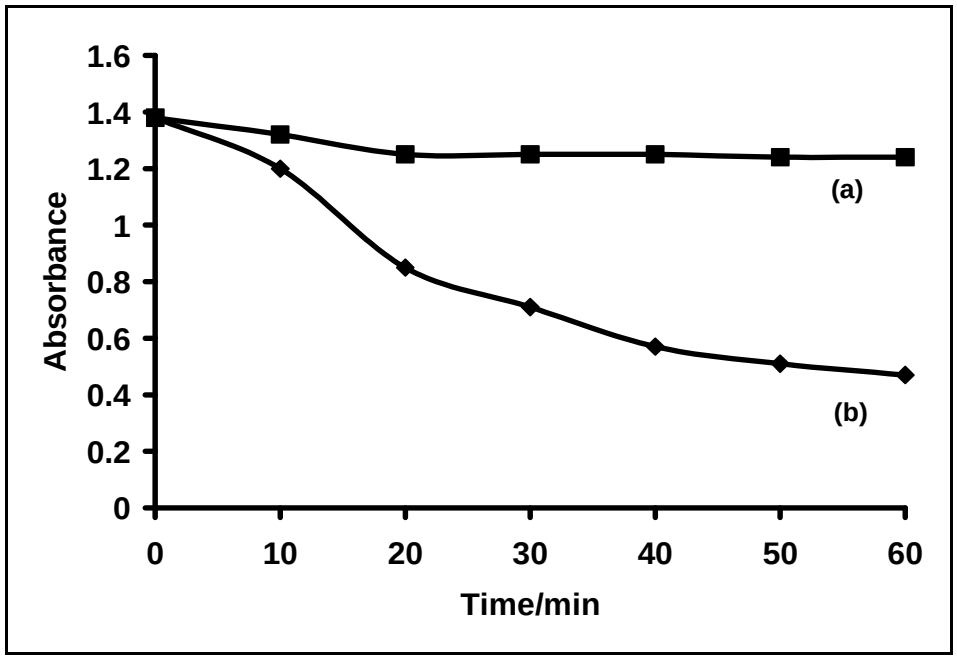

Figure 4.15: Changes in the Q band absorption for (a) $NiPcS_4$ and (b) $CoPcS_4$ during catalysis for TCP oxidation by hydrogen peroxide. $MPcS_4$ = 1% loading $H_2O_2 = 1 \times 10^{-2}$ mol L^{-1}. Starting concentration of TCP = 1×10^{-2} mol L^{-1}.

4.2 Phototransformation of chlorophenols

4.2.1 Immobilisation of MPc complexes

It is well known that the catalytic and photocatalytic activities of immobilised phthalocyanine complexes depend, amongst other factors, on the nature of the support.[314,396] Many literature reports on the immobilisation of MPc complexes onto polymer supports involved interaction between the functionalised solid polymer and a suitably functionalised MPc leading to mainly covalently bonded MPc. In this work, Amberlite® IRA-900 was used. Amberlite® IRA-900 ion exchange resin is a strongly basic, macro-reticular resin of moderately high porosity with benzyltrialkylammonium functionality and chloride moieties (Scheme 4.2a). Each of the sulphonated MPc sensitizers were attached to the resin by simply mixing it with resin beads in an aqueous solution (unbuffered). For the MOCPc complexes, pH 8 was employed in order to allow for ionisation. Scheme 4.2b presents schematic representations of the immobilised sulphonated and carboxylated MPc complexes onto Amberlite®.

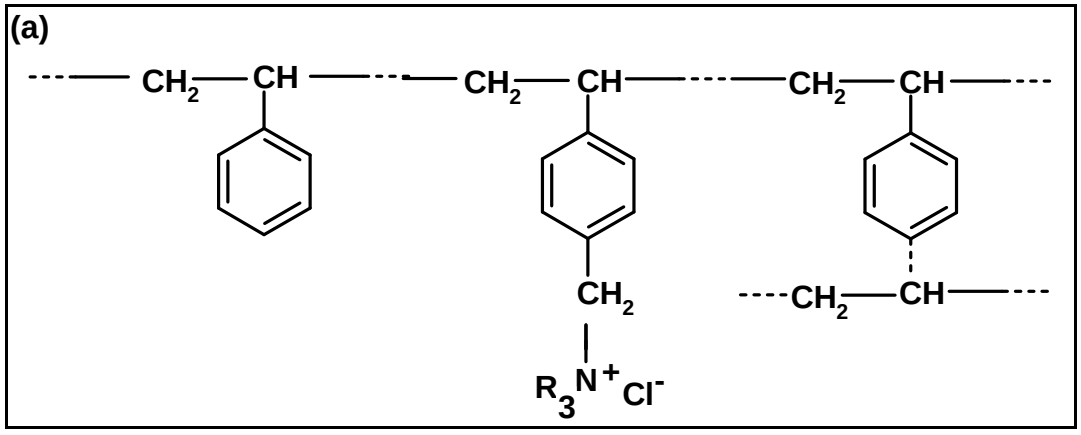

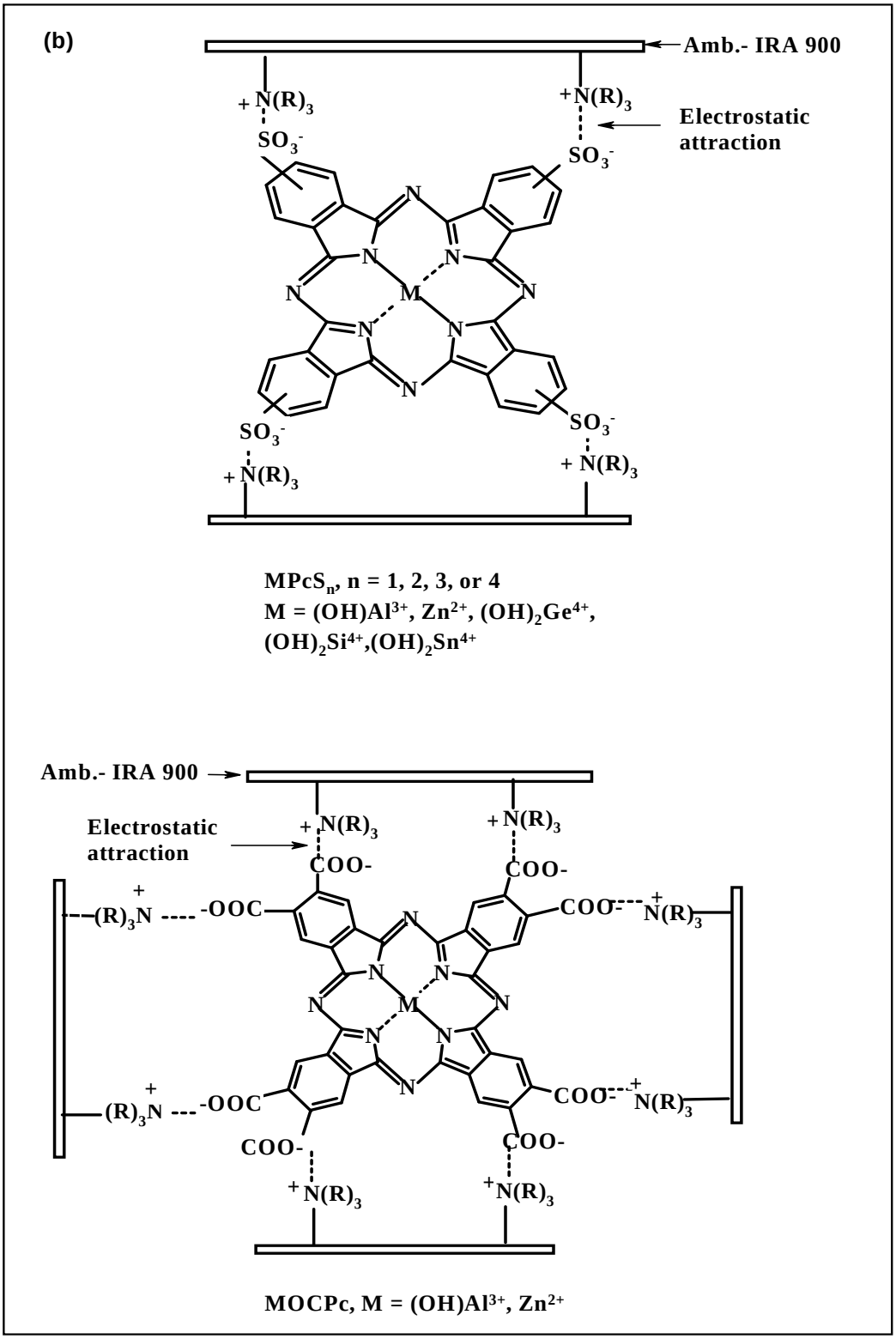

Scheme 4.1: (a) Structure of Amberlite® IRA 900 and (b) schematic representation of photosensitisers immobilised on Amberlite® IRA 900.

The immobilisation of the MPc onto the solid support was confirmed by the colour change of the polymer beads (white to light green or blue) and also by reflectance spectra measurements of the support following immobilisation. It was observed that each MPc effectively bonded to the resin and, upon bonding, these MPc complexes cannot be easily removed by washing with solvents such as water, acetonitrile, and methanol. This was confirmed by the electronic spectral measurements of the 'wash' solvents, which did not show any detectable spectral bands (B or Q bands) characteristic of the MPc after soaking the MPc-resin in the respective solvents overnight.

The concentration of the MPc immobilised onto the solid support could be estimated spectroscopically by measuring the decrease in the absorbance of the Q band of the MPc after treating it with a known amount of the Amberlite®. Figure 4.16 is an example of spectral changes observed for the MPc sensitiser during immobilisation of AlOCPc onto Amberlite®. Thus, this could conveniently be used to vary MPc loading per gram of Amberlite®.

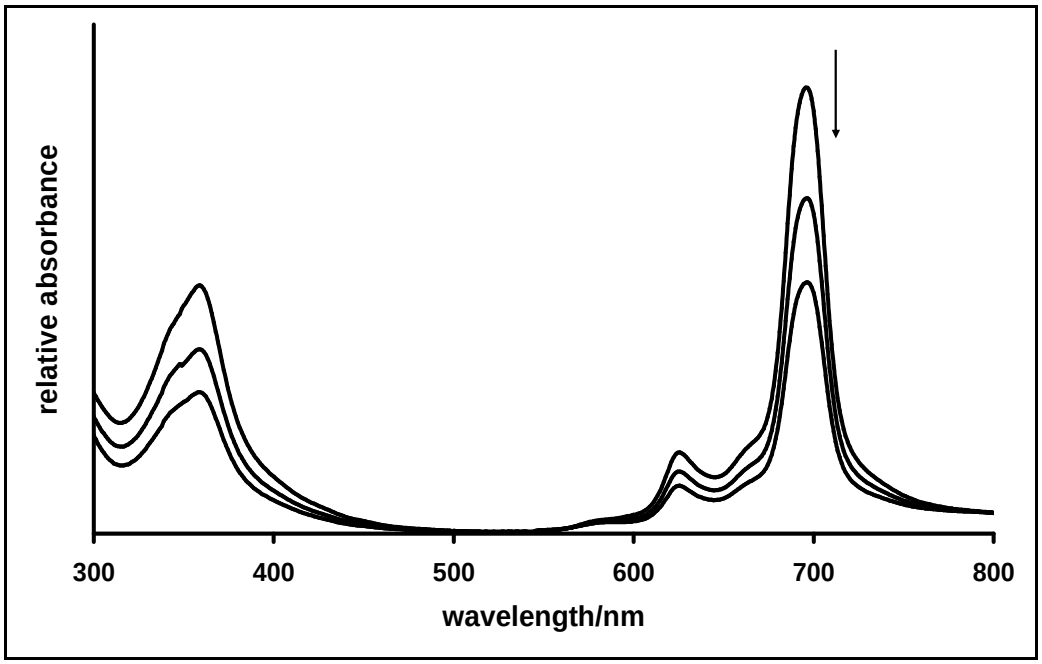

Figure 4.16: Electronic spectral changes with time of AlOCPc in aqueous (pH 8) solution during its immobilisation on Amberlite® support. Starting concentration of AlOCPc = 1.42 x 10^{-5} M. Mass of Amberlite® = 0.01 g.

As already stated, aggregation on MPc complexes is evidenced[101] by a high energy band near 620 nm, and a low energy band near 670 nm (or higher) is due to the monomeric species. The complex was mainly monomeric as expected when MPcs are immobilised. Figure 4.17 shows spectra of $AlPcS_4$ at different MPc loadings (mg MPc/ g Amberlite®), indicating that aggregation increases with increase in MPc concentration on the support as evidenced by the increase in the aggregate peak at 645 nm relative to monomer peak at 707 nm. This behaviour is due to self-association or intermolecular interactions between phthalocyanine complexes as the concentration of the immobilised MPc increases; the nature and processes that lead to this phenomenon are well described in the literature.[396-398] For studies shown in Figure 4.17, moles of the MPc photosensitizer were not calculated due to aggregation of MPc at the high concentration employed (to show aggregation effects), hence the loadings are expressed as mg MPc/ g Amberlite®.

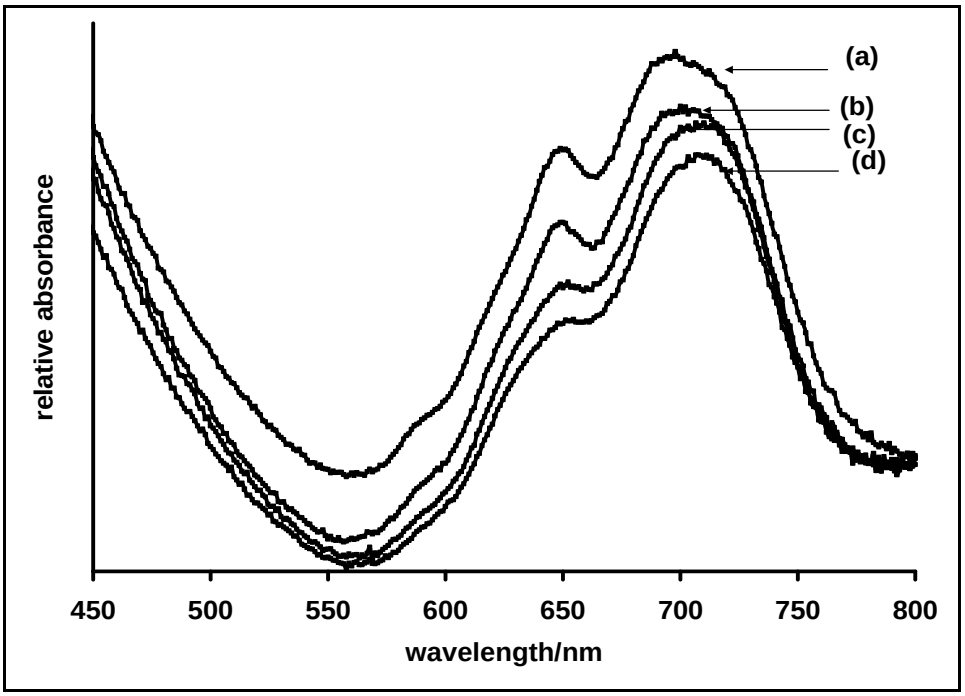

Figure 4.17: Diffuse reflectance spectra of $AlPcS_4$-Amberlite showing the effects of aggregation. Different loading on Amberlite® support (a) 1.25, (b) 1.00, (c) 0.75, (d) 0.5 $AlPcS_4$(mg)/ Amberlite®(g). The immobilisation of $AlPcS_4$ on Amberlite® was carried out in unbuffered and allowed to proceed until the Q band of the photosensitiser disappeared completely.

Figure 4.18a-c shows the diffuse reflectance spectra of the different immobilised MPc photosensitisers Amberlite®. As expected and explained before, mainly the low energy band due to the monomer is observed when the MPc complexes were immobilised onto Amberlite®. The Q bands are generally broad, this is usual for solid state electronic spectra of MPc complexes.[110-113]

A significant effect of immobilised MPc complexes (compared to solution spectra) was the shift in the Q band due to the monomeric species to lower energies (except for $ZnPcS_4$ (**26**), $SiPcS_{mix}$ (**32**) and $SnPcS_{mix}$ (**33**), Table 4.1.

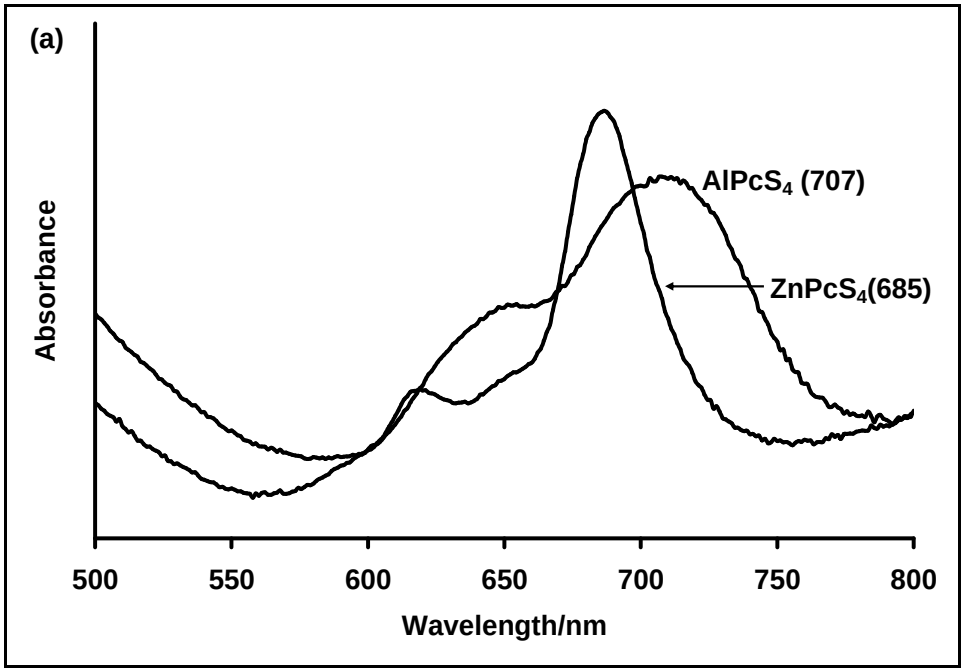
(a)
Absorbance
AlPcS4 (707)
ZnPcS4(685)
500
550
600
650
700
750
800
Wavelength/nm

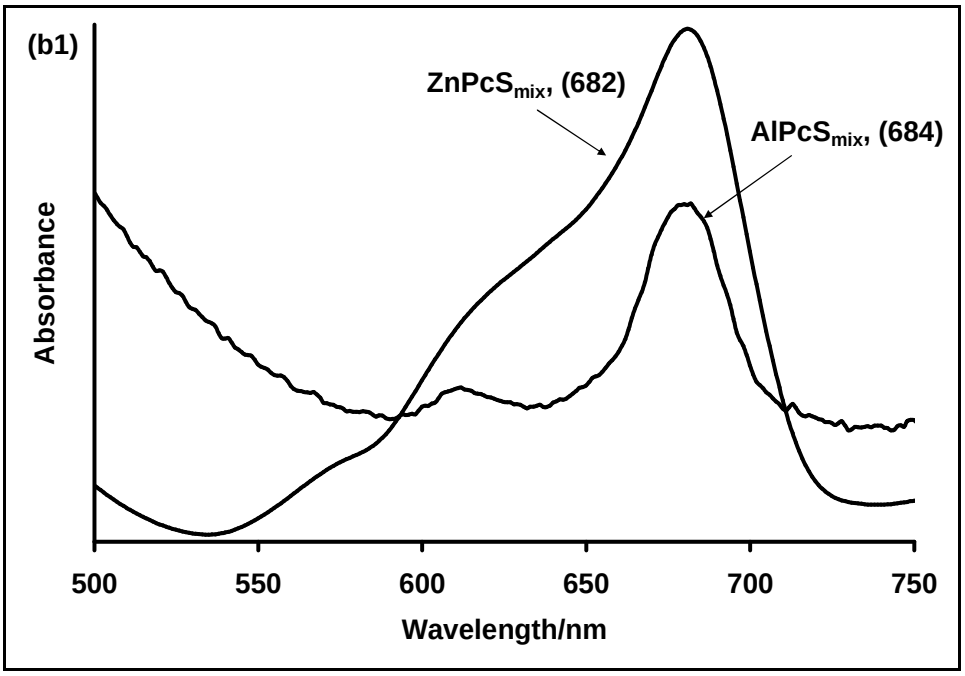
(b1)
Absorbance
ZnPcSmix, (682)
AlPcSmix, (684)
500
550
600
650
700
750
Wavelength/nm

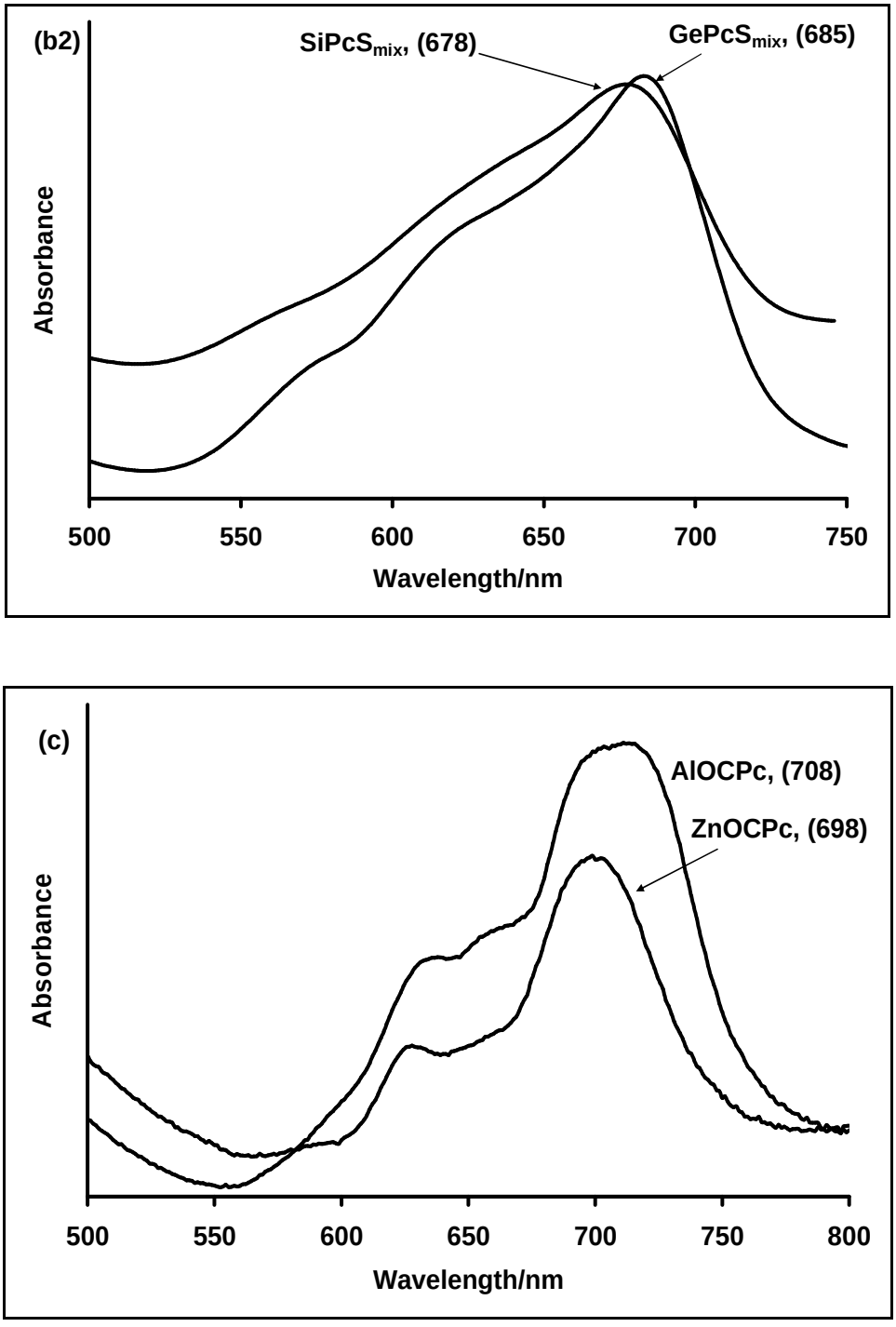

Figure 4.18: Diffuse reflectance spectra of (a) $MPcS_4$, (b) $MPcS_{mix}$ and (c) MOCPc on Amberlite.

Table 4.1: UV-Vis spectra data obtained for the MPc complexes

Catalyst	Q band in aqueous solution[a]	Q band on support[b]
$AlPcS_4$ (**25**)	660 (d), 690 (m)	707
$ZnPcS_4$ (**26**)	652 (d), 692 (m)	685
AlOCPc (**27**)	694	708
ZnOCPc (**28**)	689	698
$AlPcS_{mix}$ (**29**)	681	684
$ZnPcS_{mix}$ (**30**)	615 (d), 675 (m)	682
$GePcS_{mix}$ (**31**)	677	685
$SiPcS_{mix}$ (**32**)	685	678
$SnPcS_{mix}$ (**33**)	647 (d), 697 (m)	695

[a] Electronic absorption spectra. [b] Diffuse reflectance spectra

Such a red shift is an indication that the energy gap between the highest occupied molecular orbital (HOMO) and lowest unoccupied molecular orbital (LUMO) of the phthalocyanine is narrower than when it is in solution. The strong phthalocyanine-polymer interaction is expected to push the HOMOs of the phthalocyanine energetically up due to enhanced electron density on the π-framework caused by the tilted anionic sulphonato or carboxylic groups. Thus, the electronic transition from the low-lying filled π orbital to the π* orbital (LUMO) would occur at lower energy. Inbaraj et al[399] reported similar observation for tetrasulphometalloporphyrin complexes immobilised onto solid polystyrene support, which also was attributed to the distortion of the porphyrins from planarity.

4.2.2 Efficiency of singlet oxygen generation

All photochemical studies were restricted to 5 x 10^{-8} mol photosensitiser/ Amberlite® (0.01 g) so that the photosensitisation of the various MPcs could be compared.

The potential applications of these immobilised photosensitizers for water treatment will depend on the production rate of singlet oxygen in the aqueous system. The relative efficiencies of the generation of singlet oxygen by these sensitizers was monitored spectrophotometrically by following the decay of tetrasodium (anthracene-9, 10-diyl) dimethylmalonate (ADMA) (a singlet oxygen scavenger) at λ = 379 nm. The rate of bleaching of ADMA is directly proportional to the production rate of singlet oxygen. Figure 4.19 shows typical spectral changes observed for the degradation of ADMA during photosensitised reaction of the ZnOCPc (**28**) supported onto Amberlite® in aqueous solution. In Figure 4.19, the solution absorption spectrum of the MPc photosensitizer is not observed since MPc is immobilised on Amberlite®.

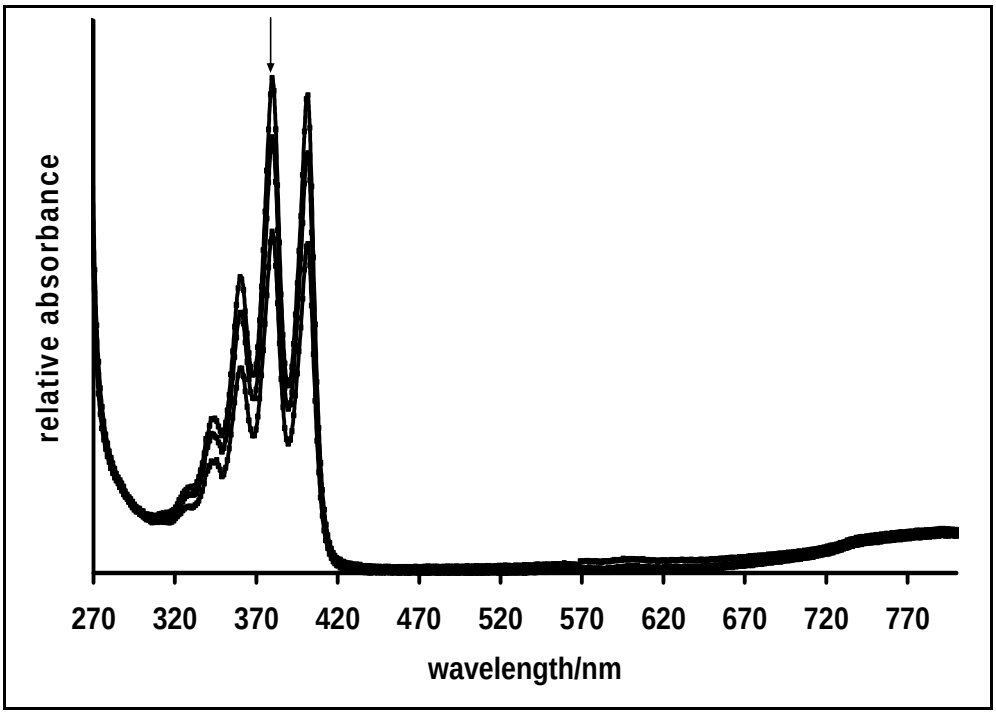

Figure 4.19: Electronic absorption spectral changes of ADMA during visible light photolysis, catalysed by ZnOCPc-Amberlite. ADMA concentration = 7.4×10^{-5} M.

Table 4.2 shows the percentage bleaching of ADMA by the photosensitizers, which is directly proportional to singlet oxygen production by the immobilised phthalocyanine complexes. From the Table 4.2, singlet oxygen generation by the photosensitisers follows the following trend: $SnPcS_{mix}$ (**33**) > ZnOCPc (**28**) > $GePcS_{mix}$ (**31**) = $SiPcS_{mix}$ (**32**) > $ZnPcS_{mix}$ (**30**) > $ZnPcS_4$ (**26**) > $AlPcS_{mix}$ (**29**) > AlOCPc (**27**) > $AlPcS_4$ (**25**). In DMF, where aggregation is expected to be minimal, Gerdes et al[49] reported the following trend: $ZnPcS_4 > SiPcS_4 > GePcS_4 > AlPcS_4$ for singlet oxygen production which is comparable to the singlet oxygen generation reported in this work (considering the same ring system and changes in the central metal), except for $ZnPcS_4$ (**26**). The participation of $^1O_2$ in the photolysis was further confirmed by the addition of sodium azide, which is a $^1O_2$

quencher, to the chlorinated phenol photolysis reaction. Photolysis did not occur with any of the immobilised MPc in the presence of sodium azide, hence confirming the participation of the singlet oxygen in this photocatalytic reaction.

Table 4.2: Singlet oxygen generation and chlorophenol percentage conversion data obtained for the MPc complexes

Catalyst	**% degradation of 7.4×10^{-5} M ADMA**	**% conversion of 1×10^{-3} M PCP**
$AlPcS_4$ (**25**)	3.8	6.2
$ZnPcS_4$ (**26**)	20.8	12.8
AlOCPc (**27**)	7.5	10.7
ZnOCPc (**28**)	41.5	29.8
$AlPcS_{mix}$ (**29**)	18.9	10.7
$ZnPcS_{mix}$ (**30**)	26.4	21.1
$GePcS_{mix}$ (**31**)	30.2	16.5
$SiPcS_{mix}$ (**32**)	30.2	24.4
$SnPcS_{mix}$ (**33**)	43.7	26.0

4.2.3 Photosensitised transformation of chlorophenols

4.2.3.1 Optimisation of phototransformation conditions

It is important to note that in the absence of immobilised photosensitizer no transformation of the chlorophenols using red light was observed following the photolysis in the Q band region of the MPc sensitiser. In order to determine the optimum amount of immobilised catalyst needed for the photosensitised transformation of the phenols, 2.5 x 10^{-3} M PCP (as an example) was photodegraded using different number of moles of the immobilised ZnOCPc, Figure 4.20. It was found that phototransformation of PCP (for 5 minutes) showed increase in the rate (determined by change in absorbance) with increase in the moles of the ZnOCPc immobilised on Amberlite® until the mole ratio of ZnOCPc (**28**) to PCP was 1 : 99. Further increase in the mole ratio did not result in the increase in the rate of phototransformation of PCP, suggesting that the best mole ratio of the immobilised MPc to PCP for a successful photodegradation reaction is approximately 1 : 99.

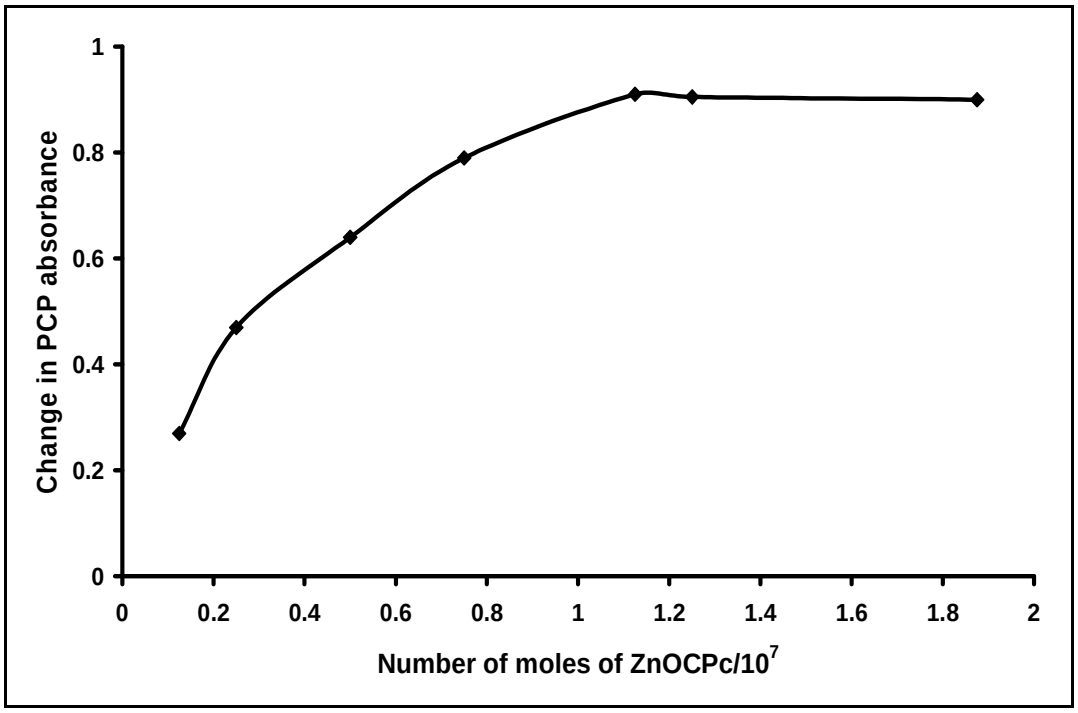

Figure 4.20: Effects of changing the concentration of ZnOCPc immobilised on Amberlite® on the % conversion of 2.5 x 10^{-3} M, PCP solution, as judged by the decrease in the absorbance spectra of the later. Photolysis time was 5 minutes.

4.2.3.2 Phototransformation of Chlorophenols

UV-Vis spectroscopy and HPLC were employed to monitor the transformation of chlorophenols. Figure 4.21 shows spectral changes which are typical for photosensitised transformation of the chlorophenols (4-CP is used as an example in Figure 4.21). As with singlet oxygen experiment, MPc loading of 5 x 10^{-8} mol g^{-1} Amberlite® was maintained for the comparative study of the photosensitised transformation of the chlorophenols (10^{-3} M). The photosensitised transformation activity with all MPc complexes followed a trend (4-CP > DCP > TCP > PCP) similar to that reported for these sensitisers in aqueous solution,[52,53] showing greater difficulty in photodegradation as the chlorine substituents increases. To compare the photosensitised efficiencies of the various immobilised MPc

complexes, PCP was chosen as a substrate. The experiment was performed at the optimised immobilised MPc: PCP mole ratio (1 : 99) at pH 10 conditions. Table 4.2 compares the percentage conversion of PCP in the presence of the MPc sensitisers and shows that the order of photoactivity of the MPc complexes was as follows: ZnOCPc (**28**) > $SnPcS_{mix}$ (**33**) > $SiPcS_{mix}$ (**32**) > $ZnPcS_{mix}$ (**30**) > $GePcS_{mix}$ (**31**) > $ZnPcS_4$ (**26**) > $AlPcS_{mix}$ (**29**) ~ AlOCPc (**27**) > $AlPcS_4$ (**25**). One of the remarkable results in this work is the high efficiency of ZnOCPc (**28**) over $SiPcS_{mix}$ (**32**) which is known for its high photocatalytic efficiency.[400] The degree of sulphonation of the $MPcS_{mix}$ did not play a major role in the photocatalytic activities of the photosensitisers, since the $MPcS_{mix}$ complexes containing more sulphonated derivatives ($GePcS_{mix}$ (**31**), $SiPcS_{mix}$ (**32**) and $AlPcS_{mix}$ (**29**)) show different catalytic activity from one another. Similarity in the trend of generation of singlet oxygen by the photocatalysis (Table 4.1) with the above trend for photodegradation of PCP was observed except for $GePcS_{mix}$ (**31**) which shows a larger rate of singlet oxygen production than $ZnPcS_{mix}$ (**30**), but shows a lower photocatalytic activity than the latter. Also $SnPcS_{mix}$ (**33**) shows a larger singlet oxygen production rate than ZnOCPc (**28**) but less catalytic activity towards the transformation of chlorinated phenols.

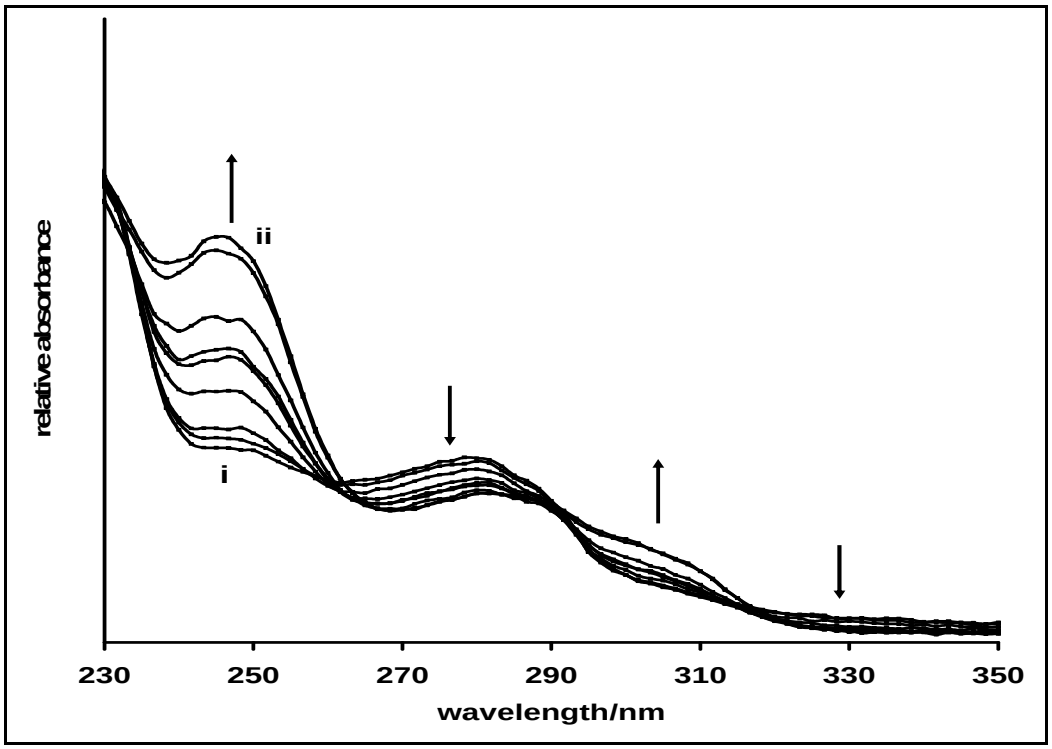

Figure 4.21: Electronic absorption spectral changes of 1 x 10^{-3} M 4-CP during its visible light photolysis in the presence of ZnOCPc-Amberlite.

Figure 4.22 and 4.23 present examples of HPLC chromatograms obtained on photolysis of the chlorophenols using PCP and DCP respectively as examples. The main products of the chlorophenol photooxidation were found to be the benzoquinone derivatives of the chlorophenols, confirmed by spiking with standard samples and by retention times. Thus, PCP gave 2,3,5,6-tetrachloro-1,4-benzoquinone(TCBQ), TCP gave 2,5-dichloro-1,4-benzoquinone (DCBQ), DCP gave 2-chloro-1,4-benzoquinone (CBQ) and 4-CP gave benzoquinone (BQ). Traces of fumaric acid (FA) were obtained for DCP (Figure 4.23).

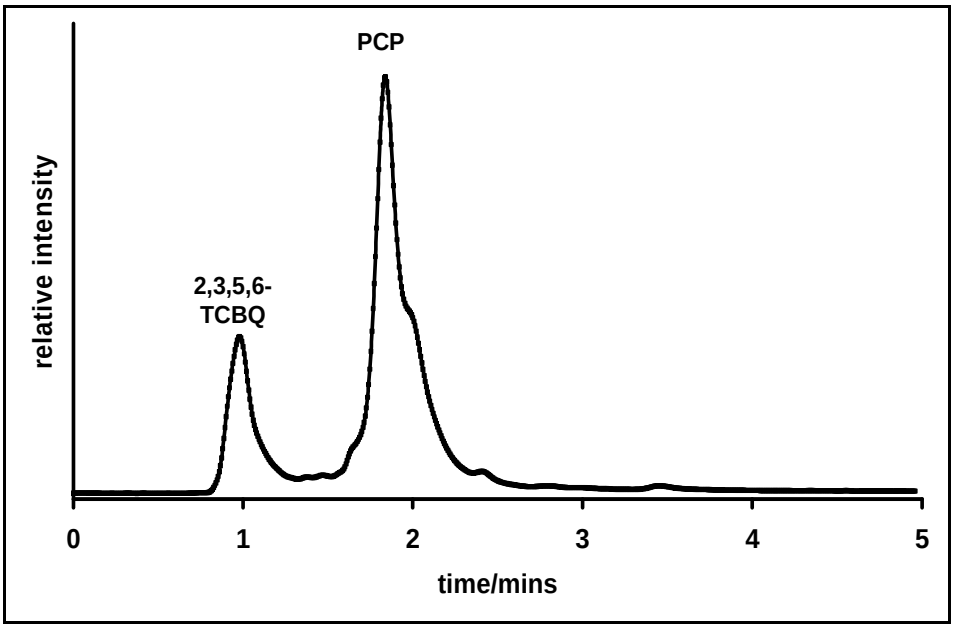

Figure 4.22: HPLC chromatogram of the reaction mixture after 1 x 10^{-3} M PCP photolysis (in the presence of ZnOCPc-Amberlite) showing formation of a new peak at t = 1 minute identified as 2,3,5,6-benzoquinone and the PCP peak at t = 1.8 minutes. TCBQ = tetrachlorobenzoquinone.

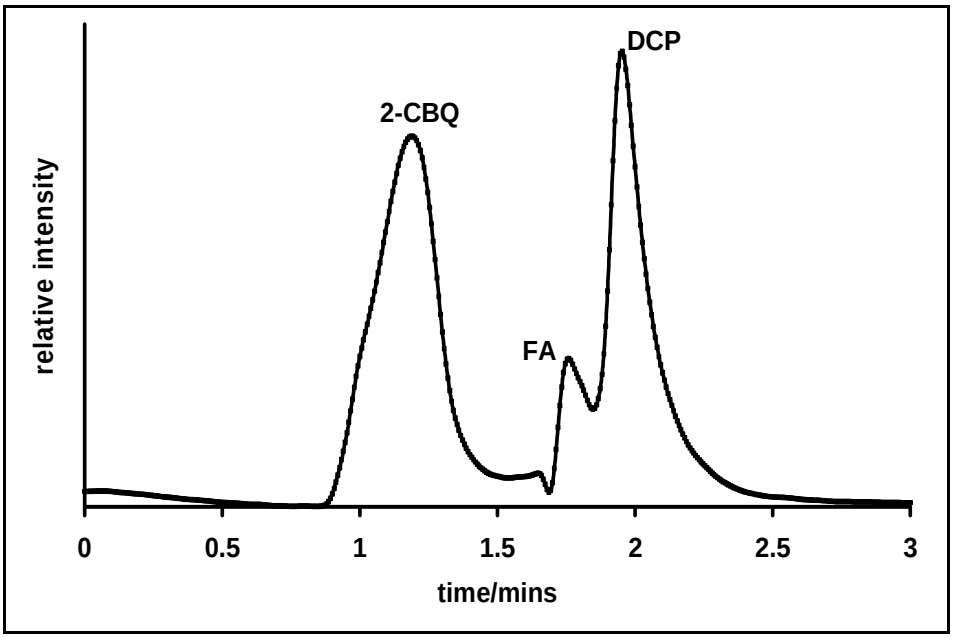

Figure 4.23: HPLC chromatogram of the reaction mixture after 10^{-3} M DCP photolysis (in the presence of ZnOCPc-Amberlite) showing formation of new peaks at t = 1.2 minutes identified as 2-chlorobenzoquinone and a peak at t = 1.8 minutes identified as fumaric acid. The DCP peak is at 1.9 minutes. CBQ = chlorobenzoquinone. FA = fumaric acid.

One of the most important factors in the large-scale application is the photostability of the photosensitisers is the ability to recycle the catalysts; three repetitive experiments were performed by re-using ZnOCPc (**28**) immobilised on Amberlite®, for fresh PCP (2×10^{-3} M) solution each time, Figure 4.24. High stability of the catalyst is observed on re-using it. Generally, it was observed that all the immobilised MPc photosensitizers could be repeatedly used for the photosensitised transformation of the chlorophenols without significant loss of activity. Under homogeneous conditions, photodegradation of 4-CP using ZnOCPc (**28**), results in the rapid degradation of this sensitiser (> 51% in 3 minutes),[52] thus making it most unsuitable for use for the photosensitised transformation of higher chlorinated phenols such as TCP and PCP. All the MPc complexes discussed in this work showed the similar stability on re-use as for observed ZnOCPc (**28**) (Figure 4.24). Compared to homogeneous conditions, the catalysts reported in this work showed superior photocatalytic properties towards the degradation of chlorinated phenols when immobilised onto Amberlite®.

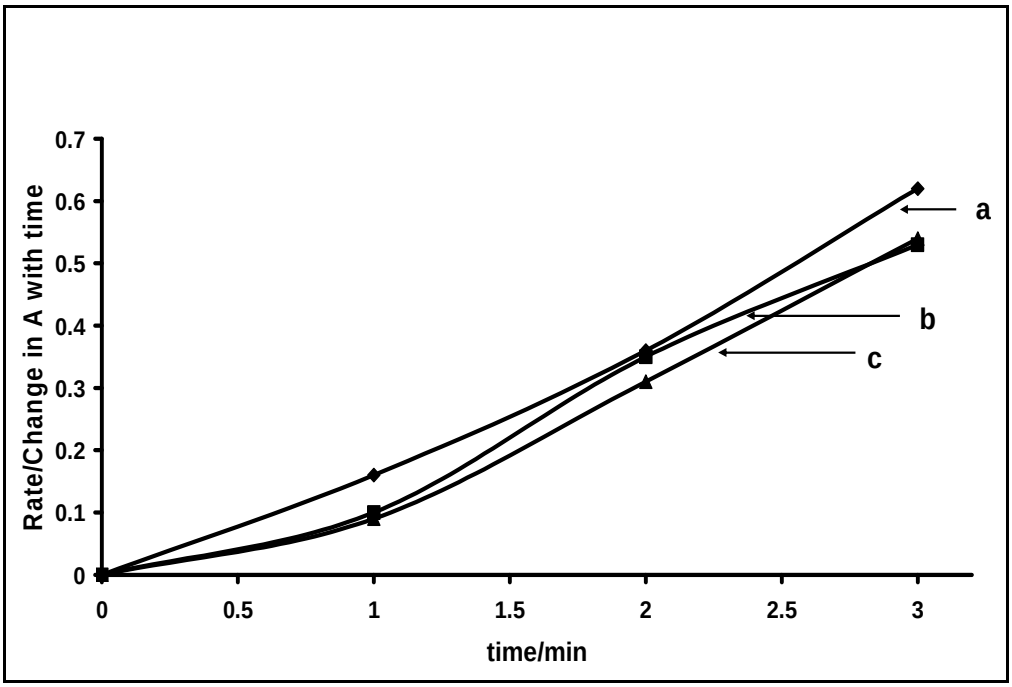

Figure 4.24: Kinetic plots (change in absorbance against time) for the photolysis of three fresh solutions of 2 x 10^{-3} M PCP performed by re-using the same ZnOCPc-Amberlite catalyst for different PCP samples: (a) fresh ZnOCPc-Amberlite catalyst, (b) re-use of the catalyst in a fresh sample of PCP solution, (c) further re-use of the same catalyst in another fresh sample of PCP solution.

4.2.4 Langmuir-Hinshelwood (L-H) kinetic model

The L-H Kinetic model has widely been employed to treat the dependency of heterogeneous photocatalytic reaction rates on the concentrations of chlorinated aromatics and other organic substrates.[328,401] L-H model (Equation 4.1) describes the competitive adsorption of substrates, reaction intermediates and chlorophenol oxidant products, and assumes that all intermediate products have the same binding characteristics to the photosensitisers as the parent substrate[328,401]:

$$\frac{1}{rate} = \frac{1}{k_r} + \frac{1}{k_r K_{ad} C^o_{sub}} \qquad (4.1)$$

where k_r is the apparent reaction rate constant, K_{ad} is the adsorption coefficient and C_{sub}^{0} is the initial concentration of the substrate (in this case PCP was used as an example). The rate refers to the degradation of the chlorophenols as judged by the disappearance of the spectra of the substrates or the reduction in the intensity of the HPLC traces.

In this work, the change in PCP UV-Vis absorbance with time was used as an example. Table 4.3 shows the kinetic parameters obtained from the plots of inverse of rate versus inverse of concentration (Figure 4.25). Relatively high degree of linearity with r^2 = 0.9387, 0.9842 and 0.9945 for the ZnOCPc (**28**), $GePcS_{mix}$ (**31**) and $ZnPcS_{mix}$ (**30**), respectively, indicating that the reactions occurred mainly on the surface of these photocatalysts. The relatively high K_{ad} values for ZnOCPc (**28**), $GePcS_{mix}$ (**31**) and $ZnPcS_{mix}$ (**30**), imply sufficient adsorption of PCP onto the catalyst. The reason for the relatively low K_{ad} values for the $AlPcS_4$ (**25**) and AlOCPc (**27**) catalysed photolysis can not be ascertained for now but low K_{ad} values are generally attributed to competition between the substrates and reaction intermediates.

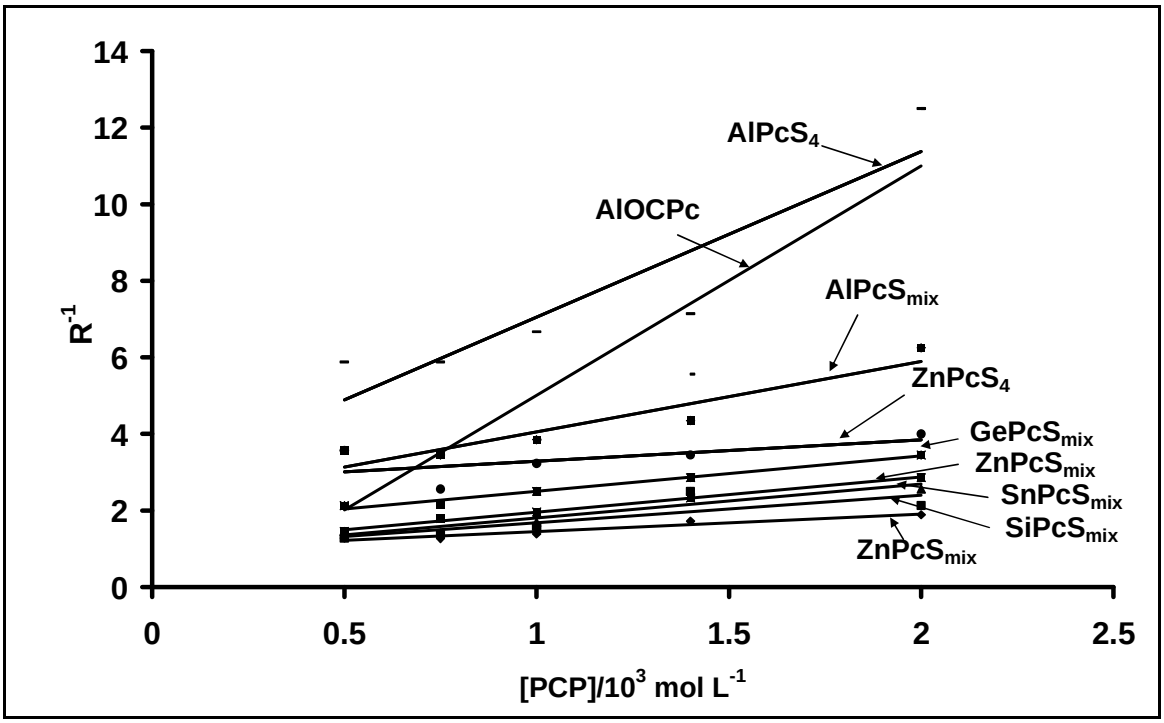

Figure 4.25: The Langmuir-Hinshelwood kinetic model plots for the photolysis of PCP.

Table 4.3: The Langmuir-Hinshelwood Kinetic Model parameter details of the photolysis of PCP.

Catalyst	**R^2 value**	**k_r**	**K_{ad}/ 10^{-3} mol^{-1} L**
$AlPcS_4$ (**25**)	0.8357	0.37	0.63
$ZnPcS_4$ (**26**)	0.8815	0.37	4.87
AlOCPc (**27**)	0.8409	1.02	0.16
ZnOCPc (**28**)	0.9387	1.01	2.15
$AlPcS_{mix}$ (**29**)	0.8912	0.45	1.21
$ZnPcS_{mix}$ (**30**)	0.9945	0.96	1.11
$GePcS_{mix}$ (**31**)	0.9842	0.63	1.72
$SiPcS_{mix}$ (**32**)	0.6507	1.04	1.34
$SnPcS_{mix}$ (**33**)	0.8561	1.09	1.03

The proposed mechanism for the photodegradation of the chlorophenols may be represented by Scheme 4.3. The singlet oxygen produced from the reaction of the photosensitisers with molecular oxygen in type II reaction discussed earlier in the introduction section (shown by equations 4.2 and 4.3) is expected to react with the chlorophenoxy ion to give chlorophenoxy anion radical. In the presence of water, an intermediate anion and hydrogen peroxide are formed and finally elimination of chloride ion (Cl^-) and formation of chlorobenzoquinone derivative occurs.[50]

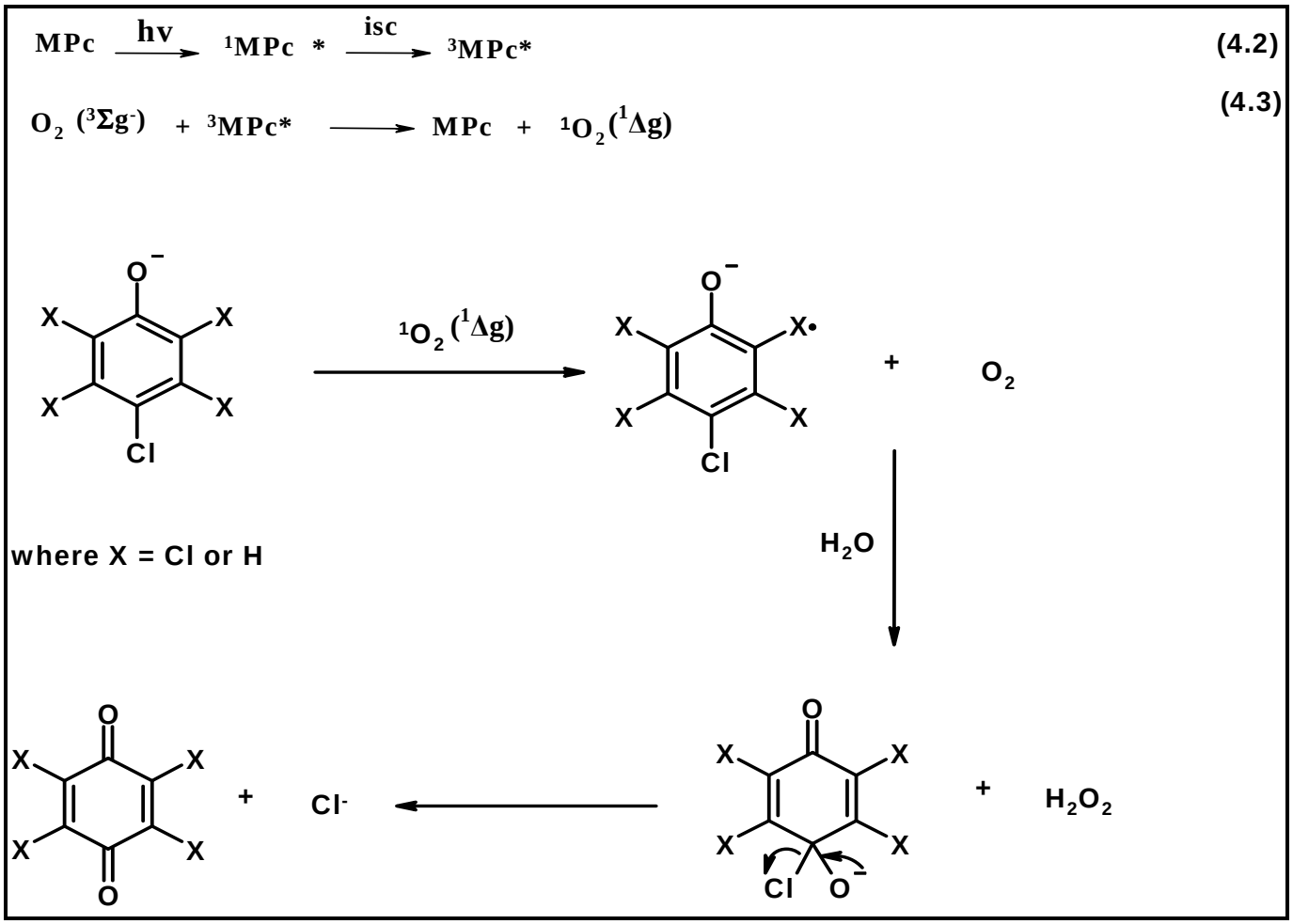

Scheme 4.2: Proposed reaction mechanism for the transformation of chlorophenols using PCP as an example.

4.3 Conclusion

In conclusion, it has been have shown in this work that the oxidation of 2-CP and TCP using $CoPcS_4$ catalyst and H_2O_2 oxidant, in different solvent conditions gives different products. In water/methanol mixture (pH 3.4), the products are phenol, benzoquinone, hydroquinone and maleic acid for 2-CP. And for TCP, the products are phenol, dichlorobenzoquinone, hydroquinone and maleic acid. In water (pH 7 or 10) the main products are dichlorobenzoquinone and benzoquinone respectively for TCP and 2-CP. There is spectroscopic evidence for the involvement of both the metal and phthalocyanine ring oxidised species in the mechanism.

Also, it has been shown in this work that various immobilised photosensitizers catalysed visible light photolysis of chlorophenols. Singlet oxygen played a major role in the photolysis reactions judging from the similar trends of the rate of singlet oxygen generation by the photosensitisers {$SnPcS_{mix}$ (**33**) > ZnOCPc (**28**) > $GePcS_{mix}$ (**31**) = $SiPcS_{mix}$ (**32**) > $ZnPcS_{mix}$ (**30**) > $ZnPcS_4$ (**26**) > $AlPcS_{mix}$ (**29**) > AlOCPc (**27**) > $AlPcS_4$ (**25**)} and the photoactivity of the MPc complexes{ZnOCPc (**28**) > $SnPcS_{mix}$ (**33**) > $SiPcS_{mix}$ (**32**) > $ZnPcS_{mix}$ (**30**) > $GePcS_{mix}$ (**31**) > $ZnPcS_4$ (**26**) > $AlPcS_{mix}$ (**29**) ~ AlOCPc (**27**) > $AlPcS_4$ (**25**)}. HPLC traces reveal that the main products of the photolysis are the benzoquinone derivatives. The L-H kinetic model also showed that for ZnOCPc, $ZnPcS_{mix}$ and $GePcS_{mix}$ catalysed photolysis, appreciable heterogeneous catalysis took place. It was observed ZnOCPc which degrades rapidly in aqueous solutions is very stable when immobilised. The results reported in this work provide a basis for development of MPc complexes for the transformation of chlorophenols in water.

CHAPTER 5

ELECTRODE MODIFICATION

In this chapter, the fabrication and characterisation of potential electrochemical sensors for chlorophenols, nitrite and sulphite are discussed. The modification of gold electrodes was carried out by two main techniques; (1) electropolymerisation and (2) self assembly technique. Figure 5.1 above shows the structures of the thiol-derivatised complexes for electrode modification.

SAM-modified gold electrodes of the complexes will be used for the electrooxidation of sulphite only; nitrite electrooxidation is not included because usually peak potential for its oxidation is around 0.7 V (vs. Ag|AgCl) which in most cases is outside the stability range of SAM though in this section the nitrite peak has been lowered to the same E_p as sulphite. Chlorophenol electrooxidation is not included because SAM desorbs in strongly alkaline medium which is the medium for chlorophenol electrooxidation.

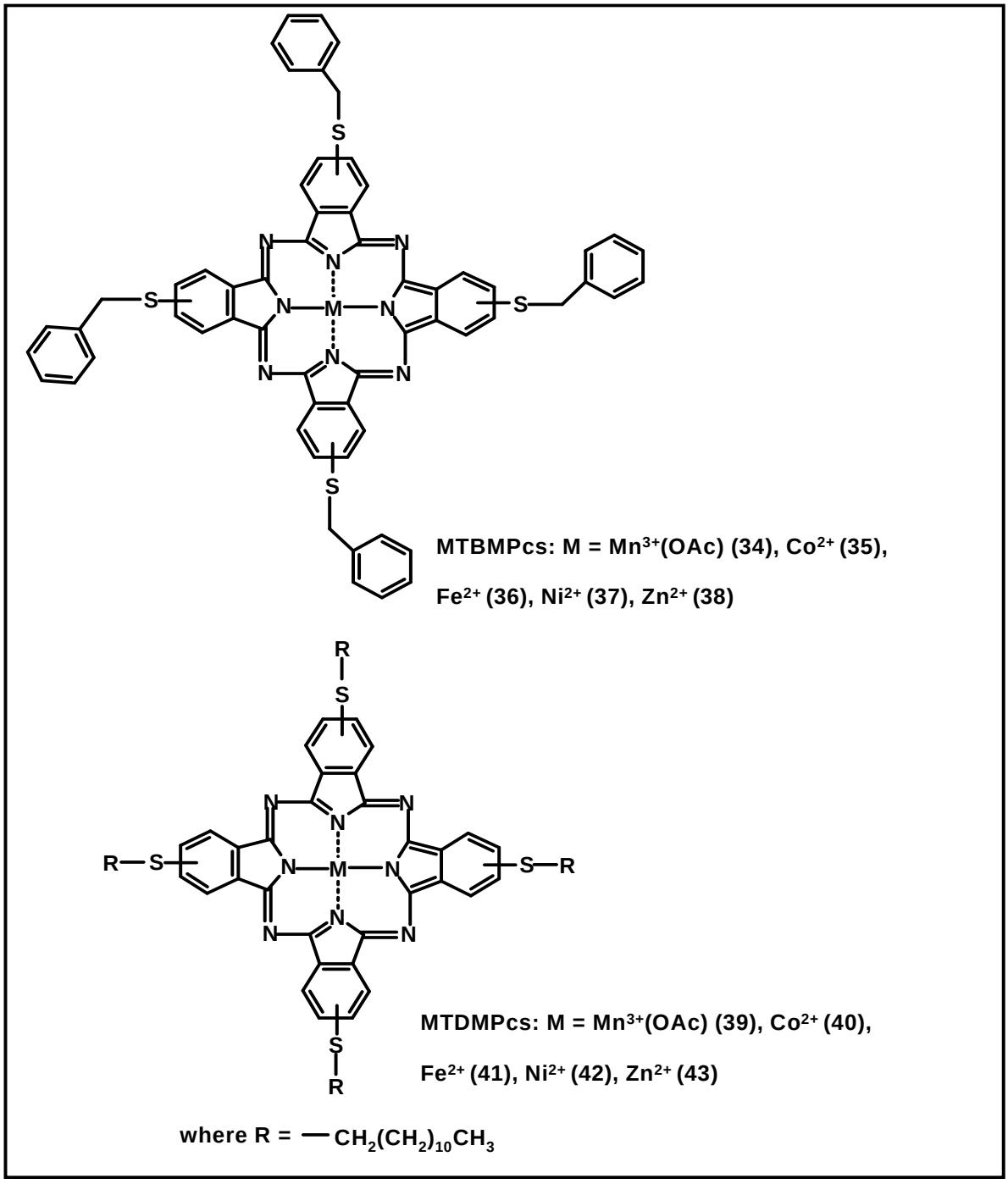

Figure 5.1: Structures of thiol-derivatised MPc complexes used for electrode modification in this thesis.

5.1 Electropolymerisation

Both Au and GC electrodes were employed for electropolymerisation but studies for NiPcs showed that polymerisation on GCE did not give good catalytic behaviour compared to polymerisation on Au electrode; hence Au was employed for all studies. The electropolymerised films on gold electrode of the thiol-derivatised MPcs (CoPc, FePcs, MnPcs and NiPcs) will be used for electrocatalysis of nitrite and chlorophenols (NiPcs only). The thiol-derivatised MPcs (M = Co^{2+}, Fe^{2+}, Mn^{3+}, Ni^{2+}) were successfully deposited on gold electrodes by electropolymerisation. Repetitive scanning of the solutions of all complexes at the potential range of -0.3 to 0.6 V (for CoPcs, FePcs and MnPcs while the range for the NiPcs was -0.5 to 1.2 V) resulted in their electrodeposition on to the gold electrode. A wider potential range was chosen for the NiPcs because there were no significant depositions of the complexes on gold electrodes when a narrower potential range was applied. For all the complexes, there were successive increases in the amplitude of peaks. Only a maximum of 30 scans was recorded for all complexes.

The differences in the peak potentials and CV shapes compared to the ones obtained in Chapter 3 are due to differences in electrodes employed; GCE was used in Chapter 3 and Au was used in this chapter. Also the difference could be due to the fact that the peaks observed after the first scan in this Chapter are due to surface confined species unlike that of species in solutions in Chapter 3 and in some cases different solvents (DMF or DCM) were employed.

5.1.1 CoPcs

There was a continuous growth in the Co^{3+}/Co^{2+} redox process with an anodic peak 0.35 V (Figure 5.2a) for complex **35**, the peak growth became less pronounced as the number of scan increases, this is due to the higher resistance to mass transport as the film thickness increased.[402] For complex **40**, there was a continuous growth of peaks at 0.06 and 0.27 V Figure 5.2b. The peak at 0.27 V is assigned to Co^{3+}/Co^{2+} redox in comparison with the solution chemistry (as already stated, the difference in the potentials could be due to the fact that peaks observed (after the first scan) in this Chapter are due to surface confined species and considering the fact that GCE was used in Chapter 3 and Au was used in this Chapter). The peak at ~0 V may be due to a reduction process and possibly polymer peak. The increase of current with scan number for complex **35** with no new peaks formed suggests electrodeposition. However for complex **40**, new peaks were formed suggesting polymerisation. Polymerisation will be due to radicals formed on oxidation with the formation of disulphide bonds (S-S). Polymerisation is most likely also occurring for complex **35**, even though new peaks are not formed, there were continuous increases in the redox peaks with scan number which are also characteristic of polymerisation. The $M^{3+}Pc/M^{2+}Pc$ couples are easier to observe in Figure 5.3a and b where the cyclic voltammograms were recorded in pH 7.4 phosphate buffer for complexes **35** and **40** respectively. It is obvious that the CVs of the modified complexes (Figure 5.3) are similar to their respective last scan CVs in Figure 5.2.

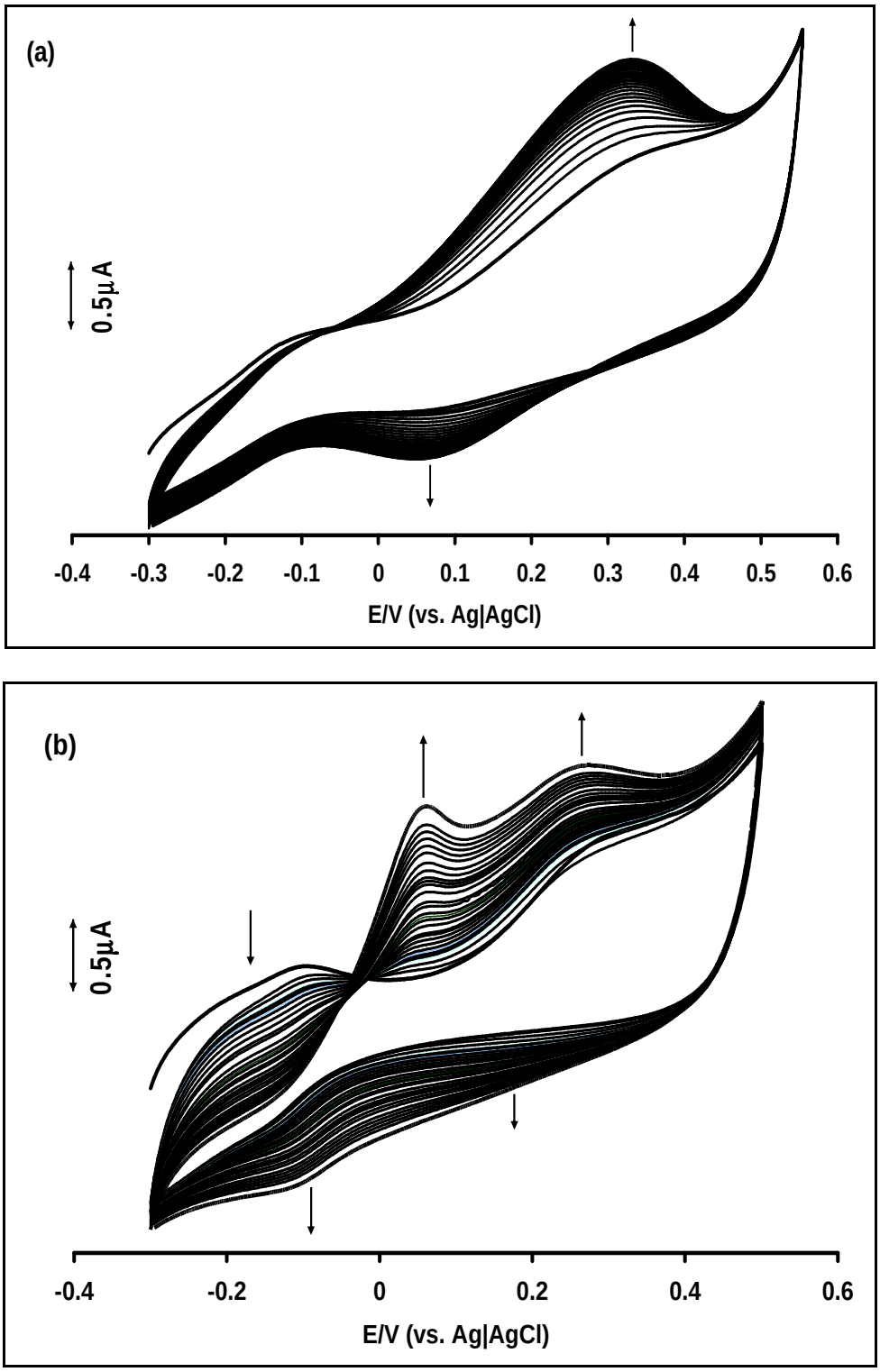

Figure 5.2: Repetitive cyclic voltamogramms of 1 mM complex (a) CoTBMPc, **35** and (b) CoTDMPc, **40** in DCM containing 0.1 M $TBABF_4$ at a gold electrode. Scan rate = 100 mV s^{-1}.

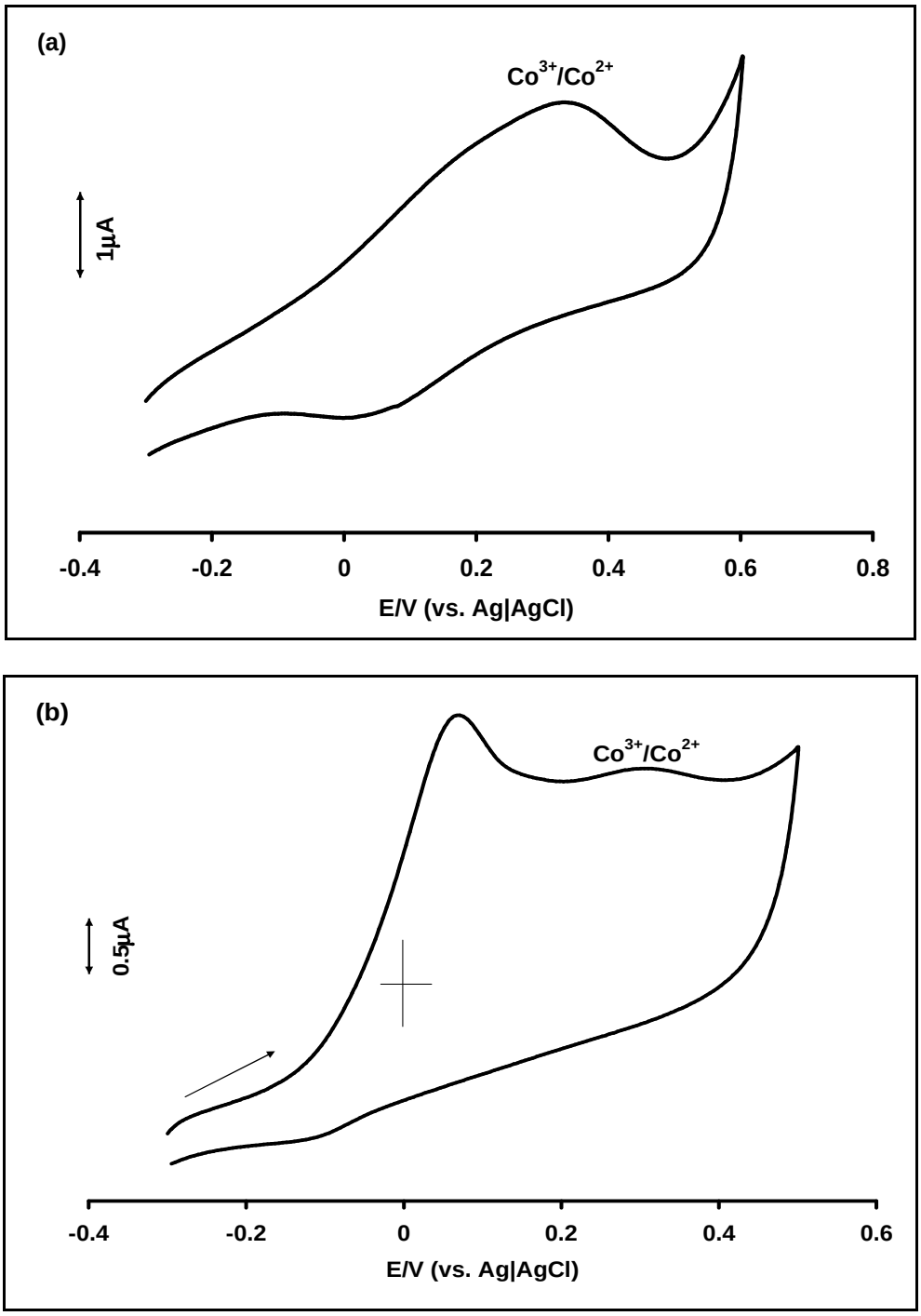

Figure 5.3: Cyclic voltamogramms of gold electrode modified with complex (a) CoTBMPc, **35** and (b) CoTDMPc, **40** in phosphate buffer pH 7.4. Scan rate = 100 mV s^{-1}.

It is important to note that there was no formation of SAM during the time it took for polymerisation. Figure 5.4 shows the Co^{3+}/Co^{2+} peaks for SAMs of complex **35** in pH 7.4 phosphate buffer. The SAM was formed in 24 hours compared to the short CV time scale in Figure 5.2 formed from polymerisation. The electrodes following polymerisation are represented as *poly*-CoTBMPc and *poly*-CoTDMPc.

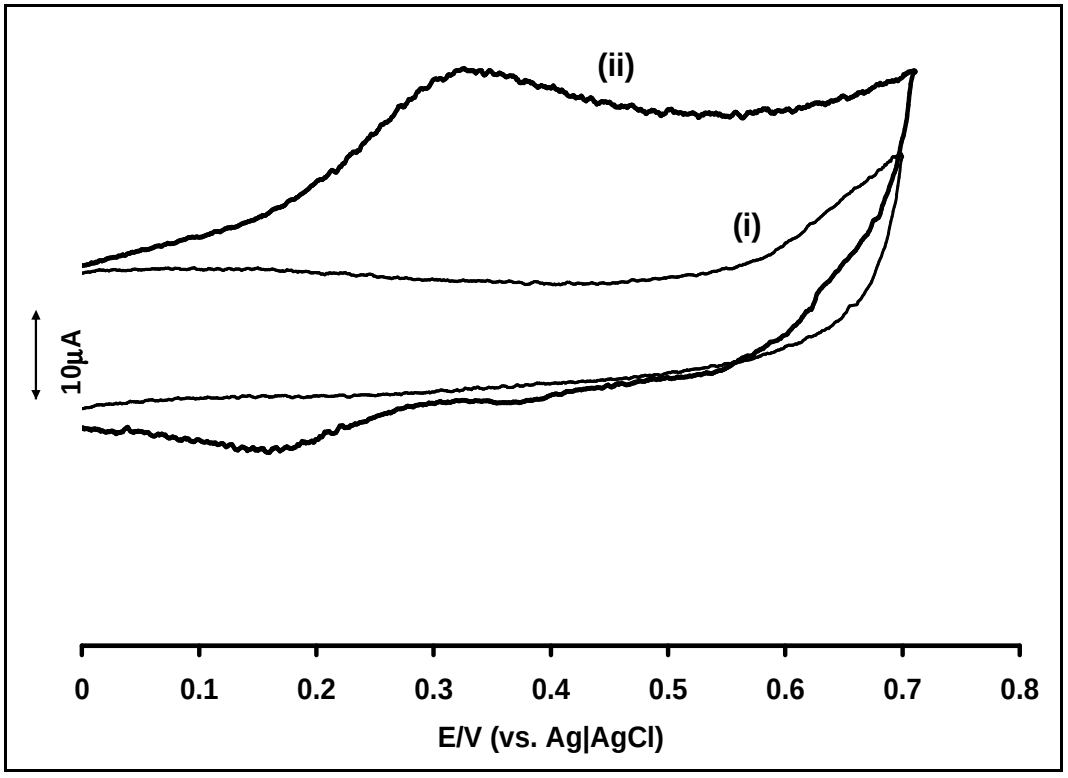

Figure 5.4: Cyclic voltammogram of (i) bare gold and (ii) SAM of complex **35** in phosphate buffer pH 7.4. Scan rate = 100 mV s^{-1}.

.

5.1.2 FePcs

Both complexes **36** and **41** showed similar behaviour in their CVs evolution during their electrodeposition on gold electrodes (Figure 5.5). There was a formation of broad anodic peak at around 0.3 V due to Fe^{3+}/Fe^{2+} which exhibited a general increase in current in the

positive potential region for both complexes. The formation of new peaks for both complexes confirms polymerisation. The peak growth became less pronounced as the number of scans increased; this is due to the higher resistance to mass transport as the film thickness increased.[402]

Figure 5.6 shows the typical cyclic voltammograms for gold electrodes modified with complexes **36** and **41** in phosphate buffer pH 7.4. The CVs show similarity with the CV of the last scans during electropolymerisation. The electrodes following polymerisation are represented as *poly*-FeTBMPc and *poly*-FeTDMPc.

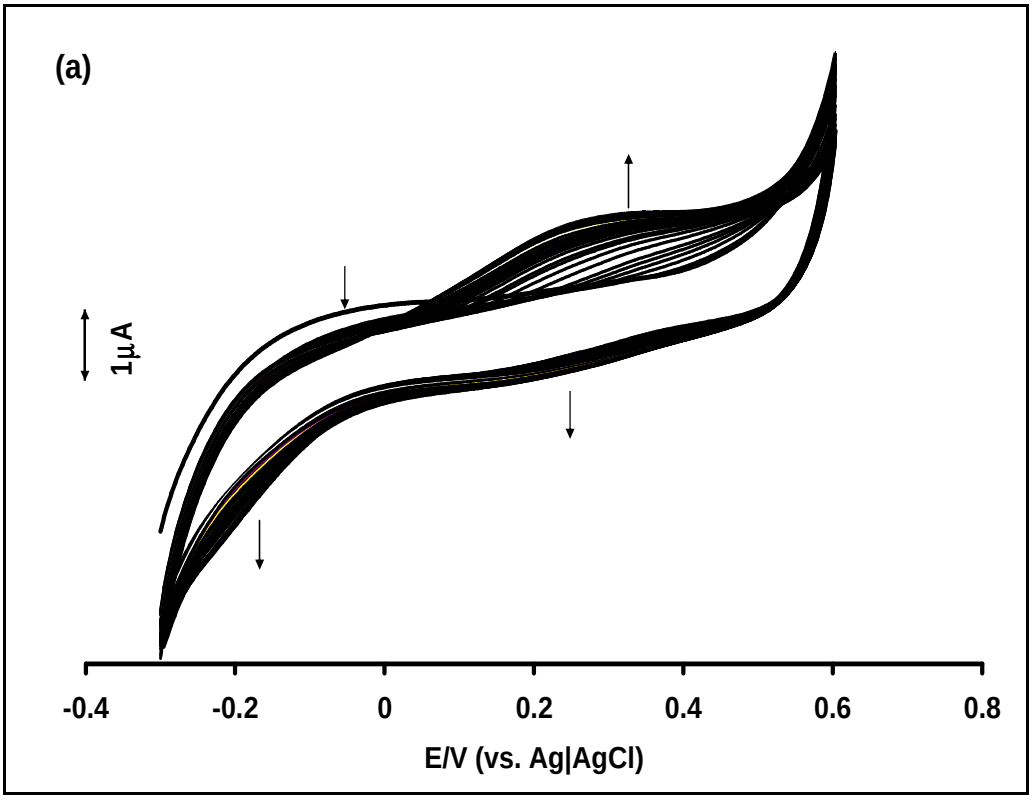

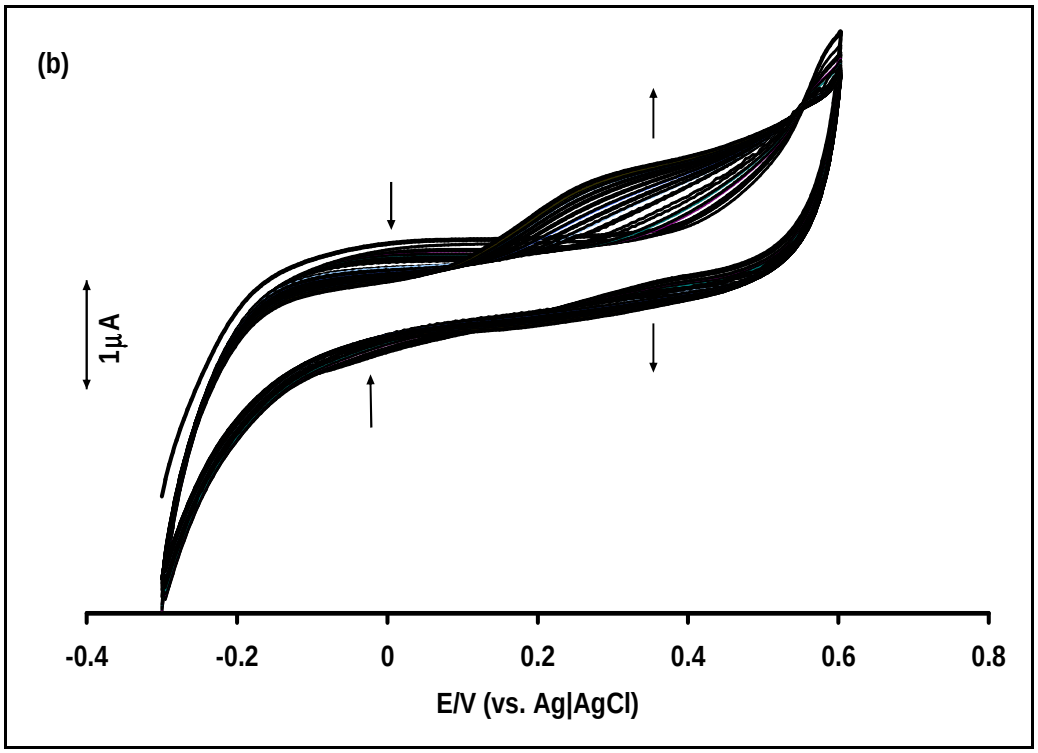

Figure 5.5: Repetitive cyclic voltamogramms of 1 mM complex (a) FeTBMPc, **36** and (b) FeTDMPc, **41** in DCM containing 0.1 M $TBABF_4$ at a gold electrode. Scan rate = 100 mV s^{-1}.

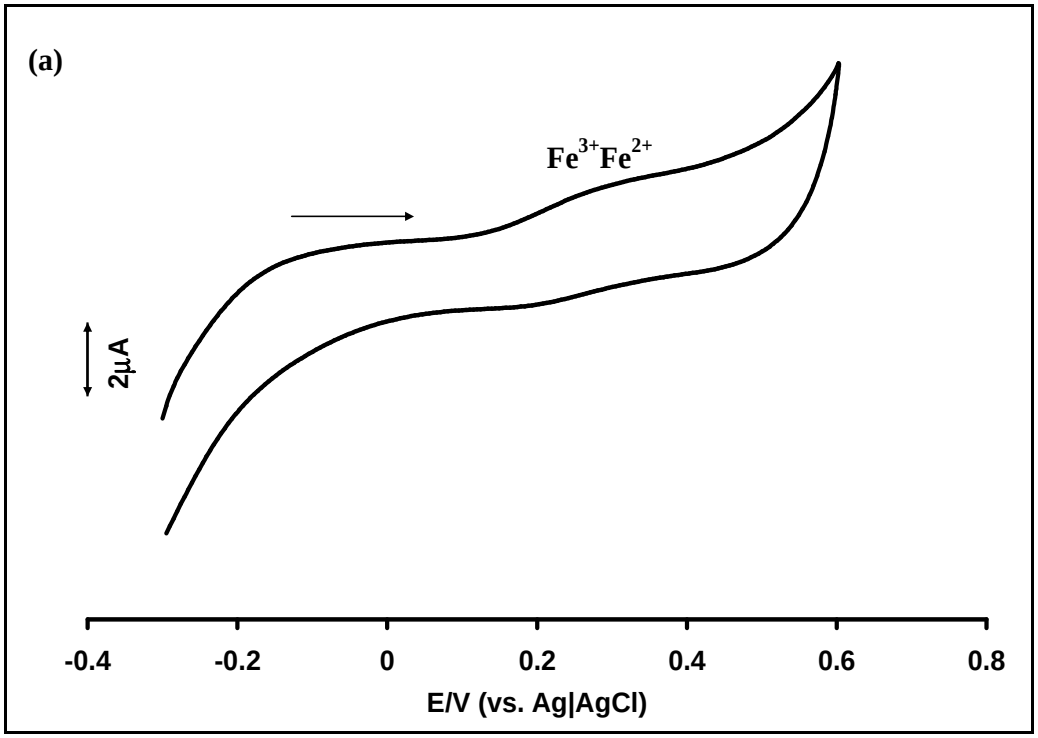

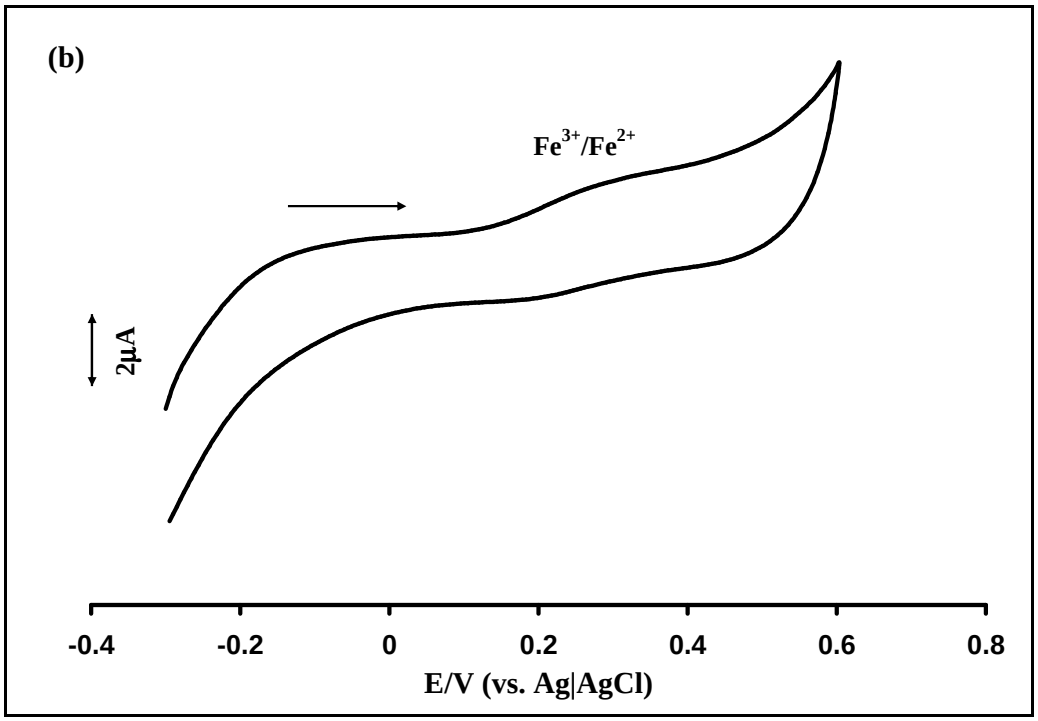

Figure 5.6: Cyclic voltamogramms of gold electrode modified with complex (a) FeTBMPc, **36** and (b) FeTDMPc, **41** in phosphate buffer pH 7.4. Scan rate = 100 mV s^{-1}.

5.1.3 MnPcs

For complex **34** (Figure 5.7a), film growth initially involved anodic peak increase around 0.17 V most likely due to Mn^{3+}/Mn^{2+} process in comparison with solution cyclic voltammetry data, which shifted to more positive potential values with scan number. The peak at 0.55 V may thus be assigned to the oxidation of the central metal (M^{4+}/M^{3+}) in comparison with solution electrochemistry (again as stated before, the difference could be due to the fact that peaks observed after the first scan in this Chapter are due to surface confined species and considering the fact that GCE was used in chapter 3 and Au was used in this chapter). The peak at 0.55 V only appeared after the 10^{th} scan (while the peak at 0.17 V began to decrease in intensity) and continued to grow up to the 30^{th} scan. For

complex **39** (Figure 5.7b), the initial voltammogram exhibited ill-defined peaks but with increase in scan rate, new anodic and cathodic peaks at 0.2 and -0.1 V emerged and continued to grow with increase in the number of scans. Formation of new peaks is an indication of polymerisation of the complexes on electrode.

MTBMPc ring based oxidation was reported at around $E_{½}$ = 1.06 V (section 3.2.3) which is far from the second oxidation reported during the electropolymerisation process and so it is logical to conclude that this is due to Mn^{4+}/Mn^{3+} process. The $M^{3+}Pc/M^{2+}Pc$ and $M^{4+}Pc/M^{3+}Pc$ couples for the complex **34** modified gold electrode are easier to observe in Figure 5.8a where the cyclic voltammogram was recorded in pH 7.4 phosphate buffer. Figure 5.8b shows the cyclic voltammogram recorded in pH 7.4 phosphate buffer for complex **39**, $M^{3+}Pc/M^{2+}Pc$ could easily be observed, the peak due to $M^{4+}Pc/M^{3+}Pc$ was not clearly observed. The electrodes following polymerisation are represented as *poly*-MnTBMPc and *poly*-MnTDMPc.

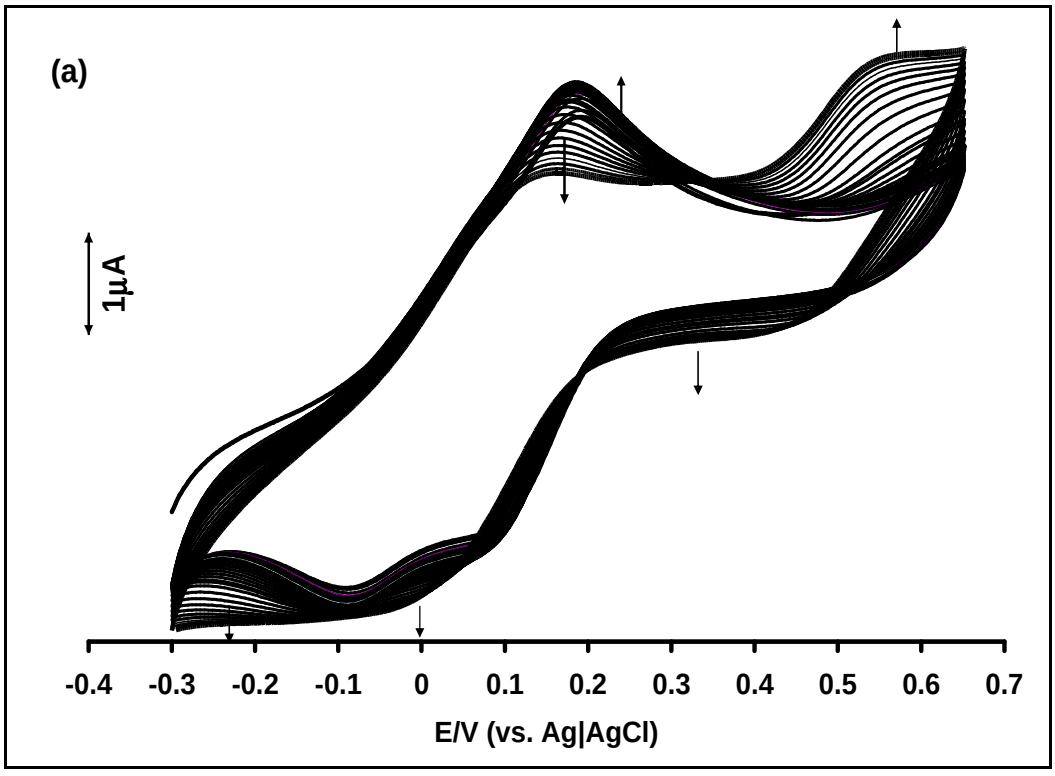

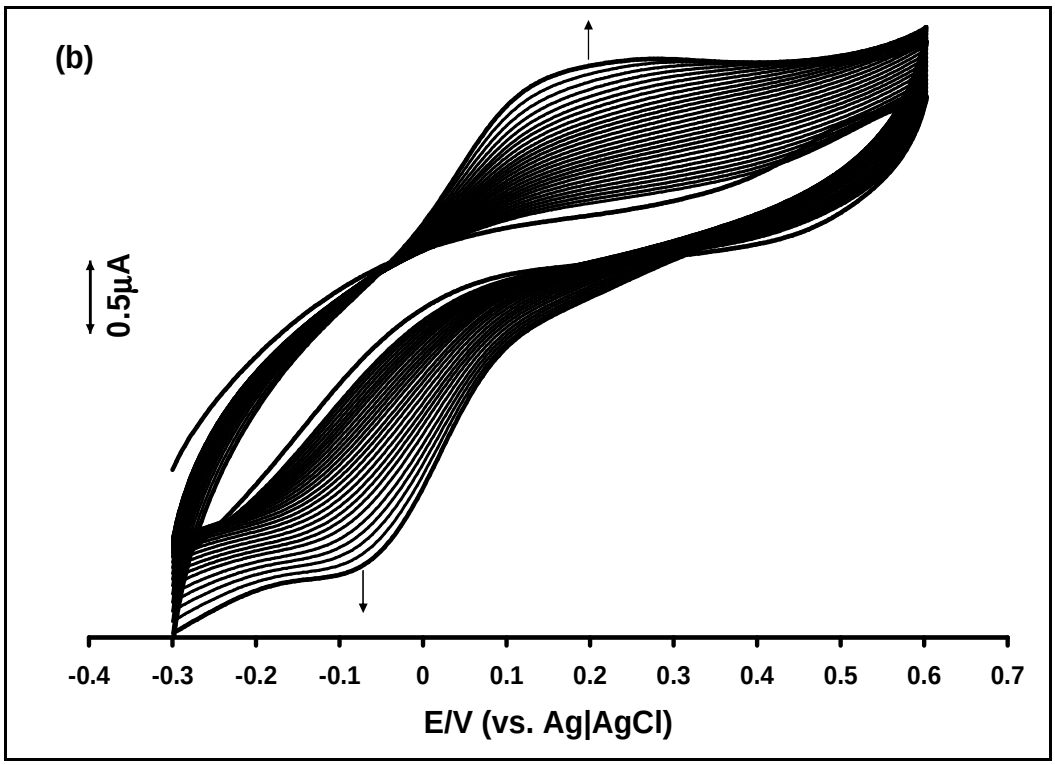

Figure 5.7: Repetitive cyclic voltamogramms of 1 mM complex (a) MnTBMPc, **34** and (b) MnTDMPc, **39** in DCM containing 0.1 M $TBABF_4$ at a gold electrode. Scan rate = 100 mV s^{-1}.

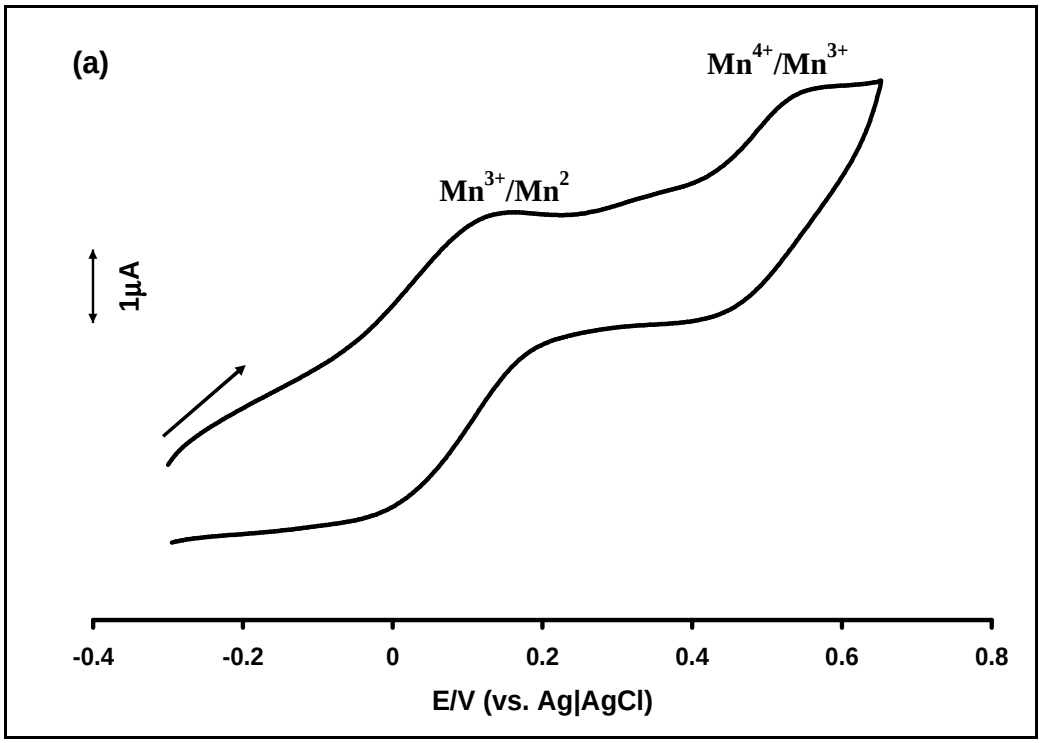

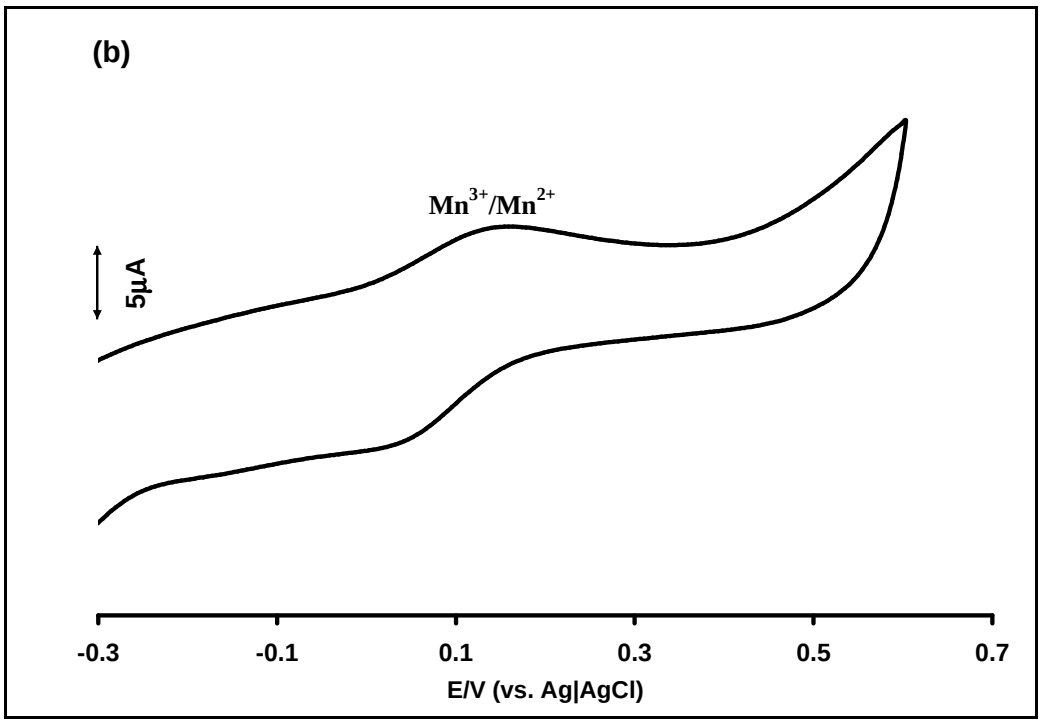

Figure 5.8: Cyclic voltamogramms of gold electrode modified with complex (a) MnTBMPc, **34** and (b) MnTDMPc, **39** in phosphate buffer pH 7.4. Scan rate = 100 mV s^{-1}.

5.1.4 NiPcs

5.1.4.1 Voltammetric characterisation

As explained before, both GC and Au electrodes were employed for the electropolymerised of NiPc complexes in order to compare the behavior of the two electrodes. Only NiTBMPc (**37**) could be deposited onto GCE, attempts to deposit NiTDMPc (**42**) on glassy carbon electrode failed. The presence of the phenyl groups in NiTBMPc (**37**) could enable π-π interaction with GCE. Figure 5.9a shows the evolution of the cyclic voltamogramms during electropolymerisation of 1 mM NiTBMPc (**37**) complex in DCM solution on gold electrode within the potential range -0.5 to 1.2 V.

Again as with all the MPcs and as stated above, there was insignificant formation of self-assembled monolayer (SAMs) of either NiTBMPc (**37**) or NiTDMPc (**42**) onto gold, SAMs of MPc complexes require hours (24 to 72 hours) to form. The general increase in currents in Figure 5.9a accompanied by shifts in the peaks is typical of polymerisation of MPc complexes onto electrodes.[403] Figure 5.9b shows selected voltammograms from Figure 5.9a, and clearly shows a new broad peak formed at ~1 V and the shift in the peak between 0.1 and 0.5 V with scan number. Figure 5.9b shows that no clear peak was observed during the first scan. On second scan, there was a formation of a polymer peak at 0.25 V and this peak shifts to more positive potentials with increase in the number of scans, this is an indication of an increase in the electrical resistance of the polymer film and that overpotential is needed to overcome the resistance.[404] The electrode following polymerisation is represented as *poly*-NiTBMPc-Au.

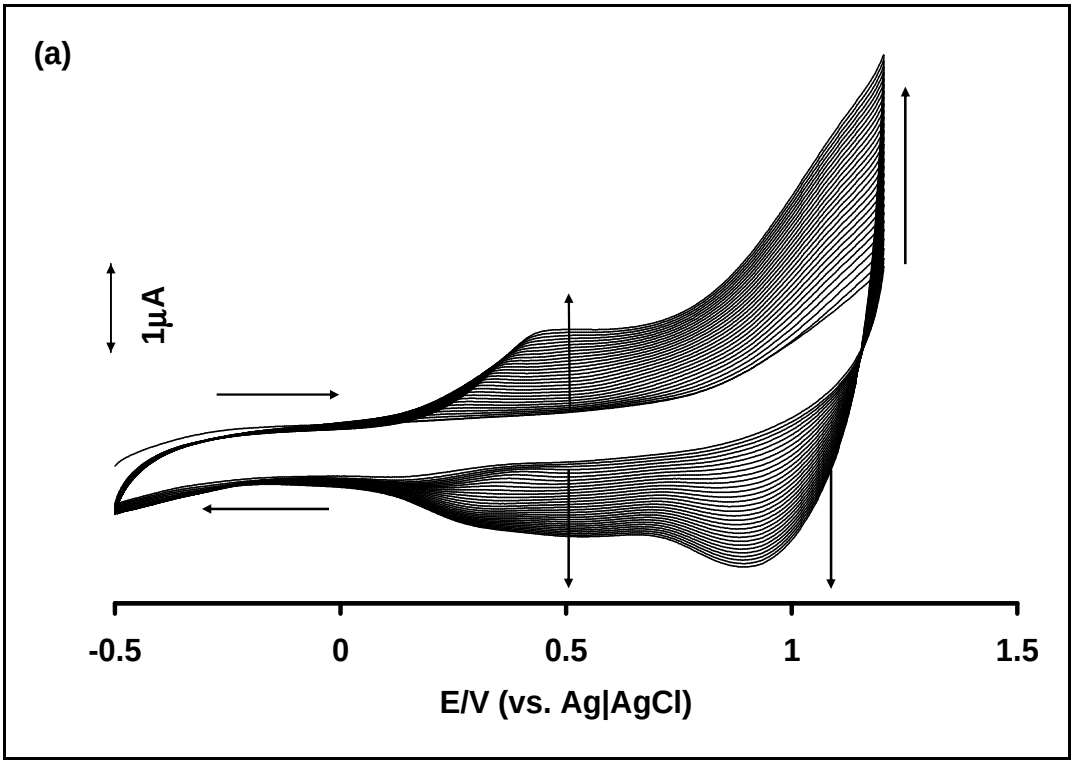

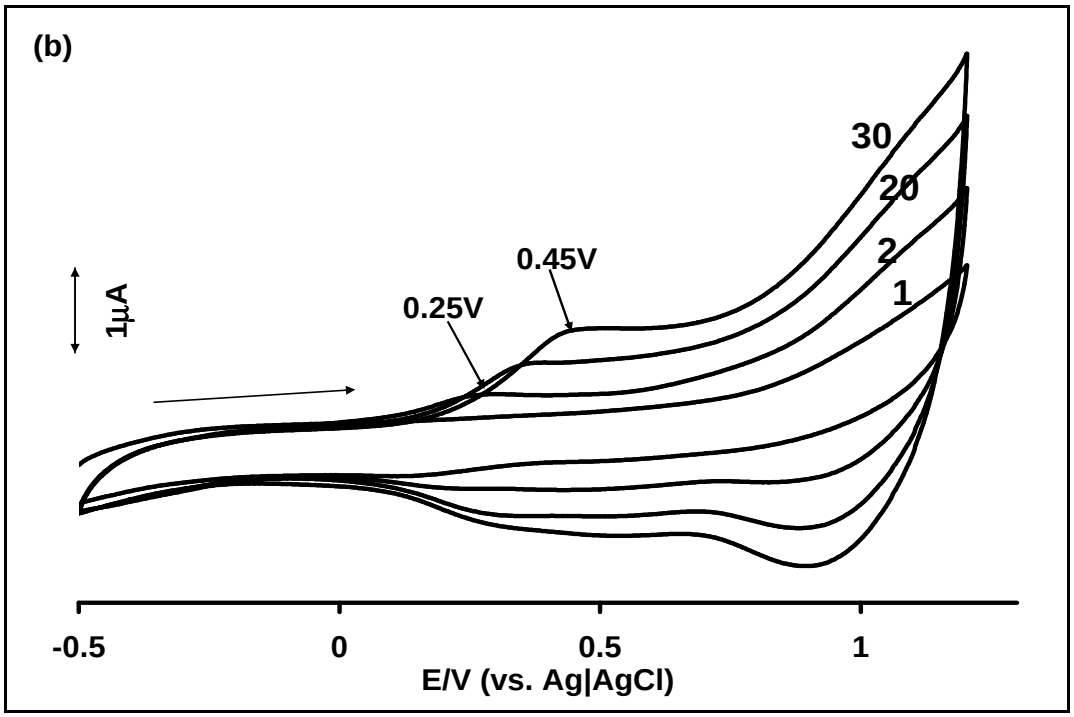

Figure 5.9: Repetitive cyclic voltamogramms of 1 mM complex (NiTBMPc, **37**) in DCM containing 0.1 M $TBABF_4$ at gold electrode. (b) Cyclic voltammograms for scan numbers 1, 2, 20 and 30 (from (a)). Scan rate: 100 mV s^{-1}.

NiTDMPc (**42**) also showed polymerisation onto the electrode (Figure 5.10a). Figure 5.10b shows selected voltammograms (1^{st} and 30^{th} scan) during the polymerisation of NiTDMPc (**42**) complex in DCM onto gold electrode. New couples were observed with cycling and after the 30^{th} scan at ~ -0.1, 0.2 and 0.72 V vs. Ag|AgCl. The resulting electrode is represented as *poly*-NiTDMPc-Au.

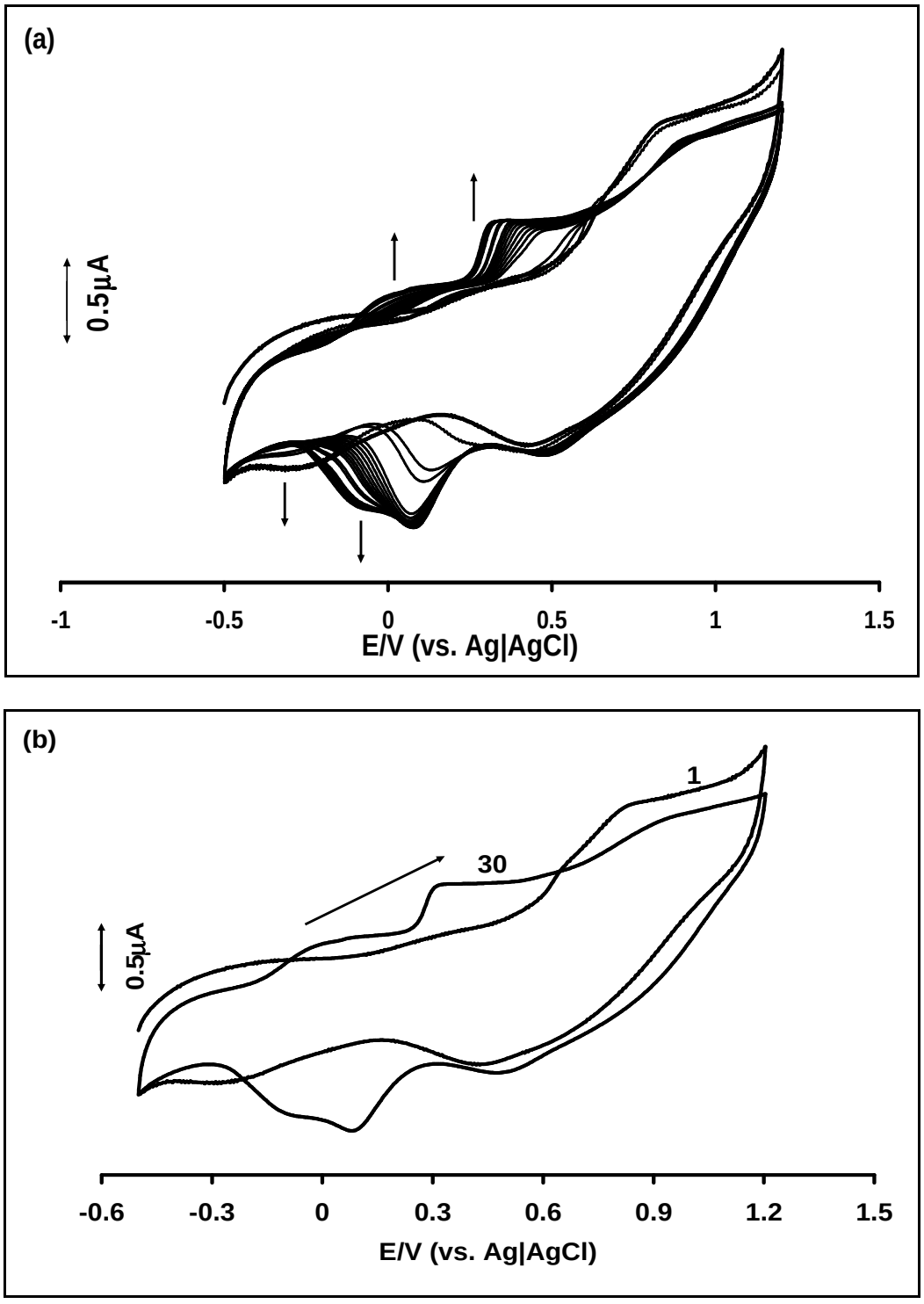

Figure 5.10: Repetitive cyclic voltamogramms of 1 mM complex (NiTDMPc, **42**) in DCM containing 0.1 M $TBABF_4$ at gold electrode. (b) Cyclic voltammograms for scan numbers 1, 2, 20 and 30 (from (a)). Scan rate: 100 mV s^{-1}.

Glassy carbon electrode was also used for the electropolymerisation of NiTBMPc. Figure 5.11 shows the evolution of the cyclic voltamogramms during the deposition of NiTBMPc complex on GCE. There were formation and progressive increase in the peaks at -1.1, -0.25, 0.32 and 0.42 V. This observation indicates electropolymerisation of the complex onto a glassy carbon electrode (represented as *poly*-NiTBMPc-GCE). As it was stated before NiTDMPc (**42**) could not be deposited onto the GCE.

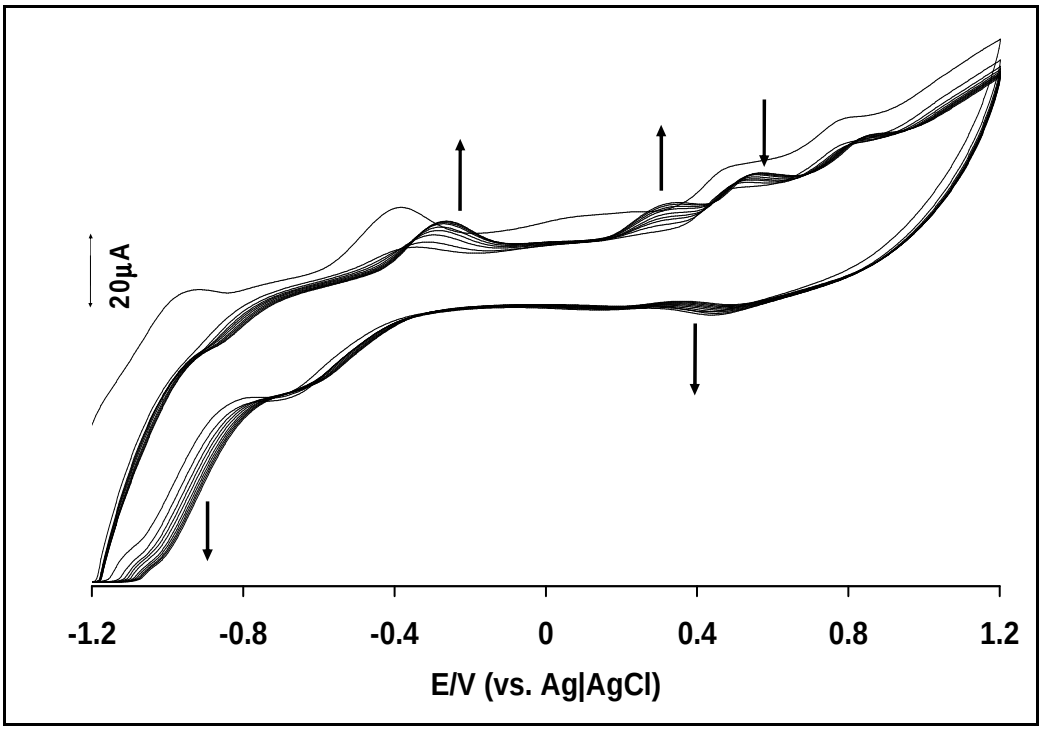

Figure 5.11: Repetitive cyclic voltamogramms of 1 mM complex (NiTBMPc, **37**) in DCM containing 0.1 M $TBABF_4$ at glassy carbon electrode. Scan rate: 200 mV s^{-1}.

Poly-NiTDMPc-Au and *poly*-NiTBMPc-Au electrodes were subjected to repetitive cycling between -0.5 and 1.2 V and the *poly*-NiTBMPc-GCE between -0.1 and 1.1 V in 0.1 M NaOH in order to transform the polymerised complexes into the O-Ni-O oxo bridged derivatives. As shown in Figure 5.12a-c, there was a formation and progressive

increase of the anodic and cathodic waves between -0.3 and 0.5 V, for all complexes. These waves are known to correspond to Ni^{3+}/Ni^{2+} redox process[254] and are an indication of the transformation of the NiTBMPc (**37**) and NiTDMPc (**42**) into the 'O-Ni-O oxo' bridged forms. The shape of the final cyclic voltammogram is very similar to those obtained with electroformed nickel macrocyclic-based films in alkaline aqueous solution[360,405,406], which are also similar to those of nickel hydroxide ($Ni(OH)_2$) electrode. The electrodes are represented as *poly*-Ni(OH)TBMPc-Au, *poly*-Ni(OH)TDMPc-Au and *poly*-Ni(OH)TBMPc-GCE. It is important to note that the Ni^{3+}/Ni^{2+} couple has not been identified electrochemically for the NiPc complexes in solution, but has been implicated in catalysis as an adsorbed polymer.[215] The high increases in the currents between 0.6 and 1.2 V is known to be due to the electrooxidation of OH^- ions to O_2 with OH radicals as intermediates, these radicals are suggested to play key role in the electrotransformation of the NiPcs to the 'oxo bridge' form,[356] with the $OH^{\cdot}$ radical facilitating the insertion of oxygen atom (O) between the NiPcs via the Ni atom. The Ni^{3+}/Ni^{2+} couple for both *poly*-Ni(OH)TDMPc-Au and *poly*-Ni(OH)TBMPc-Au, shows the cathodic peak to be much higher in magnitude than the anodic peak, while for *poly*-Ni(OH)TBMPc-GCE, the anodic and cathodic currents have almost the same magnitude. It is likely that the cathodic peak for the process using gold electrode is a combination of both Ni^{3+}/Ni^{2+} process and gold oxide reduction peaks. This was confirmed by recording the voltammogram of bare Au electrode under the same conditions as for Figure 5.12a-c, the gold oxide stripping peak was observed at ~ -0.2 V (not shown), which is the same range as the cathodic peak of the Ni^{3+}/Ni^{2+} process.

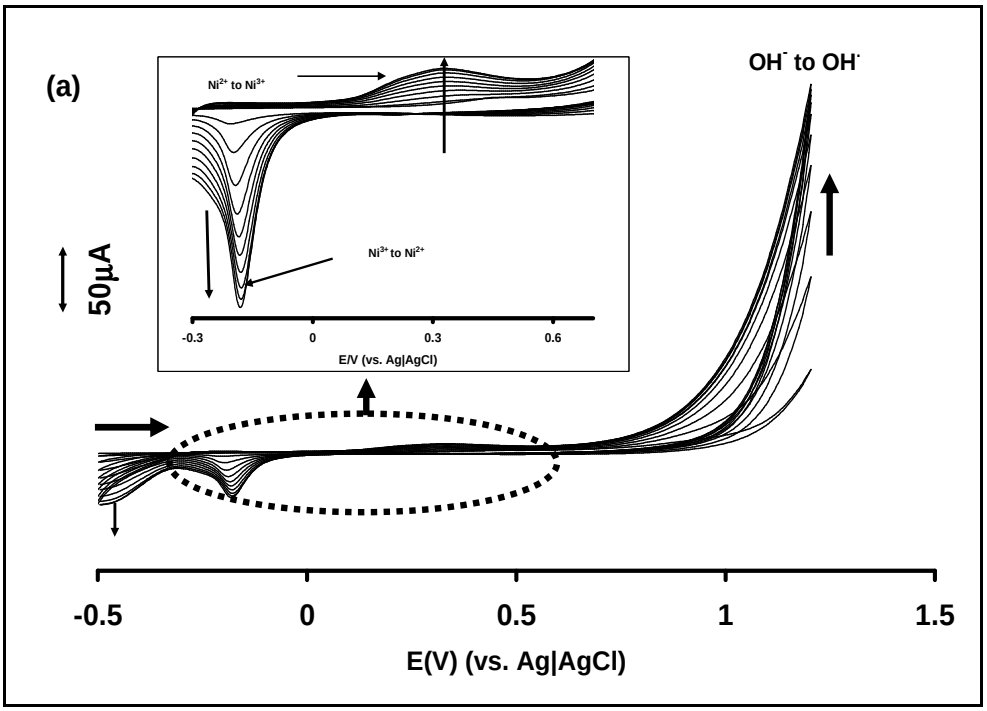
(a)
Ni2+ to Ni3+
Ni3+ to Ni2+
-0.3
0
0.3
0.6
E/V (vs. Ag|AgCl)
50µA
OH- to OH-
-0.5
0
0.5
1
1.5
E(V) (vs. Ag|AgCl)

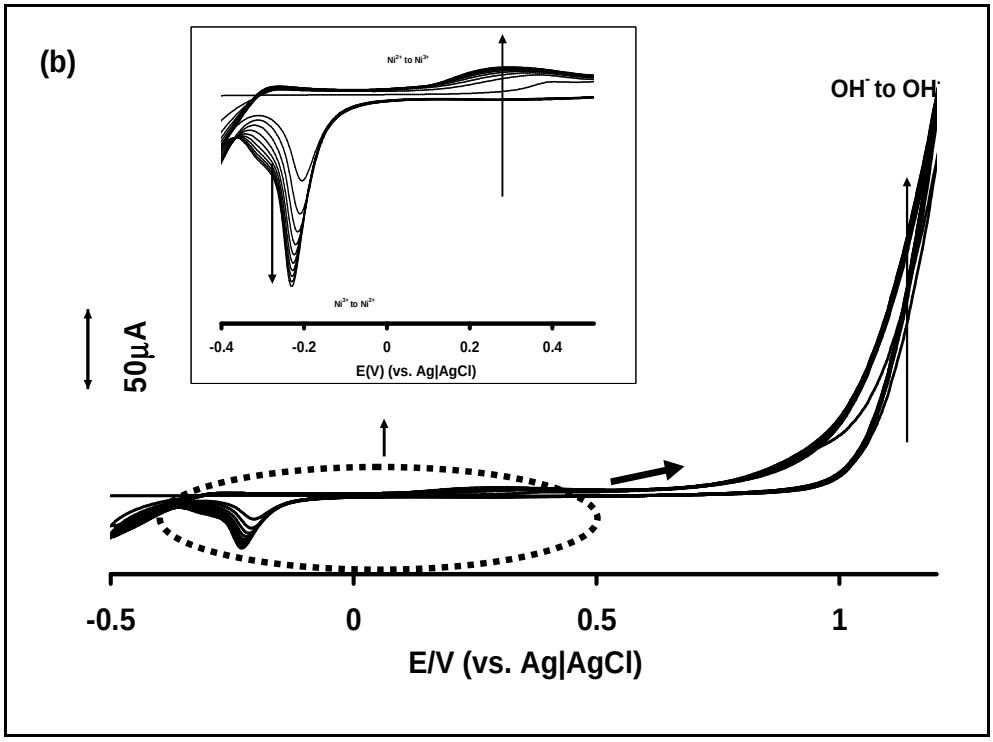
(b)
Ni2+ to Ni3+
Ni2+ to Ni2+
-0.4
-0.2
0
0.2
0.4
E(V) (vs. Ag|AgCl)
50µA
OH- to OH-
-0.5
0
0.5
1
E/V (vs. Ag|AgCl)

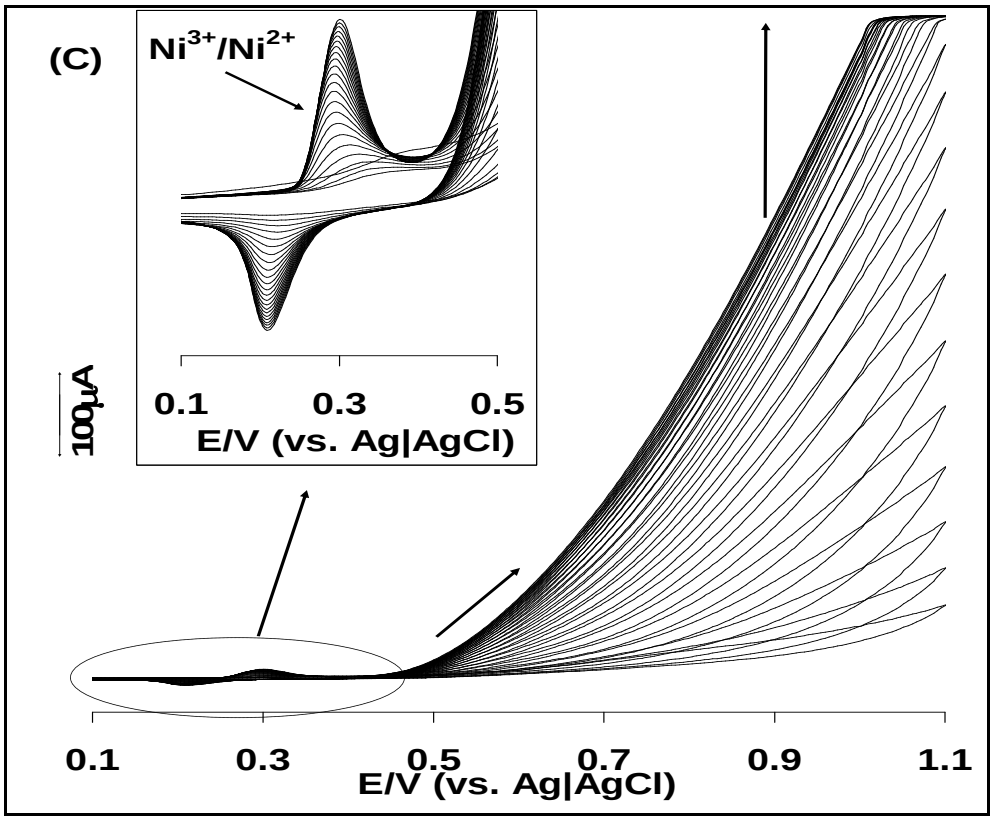

Figure 5.12: Repetitive cyclic voltamogramms of (a) *poly*-NiTBMPc-Au, (b) *poly*-NiTDMPc-Au and (c) *poly*-NiTBMPc-GCE in 0.1 M NaOH. Scan rate = 100 mV s^{-1} for (a) and (b), 200 mV s^{-1} for (c).

5.1.4.2 Electrochemical Impedance Spectroscopy (EIS) characterisation

This technique was used to characterise *poly*-NiPc-modified electrodes with different polymer thickness and *poly*-NiPc-modified electrodes with different form; *poly*-NiPc or *poly*-Ni(OH)Pc. EIS was used only for the NiPc-modified electrodes because of the importance of differentiating between the *poly*-NiPc and *poly*-Ni(OH)Pc on Au electrode. EIS technique can be used to check whether electrodes are modified or not. Generally, a bare electrode should exhibit an almost straight line for the Nyquist plot which is imaginary resistance versus the real resistance ($-Z_{im}$ vs. Z_{re}) because electrochemical reactions at such electrode surfaces are expected to be a mass diffusional limiting

electron-transfer process.[81,407] For a modified electrode, the Nyquist plot shows characteristic semi-circle pattern due to barrier to the interfacial electron-transfer.[81,407]

For each NiPc complex, three different films on gold electrodes were prepared; *poly*10-Ni(OH)Pc-Au, *poly*20-Ni(OH)Pc-Au and *poly*30-Ni(OH)Pc-Au for polymerisation scan number 10, 20 and 30 respectively and were characterised by EIS technique. Figures 5.13a and b respectively show the EIS of *poly*-Ni(OH)TBMPc and *poly*-Ni(OH)TDMPc prepared at different scan numbers. At potential regions where Ni^{2+} electrooxidation is just beginning, the impedance plots shows straight line behaviour for all modified electrodes; this behaviour have been observed before for NiPcs modified gold electrodes.[254] Thus the potential for the impedance measurements was carried out measured at 0.55 V, at this potential, Ni is present as Ni^{3+} only. The R_p values increases with scan number as shown in Table 5.1, this is an indication that the film thickness and compactness also increases.

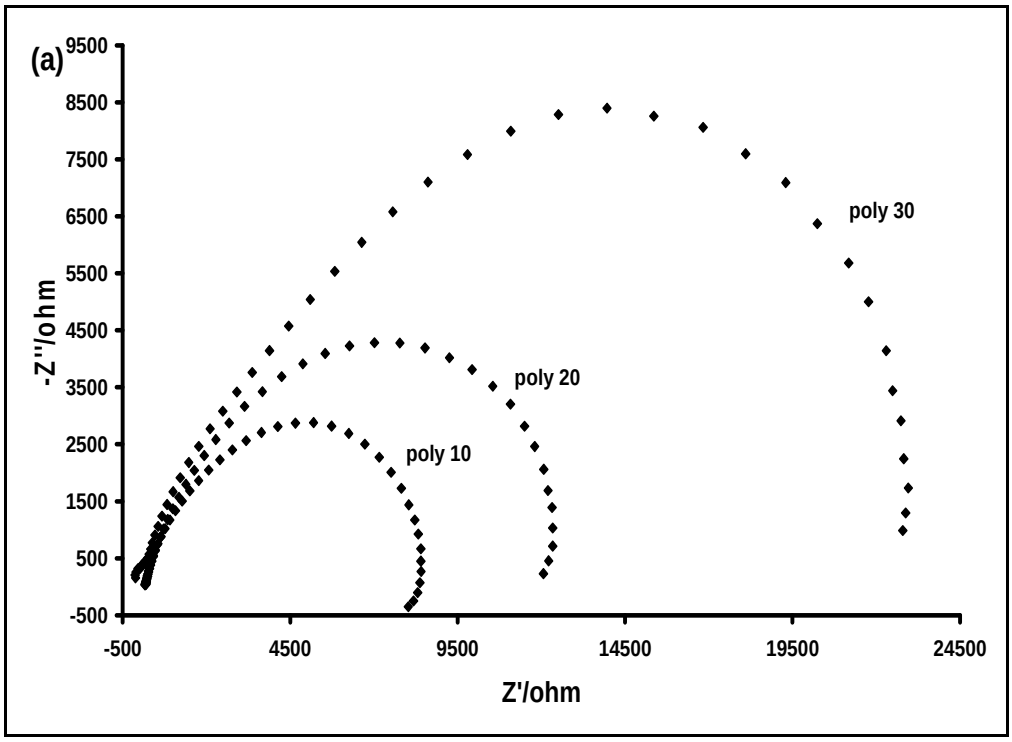

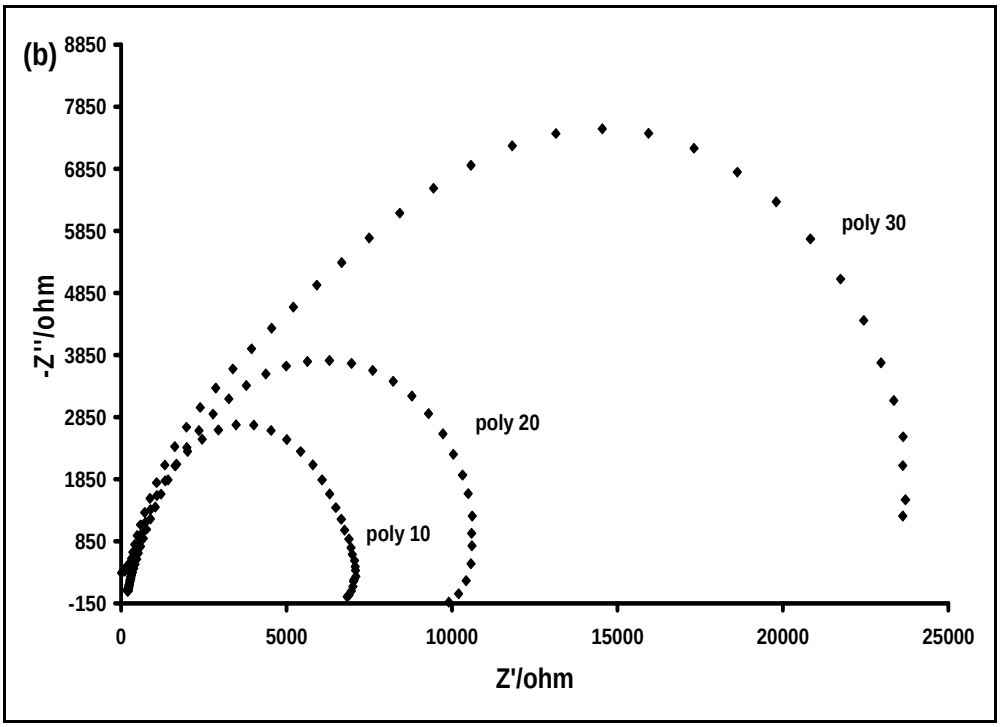

Figure 5.13: Impedance plots of (a) *poly*-Ni(OH)TBMPc-Au and (b) *poly*-Ni(OH)TDMPc-Au. (i) scan number (i) 10, (ii) 20 and (iii) 30. The electrolyte used was 0.1 M NaOH.

Table 5.1: Charge-transfer resistance (R_p) values of the *poly*-NiPcs films with different film thickness, deposited on gold electrodes.

Electrode	$R_p/10^{-4}\Omega$
Poly$_{10}$-NiTBMPc-Au	0.23
Poly$_{20}$-NiTBMPc-Au	1.06
Poly$_{30}$-NiTBMPc-Au	1.96
Poly$_{10}$-NiTDMPc-Au	0.25
Poly$_{20}$-NiTDMPc-Au	0.84
Poly$_{30}$-NiTDMPc-Au	1.27

Figure 5.14a shows the Nyquist plot for both bare gold and glassy carbon electrodes. The plots showed linearity expected from bare electrodes and this was observed at the same potentials used to measure the impedance data for modified electrodes. As shown in Figure 5.14b-d, all the NiPc-modified electrodes exhibited a semicircle plots expected when the electrodes are modified. The potentials for the impedance measurements of poly-NiTBMPc-Au, *poly*-NiTDMPc-Au and *poly*-NiTBMPc-GCE were 0.6, 0.6 and 0.5 V respectively, (Figures 5.9-5.11). These are their respective potentials closely after the formation of polymer anodic peaks while for the *poly*-Ni(OH)TBMPc-Au, *poly*-Ni(OH)TDMPc-Au and *poly*-Ni(OH)TBMPc-GCE, the potentials for the measurements are 0.5, 0.5 and 0.4 V respectively (Figures 5.12), at these potentials, Ni is present as Ni^{3+} only.

For each *poly*-NiPc-electrode and their corresponding *poly*-Ni(OH)Pc-electrode, the charge transfer resistance, R_p is higher for the latter than for the former indicating probably a more effective modification in the latter form due to the rearrangement of the NiPc complexes on the electrodes by the formation of interconnected 'O-Ni-O oxo' bridges. The R_p values are shown in Table 5.2.

Comparing GCE with Au electrode (Table 5.2) for the same NiPc complex, it shows that the former is more effectively modified judging with a large R_p values.

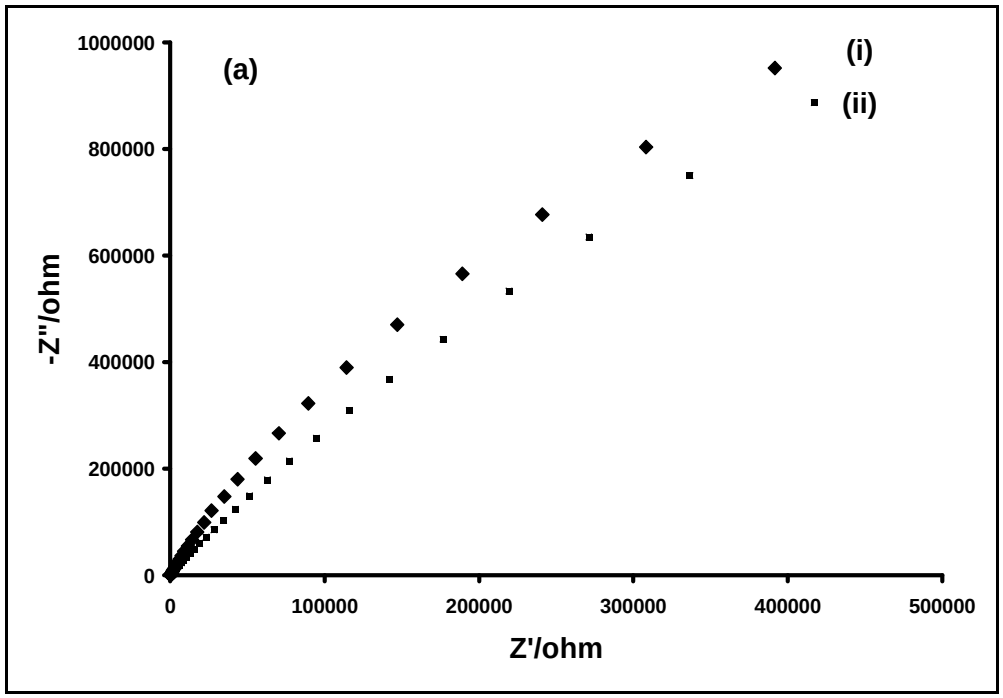
(a)
(i)
(ii)
1000000
800000
600000
400000
200000
0
-Z''/ohm
0
100000
200000
300000
400000
500000
Z'/ohm

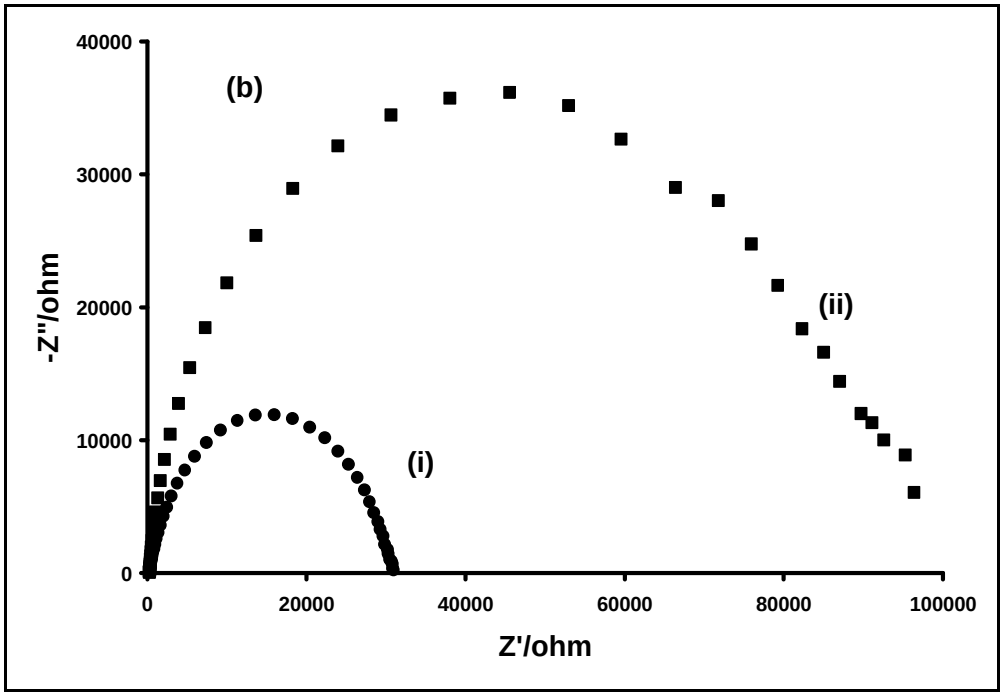
(b)
(i)
(ii)
40000
30000
20000
10000
0
-Z''/ohm
0
20000
40000
60000
80000
100000
Z'/ohm

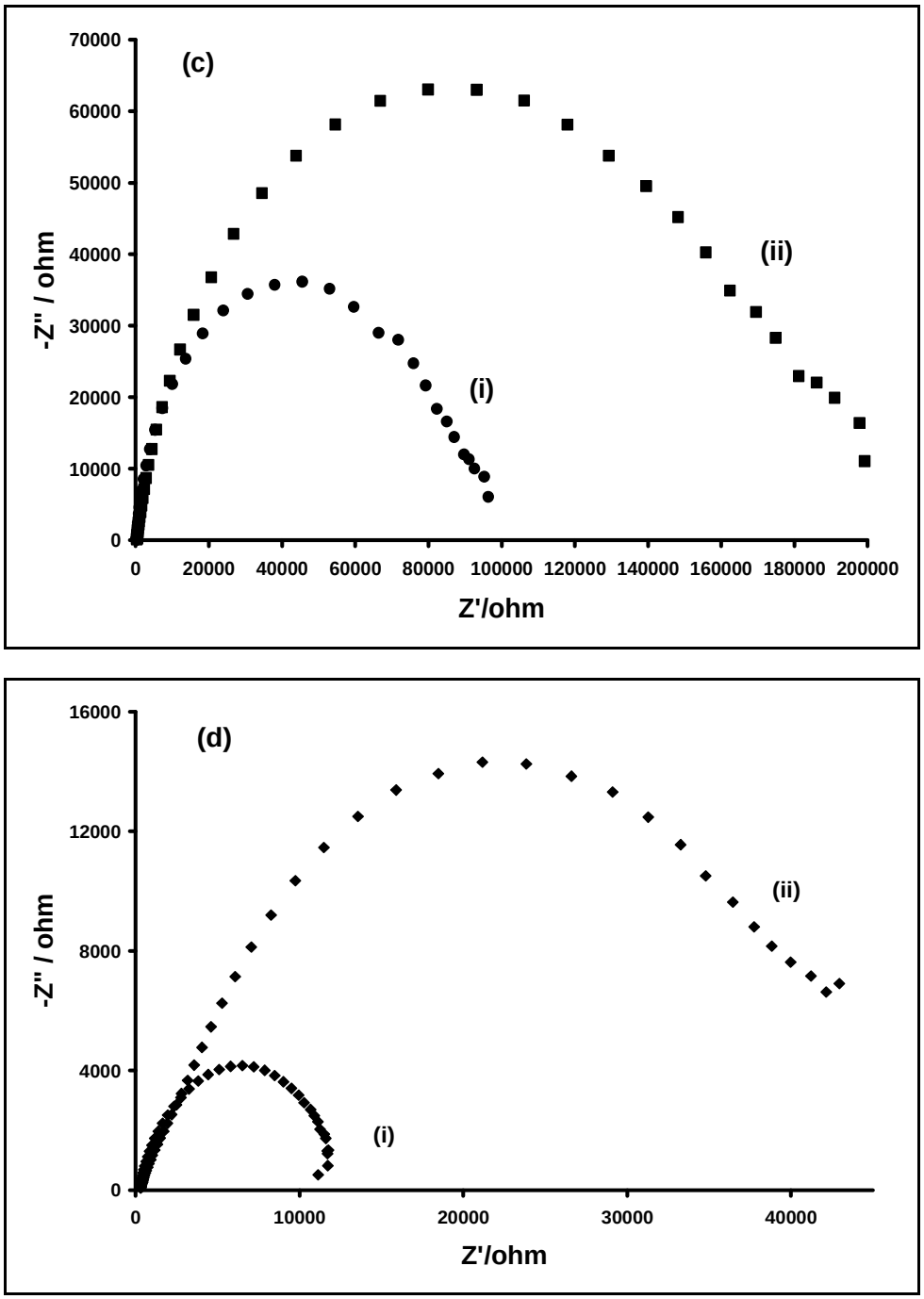

Figure 5.14: Impedance plots of (a) bare gold (i) and bare GCE (ii), (b) *poly*-NiTBMPc-Au (i) and *poly*-Ni(OH)TBMPc-Au (ii), (c) *poly*-NiTDMPc-Au (i) and *poly*-Ni(OH)TDMPc-Au (ii) and (d) *poly*-NiTBMPc-GCE (i) and *poly*-Ni(OH)TBMPc-GCE (ii). The electrolyte used was 0.1 M NaOH. Polymerisation number of scans = 30.

Table 5.2: Charge-transfer resistance (R_p) values of the *poly*-NiPcs films deposited on electrodes. Polymerisation number of scans = 30.

Electrode	$R_p/10^{-4}\Omega$
Poly-NiTBMPc-Au	3.1
Poly-Ni(OH)TBMPc-Au	9.9
Poly-NiTDMPc-Au	9.8
Poly-Ni(OH)TDMPc-Au	20
Poly-NiTBMPc-GCE	4.7
Poly-Ni(OH)TBMPc-GCE	11.8

5.1.4.3 Poly-NiPc spectral characterisation on ITO

The films were further characterised using UV-Visible spectral studies. Figure 5.15 shows the spectra of the NiTBMPc polymer films on ITO electrodes. It can be seen from Figure 5.15 that the higher the scan number, the more intense the Q band indicating more stacking as the polymerisation scan number increases. Comparing the spectrum of *poly*-Ni(OH)TBMPc with that of *poly*-NiTBMPc (Figure 5.15), the former has a sharp band at around 580 nm which is associated with the oxo bridges form of the complex.[407] Even though a broad peak at around 580 nm appeared for the *poly*-NiTBMPc, this peak is more likely to be due to the Q band shoulder as judged by the relatively blue shifted position of the Q band for *poly*-NiTBMPc.

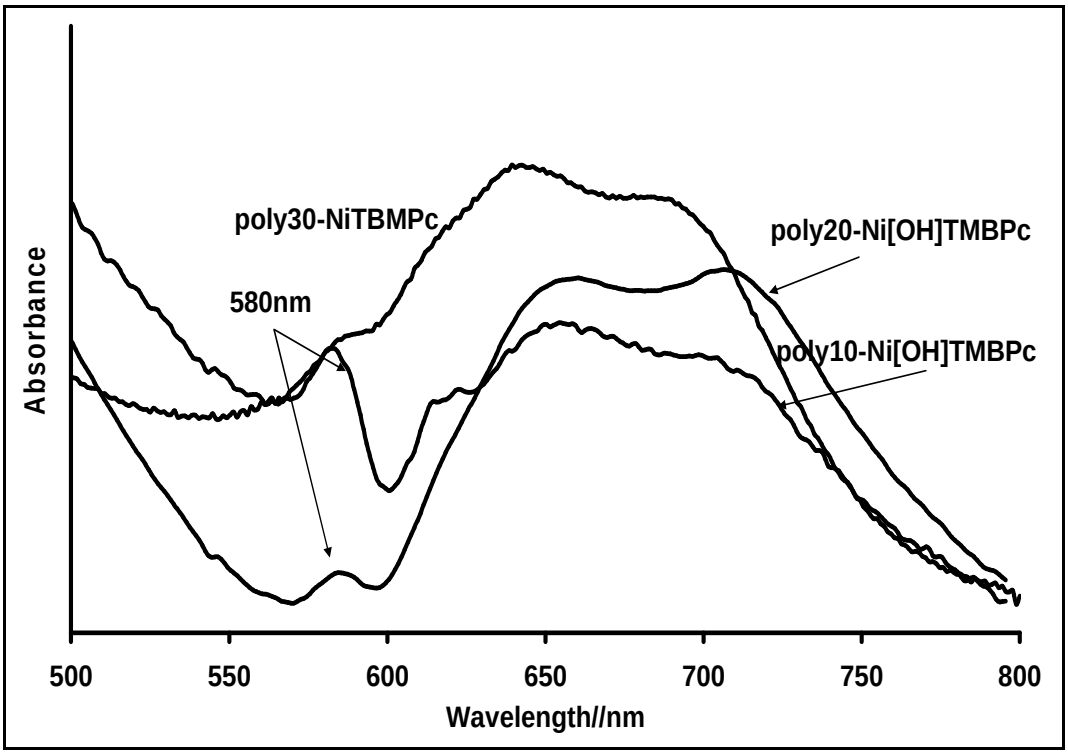

Figure 5.15: Electronic spectra of the poly-NiPc films on ITO.

5.2 Self-Assembled Monolayer

The chemosorption of thiol-derivatised MPc complexes (**34-43**) on gold electrodes was achieved by the immersion of gold electrodes in the various solutions containing the complex in DCM.

5.2.1 Optimisation of SAM formation time

An investigation of the minimum time needed for the formation of a stable and well packed SAM was conducted using $[Fe(CN)_6]^{3-}/[Fe(CN)_6]^{4-}$ couple, the cobalt analogues of these MPcs were used for the study because they catalyse this redox reaction. A well

formed CoPc-SAM of the molecules with flat orientation on the gold electrodes should be able to catalyse this redox reaction, and the currents should be of same magnitude as on bare Au electrode. The $[Fe(CN)_6]^{3-}/[Fe(CN)_6]^{4-}$ redox system occurs on cobalt (II) octabutylthiolphthalocyanine-SAM with currents and potentials similar to those observed on bare gold electrodes.[409] Also in the study of the electrocatalytic activity of adsorbed cobalt tetra-aminophthalocyanine films on vitreous carbon electrodes,[110] it was observed that both modified and unmodified electrode showed the same redox potential and almost equal peak currents intensities, for Fe^{3+}/Fe^{2+} and that the modified electrodes act as electronic conductors which allow rapid electron transfer to the solution species. It was also observed[410] that among tetraamino phthalocyanines with Co^{2+}, Cu^{2+} and Fe^{3+}, only the cobalt analog catalysed the $[Fe(CN)_6]^{3-}/[Fe(CN)_6]^{4-}$ redox reaction, this indicates the involvement of central metal, Co^{2+} in the catalysis of the redox reaction. The fact that $[Fe(CN)_6]^{3-}/[Fe(CN)_6]^{4-}$ activity on gold and modified electrodes is identical can be explained by its reversibity. Catalysis means increasing electron transfer rate but for a reversible process it is transport that determines the overall reaction rate at all applied potentials, therefore increase in electron transfer rate does not increase the overall rate. Thus, identical curves were obtained. A multi layer or non flat orientation of the molecules on gold electrodes may cause partial blockage of the central metal ion, Co^{2+} from getting exposed to the electrolyte solution. Figures 5.16a and b show the CVs of $[Fe(CN)_6]^{3-}/[Fe(CN)_6]^{4-}$ redox system at different times for SAM formation at CoTBMPc and CoTDMPc SAM modified gold electrodes. For SAM_1, SAM_6 and SAM_{18}, (where subscripts are SAM formation time), catalysis still occurred since there was no significant decrease in both anodic and cathodic currents compared to that of the bare gold electrode

and also no significant shift in the peak potentials while for SAM_{24} and SAM_{48} there was evidence of decrease in catalysis judging by both the decrease in the anodic and cathodic current and also the shift in the anodic and cathodic peak potentials. The reason why there was less catalysis of the $[Fe(CN)_6]^{3-}/[Fe(CN)_6]^{4-}$ system by the SAM_{24} and SAM_{48} could be that the remaining gold sites were filled up but not necessary in the flat orientation but vertical orientation in which just one or two of the thiol "arms" were bound to the gold sites and this can cause a partial blocking of the Co^{2+} ions from getting exposed to the electrolyte solutions. Another possibility is the formation of multilayers by ring substituents interaction through Van der Waal forces or by Co^{2+} ions coordinations, resulting in reduced electron transfer rate between the multilayers.

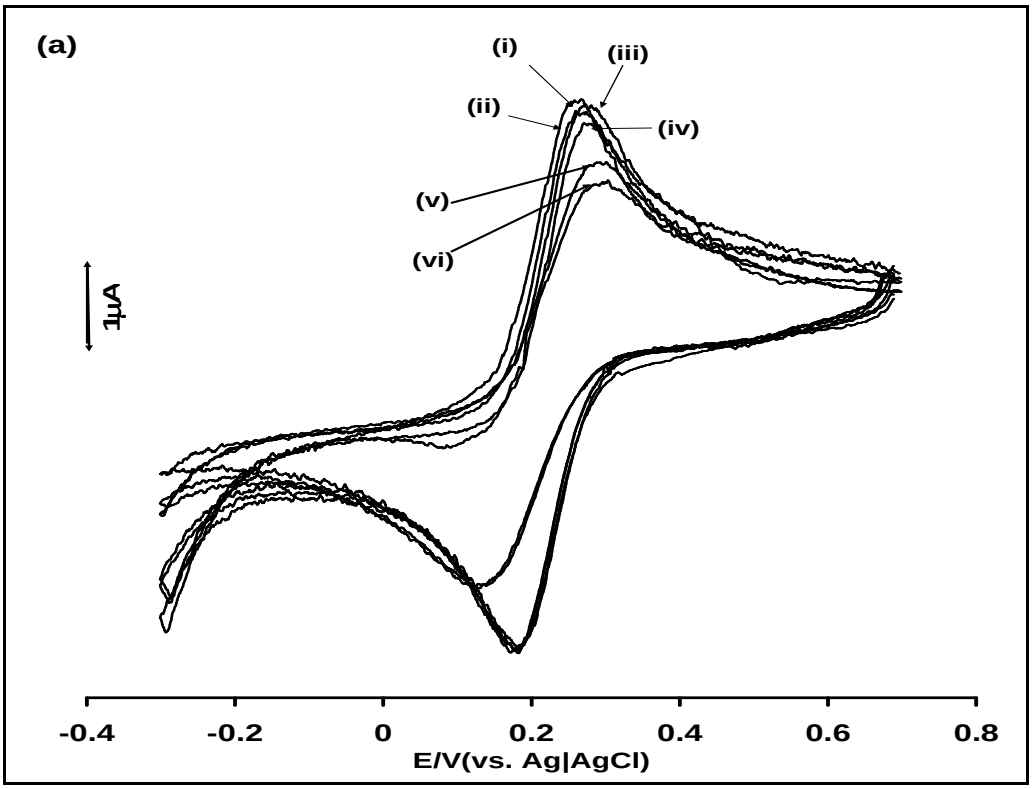

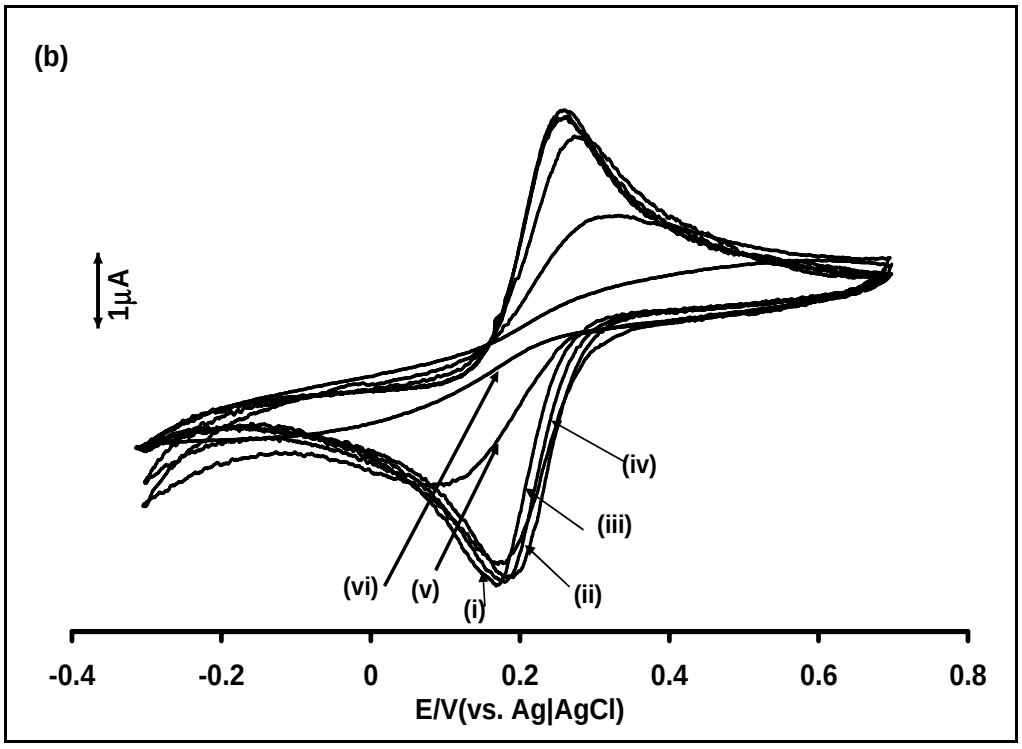

Figure 5.16: Typical comparative cyclic voltammograms showing the responses of gold electrodes at different SAM formation time (i) bare gold, (ii) 1 hour, (iii) 6 hour, (iv) 18 hour, (v) 24 hour, (vi) 48 hour with (a) CoTBMPc and (b) CoTDMPc. Electrolyte = 1 mM $K_3Fe(CN)_6$ in 0.2 M KCl. Scan rate = 50 mV s^{-1}.

At the same time, the integrity of the different SAM formed at different times were monitored using CVs of the gold oxidation/reduction in 10 mM KOH, Figures 5.17a and b show the CVs at different times for SAM formation. For all the different times, the SAMs formed blocked the Au oxide formation indicating an effective SAM formation.

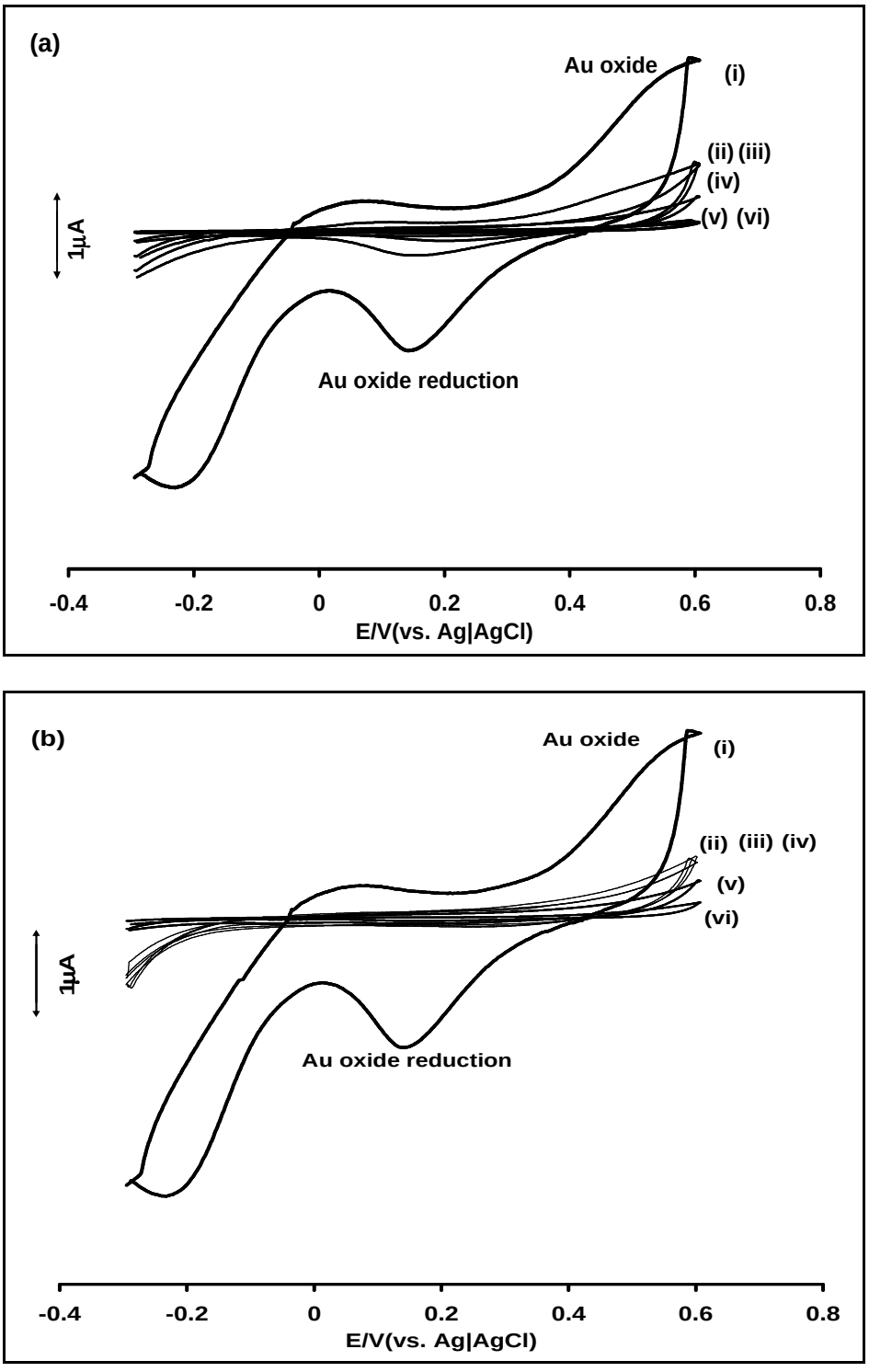

Figure 5.17: Typical comparative cyclic voltammograms showing the responses of gold electrode at different SAM formation time (i) bare gold, (ii) 1 hour, (iii) 6 hour, (iv) 18 hour, (v) 24 hour, (vi) 48 hour with (a) CoTBMPc (**35**) and (b) CoTDMPc (**40**). Electrolyte = 10 mM KOH. Scan rate = 50 mV s^{-1}.

In order to estimate the surface concentration of the complexes on gold electrodes, the real surface area of the gold electrodes was first determined using the conventional method.[201] Randles-Sevcik equation (5.1) introduced in 1.11 in chapter 1 was employed.

$$I_{pa} = (2.69 \text{ X } 10^5)\, n^{3/2} D^{1/2} v^{1/2} AC \qquad (5.1)$$

where n is the number of electron transferred (n = 1), *D* is the diffusion coefficient of $[Fe(CN)_6]^{3-}$ (7.6×10^{-6} cm^2 s^{-1}), *v* is the scan rate (0.05 V s^{-1}), A is the geometric surface area (0.0201 cm^2), C is the bulk concentration of $[Fe(CN)_6]^{3-}$ (1 mM). The surface roughness of the Au electrode used in this work was found to be 1.32 (ratio of I_{pa} (exptal.) /I_{pa} (theor.)), where I_{pa} (exptal.) is the experimental current and $I_{pa\ (}$theor.) is the current calculated using equation 5.1, using the geometrical area of the electrode. Using the surface roughness, the real surface area of the electrode was found to be 0.0279 cm^2 (roughness factor multiply by theoretical surface area).

For the estimation of the surface concentration of complexes on gold electrode, the charge difference between the bare gold (Q_{Bare}) and the Au modification with complexes (Q_{SAM}) (Figure 5.17, 18 hours SAM time) was determined. This is proportional to the fraction of the gold sites covered by the SAMs of complexes and corresponds to three times the amount of gold sites that are covered with the MPc-SAM, following the equation (5.2):

$$Au.H_2O + 2H_20 \rightleftharpoons Au(OH)_3 + 3H^+ + 3e^- \qquad (5.2)$$

This fraction is thus divided by three to get the charge proportion to gold sites covered with CoPc-SAM. The amount of gold sites covered by the MPc-SAM is then divided by four (each CoPc is assumed to consume four gold sites) and then divided by 0.0279 cm^{-2} which is the geometric area of the gold electrode surface to get the charge density

proportional to each CoPc molecule, these values can then be converted to the corresponding surface concentration in mol cm^{-2} is determined by dividing them by the Faraday constant (96485 C mol^{-1}). The surface concentration in number of molecules per area in cm^2 by simply multiplying the $\Gamma_{MPc\ (mol\ cm\text{-}2)}$ with the Avogadro's constant (N_A) and finally the inverse of the concentration in molecules per $Å^2$ correspond to the approximate surface area occupied per molecule. For a monolayer on gold electrode, the surface concentration of phthalocyanine complexes with flat orientation is approximately 1 x 10^{-10} mol cm^{-2}.[89,409] Table 5.3 shows the various approximate surface concentration values in mol cm^{-2} and the corresponding approximate gold surface area occupied per molecule ($Å^2$) for various CoPc-SAMs formed at different times. For cobalt macrocycles adsorbed as monolayers in the octopus configuration,[409,411] the surface concentrations are in the range ~1 x 10^{-10} mol cm^{-2}.

Table 5.3: Comparative surface concentration and approximate gold surface area occupied per molecule ($Å^2$) for the CoPcs-SAMs formed at different times

Time (hour)	**CoTBMPc (35), Γ (10^{10} mol cm^{-2})[a]**	**CoTDMPc (40), Γ (10^{10} mol cm^{-2})[a]**
1	0.42, (395)	0.44, (377)
6	0.67, (248)	0.72, (231)
18	0.86, (193)	0.91, (182)
24	1.18, (141)	1.37, (121)
48	1.38, (120)	1.49, (111)

[a] numbers in brackets are the approximate gold surface areas occupied per molecules ($Å^2$)

For both complexes, SAM_1 and $SAM_{6,}$ a significantly less surface concentration compared to the ~1 x 10^{-10} mol cm^{-2} value for monolayers were obtained while SAM_{18} concentration values for both complexes are within the monolayer concentration range.

Both complexes, SAM_{24} and SAM_{48} surface concentration values are higher than that of SAM_{18}, as stated before, this may probably be due to the filling up of the remaining gold sites but not necessary in the octopus orientation but vertical orientation in which there will be one or two of the thiol 'arms' involved in the binding to the gold sites. At all times for SAM formation, the surface concentration value of the SAM formed by the CoTDMPc (**40**) is larger than the CoTBMPc (**35**) counterpart, also from Figures 5.16a and b there were less catalysis of Fe^{3+}/Fe^{2+} by the CoTDMPc SAM compared to their CoTBMPc counterparts for both SAM_{24} and SAM_{48}. The influence of the ring substituents could be responsible for these observations, long chain alkanethiols are known to form closely packed SAM on gold electrodes and in addition, the C_{12} alkyl chain could cause more blocking of Co^{2+} than the benzylmercapto groups of the CoTBMPc (**35**).

The minimum time required for a closely packed SAM to be formed based on the characterisations above can be estimated as 18 hours since monolayers were formed at this time judging by the Γ_{MPc} calculated and further confirmed by SAM_{18} catalyses of Fe^{3+}/Fe^{2+} reaction. This time was then used for the formation of SAMs of the other complexes. Table 5.4 shows the SAM parameters, approximate surface concentration (mol cm^{-2}) and corresponding approximate gold surface area occupied per molecule ($Å^2$) for all the SAM formed by the MPc complexes after 18 hours. It is very clear that for all the complexes, well packed SAMs were formed with surface concentrations values within the monolayers values ($0.78 – 0.92 \times 10^{-10}$ mol cm^{-2}) in which the molecules are lying in octopus configuration on the gold electrode surface and occupying approximately 200 $Å^2$ per molecule.

It is possible that not all of the four substituents are attached; hence the Γ_{MPc} values are a rough estimate. Thus a second method for determining Γ_{MPc} value was employed using Equation 5.3 introduced in Chapter 1 as equation 1.20:

$$\Gamma_{MPc} = \frac{Q}{nFA} \qquad (5.3)$$

where Q is the background corrected electric charge of the anodic peaks in Figure 5.17, A is the real electrode surface area, and the other symbols have their usual meaning. The surface concentrations (Γ_{MPc}) were not too different from those obtained in the first method, Table 5.4. The Γ_{MPc} values were found to range from 0.83 to 1.04 x 10^{-10} mol cm^{-2} confirming monolayer formation. Generally, the surface concentration value of the SAM formed by the MTDMPc is larger than the MTBMPc counterparts, Table 5.4. This might be due to the influence of the ring substituents as explained above.

A good way of measuring how well SAM has isolated the gold electrode from the electrolyte solution is the so called ion barrier factor, Γ_{ibf} which can be obtained by equation 5.4 introduced in Chapter 1 as equation 1.24:

$$\Gamma_{ibf} = 1 - Q_{SAM}/Q_{Bare} \qquad (5.4)$$

where Q_{Bare} and Q_{SAM} are the total charges produced under the peak due to the reduction at the bare and at SAM modified gold electrodes. Figure 5.17 (18 hours SAM time) was used for the calculations. The Γ_{ibf} values calculated for the different SAM formation times are close to unity as shown in Table 5.4, and this implies that the SAMs are effective in providing barriers to ion and solvent permeability.

Table 5.4: Comparative surface concentration and approximate gold surface area occupied per molecule ($Å^2$) for the various MPcs-SAMs**.** SAM formation time = 18 hours.

MPc complex	Γ, (10^{10} mol cm^{-2})[a]	Γ, (10^{10} mol cm^{-2})[b]	Γ_{ibf}
CoTBMPc (**35**)	0.86, (194)	0.89	0.98
CoTDMPc (**40**)	0.91, (182)	1.02	0.96
FeTBMPc (**36**)	0.74, (224)	0.83	0.99
FeTDMPc (**41**)	0.78, (213)	0.85	0.99
MnTBMPc (**34**)	0.69, (241)	0.78	0.97
MnTDMPc (**39**)	0.78, (213)	0.94	0.99
NiTBMPc (**37**)	0.87, (191)	1.02	0.96
NiTDMPc (**42**)	0.92, (180)	1.04	0.99
ZnTBMPc (**38**)	0.79, (210)	-	0.97
ZnTDMPc (**43**)	0.82, (202)	-	0.98

[a] method 1 using equation 5.2, numbers in brackets are the approximate gold surface areas occupied per molecules ($Å^2$), [b]method 2 using equation 5.3

5.2.2 Blocking characteristics of the faradaic reactions by MPc-SAMs

In a separate set of experiments, the self assembled monolayer films of the complexes on gold electrodes were characterised using the following well established Faradaic processes;[231,242] gold surface oxidation, solution redox chemistry of $[Fe(H_2O)_6]^{3+}$/ $[Fe(H_2O)_6]^{2+}$ and underpotential deposition (UPD) of copper. Figure 5.17 was employed for Au oxide reaction. Figure 5.18a and b respectively show typical cyclic voltammograms of (a) 1 mM $Fe(NH_4)(SO_4)_2$ in 1 mM $HClO_4$ electrolyte and (b) 1 mM $CuSO_4$ in 0.5 M H_2SO_4 electrolyte at (i) bare gold electrode and (ii) complex **35** (as an

example) modified gold electrode at a scan rate of 100 mV s^{-1}. In Figures 5.17 and 5.18, the modified electrodes inhibited the Faradaic processes showing that the SAM formed on the gold electrodes are stable, well packed and defect free, as evidenced first by inhibition of the gold oxidation, Figure 5.17 and decrease in the corresponding reduction peak after SAM formation. Secondly, it is clear that the quasi reversible redox reaction $[Fe(H_2O)_6]^{3+}/[Fe(H_2O)_6]^{2+}$ which occurred at the bare gold electrode is inhibited at complex **35**-SAM modified Au electrodes, Figure 5.18a. In Figure 5.18a, the Fe^{3+}/Fe^{2+} redox peak lost its shape and intensity on SAM electrodes. This is a good indication that the SAM formed isolates the gold surface from the electrolyte solution. And finally the copper deposition process was inhibited by the SAMs in Figure 5.18b, complex **35** (as an example). The UDP of Cu and the stripping peaks occurred at about -0.45 and -0.1 V respectively at the bare gold electrode as shown in Figure 5.18b. These peaks did not appear in the CVs obtained at complex **35**-SAM gold electrodes clearly showing that the CoPc-SAMs formed is well packed and almost free from pinholes and defects. Similar results in both experiments were also obtained for the other MPcs-SAM electrodes.

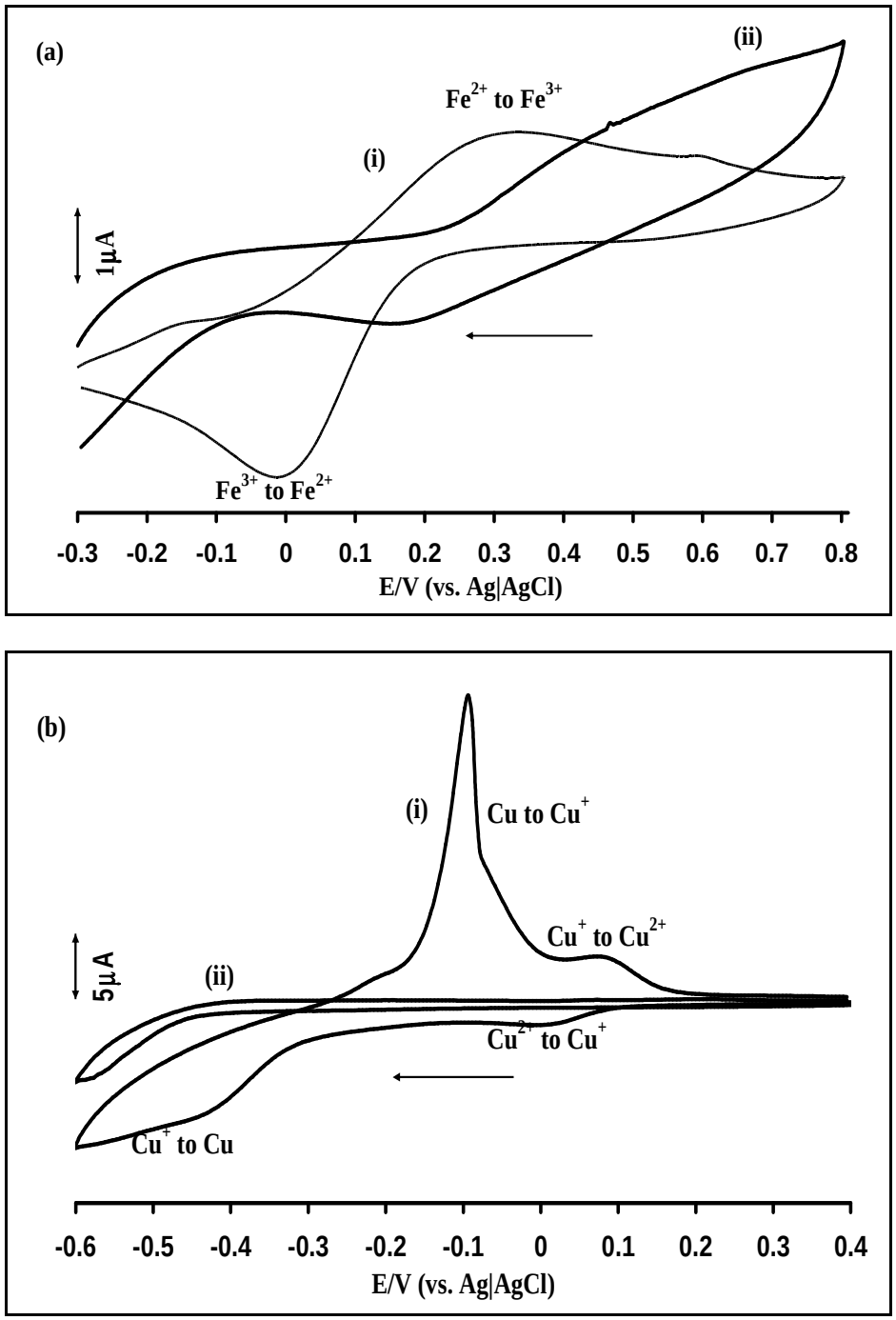

Figure 5.18: Typical cyclic voltammograms of (a) 1 mM $Fe(NH_4)(SO_4)_2$ in 1 mM $HClO_4$ electrolyte and (b) 1 mM $CuSO_4$ in 0.5 M H_2SO_4 electrolyte at (i) bare gold electrode, (ii) complex **35** modified gold electrode. Scan rate = 100 mV s^{-1}.

5.2.3 Oxidation redox couples of the MPc-SAM electrodes

The positions of the oxidation redox peaks of the complexes on gold electrodes were determined in phosphate buffers pH 4 and 7.4; the latter is essential since these modified electrodes were fabricated for the electrocatalysis of sulphite oxidation in phosphate buffers pH 7.4.

Figures 5.19a-d respectively show the typical CVs of the MPc-SAMs of CoPcs, FePcs, MnPcs and NiPcs in phosphate buffer pH 7.4. Both metal and ring based redox peaks were observed for the CoPcs, FePcs and MnPcs while only the ring based ones were observed for the NiPcs. NiPc complexes are known to often show metal based redox inactivity and so this could be the reason for the non appearance of Ni^{3+}/Ni^{2+} peak. The plots of peak currents, I_p (M^{3+}/Mn^{2+} for CoPcs and FePcs, M^{4+}/M^{3+} for MnPcs and Pc^{-}/Pc^{2-} for NiPcs) versus the scan rates (Figures 5.19a-d insets) were linear showing that the complexes are surface confined onto the gold electrodes.[201] The peaks are generally broad characteristics of surface confined species redox peaks; this can be attributed to the fact that the redox reactions may be kinetically hindered.[412]

The redox peaks were also observed in phosphate buffer pH 4, Figure 5.20 shows the CVs of the CoPc complexes (as an example).

Table 5.5 shows the redox peaks of all complexes in phosphate buffer pH 4 and 7.4.

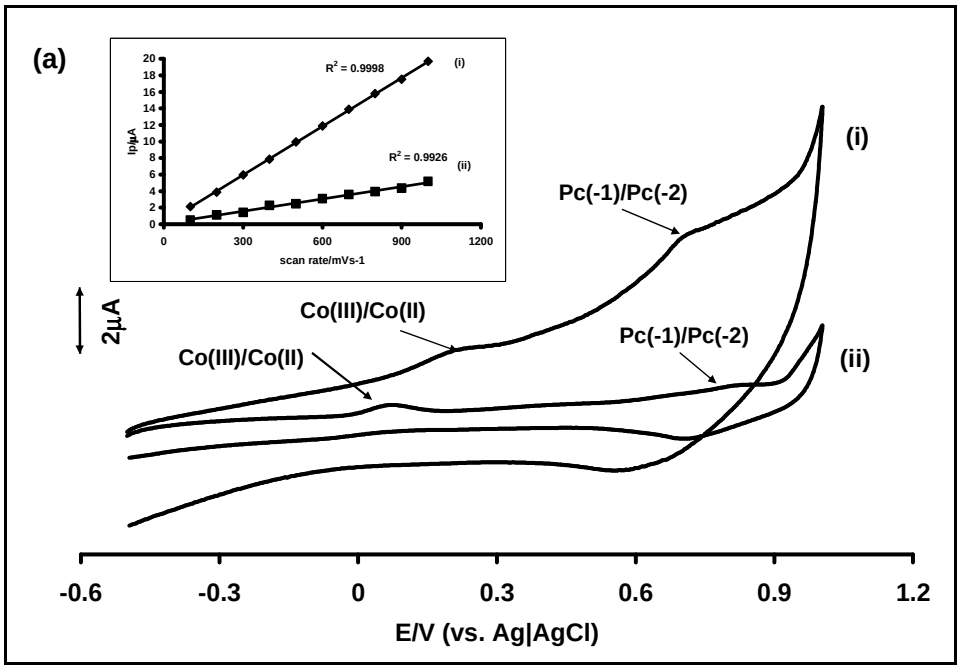
(a)
R² = 0.9998
(i)
R² = 0.9926
(ii)
Ip/μA
scan rate/mVs-1
Pc(-1)/Pc(-2)
(i)
2μA
Co(III)/Co(II)
Co(III)/Co(II)
Pc(-1)/Pc(-2)
(ii)
-0.6
-0.3
0
0.3
0.6
0.9
1.2
E/V (vs. Ag|AgCl)

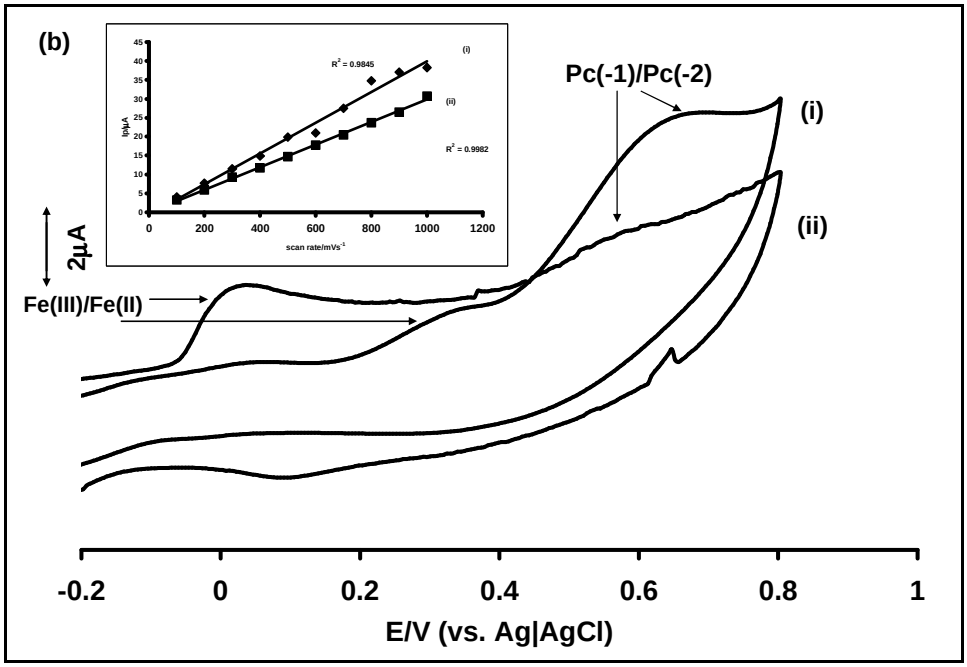
(b)
R² = 0.9845
(i)
(ii)
R² = 0.9982
Ip/μA
scan rate/mVs⁻¹
Pc(-1)/Pc(-2)
(i)
(ii)
2μA
Fe(III)/Fe(II)
-0.2
0
0.2
0.4
0.6
0.8
1
E/V (vs. Ag|AgCl)

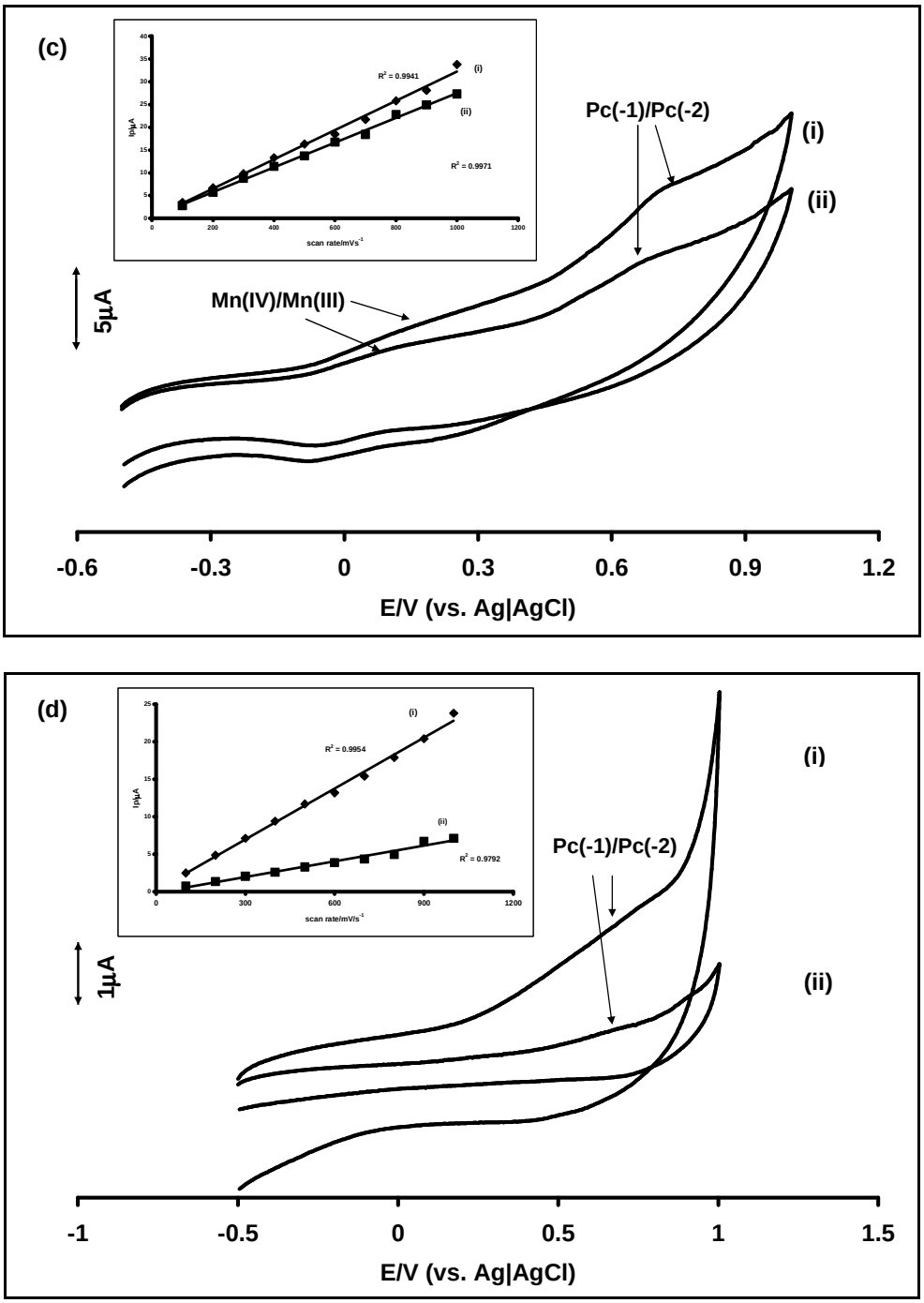

Figure 5.19: Cyclic voltammograms of the complexes in phosphate buffer pH 7.4, (a) CoPcs, (b) FePcs, (c) MnPcs and (d) NiPcs. Curve (i) MTBMPc and (ii) MTDMPc. Scan rate = 100 mV s^{-1}.

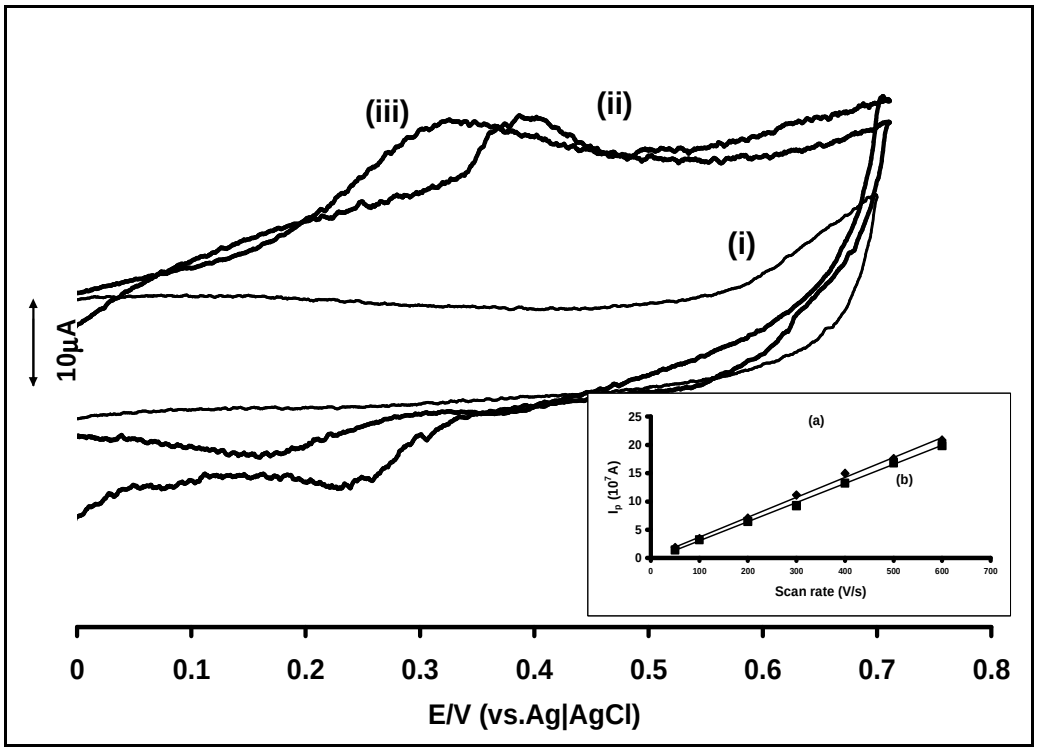

Figure 5.20: Comparative cyclic voltammograms obtained at (i) bare gold electrode, (ii) CoTBMPc-SAM gold electrode and (iii) CoTDMPc-SAM gold electrode in phosphate buffer pH 4. Inset is the plot of anodic peak currents (a) CoTBMPc and (b) CoTDMPc versus scan rate. Scan rate = 100 mV s^{-1}.

Table 5.5: Comparative anodic peaks (V) vs. Ag|AgCl of all MPcs-SAM Au electrodes in phosphate buffers pH 4 and 7.4.

MPc complex	**E (V), Peak assignment pH 4**		**E (V), Peak assignment in pH 7.4**	
CoTBMPc (**35**)	0.40	Co^{3+}/Co^{2+}	0.23	Co^{3+}/Co^{2+}
CoTDMPc (**40**)	0.33	Co^{3+}/Co^{2+}	0.10	Co^{3+}/Co^{2+}
FeTBMPc (**36**)	0.45	Fe^{3+}/Fe^{2+}	0.08	Fe^{3+}/Fe^{2+}
FeTDMPc (**41**)	0.41	Fe^{3+}/Fe^{2+}	0.31	Fe^{3+}/Fe^{2+}
MnTBMPc (**34**)	0.35	Mn^{4+}/Mn^{3+}	0.11	Mn^{4+}/Mn^{3+}
MnTDMPc (**39**)	0.20	Mn^{4+}/Mn^{3+}	0.13	Mn^{4+}/Mn^{3+}
NiTBMPc (**37**)	none [a]	none [a]	(0.66)	(Pc^{-}/Pc^{2-})
NiTDMPc (**42**)	none [a]	none [a]	(0.70)	(Pc^{-}/Pc^{2-})

[a]no peaks observed

Lastly, the stability of the MPcs-SAM was also studied, this was done as a function of pH and applied potential. The immobilised films showed high stability from pH 2 to 9 in the potential window -0.2 to +0.8 V. However, at potentials outside this window SAM desorption occurred. These thiol derivatised metallophthalocyanine complexes SAM modified gold electrodes showed stability with no detectable desorption when they were stored for over a period of one month in both pH 4 and pH 7 phosphate buffers.

5.3 Conclusion

In conclusion, newly synthesised thiol derivatised complexes, (MTBMPc and MTDMPc, M = Co^{2+}, Fe^{2+}, Mn^{3+} and Ni^{2+}) were successfully deposited on gold electrodes by electropolymerisation. The cyclic voltammogram evolution during electropolymerisation showed that the complexes were electropolymerised on Au electrodes. In addition, electropolymerisation of the complexes on Au electrodes were confirmed by similarity of the CVs of last scans of the electropolymerisation with the corresponding CVs in phosphate buffer pH 7.4 solution. The films of the NiPc derivatives were electro-transformed in aqueous 0.1 M NaOH solution to the 'O-Ni-O oxo' bridged form. For both complexes, films with different thicknesses were prepared and characterised by electrochemical impedance spectroscopy and the results showed typical behaviour for modified electrodes with increasing charge transfer resistance values, R_p with polymer thickness. Also, electrodes with *poly*-Ni(OH)Pcs films exhibited higher charge transfer resistance values, R_p than their corresponding *poly*-NiPcs films counterparts. Spectroelectrochemical method using ITO was also used for the characterisation of the NiPc films and this method differentiated between the *poly*-NiPc and *poly*-Ni[OH]Pc films.

The complexes (MTBMPc and MTDMPc, M = Co^{2+}, Fe^{2+}, Mn^{3+} Ni^{2+} and Zn^{2+}) were successfully used to modify gold electrodes by self assembled monolayer (SAM) technique. The self assembled films are stable and showed blocking characteristics towards the following Faradaic processes; gold surface oxidation, underpotential deposition (UPD) of copper and solution redox chemistry of $[Fe(H_2O)_6]^{3+}$/ $[Fe(H_2O)_6]^{2+}$. As evidenced from the voltammetric study, formation of stable, well packed and defect

free SAMs of benzyl- and dodecyl-mercapto tetra substituted first transition metal phthalocyanines complexes on gold electrodes is possible. Using the $[Fe(CN)_6]^{-3}$ /$[Fe(CN)_6]^{-4}$ redox system as a guide, it was shown that a possible change in molecules orientation from flat to vertical or multilayer form with increase in SAM formation time to 24 hours and above occurred. For the fist time, CV technique was used to optimise the time needed for SAM formation. Ring substituents influenced the blocking characteristics of the CoPcs-SAM towards $[Fe(CN)_6]^{-3}$/$[Fe(CN)_6]^{-4}$ redox process, CoTDMPc with dodecylmercapto ring substituents showing more blocking characteristic than that of CoTDMPc with benzylmercapto ring substituents.

CHAPTER 6

ELECTROCATALYTIC PROPERTIES

This chapter deals with the electrooxidation of the following pollutants: chlorophenols, nitrite and sulphite. These molecules were electrooxidised using thiol-derivatised MPc complexes modified on gold electrodes as catalysts. As earlier mentioned and explained in Chapter 5, for electropolymerisation, chlorophenols and nitrite will be studied while for SAMs, only sulphite will be studied.

6.1 Electrocatalytic oxidation of Chlorophenols with *poly*-NiPc films

Only the catalysis by the *poly*-NiPc-Au films are presented in this thesis, other *poly*-MPc-Au films showed insignificant catalysis.

6.1.1 Nature of the *poly*-NiPc films

Figure 6.1 shows the CVs of 1 mM (a) 4-CP in 0.1 mM NaOH at (i) unmodified gold electrode; (ii) *poly*-NiTBMPc-Au; (iii) *poly*-NiTDMPc-Au; (iv) *poly*-Ni(OH)TBMPc-Au; (iv) *poly*-Ni(OH)TDMPc-Au. A broad peak was obtained on unmodified electrode at ~ 0.4 V. It can be seen that the modified electrodes showed better catalytic behaviour towards 4-CP electrooxidation than the unmodified gold electrodes as judged by the shift in the potential to less positive values and the large increase in peak current. *Poly*-Ni(OH)TBMPc-Au and *poly*-Ni(OH)TDMPc-Au performed better than their corresponding *poly*-NiPc-Au electrodes as the catalytic peaks shifted to less positive potential from 0.34 to 0.33 V for both electrodes and there was larger increase in currents as follows: 12.1 µA (for *poly*-NiTBMPc) to 14.6 µA (for *poly*-Ni(OH)TBMPc) and 11.1 µA (for *poly*-NiTDMPc) to 14.0 µA (for *poly*-Ni((OH)TDMPc). The mechanism behind

the catalytic activity improvement of the electrooxidation processes when the nickel macro complexes are transformed to the 'O-Ni-O oxo form' is not fully understood, but Ni^{3+}/Ni^{2+} redox process maybe playing a key role in the reaction. As shown in Figure 5.12 (Chapter 5), the Ni^{2+} to Ni^{3+} peaks occur at around 0.2 to 0.3 V which is the same potential range for 4-CP oxidation and it can be seen in Figure 6.1a that the Ni^{3+}/Ni^{2+} redox is around 0.2 V and it appears as a shoulder to 4-CP oxidation peak for the *poly*-Ni(OH)TBMPc-Au and *poly*-Ni(OH)TDMPc-Au electrodes only (curves iv and v).

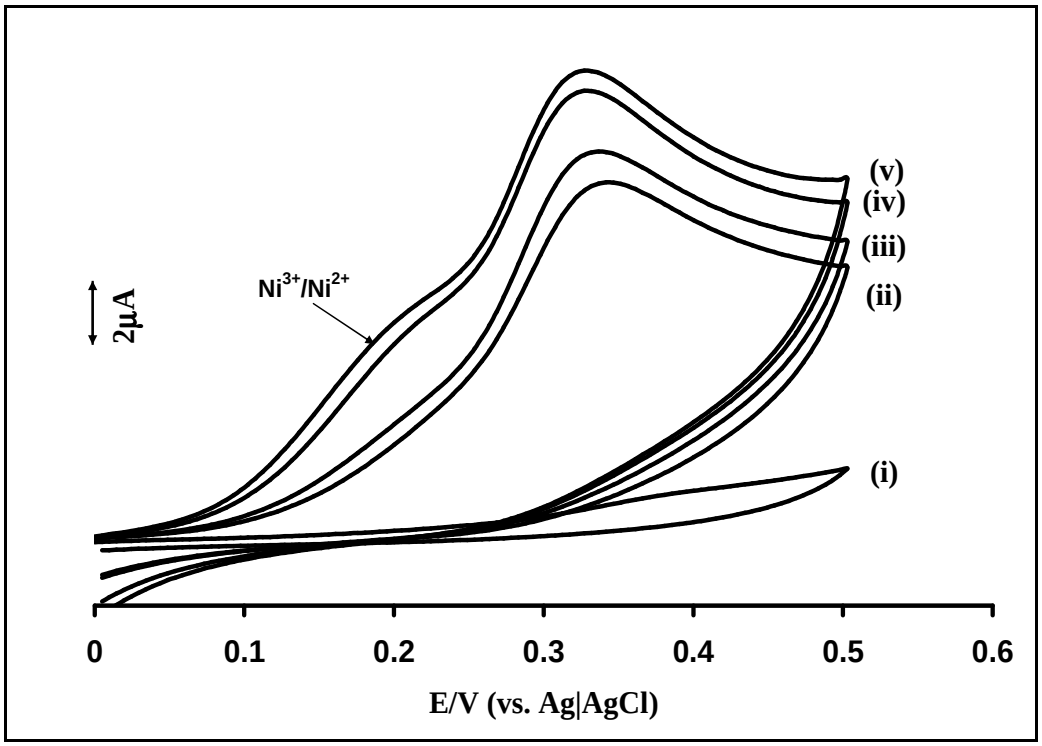

Figure 6.1: Cyclic voltammograms of 1 mM 4-CP in 0.1 mM NaOH at (i) unmodified gold electrode; (ii) *poly*-NiTBMPc-Au; (iii) *poly*-NiTDMPc-Au; (iv) *poly*-Ni(OH)TBMPc-Au; (iv) *poly*-Ni(OH)TDMPc-Au.

In the case of TCP electrooxidation, the potential peak shift was from 0.55 to 0.53 V and 0.55 to 0.50 V for *poly*-Ni(OH)TBMPc-Au and *poly*-Ni(OH)TDMPc-Au respectively,

compared with their *poly*-NiPc counterparts (Figure 6.2). The CVs (Figure 6.2) showing TCP electrooxidation by *poly*-Ni(OH)TBMPc-Au and *poly*-Ni(OH)TDMPc-Au (curves iv and v respectively) also have broad anodic peaks of the Ni^{3+}/Ni^{2+} redox process at around 0.3 V partially overlapping with the TCP anodic peak.

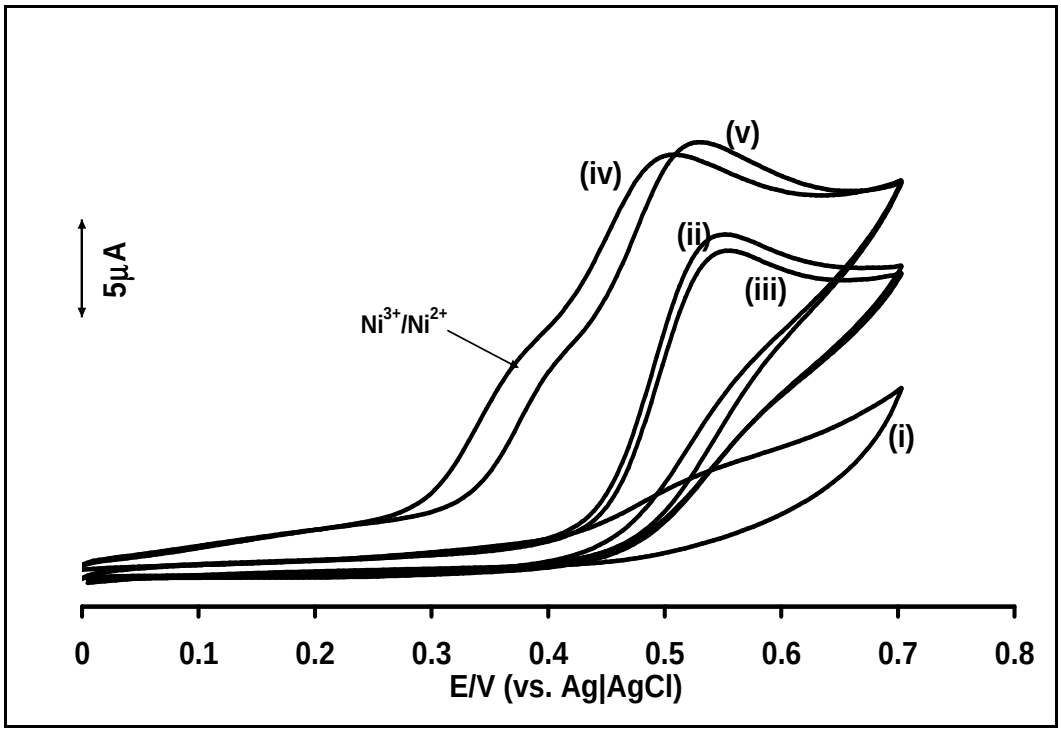

Figure 6.2: Cyclic voltammograms of 1mM TCP in 0.1 mM NaOH at (i) unmodified gold electrode; (ii) *poly*-NiTBMPc-Au; (iii) *poly*-NiTDMPc-Au; (iv) *poly*-Ni(OH)TBMPc-Au; (iv) *poly*-Ni(OH)TDMPc-Au.

6.1.2 Effects of poly-NiPc film thickness

The effect of film thickness on the electrocatalytic efficiency of the modified electrodes was investigated; the film thickness is expected to increase with the number of scans during polymerisation as long as the CV peaks are increasing in intensities. For both complexes, three different *poly*-Ni(OH)Pc-Au using different scan numbers were

prepared; *poly*10-Ni(OH)Pc-Au, *poly*20-Ni(OH)Pc-Au and *poly*30-Ni(OH)Pc-Au for polymerisation scan number 10, 20 and 30 respectively.

One major problem with electrooxidation of chlorophenols is the often irreversible passivation of the electrode by the oxidation products. The suppressing effect of film thickness on passivation was investigated, Figures 6.3 a and b respectively show the CVs for 4-CP oxidation at 'poly 10', 'poly 20' and 'poly 30' for Ni(OH)TBMPc (a) and Ni(OH)TDMPc (b) films on gold electrode (where 'poly number' is the polymerisation scan number). With increase in the polymerisation scan number, higher current and at the same time less positive potentials were obtained for 4-CP oxidation. This shows that catalytic activities increase as the film thickness increases. This can be explained by the fact that there will be more catalytic sites as the film thickness increases.

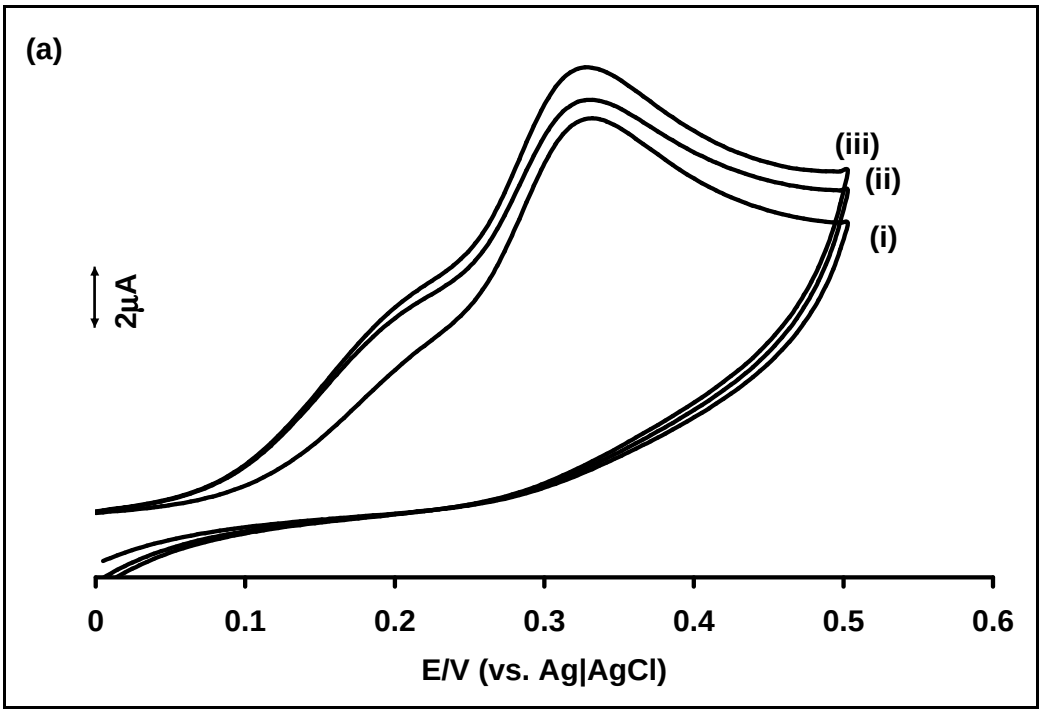

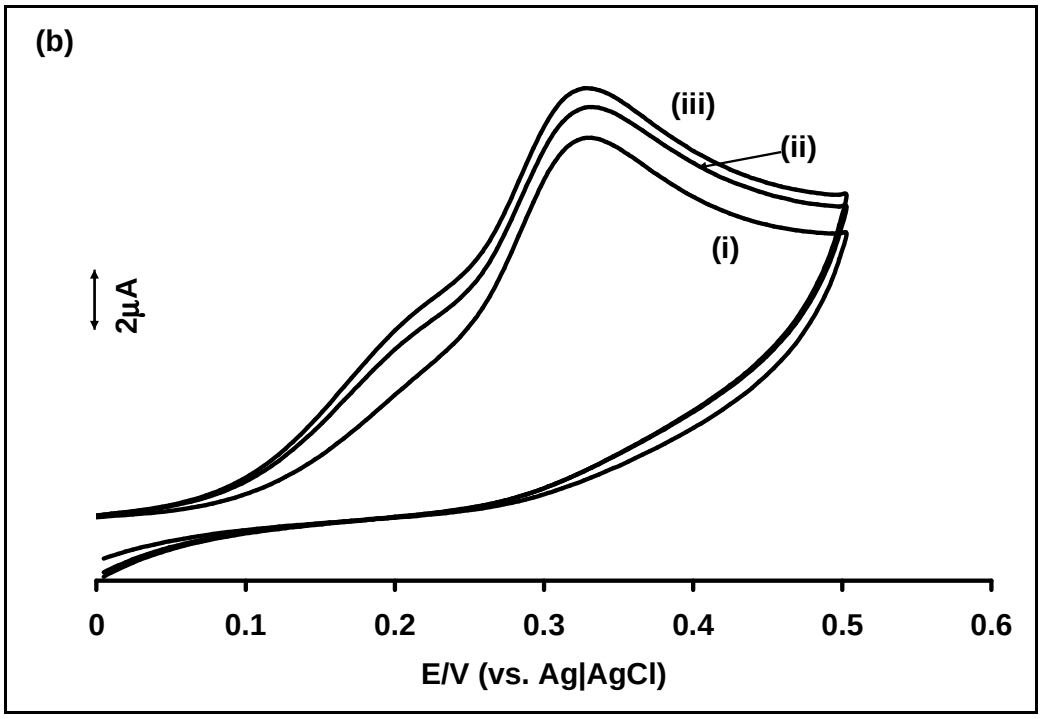

Figure 6.3: Cyclic voltammograms of 1 mM 4-CP catalysed by (a) *poly*-Ni(OH)TBMPc-Au and (b) *poly20*-Ni(OH)TDMPc-Au. Polymerisation number (i) 10, (ii) 20, (iii) 30. The electrolyte used was 0.1 M NaOH.

Figures 6.4 and 6.5 show the passivation of the modified electrodes following oxidation of 4-CP, using *poly*30-Ni(OH)TBMPc-Au (Figure 6.4a), *poly*20-Ni(OH)TBMPc-Au (Figure 6.4b) and *poly*10-Ni(OH)TBMPc-Au (Figure 6.4c); and *poly*30-Ni(OH)TDMPc-Au (Figure 6.5a, *poly*20-Ni(OH)TDMPc-Au (Figure 6.5b) and *poly*10-Ni(OH)TDMPc-Au (Figure 6.5c). In Figures 6.4 and 6.5, curves (i) are the first scans in chlorophenol solutions, curves (ii) are curves obtained after the second scan in chlorophenol solutions and curves (iii) were observed after the modified electrodes from (ii) were rinsed (for five minutes) in phosphate buffer and CV of the chlorophenols recorded as in (i). Curves (iii) show that there was recovery of the oxidation currents following rinsing with phosphate buffer. For both Ni(OH)TBMPc-Au and Ni(OH)TDMPc-Au electrodes, the largest

recovery was obtained for films formed by 30 scans, and the least for 10 polymerisation scans, Table 6.1.

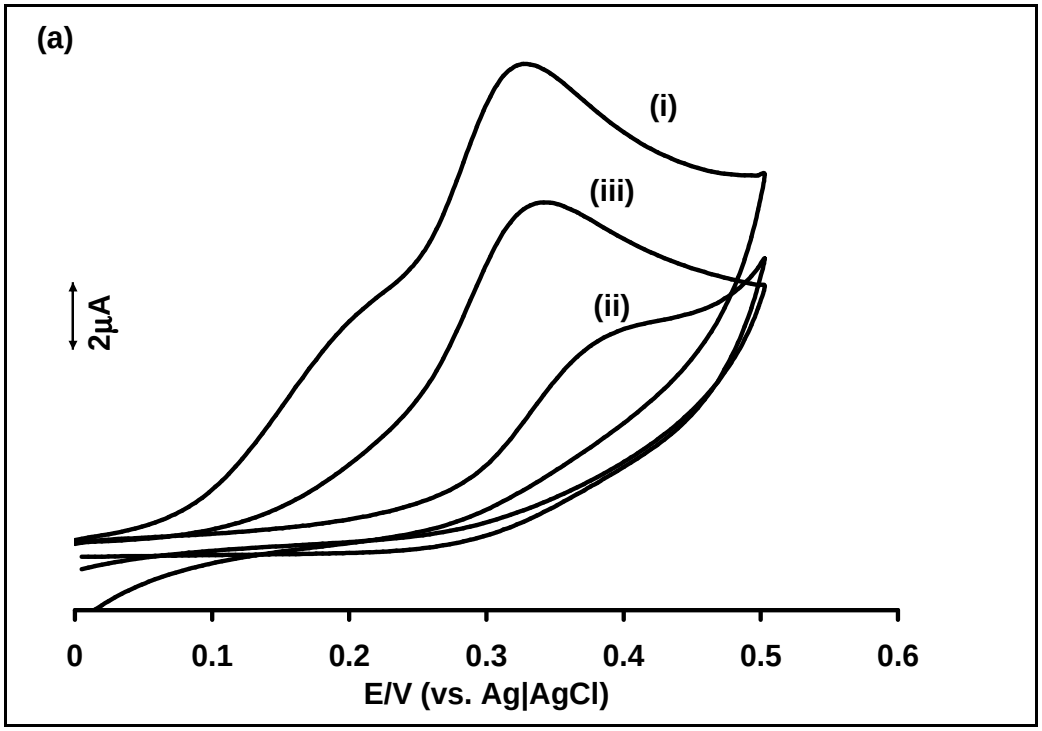

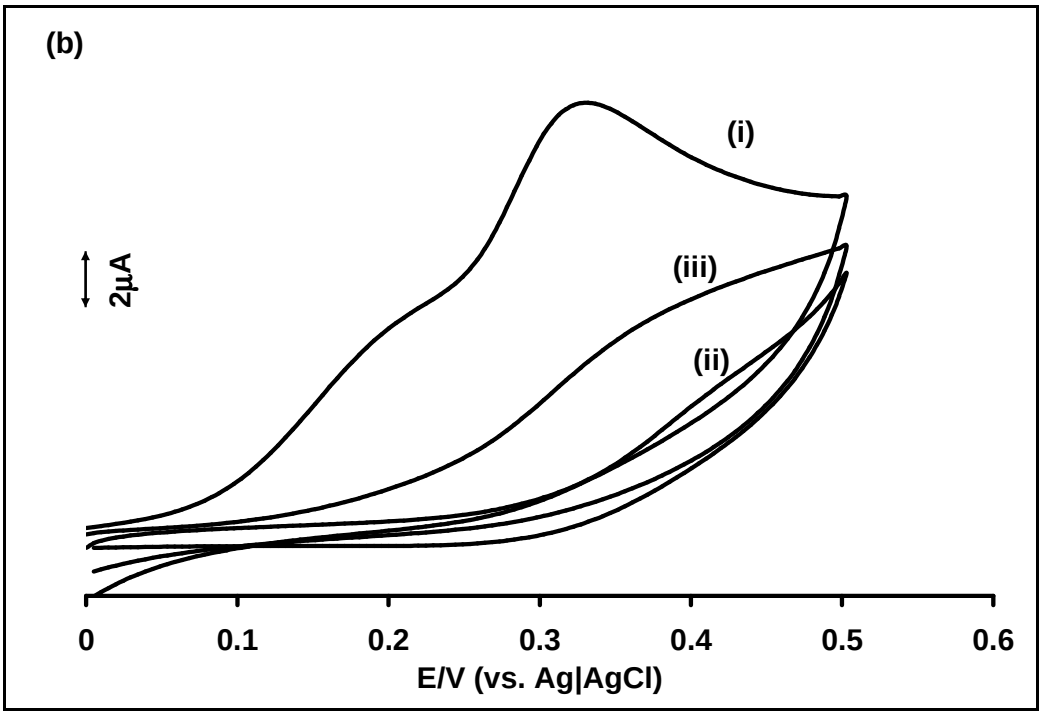

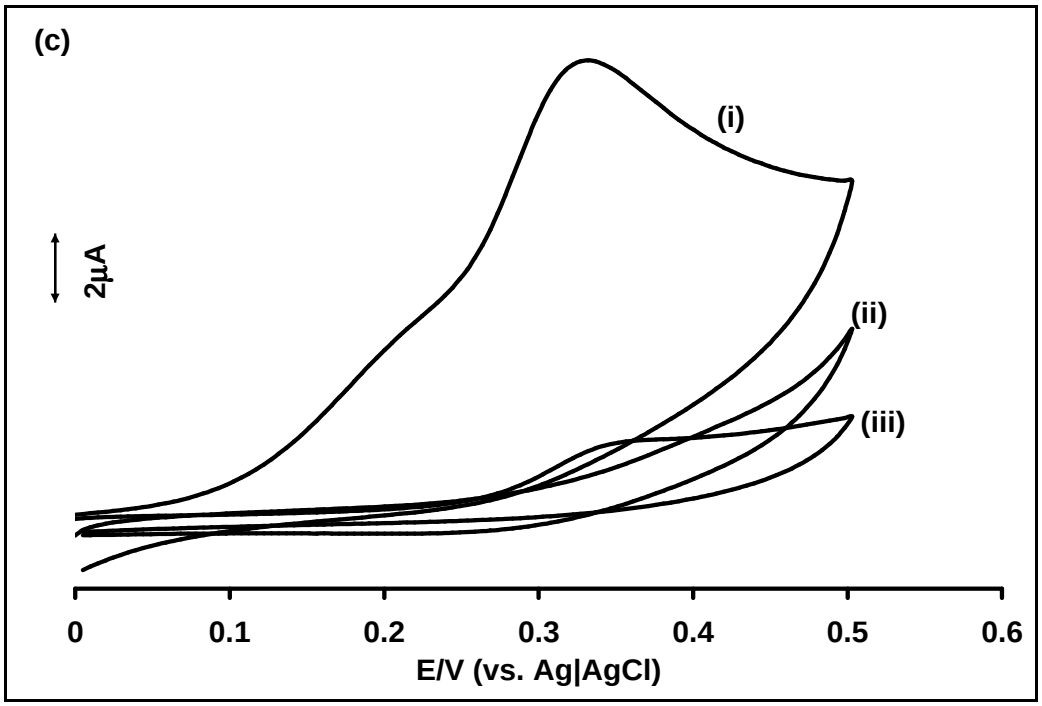

Figure 6.4: Cyclic voltammograms of 1 mM 4-CP catalysed by (a) *poly30*-Ni(OH)TBMPc-Au, (b) *poly20*-Ni(OH)TBMPc-Au and (c) *poly10*-Ni(OH)TBMPc-Au. Curve (i) First scan, (ii) second scan and (iii) second scan after rinsing the electrode (for 5 minutes) in phosphate buffer (pH 7.4). The electrolyte used was 0.1 M NaOH.

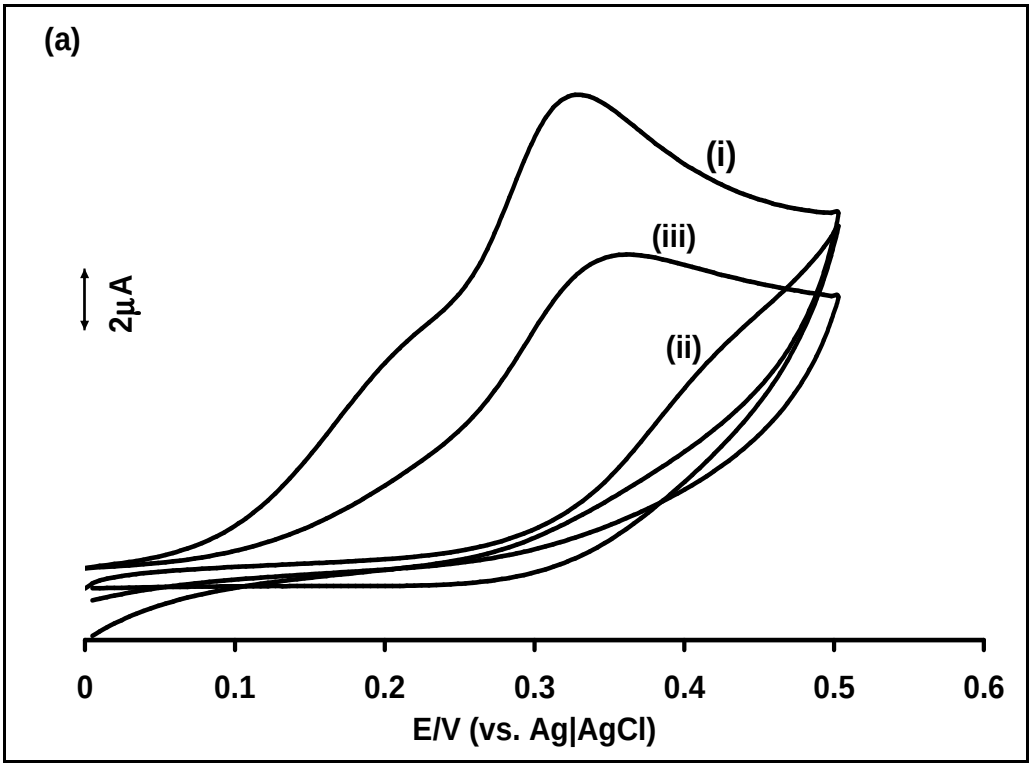

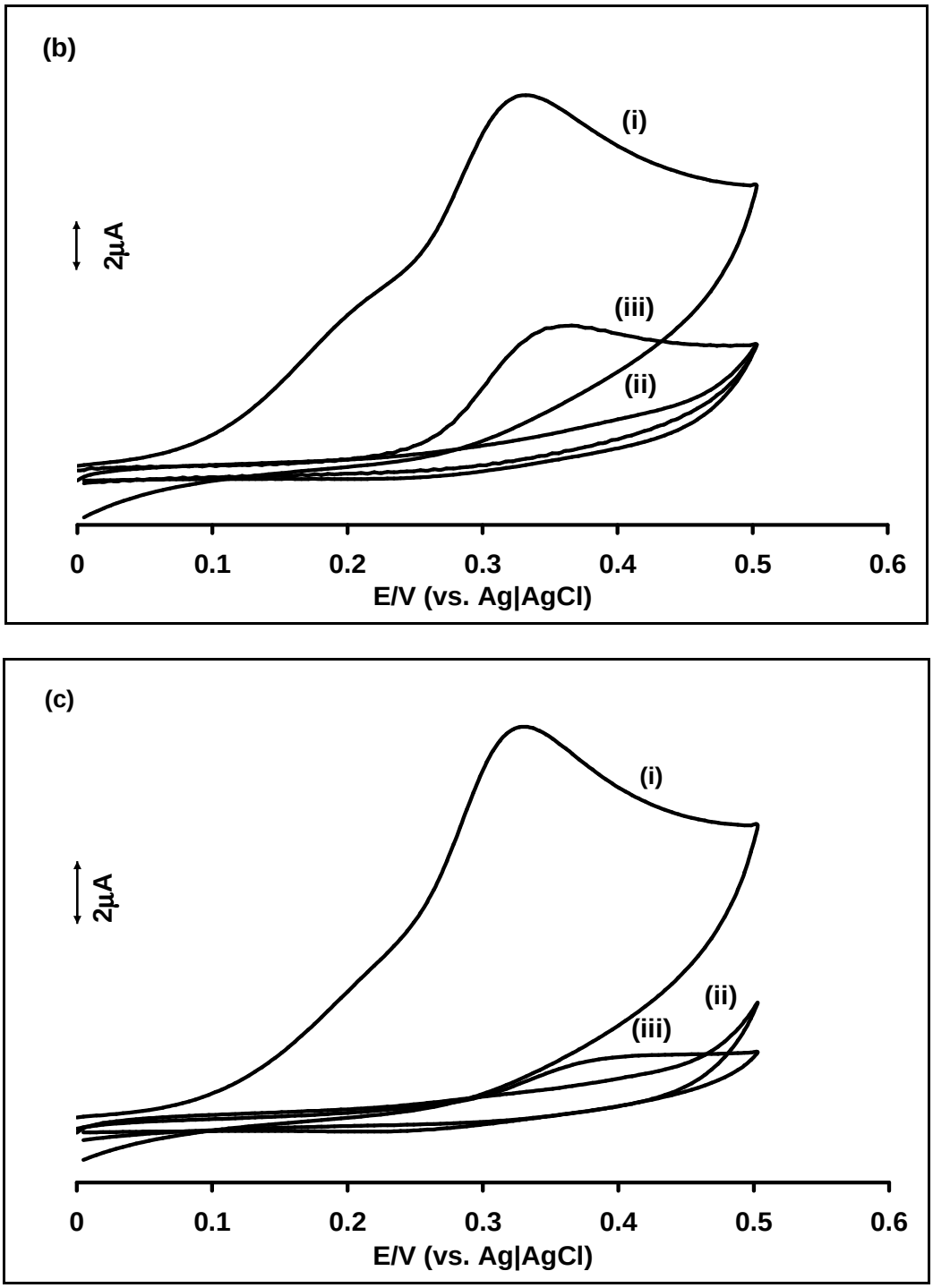

Figure 6.5: Cyclic voltammograms of 1 mM 4-CP catalysed by (a) *poly30*-Ni(OH)TDMPc-Au, (b) *poly20*-Ni(OH)TDMPc-Au and (c) *poly10*-Ni(OH)TDMPc-Au. Curve (i) First scan, (ii) second scan and (iii) second scan after rinsing the electrode (for 5 minutes) in phosphate buffer (pH 7.4). The electrolyte used was 0.1 M NaOH.

These studies were done in triplicate and the errors are shown in Table 6.1. The recovery increases with the number of polymerisation scans hence the film thickness (Table 6.1), showing that resistance to electrode passivation increases as the film thickness increases. This can also be explained by the fact that in addition to increase in catalytic sites as the film thickness increases, the electrode films maybe more porous attributed to the complex nature of the ring substituents of both complexes which are bulky, allowing passage of the chlorophenol molecules. The chlorophenol polymers are known to be thick and non-porous.[362,363] The bulky nature of the ring substituents may make the chlorophenols polymers to be irregular and thus porous, making the films on the gold electrodes to be difficult to deactivate.[361]

Table 6.1: Percent recovery (after rinsing in phosphate buffer, pH 7.4) of the electrodes following fouling for the electrooxidation of 1 mM 4-CP.

Electrode	**% Recovery**
Poly$_{10}$-Ni(OH)TBMPc-Au	15.7 (±1.2)
Poly$_{20}$-Ni(OH)TBMPc-Au	52.1 (±2.3)
Poly$_{30}$-Ni(OH)TBMPc-Au	71.2 (±2.6)
Poly$_{10}$-Ni(OH)TDMPc-Au	15.8 (±1.6)
Poly$_{20}$-Ni(OH)TDMPc-Au	38.1 (±1.8)
Poly$_{30}$-Ni(OH)TDMPc-Au	66.1 (±2.4)

6.1.3 Reaction mechanism

Studies such as variation of peak current, I_p with chlorophenol concentration and mechanistic studies such as Tafel plots were not done for chlorophenols because of the problem of passivation of electrodes but were carried out for both nitrite and sulphite. Also studies of the spectroscopic interaction between chlorophenols and NiPc complexes were not carried because of lack of a common solvent for both chlorophenols and the thiol-derivatised complexes.

The chlorophenols will be in the deprotonated forms because the electrolyte is strongly alkaline (0.1 M NaOH) and so it is in this form that the reaction mechanism will be based on. The proposed reaction mechanism is shown in Scheme 6.1. There are likely to be two competing processes taking place during the electrooxidation of 4-chlorophenol (4-CP);

(1.) Dimerisation of chlorophenols with the possibility of the formation of polymer (equations 6.1-6.3). The first step is the electrooxidation of the deprotonated 4-chlorophenol to form 4-chlorophenoxy radical (equation 6.1),[351,352] the radical is resonance stabilised (equation 6.2) and thus its head to head coupling reaction via oxygen atoms is feasible (equation 6.3).

(2.) Ni^{3+}/Ni^{2+} electrocatalysed oxidation of 4-chlorophenol to form oxidised products such as benzoquinones (equations 6.4, 6.5).

The first step is the electrochemical oxidation of Ni^{2+} to Ni^{3+} (equation 6.4) followed by the reaction of Ni^{3+} with deprotonated 4-chlorophenol in the presence of water molecules from electrolyte to form benzoquinone (equation 6.5). The better catalysis observed for the *poly*-Ni(OH)TBMPc-Au and *poly*-Ni(OH)TDMPc-Au electrodes than their *poly*-NiTBMPc-Au and *poly*-NiTDMPc-Au electrodes counterparts respectively could be

explained by the fact that the former have Ni^{3+}/ Ni^{2+} redox process, due to activation while the latter have no Ni^{3+}/ Ni^{2+} redox process and thus making reactions in equations 6.4, 6.5 more feasible for the former. The possibility of Ni^{3+}/ Ni^{2+} redox process catalysing 4-CP oxidation is strongly supported by the fact that the peaks associated with Ni^{2+} to Ni^{3+} overlap with the 4-CP oxidation peaks.

Similar reactions are expected for trichlorophenol (TCP) electrooxidation reaction mechanism catalysed by NiPc-Au electrodes.

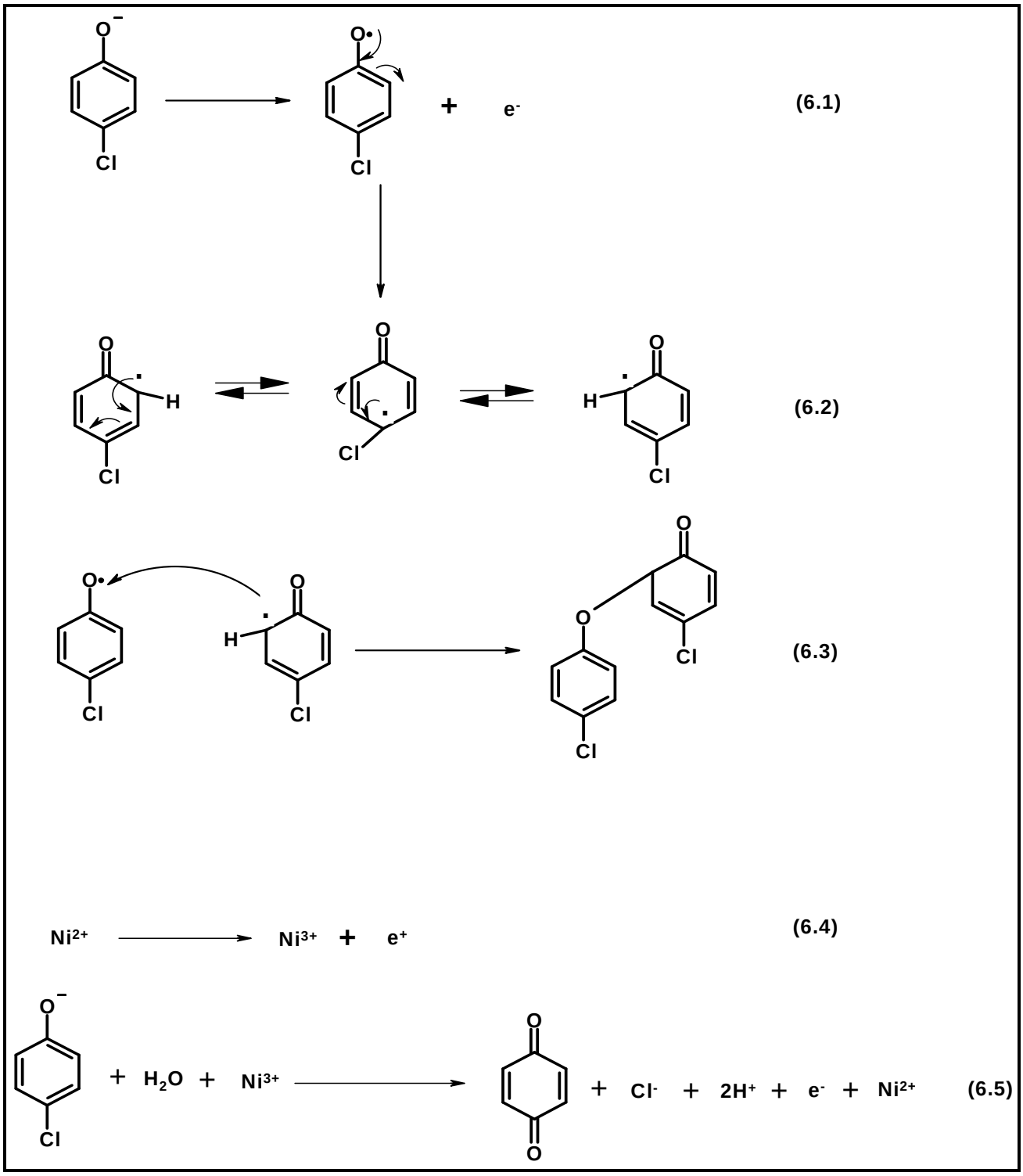

Scheme 6.1: Proposed reaction mechanism for electrooxidation processes of 4-chlorophenol

6.2 Electrocatalytic oxidation of Nitrite

6.2.1 Voltammetric Studies on MTBMPc and MTDMPc

Since the nitrite determination will be performed under pH 7.4 conditions, the voltammograms of the *poly*-Ni(OH)TDMPc-Au and *poly*-Ni(OH)TBMPc-Au were recorded in pH 7.4 buffer, Figure 6.6a and b. The Ni^{3+}/Ni^{2+} peaks were observed at different potential values in pH 7.4 compared to 0.1 M NaOH shown in Figure 5.12. For *poly*-Ni(OH)TBMPc-Au, the Ni^{3+}/Ni^{2+} peaks shifted from -0.20 (cathodic) and ~0.30 V (anodic) in 0.1 M NaOH to 0.20 and ~ 0.70 V, respectively. For *poly*-Ni(OH)TDMPc-Au, the Ni^{3+}/Ni^{2+} peaks shifted from -0.28 V (cathodic) and ~0.3 V (anodic) in 0.1 M NaOH to 0.30 and ~ 0.80 V, respectively. Thus a large shift to more positive potentials occurred with decrease in pH.

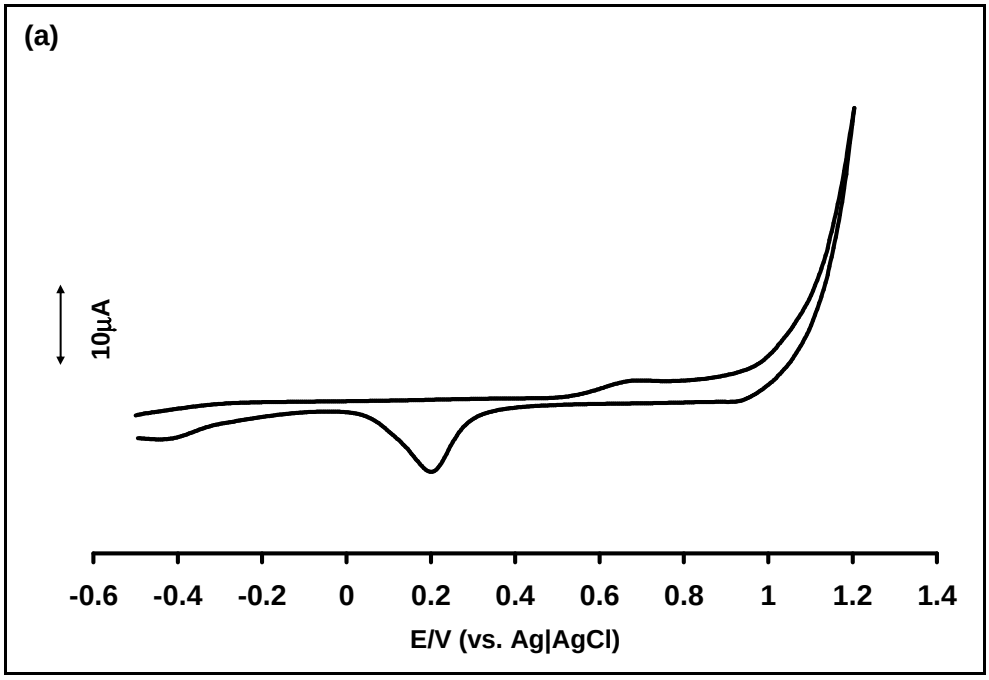

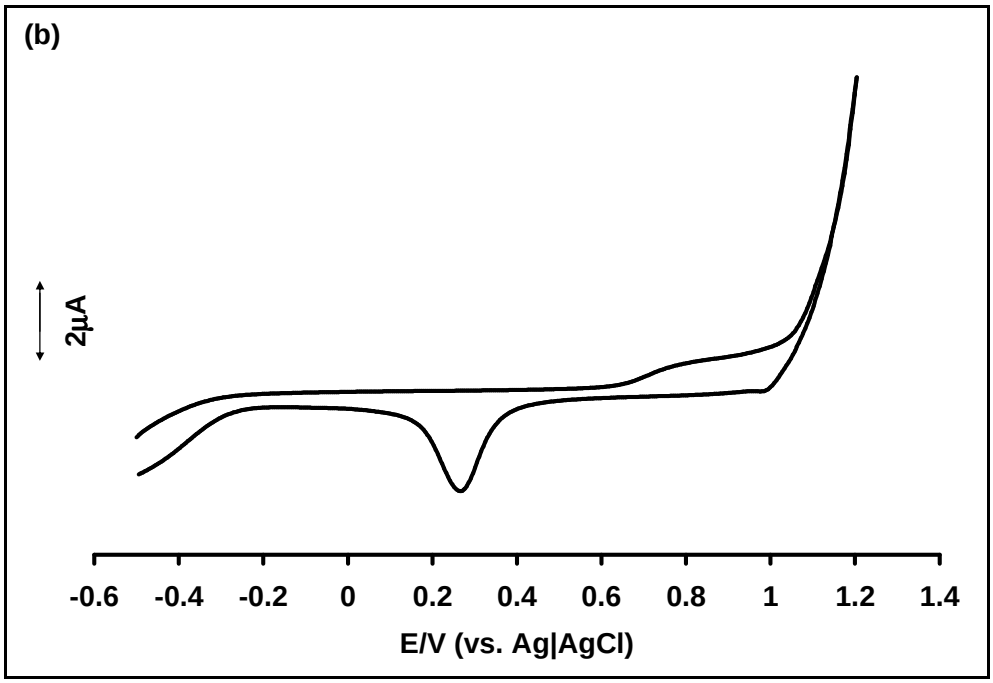

Figure 6.6: Typical cyclic voltammogram of (a) *poly*-Ni(OH)TBMPc-Au and (b) *poly*-Ni(OH)TDMPc-Au in pH 7.4 buffer.

Figure 6.7 showed the comparative cyclic voltammograms for the catalytic activities of gold electrodes modified with the MTBMPc and MTDMPc complexes towards nitrite electrooxidation. The increasing order of activity based on the positions of the catalytic peak potential E_p (Table 6.2) is as follows; complex **42** < complex **37** < Ni(OH)TDMPc< complex **39** < complex **40** < Ni(OH)TBMPc < complex **34** < complex **35** < complex **41** < complex **36** while in terms of the catalytic peak current, I_p the order is as follows; complex **39** < complex **40** < complex **42** < complex **34** < complex **36** < complex **37** < Ni(OH)TDMPc < complex **41** < complex **35** < Ni(OH)TBMPc.

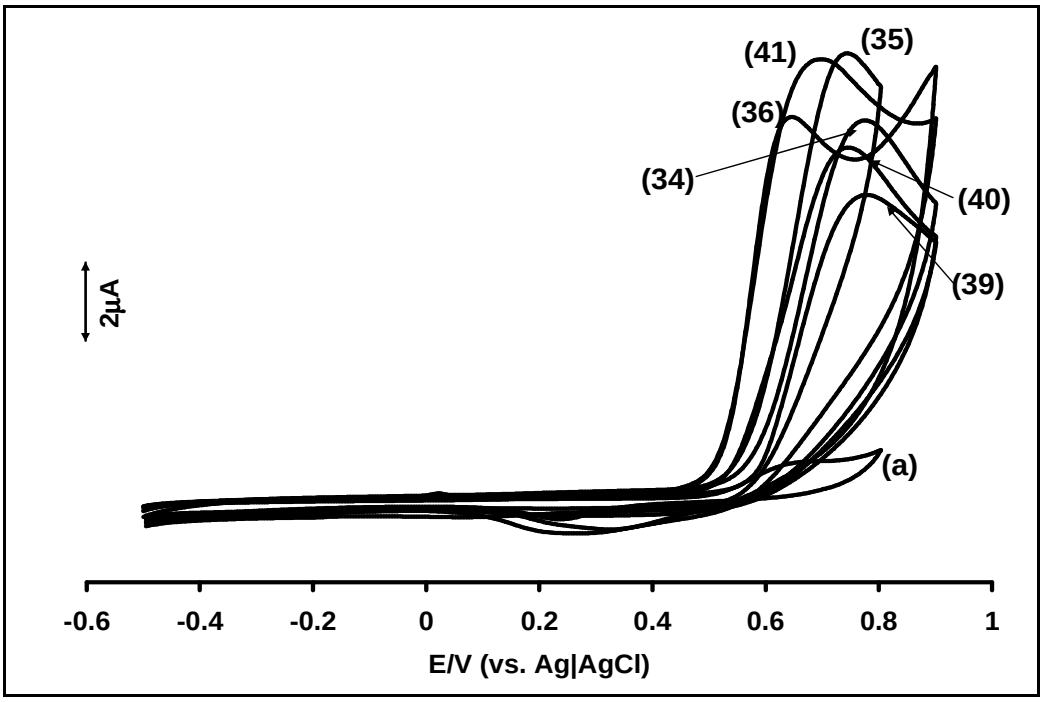

Figure 6.7: Cyclic voltamogramms for 1 mM nitrite oxidation in phosphate buffer pH 7.4 solution at (a) an unmodified au electrode, complex (b) **35**, (c) **40**, (d) **36**, (e) **41**, (f) **34**, (g) **39**. Scan rate = 100 mV s^{-1}.

From these trends, it can be concluded that the FePc and CoPc complexes performed best and MnPcs were the worst in terms of potential. But in terms of current enhancement Ni(OH)TBMPc performed the best. This trend (in terms of the peak potential) in electrocatalytic activity has been observed before[413] for NO electrooxidation on carbon fibre microelectrodes modified with CoPc, FePc and MnPc. In comparison to literature,[63,214,287,365-369] (Table 1.8, Introduction section), 0.66 V peak potential value obtained for complex **36** modified Au electrode is the lowest value for peak potential reported for MPc or metalloporphyrin modified electrode for nitrite electrooxidation.

Table 6.2: Mechanistic feature of the nitrite oxidation on *poly*-MPc modified Au electrode

Modified electrodes	**E_p (V) $M^{III}Pc/M^{II}Pc$ (vs. Ag|AgCl)**	**E_p (V) (vs. Ag|AgCl)**	**I_p (µA)**	**Sensitivity (µA mM^{-1})**	**b (mV dec^{-1})**	**α**	***k***	**n_t**
CoTBMPc (**35**)	0.35	0.75	11.2	7.3 (±0.2)	154	0.61	0.063	2.1
CoTDMPc (**40**)	~ 0.3	0.77	8.7	7.1 (±0.1)	114	0.52	0.27	1.52
FeTBMPc (**36**)	~ 0.3	0.66	9.6	9.6 (±0.2)	166	0.64	0.0064	1.86
FeTDMPc (**41**)	~ 0.3	0.71	11.1	9.9 (±0.2)	123	0.51	0.111	1.83
MnTBMPc (**34**)	0.15 (~0.5)[a]	0.76	9.5	7.6 (±0.3)	70.4	0.14	0.20	1.2
MnTDMPc (**39**)	0.20	0.79	7.7	6.9 (±0.2)	55	0	98	1.0
NiTBMPc (**37**)	0.4[b]	0.82	9.9	6.0 (±0.2)	250	0.76	0.006	1.99
NiTDMPc (**42**)	0.6[b]	0.87	9.3	3.3 (±0.1)	258	0.77	0.006	1.1
Ni[OH]TB MPc	~ 0.7	0.76	13	12.6 (±0.9)	186	0.72	0.006	2.25
Ni[OH]TD MPc	~ 0.8	0.81	11	11.1 (±0.8)	226	0.73	0.022	2.45

[a] number in brackets are for Mn^{4+}/Mn^{3+}, [b] ring based process

As stated already, the film thickness can be controlled by varying the electropolymerisation scan number; Figure 6.8 shows the effect of film thickness of CoTBMPc-Au electrode on the catalytic efficiency towards nitrite oxidation. It can be seen that the catalytic activity towards nitrite ion oxidation increased as the number of scans increased; CoTBMPc-10 Au (E_p 0.79 V, I_p 3.0 μA) < CoTBMPc-20 Au (E_p 0.77 V, I_p 3.4 μA) < CoTBMPc-30 Au (E_p 0.76 V, I_p 4.1 μA), where the numbers refer to number of deposition scans. This was also observed above for chlorophenol oxidation; again this trend can be explained by the fact that an increase in the scan number increases the number of active sites on the electrode surface.

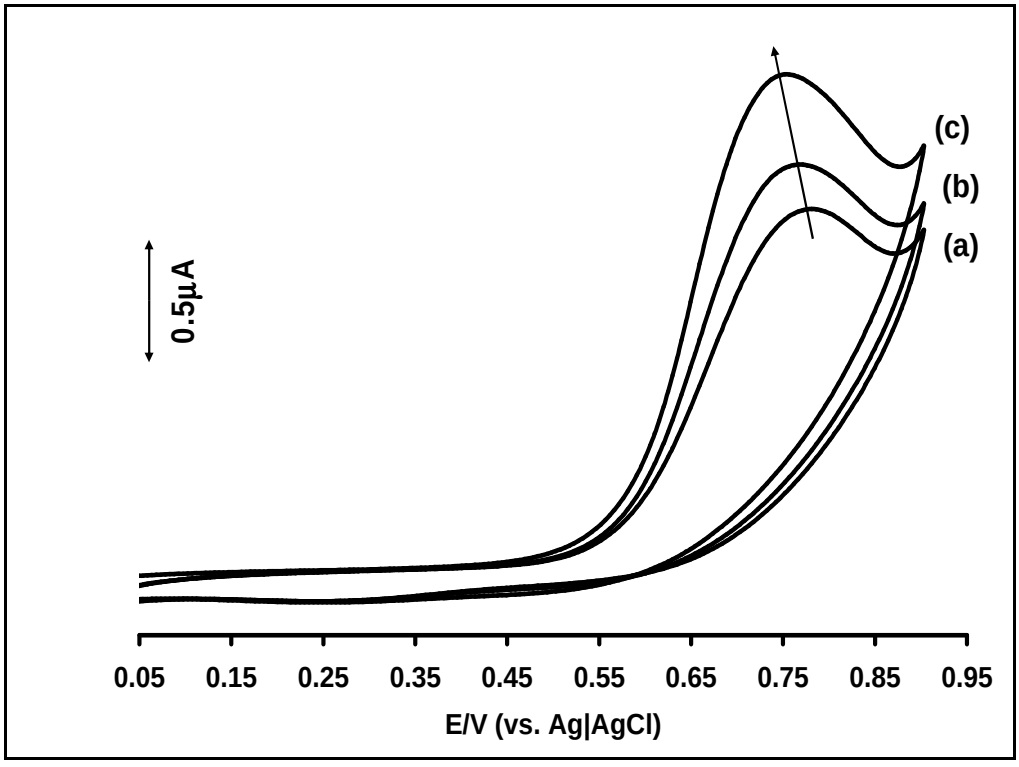

Figure 6.8: Cyclic voltamogramms for 0.5 mM nitrite oxidation in phosphate buffer pH 7.4 solution at CoTBMPc (complex **35**) poly-Au, poly number (a) 10, (b) 20, (c) 30.

In terms of resistance to electrode surface passivation, all the modified electrodes exhibited some resistance to passivation in that only small decreases in currents on cycling were observed after the first scan, Figure 6.9. The % decrease between the first and second scan range from 2.6 – 14.6% while for the subsequent scans they were less than 7%.

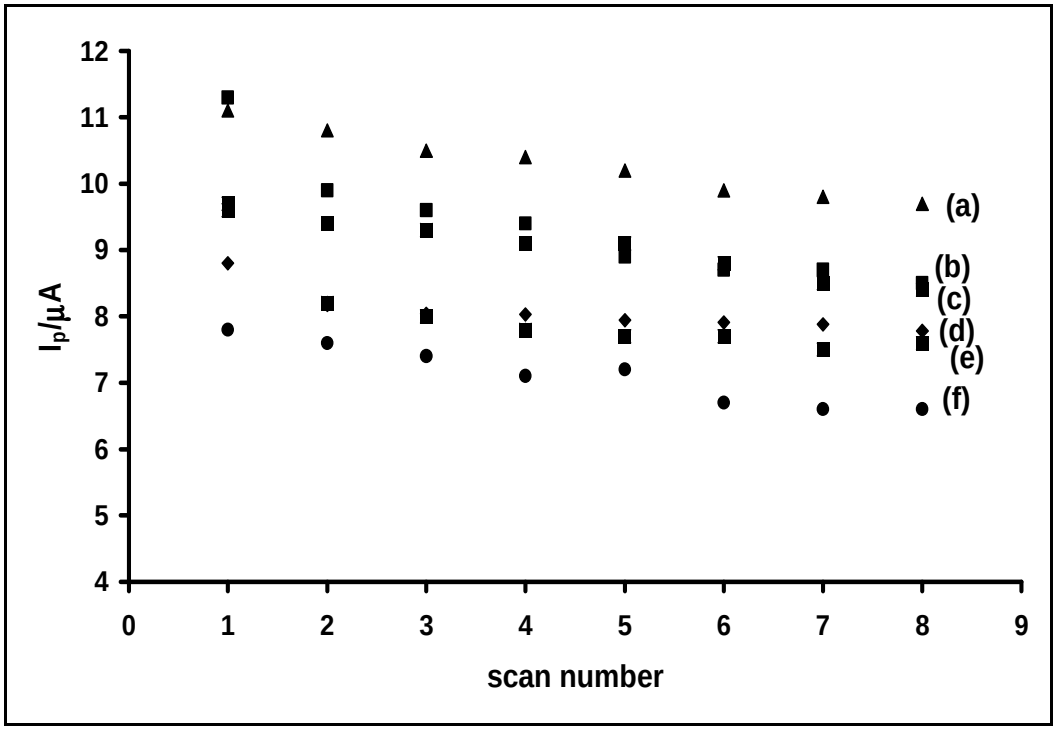

Figures 6.9: The variation of peak currents with scan number for the voltammetric response of 1 mM NO_2^- on (a) complex **35**, (b) complex **41**, (c) complex **36**, (d) complex **34**, (e) complex **40**, (f) complex **39**-poly 30 on gold electrode. Buffer = pH 7.4. Scan rate = 100 mV s^{-1}.

Within the concentration range chosen for the catalytic studies in this work (i.e. 1.0 x 10^{-4} – 1.0 x 10^{-3} mol L^{-1}), a linear relationship was observed between the catalytic currents and the nitrite concentrations (Figure 6.10). From the slopes of the plots in Figure 6.10, high sensitivities ranging from 6.9 to 9.9 µA mM^{-1} were obtained, Table 6.2.

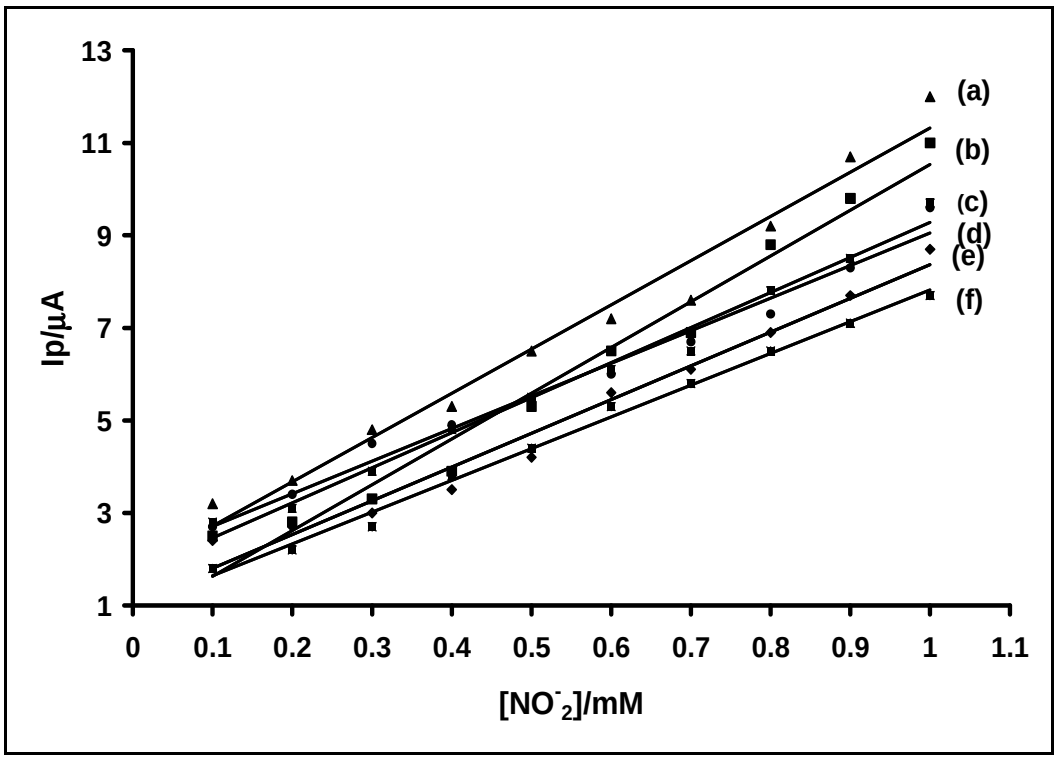

Figures 6.10: Plot of I_p vs. $[NO_2^-]$ (a) **35**, (b) **41** (c) **36** (d) **34** (e) **40** (f) **39**.

In order to determine the Tafel slopes, the usual equation (Equation 6.6) for a totally irreversible process was employed[123]

$$E_p = \frac{2.3RT}{2(1-\alpha)nF}\log\nu + K \qquad (6.6)$$

where ν is the scan rate, α is the transfer coefficient, n is the number of electrons involved in the rate determining step, K is the intercept. Plots of E_p vs. log ν (Figure 6.11a) gave linear relationships. The Tafel slopes, b ranging from 55 to 258 mV dec^{-1} were obtained, Table 6.2. A Tafel slope of 120 mV dec^{-1} suggests the involvement of one electron in the rate determining step whereas the value of 60 mV dec^{-1} indicates that a fast one electron transfer is followed by a slow chemical step.[63] Thus for FePc, NiPc and

CoPc derivatives in Table 6.2, with Tafel slopes close to 120 mV dec^{-1} or larger, the first one electron transfer is the rate limiting step. While for MnPc derivatives the one electron step is followed by a slow chemical rate determining step. The linear relationships in Figure 6.11a (R^2 ranging from 0.98 to 0.99) indicate that the electrocatalytic oxidation of nitrite is irreversible.[63] For NiPc derivatives Tafel slopes are significantly higher than 120 mV dec^{-1} indicating interaction between nitrite ions and the NiPc complexes or chemical reactions coupled with electrochemical steps.[414]

The values of α are listed in Table 6.2. α values at approximately 0.5 indicate that there is an equal probability that the reaction activated transition state can form either products or reactants. This holds for the CoPc and FePc derivatives, Table 6.2. α values of approximately 1 imply that the reaction equilibrium favours product formation only, and α values of zero imply the reactants are favoured. Indeed for MnPc derivatives α were close to zero indicating that product formation is not favoured. For NiPc derivatives α approached 1 suggesting product formation is favoured.

The heterogeneous electron transfer coefficient, *k*, was obtained from Equation 6.7.[123]

$$K = E^{o'} + \frac{RT}{(1-\alpha)nF} \times \left[0.78 + \frac{2.3}{2} \log\left(\frac{(1-\alpha)nFD}{k^2 RT} \right) \right] \qquad (6.7)$$

where $E^{0'}$ is the formal potential, D is the diffusion coefficient and the remaining symbols are as they were described above. Using D = 2.1 x 10^{-5} cm^2 s^{-1} for nitrite ion,[288] the values of the constant k were obtained and they varied considerably, Table 6.2. In general the values of *k* were higher for the MTDMPc compared to the corresponding MTBMPc (except for NiTBMPc and NiTDMPc), showing that the former (containing dodecyl mercapto) are more efficient in electron transfer. The k values for NiPc and for

FeTBMPc complexes were very low suggesting a slow electron transfer. Fastest electron transfer was obtained for MnTDMPc.

The total number of electrons (n_t) involved in the electrocatalytic oxidation of nitrite was evaluated according to Equation 6.8, which is valid for totally irreversible electrode processes:[123]

$$I_p = 2.99\times10^5 n_t[(1-\alpha)n]^{1/2} AC_o D^{1/2} v^{1/2} \qquad (6.8)$$

where A is the area of the electrode in cm^2, C_o is the concentration of the electroactive reactant in mol cm^{-3}. From Figure 6.11b, it can be seen that there is a linear (R^2 ranging from 0.97 to 0.99) relationship between the peak current and square root of the scan rate (Equation 6.8), indicating that the nitrite electrocatalytic oxidation is diffusion controlled. The values of overall number of electrons transferred (n_t) were determined using equation 6.8 and were close to 2 for the CoPc, NiPc and FePc complexes hence confirming that a total of 2 electrons are transferred during the catalytic oxidation of nitrite. The n_t values were close to 1 for the MnPc complexes. Thus, different final products are formed when MnPc derivatives are employed compared to FePc, NiPc and CoPc derivatives.

Figure 6.11c further confirms that the electrooxidation of nitrites by all the modified electrodes is a catalytic processes judging by the pattern of curves obtained which is typical of catalytic processes.[63]

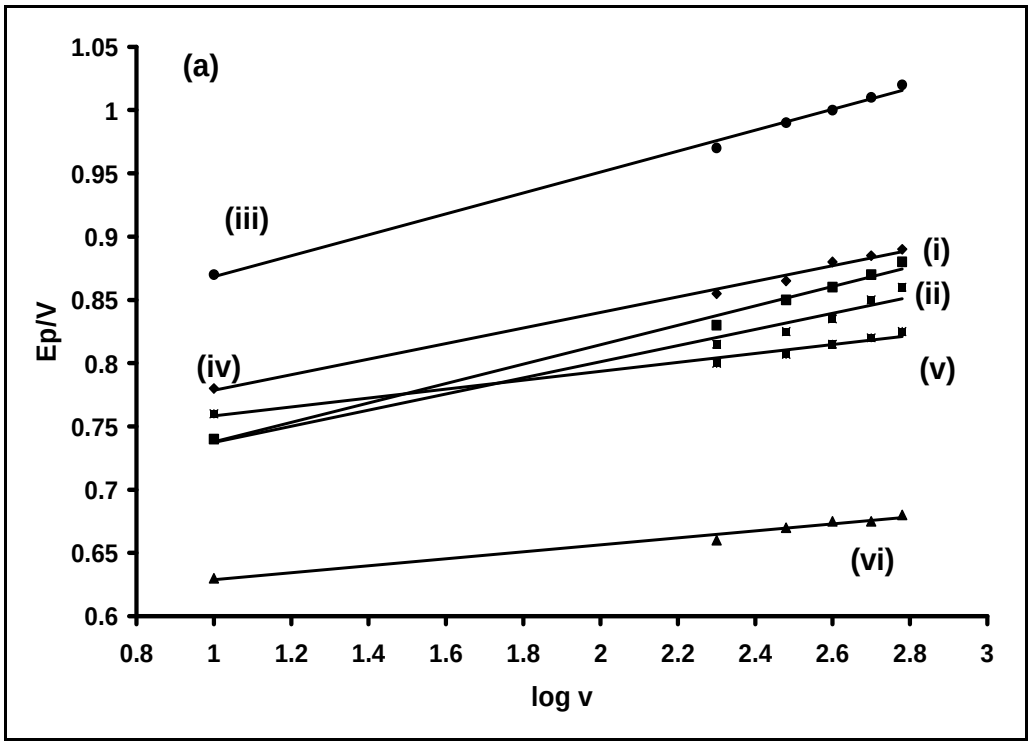
(a)
(iii)
(i)
(ii)
(iv)
(v)
(vi)
Ep/V
log v
1.05
1
0.95
0.9
0.85
0.8
0.75
0.7
0.65
0.6
0.8
1
1.2
1.4
1.6
1.8
2
2.2
2.4
2.6
2.8
3

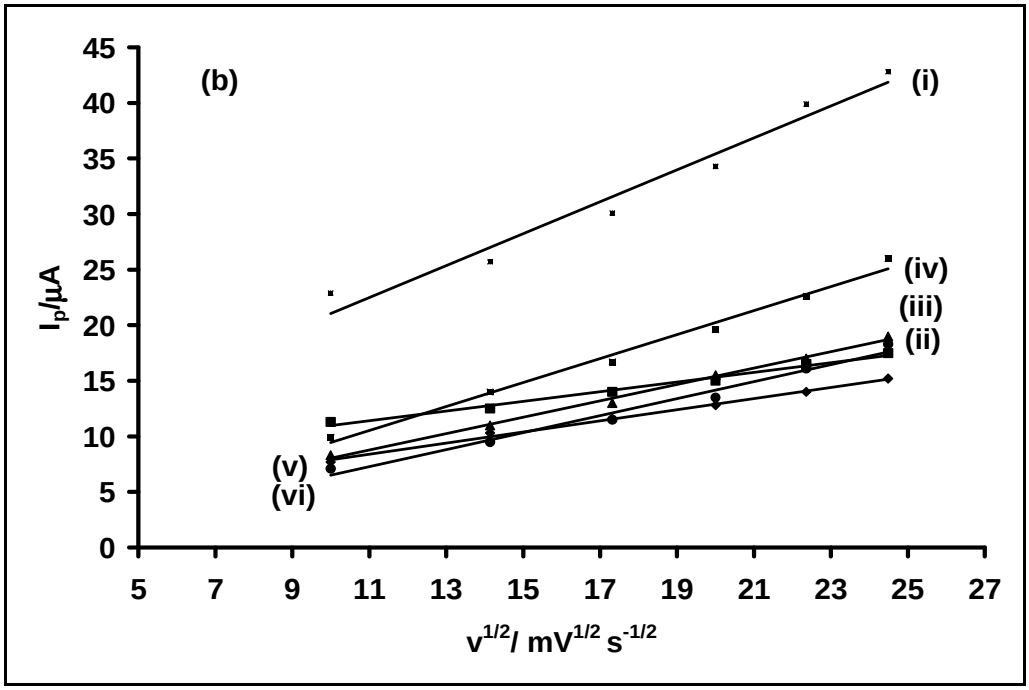
(b)
(i)
(iv)
(iii)
(ii)
(v)
(vi)
$I_p/\mu A$
$v^{1/2}/ mV^{1/2} s^{-1/2}$
45
40
35
30
25
20
15
10
5
0
5
7
9
11
13
15
17
19
21
23
25
27

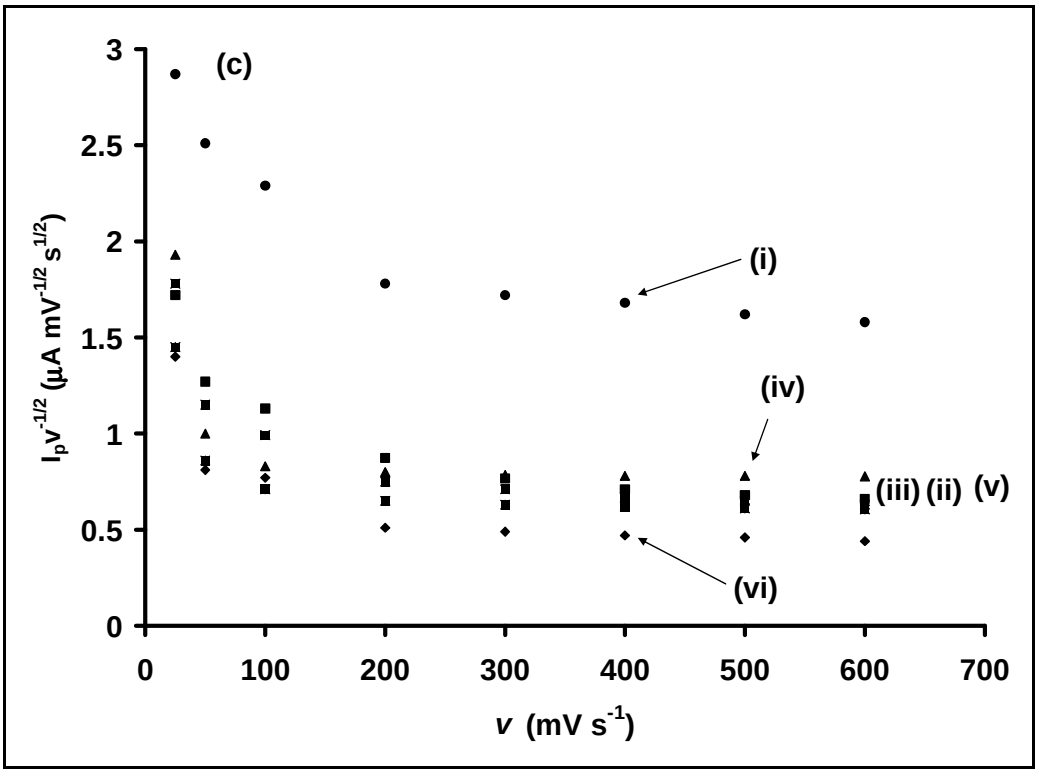

Figures 6.11: Electrooxidation of 1 mM nitrite in phosphate buffer on *poly*-MPc, (a) E_p vs. log *v*, (b) I_p vs. $v^{1/2}$, (c) $I_p v^{1/2}$ vs. *v*. *Poly*-MPc: (i) **35**, (ii) **40**, (iii) **36**, (iv) **41**, (v) **34**, (vi) **39** modified Au electrode.

6.2.2 Spectroscopic studies of interaction between nitrite and MTBMPc and MTDMPc (M = Co^{2+}, Fe^{2+} and Mn^{3+})

In order to further understand the mechanism for the catalytic oxidation of nitrite, changes in the electronic spectra of MnTBMPc (**34**), CoTBMPc (**35**) and FeTBMPc (**36**) in DMSO on addition of nitrite were monitored. As can be seen from the Figures 6.12-6.14, nitrite reaction with the complexes depends on the type of central metal ion. For complex **35** which has Co^{2+} as the central metal ion, on addition of nitrite, the Q band shifted from 670 to 690 nm (Figure 6.12a). These changes occurred with very clear isobestic points showing that only two species are involved during the reaction. Such

changes could be associated with either axial coordination of ligands to MPc complexes, or oxidation of the central metal in $Co^{2+}Pc$ to $Co^{3+}Pc$.[101,415] Addition of a reducing agent to solutions of complex **35** at the end of the reaction in Figure 6.12a, resulted in the reduction of the complex (Figure 6.12b) to a $Co^{+}Pc$ species with a typical[101] band charge transfer band at 480 nm and a weaker Q band at 715 nm. There was no regeneration of the original peak in Figure 6.12a at 670 nm, showing that the observed changes in Figure 6.12a are not due to oxidation of $Co^{2+}Pc$ to $Co^{3+}Pc$, but due to axial ligand (nitrite) coordination to the complex. Similar spectral changes were observed for complex **40**.

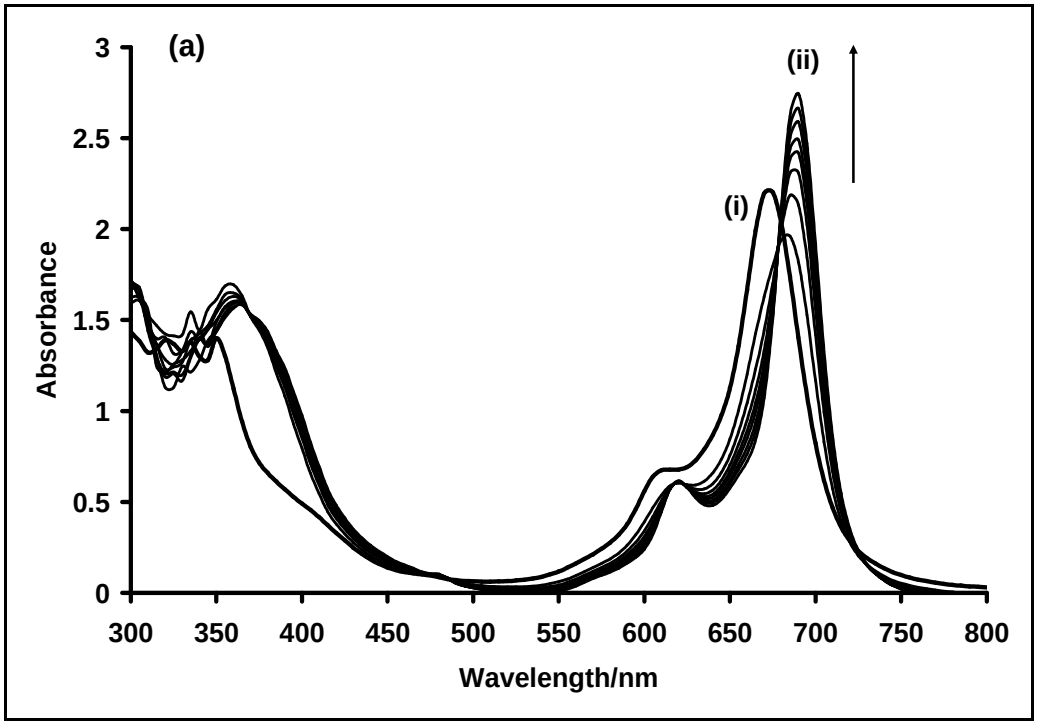

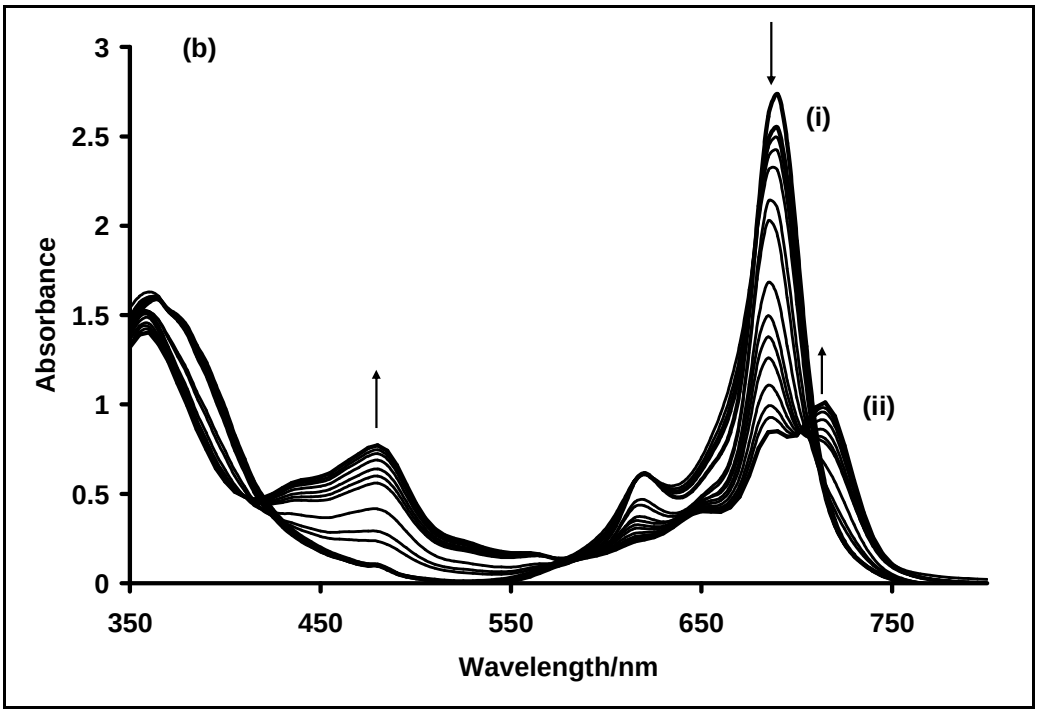

Figure 6.12: Electronic spectral changes of (a) complex **35** on addition of 1 mM nitrite solution in DMSO to approx. 2 µM solution of the complex in DMSO. (i) initial spectrum, (ii) final spectrum after 20 minutes. (b) on addition of $NaBH_4$ to the final spectrum in (a). Concentration of (i) complex in DMSO = 1 µM and (ii) nitrite in DMSO = 1 µM.

Even though these studies were done in solution, they give some idea of the possible mechanism for the electrocatalytic oxidation of nitrite. Thus the catalytic oxidation of nitrite using the CoPc complexes occurs by inner sphere mechanism and may be represented in equations 6.9 to 6.11 (Scheme 6.2):

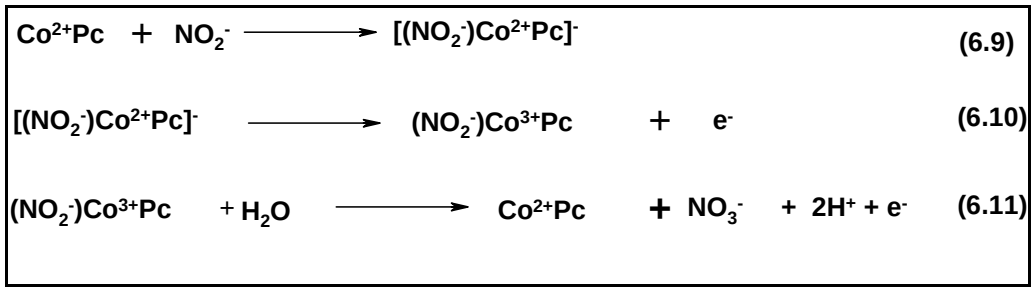

Scheme 6.2: Proposed reaction mechanism for CoPcs-modified gold electrode electrooxidation of nitrite

Equation 6.9 is proposed on the basis of coordination of nitrite to complexes as shown by Figure 6.12. The Tafel plots showed that the first one-electron transfer is the rate limiting step, hence suggesting equation 6.10 to be rate limiting reaction. A comparison between the cyclic voltammograms for the adsorbed complexes in Figure 5.3 (which show the metal oxidation couples at pH 7.4) with the nitrite oxidation in Figure 6.7 (also in pH 7.4) shows a broad peak for Co^{3+}/Co^{2+} at around 0.2–0.4 V, very close to the foot of the wave for nitrite oxidation, hence this couple catalyses nitrite oxidation. Equation 6.11 is proposed since the total number of electrons involved is 2 and the likely product is nitrate.

Figure 6.13 shows the spectral changes observed on addition of nitrite to solutions of complex **36,** containing Fe^{2+} as the central metal ion. The complex shows aggregation as evidenced by appearance of a high energy peak at 640 nm. As already stated, aggregation in MPc complexes is typified by a broadened or split Q band, with the high energy band being due to the aggregate and the low energy band due to the monomer. For complex **36**, the peak at 640 nm in Figure 6.13 shows a spectrum typical of stacked monomer in FePc complexes which is normally observed near 630 nm. A broad band was observed at 665

nm due to the monomer. On addition of nitrite to solutions of complex **36** in DMSO, Q band due to the aggregated species at 640 nm shifted to 635 nm while the monomer peak at 665 nm sharpened, and both peaks increased in intensity. The slight shift in wavelength from 640 to 635 nm is associated[101] with axial ligation in MPc complexes. Oxidation in FePc complexes is accompanied by a split in the Q band and a shift of one of the components to low energy. The spectral changes observed in Figure 6.13 are not due to oxidation. This was confirmed by addition of reducing agents such as sodium borohydride, which did not result in the regeneration of the original spectrum in Figure 6.13. Thus the spectral changes shown in Figure 6.13 suggest coordination of nitrite. The catalytic oxidation of nitrite by the monomer will be similar to equations 6.9 to 6.11 for the CoPc derivatives. The FePc complexes, also show the Fe^{3+}/Fe^{2+} around 0.2 – 0.4 V (comparing Figure 6.7 and 5.6), hence this couple catalyses nitrite oxidation.

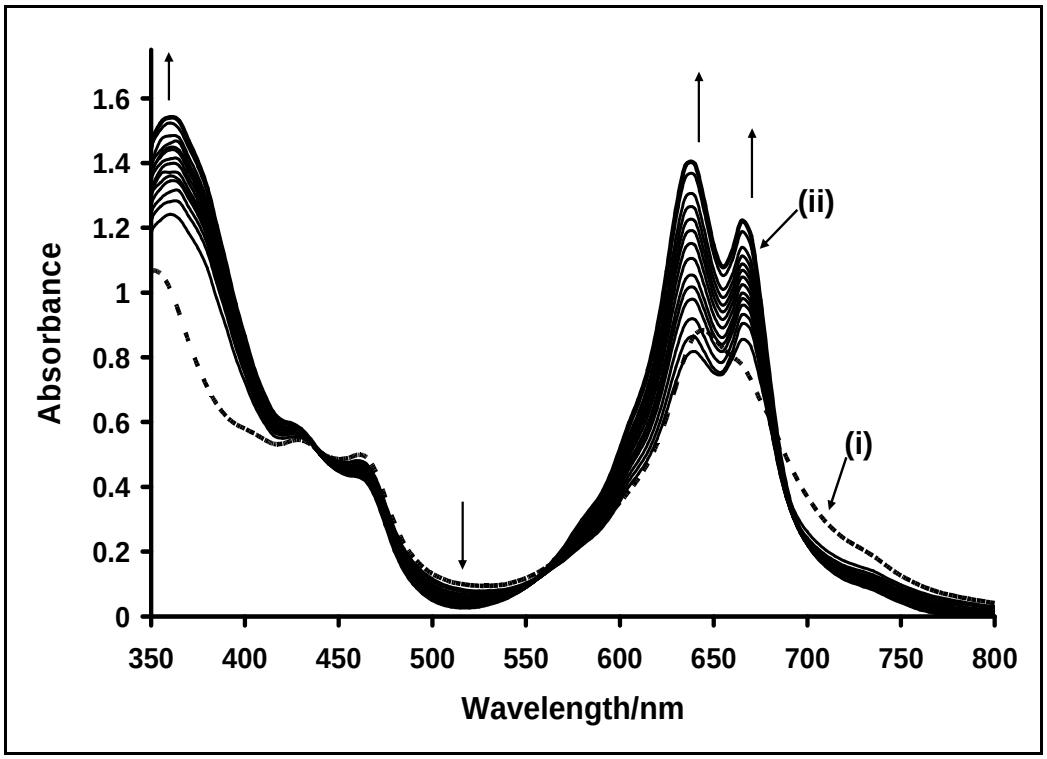

Figure 6.13: Electronic spectral changes of complex **36** on addition of 1 mM nitrite solution in DMSO to approx. 2 µM solution of the complexes in DMSO. (i) initial spectrum, (ii) final spectrum after 20 minutes. Concentration of (i) complex in DMSO = 1 µM and (ii) nitrite in DMSO = 1 µM.

The interaction of complex **34,** containing Mn^{3+} with nitrite ions resulted in spectral changes shown in Figure 6.14, which are typical of reduction of Mn^{3+}Pc (with Q band at 750 nm) to Mn^{2+}Pc (Q band at 680 nm). These spectral changes are accompanied by coordination as judged by the initial shift of the Q band Mn^{3+}Pc from 750 to 745 nm before the decrease in the 745 nm and the increase in the 680 nm band.

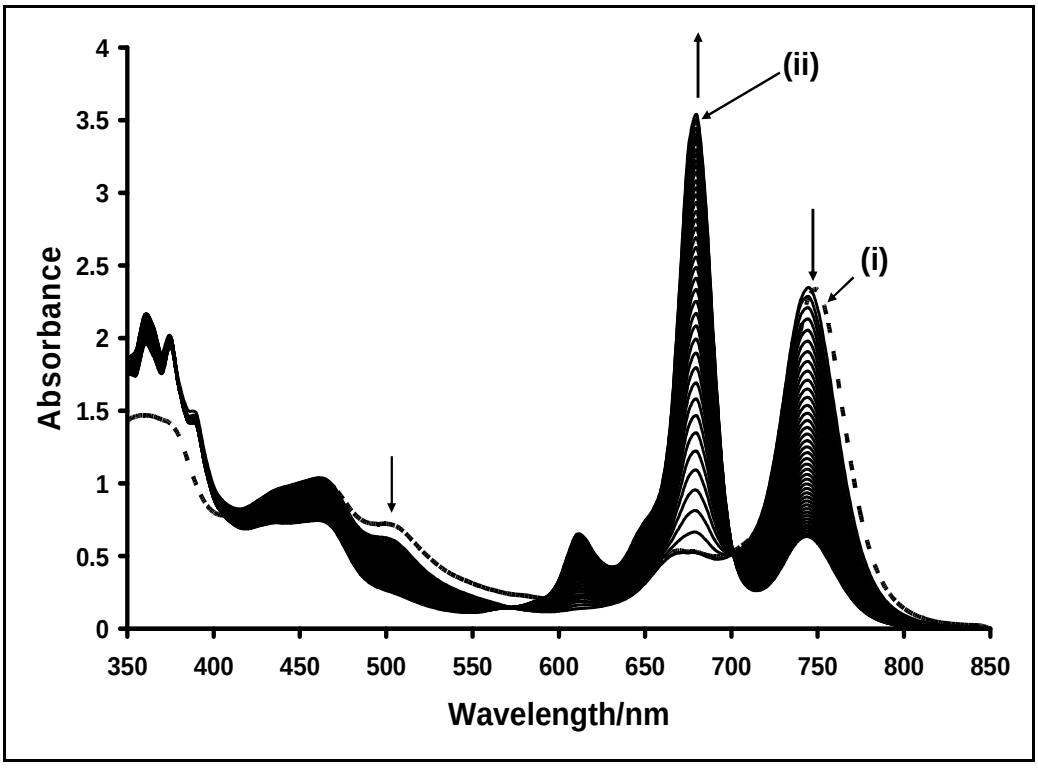

Figure 6.14: Electronic spectral changes of complex **34** on addition of 1 mM nitrite solution in DMSO to approx. 2 µM solution of the complexes in DMSO. (i) initial spectrum, (ii) final spectrum after 6 hours.

Reduction was confirmed by addition of oxidants such as bromine which resulted in the decrease in the absorption band at 680 nm and the increase in the Q band due to $Mn^{3+}Pc$ (not shown). The catalytic oxidation of nitrite by the MnPc complexes may be represented by equations 6.12 to 6.14, Scheme 6.3.

$(AcO^-)Mn^{3+}Pc$	+	NO_2^-	⟶	$(NO_2^-)Mn^{3+}Pc$	+	AcO^-	**(6.12)**
$(NO_2^-)Mn^{3+}Pc$			⟶	$Mn^{2+}Pc$	+	NO_2	**(6.13)**
$Mn^{2+}Pc$			⟶	$[Mn^{3+}Pc]^+$	+	e^-	**(6.14)**

Scheme 6.3: Proposed reaction mechanism for MnPcs-modified gold electrode electrooxidation of nitrite

Equation 6.12 is proposed due to spectral changes shown in Figure 6.14, whereby a shift of 5 nm is observed on the spectrum of the $Mn^{3+}Pc$ species at 750 nm immediately following the addition of nitrite. Equation 6.13 is proposed as a result of the reduction of the $Mn^{3+}Pc$ complexes to the $Mn^{2+}Pc$ species on addition of nitrite. Equation 6.14 is suggested since the $Mn^{2+}Pc$ species is formed in the presence of nitrite and the electrochemical oxidation will occur from this species. However, the formation of the $Mn^{2+}Pc$ species is very slow; it took 6 hours to obtain the spectral changes shown in Figure 6.14. Hence the reduction of $Mn^{3+}Pc$ is not expected to occur within the time scale of cyclic voltammetry and the most likely mechanism is that involving the $Mn^{4+}Pc/Mn^{3+}Pc$ couple which would catalyse nitrite oxidation before the $Mn^{3+}Pc$ is reduced resulting in a mechanism shown by equations 6.15 to 6.17 (Scheme 6.4):

$\mathbf{(AcO^-)Mn^{3+}Pc + NO_2^- \longrightarrow (NO_2^-)Mn^{3+}Pc + AcO^-}$		**(6.15)**
$\mathbf{(NO_2^-)Mn^{3+}Pc \longrightarrow [(NO_2^-)Mn^{4+}Pc]^+ + e^-}$		**(6.16)**
$\mathbf{[(NO_2^-)Mn^{4+}Pc]^+ \longrightarrow [Mn^{3+}Pc]^+ + NO_2}$		**(6.17)**

Scheme 6.4: Proposed reaction mechanism for MnPcs-modified gold electrode electrooxidation of nitrite

The latter mechanism is proposed on the basis that the oxidation of nitrite is in the potential region for the $Mn^{4+}Pc/Mn^{3+}Pc$ couple, (compare Figure 6.7 and 5.8a). Mn^{4+}/Mn^{3+} peak is around 0.5 V which is at the foot of the nitrite oxidation. In the case of MnPc derivatives, the formation of NO_2, which requires one electron, would be the last step, since the total number of electrons was found to be one (Table 6.2). Moreover, the fact that the Tafel slopes for the MnPcs derivatives is close to 60 mV dec^{-1} indicates that

the fast electron transfer step in equation 6.16 is followed by the slow chemical step represented by equation 6.17. The worse catalytic performance of the MnPcs derivatives compared to the FePc and CoPc derivatives is supported by the close to zero values of α for the MnPcs which as earlier described indicate that product formation is not favoured.

6.2.3 Catalytic effect of the different forms of NiPc complexes

The electrooxidation of nitrite by the NiPcs modified electrodes was carried out in separate experiments; the main aim is to investigate the effect of the nature of the NiPc complexes on catalytic activities.

Figure 6.15 shows the cyclic voltamogramms of 1 mM nitrite in phosphate buffer (pH 7.4) at (a) an unmodified gold electrode, (b) *poly*-NiTDMPc-Au electrode, (c) *poly*-NiTBMPc-Au electrode, (d) *poly*-Ni(OH)TDMPc-Au electrode and (e) *poly*-Ni(OH)TBMPc-Au electrode.

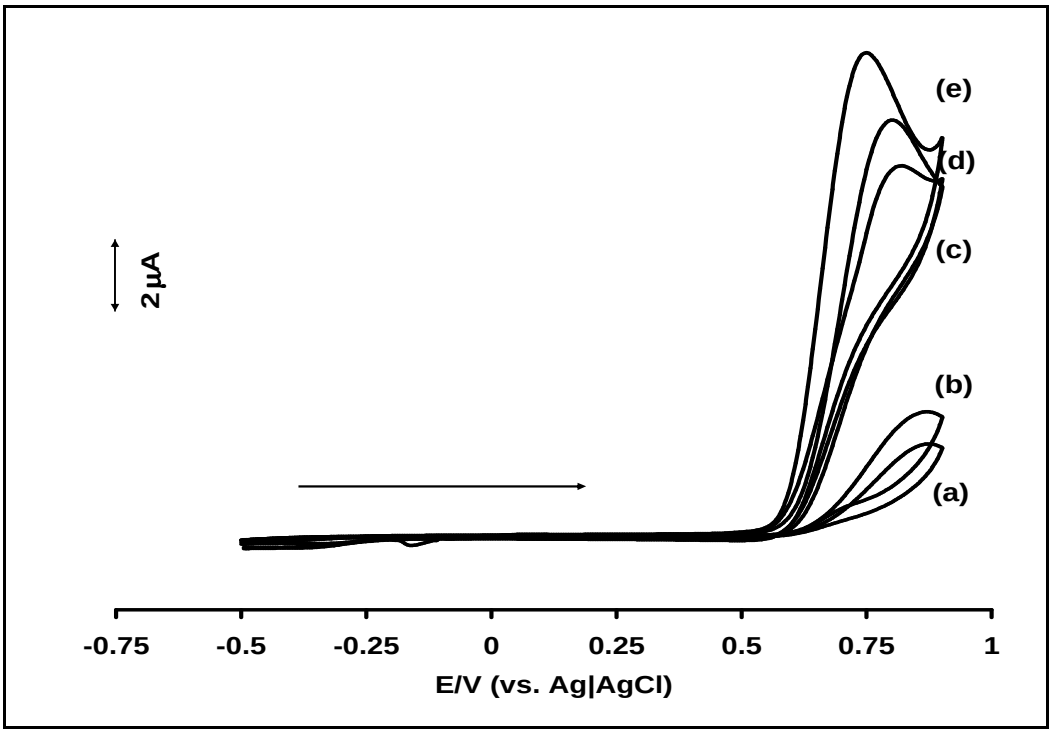

Figure 6.15: Cyclic voltamogramms for 1 mM nitrite oxidation in phosphate buffer pH 7.4 solution at (a) an unmodified Au electrode, (b) *poly*-NiTDMPc-Au, (c) *poly*-NiTBMPc-Au, (d) *poly*-Ni(OH)TDMPc-Au and (e) *poly*-Ni(OH)TBMPc-Au. Scan Rate = 100 mV s^{-1}

From Figure 6.15, it can be concluded that:

(1) Better catalysis occurred when the gold electrode was modified with the complexes judging from the shifting of peak potential to less positive values (from 0.89 to 0.83 V for NiTBMPc) and higher peak currents for the modified electrodes compared to the unmodified gold electrode.

(2) Both complexes increased their activities for nitrite electrooxidation when they were transformed to the 'O-Ni-O oxo form', as judged by shifts of the peak potential to the less positive values, for the 'O-Ni-O' form (from 0.85 to 0.80 V for NiTDMPc, and from 0.83 to 0.76 V for NiTBMPc).

(3) NiTBMPc modified gold electrodes showed better catalytic activities than the NiTDMPc modified gold electrodes both before and after transformation to 'O-Ni-O oxo form', as judged by increase in currents and a shift to less positive potentials.

In terms of resistance to electrode surface passivation, surprisingly there were not significant differences between the various electrodes, all the modified electrodes showed resistance to passivation as shown in Figure 6.16, which shows only small decreases in currents with scan numbers. The % decrease between the first and second scan range from 7.1 – 14.5% while for the subsequent scans they were less than 4%.

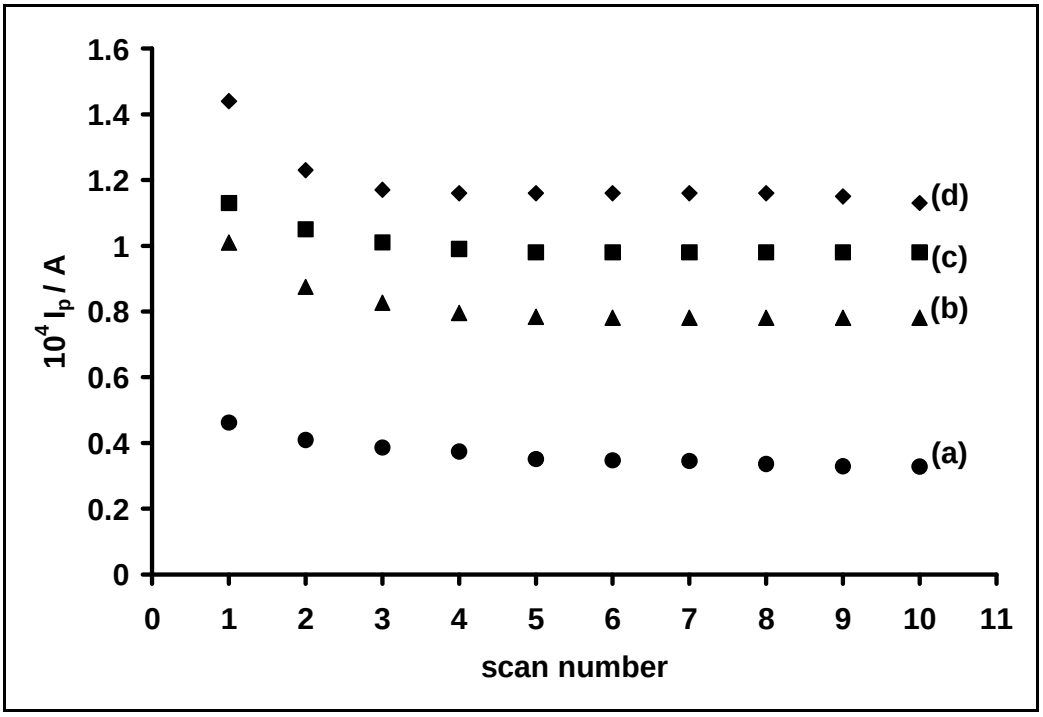

Figure 6.16: The variation of peak currents with scan number for the voltammetric response of 1 mM NO_2^- on (a) *poly*-NiTDMPc-Au, (b) *poly*-NiTBMPc-Au, (c) *poly*-Ni(OH)TDMPc-Au and (d) *poly*-Ni(OH)TBMPc-Au. Buffer = pH 7.4. Scan rate = 100 mV s^{-1}.

Figure 6.17 shows the variation of peak currents with nitrite concentration at various poly-NiPc-Au electrodes. In the concentration range chosen for the catalytic studies in this work (i.e., 1.0 µM – 1.0 mM), a linear relationship between the catalytic currents and the nitrite concentrations was observed, resulting in slopes (sensitivities) of 6.0 (± 0.2) µA mM^{-1}, 3.3 (± 0.1) µA mM^{-1}, 12.6 (± 0.9) µA mM^{-1} and 11.1 (± 0.8) µA mM^{-1} for *poly*-NiTBMPc-Au and poly-NiTDMPc-Au, *poly*-Ni(OH)TBMPc-Au and poly-Ni(OH)TDMPc-Au respectively, Table 6.2.

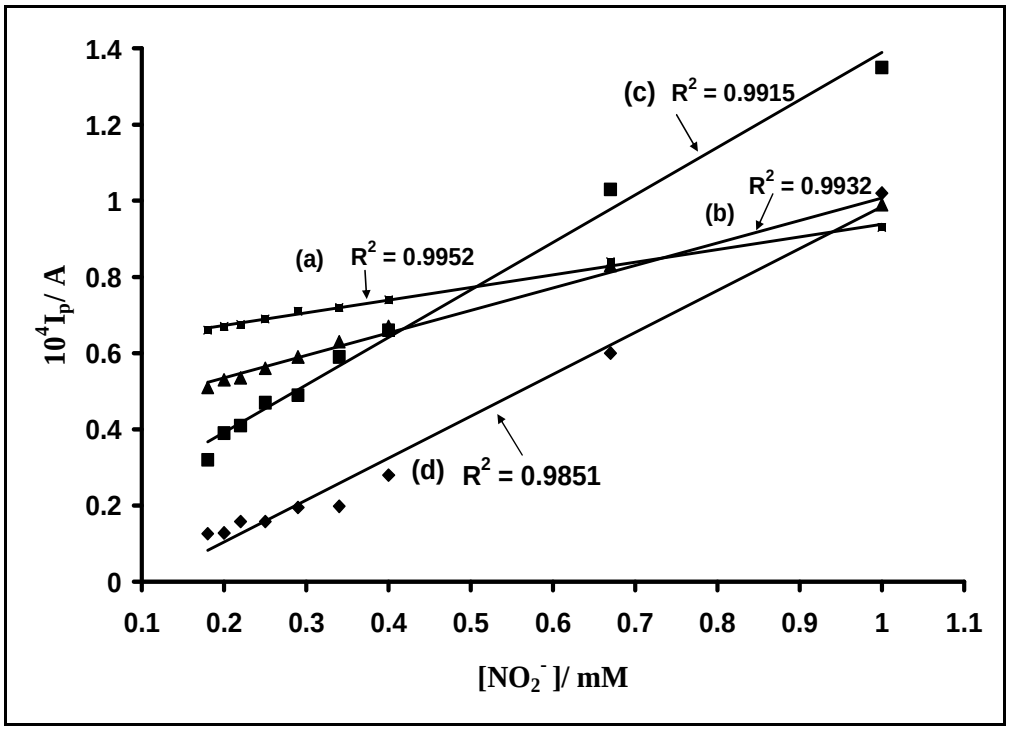

Figure 6.17: The variation of peak currents with nitrite concentration for the voltammetric response on (a) *poly*-NiTBMPc-Au, (b) *poly*-NiTDMPc-Au, (c) *poly*-Ni(OH)TBMPc-Au and (d) *poly*-Ni(OH)TDMPc-Au. Buffer = pH 7.4. Scan rate = 100 mV s^{-1}.

Figure 6.18a shows the typical cyclic voltamogramms for 1 mM NO_2^- electrooxidation at different scan rates while Figure 6.18b shows the plot of E_p vs. log *v* for electrooxidation of 1 mM nitrite solution in phosphate buffer pH 7.4 at all the *poly*-NiPc-Au electrodes. For all the *poly*-NiPc-Au electrode catalysis of nitrite oxidation, the peak potentials shifted with the log of scan rate as shown in Figure 6.18b. This trend indicates that the electrocatalytic oxidation of nitrite is irreversible.[406] Figure 6.18c shows that there is a linear relationship between the peak current, I_p and square root of the scan rate, indicating that the nitrite electrocatalytic oxidation is diffusion controlled. Figure 6.18d further confirms that the electrooxidation of nitrite by all the *poly*-NiPc-Au electrodes are a catalytic processes judging by the pattern of curves obtained which is typical of catalytic processes.[63] It should be noted that the observations reported for the catalytic oxidation of nitrite by *poly*-NiPc-Au electrodes was also observed for *poly*-Ni(OH)TBMPc-GCE, except that the peak potential did not shift to the less positive potentials with nitrite concentration as expected.

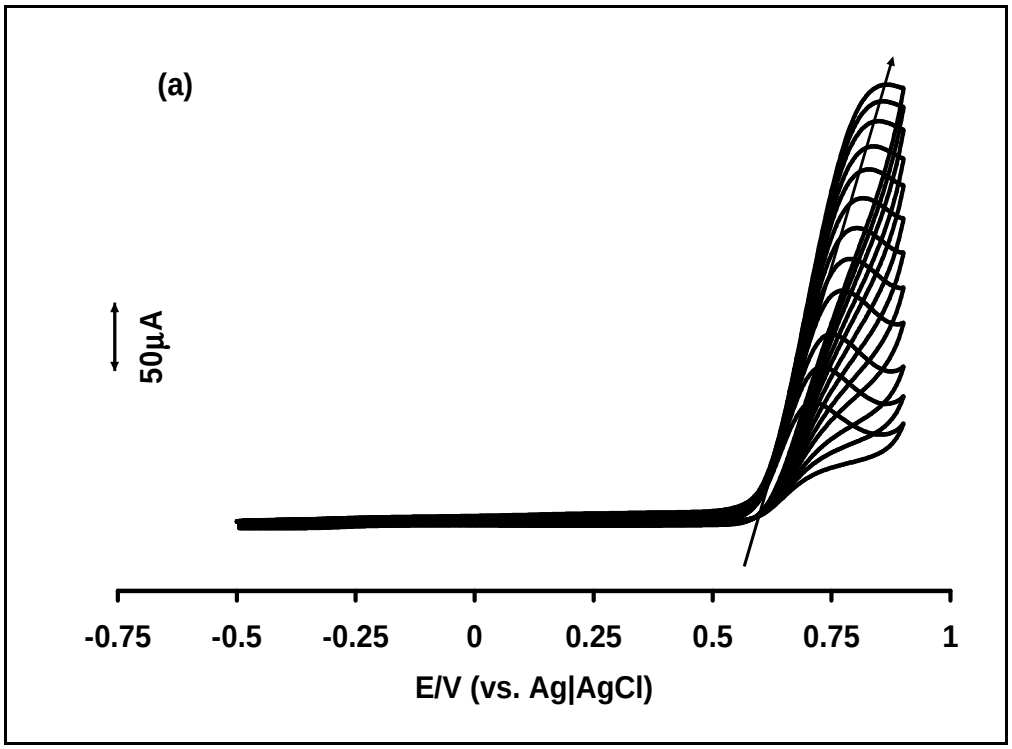
(a)
50µA
-0.75
-0.5
-0.25
0
0.25
0.5
0.75
1
E/V (vs. Ag|AgCl)

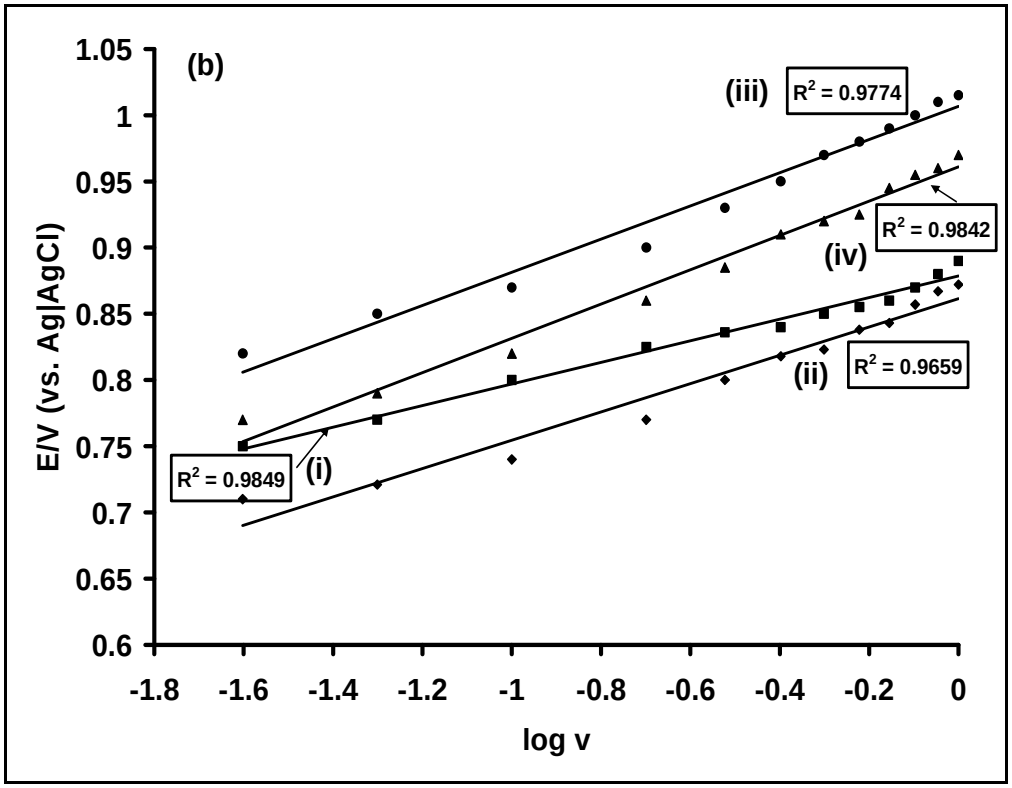
(b)
1.05
1
0.95
0.9
0.85
0.8
0.75
0.7
0.65
0.6
E/V (vs. Ag|AgCl)
-1.8
-1.6
-1.4
-1.2
-1
-0.8
-0.6
-0.4
-0.2
0
log v
(iii)
R2 = 0.9774
R2 = 0.9842
(iv)
(ii)
R2 = 0.9659
R2 = 0.9849
(i)

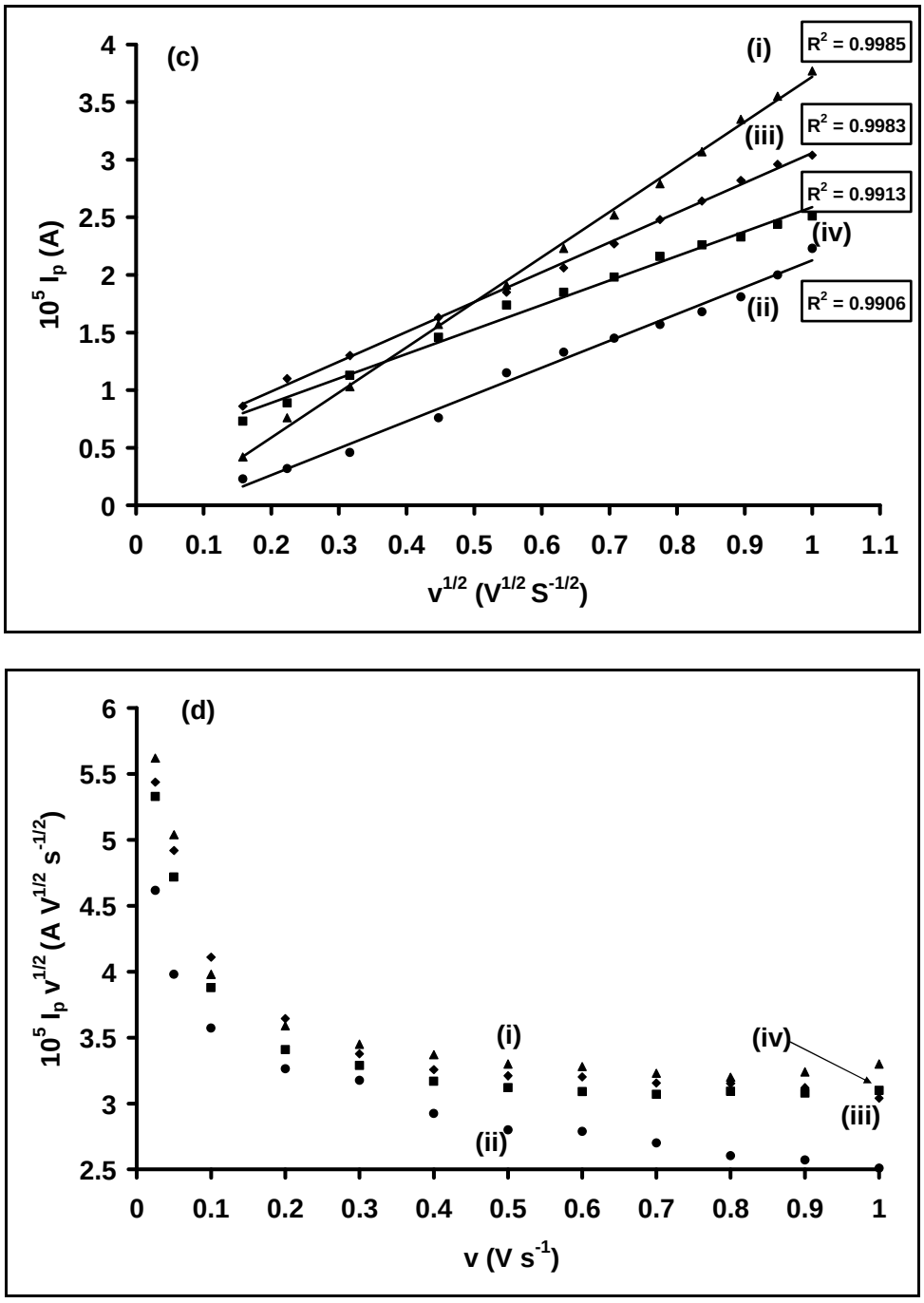

Figure 6.18: (a) Cyclic voltamogramms of electrooxidation of 1 mM nitrite at different scan rates catalysed by *poly*-Ni(OH)TBMPc-Au electrode (b) Plot of E_p vs. log *v* (c) Plot of Ip vs. $v^{1/2}$ and (d) Plot of $I_p v^{-1/2}$ vs. *v* for electrooxidation of 1 mM nitrite solution in phosphate buffer pH 7.4 on (i) *poly*-NiTBMPc-Au and (ii) *poly*-NiTDMPc-Au, (iii) *poly*-Ni(OH)TBMPc-Au and (iv) *poly*-Ni(OH)TDMPc-Au.

The mechanism behind the improvement in catalytic activities when the nickel macro complexes are transformed to the 'O-Ni-O oxo form' is not fully understood, but Ni^{3+}/Ni^{2+} redox process maybe playing a key role in the reaction, with the possibility that Ni^{3+} produced from electrooxidation of Ni^{2+} reacts with nitrite ions resulting in the oxidation of nitrite to nitrate and Ni^{3+} getting reduced back to Ni^{2+} in the process (Scheme 6.3). The catalytic oxidation of nitrite occurs in the same potential range as the anodic component of the Ni^{3+}/Ni^{2+} process in pH 7.4 buffer (comparing Figure 6.6 and 6.15). The spectroscopic studies (Figure 6.19) of the interaction of complex **37** with nitrite did not prove any transformation of the complex; this might be due to the fact that NiPc complexes are square planar and show no coordination of axial ligands. The calculation of the total number of electron transferred was found to be approximately 2 for all the electrodes with the exception of *poly*-NiTDMPc-Au electrode which was found to be 1 electron (Table 6.2). Equations shown in Scheme 6.5 are likely to be the reaction mechanism for the *poly*-NiTBMPc-Au, *poly*-Ni(OH)TBMPc-Au and *poly*-Ni(OH)TDMPc-Au derivatives with the exception of *poly*-NiTDMPc-Au electrodes. Coordination of nitrite to NiPc complexes was not proved so an outer sphere mechanism is proposed in Scheme 6.5. For *poly*-NiTDMPc-Au electrodes, similar reaction mechanism for the MnPc derivatives in Scheme 6.4 which led to NO_2 as the product could also be proposed.

$$Ni^{2+}Pc^{2-} \longrightarrow [Ni^{3+}Pc^{2-}]^{+} + e^{-} \quad (6.18)$$

$$[Ni^{3+}Pc^{2-}]^{+} + NO^{-}_{2} + H_2O \longrightarrow Ni^{2+}Pc^{2-} + NO^{-}_{3} + 2H^{+} + e^{-} \quad (6.19)$$

Scheme 6.5 Proposed reaction mechanism for NiPcs-modified gold electrode electrooxidation of nitrite

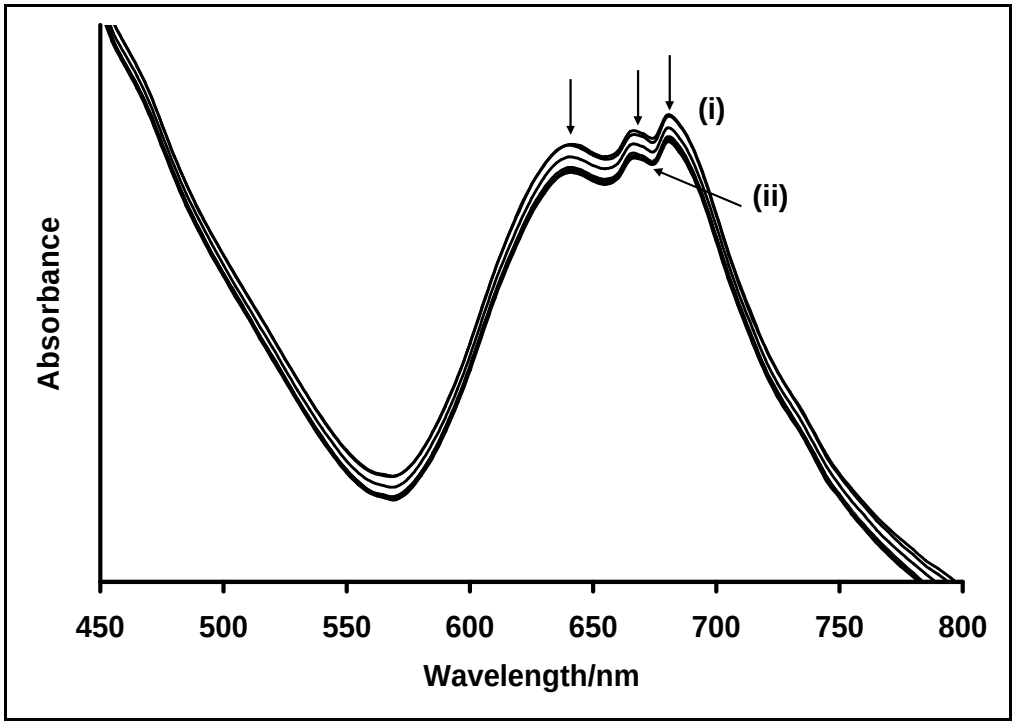

Figure 6.19: Electronic spectral changes of (a) complex **37** on addition of 1 mM nitrite solution in DMSO to approx. 2 µM solution of the complexes in DMSO. (i) initial spectrum, (ii) final spectrum after 20 minutes. Concentration of (i) complex in DMSO = 1 µM and (ii) nitrite in DMSO = 1 µM.

6.3 Electrocatalytic oxidation of Sulphite on MPc-SAM

Figure 6.20 shows the cyclic voltamogramms of 1 mM sulphite in phosphate buffer (pH 7.4) at (i) an unmodified gold electrode and on SAMs of complexes (ii) **35**, (iii) **40**, (iv) **36**, (v) **41**, (vi) **34**, (vii) **39**, (viii) **37** and (ix) **42**. All the complexes-SAM electrodes showed catalysis judging by the significant increase in the peak currents. The oxidation peak for sulphite at unmodified gold electrode was a slow redox reaction with a catalytic potential peak, E_p at around 0.59 V. With the exception of the NiPcs-SAM, the E_p was significantly lowered by all the complexes-SAM electrodes indicating catalysis, Table 6.3.

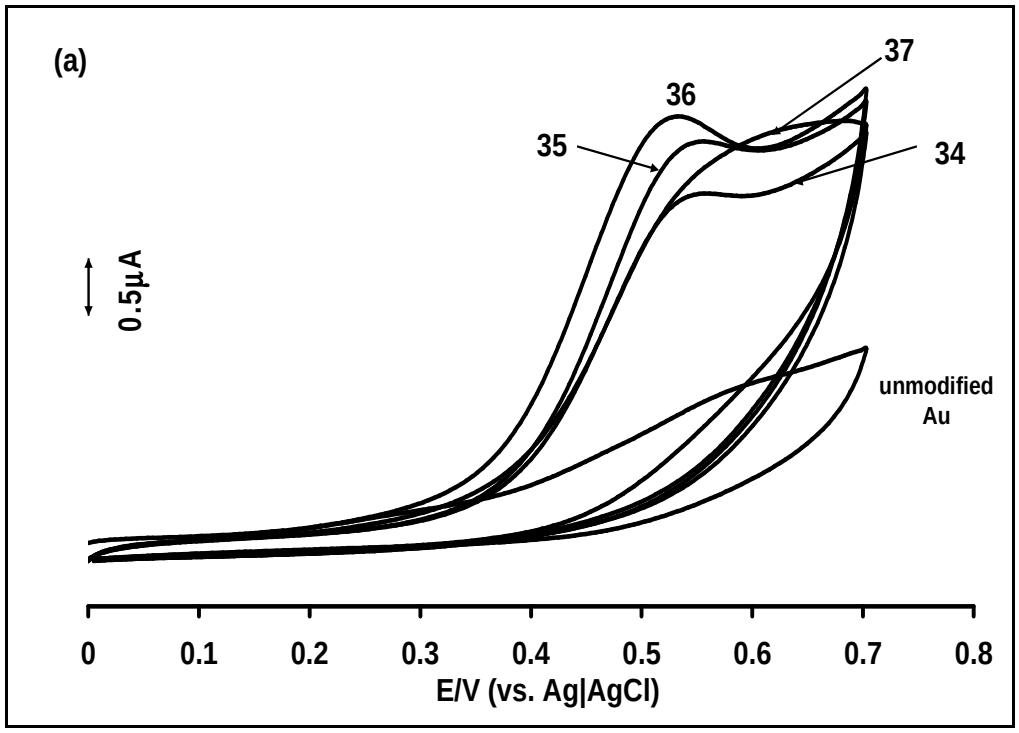

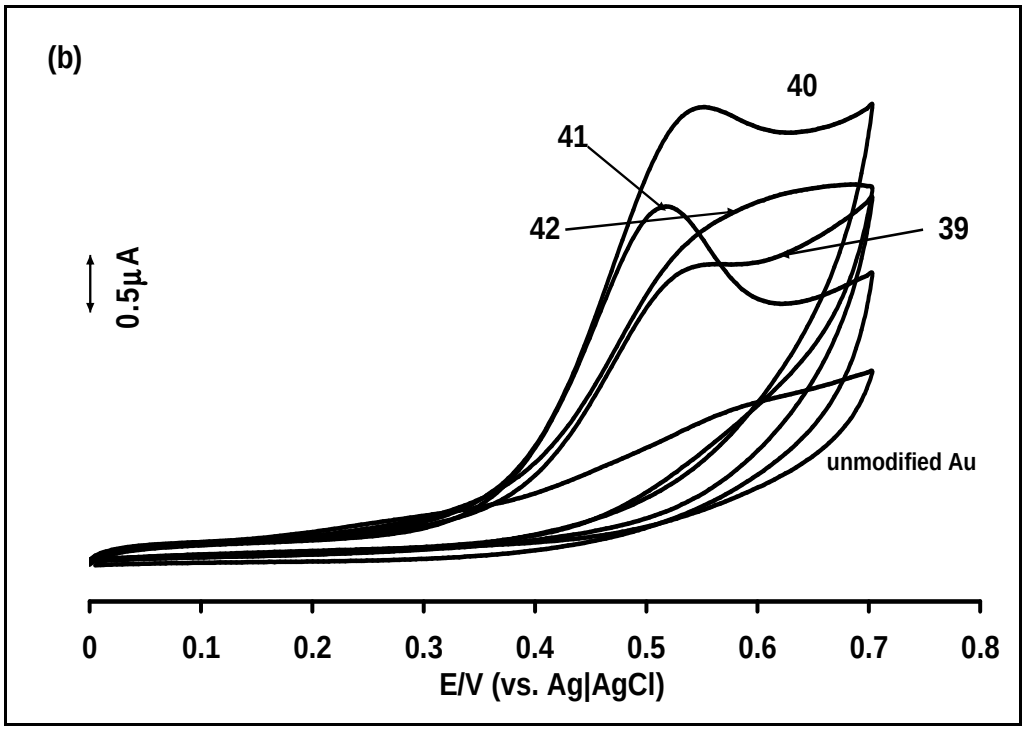

Figure 6.20: Cyclic voltamogramms for 1 mM sulphite oxidation in phosphate buffer pH 7.4 solution at (i) unmodified gold electrode, (**a**) complex (ii) **34**, (iii) **35**, (iv) **36**, (v) **37**, (**b**) (vi) **39**, (vii) **40**, (viii) **41** and (ix) **42.**

The order of catalytic activity in terms of decreasing peak current, I_p/ µA is as follows complex **40** (3.8) > complex **36** (3.3) > complex **37** (3.2) > complex **35** (3.1) ~ complex **42** (3.1) > complex **41** (2.9) > complex **34** (2.7) > complex **39** (2.4) while in terms of peak potential, E_p/V is as follows complex **37** (0.64) ~ complex **42** (0.63) < complex **40** (0.55) ~ complex **39** (0.54) ~ complex **34** (0.54) ~ complex **35** (0.54) < complex **36** (0.53) < complex **41** (0.52), Table 6.3.

Table 6.3: Mechanistic feature of the sulphite oxidation on MPc-SAM modified Au electrode

Complex	E_p (V) $M^{III}Pc/M^{II}Pc$ (vs. Ag|AgCl)[a]	E_p (V)/ (vs. Ag|AgCl)	I_p (µA)	Sensitivity (µA mM^{-1})	b	α	*k*	n_t
CoTBMPc (**35**)	0.23	0.54	3.1	2.96	110	0.45	0.00688	4.1
CoTDMPc (**40**)	0.10	0.55	3.8	2.82	144	0.59	0.00597	4.6
FeTBMPc (**36**)	0.08	0.53	3.3	1.94	236	0.75	0.00356	4.5
FeTDMPc (**41**)	0.31	0.52	2.9	3.05	264	0.73	0.00254	3.8
MnTBMPc (**34**)	0.11	0.54	2.7	2.51	224	0.73	0.00417	4.3
MnTDMPc (**39**)	0.13	0.54	2.4	2.72	239	0.75	0.00381	4.5
NiTBMPc (**37**)	(0.66)[b]	0.63	3.2	1.68	139	0.56	0.00212	4.2
NiTDMPc (**42**)	(0.70)[b]	0.62	3.1	2.10	140	0.57	0.00253	4.5

[a]E_p values from Table 5.5 in pH 7.4 buffer, [b]ring based redox process in brackets

It should be stated that the catalytic performance of the CoPc, FePc and MnPc derivatives in terms of lowering the E_p values for sulphite electrooxidation is comparable and better than most reported in literature.[365,367,370-373] The catalytic activities of the complexes-SAM modified electrodes were also studied for lower concentration (1 µM) sulphite electrooxidation, Figure 6.21. The unmodified gold electrode (curve i) hardly showed any catalytic activity in Figure 6.21 while for the oxidation of sulphite by selected complexes-SAM modified electrodes, there were significant increases in the peak currents; this observation shows that these modified electrodes are potential sensors for real samples applications.

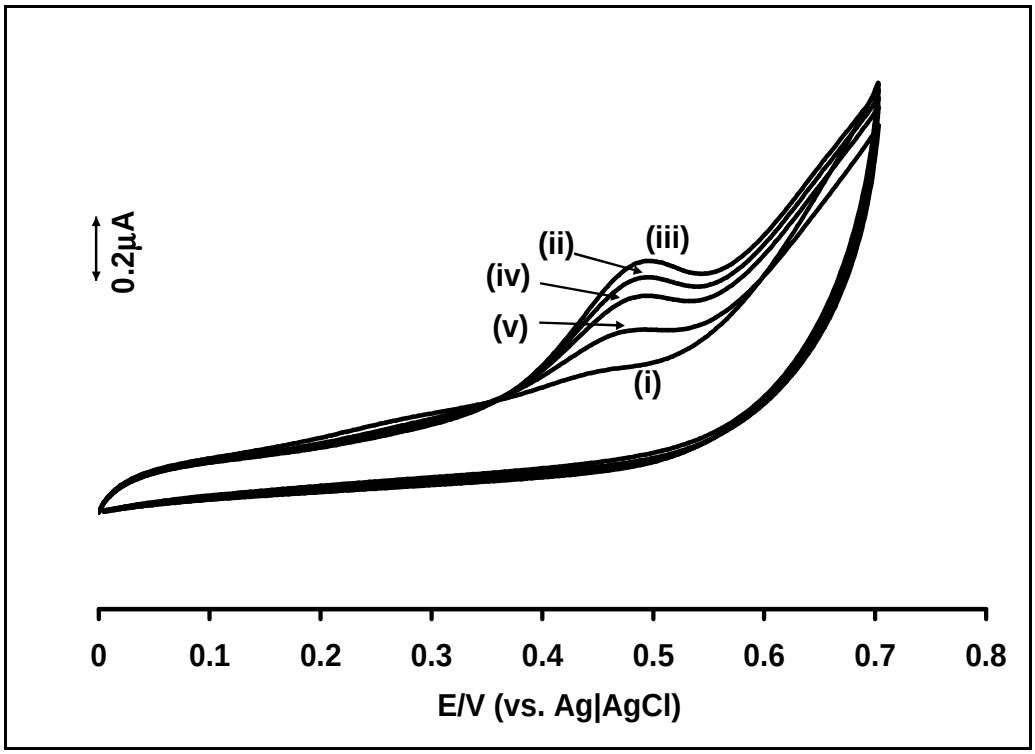

Figure 6.21: Cyclic voltamogramms for 1 µM sulphite oxidation in phosphate buffer pH 7.4 solution at (i) unmodified gold electrode, complex (ii) **35**, (iii) **36**, (iv) **34** and (v) **37**.

As shown in Figure 6.22, there were linear relationships between the catalytic currents and the sulphite concentrations for the concentration range chosen for the catalytic studies in this work (i.e. 0.1–1.0 mM), resulting to slopes (sensitivities) ranging from 1.68 to 2.96 µA mM^{-1} for the various electrodes, Table 6.3.

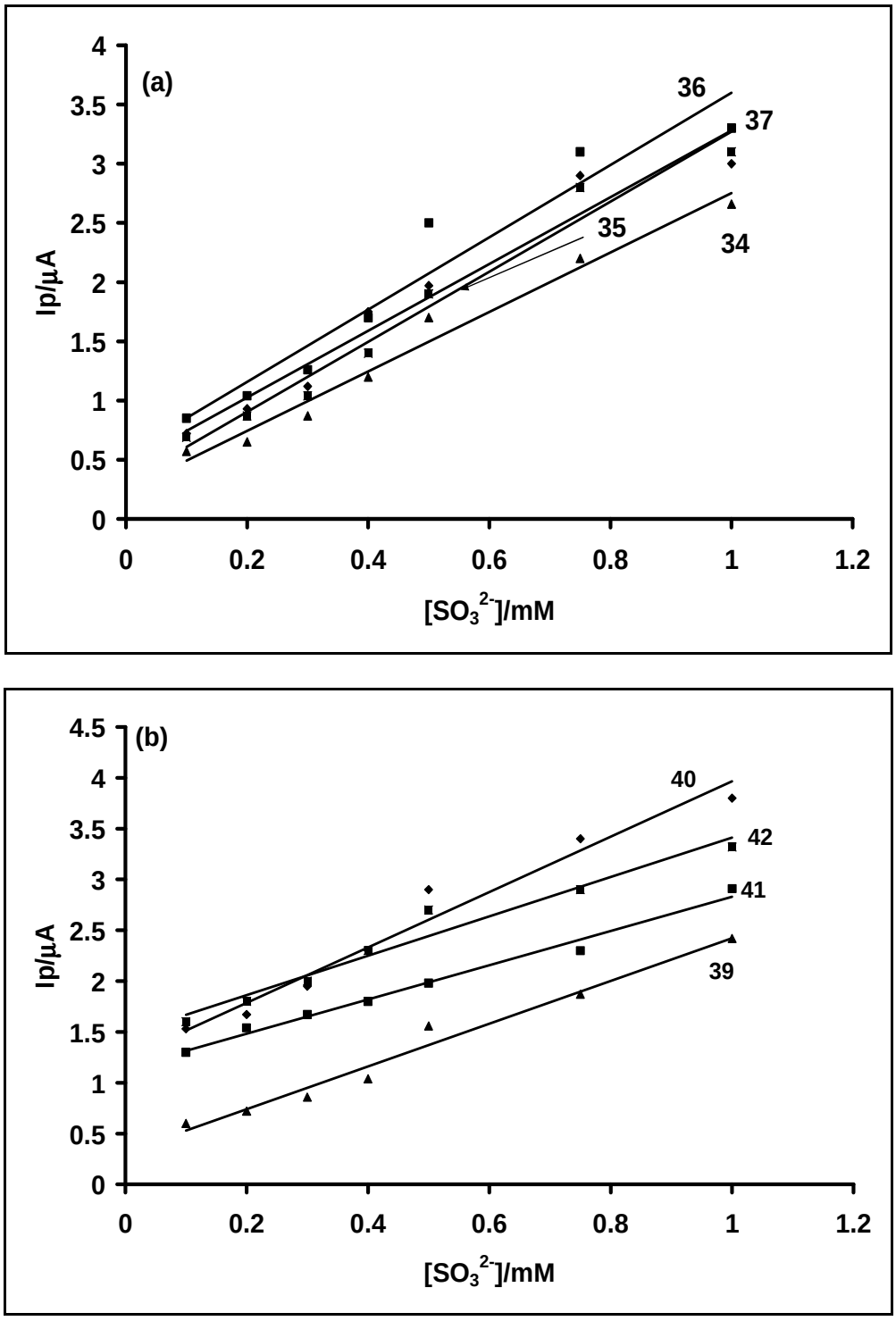

Figure 6.22: Plots of I_p vs. $[SO_3^{2-}]$ at complex (**a**) (i) **34**, (ii) **35**, (iii) **36**, (iv) 37, (**b**) (v) **39**, (vi) **40**, (vii) **41** and (vii) **42**. Scan rate = 100 mV s^{-1}.

In terms of resistance to electrode surface passivation, there were no significant differences between the various electrodes, all the modified electrodes showed high resistance to passivation as shown in Figure 6.23, which shows only small decreases in current with scan number and mainly observed between the first and second scan. The % decrease between the first and second scan range from 3.3 – 11.5% while for the subsequent scans they were less than 5%.

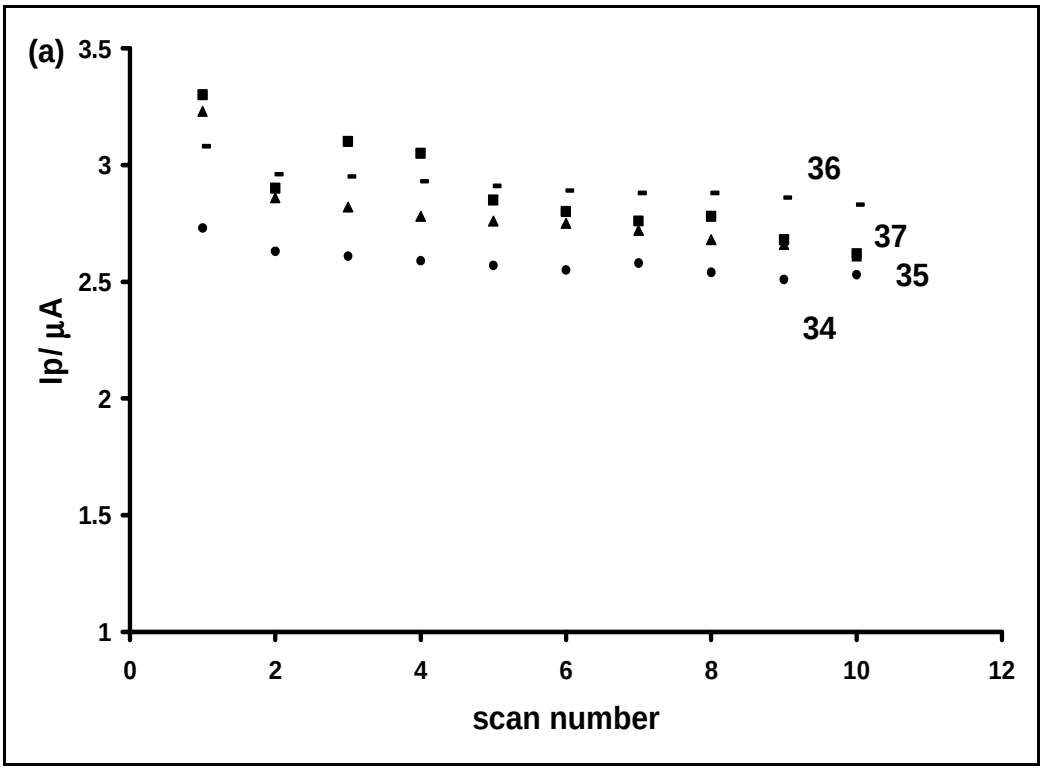

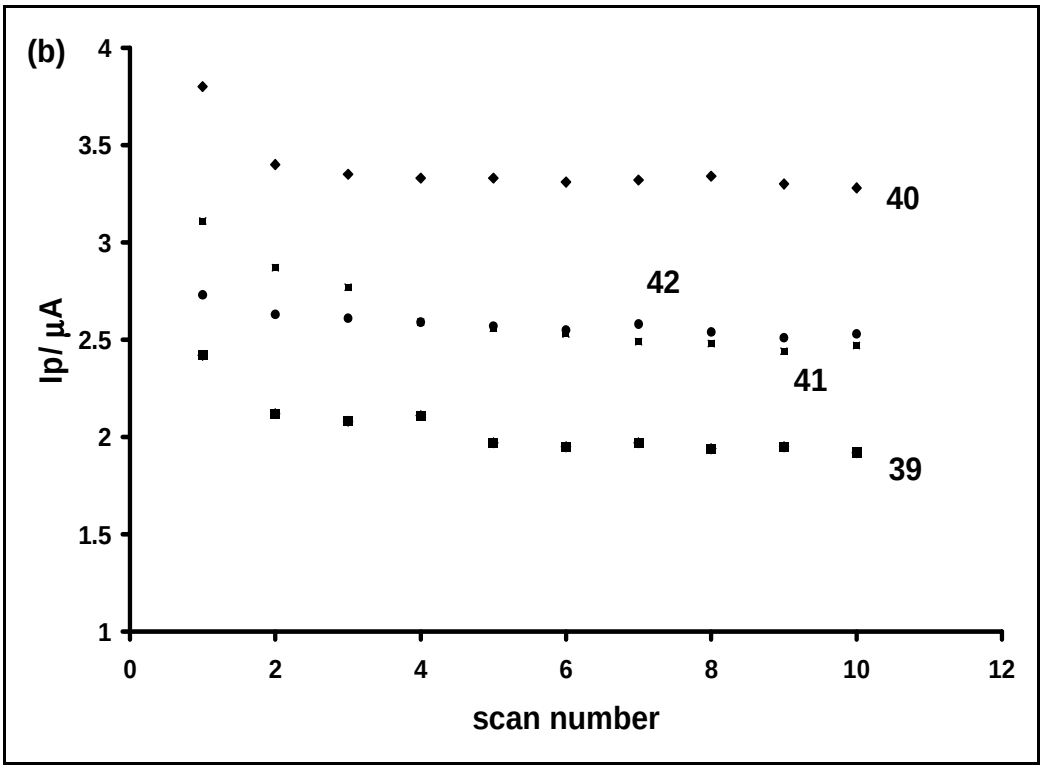

Figure 6.23: Plots of I_p vs. number of scans for repetitive cycling of 1 mM sulphite at complex (**a**) **34, 35**, **36, 37** (**b**) **39**, **40**, **41, 42.** Scan rate = 100 mV s^{-1}.

Figure 6.24a shows the cyclic voltamogramms of electrooxidation of 1 mM sulphite at different scan rates catalysed by complex **40**-SAM electrode as an example, it is clear that the E_p shifted positively with increase in scan rate. For all complexes-SAM catalysis of sulphite oxidation, the peak potentials shifted linearly with the log of scan rate as shown in Figure 6.24b, this indicates that the electrocatalytic oxidation of sulphite is irreversible[406] and this is in agreement with the pattern of the sulphite oxidation CV peaks which did not show any cathodic return peak. Using Figure 6.24b and equation 6.6, Tafel slopes calculated for both CoPc and NiPc were close to 120 mV dec^{-1} while for the FePc and MnPc derivatives, they were higher than 200 mV dec^{-1}. Thus for CoPc and NiPc derivatives, the Tafel slopes close to 120 mV dec^{-1} indicate that the first one electron

transfer is the rate limiting step. While for FePc and MnPc derivatives, the slopes of 224 to 264 mV dec^{-1} imply that there were strong interactions between sulphite ions and the complexes or chemical reactions coupled with electrochemical steps.[414] The α values obtained for both CoPc and NiPc derivatives are approximately 0.5 (Table 6.3) while for the FePc and MnPc derivatives the α values are greater than 0.5. This observation for the CoPc and NiPc derivatives imply that the reaction equilibrium favours both reactants and products while for the FePc and MnPc derivatives, the reaction equilibrium favours the products more than the reactants. The diffusion coefficient (*D*) for sulphite is 2.3 x 10^{-5} cm^2 s^{-1}.[416] In general, the values of k (Table 6.3, equation 6.7) were higher for the CoPc, FePc and MnPc derivatives compared to the corresponding NiPc derivatives, this may imply that the former are more efficient in electron transfer than the latter. Figure 6.24c shows that there is a linear relationship between the peak current and square root of the scan rate, indicating that the sulphite electrocatalytic oxidation is diffusion controlled. Using equation 6.8, total number of electrons (n_t) calculated for all the electrodes oxidation of sulphite are in the range 3.8-4.6 (Table 6.3). The higher number of electrons obtained for all the MPc complexes could be due to the fact that there may be electrooxidation of the other form of SO_3^{2-} such as hydrogen sulphite, (HSO_3^-) in pH 7.4.[289] Figure 6.23d further confirmed that the electrooxidation of sulphite by the complexes-SAM modified gold electrodes is a catalytic process judging by the pattern of curves obtained which is typical of catalytic processes.[63]

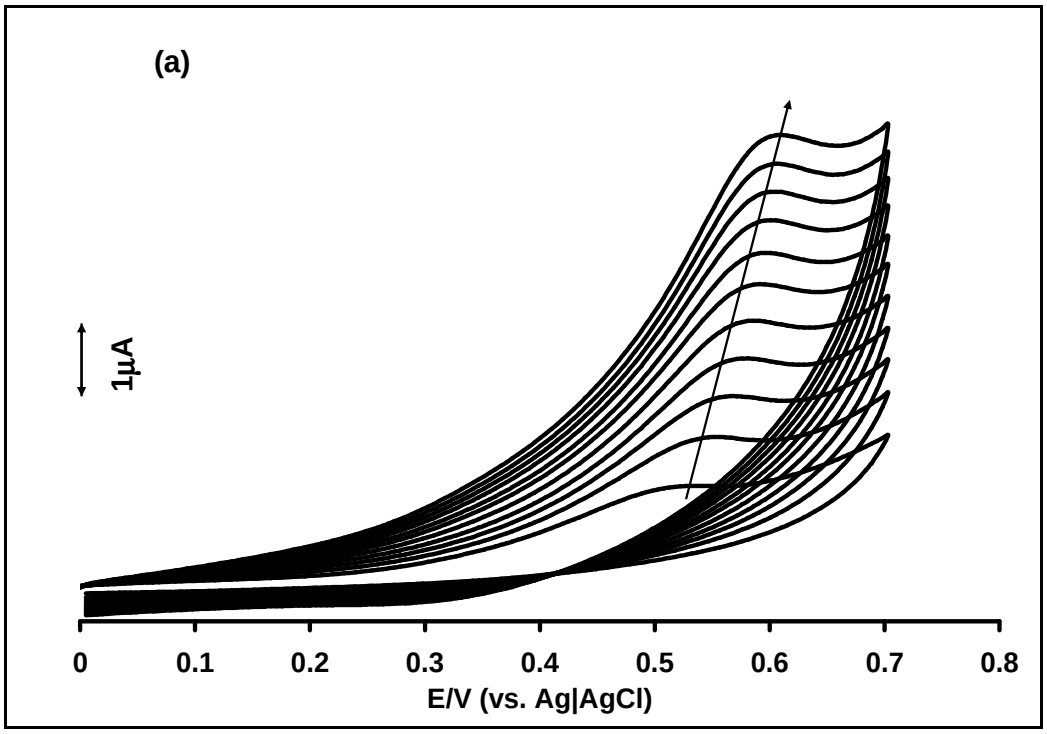
(a)
1µA
0
0.1
0.2
0.3
0.4
0.5
0.6
0.7
0.8
E/V (vs. Ag|AgCl)

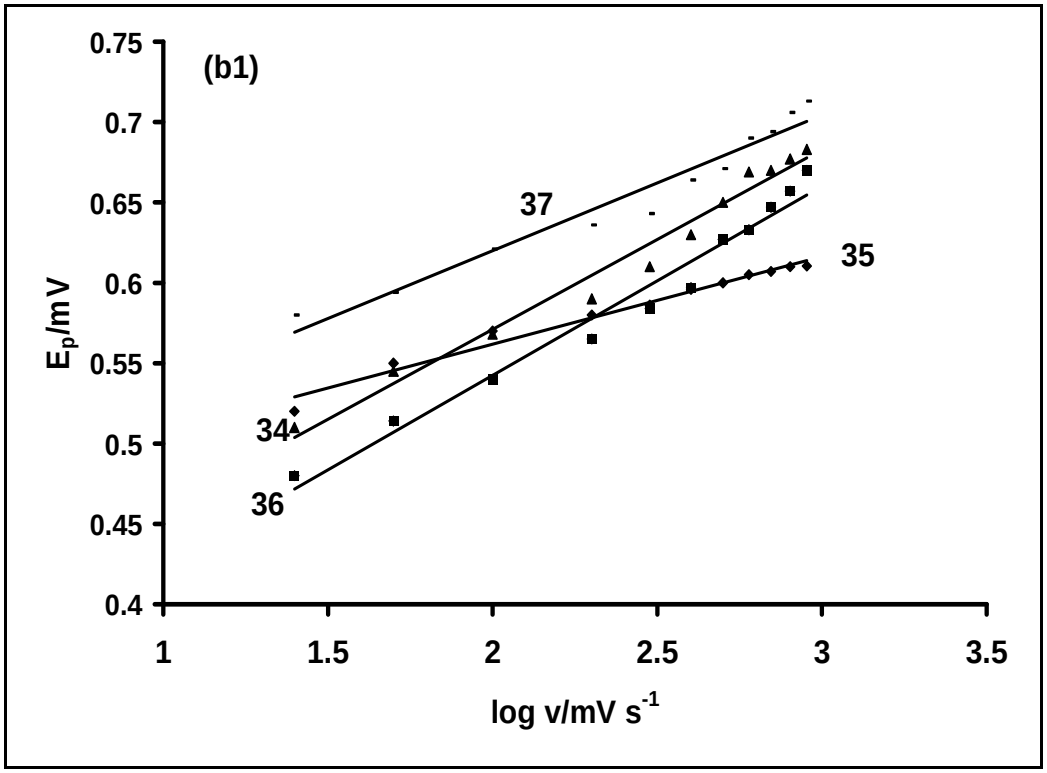
(b1)
0.75
0.7
0.65
0.6
0.55
0.5
0.45
0.4
E_p/mV
37
35
34
36
1
1.5
2
2.5
3
3.5
log v/mV s^{-1}

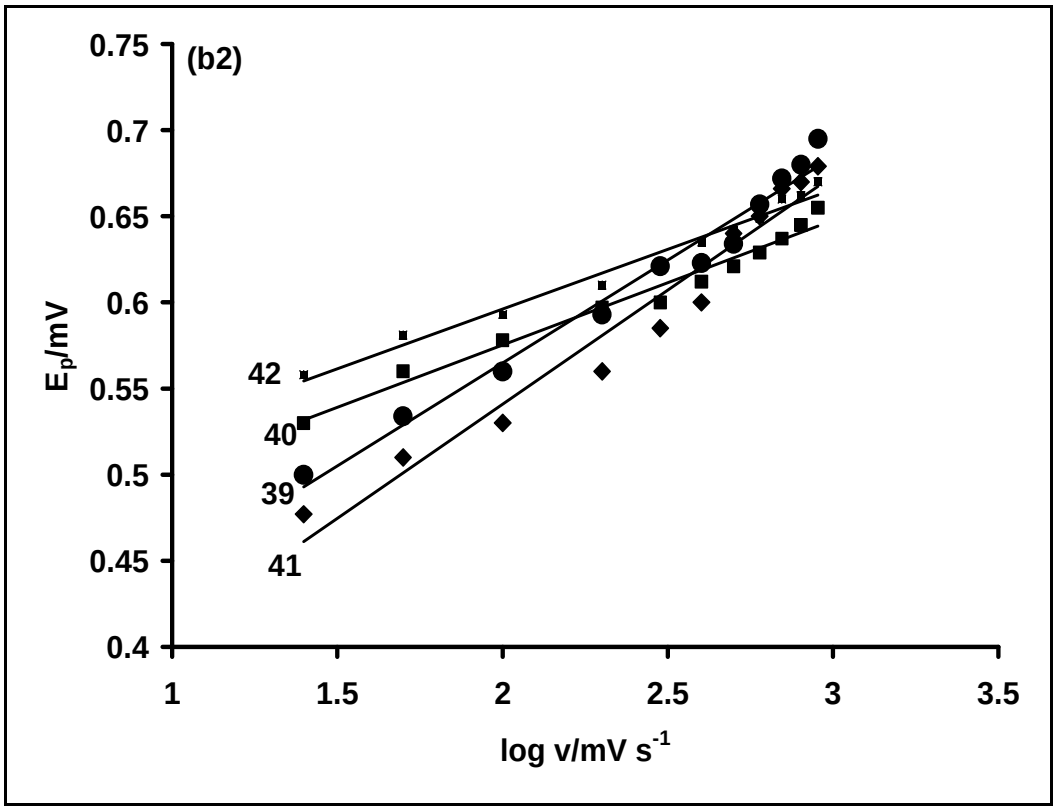
(b2)
0.75
0.7
0.65
0.6
0.55
0.5
0.45
0.4
E_p/mV
42
40
39
41
1
1.5
2
2.5
3
3.5
log v/mV s^{-1}

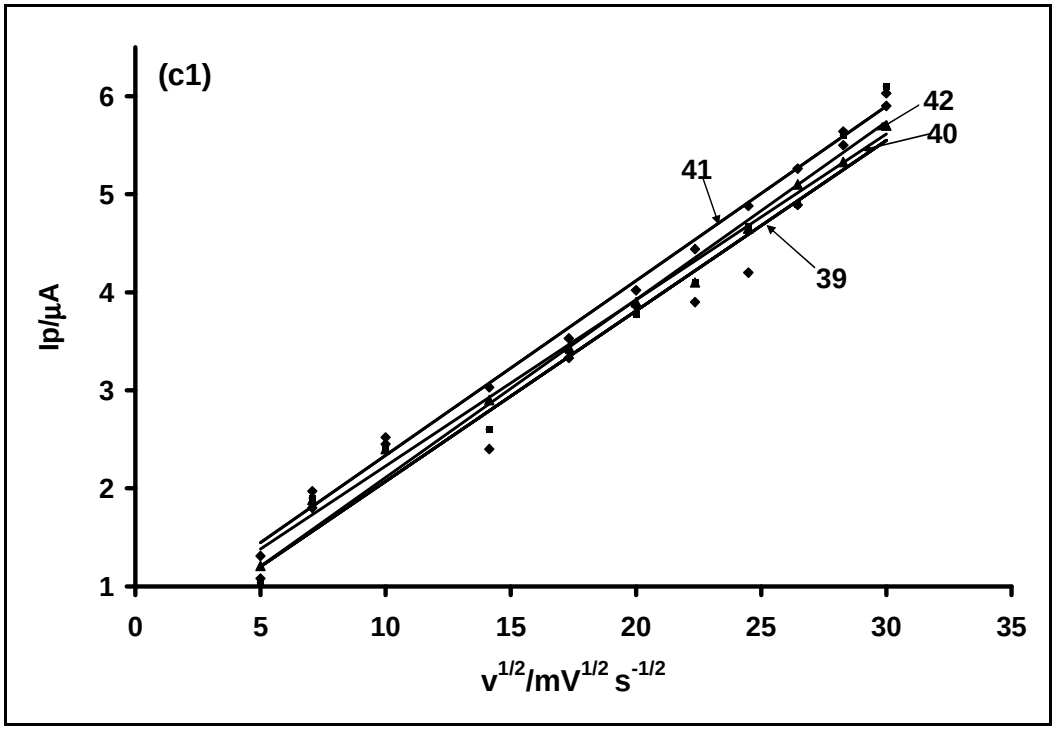
(c1)
6
5
4
3
2
1
Ip/µA
42
40
41
39
0
5
10
15
20
25
30
35
$v^{1/2}$/$mV^{1/2}$ $s^{-1/2}$

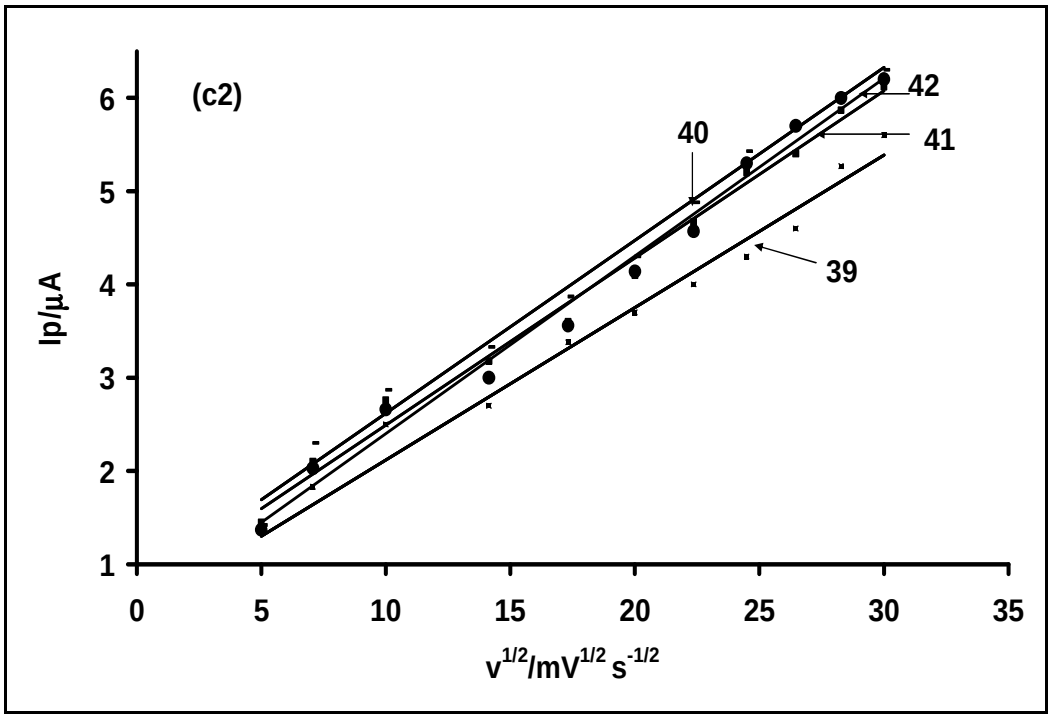
(c2)
42
40
41
39
Ip/µA
6
5
4
3
2
1
0
5
10
15
20
25
30
35
v^1/2/mV^1/2 s^-1/2

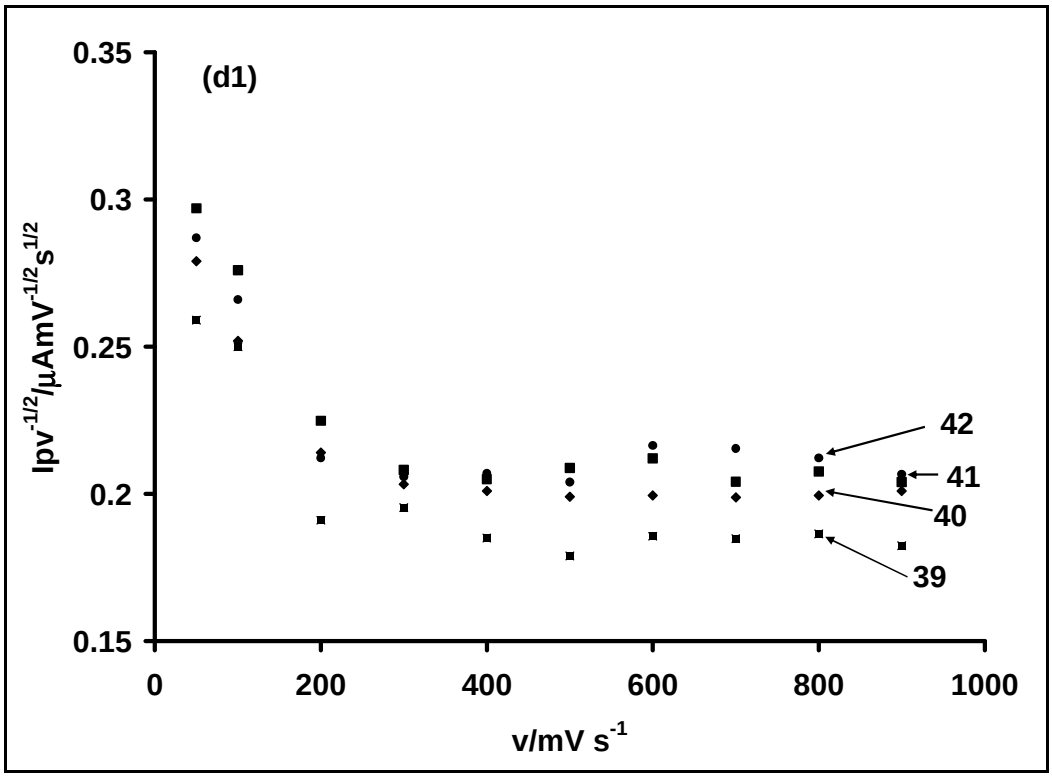
(d1)
0.35
0.3
0.25
0.2
0.15
Ipv^-1/2/µAmV^-1/2s^1/2
42
41
40
39
0
200
400
600
800
1000
v/mV s^-1

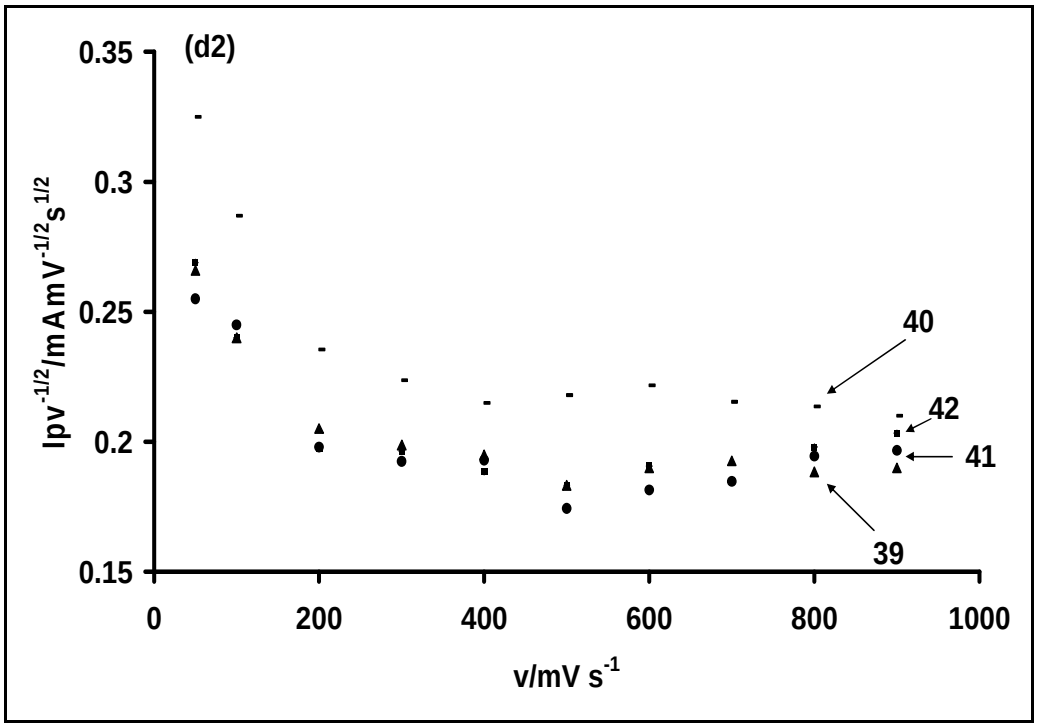

Figure 6.24: (a) Typical cyclic voltamogramms of electrooxidation of 1 mM sulphite at different scan rates catalysed by complex **41**-SAM electrode. Plots of (b) E_p vs. log *v*, (c) I_p vs. $v^{1/2}$ (d) I_p $v^{-1/2}$ vs. *v* for electrooxidation of 1 mM sulphite with complexes (i) **34**, (ii) **35**, (iii) **36**, (iv) **37**, (v) **39**, (vi) **40**, (vii) **41** and (viii) **42** in phosphate buffer pH 7.4

From Figure 6.20, the foot of the oxidation wave for sulphite electrooxidation occurred at around 0.3 V, at this potential metal based oxidation occurs (Table 6.3) for the CoPcs, FePcs and MnPcs, Scheme 6.6, equation 6.21 and 6.23. The next step would be the chemical reaction between the highly oxidising M^{3+}Pc species for the CoPcs and FePcs (M^{4+}Pc species for MnPcs) with sulphite ions which are highly reducing with the participation of water molecules from phosphate buffer pH 7.4 (Scheme 6.6, equations 6.22 and 6.24). The mechanism is very feasible and most likely to occur since the metal based oxidation peaks of the complexes are within the foot of the oxidation wave for sulphite oxidation. Similar mechanisms have been proposed before.[370,417,418] In the case of

NiPcs, as shown in Figure 5.19d, Chapter 5, metal based oxidation was not observed unless they are transformed into 'Ni oxo bridge form' which is not the case for SAMs. In addition, the NiPcs-SAMs have the more positive E_p values for sulphite catalytic peak relative to other MPcs. The mechanism for the NiPcs-SAMs catalysed sulphite electrooxidation is most likely to be a ring based one and is proposed in Scheme 6.6, equations 6.25 and 6.26. As stated above the involvement of more than 2 electrons could be due to electrooxidation of other forms of sulphite.

Spectroscopic interaction of sulphite and the complexes were not carried out because of lack of common solvent for both sulphite ions and the complexes.

$$2M^{2+}Pc \longrightarrow 2[M^{3+}Pc]^{+} + 2e^{-} \quad (6.21)$$

$$2[M^{3+}Pc]^{+} + SO_3^{2-} + H_2O \longrightarrow 2M^{2+}Pc + SO_4^{2-} + 2H^{+} \quad (6.22)$$

where M is Co, Fe

$$2Mn^{3+}Pc \longrightarrow 2[Mn^{4+}Pc]^{+} + 2e^{-} \quad (6.23)$$

$$2[Mn^{4+}Pc]^{+} + SO_3^{2-} + H_2O \longrightarrow 2Mn^{3+}Pc + SO_4^{2-} + 2H^{+} \quad (6.24)$$

$$2Ni^{2+}Pc^{2-} \longrightarrow 2Ni^{2+}Pc^{-} + 2e^{-} \quad (6.25)$$

$$2Ni^{2+}Pc^{-} + SO_3^{2-} + H_2O \longrightarrow 2Ni^{2+}Pc^{2-} + SO_4^{2-} + 2H^{+} \quad (6.26)$$

Scheme 6.6: Proposed reaction mechanism for Co, Fe, Mn, NiPcs-modified gold electrode electrooxidation of sulphite

6.4 Conclusion

In conclusion, it has been shown in this work that Au electrodes modified with NiTBMPc and NiTDMPc complexes exhibited electrocatalytic activity towards the oxidation of 4-CP and TCP, and their catalytic activities improved in terms of increase in peak current and shift to less positive peak potentials when they were transformed to the *poly*-Ni(OH)TBMPc and *poly*-Ni(OH)TDMPc respectively indicating the participation of Ni^{3+}/Ni^{2+} redox process in the catalytic process and increase in film thickness increased the anti-fouling ability of the films and this could be attributed to complex nature of the films due to the bulky nature of the substituents.

It has been shown in this work that Au electrodes modified by electropolymerisation with Co^{2+}, Fe^{2+} and Mn^{3+} tetrakis (benzylmercapto) and tetrakis (dodecylmercapto) phthalocyanines exhibited electrocatalytic activity towards the oxidation of nitrite. A linear relationship between the peak current, I_p and nitrite concentration was observed for all the modified complexes, with sensitivities ranging from 6.9 to 9.9 μA mM^{-1}. In comparison with literature, FeTBMPc gave the best catalysis of E_p (0.66 V vs. Ag|AgCl) for nitrite oxidation. It was shown that the interaction between the complexes and nitrite depended on the central metal ions of the MPcs. Cyclic voltammetry and spectroscopic evidences provided insights into the mechanistic aspect of nitrite electrooxidation. For CoPc, FePc, NiPc derivatives, the total number of electron transfer was found to be 2 while for the MnPc derivatives, it was found to be 1. From the Tafel slope values, CoPc, NiPc and FePc derivatives suggest the first one electron transfer is the rate limiting step. For the MnPc derivatives, the one electron step is followed by a slow rate determining-chemical step. Lastly, for the NiPc derivatives, Tafel slopes higher than 120 mV dec^{-1}

were obtained which indicate strong interaction between nitrite ions and the NiPc complexes or chemical reactions coupled with electrochemical steps. High stabilities were exhibited by these modified electrodes even after repeated use. Also, Au electrodes modified with *poly*-NiTBMPc and *poly*-NiTDMPc complexes modified exhibited improved electrocatalytic when they were transformed to the *poly*-Ni(OH)TBMPc and *poly*-Ni(OH)TDMPc, respectively, indicating the importance of Ni^{3+}/Ni^{2+} redox process.

It has been shown in this work that Au electrodes modified by SAM technique with Co^{2+}, Fe^{2+}, Ni^{2+} and Mn^{3+} tetrakis benzylmercapto and dodecylmercapto phthalocyanine complexes exhibited electrocatalytic activity towards the oxidation of sulphite. The order of catalytic activity (E_p) was found to be FePcs > MnPcs ~ CoPcs > NiPcs with the involvement of metal based redox processes of the CoPcs, FePcs and MnPcs but ring based ones for NiPcs. A linear relationship with a high sensitivity between the peak current, I_p and sulphite concentration was observed for all the modified complexes. Mechanistic studies of the sulphite electrooxidation using cyclic voltammetry gave for all the complexes high number of electrons in the range 3.8-4.6 indicating the possible electrooxidation of other sulphite form (e.g. HSO_3^-). Tafel slopes obtained for both CoPc and NiPc were close to 120 mV dec^{-1} indicating that the first one electron transfer is the rate limiting step. While for FePc and MnPc derivatives, they were higher than 200 mV dec^{-1} which indicate strong interaction between nitrite ions and the NiPc complexes or chemical reactions coupled with electrochemical steps.

CHAPTER 7

GENERAL CONCLUSIONS and FUTURE PERSPECTIVE

7.1 General Conclusions

In conclusion, the synthesis, spectroscopic, and electrochemical characterisation of thiol substituted CoPc, FePc, MnPc, NiPc and ZnPc derivatives are presented. High yields with satisfactorily spectroscopic and electrochemical characterisation were obtained. As expected first oxidation and reduction processes in CoPc, FePc and MnPc complexes occurred at the central metal and the ZnPc derivatives exhibited ring based processes only. For the MnPc derivatives, three quasi reversible peaks were observed, one metal based and two ring based redox couples. The complex MnTDMPc which has a more red shifted Q band in DCM was easier to reduce than the complex MnTBMPc and the other way around for oxidation, confirming the influence of electron donating ability of the ring substituents on the positions of the redox couples. Spectroelectrochemistry confirmed the first oxidation and reduction redox couples for CoPc, FePc and MnPc to be metal based redox processes. Spectroelectrochemistry also confirmed that the redox couple (**II**) for both MnPc derivatives as a metal based reduction of Mn^{3+}Pc to Mn^{2+}Pc thus confirming the original state of the complexes as Mn^{3+}(Ac)Pc. For the first time, spectroelectrochemistry gave spectral evidence for the formation of Ni^{2+}/Ni^{+} process in a NiPc complex. The voltammetric characteristic Mn^{4+}Pc species and the spectra of Ni^{+}, Fe^{+} and Co^{+} phthalocyanine complexes are not well known, thus this work further gives some insight into the spectra of the latter three species which would be helpful to other researchers.

It was shown in this work that the oxidation of 2-CP and TCP using $CoPcS_4$ catalyst and H_2O_2 oxidant, in different solvent conditions gives different products. Spectroscopic evidence for the involvement of both the metal and phthalocyanine ring oxidised species

in the mechanism was obtained. Also, it was shown that various immobilised photosensitizers catalysed visible light photolysis of chlorophenols. Almost similar trends were obtained for both singlet oxygen generation and photoactivity of the MPc complexes indicating that singlet oxygen played a major role in the photolysis reactions. HPLC traces reveal that the main products of the photolysis are the benzoquinone derivatives. Significant improvement in ZnOCPc which degrades rapidly in aqueous solutions was obtained when immobilised on Amberlite®. The results reported in this work provide a basis for development of MPc complexes for the transformation of chlorophenols in water.

Thiol derivatised complexes, (MTBMPc and MTDMPc, M = Co^{2+}, Fe^{2+}, Mn^{3+} and Ni^{2+}) were successfully deposited on gold electrodes by electropolymerisation. The cyclic voltammogram evolution during electropolymerisation showed that the complexes were electropolymerised on Au electrodes. In addition, electropolymerisation of the complexes on Au electrodes were confirmed by similarity of the CVs of last scans of the electropolymerisation with the corresponding CVs in phosphate buffer pH 7.4 solution. The films of the NiPc derivatives were electro-transformed in aqueous 0.1 M NaOH solution to the 'O-Ni-O oxo' bridged form. For both complexes, films with different thickness were prepared and characterised by EIS and the results showed typical behaviour for modified electrodes with increasing charge transfer resistance values, R_p with polymer thickness. Also, electrodes with *poly*-Ni(OH)Pcs films exhibited higher charge transfer resistance values, R_p than their corresponding *poly*-NiPcs films counterparts. Spectroelectrochemical characterisation on indium tin oxide (ITO) data distinguished between *poly*-NiPc and *poly*-Ni(OH)Pc films. The complexes (MTBMPc

and MTDMPc, M = Co^{2+}, Fe^{2+}, Mn^{3+} Ni^{2+} and Zn^{2+}) were successfully used to modify gold electrodes by self assembled monolayer (SAM) technique. The self assembled films showed blocking characteristics towards well known Faradaic processes indicating formation of stable, well packed and defect free SAMs. Using the $[Fe(CN)_6]^{-3}/[Fe(CN)_6]^{-4}$ redox system as a guide, it was shown that a possible change in molecules orientation from flat to vertical or multilayer form with increase in SAM formation time to 24 hours and above occurred. First examples of SAM formation time optimisation were carried out using CV technique. The nature of the ring substituents of the MPcs was found to influence the blocking characteristics of the CoPc-SAMs towards $[Fe(CN)_6]^{-3}/[Fe(CN)_6]^{-4}$ redox process.

It was shown in this work that the nature of *poly*-NiPc-Au electrodes modified (electropolymerisation) with NiTBMPc and NiTDMPc complexes influenced the electrocatalytic activity towards the oxidation of 4-CP and TCP and this indicates the importance of Ni^{3+}/Ni^{2+} redox process in the catalytic process. Increase in film thickness increased the anti-fouling ability of the films. This is a significant contribution towards finding suitable electrocatalysts and sensors with effective antifouling ability for chlorophenols analysis. Au electrodes modified by electropolymerisation with Co^{2+}, Fe^{2+} and Mn^{3+} tetrakis (benzylmercapto) and tetrakis (dodecylmercapto) phthalocyanines exhibited electrocatalytic activity towards the oxidation of nitrite. A linear relationship between the peak current, I_p and nitrite concentration was observed for all the modified complexes. In comparison with literature, better catalyses were observed in this work in terms of less positive values of the peak potential for nitrite electrooxidation. It was shown that the interaction between the complexes and nitrite depended on the central

metal ions of the MPcs. Cyclic voltammetry and spectroscopic studies provided insights into the mechanistic aspect of nitrite electrooxidation. The studies showed that the reaction mechanism strongly depends on the central metal ions of the thiol-derivatised MPc complexes. High stabilities were exhibited by these modified electrodes even after repeated use. These modified electrodes are therefore potential electrodes for the development of suitable electrocatalysts for nitrite oxidation as well as in the fabrication of nitrite electrochemical sensors. Also like in the case of chlorophenol electrooxidation, the NiPc derivatives exhibited better electrocatalytic activities after they were transformed to the *poly*-Ni(OH)TBMPc and *poly*-Ni(OH)TDMPc. In addition, high stability exhibited by these modified electrodes even after repeated use make the modified electrodes as potential electrodes for the development of suitable electrocatalysts for nitrite oxidation as well as in the fabrication of nitrite electrochemical sensors. It was shown that Au electrodes modified by SAM technique with Co^{2+}, Fe^{2+}, Ni^{2+} and Mn^{3+} tetrakis benzylmercapto and dodecylmercapto phthalocyanine complexes exhibited electrocatalytic activity towards the oxidation of sulphite. Metal based redox catalysis (CoPcs, FePcs and MnPcs) were more efficient than the ring based ones (NiPcs). A linear relationship between the peak current, I_p and sulphite concentration and high stability exhibited by these modified electrodes even after repeated use make the modified electrodes as potential electrodes for the development of suitable electrocatalysts for sulphite oxidation as well as in the fabrication of sulphite electrochemical catalysts and sensors. Mechanistic studies of the sulphite electrooxidation using cyclic voltammetry gave for all the complexes high number of electrons in the range 3.8-4.6 indicating the possible electrooxidation of other forms of

sulphite e.g. HSO_3^-; more investigation into this will be an interesting future work. Tafel slopes revealed that CoPcs and NiPcs catalysis involve first one electron transfer as the rate limiting step and for FePcs and MnPcs, they were strong interaction between sulphite and the complexes judging by the high values of the Tafel slopes.

7.2 Future Perspective

Future work on these newly synthesised thiol-derivatised MPc complexes may include exploring their versatility (their abilities to form SAMs and polymer films on gold electrodes) in applications as electrocatalysts and sensors for biologically and environmentally important molecules. Further characterisation of the complexes films on Au electrodes using surface techniques such as X-ray photoelectron spectroscopy (XPS) and atomic force microscopy (AFM) will be an interesting future work. Finally, the MTBMPc derivatives (benzyl mercapto group) of the thiol-derivatised MPc complexes are potential precursors for synthesis of MPcs with S-H groups as ring substituents.

References:

1. N.B. Mckeown in *Phthalocyanine Materials: Synthesis, Structure and Function.* Chemistry of Solid State Materials, Cambridge University Press, New York, 1998.
2. *Phthalocyanines: Properties and Applications,* C.C. Leznoff and A.B.P. Lever, Eds., VCH Publishers, New York, Vols. **1-4**, 1989, 1993, 1993, 1996.
3. R.P. Linstead, *J. Chem. Soc.,* 1934, 1016.
4. J.M. Robertson and I. Woodward, *J. Chem. Soc.,* 1936, 219.
5. F. Mosser and A.L. Thomas, *The Phthalocyanines*, Eds., CRS Press: Boca Raton, F.L. 1983.
6. M. Gouterman, In D. Dolphin, Ed., *The Porphyrins, Physical Chemistry, Part A*, Vol. **3**, Academic Press: New York, 1978; pp. 1-165.
7. F.R. Fan and L.R. Faulkner, *J. Am. Chem. Soc*., 1979, **101**, 4779.
8. T. Nyokong, Z. Gasyna and M.J. Stillman, *Inorg. Chem.,* 1987, **26**, 548.
9. J. Simon and P. Bassoul, *Phthalocyanine: Properties and Applications,* Leznoff, C.C., Lever, A.B.P., Eds. V.H.S. Publishers: New York, 1989.
10. R.K. Sen, J. Zagal and E. Yerger, *Inorg. Chem*., 1977, **16**, 3379.
11. J. Limson and T. Nyokong, *Electroanalysis*, 1997, **9**, 255.
12. K. Hanabusa and H. Sharai in *Phthalocyanines: Properties and Applications*, eds. A.P.B. Lever and C.C. Leznoff, VHC Publishers, New York, 1993, Vol.**2**.
13. H. Kasuga in *Phthalocyanine: Properties and Applications,* Eds. A.P.B. Lever and C.C. Leznoff, VCH Publishers, New York, 1996, Vol.**4**.
14. B. Meunier and A. Sorokin, *Acc. Chem. Res*., 1997, **30**, 470.

15. M. Thamae and T. Nyokong, *J. Electroanal. Chem*., 1999, **470**, 126.

16. K. Morishige, S. Tomoyasu and G. Iwano, *Langmuir*, 1997, **13**, 5184.

17. A.W. Snow and W.R. Barger in *Phthalocyanines: Properties and Applications* eds. A.P.B. Lever and C.C. Leznoff, VCH Publishers, New York, 1989, Vol.**1**.

18. E. Ben-Hur and I. Rosenthal, *Int. J. Radiat. Biol*., 1985, **47**, 145.

19. E. Ben-Hur and I. Rosenthal, *J. Photochem. Photobiol*., 1985, **42**, 129.

20. I. Rosenthal and E. Ben-Hur, *in Phthalocyanine: Properties and Applications*, eds. A.P.B. Lever and C.C. Leznoff, VCH Publishers, New York, 1989, Vol.**1**.

21. D. Phillips, *Pure Appl. Chem*., 1995, **67**, 117.

22. I.J. MacDonald and T. Dougherty, *J. Porphyrins Phthalocyanines*, 2001, **5**, 105.

23. P. Gregory, *J. Porphyrins Phthalocyanines*, 1999, **3**, 468.

24. P. Gregory in *High Technology Applications of Organic Colorants*, Plenum Press, New York, 1991.

25. N.B. McKeown, *Chem. Ind*., 1999, 92.

26. G.C.S. Collins and D.J. Schiffrin, *J. Electroanal. Chem*., 1982, **139**, 335.

27. M.M. Nicholson in *Phthalocyanine: Properties and Applications*, eds. A.P.B. Lever, C.C. Leznoff, VCH Publishers, New York, 1993. Vol. **3**.

28. N. Toshina and T. Tominaga, *Bull. Chem. Soc. Jpn.*, 1996, **69**, 2111.

29. J.E. Kuder, *J. Imaging Sci*., 1988, **32**, 51.

30. R. Ao, L. Kummert and D. Haarer, *Adv. Mater*., 1995, **5**, 495.

31. S. Nalwa and J.A. Shirk in *Phthalocyanine: Properties and Applications*, eds. A.P.B. Lever and C.C. Leznoff, VCH Publishers, New York, 1993, Vol. **4**.

32. D.K.P. Ng, Y.-O. Yeung, W.K. Chan and S.-C. Yu, *Tet. Lett.*, 1997, **38**, 6701.

33. D. Worhle and D. Meissener, *Adv. Mater*., 1991, **3**, 129.

34. D. Worhle, L. Kreienhoop and D. Schlettwein in *Phthalocyanine: Properties and Applications*, eds. A.P.B. Lever and C.C. Leznoff, VCH Publishers, New York, 1996, Vol.**4**.

35. A.B.P. Lever, M.R. Hempstead, C.C. Leznoff, W. Lui, M. Melnik, W.A. Nevin and P. Seymour, *Pure Appl. Chem*., 1986, **58**, 1467.

36. B. Simic-Glavaski in *Phthalocyanine: Properties and Applications*, eds. A.P.B. Lever and C.C. Leznoff, VCH Publishers, New York, 1993, Vol.**3**.

37. J. Simon and J.J. Andre, *Mol. Semicond.*, Springer, Berlin, 1985.

38. J. Simon and T. Toupance in *Comprehensive Supramolecular Chemistry*. Vol. **10**, Supramolecular Technology, Ed. D.N. Reinhoudt, Pergamon, London, 1996.

39. M. Iwamoto, *J. Mater. Chem*., 2000, **10**, 99.

40. S. Vilakazi and T. Nyokong, *Polyhedron*, 2000, **19**, 229.

41. A. Sorokin and B. Meunier, *J. Chem. Soc. Chem. Commun*., 1994, 1799.

42. A. Sorokin, S. De Suzzoni-Dezard, D. Poullain, J.P. Noel and B. Meunier, *J. Am. Chem. Soc.*, 1996, **118,** 7410.

43. A. Hadasch, A. Sorokin, A. Rabion, L. Fraisse and B. Meunier, *Bull Soc. Chim. Fr.*, 1997, **134,** 1025.

44. A. Hadasch, A. Sorokin, A. Rabion and B. Meunier, *New J. Chem.*, 1998, 45.

45. K. Kasuga, K. Mori, T. Sugimore and M. Handa, *Bull. Chem. Soc. Jpn.*, 2000, **73**, 939.

46. M. Sanchez, A. Hadasch, R.T. Fell and B. Meunier, *J. Cat*., 2001, **202**, 177.

47. A.M. Volodin, *Catal. Today*, 2000, **58**,103.

48. N. Nensala, T. Nyokong, *Polyhedron*, 1997, **16,** 2971.

49. R. Gerdes, D. Wohrle, W. Spiller, G. Schneider, G. Schnurpfeil and G.J. Schulz-Ekloff, *J. Photochem. Photobiol. A: Chem.*, 1997, **111,** 65.

50. Y.I. Skurlatov, L.S. Ernestova, E.V. Vichutinskaya, D.P. Samsonov, I.V. Semenov, I.Y. Rod'ko, V.O. Shvidky, R.I. Pervunina and T.J. Kemp, *J. Photochem. Photobiol.*, 1997, **107**, 207.

51. T. Ichinohe, H. Miyasaka, A. Isoda, M. Kimura, K. Hanabusa and H. Shirai, *React. Funct. Polym.*, 2000, **43**, 63.

52. K. Ozoemena, N. Kuznetsova and T. Nyokong, *J. Photochem. Photobiol. A: Chem.*, 2001, **139**, 217.

53. K. Ozoemena, N. Kuznetsova and T. Nyokong, *J. Mol. Catalysis A: Chem.*, 2001, **176,** 29.

54. J.D. Spikes, *J. Photochem. Photobiol.* 1986, **43**, 691.

55. O. Oda, S.-I. Ogura and I. Okura, *J. Photochem. Photobiol. B: Biology*, 2000, **59**, 20.

56. M.P. De Filippis, D. Dei, L. Fantetti and G. Roncucci, *Tet. Lett*., 2000, **41**, 9143.

57. J.W. Owens and M. Robins, *J. Porphyrins Phthalocyanines*, 2001, **5**, 460.

58. K.I. Ozoemena, P.Westbroek and T. Nyokong, *Electrochem. Commun.*, 2001, **3**, 529.

59. F. Bedioui, Y. Bouhier, C. Sorel, J. Devynck, L. Coche-Guerente, A. Deronzier and J.C. Montet, *Electrochim. Acta,* 1993, **38,** 2485.

60. J. Obirai and T. Nyokong, *Electrochim. Acta*, 2004, **49,** 1417.

61. J.H. Zagal, *Coord. Chem. Rev.*, 1992, **119**, 89.

62. F.J. Fenoy, P. Ferrer, L. Carbonell and M. García-Salom, *Hypertension.*, 1995, **25**, 408.

63. C.A. Caro, F. Bedioui and J.H. Zagal, *Electrochim.* Acta, 2002, **47**, 1489.

64. S. Griveau, M. Gulppi, F. Bedioui and J.H. Zagal, *Solid State Ionics*, 2004, **169**, 59.

65. L.J. Huffman, D.J. Prugh, L. Millecchia, K.C. Schuller, S. Cantrell and D.W. Porter, *J. Biosci.*, 2003, **28**, 29.

66. L.J. Ignarro, R.E. Byrns, G.M. Buga, K.S. Wood and G. Chaudhuri, *J. Pharmacol. Exp. Ther*., 1988, **244**, 181.

67. K.I. Ozoemena, P. Westbroek and T. Nyokong, *Electroanalysis*, 2003, **15,** 1762.

68. D. Wohrle, G. Schnurpfeil and G. Knothe, *Dyes and Pigments*, 1992, **18**, 91.

69. A. Lützen, S.D. Starnes, D.M. Rudkevich and J. Rebeck Jr, *Tet. Lett.*, 2000, **41**, 3777.

70. F. Yilmaz, D. Atilla and V. Ahsen, *Polyhedron*, 2004, **23**, 1931.

71. M. Brewis, M. Helliwell, N.B. McKeown, S. Reynolds and A. Shawcross, *Tet. Lett.*, 2001, **42**, 813.

72. P. Yiru, H. Fenghua, L. Zhipeng, C. Naisheng and H. Jinling, *Inorg. Chem. Commun.* 2004, **7**, 967.

73. M. Brewis, G.J. Clarkson, P. Humberstone, S. Makhseed and N.B. Mckeown, *Chem. Eur. J.*, 1998, **4**, 1633.

74. N.B. Mckeown, I. Chambrier and M.J. Cook, *J. Chem. Soc. Perkin Trans.*, 1990, **1**, 1169.

75. H. Vollman: *In Chemistry of Synthetic Dyes*. Venkataraman, K. Ed.; Academic Press: New York, 1971; pp. 283-311.

76. J.H. Weber and D.H. Busch, *Inorg. Chem*., 1965, **4**, 469.

77. S.V. Kudrevich, M.G. Galpern and J.E. van Lier, *Synthesis*, 1993, 779.

78. K. Sakamoto and E. Ohno, *Prog. Org. Coating*, 1997, **31**, 139.

79. M. Ambroz, A. Beeby, A.J. MacRobert, M.S.C. Simpson, R.K. Svensen and D. Phillips, *J. Photochem. Photobiol. B:* 1991, **9**, 87.

80. A.W. Snow, J.R. Griffith and N.P. Marullo, *Macromolecules*, 1984, **17,** 1614.

81. A.G. Gurek and O. Bekaroglu, *J. Chem. Soc. Dalton Trans.*, 1994, 1419.

82. K.I. Ozoemena and T. Nyokong, *Electrochim. Acta*, 2002, **47**, 4035.

83. K. Takahashi, M. Kawashima, Y. Tomita and M. Itoh, *Inorg. Chim. Acta.*, 1995, **232**, 69.

84. A.G. Gurek, V. Ahsen, F. Heinemann and P. Zugenmaier, *Mol. Cryst. Lig. Cryst*. 2000, **338,** 75.

85. S. Dabak, F. Heinemann, V. Ahsen and P. Zugenmaier, *New J. Chem.*, 2004, **28,** 693.

86. I. Chambrier, M.J. Cook and D.A. Russell, *Synthesis*, 1995, 1283.

87. M.J. Cook, R. Hersans, J. McMurdo and D.A. Russell, *J. Mater. Chem*., 1996, **6**, 149.

88. T.R.E. Simpson, D.J. Revell, M.J. Cook and D.A. Russell, *Langmuir*, 1997, **13**, 460.

89. D.J. Revell, I. Chambrier, M.J. Cook and D.A. Russell, *J. Mater. Chem.*, 2000, **10**, 31.

90. M.J. Cook, *Pure Appl. Chem.* 1999, **71**, 2145.

91. Z. Li and M. Lieberman, *Supramol. Science*, 1998, **5**, 485.

92. Z. Li and M. Lieberman in *Fundamental and Applied Aspects of Chemically Modified Surfaces*, eds. J.P. Blitz and C.B. Little, Royal Soc. Chem., Lettchworth, U.K. 1999; p.24-35.

93. Z. Li, M. Lieberman and W. Hill, *Langmuir*, 2001, **17**, 4887.

94. A.R. Ozkaya, A.G. Gurek, A. Gul and O. Bekaroglu, *Polyhedron*, 1997, **16,** 1877.

95. F. Matemadombo, M.D. Maree, K.I. Ozoemena, P. Westbroek and T. Nyokong, *J. Porphyrin Phthalocyanines*, 2005, **9,** 484.

96. I. Gurol, V. Ahsen and O. Bekaroglu, *J. Chem. Soc. Dalton Trans*., 1994, 497.

97. Z.A. Bayir, E. Hamuryudan, A.G. Gurek and O. Bekaroglu, *J. Porphyrins Phthalocyanines*, 1997, **1,** 349.

98. D.J. Revell, I. Chambrier, M.J. Cook and D.A. Russell, *J. Mater. Chem.*, 2000, **10**, 31.

99. M. Nicolau, B. del Rey, T. Torres, C. Mingotaud, P. Delhaes, M.J. Cook and S.C. Thorpe, *Synthetic Metals* 1999, **102,** 1462.

100. P. Tau and T. Nyokong, *Dalton Trans.*, 2006, 4482.

101. M.J. Stillman and T. Nyokong in *Phthalocyanines: Properties and Applications*, eds. C.C. Leznoff and A.B.P. Lever, VCH Publishers, New York, 1989, Vol.**1**.

102. A.B.P. Lever, *Adv. Inorg. Radiochem*., 1965, **7**, 28.

103. T.H. Huang, K.E. Reickhoff and E.M. Voight, *J. Chem. Phys.*, 1982, **77**, 3424.

104. W.A. Nevin, W. Liu, S. Greenberg, M.R. Hempstead, S.M. Maruccio, M.M. Melnik, C.C. Leznoff and A.B.P. Lever, *Inorg. Chem*., 1987, **26**, 291.

105. Z. Li and M. Lieberman, *Inorg. Chem*., 2001, **40**, 932.

106. K. Kasuga and M. Tsutsui, *Coord. Chem. Rev*., 1980, **32**, 67.

107. N. Nensala and T. Nyokong, *Polyhedron*, 1996, **15**, 867.

108. N. Nensala and T. Nyokong, *Polyhedron*, 1998, **17**, 3467.

109. O.T.E. Sielcken, M.M. van Tilborg, M.F.M. Rocks, R. Hendricks, W. Drenth and R.J.M. Nolte, *J. Am. Chem. Soc*., 1987, **109**, 4261.

110. S. Griveau, J. Pavez, J.H. Zagal and F. Bedioui, *J. Electroanal. Chem.*, 2001, **497**, 75.

111. J. Prekumar and R. Ramaraj, *J. Photochem. Photobiol. A: Chem.*, 1998, **110,** 53.

112. S.L. Buell and J.N. Demas, *J. Phys. Chem.*, 1983, **87,** 4675.

113. R. Gerdes, O. Bartels, G. Schneider, D.W¨ohrle and G. Schulz-Ekloff, *Polym. Adv. Technol.*, 2001, **12,** 152.

114. W.J. Kroenke and M.E. Kenney, *Inorg. Chem.*, 1964, **3**, 696.

115. A.N. Sidorov and I.P. Kotlyar, *Opt. I. Spektr.*, 1961, **11**, 175.

116. R.M. Negri, A. Zalts, E.S. Roman, P. Aramendia and S.E. Braslavsky, *Photochem. Photobiol.*, 1991, **53**, 317.

117. M.G. Lagorio, L.E. Dicelio and E.S. Roman, *J. Photochem. Photobiol. A: Chem*., 1993, **71**, 153.

118. J.R. Harbour, J. Tromp and M.L. Hair, *J. Am. Chem. Soc*., 1980, **102**, 1874.

119. J.R. Darwent, P. Douglas, A. Harriman, G. Porter and M.-C. Richoux, *Coord. Chem. Rev*., 1982, **44**, 83.

120. E.A. Lissi, M.V. Encinas, E. Lemp and M.A. Rubio, *Chem. Rev*., 1993, **93**, 699.

121. D.B. Hibbert, *Introduction to Electrochemistry,* Macmillan, London, 1993.

122. A.E. Kaifer and M. Gomez-Kaifer, *Supramol. Electrochem.*, Willey, VCH, New York, 1999.

123. A.J. Bard and L.R. Faulkner, *Electrochemical Methods: Fundamentals and Applications,* John Willey & Sons, 1996.

124. D.G. Davis, *in D. Dolphin, Ed., Physical Chemistry: The porphyrins, Part A*, Vol. **III**. Academic Press, NY, 1978, Ch. 4.

125. E.R. Brown and R.F. Large, *in Physical Methods of Chemistry, Vol.1-Part IIA: Electrochemical Methods*, eds. A. Weissberger and B. Rossiter, Willey-Interscience, New York, 1971.

126. J.E.B. Randles, *Trans. Faraday Soc*., 1948, **44**, 327.

127. P.A. Christenson and A. Hamnet, *Techniques and Mechanisms in Electrochemistry*, 1st ed, Blackie Academic and Professional, London, 1994.

128. R.S. Nicholson and I. Shain, *Anal. Chem.,* 1964, **36**, 1351.

129. A. Sevcik, *Coll. Czech. Chem. Comm*., 1958, **13**, 349.

130. W.R. Heineman and P.T. Kissinger in *Laboratory Techniques in Electroanalytical Chemistry, 2nd ed., eds.* P.T. Kissinger and W.R. Heineman, Marcel Dekker Inc., New York, 1996.

131. J. Wang, *Analytical Electrochemistry*, VCH Publishers Inc., New York, 1994.

132. J. Wang, D.B.Luo, P.A.M. Farias and J.S. Mahmoud, *Anal. Chem.*, 1985, **57**, 158.

133. J.G. Osteryoung, *Acc. Chem. Res*., 1993, **26**, 77.

134. J.G. Osteryoung and R.A. Osteryoung, *Anal. Chem*., 1985, **57**, 101A.

135. R. Cieslinski and N.R. Amstrong, *Anal. Chem.*, 1979, **51**, 565.

136. M. Krejčik, M. Deněk and F. Hartl, *J. Electroanal. Chem*., 1991, **317**, 179.

137. S. Besnes, A. Ltaief, K. Reybier, L. Ponsonner, N. Jaffrezic, J, Davenas and H.B. Ouada, *Synthetic Metals*, 2003, **138**, 197.

138. R.W. Murray, W.R. Heinemann and G.W. O'Dom, *Anal. Chem*., 1967, **39**, 1666.

139. M. Petek, T.E. Neal and R.W Murray, *Anal. Chem*., 1971, **43**, 1069.

140. W.J. Blaedel and S.L. Boyer, *Anal. Chem.*, 1973, **45**, 258.

141. D. Lexa, J.M. Saveant and J. Zickler, *J. Am. Chem. Soc*, 1977, **99**, 2786.

142. H.B. Mark Jr. and B.S. Pons, *Anal. Chem*., 1966, **38**, 119.

143. D.R. Tallant and D.H. Evans, *Anal. Chem*., 1969, **41**, 835.

144. F. Beck, *J. Appl. Electrochem.*, 1977, **7**, 191.

145. J.F. Myers, R.G.W. Canham and A.B.P. Lever, *Inorg. Chem*., 1975, **14**, 461.

146. D.W. Clack and J.R. Yandle, *Inorg. Chem*., 1972, **11**, 1739.

147. D.W. Clack, N.S. Hush and I.S. Woosley, *Inorg. Chim. Acta*, 1976, **19**, 129.

148. L.D. Rollman and R.T. Iwamoto, *J. Am. Chem. Soc*., 1968, **90**, 1455.

149. D.W. Clack and N.S. Hush, *J. Am. Chem. Soc.*, 1965, **87**, 4238.

150. R.H. Felton and H. Linschitz, *J. Am. Chem. Soc*., 1966, **88**, 1113.

151. P. Tau, T. Nyokong, *Electrochim. Acta*, 2006 (in press).

152. A. Louati, M.E.I. Meray, J.J. Andre, J. Simon, K.M. Kadish, M. Gross and A. Giraurdeau, *Inorg. Chem.*, 1985, **24**, 1175.

153. R.O. Loufty and C. Chang, *J. Chem. Phys*., 1980, **73**, 2902.

154. C.C. Leznoff, S. Greenberg, S.M. Marcuccio, P.C. Minor, P. Seymour and A.B.P. Lever, *Inorg. Chim. Acta*, 1984, **89**, L35.

155. A.B.P. Lever, S.R. Pickens, P.C. Minor, L. Licoccia, B.S. Ramaswamy and K. Magnell, *J. Am. Chem. Soc*., 1981, **103**, 6800.

156. R.J. Blagrove, Austr., *J. Chem*., 1973, **26**, 472.

157. W. Liu, M.R. Hempstead, W.A. Nevin, M. Melnik, A.B.P. Lever and C.C. Leznoff, *J. Chem. Soc. Dalton Trans*., 1987, 2511.

158. R. Jalinsky, *J. Electrochem. Soc.*, 1965, **112**, 526.

159. R. Jalinsky, *Nature*, 1964, **201**, 1212.

160. A.B.P. Lever, *J. Porphyrins Phthalocyanines*, 1999, **3**, 488.

161. N. Grootboom and T. Nyokong, *Anal. Chim. Acta*, 2001, **432**, 49.

162. J.H. Zagal, M.A. Gulppi and G. Cárdenas-Jirón, *Polydehron*, 2000, **19**, 2255.

163. N. Kobayashi and W.A. Nevin, *Appl. Organomet. Chem.*, 1996, **10**, 579.

164. C.A. Caro, F. Bedioui, M.A. Páez, G.I. Cárdenas-Jirón, J.H. Zagal, *J. Electrochem. Soc.*, 2004, **151,** E32.

165. R.F. Lane and A.T. Hubbard, *J. Phys. Chem*., 1973, **77**, 1401.

166. R.A. Durst, A.J. Baumner, R.W. Murray, R.P. Buck and C.P. Andrieux, *IUPAC Recommendation*, *Pure and Appl. Chem*., 1997, **69**, 1317.

167. C.M. Elliot and R.W. Murray, *Anal. Chem*., 1976, **48**, 1247.

168. B.F. Watkins, J.R. Behling, E. Kariv and L.L. Miller, *J. Am. Chem. Soc*., 1975, **97**, 3549.

169. L. Netzer and J. Sagiv, *J. Am. Chem. Soc.*, 1983, **105**, 674.

170. J. Wang, T. Golden, K. Varughese and I. El-Rayes, *Anal. Chem.*, 1989, **61**, 509.

171. M.B. Gilbert and D.J. Curran, *Anal. Chem*., 1986, **58**, 1028.

172. T.J. Mafatle and T. Nyokong, *J. Electroanal. Chem*., 1996, **408**, 213.

173. J. Oni, P. Westbroek and T. Nyokong, *Electrochem. Commun.*, 2001, **3**, 524.

174. J.B. Kerr, L.L. Miller and M.R. Van De Mark, *J. Am. Chem. Soc.*, 1980, **102**, 3383.

175. M.F. Dautartas, J.F. Evans and T. Kuwana, *Anal. Chem.*, 1978, **51**, 104.

176. N. Oyama and F.C. Anson, *J. Am. Chem. Soc.*, 1979, **101**, 739.

177. A.H. Schroeder and F.B. Kaufman, *J. Electroanal. Chem.*, 1980, **133**, 209.

178. F.B. Kaufman, A.H. Schroeder, E.M. Engler, S.R. Kraimer and J.Q. Chambers, *J. Am. Chem. Soc.*, 1980, **102**, 483.

179. M.J. Cook and A. JafariFini, *J. Mater. Chem*., 1997, **7**, 5.

180. P. Daun and R.W. Murray, *J. Phys. Chem.*, 1981, **85**, 389.

181. M.J. Cook, *J. Mater. Chem*., 1996, **6**, 677.

182. M.J. Cook, D.A. Mayes and R.H. Poynter, *J. Mater. Chem*., 1995, **5,** 2233.

183. B.M. Hassan, H. Li and N.B. Mckeown, *J.Mater. Chem*., 2000, **10,** 39.

184. A. Volkov, G. Tourillon, P.C. Lacaze and J.-E. Dubois, *J. Electroanal. Chem*., 1980, **115**, 279.

185. A.F. Diaz and J.A. Logan, *J. Electroanal. Chem.*, 1980, **111**, 111.

186. A.F. Diaz, J.I. Castillo, J.A. Logan and W.-Y. Lee, *J. Electroanal. Chem.*, 1981, **129**, 115.

187. E.M. Genies, G. Bidan and A.F. Diaz, *J. Electroanal. Chem*., 1983, **149**, 101.

188. R.M. Penner and C.R. Martin, *J. Electrochem. Soc*., 1986, **133**, 300.

189. K.K. Kanazawa, A.F. Diaz, R.H. Geiss, W.D. Gill, J.F. Kwak, J.A. Logan, J.F. Rabolt and G.B. Street, *J. Chem. Soc.* 1979, 854.

190. H.D. Abruna, P. Denisevich, M. Umana, T.J. Meyer and R.W. Murray, *J. Am. Chem. Soc.*, 1981, **103**, 1.

191. P. Denisevich, H.D. Abruna, C.R. Leidner, T.J. Meyer and R.W. Murray, *Inorg. Chem.*, 1982, **21**, 2153.

192. K.W. Willman and R.W. Murray, *J. Electroanal. Chem.*, 1982, **133**, 211

193. B.F.Y. Yan Hin and C.R. Lower, *Sens. Actuators B*, 1992, **7**, 339.

194. G. Bidan, *Sens. Actuators B*, 1992, **6**, 45.

195. G. Harsãnyi, *Sensors in Biomedical Applications. Fundamentals, Technology and Applications*, Techonic Publishing Co. Inc. Lanchester, 2000, chapt. 2.

196. A.J. Downard, *Electroanalysis*, 2000, **12,** 1085.

197. T-F. Kang, G-L. Shen and R-Q, Yu, *Anal. Chim. Acta*, 1997, **356**, 245.

198. M.A. Ruiz, M.G. Blazquez and J.M. Pingarron, *Anal. Chim. Acta*, 1995, **305**, 49.

199. P.S. Vukusic and J.R. Sambles, *Thin Solid Films*, 1992, **221,** 311.

200. A. Ulman, *An Introduction to Ultrathin Organic Films: From Langmuir-Blodgett to Self-assembly*, Academic Press, San Diego, 1991.

201. H.O. Finklea in *Electroanalytical Chemistry*, A.J. Bard and I. Rubinstein, Eds., Marcel Dekker: New York, 1996; Vol. **19**, pp109-335.

202. H.O. Finklea in; R.A. Meyers, Eds., *Encyclopaedia of Analytical Chemistry: Applications, Theory and Instrumentations*, Vol. **11**, Wiley, Chichester, 2000, p. 10090.

203. M.D. Imisides, R. John, P.J. Riley and G.G. Wallace, *Electroanalysis*, 1991, **3**, 879.

204. H. Li and T.F. Guarr, *J. Chem. Soc. Chem. Commun.*, 1989, 832.

205. F. Xu, H. Li, Q. Peng and T.F. Guarr, *Synth. Met.*, 1993, **55-57**, 1668.

206. F. Xu, H. Li, S.J. Cross and T.F. Guarr, *J. Electroanal. Chem.*, 1994, **368,** 221.

207. C.R. Martin and C.A. Foss Jr., in *Laboratory Techniques in Electroanalytical Chemistry*, 2nd ed., P.T. Kissinger and W.R. Heineman, (Eds), Marcel Dekker Inc., New York, 1996.

208. E.W. Paul, A.J. Ricco and M.S. Wrighton, *J. Phys. Chem*. 1985, **89**, 1441.

209. Y.-B. Shim and S.-M. Park, *J. Electrochem. Soc*., 1997, **144**, 3027.

210. H.J. Lee, S.-Y. Cui and S.-M. Park, *J. Electrochem. Soc.*, 2001, **148**, D139.

211. T. Nyokong and F. Bedioui, *J. Porphyrins Phthalocyanines*, 2006, In press.

212. E. Trullund, P. Ardies, M.J. Aguirre, S.R. Biaggio and R.C. Rocha-Filho, *Polyhedron*, 2002, **72,** 285.

213. S. Griveau, M. Gulppi, J. Pavez, J.H. Zagal and F. Bedioui, *Electroanalysis*, 2003, **15**, 779.

214. J. Obirai and T. Nyokong, *J. Electroanal. Chem*., 2004, **573**, 77.

215. A. Goux, F. Bedioui, L. Robbiola and M. Pontie, *Electroanalysis*, 2003, **15,** 696.

216. N. Pereira-Rogrigues, J. Obirai, T. Nyokong and F. Bedioui, *Electroanalysis*, 2005, **17,** 186.

217. J. Obirai, F. Bedioui and T. Nyokong, *J. Electroanal. Chem*., 2005, **576**, 323.

218. J. Obirai, N. Pereira-Rogrigues, F. Bedioui and T. Nyokong, *J. Porphyrins Phthalocyanines*, 2003, **7**, 508.

219. C. de la Funte, M.D. Vazquez, M.L. Tascon, M.I. Gomez and S. Batanero, *Talanta*, 1997, **44**, 685.

220. P. Janda, J. Weber, L. Dunsch and A.B.P. Lever, *Anal. Chem.*, 1996, **68**, 960.

221. Y.-H, Tse, P. Janda and A.B.P. Lever, *Anal. Chem.*, 1994, **66**, 384.

222. D.L. Pilloud, X. Chen, P.L. Dutton and C.C. Moser, *J. Phys. Chem. B*, 2000, **104**, 2868.

223. J. Sagiv, *J. Am. Chem. Soc*., 1980, **102**, 92.

224. E.E. Polymeropoulos and J. Sagiv, *J. Chem. Phys.*, 1978, **69**, 1836.

225. R. Maoz, and J. Sagiv, *J. Colloid. Interface Sci.*, 1984, **100**, 465.

226. H.O. Finklea, L.R. Robinson, A. Blackburn, B. Richter, D. Allara and T. Bright, *Langmuir*, 1986, **2**, 239.

227. D.L. Allara and R.G. Nuzzo, *Langmuir*, 1985, **1**, 45.

228. D.L. Allara and R.G. Nuzzo, *Langmuir*, 1985, **1**, 52.

229. R.G. Nuzzo and D.L Allara, *J. Am. Chem. Soc*., 1983, **105**, 4481.

230. M.D. Porter, T.B. Bright, D. Allara and C.E.D. Chidsey, *J. Am. Chem. Soc*., 1987, **109**, 3559.

231. E. Sabatani and I. Rubinstein, *J. Phys. Chem.*, 1987, **91**, 6663.

232. C.D. Bain and G.M. Whitesides, *J. Am. Chem. Soc.*, 1988, **110**, 3665.

233. C.D. Bain and G.M. Whitesides, *J. Am. Chem. Soc.*, 1988, **110**, 6560.

234. C.A. Widrig, C. Chung and M.D. Porter, *J. Am. Chem. Soc*., 1991, **310**, 335.

235. A. Dalmia, C.C. Liu and R.F. Savinell, *J. Electroanal. Chem*., 1997, **430**, 205.

236. C-J. Zhong, R.C. Brush, J. Anderegg and M.D. Porter, *Langmuir,* 1999, **15**, 518.

237. P. Diao, D. Jiang, X. Cui, D. Gu, R. Tong and B. Zhong, *J. Electroanal. Chem.*, 1999, **464**, 61.

238. W. Yang, J.J. Gooding and D.B. Hibbert, *J. Electroanal. Chem*., 2001, **516**, 10.

239. R.G. Nuzzo, B.R. Zegarski and L.H. Dubois, *J. Am. Chem. Soc*., 1987, **109**, 733.

240. L.H. Dubois and R.G. Nuzzo, *Ann. Rev. Phys. Chem*., 1992, **43**, 437.

241. C.D. Bain, E.B. Troughton, Y.-T. Tao, J. Evall, G.M. Whitesides and R.G. Nuzzo, *J. Am. Chem. Soc.*, 1989, **111**, 321.

242. D. Losic, J.G. Shapter and J.J. Gooding, *Langmuir*, 2001, **17**, 3307.

243. K.I. Ozoemena and T. Nyokong, *J. Electroanal. Chem*., 2005, **579**, 283.

244. K.I. Ozoemena and T. Nyokong, *Electrochim. Acta,* 2006, **51,** 2669.

245. K.I. Ozoemena and T. Nyokong, *Talanta*, 2005, **67**, 162.

246. P.N. Mashazi, K.I. Ozoemena and T. Nyokong, *Electrochim. Acta,* 2006, **52,** 177.

247. D.E. Smith, *Crit. Rev. Anal. Chem.,* 1971, **2**, 248.

248. D.E. Smith, *Anal. Chem.,* 1976, **48**, 221.

249. J.R. Macdonald, Ed., *Impedance Spectroscopy Emphasizing Solid Materials and Systems*, Wiley/Interscience, New York, 1987.

250. C. Gabrielli, *Identification of Electrochemical Processes by Frequency Response Analysis*, Technical Report No. 004/83, SOLARTRON Instruments, Farmborough, UK, 1984.

251. D.D. Macdonald and M.C.H. McKubre, *Mod. Asp. Electrochem*., 1982, **14**, 61.

252. E. Katz and I. Wilner, *in: Ultrathin Electrochemical Chemo- and Biosensors. Technology and Performance*, V.M. Mirsky Ed. Springer- Verlag, New York, 2004, pp. 68–116, Chapter 4.

253. R.K. Shervedani and S.A. Mozaffari, *Surf. Coatings Technol.*, 2005, **198**, 123.

254. M.S. Ureta-Zanartu, A. Alarcon, C. Berrios, G.I. Cardenas-Jiron, J. Zagal and C. Gutierrez, *J. Electroanal. Chem.*, 2005, **580,** 94.

255. A. Lasia and A. Rami, *J. Electroanal. Chem.*, 1990, **294**, 123.

256. B. Boukamp, *Solid State Ionics*, 1986, **18**, 136.

257. B. Boukamp, *Solid State Ionics*, 1986, **20**, 31.

258. E.T. McAdams, A. Lackmier, J.A. Mclaughlin, D. McKen and J. Jossinet, *Biosens. Bioelectron*., 1995, **10,** 1429.

259. R.K. Mendes, R.S. Freire, C.P. Fonseca, S. Neves and L.T. Kubota, *J. Braz. Chem. Soc.*, 2004, **15,** 849.

260. M.J. Christopher and T.J. Cardwell, *Anal. Chim. Acta*, 1996, **323,** 39.

261. O. Jauregui and M.T. Galceran, *Anal. Chim. Acta*, 1997, **340,** 191.

262. D. Liu, K. Thompson and K.L.E. Kaiser, *Bull. Environ. Contam. Toxicol*., 1982, **24**, 130.

263. H. Saito, M. Sudo, T. Shigeoka and F. Yamauchi, *Envir. Toxic. Chem.*, 1991, **10**, 235.

264. M. Czaplicka, *Sci. Total Environ.*, 2004, **322,** 21.

265. M. Alexander, *Science,* 1981, **211,** 132.

266. W. Reineke, *in: Microbial Degradation of Aromatic Compounds*, D.T. Gibson Eds., Marcel Dekker, New York, 1984, p. 319.

267. B. Winter and W. Zimmermann, *in: Metal Ions in Biological Systems*, Vol.**28**, H. Sigel, A. Sigel, Eds., Marcel Dekker, New York, 1992, p. 157.

268. T. Pandiyan, O. Martinez Rivas, J. Orozco Martinez, G. Burillo Amazcua and M.M. Martinez-Carillo, *J. Photochem. Photobiol. A: Chem.*, 2002, **146**, 144.

269. M.L. Hitchman, R.A. Spackman, N.C. Ross and C. Agra, *Chem. Soc. Rev.*, 1995, **24**, 423.

270. N.S. Bryan, *Free Radical Biol. Med.*, 2006, **41,** 691.

271. E.T. Reichert and S.W. Mitchell, *Am. J. Med. Sci.* 1980, **159,** 158.

272. C.J. Hunter, *Nat. Med.*, 2004, **10**, 1122.

273. A.V. Kozlov, *Shock*, 2001, **15,** 366.

274. K.K. Chen and C.L. Rose, *JAMA*, 1952, **149,** 113.

275. C.L. Walters, *Oncology,* 1980, **37,** 289.

276. W. Lijinsky and S.S. Epstein, *Nature,* 1970, **225,** 21.

277. I.A. Wolf and A.E. Wasserman, *Science,* 1972, **177,** 15.

278. K.K. Choi and K.W. Fung, *Analyst,* 1980, **105,** 241.

279. H.H. Comly, *JAMA,* 1945, **129**, 112.

280. W.E. Donohoe, *Paediatrics,* 1949, **3**, 308.

281. H.I. Lecks, *Am. J. Dis. Child.,* 1950, **79,** 117.

282. G.M. Greenway, S.J. Haswell and P.H. Petsul, *Anal.Chim. Acta,* 1999, **387,** 1.

283. M.I.H. Helaleh and T. Korenaga, *J. Chromatogr. B,* 2000, **744,** 433.

284. X. Cai and Z. Zhao, *J. Electroanal. Chem.,* 1988, **252**, 361.

285. J.E. Newbry and M.P.L. de Haddad, *Analyst,* 1985, **110,** 81.

286. M. Trojanowicz, W. Matuszewski and B. Szostek, *Anal. Chim. Acta*, 1992, **261**, 391.

287. Z-H Wen and T-F Kang, *Talanta,* 2004, **62**, 351.

288. M.H. Pournaghi-Azar and H. Dastangoo, *J. Electroanal. Chem.,* 2004, **567,** 211.

289. A.F. Gunnison, *Fd. Cosmet. Toxicol.,* 1981, **19**, 667.

290. H. Pfanz, E. Martinoia, O.L. Lange and U. Heber, *Plant Physiol.,* 1987, **85**, 928.

291. Z. Miszalski and H. Ziegler, *Z. Naturforsch.*, 1989, **44,** 509.

292. G.D. Peise and S.F. Yang, *Biochemical and physiological effects of SO_2 on non-photosynthetic process in plants,* in W.E. Winner, H.A. Mooney, R.A.

Goldstein (Eds.), Sulphur dioxide and Vegetation, Stanford University Press, 1985, pp. 148.

293. C. Bowler, M. Van Montagu and D. Inze, *Annu. Rev. Plant Physiol. Plant Mol. Biol.*, 1992, **43**, 83.

294. R.G. Alscher, J.L. Donahue and C.L. Cramer, *Physiol. Plant.*, 1997, 224.

295. A. Safavi and B. Haghighi, *Talanta*, 1997, **44**, 1009.

296. S. Williams, Official methods of the AOAC. Arlington, V.A: *Association of Official Chemists Incorporation.* 14th Eds., Method 20, 1984, p.123.

297. C. Anderson, C.R. Warners, D.H. Daniel and K.L. Padgett, *J. Ass. Official Anal. Chem.*, 1986, **69**, 14.

298. J. Sadecke and J. Polonski, *J. Chromatography A*, 1999, **834,** 401.

299. V.C. Trenerry, *Food chemistry*, 1996, **55** 299.

300. D.R. Shankran, N. Uehera and T. Kato, *Sens. and Actuators B*, 2002, **87,** 442.

301. D.R. Shankran and S. Sriman, *Sensors and Actuators B*, 1999, **55,** 191.

302. M. Kimura and H. Shirai: *The Porphyrin Handbook*, K.M. Kadish, K.M. Smith, R. Guilard, Eds., *Applications of Phthalocyanines*, Vol. **19**, 151-177.

303. P. Karlson, *Biochemie Georg Thieme Verlag*, Stuttgart, 1962; pp.67.

304. H. Euler and K. Josephson, *Liebigs Ann. Chem*. 1927, **456**, 111.

305. M.L. Kremer, *Nature*, 1965, **205**, 384.

306. M.L. Kremer, *Trans. Faraday Soc*. 1965, **61**, 1453.

307. R. Gatt and M.L. Kremer, *Trans. Faraday Soc.* 1968, **64**, 721.

308. P. Waldmeier and H. Sigel, *Chimia (Aarau)*, 1970, **24**, 195.

309. H. Sigel, *Angew. Chem*. 1969, **81**, 161.

310. P. Waldmeier and H. Sigel, *Inorg. Chem. Acta*, 1971, **5**, 659.

311. B.C. Saunders, *Inorganic Biochemistry*. Eichhorn, G.L., Ed.; Elsevier: Amsterdam, 1973; Vol. **2**, p.989.

312. J.A. Cowan, *Inorganic Biochemistry, An Introduction*, VCH: New York, 1993.

313. H. Shirai, A. Maruyama, M. Konishi and N. Hojo, *Makromol. Chem*, 1980, **181**, 1003.

314. V. Iliev and A. Ileva, *J. Mol. Catal. A.*, 1995, **103**, 147.

315. V. Iliev, A. Ileva and L. Bilyarska, *J. Mol. Catal. A.*, 1997, **126**, 99.

316. M.R. Hoffman and B.C.H. Lim, *Environ. Sci. Technol*., 1979, **13**, 1406.

317. S.D. Boyce, M.R. Hoffman, P.A. Hong and L.M. Moberly, *Environ. Sci. Technol.*, 1983, **13**, 1406.

318. P.A. Hong, S.D. Boyce and M.R. Hoffman, *Environ. Sci. Technol.*, 1989, **23**, 533.

319. A. Kotronarou and M.R. Hoffman, *Environ. Sci. Technol.*, 1991, **25**, 533.

320. R. Belal and B. Meunier, *J. Mol. Catal.*, 1988, **44**, 187.

321. E. Larsen and A. Jorgensen, *Acta Chem Scandinavica*, 1989, **43**, 259.

322. N. Ito, T. Etoh, H. Hagiwara and M. Kato, *Synthesis*, 1997, 153.

323. A. Sorokin, J-L, Seris and B. Meunier, *Science*, 1995, **268**, 1163.

324. M. Sanchez, A. Hadasch, A. Rabion and B. Meunier, *Surf. Chem. Cat.*, 1999, **2**, 241.

325. M. Nowakowska and K. Szczubialka, *J. Photochem. Photobiol.*, 1995, **91,** 81.

326. M. Nowakowska, K. Szczubialka and S. Zapotoczny, *J. Photochem. Photobiol.,* 1996, **97,** 93.

327. S. Vollmuth, A. Zajc and R. Niessner, *Environ. Sci. Technol.*, 1994, **28,** 1145.

328. H. Al-Ekabi and N. Serpone, *J. Phys. Chem*., 1988, **92**, 5726.

329. H. Al-Ekabi, N. Serpone, E. Pelizzetti, C. Minero, M.A. Fox and R.B. Draper, *Langmuir*, 1989, **5**, 250

330. G. Al-Sayyed, J.-C. D'Oliveira and P. Pichat, *J. Photochem. Photobiol. A: Chem.*, 1991, **58**, 99.

331. A. Mills and S. Morris, *J. Photochem. Photobiol. A: Chem*., 1993, **71**, 75.

332. A. Mills, S. Morris and R. Davies, *J. Photochem. Photobiol. A: Chem.*, 1993, **70**, 183.

333. A. Mylonas and E. Papaconstantinou, *J. Mol. Catal.*, 1994, **92**, 267.

334. U. Stafford, K.A. Gray and P.V. Kamat, *J. Phys. Chem.*, 1994, **98**, 6343.

335. A. Mills and R. Davies, *J. Photochem. Photobiol. A: Chem*., 1995, **85**, 173.

336. A. Haarstrick, O. M. Kut and E. Heinzle, *Environ. Sci. Tech*., 1996, **30**, 817.

337. J.M. Kesselman, O. Weres, N.S. Lewis and M.R. Hoffman, *J. Phys. Chem. B*, 1997, **101**, 2637.

338. E. Leyva, E. Moctezuma, M.G. Ruiz and L. Torres-Martinez, *Catal. Today*, 1998, **40**, 367.

339. X. Li, J. W. Cubbage, T.A. Tetzlaff and W.S. Jenks, *J. Org. Chem*., 1999, **64**, 8509.

340. X. Li, J.W. Cubbage and W.S. Jenks, *J. Org. Chem*., 1999, **64**, 8525.

341. A. Harriman, G. Poter and M.C. Richoux, *Coord. Chem. Rev.*, 1982, **44**, 83.

342. X. Tao, W. Ma, J. Li, Y. Huang, J. Zhao and J.C. Yu, *Chem. Commun*., 2003, 80.

343. N. Nensala and T. Nyokong, *J. Mol. Catal. A: Chemical*, 2000, **164,** 69.

344. M. Hu, Y. Xu and J. Zhao, *Langmuir*, 2004, **20**, 119.

345. T. Nyokong, in: Entitled: *N_4-macrocyclic metal complexes: electrocatalysis, electrophotochemistry, and biomimetic electrocatalysis* (Eds. J.H. Zagal, F. Bedioui, J-P. Dodelet) Springer, New York, 2006, Chpt. 7.

346. M. Gattrell and D.W. Kirk, *J. Electrochem. Soc.*, 1992, **139,** 2736.

347. M. Gattrell and B. MacDougall, *J. Electrochem. Soc*., 1999, **146**, 3335.

348. Z. Ezerskis and Z. Jusys, *J. Appl. Electrochem.*, 2001, **31,** 1117.

349. Z. Ezerskis and Z. Jusys, *J. Appl. Electrochem.*, 2002, **32,** 49.

350. M.S. Ureta-Zanartu, P. Bustos, M.C. Diez, M.L. Mora and C. Gutierrez, *Electrochim. Acta*, 2001, **46,** 2545.

351. R.C. Koile and D.C. Johnson, *Anal. Chem.*, 1979, **51,** 741.

352. T. Bejerano, C. Forgacs and E. Gileadi, *J. Electroanal. Chem.*, 1970, **27,** 69.

353. A. Merz, *in: Topics in Current Chemistry, Electrochemistry IV*, vol. **152**, E. Steckhan Eds., Springer, Berlin, 1990, p. 49.

354. P. Guo, T.-W. Hui, K.-C. Wong and K.-K. Shiu, *J. Electroanal. Chem.*, 2001, **498,** 142.

355. M. Mnariquez, J.L. Bravo, S. Gutierrez-Grandos, S.S. Succar, C. Bied-Charreton, A.A. Ordaz and F. Bedioui, *Anal. Chim. Acta.*, 1999, **378,** 159.

356. G. Roslonek and J. Taraszewska, *J. Electroanal. Chem.*, 1992, **325,** 285.

357. T.R.I. Cataldi, D. Centonze and G. Ricciardi, *Electroanalysis*, 1995, **7**, 312.

358. T.R.I. Cataldi, E. Desimoni, G. Ricciardi and L. Francesco, *Electroanalysis*, 1995, **7,** 435.

359. T.J. Mafatle and T. Nyokong, *Anal. Chim. Acta* 1997, **354**, 307.

360. J. Obirai and T. Nyokong, *J. Electroanal. Chem*., 2005, **576**, 323.

361. M.S. Ureta-Zanartu, C. Berrios, J. Pavez, J. Zagal, C. Gutierrez and J.F. Marco, *J. Electroanal. Chem*., 2003, **553**, 147.

362. F. Beck, *Electrochim. Acta*, 1986, **31,** 201.

363. G. Mengoli and M. Musiani, *Electrochim. Acta*, 1988, **33,** 839.

364. N. Chebotareva and T. Nyokong, *J. Appl. Electrochem.,* 1997, **27**, 975.

365. K. Araki, L. Angnes, C.M.N. Azevedo and H.E. Toma, *J. Electroanal. Chem*., 1995, **397**, 205.

366. J.R. Caetano da Rocha, L. Angnes, M. Bertotti, K. Araki and H.E. Toma, *Anal. Chim. Acta* 2002, **452**, 23.

367. C.M.N. Azevedo, K. Araki, L. Angnes and H.E. Toma, *Electroanalysis*, 1998, **10,** 467.

368. H.L. Winnischofer, L. de Souza, K. Araki and H.E. Toma, *Anal. Chim. Acta* 2003, **480**, 97.

369. S.-M. Chen and S.-V, Chen, *Electrochim. Acta*, 2003, **48**, 4049.

370. S.-M. Chen, *J. Electroanal. Chem.,* 1996, **407,** 123.

371. I. Mayer, M.N. Eberlin, D.M. Tomazela, H.E. Toma and K. Araki, *J. Mex. Soc.*, 2005, **49,** 180.

372. S. Kim, *Bull. Korean Chem. Soc*., 2002, **23,** 1842.

373. S.-M. Chen, *J. Electroanal. Chem.,* 1996, **432,** 101.

374. C.W. Dirk, T. Inabe, K.F. Schoch Jr. and T.J. Marks, *J. Am. Chem. Soc.*, 1983, **105**, 1539.

375. D. Wöhrle, M. Eskes, K. Shigehara and A. Yamada, *Synthesis*, 1993, 194.

376. F. Hartl and K.M. Deněk, *J. Electroanal. Chem.*, 1991, 317, 179.

377. A. Ogunsipe and T. Nyokong, *J. Porphyrins Phthalocyanines*, 2005, **9,** 121.

378. R. Bounett, *Chemical Aspects of Photodynamic Therapy*, Gordon and Breach Science, Amsterdam (2000).

379. M. Kandaz, M.N.U. Yaraşir, A. Koca and Ő. Bekaroğlu, *Polyhedron*, 2002, **21,** 255.

380. J. Obirai and T. Nyokong, *Electrochim. Acta*, 2005, **50,** 3296.

381. C.C. Leznoff, L.S. Black, A. Hiebert, P.W. Causey, D. Christendat and A.B.P. Lever, *Inorg. Chim. Acta*, 2006, **359,** 2690.

382. T. Fukuda, S. Homma and N. Kobayashi, *Chem. Eur. J.*, 2005, **11**, 5205.

383. T. Fukuda, S. Homma and N. Kobayashi, *Tet. Lett.*, 2005, **46**, 2907.

384. M.J. Stillman *in Phthalocyanines: Properties and Applications*, vol. 3, Lever ABP and Leznoff CC, Eds., VCH Publishers: New York, 1993; 227-296.

385. A.B.P. Lever, E.L. Milaeva, G. Speier in Phthalocyanines: Properties and Applications, vol. 3, Leznoff CC and Lever ABP (Eds.). VCH Publishers: New York, 1993; Chapter 1; pp1 – 69.

386. K. Ban, K. Nishizawa, K. Ohta and H. Shirai, *J. Mater. Chem.*, 2000, **10,** 1083.

387. D. Worhle and V. Schmidt, *J. Chem. Soc. Dalton. Trans.*, 1988, 549.

388. J. Mack and M.J. Stillman, *J. Porphyrins Phthalocyanines*, 2001, **5** 67.

389. P.G. Tratnyek and J. Holgne, *Environ. Sci. Technol.*, 1991, **25,** 1596.

390. T. Schmidt, W. Hartung and F. Wasgestian, *Inorg. Chim. Acta*, 1998, **274,** 126.

391. S. Seelan and A.K. Sinha, *Appl. Cat. A: Gen.*, 2003, **238,** 201.

392. E.F. Perez, G. de Oliveira-Neto, A.A. Tanaka and L.T. Kubota, *Electroanalysis*, 1998, **10**, 111.

393. C. de-la-Fuente, J.A. Acuna, M.D. Vazquez, M.L. Tascon and P. Sanchez-Batanero, *Talanta*, 1999, **49,** 441.

394. J. Riber, C. de-la-Fuente, M.D. Vazquez, M.L. Tascon and P. Sanchez-Batanero, *Talanta* 2000, **52**, 241.

395. T. Malinski, in *Porphyrin Handbook, Applications: Past, Present and Future*, K.M. Kadish, K.M. Smith, R. Guilard, eds., Academic Press, New York, (2000), vol. **6**, chapt. 44, pp 231.

396. V. Iliev and D. Tomova, *Catalysis Comm.*, 2002, **3,** 287.

397. G. Schneider, D. Wöhrle, W. Spiller, J. Stark and G. Schulz-Ekloff, *Photochem. Photobiol.*, 1994, **60,** 333.

398. T. Buck, H. Bohlen, D. Wöhrle, G. Schulz-Ekloff and A.J. Andreev. *Mol. Catal.*, 1993, **80,** 253.

399. I.J. Inbaraj, M.V. Vinodu, R.G. Gandhidasan, R. Murugesan and M. Padmanbhan, *J. App. Polym. Sc.*, 2003, **89,** 3925.

400. D. Wöhrle, O. Surorova, R. Gerdes, O. Bartels, L. Lapok, N. Baziakina, S. Makarov and A. Slodek, *J. Porphyrins Phthalocyanines*, 2004, **8,** 1020.

401. D.D. Dionysiou, A.P. Khodadoust, A.M. Kern, M.T. Suidan, I. Baudin and J.-M. Laîné, *Appl. Catal. B: Environmental*, 2000, **24,** 139.

402. H.S. Sharman and S.-M. Park, *J. Electrochem. Soc.*, 2004, **151,** 61.

403. J. Obirai and T. Nyokong, *J. Electroanal. Chem.*, 2004, **573,** 77.

404. T.F. Otero and E.D. Larreta-Azelain, *Polymer*, 1988, **29,** 1522.

405. F. Bedioui, S. Trevin, J. Devynck, F. Lantoine, A. Brunet and M-A. Devynck, *Biosens. Bioelectron.*, 1996, **12,** 205.

406. T. Malinsky and Z. Taha, *Nature*, **358,** 1992, 676.

407. J. Poerschmann, Z. Zhang, F.D. Kopinke and T. Pawliszyn, *Anal. Chem.*, 1997, **69,** 597.

408. F. Hahn, B. Beden, M.J. Croissant and C. Lamy, *Electrochim. Acta*, 1986, **31**, 335.

409. K. Ozoemena, P. Westbroek and T. Nyokong, *J. Porphyrins Phthalocyanines*, 2002, **6,** 98.

410. M.P. Somashekarappa, J. Keshavayya and S. Sampath, *Pure Appl. Chem.*, 2002, **74**, 1609.

411. D.A.Van Galen and M. Majda, *Anal. Chem.*, 1998, **60**, 1549.

412. Q. Zhang, D. Huang and Y. Liu, *Synth. Met.*, 2003, **137,** 989.

413. S.L. Vilakazi and T. Nyokong, *J. Electroanal. Chem.*, 2001, **512,** 56.

414. B. Wermeckers and F. Beck, *Electrochim. Acta*, 1985, **30**, 1491.

415. N. Chebotareva and T. Nyokong, *J. Coord. Chem.*, 1997, **46,** 435.

416. A. Salimi, S. Pourbeyram and M.K. Amini, *Analyst*, 2002, **127**, 1649.

417. D.R. Shankaran and S.S. Narayanan, *Sensors and Actuators B,* 1999, **55,** 191.

418. I. Mayer, M.N. Eberlin, D.A. Tomazela, H.E. Toma and K. Araki, *J. Braz. Chem. Soc.*, 2005, **16,** 418.